ON WAVE-WAVE INTERACTIONS ON THE OCEAN SURFACE

by

MAMOUN NACIRI

DIPLOME D'INGENIEUR CIVIL DES PONTS ET CHAUSSEES
1985

MASTER OF SCIENCE, MASSACHUSETTS INSTITUTE OF TECHNOLOGY
1987

SUBMITTED TO THE DEPARTMENT OF CIVIL ENGINEERING
IN PARTIAL FULFILLMENT OF THE REQUIREMENTS
FOR THE DEGREE OF

DOCTOR OF PHILOSOPHY IN CIVIL ENGINEERING
at the
MASSACHUSETTS INSTITUTE OF TECHNOLOGY
February, 1992

Signature of the Author _____
Department of Civil Engineering
September, 27th 1991

Certified by _____
Chiang C. Mei
Professor of Civil Engineering
Thesis Supervisor

Accepted by _____
Eduardo Kausel
Chairman, Department
Committee on Graduate Students

ON WAVE-WAVE INTERACTIONS ON THE OCEAN SURFACE

by
MAMOUN NACIRI

Submitted to the department of Civil Engineering
on September 27th, 1991 in partial fulfillment of the requirements
for the degree of Doctor of Philosophy
in Civil Engineering

ABSTRACT

Part 1
Bragg scattering of sound from a line source by surface waves

The strong scattering of plane sound waves from a line source in a waveguide is analysed for a hard bottom and a soft undulatory surface representing one or two uniform surface waves. If the waveguide is shallow enough, it only sustains one acoustic propagating mode. The near field of a line source is then approximated by two outgoing plane sound waves. In the presence of one surface wave, sound is radiated and scattered in the same two directions. When two surface waves are present, each outgoing sound wave is, in general, scattered in two new directions in the horizontal plane. Furthermore, if the two surface waves satisfy one of two geometrical criteria, multiple scattering occurs and sound is resonantly scattered in a third new direction. Evolution equations are deduced for the sound wave envelopes, and the corresponding far field is asymptotically matched with the near field of the source. These envelopes are strongly dispersive and propagate in many directions.

Part 2
Interactions of short and long waves on the sea surface

The evolution of a weakly nonlinear short wave interacting with a long gravity wave is investigated using a formulation based on Lagrangian variables. The ratio of the long to short wave wavenumbers is assumed to be very small $\frac{K}{k} \ll 1$. Both coplanar and non-coplanar interactions are examined.

In Chapter I, the long wave is a weakly nonlinear irrotational Stokes wave. The amplitude modulation of the short wave is found to be the product of a factor already deduced by Longuet-Higgins & Stewart(1960) and a factor satisfying the nonlinear Schrödinger equation.

In Chapter II, we allow the long wave to assume a finite amplitude. Gerstner's exact solution in Lagrangian variables is chosen for simplicity. Analytical results on the modulation of short waves agree fairly well with existing theories which rely on numerically obtained long waves. The evolution of short waves is described by a nonlinear Schrödinger equation with explicit time-periodic coefficients. Analysis of the stability of uniform short waves to sideband disturbances shows the appearance of additional bands of instability. Numerical results from both the nonlinear evolution and a lower order dynamical system suggest that the evolution of a uniform short wave disturbed by its most unstable sideband can become chaotic when the short wave slope increases and (or) when the long to short wave frequency ratio decreases.

In Chapter III, the short waves are incident at an angle θ relative to the steep Gerstner wave. The linear modulation of the short waves is analysed for finite θ. For small θ, the nonlinear evolution of the short wave envelope is described by a two-dimensional Schrödinger equation with explicit time-periodic coefficients. The Benjamin-Feir stability of uniform short waves to two-dimensional sidebands shows the proliferation of instability bands in addition to the single instability strip found in the absence of long waves.

Thesis Supervisor: Chiang C. Mei
Title: Professor of Civil Engineering

It is only after you have come to know the surface of things
that you can venture to seek what is underneath.
But the surface of things is inexhaustible.

Italo Calvino

Palomar (1983)

To Amal

ACKNOWLEDGMENTS

I am greatly indebted to my advisor Chiang C. Mei. Without his continuous support, invaluable insights and communicative enthusiasm, much of the present work would not have been possible. These years at MIT have been full of challenge and excitement, thanks to you Chiang.

I thank the members of my thesis committee for their contributions. I am especially grateful to Professor Jack Wisdom for long discussions and for his class on solar dynamics which proved to be very useful. Many thanks also to Professor George V. Frisk for contributing the experience of an acoustician.

We thank the National Science Foundation, Fluid Mechanics and Ocean Engineering (Grant MSME8813121) and the Office of Naval Research, Fluid Mechanics Program (N00014-87-K-0121 and N00014-90-J-1163) for supporting this research.

Very special thanks go to my wife Amal for the support, encouragement and care she provided since we met and even more so during the last stressful months of my dissertation.

Many thanks go to my friends in Parsons Laboratory who have made this place special to me.

Finally, I would like to thank my parents for showing me the value of higher education. Their efforts, I think, have born fruit.

TABLE OF CONTENTS

PART 2
INTERACTIONS OF SHORT AND LONG WAVES ON THE SEA SURFACE

Chapter II: Two-Dimensional Interactions of Weak Short Waves and a Finite Amplitude Long Wave

Part 1
BRAGG SCATTERING OF SOUND FROM A LINE SOURCE BY SURFACE WAVES

Notations for Part 1

A	Envelope of the right going sound wave.
$A^{\pm}$	Envelope of the right going sound wave for the $\pm$ radiation problems.
$\tilde{A}^{+}$	Fourier transform of the envelope of the right going sound wave in the "+" radiation problem.
$\mathcal{A}^{\gtrless}_{n,j}$	Discretized envelope of the right going sound wave in the $\pm$ half planes at location $j\Delta x$ and time $n\Delta t$.
B	Envelope of the left going sound wave.
B_i	Envelope of the i-th left going sound wave.
$B^{\pm}$	Envelope of the left going sound wave for the $\pm$ radiation problems.
$\tilde{B}^{+}$	Fourier transform of the envelope of the scattered sound wave in the "+" radiation problem.
$\tilde{B}_i^{+}$	Fourier transform of the envelope of the i-th scattered sound wave in the "+" radiation problem.
$\mathcal{B}^{\gtrless}_{i_{n,j}}$	Discretized envelope of the i-th scattered sound wave in the $\pm$ half planes at location $j\Delta x$ and time $n\Delta t$.
C	Velocity of sound in water.
C_ℓ	Phase velocity of acoustic mode ℓ .
C_{g_ℓ}	Group velocity of acoustic mode ℓ .
C_{g_A}	Normalized group velocity associated with the sound envelope A.
C_{g_B}	Normalized group velocity associated with the sound envelope B.
$C_{g_{B_i}}$	Normalized group velocity associated with the sound envelope B_i.
C_{g_x}	Diagonal matrix formed by the x-component of the group velocities associated with the sound envelopes.
C_{g_y}	Diagonal matrix formed by the y-component of the group velocities associated with the sound envelopes.
D	Amplitude of a uniform surface wave.
D_i	Amplitude of the i-th uniform surface wave.
$\mathcal{D}$	Directionality of the acousitc field of a line source.
f	Envelope of the radiated sound from the line source.
h	Water depth.
I	Identity matrix.
k	Acoustic wavenumber.
$\vec{k}_i$	Horizontal wavenumber of the i-th scattered sound wave.
k_w	Wavenumber of the surface wave.
k_{w_i}	Wavenumber of the i-th surface wave.
ℓ	Acoustic mode number.
L	Complex amplitude along the line source of sound.
$\tilde{L}$	Fourier amplitude along the line source of sound.
m	x-component of the surface wave wavenumber vector.
m_i	x-component of the i-th surface wave wavenumber vector.
n	y-component of the surface wave wavenumber vector.
n_i	y-component of the i-th surface wave wavenumber vector.

N	Matrix of coupling frequencies.
p	Pressure field.
P	Eigenvalue matrix.
U	Vector of sound envelopes.
$\tilde{U}$	Fourier transform of the vector of sound envelopes.
$U^{\gtrless}_{n,j}$	Discretized vector of sound envelopes in the $\pm$ half planes.
S	Phase function of the right going radiated sound wave.
S_i	Phase function of the i-th scattered sound wave.
t	Time variable.
t_1	Stretched time variable.
T	Normalized time variable.
x	Horizontal space variable.
x_1	Horizontal stretched space variable.
X	Normalized horizontal space variable.
y	Horizontal transverse space variable.
y_1	Horizontal transverse stretched space variable.
Y	Reduced transverse coordinate.
z	Vertical spatial variable.
z_0	Depth of the line source.
α	Normalized coupling frequency.
α_i	Normalized coupling frequency dur to the i-th surface wave.
β	Parameter defined as $\alpha/\Lambda\cos\theta$.
γ	Vertical dependence of the outgoing sound wave.
γ_i	Vertical dependence of the i-th scattered sound wave.
δ	Dirac's generalized function.
ϵ	Small parameter scaling as the surface wave slope.
ζ	Free surface elevation.
ζ_1	Contribution of the free surface elevation at $\mathcal{O}(\epsilon)$.
η	Vertical component of the acoustic wavenumber.
η_ℓ	Vertical component of the acoustic wavenumber for the ℓ-th mode.
θ	Incidence angle of sound relative to the x-axis.
θ_i	Inclination of the i-th surface wave relative to the x-axis.
Θ	Angle variable in the evaluation of the contour integral.
κ_ℓ	Horizontal wavenumber of the ℓ-th evanescent mode
λ	Acoustic wavelength.
Λ	Normalized group velocity for acoustic mode 0.
μ	x-component of the modulational wavenumber.
ν	y-component of the modulational wavenumber.
ξ	Horizontal component of the acoustic wavenumber vector.
ξ_ℓ	Horizontal component of the wavenumber vector for the ℓ-th acoustic mode.
π	3.14159265 ...
Π	Strength of the line source.
ρ_o	Density of water.
σ	Modulational frequency of sound envelopes.

σ_i	i-th modulational frequency of sound envelopes.
Φ	Sound potential in the far field of the source.
Φ_i	Sound potential in the far field of the source at $\mathcal{O}(\epsilon^i)$.
$\vec{\chi}$	Modulational vector for sound envelopes.
ψ	Slowly varying sound potential in the near field of the line source.
ψ_i	Contribution to ψ at $\mathcal{O}(\epsilon^i)$.
Ψ	Sound potential in the near field of the line source.
ω	Radian frequency of monochromatic sound.

1. INTRODUCTION

1.1. Literature Review

The literature on sound scattering by sea waves is immense. An exhaustive account will not be given here. Instead, we shall focus on some aspects directly relevant to our study. For a survey of the literature on the scattering of sound by the ocean surface, the reader is referred to the review article by Fortuin(1970) and to the book by Brekhovskikh & Lysanov(1982).

Non-resonant scattering

Ever since the well-known contribution of Lord Rayleigh, considerable work has been done on the scattering of sound by a periodic surface. Despite the apparent simplicity of the scatterer, the analysis can be very complicated, cf. Uretsky(1954), Holford(1981b), Chuang *et al.*(1981) and DeSanto(1981). However, the sea surfaces of practical interest in sound scattering applications are often very rough and irregular. This precludes in general an exact analytical solution for the scattering problem. Instead, one usually adopts one of two types of approximations. The first is the *small waveheight approximation* under which the maximum excursion, a, of the surface must be less than both the radiation wavelength λ and the surface principal radii of curvature or equivalently the surface wavelength λ_w. Rice(1951) was one of the first to formulate the Method of Small Perturbation (MSP). Its realm of validity can be summarized in terms of the Rayleigh number by $P = 2k\sigma\cos\theta \ll 1$ where $k = \frac{2\pi}{\lambda}$, σ and θ are respectively the sound wavenumber, the rms waveheight and the incidence angle measured from the vertical. Extensive applications of this method can be found in Feinberg(1961) and Bass & Fuks(1978).

The second type of approximation is the *tangent plane approximation*, or Kirchhoff approximation after the Kirchhoff principle in diffraction theory. Here the surface wave can be of finite amplitude, *i.e.*, a and λ_w are comparable. It is however required that the radiation wavelength be much smaller than the local radii of curvature r_c so that within a few wavelengths λ from a given point, the surface can be well approximated by its local tangent plane. There must be a restriction on

the incidence angle in order to avoid shadowing or multiple scattering phenomena. These requirements are summarized by the condition $2kr_c \cos\theta \gg 1$.

In reality, the ocean surface is composed of scales ranging from a few centimeters for capillary waves to hundreds of meters for long gravity waves and swells. Under the simple description of the ocean surface known as the two-scale model, the shorter waves satisfy $2k\sigma \cos\theta \ll 1$ and the longer waves $2kr_c \cos\theta \gg 1$ (see Wright(1968) and Bass *et al* (1968)). Extensive references can be found in Brekhovskikh & Lysanov(1982) and McDaniel & Gorman(1983).

Realistic ocean wave fields also include many directions of propagation. Lakhtakia *et al* (1985), for instance, assumed a partially illuminated doubly periodic steady surface in a semi-infinite space and analysed the weak scattering of a plane incident wave. Holford(1981a) considered the scattering by two gravity waves propagating at right angle. The author concludes that "in addition to the characteristic directions associated with the two individual surface waves, there is a multiplicity of cross coupled directions which can contribute to the received energy ...". However, his theory does not go into such mechanism in detail.

Resonant scattering

In most of the literature mentioned above, the scattered field is assumed to be small compared to the incident field, *i.e.*, a correction term in a perturbation series solution. However, this is not always true. Medwin *et al* (1986) have reported that sound scattered from a point source by a specific kind of rough surface may have a cylindrical spreading. This *boundary wave* therefore dominates the spherically spreading incident sound wave for ranges $kr \gg 1$.

Another situation where the scattered field is no longer weak is that of Bragg resonance. Much of the literature on this topic is concerned with sound in ducts with variable cross-section. Samuels(1959) considered a hard walled waveguide with two rough boundaries described by their autocorrelation function. He then expresses the spectrum of the fluctuating pressure in terms of the wavenumber spectrum of the wall roughness. However, when applying this formulation to sinusoidally undulated walls, the perturbation breaks down near resonance and the solution is

not uniformally valid. Salant(1973) studied a hard walled waveguide with sinusoidal in or out of phase undulations. A regular perturbation expansion is adopted. Again, in the vicinity of resonance, the scattered field can outgrow the incident field in contradiction with the perturbation series assumption.

Nayfeh(1974) and Nayfeh & Asfar(1974) solved Salant's problem by a perturbation series method coupled with a multiple scale analysis and thus obtained a uniformally valid solution. Resonance is allowed to be met approximately with the introduction of a detuning parameter. It is found that the behavior of modal amplitudes is governed by a set of coupled ordinary differential equations for the envelopes. Nayfeh & Kandil(1978) also considered a cylindrical hard walled duct whose radius perturbation is a superposition of sine waves. The analysis followed the steps of Nayfeh(1974). More recently, Anand & George(1986) considered an isovelocity ocean with a sinusoidal moving free surface, pressure-release boundary conditions are imposed on the free surface and on the sea bottom. The authors include in their first order solution a Doppler shift due to the surface motion. Since the ratio of surface wave to sound wave frequency is usually very small, their theory which omits other second order effects such as nonlinearity on the free surface, is rather questionable.

Recently Naciri(1987) and Mei & Naciri(1991) developed a theory for the Bragg scattering of sound waves by a long crested ocean free surface. They allowed the amplitudes of both the sound and surface waves to vary slowly in space and time and examined the influence of the sea surface spectrum on the scattered sound. In particular, they studied the case where the sea wave is modulated by a slowly varying current.

With a view to explaining the presence of secondary peaks in the Doppler spectrum of Crombie(1955), Hasselmann(1966) proposed a scattering mechanism based on the general theory of wave-wave interactions whereby two gravity waves propagating in different directions may interact and give rise to a forced wave satisfying the Bragg resonance condition. Since the forced surface wave with wavenumber $k_{w_1} \pm k_{w_2}$ and frequency $\omega_{w_1} \pm \omega_{w_2}$ does not satisfy the dispersion relation for deep water gravity waves (Phillips, 1977), its amplitude remains a second order

quantity. The corresponding scattered sound envelope is therefore expected to be smaller than the scattered sound from one surface wave. Barrick(1972) allowed for similar wave-wave interactions in the context of the scattering of radio waves by a two-dimensional ocean surface.

1.2. Objectives of the Present Work

We are concerned here with a waveguide, whose free surface is corrugated due to the presence of uniform periodic surface waves extending throughout all space ($|x| < \infty$) and whose bottom is flat and impenetrable. This is of course an idealization since in reality other complex factors are known to exist in shallow seas such as bottom dissipation through a layer of sediment or radiation losses to the deformable sea bed. We are interested in a strong scattering mechanism which can be more easily detected even if losses at the bottom are not negligible.

For the acoustic and surface waves of interest (see Appendix A), the ratio of surface to sound wave frequency is small enough to assume legitimately that the free surface is frozen in time and that gravity effects are negligible. On the water surface, a pressure release boundary condition is adopted. A line source located at $(x, z) = (0, z_0)$ emits monochromatic sound waves with wavenumber k and radian frequency ω. The source envelope is gradually turned on and then tapered off, after a long time interval ($\omega t \gg 1$). The waveguide is shallow enough to sustain only one propagating acoustic mode. In the neighborhood of the sound source ($k|x| \leq \mathcal{O}(1)$), the presence of the corrugated surface wave is negligible and the near field can eventually be approximated by two outgoing plane sound waves propagating to the left and to the right. In the far field ($k|x| \gg 1$) where the undulations of the free surface are important, the envelopes of the scattered sound waves are governed by a set of coupled asymptotic equations. The near and far field are then connected with matched asymptotics.

In §2 , the line source radiates two outgoing sound waves at angles θ and $\pi - \theta$ relative to the positive x-axis. The ocean surface consists here of one wave only which propagates along the x-axis. The outgoing sound waves at angle θ ($\pi - \theta$)

resonates with the surface wave giving rise to a scattered sound wave in the direction $\pi - \theta$ (θ). An analytical solution for the envelope of the left and right propagating sound waves is then derived. The influence of θ on the evolution of the sound envelope is investigated.

In §3, the ocean surface consists of two surface waves propagating in arbitrary directions. The sound source now radiates two opposite and outgoing sound waves in the $\pm$ x-directions. In general (*Case 1*), each outgoing sound wave resonates with the two surface waves yielding two scattered sound waves each. Sound therefore propagates in a total of six directions. If, however, the surface waves intersect at right angle (*Case 2*) or if one surface wave is collinear to an outgoing sound wave (*Case 3*) multiple scattering occurs owing to a forced surface wave as described earlier by Hasselman(1966). Sound propagates then in two sets of opposite directions, one of which being the $\pm$ x-axes. Asymptotic equations for the corresponding envelopes are deduced for the acoustic far field. Dispersion effects in the sound envelopes are analysed in §4.

The near field of the line source is then connected to its far field by asymptotic matching. To investigate the transient evolution of the sound envelopes, a numerical method is employed while the sound source is active. A Fourier method is then used to compute the envelopes for larger times. It is found, for instance, that the envelope of a right propagating scattered sound wave may propagate both to the right and to the left owing to the coupling from the undulatory free surface of the waveguide.

A detailed description of our results and conclusions is given in the general summary at the end of Part 1.

2. EVOLUTION OF THE ACOUSTIC FIELD OF A SOUND SOURCE IN THE PRESENCE OF ONE UNIFORM SURFACE WAVE.

2.1. Bragg Scattering in an Underwater Sound Channel

2.1.1 *Governing equations*

Consider an underwater sound channel of constant depth h and characterized by a pressure release boundary condition at the free surface and a hard boundary condition at the impenetrable bottom. The acoustic pressure is defined in terms of the velocity potential Φ as

$$p = -\rho_0 \frac{\partial \Phi}{\partial t} \tag{2.1}$$

where ρ_0 is the static density of water assumed to be constant. For relatively weak acoustic intensities, the potential Φ is governed by the linearized wave equation

$$\nabla^2 \Phi - \frac{1}{C^2} \frac{\partial^2 \Phi}{\partial t^2} = 0 \qquad -h < z < \zeta \tag{2.2}$$

where C is the velocity of sound in water. The bottom boundary condition is

$$\frac{\partial \Phi}{\partial z} = 0 \qquad z = -h \tag{2.3}$$

In the presence of a train of gravity waves, the pressure must vanish at the free surface $z = \zeta(x, y, t)$, *i.e.*

$$\Phi(x, y, z, t) = 0 \qquad z = \zeta \tag{2.4}$$

Provided that the amplitude of the gravity wave is small compared to both the acoustic and the surface wave wavelengths, we may Taylor expand (2.4) around the mean sea level

$$\Phi(x, y, z, t) + \zeta \Phi_z(x, y, z, t) = \mathcal{O}(\zeta^2) \tag{2.5}$$

A solution of (2.2), (2.3) and (2.5) is sought in perturbation series of ϵ

$$\Phi = \Phi_0 + \epsilon \Phi_1 + \mathcal{O}(\epsilon^2) \qquad \zeta = \epsilon \zeta_1 + \mathcal{O}(\epsilon^2) \tag{2.6a - b}$$

Since the acoustic waves interact with and are resonated by the undulatory free surface, slowly varying scales must be introduced

$$(x_1, y_1, t_1) = \epsilon(x, y, t) \tag{2.7}$$

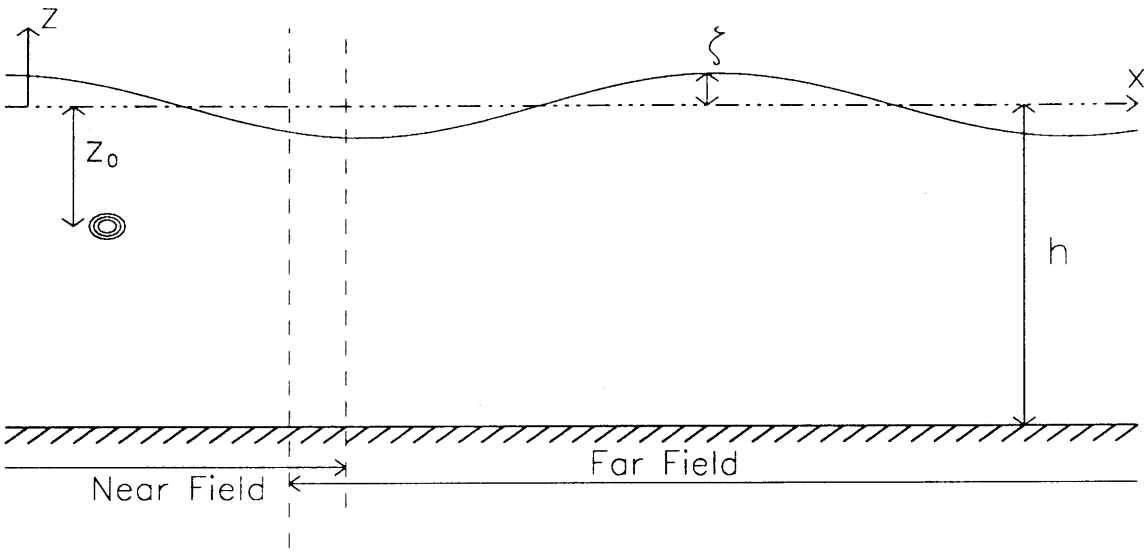

Figure 2.1: Geometry of the acoustic waveguide.

From the substitution of $(2.6a-b)$ in the governing equations, we obtain at $\mathcal{O}(1)$

$$\nabla^2\Phi_0 - \frac{1}{C^2}\frac{\partial^2\Phi_0}{\partial t^2} = 0 \tag{2.8a}$$

$$\frac{\partial\Phi_0}{\partial z} = 0 \qquad z = -h, \qquad \Phi_0 = 0 \qquad z = 0 \tag{2.8b-c}$$

Let the solution consist of two plane acoustic waves one of which is propagating at an angle θ relative to the x-axis, *i.e.*

$$\Phi_0(x,y,z,t,x_1,y_1,t_1) = \left\{A(x_1,y_1,t_1)e^{iS} + B(x_1,y_1,t_1)e^{iS_1}\right\}\cos\eta(z+h) \tag{2.9a}$$

The first term represents the incident wave where the phase function S is defined by

$$S = \xi(x\cos\theta + y\sin\theta) - \omega t \tag{2.9b}$$

and

$$\xi^2 + \eta^2 = k^2 = \frac{\omega^2}{C^2} \tag{2.9c}$$

where k and ω are respectively the acoustic wavenumber and radian frequency. The second term in $(2.9a)$ represents the resonantly scattered wave. The phase function S_1 is yet unknown and awaits the analysis of resonance.

Let us first analyse the incident wave. Satisfaction of $(2.8c)$ requires that $\cos\eta h$ vanish, *i.e.*

$$\eta_\ell h = (\ell + \frac{1}{2})\pi \qquad \ell = 0,1,\ldots \tag{2.10}$$

where ℓ refers to the acoustic mode. To ensure propagation

$$\xi_\ell^2 = k^2 \left[1 - (\ell + \frac{1}{2})^2 \frac{\pi^2}{k^2 h^2} \right] \tag{2.11}$$

must be positive. For large normalized water depths kh, several propagating modes are sustained. However, when $\frac{\pi}{2} \leq kh \leq \frac{3\pi}{2}$, there is only one propagating mode ($\ell = 0$) while $\ell > 0$ correspond to evanescent modes.

For a propagating mode ℓ, the constant phase lines propagate in the horizontal plane at the phase velocity

$$C_\ell = \frac{\omega}{\xi_\ell} = \frac{C}{\sqrt{1 - \left[(\ell + \frac{1}{2}) \frac{\pi}{kh} \right]^2}} \tag{2.12}$$

Note that the phase velocity C_ℓ is greater than C and may become infinite in the vicinity of cutoff. The group velocity, *i.e.* the velocity at which energy travels in the horizontal direction is defined by

$$C_{g_\ell} = \frac{\partial \omega}{\partial \xi_\ell} = C \sqrt{1 - \left[(\ell + \frac{1}{2}) \frac{\pi}{kh} \right]^2} \tag{2.13}$$

Note that the group velocity is always finite and less than C. More importantly, (2.12) and (2.13) show that, for a given mode ℓ, different sound wave wavelengths propagate at different speeds. The waveguide is therefore dispersive. For simplicity, we assume that $\ell = 0$ is the only propagating mode.

The governing equations at $\mathcal{O}(\epsilon)$ are

$$\nabla^2 \Phi_1 - \frac{1}{C^2} \frac{\partial^2 \Phi_1}{\partial t^2} = -2 \nabla_1 \cdot \nabla \Phi_0 + \frac{2}{C^2} \frac{\partial^2 \Phi_0}{\partial t \partial t_1}. \tag{2.14a}$$

$$\frac{\partial \Phi_1}{\partial z} = 0 \qquad z = -h, \qquad \Phi_1 = -\zeta_1 \frac{\partial \Phi_0}{\partial z} \qquad z = 0 \tag{2.14b-c}$$

For the acoustic and surface wave wavelengths considered here, the ratio of sound frequency to surface wave frequency is very large (see Appendix A), therefore justifying the frozen surface assumption, *i.e.*

$$\zeta_1 = \frac{1}{2} D e^{imx} + (*) \tag{2.14d}$$

where m is the wavenumber and D the amplitude of a gravity wave propagating along the x-axis. Substitution of $(2.14d)$ in $(2.14c)$ yields

$$\Phi_1 = \frac{\eta_0}{2}(De^{imx} + D^*e^{-imx})(Ae^{iS} + Be^{iS_1}) \qquad z = 0 \tag{2.15}$$

We proceed to analyse the resonance condition on the basis of (2.15).

2.1.2. *Resonance condition and evolution equations*

The analysis of resonance follows that of Naciri & Mei(1988) for surface waves propagating over a doubly sinusoidal bottom topography. The following two phase functions arise from (2.15)

$$S \pm mx = (\xi_0 \cos\theta \pm m)x + \xi_0 \sin\theta y - \omega t \tag{2.16}$$

Any of these two phase functions corresponds to an acoustic mode provided that it satisfies the homogeneous equation $(2.8a)$, *i.e.*

$$|\nabla(S \pm mx)|^2 = (\xi_0 \cos\theta \pm m)^2 + (\xi_0 \sin\theta)^2 = \xi_0^2 \tag{2.17a}$$

this can be rewritten as

$$\begin{cases} (\xi_0 \cos\theta \pm m)^2 + (\xi_0 \sin\theta \pm n)^2 = \xi_0^2 \\ n = 0 \end{cases} \tag{2.17b}$$

Geometrically, $(2.17b)$ can be interpreted as the intersection of the m-axis with a circle of radius ξ_0 centered at one of he following four points $(\mp\xi_0 \cos\theta, \mp\xi_0 \sin\theta)$. Upon choosing the negative signs in $(2.17b)$, the circle is centered at $(\xi_0 \cos\theta, \xi_0 \sin\theta)$ as shown in figure 2.2 and the corresponding solution is

$$m = 2\xi_0 \cos\theta \tag{2.18}$$

The sign combination $(-,+)$ in $(2.17b)$ yields also the solution (2.18). On the other hand, the combinations $(+,\pm)$ yield $m = -2\xi_0 \cos\theta$ which is equivalent to (2.18) since the sense of propagation of the surface wave is irrelevant when the free surface is assumed to be frozen. In view of (2.18), the expression of the new phase function may now be deduced

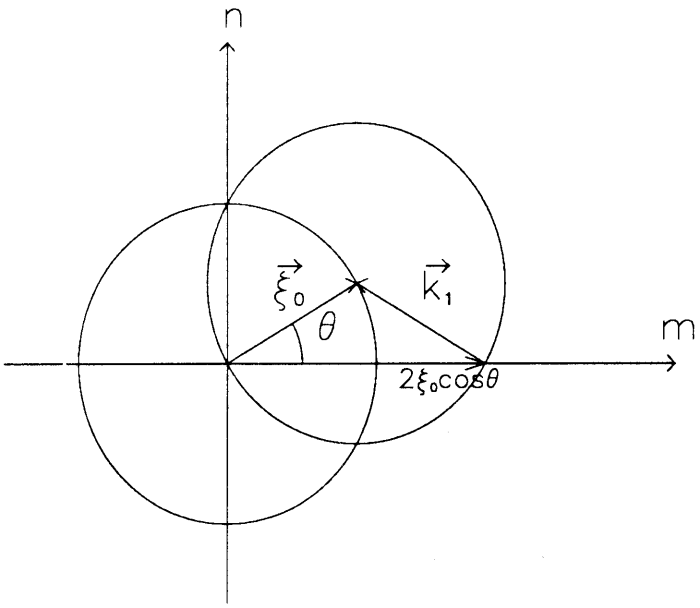

Figure 2.2: Geometrical interpretation of the resonance condition for the scattered sound wave in the (m,n) wavenumber domain. $\vec{\xi}_0$ and $\vec{k}_1$ are respectively the horizontal wavenumber vectors of the incident and scattered sound waves.

$$S_1 = S - 2\xi_0 \cos\theta x = \xi_0(-x\cos\theta + y\sin\theta) - \omega t \tag{2.19}$$

Substitution of (2.18) and (2.19) in (2.15) yields

$$\Phi_1 = \frac{\eta_0}{2}(DBe^{iS} + D^*Ae^{iS_1}) + \text{NRT} \tag{2.20}$$

after omitting the Non-Resonant Terms. Let us seek a solution for Φ_1 in the form

$$\Phi_1 = \gamma(z)e^{iS} + \gamma_1(z)e^{iS_1} \tag{2.21}$$

Then, from $(2.13a-b)$ and (2.20), $\gamma(z)$ satisfies

$$\frac{\partial^2\gamma}{\partial z^2} + \eta_0^2\gamma = -2i\frac{k}{C}\{\frac{\partial A}{\partial t_1} + \frac{\xi_0}{k}C\cos\theta\frac{\partial A}{\partial x_1} + \frac{\xi_0}{k}C\sin\theta\frac{\partial A}{\partial y_1}\}\cos\eta_0(z+h) \tag{2.22a}$$

and the boundary conditions

$$\frac{\partial\gamma}{\partial z} = 0 \qquad z = -h, \qquad \gamma = \frac{\eta_0}{2}DB \qquad z = 0 \tag{2.22b-c}$$

Since $\cos\eta_0(z+h)$ is a solution of the homogeneous problem, a solvability condition must be enforced

$$\int_{-h}^{0}(\frac{\partial^2\gamma}{\partial z^2}+\eta_0^2\gamma)\cos\eta_0(z+h)dz = \left[\frac{\partial\gamma}{\partial z}\cos\eta_0(z+h) - \gamma\frac{\partial}{\partial z}(\cos\eta_0(z+h))\right]_{-h}^{0} \tag{2.23}$$

Straightforward integration yields an equation describing the evolution of the sound amplitude A over long time and spatial scales:

$$\frac{\partial A}{\partial t_1} + \frac{\xi_0}{k} C \cos\theta \frac{\partial A}{\partial x_1} + \frac{\xi_0}{k} C \sin\theta \frac{\partial A}{\partial y_1} = \frac{i}{2} \frac{\eta_0^2 C}{kh} DB \tag{2.24}$$

Likewise, $\gamma_1(z)$ satifisfies

$$\frac{\partial^2 \gamma_1}{\partial z^2} + \eta_0^2 \gamma_1 = -2i \frac{k}{C} \left\{ \frac{\partial A}{\partial t_1} - \frac{\xi_0}{k} C \cos\theta \frac{\partial A}{\partial x_1} + \frac{\xi_0}{k} C \sin\theta \frac{\partial A}{\partial y_1} \right\} \cos\eta_0(z+h) \tag{2.25a}$$

along with the bottom and free surface boundary condition

$$\frac{\partial \gamma_1}{\partial z} = 0 \qquad z = -h, \qquad \delta_1 = \frac{\eta_0}{2} D^* A \qquad z = 0 \tag{2.25b-c}$$

Solvability condition yields the evolution equation for B

$$\frac{\partial B}{\partial t_1} - \frac{\xi_0 C}{k} \cos\theta \frac{\partial B}{\partial x_1} + \frac{\xi_0 C}{k} \sin\theta \frac{\partial B}{\partial y_1} = \frac{i}{2} \frac{\eta_0^2 C}{kh} D^* A \tag{2.26}$$

Upon normalizing the spacial coordinates by the acoustic wavelength k and time by the sound radian frequency ω, (2.24) and (2.26) become

$$\frac{\partial A}{\partial t_1} + \Lambda \cos\theta \frac{\partial A}{\partial x_1} + \Lambda \sin\theta \frac{\partial A}{\partial y_1} = i\alpha B \tag{2.27a}$$

and

$$\frac{\partial B}{\partial t_1} - \Lambda \cos\theta \frac{\partial B}{\partial x_1} + \Lambda \sin\theta \frac{\partial B}{\partial y_1} = i\alpha^* A \tag{2.27b}$$

where

$$\Lambda \equiv \sqrt{1 - \left[\frac{\pi}{2kh}\right]^2} \qquad \alpha \equiv \frac{1}{2} \frac{\eta_0^2}{kh} D \tag{2.28a-b}$$

Note that α is has the dimension of a frequency. This coupling frequency decreases with the normalized water depth kh. Shallow acoustic waveguides are therefore more efficient scatterers. Simple manipulations of $(2.27a-b)$ yield

$$\frac{\partial}{\partial t_1} \left[|A|^2 + |B|^2 \right] + \nabla \cdot \left[\vec{C}_{g_A} |A|^2 + \vec{C}_{g_B} |B|^2 \right] = 0 \tag{2.29}$$

where

$$\vec{C}_{g_{A,B}} = \Lambda(\pm\cos\theta, \sin\theta) \tag{2.30a-b}$$

Eq. (2.29) represents the conservation of sound intensity and will be used later to check the accuracy of numerical computations.

2.2. Near Field of a Line Source in an Underwater Sound Channel

In the underwater sound channel previously described, we consider a horizontal line source located at $(x, z) = (0, z_0)$ and whose elements have a complex amplitude $L(y)$. When $L(y) = 1$, the acoustic field of the line source can be approximated by two outgoing plane sound waves propagating in the $\pm$ x-directions (normal radiation). When $L(y) = e^{-ipy}$, the outgoing plane sound waves are inclined relative to the x-axis (oblique radiation). We also allow the source strength to be slowly modulated in time. The governing equations for the sound potential Ψ for an arbitrary function $L(y)$ are

$$\nabla^2\Psi - \frac{1}{C^2}\frac{\partial^2\Psi}{\partial t^2} = \delta(x)\delta(z - z_0)L(y)\Pi f(t_1)e^{-i\omega t} \qquad -h < z < 0 \qquad (2.31a)$$

$$\frac{\partial\Psi}{\partial z} = 0 \qquad z = -h, \qquad \Psi = 0 \qquad z = \zeta \qquad (2.31b - c)$$

where ∇ is the three-dimensional gradient $(\frac{\partial}{\partial x}, \frac{\partial}{\partial y}, \frac{\partial}{\partial z})$, $f(t_1)$ represents the slowly modulated amplitude of the sound source and Π its maximum strength. We seek a solution of the form:

$$\Psi = \psi(x, y, z, t_1)e^{-i\omega t} + c.c. \qquad (2.32a)$$

and represent ψ as a perturbation series of ϵ:

$$\psi = \psi_0 + \epsilon\psi_1 + \mathcal{O}(\epsilon^2) \qquad (2.32b)$$

In view of the series expansion $(2.6b)$, the leading order potential ψ_0 satisfies

$$\nabla^2\psi_0 + k^2\psi_0 = \Pi f(t_1)\delta(x)\delta(z - z_0)L(y) \qquad -h < z < 0 \qquad (2.33a)$$

$$\frac{\partial\psi_0}{\partial z} = 0 \qquad z = -h, \qquad \psi_0 = 0 \qquad z = 0 \qquad (2.33b - c)$$

In order to solve $(2.33a - c)$, it is convenient to introduce the Fourier transform pair with respect to x:

$$\tilde{u}(\mu) = \int_{-\infty}^{\infty} e^{-i\mu x}u(x)dx \qquad u(x) = \frac{1}{2\pi}\int_{-\infty}^{\infty} e^{i\mu x}\tilde{u}(\mu)d\mu \qquad (2.34a)$$

and likewise the Fourier transform pair with respect to y:

$$\hat{v}(\nu) = \int_{-\infty}^{\infty} e^{-i\nu y}v(y)dy \qquad v(y) = \frac{1}{2\pi}\int_{-\infty}^{\infty} e^{i\nu y}\hat{v}(\nu)d\nu \qquad (2.34b)$$

In the Fourier domain, eqs. $(2.33a-c)$ become

$$\frac{\partial^2\hat{\tilde{\psi}}_0}{\partial z^2}+(k^2-\mu^2-\nu^2)\hat{\tilde{\psi}}_0=\Pi f(t_1)\delta(z-z_0)\hat{L}(\nu) \qquad -h<z<0 \qquad (2.35a)$$

$$\frac{\partial\hat{\tilde{\psi}}_0}{\partial z}=0 \qquad z=-h, \qquad \hat{\tilde{\psi}}_0=0 \qquad z=0 \qquad (2.35b-c)$$

Solution of $(2.35a-c)$ is straightforward:

$$\hat{\tilde{\psi}}_0(\mu,\nu,z,t_1)=\hat{L}(\nu)\Pi f(t_1)\frac{\cos\sqrt{k^2-\mu^2-\nu^2}(z_<+h)}{\cos\sqrt{k^2-\mu^2-\nu^2}h}\frac{\sin\sqrt{k^2-\mu^2-\nu^2}z_>}{\sqrt{k^2-\mu^2-\nu^2}} \qquad (2.36a)$$

where

$$\begin{cases} z_< = \min(z,z_0) \\ z_> = \max(z,z_0) \end{cases} \qquad (2.36b)$$

The inverse transform is

$$\psi_0(x,y,z,t_1)=\frac{1}{4\pi^2}\int_{-\infty}^{\infty}d\mu\int_{-\infty}^{\infty}d\nu e^{i\mu x+i\nu y}\hat{\tilde{\psi}}_0(\mu,\nu,z,t_1) \qquad (2.37)$$

It is convenient to introduce the polar coordinates

$$\mu=\xi\cos\Theta \qquad \nu=\xi\sin\Theta \qquad (2.38)$$

where Θ, the angle of the sound wavenumber vector with the x-axis, varies within $[-\frac{\pi}{2},\frac{3\pi}{2}]$. The potential ψ_0 becomes

$$\psi_0(x,y,z,t_1)=\frac{\Pi f(t_1)}{4\pi^2}\int_0^{\infty}d\xi\xi\int_{-\frac{\pi}{2}}^{\frac{3\pi}{2}}d\Theta e^{i\xi(x\cos\Theta+y\sin\Theta)}\hat{L}(\xi\sin\Theta)\times$$

$$\frac{\cos\sqrt{k^2-\xi^2}(z_<+h)}{\cos\sqrt{k^2-\xi^2}h}\frac{\sin\sqrt{k^2-\xi^2}z_>}{\sqrt{k^2-\xi^2}} \qquad (2.39)$$

Simple symmetry considerations yield

$$\psi_0(x,y,z,t_1)=\frac{\Pi f(t_1)}{4\pi^2}\int_{-\frac{\pi}{2}}^{\frac{\pi}{2}}d\Theta\int_{-\infty}^{\infty}d\xi|\xi|\,e^{i\xi(x\cos\Theta+y\sin\Theta)}\hat{L}(\xi\sin\Theta)\times$$

$$\frac{\cos\sqrt{k^2-\xi^2}(z_<+h)}{\cos\sqrt{k^2-\xi^2}h}\frac{\sin\sqrt{k^2-\xi^2}z_>}{\sqrt{k^2-\xi^2}} \qquad (2.40)$$

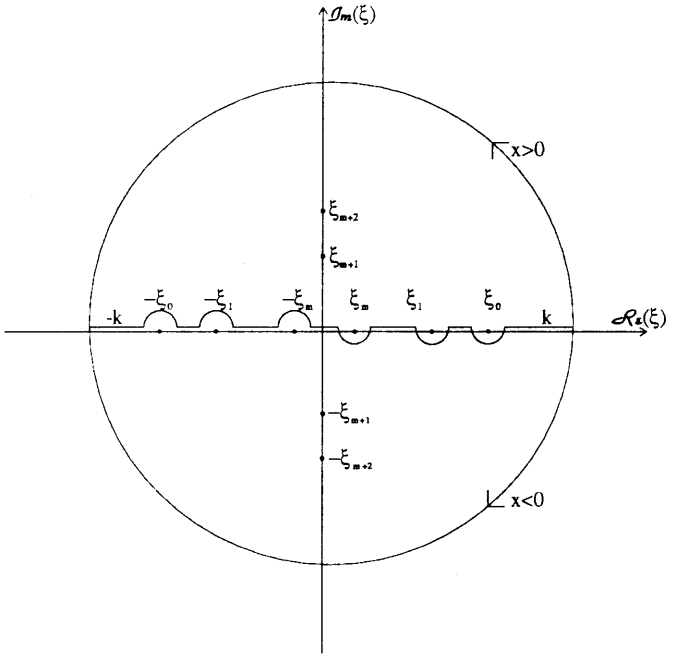

Figure 2.3: Contour in the complex ξ plane used to perform the integration of (2.37).

Let us extract further physical information from the formal solution (2.40). The poles of the ξ-integral are located in the complex ξ-plane at the zeros of

$$\cos\sqrt{k^2-\xi^2}h = 0 \tag{2.41}$$

Eq. (2.41) admits an infinite number of discrete roots characterized by

$$\sqrt{1-\left(\frac{\xi_\ell}{k}\right)^2} = (\ell+\frac{1}{2})\frac{\pi}{kh} \qquad \ell = 0,1,2,\ldots \tag{2.42}$$

Note that for $\ell = 0,1,\ldots\bar{\ell}$, where $\bar{\ell}$ is the integer part of $\left(\frac{kh}{\pi}-\frac{1}{2}\right) \geq 0$, ξ_ℓ is real and thus corresponds to a propagative mode. In particular, if $\frac{\pi}{2} < kh < \frac{3\pi}{2}$, $\bar{\ell} = 0$ and the waveguide sustains only one propagating mode.

For $\ell > \bar{\ell}$, it is clear that solutions of (2.42) become purely imaginary *i.e.* $\xi_\ell = i\kappa_\ell$ such that

$$\sqrt{1+\left(\frac{\kappa_\ell}{k}\right)^2} = (\ell+\frac{1}{2})\frac{\pi}{kh} \qquad \ell > \bar{\ell} \tag{2.43}$$

The countable set $\{\xi_\ell\}_{\ell>\bar{\ell}}$ corresponds to evanescent modes in the x-direction.

In the complex ξ-plane, the contour of integration used to evaluate (2.40) is indented in order to satisfy the radiation condition, cf. figure 2.3. For $x > 0$, the

contour is closed above the real axis, thus including the singularities at $\{\xi_\ell\}_{n=0,\bar{\ell}}$ and $\{\kappa_\ell\}_{\ell=\bar{\ell}+1,\infty}$. For $x < 0$ however, the contour of integration is closed below the real axis, thus including singularities $\{-\xi_\ell\}_{\ell=0,\bar{\ell}}$ and $\{-\eta_\ell\}_{\ell=\bar{\ell}+1,\infty}$. Straightforward application of the residue theorem yields the expression of $\psi_0(x,y,z,t)$

$$\psi_0(x,y,z,t_1) = -\frac{\Pi f(t_1)}{2\pi h}\Bigg\{$$

$$i\sum_{\ell=0}^{\bar{\ell}} \sin\sqrt{k^2-\xi_\ell^2}z \ \sin\sqrt{k^2-\xi_\ell^2}\ z_0 \int_{-\frac{\pi}{2}}^{\frac{\pi}{2}} d\Theta\ e^{i\xi_\ell(|x|\cos\Theta+y\sin\Theta)}\hat{L}(\xi_\ell\sin\Theta) \quad +$$

$$+\sum_{\ell=\bar{\ell}+1}^{\infty} \sin\sqrt{k^2+\kappa_\ell^2}z \ \sin\sqrt{k^2+\kappa_\ell^2}z_0 \int_{-\frac{\pi}{2}}^{\frac{\pi}{2}} d\Theta\ e^{-\kappa_\ell(|x|\cos\Theta+y\sin\Theta)}\hat{L}(i\kappa_\ell\sin\Theta)\Bigg\} \tag{2.44}$$

At the outer stretch of the near field, $k|x| \gg 1$, the evanescent modes become negligible and only the propagative modes remain. In particular, if $\frac{\pi}{2} < kh < \frac{3\pi}{2}$, only one propagating mode is sustained by the sound channel and ψ_0 becomes

$$\psi_0(x,y,z,t_1) \simeq i\frac{\Pi f(t_1)}{h}\cos\sqrt{k^2-\xi_0^2}(z+h)\ \sin\sqrt{k^2-\xi_0^2}\ z_0 \ \ \mathcal{D}(x,y,\xi_0) \tag{2.45a}$$

where $\mathcal{D}$ decribes the directionality of the sound field:

$$\mathcal{D}(x,y,\xi_0) = \frac{1}{2\pi}\int_{-\frac{\pi}{2}}^{\frac{\pi}{2}} d\Theta\ e^{i\xi_0(|x|\cos\Theta+y\sin\Theta)}\hat{T}(\xi_0\sin\Theta) \tag{2.45b}$$

where ξ_0 is given by (2.11) with $\ell = 0$. We assume for simplicity that

$$\Pi = \frac{\xi_0 h}{\sin\sqrt{k^2-\xi_0^2}\ z_0} \tag{2.45c}$$

2.2.1. *Normal radiation*

In order to generate plane outgoing sound waves in the $\pm$ x-directions, $L(y)$ is identically equal to unity. Consequently, its Fourier transform is

$$\hat{L}(\nu) = 2\pi\delta(\nu) \tag{2.46a}$$

Evaluation of the directionality function $\mathcal{D}$ yields

$$\mathcal{D}(x,y,\xi_0) = \int_{-\frac{\pi}{2}}^{\frac{\pi}{2}} d\Theta\ e^{i\xi_0(|x|\cos\Theta+y\sin\Theta)}\delta(\xi_0\sin\Theta) = \frac{1}{\xi_0}e^{i\xi_0|x|} \tag{2.46b}$$

and the asymptotic expression of the near field of the sound source for $k|x| \gg 1$ is

$$\psi_0(x,y,z,t_1) \simeq if(t_1)\cos\sqrt{k^2-\xi_0^2}(z+h)\, e^{i\xi_0|x|} \tag{2.47}$$

2.2.2. *Oblique radiation*

Generation of sound waves oblique at an angle θ with respect to the x-axis requires that $L(y) = e^{i\xi_0 y\sin\theta}$, *i.e.*, that its Fourier transform be

$$\hat{L}(\nu) = 2\pi\delta(\nu - \xi_0\sin\theta) \tag{2.48a}$$

The corresponding directionality function $\mathcal{D}$ is readily deduced

$$\begin{aligned}\mathcal{D}(x,y,\xi_0) &= \int_{-\frac{\pi}{2}}^{\frac{\pi}{2}} d\Theta\; e^{i\xi_0(|x|\cos\Theta+y\sin\Theta)}\delta\left[\xi_0(\sin\Theta-\sin\theta)\right] \\ &= \frac{1}{\xi_0\cos\theta}e^{i\xi_0(|x|\cos\theta+y\sin\theta)}\end{aligned} \tag{2.48b}$$

The array therefore generates plane waves propagating in the $(\pm\cos\theta, \sin\theta)$ directions, the corresponding sound potential yields

$$\psi_0(x,y,z,t_1) \simeq i\frac{f(t_1)}{\cos\theta}\cos\sqrt{k^2-\xi_0^2}(z+h)\; e^{i\xi_0(|x|\cos\theta+y\sin\theta)} \tag{2.49}$$

Expressions (2.47) and (2.49) represent the outer approximation of the near field of the sound source.

2.3. Asymptotic Matching of the Near and Far Fields

In this section the outgoing sound waves emitted from the line source propagate at an angle θ with respect to the x-axis. The sound potential in the farfield, *i.e.* far to the left or to the right of the line source, is described by

$$\begin{aligned}\Phi_0(x,x_1,y,y_1,z,t,t_1) = \big[&A(x_1,y_1,t_1)e^{i\xi_0(x\cos\theta+y\sin\theta)}+ \\ &+B(x_1,y_1,t_1)e^{i\xi_0(-x\cos\theta+y\sin\theta)}\big]e^{-i\omega t}\cos\sqrt{k^2-\xi_0^2}(z+h)+(*)\end{aligned} \tag{2.50}$$

where A and B are the envelopes of the scattered sound waves. Their evolution is governed by $(2.27a-b)$.

In the near field of the source, the potential is

$$\psi_0(x,y,z,t_1) = i\frac{f(t_1)}{\cos\theta}\cos\sqrt{k^2-\xi_0^2}(z+h)e^{i\xi_0(|x|\cos\theta+y\sin\theta)} + (*) \qquad (2.51)$$

We now match the amplitude of the right going wave of the near field with the right going wave of the far field in the positive x-range:

$$A(x_1 = 0^+, t_1) = \frac{if(t_1)}{\cos\theta} \qquad (2.52)$$

Likewise, we find

$$A(x_1 = 0^-, t_1) = 0 \qquad (2.53)$$

Eqs. (2.52)-(2.53) imply that the discontinuity accross $x_1 = 0$ is

$$A(x_1 = 0^+, t_1) - A(x_1 = 0^-, t_1) = \frac{if(t_1)}{\cos\theta} \qquad (2.54)$$

The discontinuity (2.54) can be incorporated to $(2.27a)$ by adding an impulse function in its right hand side:

$$\frac{\partial A}{\partial t_1} + \Lambda\cos\theta\frac{\partial A}{\partial x_1} + \Lambda\sin\theta\frac{\partial A}{\partial y_1} = i\alpha B + i\Lambda\delta(x_1)f(t_1) \qquad (2.55a)$$

By a similar argument, we obtain the evolution equation for B:

$$\frac{\partial B}{\partial t_1} - \Lambda\cos\theta\frac{\partial B}{\partial x_1} + \Lambda\sin\theta\frac{\partial B}{\partial y_1} = i\alpha A + i\Lambda\delta(x_1)f(t_1) \qquad (2.55b)$$

Eqs. $(2.55a-b)$ describe, for all x_1, the long time evolution of two oblique outgoing sound waves scattered by a long crested uniform surface wave.

The far field radiation-scattering problem is now fully characterized by the governing equations $(2.55a-b)$, the initial and boundary conditions:

$$A(x_1, t_1 = 0) = B(x_1, t_1 = 0) = 0 \quad A(x_1 = \pm\infty, t_1) = B(x_1 = \pm\infty, t_1) = 0 \quad (2.56)$$

and the specification of the source amplitude $f(t_1)$.

Owing to linearity, the foregoing problem may be regarded as the superposition of two problems: a right-radiation problem where the source emits sound in the positive x-direction only (referred to by the "+" superscript) and a left-radiation problem where sound is beamed towards the negative x-direction (referred to by

the "-" superscript). The governing equations for the right-radiation problem are easily deduced

$$\frac{\partial A^+}{\partial t_1} + \Lambda\cos\theta\frac{\partial A^+}{\partial x_1} + \Lambda\sin\theta\frac{\partial A^+}{\partial y_1} = i\alpha B^+ + i\Lambda\, f(t_1)\delta(x_1) \qquad (2.57a)$$

$$\frac{\partial B^+}{\partial t_1} - \Lambda\cos\theta\frac{\partial B^+}{\partial x_1} + \Lambda\sin\theta\frac{\partial B^+}{\partial y_1} = i\alpha A^+ \qquad (2.57b)$$

with homogeneous initial and boundary conditions. Similarly, the left-radiation problem is defined by

$$\frac{\partial A^-}{\partial t_1} + \Lambda\cos\theta\frac{\partial A^-}{\partial x_1} + \Lambda\sin\theta\frac{\partial A^-}{\partial y_1} = i\alpha B^- \qquad (2.58a)$$

$$\frac{\partial B^-}{\partial t_1} - \Lambda\cos\theta\frac{\partial B^-}{\partial x_1} + \Lambda\sin\theta\frac{\partial B^-}{\partial y_1} = i\alpha A^- + i\Lambda\, f(t_1)\delta(x_1) \qquad (2.58b)$$

subjected to the same initial and boundary conditions. It is clear that the solution of $(2.55a-b)$ is simply

$$A(x_1,y_1,t_1) = A^+(x_1,y_1,t_1) + A^-(x_1,y_1,t_1) \qquad (2.59a)$$

$$B(x_1,y_1,t_1) = B^+(x_1,y_1,t_1) + B^-(x_1,y_1,t_1) \qquad (2.59b)$$

Furthermore, note that the right- and left-radiation problems are mirror images of each others, *i.e.*

$$A^-(x_1,y_1,t_1) = B^+(-x_1,y_1,t_1) \qquad B^-(x_1,y_1,t_1) = A^+(-x_1,y_1,t_1) \qquad \forall x_1,y_1,t_1 \qquad (2.60a-b)$$

Substitution of $(2.60a-b)$ into $(2.59a-b)$ yields

$$A(x_1,y_1,t_1) = A^+(x_1,y_1,t_1) + B^+(-x_1,y_1,t_1) \qquad (2.61a)$$

$$B(x_1,y_1,t_1) = B^+(x_1,y_1,t_1) + A^+(-x_1,y_1,t_1) \qquad (2.61b)$$

In view of $(2.61a-b)$, we only need to solve the right-radiation problem. The solution to $(2.55a-b)$ with the appropriate boundary conditions follows easily by superposition.

2.4. An analytical solution for A^+ and B^+

Consider the following shift of variables

$$X = x_1 \quad Y = y_1 - \Lambda \sin\theta \; t_1 \quad T = t_1 \tag{2.62a - c}$$

Substitution of $(2.62a - c)$ in $(2.57a - b)$ yields

$$\frac{\partial A^+}{\partial T} + \Lambda \cos\theta \frac{\partial A^+}{\partial X} = i\alpha B^+ + i\Lambda \; f(T)\delta(X) \tag{2.63a}$$

$$\frac{\partial B^+}{\partial T} - \Lambda \cos\theta \frac{\partial B^+}{\partial X} = i\alpha A^+ \tag{2.63b}$$

Let μ be the Fourier variable associated with X. Transformation of $(2.63a - b)$ yields the following matrix ordinary differential equation

$$\frac{\partial \tilde{U}}{\partial T} = i \begin{pmatrix} -\Lambda\mu\cos\theta & \alpha \\ \alpha & \Lambda\mu\cos\theta \end{pmatrix} \tilde{U} + iV(T) \tag{2.64}$$

where $\tilde{U}$ and $V(T)$ are the vector of unknowns and the forcing vector respectively defined by

$$\tilde{U}(\mu, T) = \begin{pmatrix} \tilde{A}^+(\mu, T) \\ \tilde{B}^+(\mu, T) \end{pmatrix} \qquad V(T) = \begin{pmatrix} \Lambda f(T) \\ 0 \end{pmatrix} \tag{2.65b - c}$$

The homogeneous part of (2.64) admits the following solution

$$\tilde{U}(\mu, T) = c_1 \begin{pmatrix} \alpha \\ \Lambda\cos\theta(\mu + \sqrt{\mu^2 + \beta^2}) \end{pmatrix} e^{i\Lambda\cos\theta\sqrt{\mu^2+\beta^2}T} +$$

$$+ \; c_2 \begin{pmatrix} \alpha \\ \Lambda\cos\theta(\mu - \sqrt{\mu^2 + \beta^2}) \end{pmatrix} e^{-i\Lambda\cos\theta\sqrt{\mu^2+\beta^2}T} \tag{2.66}$$

where $\beta = \frac{\alpha}{\Lambda\cos\theta}$. Upon using the method of variation of parameters, the unknown coefficients $c_{1,2}$ in (2.66) are computed

$$c_1(T) = -\frac{i}{\beta\cos\theta} \frac{\mu - \sqrt{\mu^2 + \beta^2}}{2\sqrt{\mu^2 + \beta^2}} \int_0^T e^{-i\Lambda\cos\theta\sqrt{\mu^2+\beta^2}\tau} f(\tau) d\tau \tag{2.67a}$$

$$c_2(T) = \frac{i}{\beta\cos\theta} \frac{\mu + \sqrt{\mu^2 + \beta^2}}{2\sqrt{\mu^2 + \beta^2}} \int_0^T e^{i\Lambda\cos\theta\sqrt{\mu^2+\beta^2}\tau} f(\tau) d\tau \tag{2.67b}$$

where use has been made of the homogeneous initial condition for $\tilde{U}$. Substitution of $(2.67a - b)$ in (2.66) yields the sound amplitude in the Fourier domain

$$\tilde{A}^+(\mu, T) = i\Lambda \int_0^T f(\tau) \cos\left[\Lambda\cos\theta\sqrt{\mu^2 + \beta^2}(T - \tau)\right] d\tau \quad +$$

$$+ \quad \Lambda\mu \int_0^T f(\tau) \frac{\sin\left[\Lambda \cos\theta \sqrt{\mu^2+\beta^2}(T-\tau)\right]}{\sqrt{\mu^2+\beta^2}} d\tau \tag{2.68a}$$

and

$$\tilde{B}^+(\mu,T) = -\frac{\alpha}{\cos\theta} \int_0^T f(\tau) \frac{\sin\left[\Lambda \cos\theta \sqrt{\mu^2+\beta^2}(T-\tau)\right]}{\sqrt{\mu^2+\beta^2}} d\tau \tag{2.68b}$$

By inverse Fourier transform, the sound amplitudes in the physical domain are obtained. Thus, the left going sound wave B^+ is

$$B^+(X,T) = -\frac{\alpha}{2\pi\cos\theta} \int_{-\infty}^{\infty} d\mu e^{i\mu X} \int_0^T d\tau f(\tau) \frac{\sin[\Lambda \cos\theta \sqrt{\mu^2+\beta^2}(T-\tau)]}{\sqrt{\mu^2+\beta^2}} \tag{2.69}$$

which, owing to the evenness of the integrand, simplifies to

$$B^+(X,T) = -\frac{\alpha}{\pi\cos\theta} \int_0^T d\tau f(\tau) \int_{-\infty}^{\infty} d\mu \cos\mu X \frac{\sin[\Lambda \cos\theta \sqrt{\mu^2+\beta^2}(T-\tau)]}{\sqrt{\mu^2+\beta^2}} \tag{2.70}$$

The μ-integral can be evaluated analytically (Erdelyi *et al*, 1953), yielding

$$B^+(X,T) =$$

$$-\frac{\alpha}{2\cos\theta} \int_0^T d\tau f(\tau) J_0\left[\beta\sqrt{\Lambda^2\cos^2\theta(T-\tau)^2 - X^2}\right] H\left[\Lambda\cos\theta(T-\tau) - |X|\right]$$

$$= -\frac{\alpha}{2\cos\theta} \int_0^T d\tau f(T-\tau) J_0\left[\beta\sqrt{\Lambda^2\cos^2\theta\tau^2 - X^2}\right] H(\Lambda\cos\theta\ \tau - |X|) \tag{2.71}$$

Equation (2.71) can also be written as

$$B^+(X,T) = -\frac{\alpha}{2\cos\theta} H(T - \frac{|X|}{\Lambda\cos\theta}) \int_{\frac{|X|}{\Lambda\cos\theta}}^T d\tau f(T-\tau) J_0(\alpha\sqrt{\tau^2 - (\frac{X}{\Lambda\cos\theta})^2}) \tag{2.72}$$

Note that $B^+(X,T)$ is even in X and clearly continuous across $X = 0$.

Similarly, we evaluate the inverse Fourier transform of $\tilde{A}^+$ given by (2.68a). Integration by parts of the first integral in (2.68a) yields

$$\int_0^T f(\tau)\cos\left[\Lambda\sqrt{\mu^2+\beta^2}(T-\tau)\right] d\tau = \frac{1}{\Lambda} \int_0^T \frac{\sin\left[\Lambda\sqrt{\mu^2+\beta^2}(T-\tau)\right]}{\sqrt{\mu^2+\beta^2}} \frac{df}{dT}(\tau) d\tau \tag{2.73}$$

where use has been made of $f(0) = 0$. Upon comparing (2.73) with (2.68b), one deduces straightforwardly the inverse Fourier transform of (2.73)

$$\frac{i}{2}H(T-\frac{|X|}{\Lambda\cos\theta})\int_{\frac{|X|}{\Lambda\cos\theta}}^{T}d\tau\frac{df}{dT}(T-\tau)J_0(\alpha\sqrt{\tau^2-(\frac{X}{\Lambda\cos\theta})^2}) \tag{2.74}$$

The inverse Fourier transform of the second term in (2.68a) is

$$\mathcal{A}(X,T)=\frac{\Lambda}{2\pi}\int_0^T d\tau f(\tau)\int_{-\infty}^{\infty}d\mu\ \mu e^{i\mu X}\frac{\sin\Lambda\sqrt{\mu^2+\beta^2}(T-\tau)}{\sqrt{\mu^2+\beta^2}} \tag{2.75}$$

Since

$$\int^X\mathcal{A}(x',T)dx'=\frac{\Lambda}{2\pi i}\int_0^T d\tau f(\tau)\int_{-\infty}^{\infty}d\mu e^{i\mu X}\frac{\sin\Lambda\sqrt{\mu^2+\beta^2}(T-\tau)}{\sqrt{\mu^2+\beta^2}}$$

$$=-\frac{i\Lambda}{2}H(T-\frac{|X|}{\Lambda\cos\theta})\int_{\frac{|X|}{\Lambda\cos\theta}}^{T}d\tau f(T-\tau)J_0(\alpha\sqrt{\tau^2-(\frac{X}{\Lambda\cos\theta})^2}) \tag{2.76}$$

We obtain the inverse Fourier of the second integral in (2.68a) by differentiating (2.76) with respect to X

$$\frac{i}{2}H(T-\frac{|X|}{\Lambda\cos\theta})\Big\{\mathrm{sign}(X)f(T-\frac{|X|}{\Lambda\cos\theta})+$$

$$-\beta X\int_{\frac{|X|}{\Lambda\cos\theta}}^{T}d\tau f(T-\tau)\frac{J_1(\alpha\sqrt{\tau^2-(\frac{X}{\Lambda\cos\theta})^2})}{\sqrt{\tau^2-(\frac{X}{\Lambda\cos\theta})^2}}\Big\} \tag{2.77}$$

In summary, the rightward sound amplitude is the sum of (2.74) and (2.77)

$$A^+(X,T)=H(T-\frac{|X|}{\Lambda\cos\theta})\frac{i}{2}\Big\{\mathrm{sign}(X)f(T-\frac{|X|}{\Lambda\cos\theta})+$$

$$+\int_{\frac{|X|}{\Lambda\cos\theta}}^{T}d\tau\frac{df}{dt}(T-\tau)J_0(\alpha\sqrt{\tau^2-(\frac{X}{\Lambda\cos\theta})^2})+$$

$$-\beta X\int_{\frac{|X|}{\Lambda\cos\theta}}^{T}d\tau f(T-\tau)\frac{J_1(\alpha\sqrt{\tau^2-(\frac{X}{\Lambda\cos\theta})^2})}{\sqrt{\tau^2-(\frac{X}{\Lambda\cos\theta})^2}}\Big\} \tag{2.78}$$

One can easily verify that (2.78) satisfies the specified discontinuity at $X = 0$. Substitution of the solution to the right-radiation problem (2.78) and (2.72) in (2.60$a-b$) yields the solution of the left-radiation problem

$$A^-(X,T)=B^+(-X,T)=$$

$$-\frac{\alpha}{2}H(T-\frac{|X|}{\Lambda\cos\theta})\int_{\frac{|X|}{\Lambda\cos\theta}}^{T}d\tau f(T-\tau)J_0(\alpha\sqrt{\tau^2-(\frac{X}{\Lambda\cos\theta})^2}) \qquad (2.79a)$$

$$B^-(X,T)=A^+(-X,T) \;=\; \frac{i}{2}H(T-\frac{|X|}{\Lambda\cos\theta})\{-\mathrm{sign}(X)f(T-\frac{|X|}{\Lambda\cos\theta}) \;+$$

$$+\quad\int_{\frac{|X|}{\Lambda}}^{T}d\tau\frac{df}{dT}(T-\tau)J_0(\alpha\sqrt{\tau^2-(\frac{X}{\Lambda\cos\theta})^2}) \;+$$

$$+\beta X\int_{\frac{|X|}{\Lambda}}^{T}d\tau f(T-\tau)\frac{J_1(\alpha\sqrt{\tau^2-(\frac{X}{\Lambda\cos\theta})^2})}{\sqrt{\tau^2-(\frac{X}{\Lambda\cos\theta})^2}}\} \qquad (2.79b)$$

Finally, when sound is emitted in both directions, we deduce the solution to $(2.54a-b)$ by superposition

$$\begin{pmatrix}A(X,T)\\B(X,T)\end{pmatrix}=\frac{1}{2}H(T-\frac{|X|}{\Lambda\cos\theta})\Big\{$$

$$\pm i\;\mathrm{sign}(X)f(T-\frac{|X|}{\Lambda\cos\theta}) \quad+\quad i\int_{\frac{|X|}{\Lambda\cos\theta}}^{T}d\tau\frac{df}{dT}(T-\tau)J_0(\alpha\sqrt{\tau^2-(\frac{X}{\Lambda\cos\theta})^2})+$$

$$\mp i\beta X\int_{\frac{|X|}{\Lambda}}^{T}d\tau f(T-\tau)\frac{J_1(\alpha\sqrt{\tau^2-(\frac{X}{\Lambda\cos\theta})^2})}{\sqrt{\tau^2-(\frac{X}{\Lambda\cos\theta})^2}}+$$

$$-\alpha\int_{\frac{|X|}{\Lambda\cos\theta}}^{T}d\tau f(T-\tau)J_0(\alpha\sqrt{\tau^2-(\frac{X}{\Lambda\cos\theta})^2})\Big\} \qquad (2.80)$$

For given X and T, the integrals are evaluated using the Euler-Maclaurin sum formula (cf. Bender & Orszag, 1978).

2.5. Numerical Results

The evolution of the scattered sound amplitudes has been computed for the right, left and two-way radiation problems. The carrier frequency of the sound source is taken to be 30Hz, the normalized water depth 1.65. With these parameters, only one propagating mode is sustained by the waveguide and the acoustic wavelength is 50 meters. Moreover, when $\theta=0$, the surface gravity wave causing Bragg resonance has a wavelength of about 83 meters. Its slope is assumed to be 0.1. The parameters

Λ and α are then evaluated from $(2.28a-b)$ with $\Lambda \simeq 0.306$, and $\alpha \simeq 0.449$. Finally, the modulation of the sound source amplitude is described by

$$f(t_1) = \begin{cases} \sin^2 \frac{\pi T}{2} & \text{if } T \leq 2 \\ 0 & \text{if } T > 2 \end{cases} \tag{2.82}$$

Note that both $f(T)$ and its first derivative are continuous at $T = 2$ insuring a smooth transition.

2.5.1. *The collinear case:* $\theta = 0$

The scattered sound amplitudes for the right-radiation problem are plotted in figure 2.4a-b. The right going pulse propagates at speed $\Lambda = 0.3$ and disperses, giving rise to trailing pulses 0†. Note also the mild front propagating at speed $-\Lambda$. Right-going sound waves $|A^+|$ ensonify a wedge delimited by the lines $X = \pm\Lambda T$. The left going scattered sound amplitude $|B^+|$ is even in X despite the obvious asymmetry of the right-radiation problem. Note also the crescent like structures appearing in both $|A^+|$ and $|B^+|$ arising as the trailing waves behind the two propagating fronts merge together.

It is interesting to point out that, as in the case of gravity waves propagating on a variable topography (see Mei(1989)), the carrier wave and its envelope can propagate in opposite directions.

Next, the scattered sound amplitudes for the left radiation problem are presented in figures 2.5a-b. The amplitude $|A^-|$ plays the role of $|B^+|$ in the right-radiation problem, $|A^-|$ is thus the mirror image of *i.e.* identical to $|B^+|$ since the latter is even in X. The amplitude $|B^-|$ is on the other hand, the mirror image of $|A^+|$ and thus consists of a dispersive pulse propagating to the left at speed $-\Lambda$.

Consider now the two-way radiation problem, the amplitude $|A|$ of the right going sound wave is given by

$$|A(X,T)| = \sqrt{|A^+(X,T)|^2 + |B^+(-X,T)|^2} \tag{2.83a}$$

† This behavior is expected since the governing equations for A^+ and B^+ are known to reduce, in the absence of a sound source, to the dispersive Klein-Gordon equation.

and likewise, the amplitude $|B|$ of the left going sound wave is

$$|B(X,T)| = \sqrt{|B^+(X,T)|^2 + |A^+(-X,T)|^2} \qquad (2.83b)$$

after noticing that A^+ and B^+ are respectively purely imaginary and real. Amplitudes $(2.83a-b)$ are plotted in figures 2.6a-b. The two figures are clearly mirror images of each other. Again, we point out the presence of dispersive trailing waves behind both propagating fronts.

Owing to the conservation of sound intensity (2.29), it is clear that, as time elapses, the maximum sound intensity decreases to zero as the original intensity spreads out over an increasing stretch.

2.5.2. *The oblique case:* $\theta \neq 0$

We assume now that the line source radiates plane waves at an angle $\theta = \frac{\pi}{6}$, $\frac{\pi}{4}$ and $\frac{\pi}{3}$. For each incidence angle, the results of the right-radiation and two-way radiation problems are plotted in figures 2.7a-d, 2.8a-d and 2.9a-d. The obliqueness θ determines the speeds of propagation, $\pm\Lambda\cos\theta$, of the right and left going fronts. The reduced propagation speed means that, at a given time T, the initial sound intensity occupies a smaller range $X \in [-\Lambda\cos\theta\, T, \Lambda\cos\theta\, T]$. As a result, the height of the incident and dispersive pulses increases with increasing incidence angle θ, as observed in figures 2.7a, 2.8a and 2.9a. In particular, the weak left propagating front and its trailing pulses observed for $|A^+|$ when $\theta = 0$ has now become significantly larger.

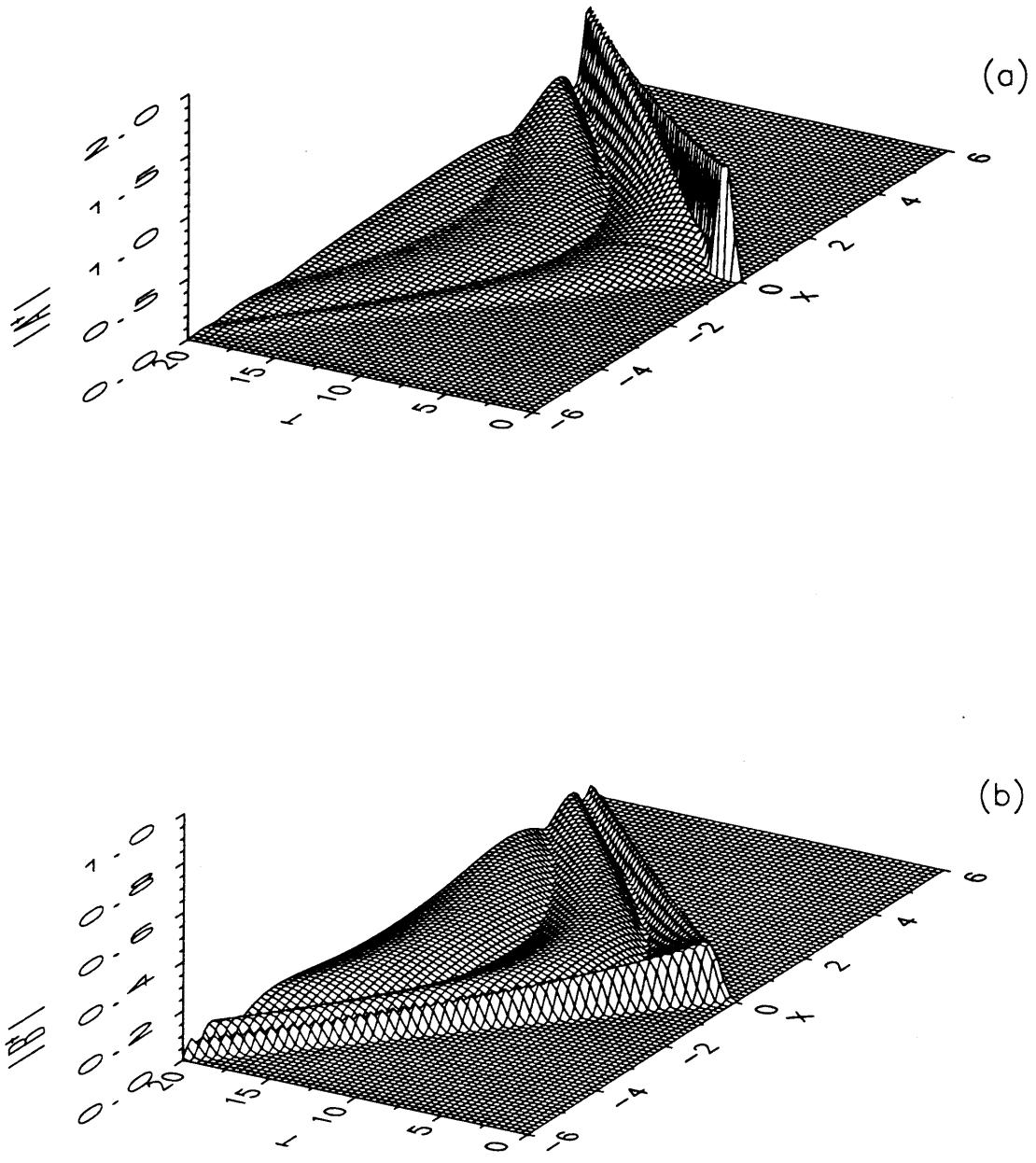

Figures 2.4a-b: Evolution of sound envelopes in the right-radiation problem with $\theta = 0$; (a) $|A^+|$, (b) $|B^+|$.

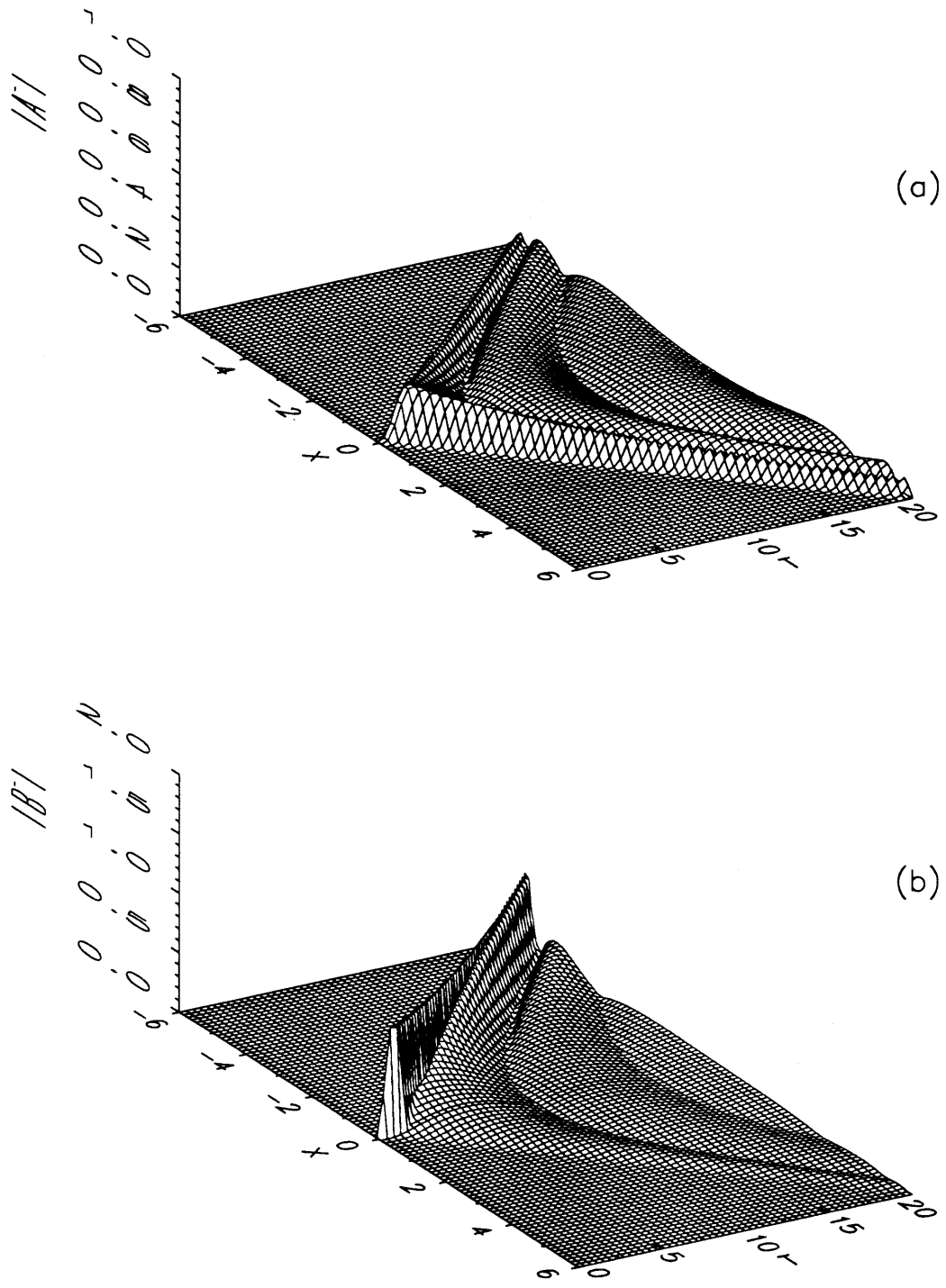

Figures 2.5a-b: Evolution of sound envelopes in the left-radiation problem with $\theta = 0$; (a) $|A^-|$, (b) $|B^-|$.

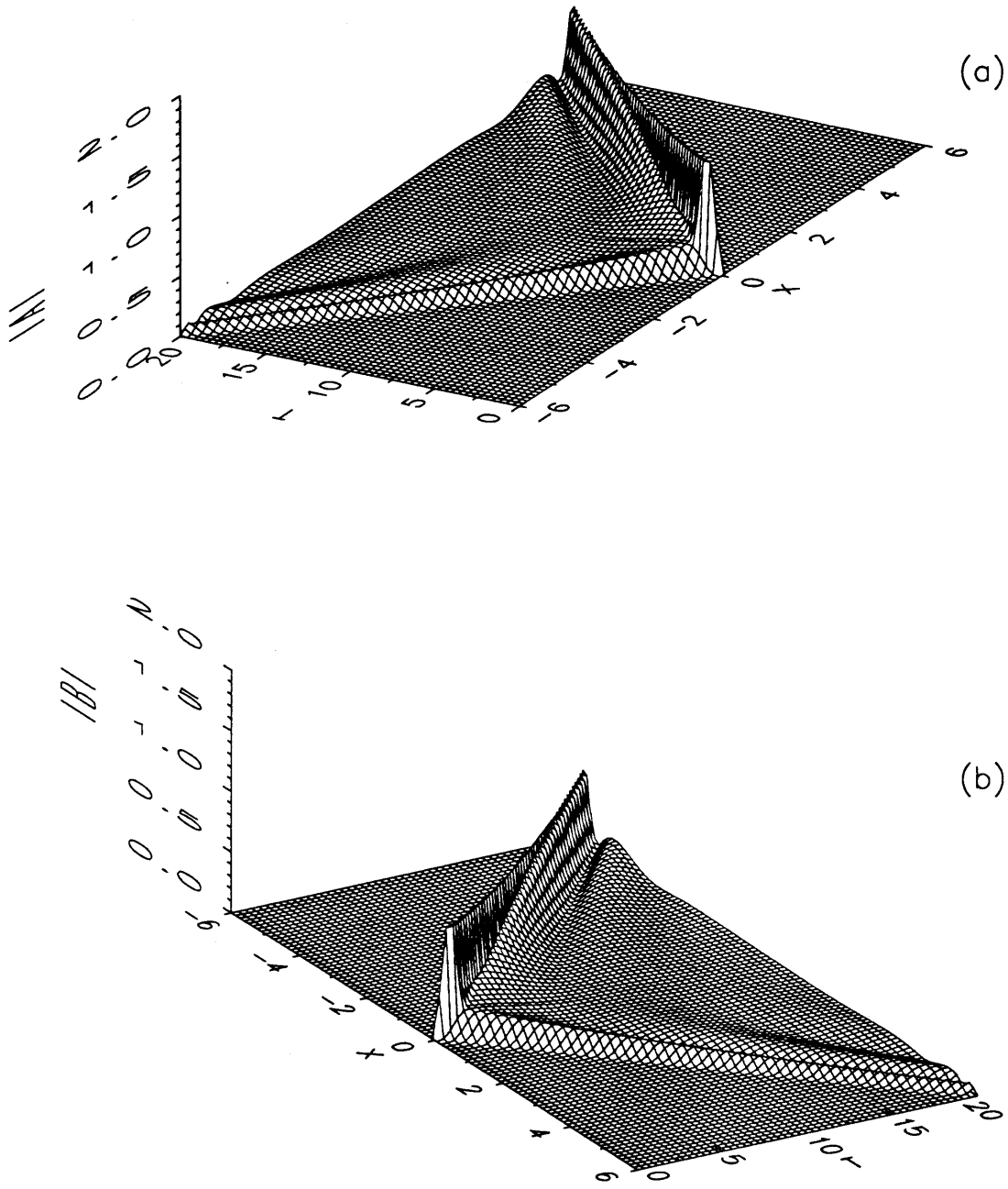

Figures 2.6a-b: Evolution of sound envelopes in the two-way radiation problem with $\theta = 0$; (a) $|A|$, (b) $|B|$.

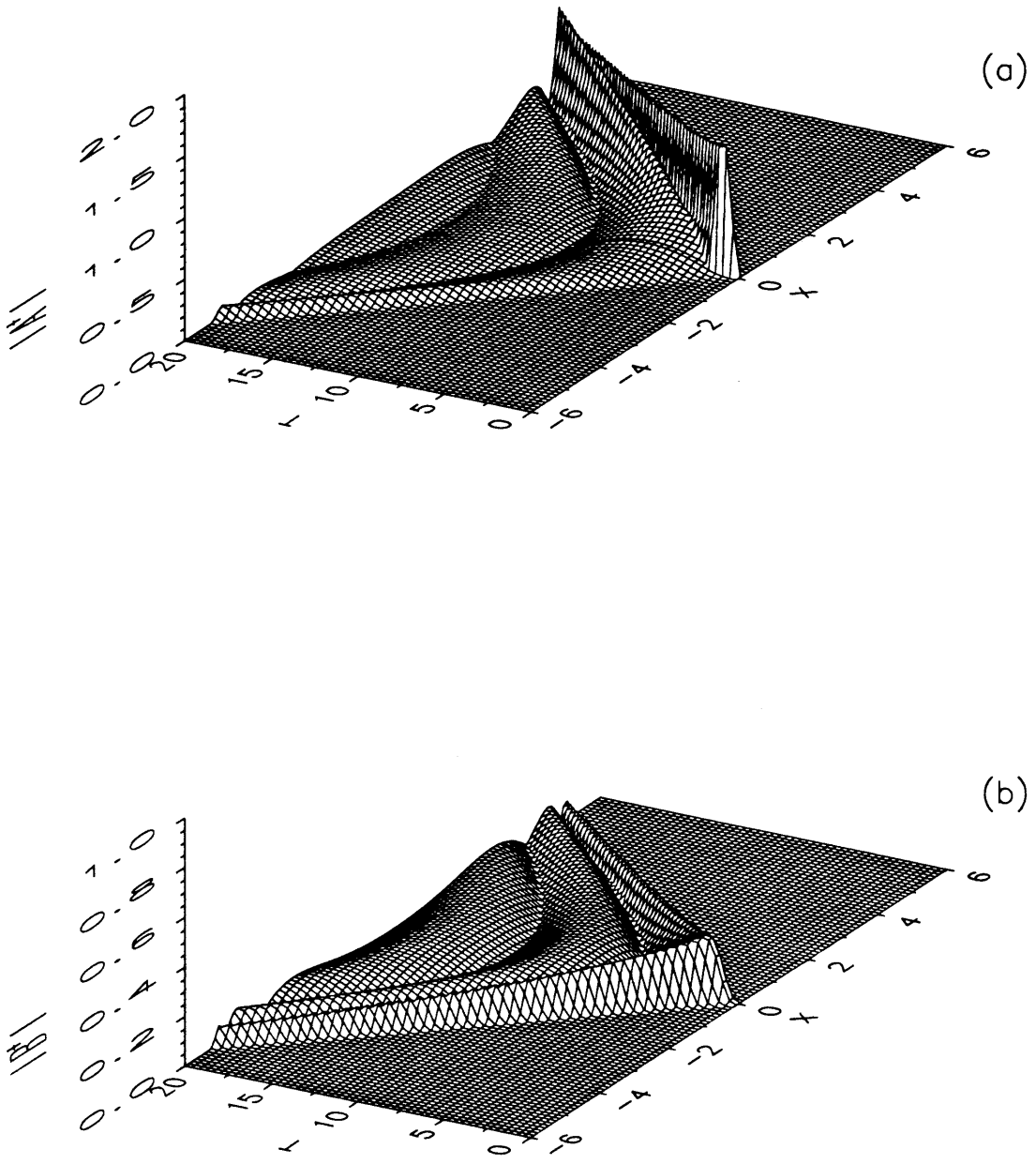

Figures 2.7a-b: Evolution of sound envelopes in the right-radiation problem with $\theta = 30°$; (a) $|A^+|$, (b) $|B^+|$.

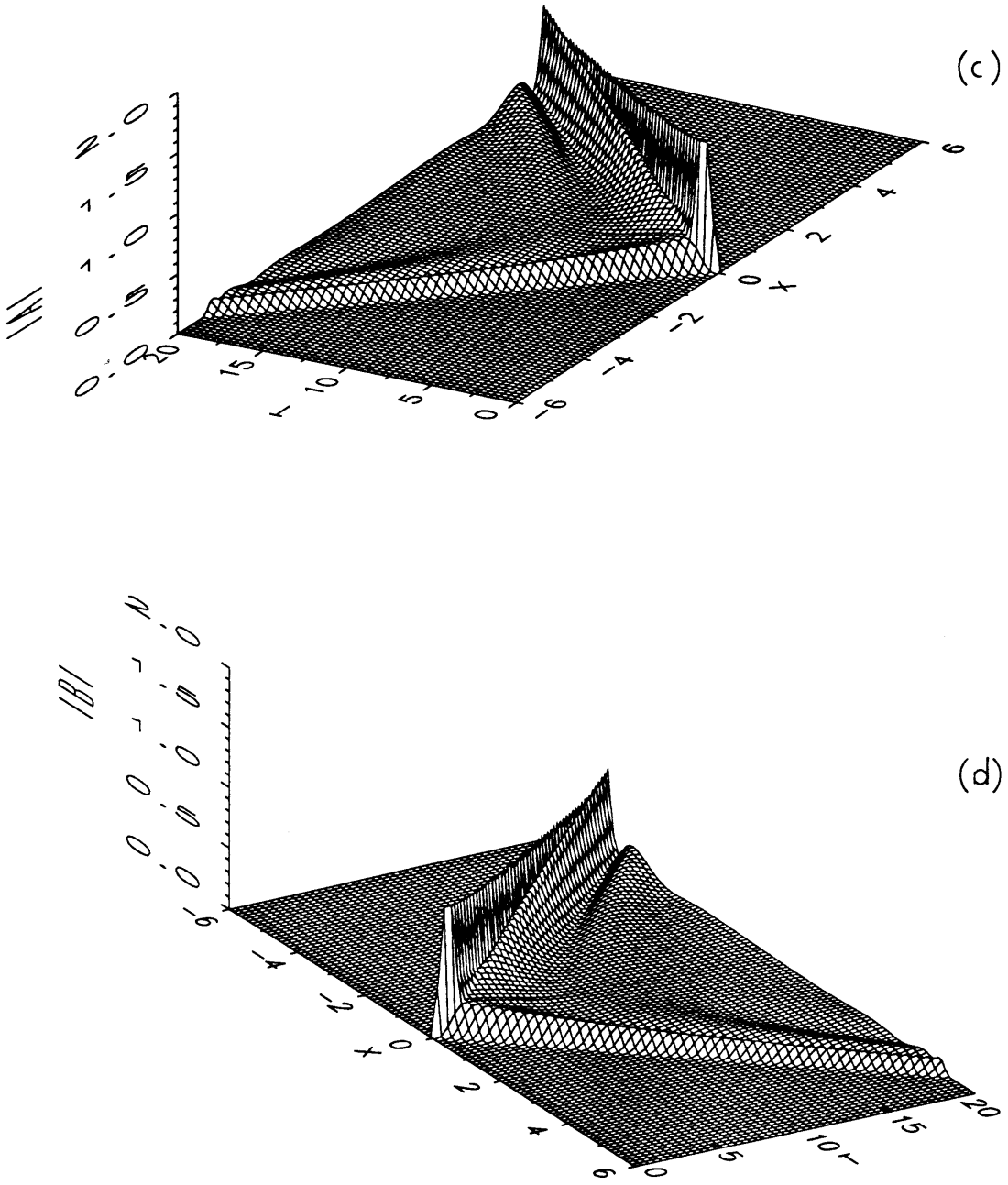

Figures 2.7c-d: Evolution of sound envelopes in the two-way radiation problem with $\theta = 30°$; (c) $|A|$, (d) $|B|$.

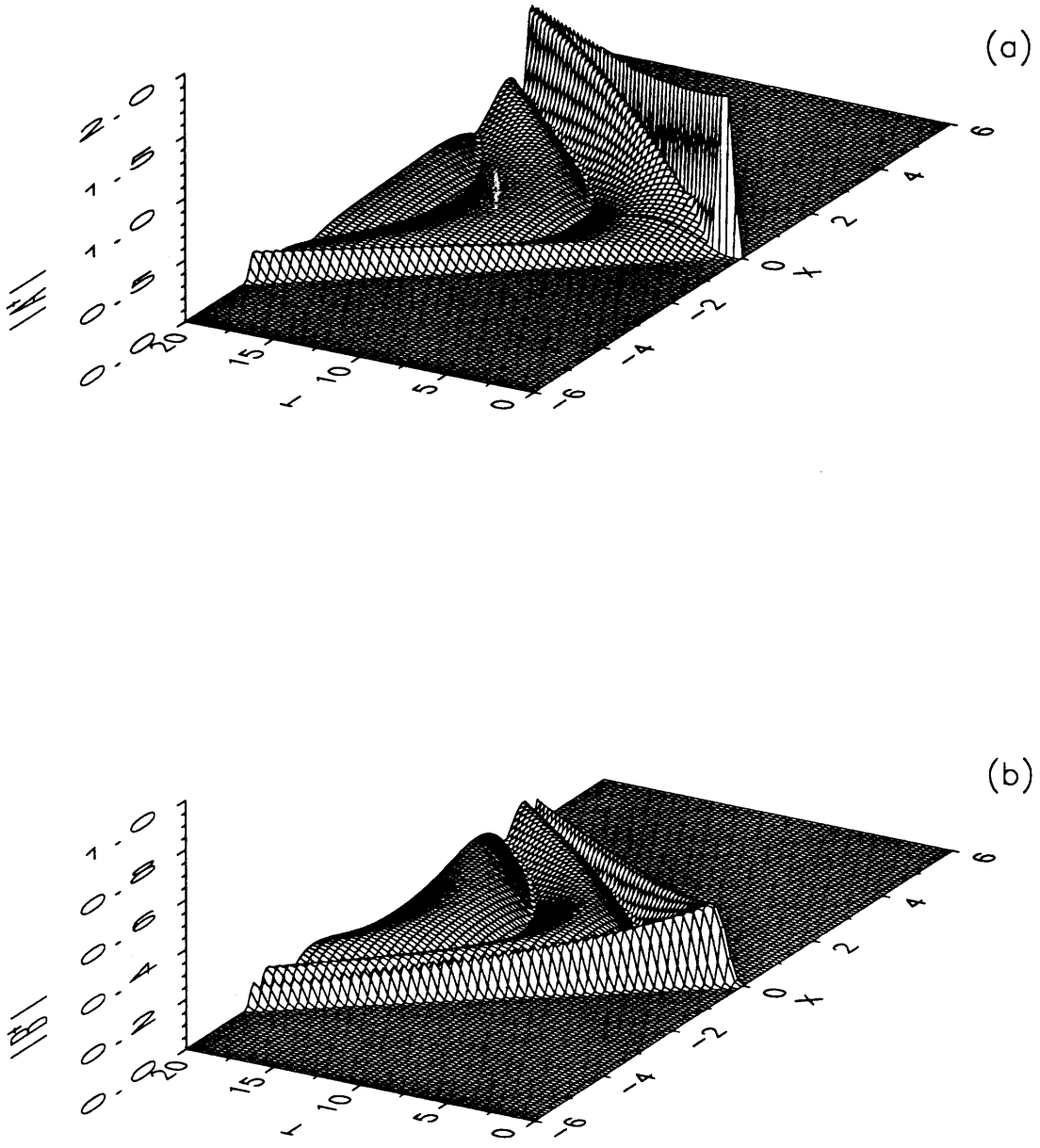

Figures 2.8a-b: Evolution of sound envelopes in the right-radiation problem with $\theta = 45°$; (a) $|A^+|$, (b) $|B^+|$.

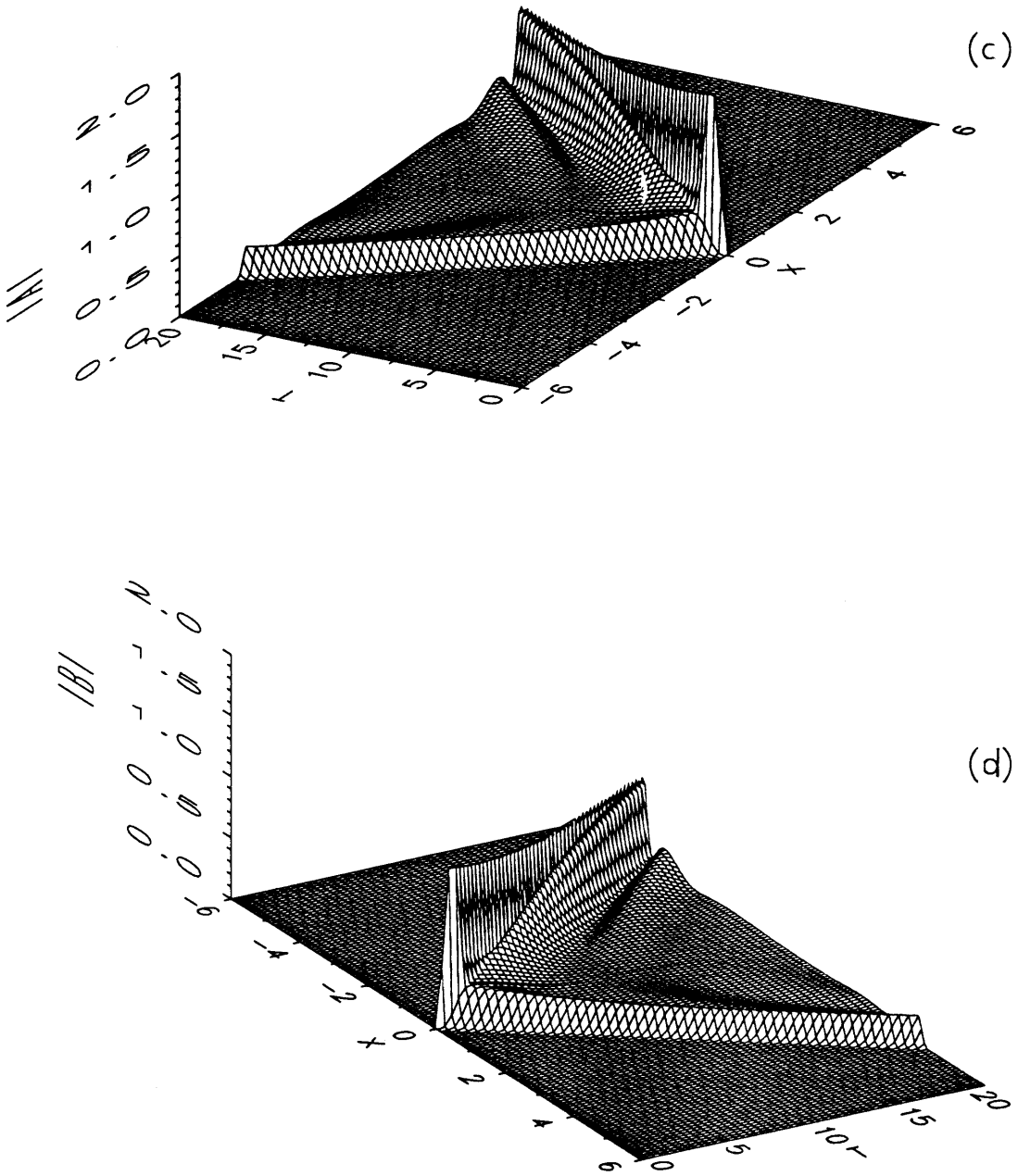

Figures 2.8c-d: Evolution of sound envelopes in the two-way radiation problem with $\theta = 45°$; (c) $|A|$, (d) $|B|$.

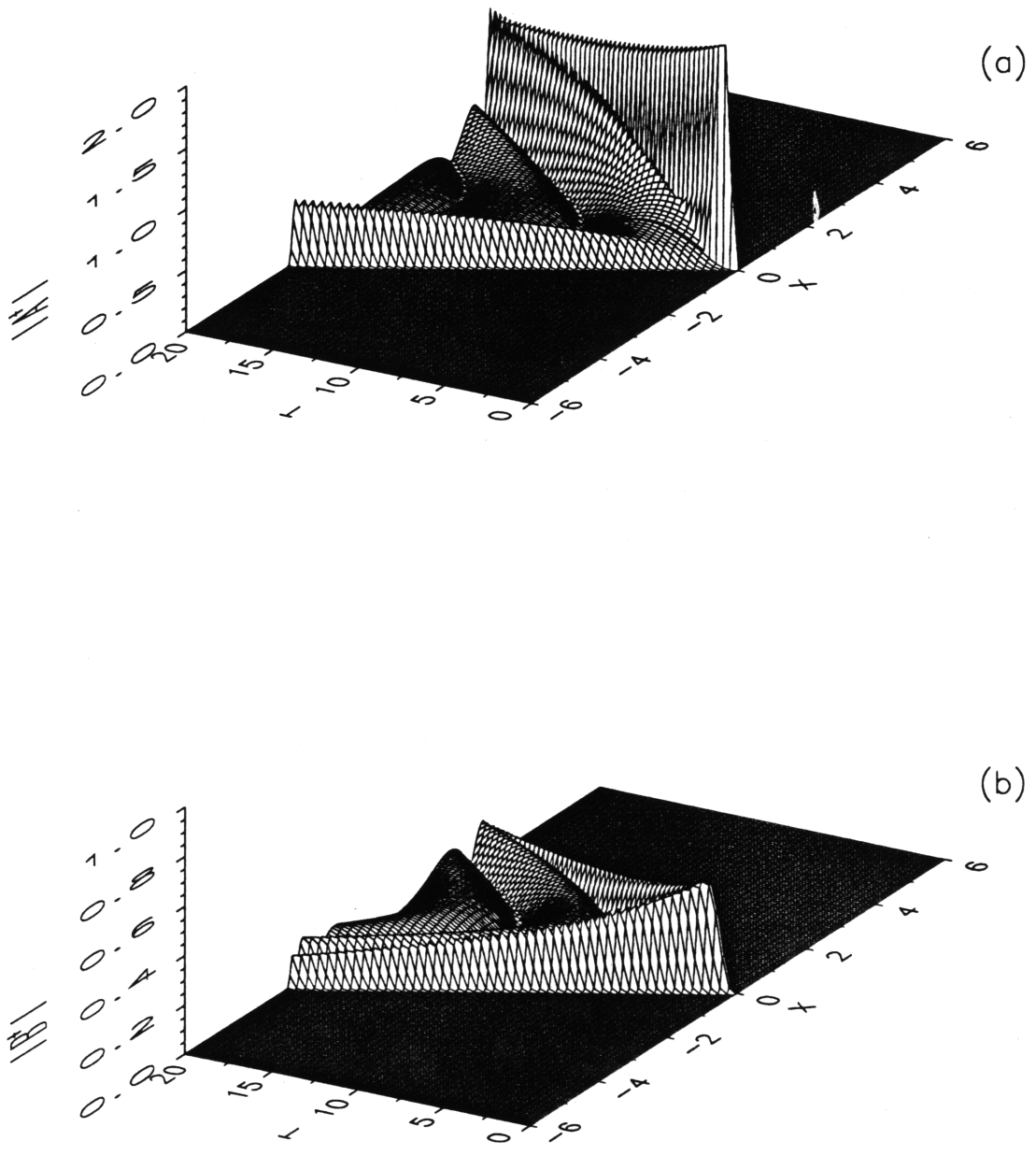

Figures 2.9a-b: Evolution of sound envelopes in the right-radiation problem with $\theta = 60°$; (a) $|A^+|$, (b) $|B^+|$.

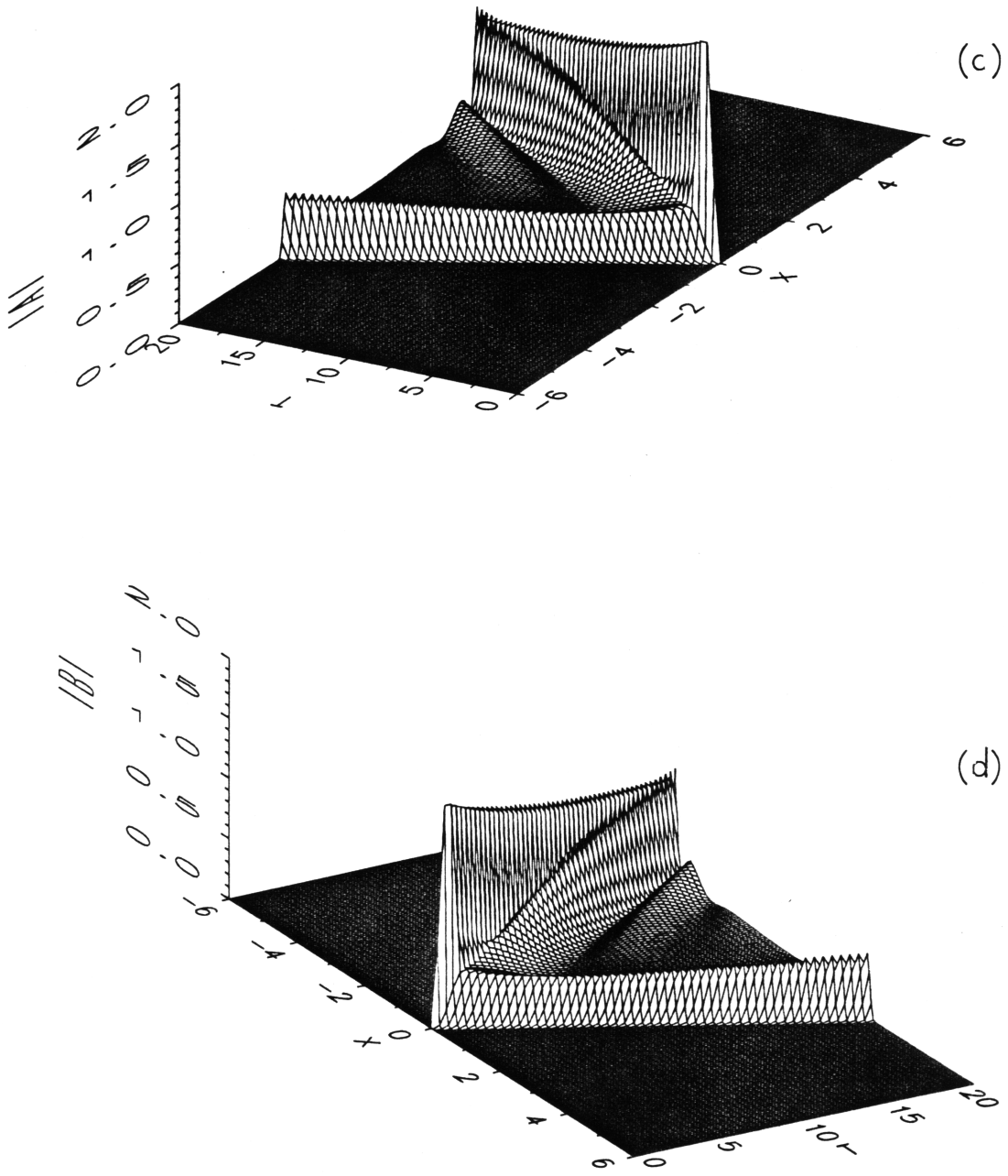

Figures 2.9c-d: Evolution of sound envelopes in the two-way radiation problem with $\theta = 60°$; (c) $|A|$, (d) $|B|$.

3. SCATTERING AND EVOLUTION OF PLANE SOUND WAVES IN THE PRESENCE OF TWO UNIFORM SURFACE WAVES.

We consider in this section an underwater sound channel whose surface is now corrugated by the presence of two uniform surface waves propagating in arbitrary directions. From now on, we assume a normal radiation as described in §2.2.1. The acoustic field of the line source is then approximated by two outgoing plane waves propagating along the ± x-axes, see (2.47).

3.1. Case 1: Two Surface Waves in Arbitrary Directions

Under the previous assumptions, the free surface elevation is described by

$$\zeta_1 = \frac{1}{2}\{D_1 e^{i\vec{k}_{w_1}\cdot\vec{r}} + D_2 e^{i\vec{k}_{w_2}\cdot\vec{r}} + (*)\}. \tag{3.1}$$

where $\vec{k}_{w_1} = (m_1, n_1)$ and $\vec{k}_{w_2} = (m_2, n_2)$ are the wavenumber vectors of the two distinct surface waves represented in figure 3.1a.

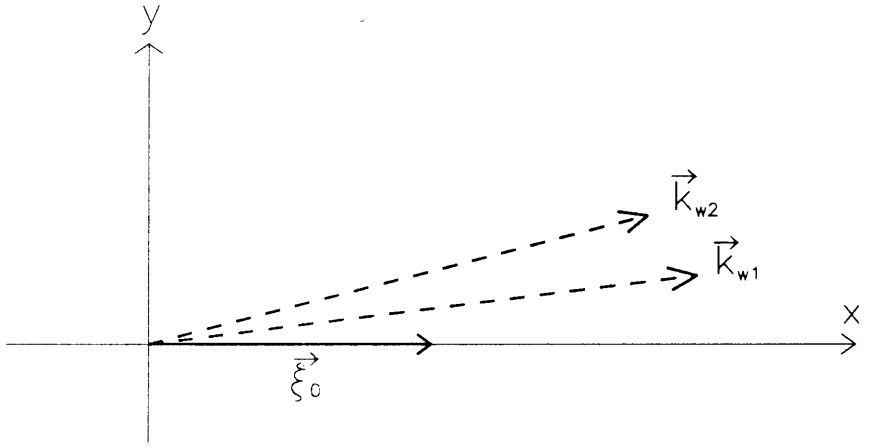

Figure 3.1a: Geometry of the sound and surface waves for *Case 1.* $\vec{\xi}_0$ represents the horizontal component of the sound wavenumber for the acoustic mode $\ell = 0$.

The incident sound wave interacts with each surface wave $\vec{k}_{w_i}$ separately triggering a strong scattered wave provided the tip of $\vec{k}_{w_i}$ falls on the circle of radius ξ_0 centered

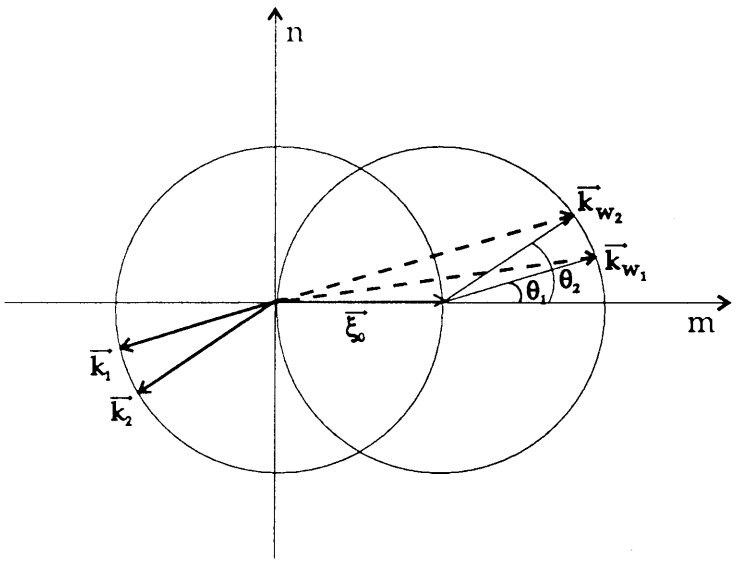

Figure 3.1b: Resonance condition for *Case 1.*

at $(\xi_0, 0)$ in the (m, n) wavenumber domain as illustrated in figure 3.1b. In total, there are three sound waves and the acoustic potential at the leading order reads

$$\Phi_0 = \{Ae^{iS} + \sum_{j=1}^{2} B_j e^{iS_j}\} \cos \eta_0 (z + h) + (*) \tag{3.2}$$

where

$$\begin{cases} S = \xi_0 x - \omega t, \\ S_1 = (\xi_0 - m_1)x - n_1 y - \omega t, \\ S_2 = (\xi_0 - m_2)x - n_2 y - \omega t. \end{cases} \tag{3.3a-c}$$

With the notations of figure 3.1b, we easily deduce

$$m_{1,2} = \xi_0(1 + \cos \theta_{1,2}) \qquad n_{1,2} = \xi_0 \sin \theta_{1,2} \tag{3.4a-b}$$

where the angles are positive counterclockwise. Comparison of $(3.3b-c)$ and $(3.4a-b)$ yields

$$S_{1,2} = -\xi_0(\cos \theta_{1,2}\ x + \sin \theta_{1,2}\ y) - \omega t \tag{3.5a-b}$$

The directions of resonant scattering

$$\vec{k}_{1,2} = \nabla S_{1,2} \tag{3.5c-d}$$

are shown in figure 3.1b. If use is made of $(3.3a)$ and $(3.5a-b)$ in $(2.14a-b)$, we obtain

$$\nabla^2 \Phi_1 - \frac{1}{C^2} \frac{\partial^2 \Phi_1}{\partial t^2} = -2i \frac{k}{C} \left[\{ \frac{\partial A}{\partial t_1} + \frac{\xi_0 C}{k} \frac{\partial A}{\partial x_1} \} e^{iS} + \right.$$

$$\{\frac{\partial B_1}{\partial t_1} - \frac{C\xi_0 \cos\theta_1}{k}\frac{\partial B_1}{\partial x_1} - \frac{C\xi_0 \sin\theta_1}{k}\frac{\partial B_1}{\partial y_1}\}e^{iS_1} +$$

$$\{\frac{\partial B_2}{\partial t_1} - \frac{C\xi_0 \cos\theta_2}{k}\frac{\partial B_2}{\partial x_1} - \frac{C\xi_0 \sin\theta_2}{k}\frac{\partial B_2}{\partial y_1}\}e^{iS_2}\Big] \cos\eta_0(z+h) + \text{NRT} \qquad (3.6)$$

$$\frac{\partial \Phi_1}{\partial z} = 0 \qquad z = -h \qquad (3.7)$$

Substitution of (3.1) and (3.2) in the boundary condition (2.14c) yields

$$\Phi_1 = \frac{\eta_0}{2}\{D_1 e^{i(m_1 x + n_1 y)} + D_2 e^{i(m_2 x + n_2 y)} + (*)\}\{Ae^{iS} + \sum_{j=1}^{2} B_j e^{iS_j}\} \quad z = 0 \quad (3.8)$$

which becomes, after multiplication:

$$\Phi_1 = \frac{\eta_0}{2}\{e^{iS}(D_1 B_1 + D_2 B_2) + e^{iS_1} D_1 A + e^{iS_2} D_2 A\} + \text{NRT} \quad z = 0 \qquad (3.9)$$

In view of (3.6), (3.7) and (3.9), a solution for Φ_1 is sought in the form:

$$\Phi_1 = \gamma(z)e^{iS} + \gamma_1(z)e^{iS_1} + \gamma_2(z)e^{iS_2} \qquad (3.10)$$

The governing equations for $\gamma(z)$ are

$$\frac{\partial^2 \gamma}{\partial z^2} + \eta_0^2 \gamma = -2i\frac{k}{C}\{\frac{\partial A}{\partial t_1} + C_g \frac{\partial A}{\partial x_1}\} \cos\eta_0(z+h) \qquad (3.11a)$$

$$\frac{\partial \gamma}{\partial z} = 0 \qquad z = -h, \qquad \gamma = \frac{\eta_0}{2}(D_1 B_1 + D_2 B_2) \qquad z = 0 \qquad (3.11b-c)$$

Since $\cos\eta_0(z+h)$ is a solution of the homogeneous problem, we must enforce solvability and apply Green's formula to γ and the solution $\cos\eta_0(z+h)$:

$$\int_{-h}^{0} (\frac{\partial^2 \gamma}{\partial z^2} + \eta_0^2 \gamma)\cos\eta_0(z+h)dz = \Big[\frac{\partial \gamma}{\partial z}\cos\eta_0(z+h) - \gamma\frac{\partial(\cos\eta_0(z+h))}{\partial z}\Big]_{-h}^{0} \qquad (3.12)$$

After use is made of $(3.11a-c)$, (3.12) becomes

$$\frac{\partial A}{\partial t_1} + \frac{\xi_0 C}{k}\frac{\partial A}{\partial x_1} = \frac{i}{2}\frac{\eta_0^2 C}{kh}(D_1 B_1 + D_2 B_2) \qquad (3.13)$$

Similarly, we obtain the governing equations for $\gamma_1(z)$:

$$\frac{\partial^2 \gamma_1}{\partial z^2} + \eta_0^2 \gamma_1 = -2i\frac{k}{C}\{\frac{\partial B_1}{\partial t_1} - \frac{\xi_0 \cos\theta_1 C}{k}\frac{\partial B_1}{\partial x_1} - \frac{\xi_0 \sin\theta_1 C}{k}\frac{\partial B_1}{\partial y_1}\} \cos\eta_0(z+h) \qquad (3.14a)$$

$$\frac{\partial \gamma_1}{\partial z} = 0 \qquad z = -h, \qquad \gamma_1 = \frac{\eta_0}{2} D_1 A \qquad z = 0 \tag{3.14b-c}$$

Again, the solvability condition is required:

$$\int_{-h}^{0} \left(\frac{\partial^2 \gamma_1}{\partial z^2} + \eta_0^2 \gamma_1\right) \cos \eta_0 (z+h) dz = \left[\frac{\partial \gamma_1}{\partial z} \cos \eta_0 (z+h) - \gamma_1 \frac{\partial \left(\cos \eta_0 (z+h)\right)}{\partial z}\right]_{-h}^{0} \tag{3.15}$$

which, owing to $(3.14a-c)$, is evaluated to

$$\frac{\partial B_1}{\partial t_1} - \frac{\xi_0 \cos \theta_1 C}{k} \frac{\partial B_1}{\partial x_1} - \frac{\xi_0 \sin \theta_1 C}{k} \frac{\partial B_1}{\partial y_1} = \frac{i}{2} \frac{\eta_0^2 C}{kh} D_1 A \tag{3.16}$$

Upon replacing index 1 by index 2, the evolution equation for B_2 is deduced:

$$\frac{\partial B_2}{\partial t_1} - \frac{\xi_0 \cos \theta_2 C}{k} \frac{\partial B_2}{\partial x_1} - \frac{\xi_0 \sin \theta_2 C}{k} \frac{\partial B_2}{\partial y_1} = \frac{i}{2} \frac{\eta_0^2 C}{kh} D_2 A \tag{3.17}$$

After normalization of the spatial variables and time respectively by k and ω, we obtain the governing equations describing the evolution of the three scattered sound amplitudes

$$\begin{cases} \frac{\partial A}{\partial t_1} + \nabla_1 \cdot (\vec{C}_{g_A} A) = i(\alpha_1 B_1 + \alpha_2 B_2), \\ \frac{\partial B_1}{\partial t_1} + \nabla_1 \cdot (\vec{C}_{g_{B_1}} B_1) = i\alpha_1 A, \\ \frac{\partial B_2}{\partial t_1} + \nabla_1 \cdot (\vec{C}_{g_{B_2}} B_2) = i\alpha_2 A, \end{cases} \tag{3.18}$$

where

$$\alpha_{1,2} = \frac{1}{2} \frac{\eta_0^2}{kh} D_{1,2} \tag{3.19}$$

and the group velocities are

$$\vec{C}_{g_A} = \Lambda \begin{pmatrix} 1 \\ 0 \end{pmatrix}, \qquad \vec{C}_{g_{B_{1,2}}} = -\Lambda \begin{pmatrix} \cos \theta_{1,2} \\ \sin \theta_{1,2} \end{pmatrix} \tag{3.20a-c}$$

It is worth commenting that scattered sound waves A, B_1 and B_2 are all coupled. Thus the resonant scattering by the two surface waves is not the mere superposition of the individual scattering by each surface wave. The magnitude of the coupling frequency α_i is expectedly proportional to the surface waveheight and to the inverse of normalized water depth kh, hence is greater for shallower seas.

Note that B_1 is only indirectly coupled to B_2 through their common coupling with A. In the special case where only one surface wave is present, *i.e.* $\vec{k}_{w1} = \vec{k}_{w2}$ and $D_1 = D_2$, we may substitute

$$B_1 = B_2 = \frac{B}{\sqrt{2}} \qquad \alpha_1 = \alpha_2 = \frac{\alpha}{\sqrt{2}} \tag{3.21a-b}$$

in (3.18) to obtain

$$\begin{cases} \frac{\partial A}{\partial t_1} + \nabla_1 \cdot (\vec{C}_{g_A} A) = i\alpha B, \\ \frac{\partial B}{\partial t_1} + \nabla_1 \cdot (\vec{C}_{g_B} B) = i\alpha A, \end{cases} \qquad (3.21c-d)$$

which were derived in Mei & Naciri(1991).

3.2. Multiple Scattering

3.2.1. *Resonance condition*

In this section, we investigate the possibility whereby two surface waves may resonate scattered sound in more than two directions. The velocity potential Φ_0 at the leading order reads

$$\Phi_0(x,y,z,t,x_1,y_1,t_1) = \left\{ A(x_1,y_1,t_1)e^{iS} + \sum_{j=1}^{3} B_j(x_1,y_1,t_1)e^{iS_j} \right\} \cos\eta_0(z+h) \qquad (3.22)$$

The free surface boundary condition at $\mathcal{O}(\epsilon)$ is deduced from (2.14c)

$$\Phi_1 = \frac{\eta_0}{2}\{D_1 e^{i\vec{k}_{w_1}\cdot\vec{r}} + D_2 e^{i\vec{k}_{w_2}\cdot\vec{r}} + (*)\}\{Ae^{iS} + \sum_{j=1}^{3} B_j e^{iS_j}\} \qquad z=0. \qquad (3.23)$$

where S corresponds to forward scattering. The phase functions S_1 and S_2 have been defined in (3.5$a-b$) and satisfy the Bragg resonance condition:

$$\left|\nabla S_i\right|^2 = \left|\vec{\xi}_0 - \vec{k}_{w_i}\right|^2 = \left|\nabla S\right|^2 = \left|\vec{\xi}_0\right|^2 \qquad i=1,2 \qquad (3.24)$$

where $\vec{\xi}_0$ designates the horizontal component of the acoustic wavenumber. Eq. (3.24) implies in vector form:

$$\left|\vec{k}_{w_i}\right|^2 - 2\vec{\xi}_0.\vec{k}_{w_i} = 0 \qquad i=1,2 \qquad (3.25)$$

In addition, S_3 corresponds to a new resonantly scattered sound wave whose direction is yet to be found. Expansion of (3.23) yields sum and difference phase functions involving S, S_1 and S_2. Since $\vec{k}_{w_1}$ and $\vec{k}_{w_2}$ play symmetric roles, it is sufficient to analyse the following scattering directions only:

$$\vec{\xi}_0 - \vec{k}_{w_2} \mp \vec{k}_{w_i} \qquad i=1,2 \qquad (3.26)$$

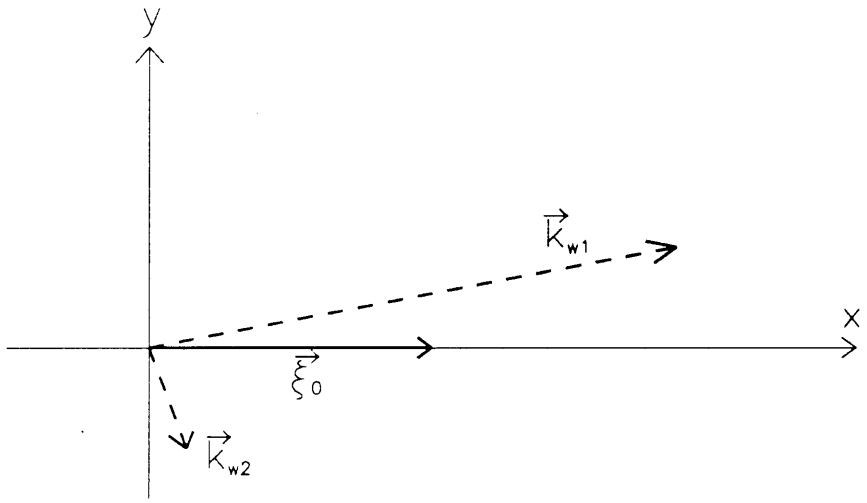

Figure 3.2a: Geometry of the sound and surface waves for *Case 2.*

The wavenumber defined in (3.26) corresponds to resonant scattering provided that

$$\left|\vec{\xi}_0 - \vec{k}_{w_2} \mp \vec{k}_{w_i}\right|^2 = \left|\vec{\xi}_0\right|^2 \qquad i = 1,2 \tag{3.27}$$

Upon using (3.24), the resonance condition (3.27) is simplified to

$$\left|\vec{k}_{w_i}\right|^2 \mp 2\vec{k}_{w_i}.(\vec{\xi}_0 - \vec{k}_{w_2}) = 0 \qquad i = 1,2 \tag{3.28}$$

Substitution of (3.25) in (3.28) yields four scenarios

$$\vec{k}_{w_i} \cdot \vec{k}_{w_2} = 0 \quad , \quad \vec{k}_{w_i} \cdot \left\{2\vec{\xi}_0 - \vec{k}_{w_2}\right\} = 0 \qquad i = 1,2 \tag{3.29a-b}$$

Let us consider first the resonance condition (3.29*a*) which can be met only when $i = 1$

$$\vec{k}_{w_1} \cdot \vec{k}_{w_2} = 0 \tag{3.30}$$

i.e. the two surface waves intersect at right angle, cf. figure 3.2a. The scattering of sound by surface waves satisfying (3.30) will be referred to as *Case 2.* The corresponding resonant scattering direction is deduced from (3.26) with the "-" sign

$$\vec{k}_3 = \vec{\xi}_0 - \vec{k}_{w_1} - \vec{k}_{w_2} \tag{3.31}$$

Simple geometrical considerations yields

$$\vec{k}_{w_1} + \vec{k}_{w_2} = 2\vec{\xi}_0 \tag{3.32}$$

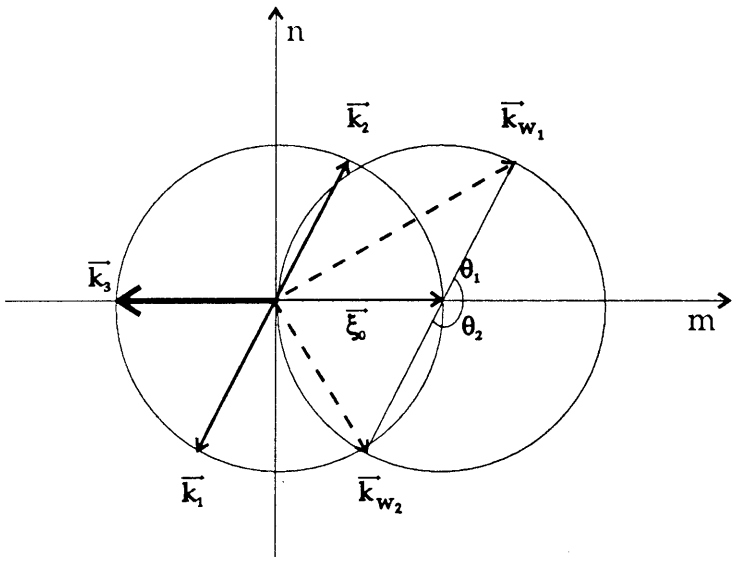

Figure 3.2b: Resonance condition for *Case 2.*

and the scattering direction (3.31) is simply

$$\vec{k}_3 = -\vec{\xi}_0 \tag{3.33}$$

as shown in figure 3.2b. The phase function associated with the third resonantly scattered sound wave is thus

$$S_3 = -\vec{\xi}_0.\vec{r} - \omega t \tag{3.34}$$

Note that A and B_3 are the amplitudes of sound waves propagating in opposite directions. The phase functions S_1 and S_2:

$$S_{1,2} = (\vec{\xi}_0 - \vec{k}_{w_{1,2}}).\vec{r} - \omega t \tag{3.35a-b}$$

can be simplified thanks to (3.32)

$$S_{1,2} = \pm(\vec{\xi}_0 - \vec{k}_{w_1}).\vec{r} - \omega t \tag{3.36a-b}$$

and therefore correspond to sound waves propagating in opposite directions. We therefore have two sets, (S, S_3) and (S_1, S_2), of sound waves propagating in opposite directions.

Consider next the resonance condition (3.29*b*). We discard $i = 2$, for it reduces to (3.25), and assume that $i = 1$:

$$\vec{k}_{w_1}.(2\vec{\xi}_0 - \vec{k}_{w_2}) = 0. \tag{3.37}$$

If $\vec{k}_{w_2} - 2\vec{\xi}_0$ is not zero, it must be perpendicular to $\vec{k}_{w_1}$. Because $2\vec{\xi}_0$ coincides with a diameter of the circle C_1, $\vec{k}_{w_2}$ is also perpendicular to $\vec{k}_{w_2} - 2\vec{\xi}_0$. Thus, we have two alternatives:

$$\vec{k}_{w_1} = \pm\vec{k}_{w_2} \tag{3.38}$$

In the first case, $\vec{k}_{w_1} = \vec{k}_{w_2}$, and there is just one surface wave. This elementary situation has been studied by Mei & Naciri(1991). The second case $\vec{k}_{w_1} = -\vec{k}_{w_2}$ is nontrivial, the corresponding free surface elevation reads

$$\zeta_1 = \frac{1}{2}\left[D_1 e^{i\vec{k}_{w1}\cdot\vec{r}} + D_2 e^{i\vec{k}_{w_2}\cdot\vec{r}} + (*)\right] = \frac{1}{2}\left[(D_1 + D_2^*)e^{i\vec{k}_{w1}\cdot\vec{r}} + (*)\right] \tag{3.39}$$

The free surface elevation (3.39) is that of a single surface wave propagating along the $\pm\vec{k}_{w_1}$ axis with amplitude $D' = D_1 + D_2^*$. Again, this case has been treated by Mei & Naciri(1991). Therefore, we need only consider

$$\vec{k}_{w_2} = 2\vec{\xi}_0 \tag{3.40}$$

which is referred to as *Case 3* (see figure 3.3a).

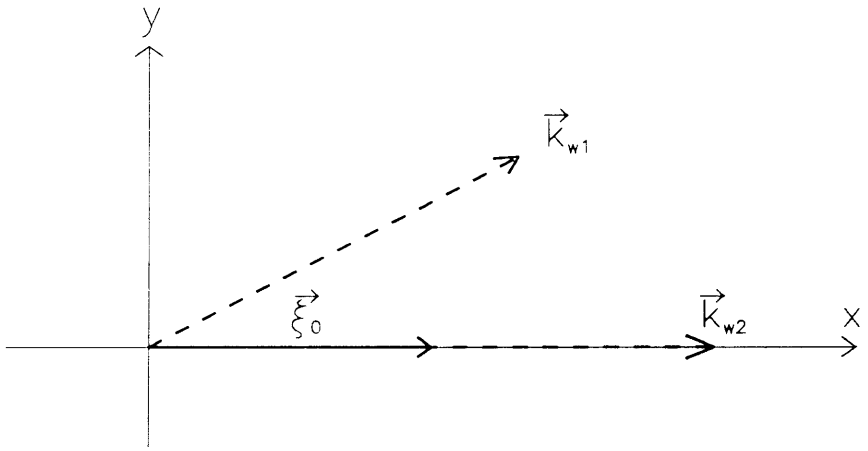

Figure 3.3a: Geometry of the sound and surface waves for *Case 3*.

The associated resonant scattering direction is deduced from (3.26) with the "+" sign

$$\vec{k}_3 = \vec{\xi}_0 - \vec{k}_{w_2} + \vec{k}_{w_1} = -(\vec{\xi}_0 - \vec{k}_{w_1}) \tag{3.41}$$

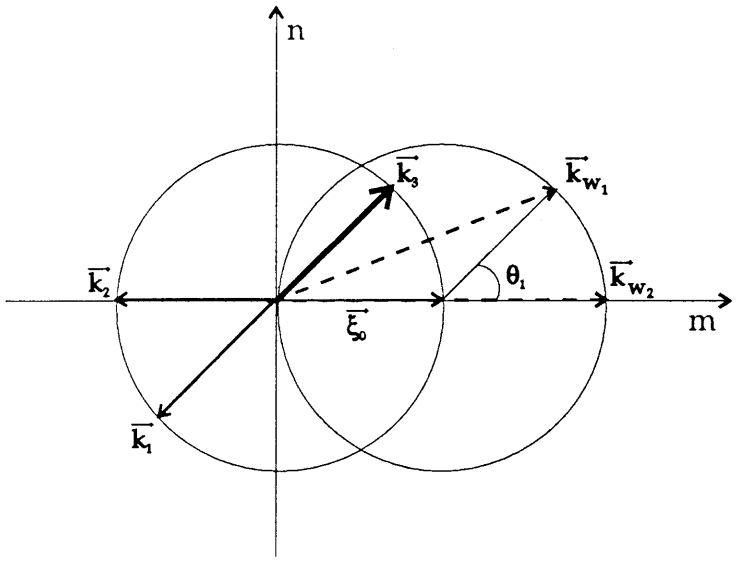

Figure 3.3b: Resonance condition for *Case 3*.

The corresponding phase function is

$$S_3 = -(\vec{\xi}_0 - \vec{k}_{w_1}).\vec{r} - \omega t \tag{3.42}$$

Under (3.40), sound is scattered in four directions. Recalling the expression of phase functions $S_{1,2}$

$$\begin{cases} S_1^- = (\vec{\xi}_0 - \vec{k}_{w_1}).\vec{r} - \omega t \\ S_2^- = -\vec{\xi}_0.\vec{r} - \omega t \end{cases} \tag{3.43a-b}$$

we again find two sets of scattered sound waves propagating in opposite directions: (S, S_2) corresponding to forward and backscattering directions and (S_1, S_3) propagating at angle θ_1 and $\pi + \theta_1$ (see figure 3.3b).

Let us try to understand better the kinematics of $\vec{k}_3$ in both *Cases 2* and *3*.

Consider first *Case 2* and $\vec{k}_3$ as defined by (3.33), cf. figure 3.4. Scattering along $\vec{k}_3$ occurs as if there were an apparent surface wave with wavenumber $\vec{k}_w = \vec{k}_{w_1} + \vec{k}_{w_2}$ in the sea. This wave cannot exist physically since it does not satisfy the surface wave dispersion relation. In other words, it is the vector sum of the two surface waves $\vec{k}_{w_1}$ and $\vec{k}_{w_2}$ with $\vec{k}_{w_1} + \vec{k}_{w_2} = 2\vec{\xi}_0$ which causes the backscattering by Bragg resonance.

Let us now examine sequentially the effect of each surface wave on the incident sound wave. Let the incident sound wave be designated by a single arrow. As

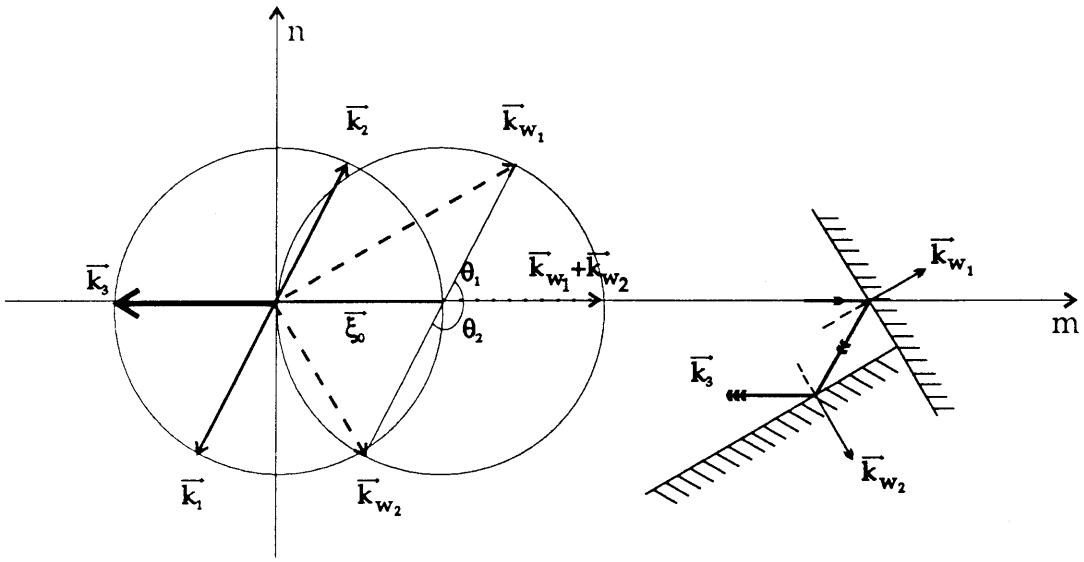

Figure 3.4: Schematic of multiple scattering for *Case 2.*

it impinges on the crest line of surface wave $\vec{k}_{w_1}$, it is reflected specularly. The resulting ray (double arrow) then impinges on a crest line of surface wave $\vec{k}_{w_2}$ and is again reflected specularly. As a result, the final ray (triple arrow) propagates in the negative x-direction as predicted by our theory. The same conclusion is reached if one begins with surface wave $\vec{k}_{w_2}$. The term *multiple scattering* is therefore appropriate for *Case 2.*

Consider next *Case 3* where one of the two surface waves is in the same direction as the incident sound wave. From eq. (3.41), Bragg scattering yields $\vec{k}_3$ as if there were a fictitious surface wave with wavenumber $\vec{k}_w = \vec{k}_{w_2} - \vec{k}_{w_1}$. Thus the vector difference of surface waves $\vec{k}_{w_1}$ and $\vec{k}_{w_2}$ is responsible for the Bragg scattering.

Referring to figure 3.5, let the incident sound wave be designated again by a single arrow, and be reflected by the crest line of surface wave $\vec{k}_{w_2} = 2\vec{\xi}_0$. The resulting ray (double arrow) then impinges on a crest line of surface wave $\vec{k}_{w_1}$ and yields a reflected ray (triple arrow) in the scattering direction predicted by our theory. Thus *Case 3* can also be regarded as a case of *multiple scattering.*

It is important to point out the fundamental difference between our multiple scattering theory and Barrick's *hydrodynamic second order scattering* introduced in the context of the scattering of HF radar by a sea spectrum. Although he considers scattering due to more than one surface wave as we do in *Case 2* and *Case 3*, his

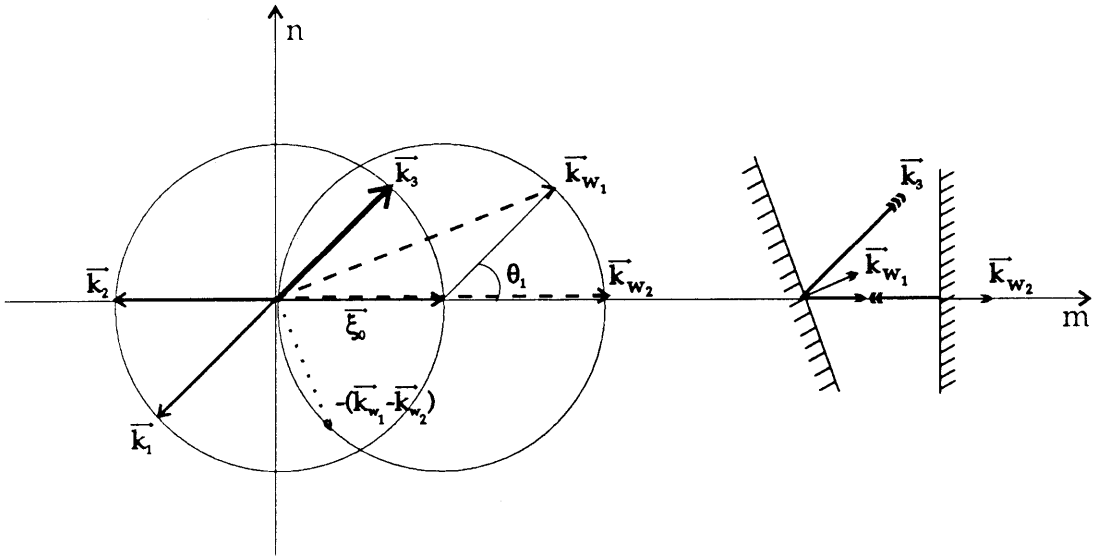

Figure 3.5: Schematic of multiple scattering for *Case 3.*

scattered field nevertheless is only second order, for it is proportional to the product of the radar wave slope and the surface wave slope. In contrast, our theory allows strong resonant scattering, and the amplitudes of the scattered amplitudes are all of comparable magnitude.

3.2.2. *Case 2: Two perpendicular surface waves*

When two surface waves intersect at right angle, sound is scattered in four directions characterized by the phase functions

$$\begin{cases} S^+ = \xi_0 x - \omega t, & S_1^- = (\xi_0 - m_1)x - n_1 y - \omega t, \\ S_2^- = (\xi_0 - m_2)x - n_2 y - \omega t, & S_3^- = -\xi_0 x - \omega t. \end{cases} \tag{3.44}$$

Substitution of (3.22) and (3.44) in ($2.14a-b$) yields after simple manipulations

$$\begin{aligned} \nabla^2\Phi_1 - \frac{1}{C^2}\frac{\partial^2\Phi_1}{\partial t^2} = -2i\frac{k}{C}\Big[& \{\frac{\partial A}{\partial t_1} + \frac{\xi_0 C}{k}\frac{\partial A}{\partial x_1}\}e^{iS} + \\ & \{\frac{\partial B_1}{\partial t_1} - \frac{\xi_0\cos\theta_1 C}{k}\frac{\partial B_1}{\partial x_1} - \frac{\xi_0\sin\theta_1 C}{k}\frac{\partial B_1}{\partial y_1}\}e^{iS_1} + \\ & \{\frac{\partial B_2}{\partial t_1} + \frac{\xi_0\cos\theta_1 C}{k}\frac{\partial B_2}{\partial x_1} + \frac{\xi_0\sin\theta_1 C}{k}\frac{\partial B_2}{\partial y_1}\}e^{iS_2} + \\ & \{\frac{\partial B_3}{\partial t_1} - \frac{\xi_0 C}{k}\frac{\partial B_3}{\partial x_1}\}e^{iS_3}\Big]\cos\eta_0(z+h) \qquad + \text{NRT} \end{aligned} \tag{3.45}$$

$$\frac{\partial \Phi_1}{\partial z} = 0 \qquad z = -h \tag{3.46}$$

From the free surface boundary condition (2.14c), we get

$$\Phi_1 = \frac{\eta_0}{2}\{(D_1B_1 + D_2B_2)e^{iS} + (D_1A + D_2B_3)e^{iS_1} +$$

$$(D_2A + D_1B_3)e^{iS_2} + (D_1B_2 + D_2B_1)e^{iS_3}\} + \text{NRT} \qquad z = 0 \tag{3.47}$$

Equations $(3.45 - 47)$ suggest the following expression for Φ_1:

$$\Phi_1 = \gamma(z)e^{iS} + \gamma_1(z)e^{iS_1} + \gamma_2(z)e^{iS_2} + \gamma_3(z)e^{iS_3} + \text{NRT} \tag{3.48}$$

Upon substituting (3.48) into $(3.45 - 47)$ and separating the phases, the governing equations for $\gamma(z)$ and $\gamma_j(z)$ are obtained.

e^{iS}:

$$\frac{\partial^2 \gamma}{\partial z^2} + \eta_0^2\gamma = -2i\frac{k}{C}\Big\{\frac{\partial A}{\partial t_1} + \frac{\xi_0 C}{k}\frac{\partial A}{\partial x_1}\Big\}\cos\eta_0(z+h) \tag{3.49a}$$

$$\frac{\partial \gamma}{\partial z} = 0 \qquad z = -h, \qquad \gamma = \frac{\eta_0}{2}(D_1B_1 + D_2B_2) \qquad z = 0 \tag{3.49$b-c$}$$

The solvability condition of γ yields

$$\frac{\partial A}{\partial t_1} + \frac{\xi_0 C}{k}\frac{\partial A}{\partial x_1} = \frac{i}{2}\frac{\eta_0^2 C}{kh}(D_1B_1 + D_2B_2) \tag{3.50}$$

e^{iS_1}:

$$\frac{\partial^2 \gamma_1}{\partial z^2} + \eta_0^2\gamma_1 = -2i\frac{k}{C}\Big\{\frac{\partial B_1}{\partial t_1} - \frac{\xi_0\cos\theta_1 C}{k}\frac{\partial B_1}{\partial x_1} - \frac{\xi_0\sin\theta_1 C}{k}\frac{\partial B_1}{\partial y_1}\Big\}\cos\eta_0(z+h) \tag{3.51a}$$

$$\frac{\partial \gamma_1}{\partial z} = 0 \qquad z = -h, \qquad \gamma_1 = \frac{\eta_0}{2}(D_1A + D_2B_3) \qquad z = 0 \tag{3.51$b-c$}$$

The solvability condition results in

$$\frac{\partial B_1}{\partial t_1} - \frac{\xi_0 C}{k}\cos\theta_1\frac{\partial B_1}{\partial x_1} - \frac{\xi_0 C}{k}\sin\theta_1\frac{\partial B_1}{\partial y_1} = \frac{i}{2}\frac{\eta_0^2 C}{kh}(D_1A + D_2B_3) \tag{3.52}$$

e^{iS_2}:

$$\frac{\partial^2 \gamma_2}{\partial z^2} + \eta_0^2\gamma_2 = -2i\frac{k}{C}\Big\{\frac{\partial B_2}{\partial t_1} + \frac{\xi_0\cos\theta_1 C}{k}\frac{\partial B_2}{\partial x_1} + \frac{\xi_0\sin\theta_1 C}{k}\frac{\partial B_2}{\partial y_1}\Big\}\cos\eta_0(z+h) \tag{3.53a}$$

$$\frac{\partial \gamma_2}{\partial z} = 0 \qquad z = -h, \qquad \gamma_2 = \frac{\eta_0}{2}(D_2A + D_1B_3) \qquad z = 0 \tag{3.53$b-c$}$$

From the solvability condition, we obtain

$$\frac{\partial B_2}{\partial t_1} + \frac{\xi_0 C}{k}\cos\theta_1 \frac{\partial B_2}{\partial x_1} + \frac{\xi_0 C}{k}\sin\theta_1 \frac{\partial B_2}{\partial y_1} = \frac{i}{2}\frac{\eta_0^2 C}{kh}(D_2 A + D_1 B_3) \tag{3.54}$$

e^{iS_3}:

$$\frac{\partial^2 \gamma_3}{\partial z^2} + \eta_0^2 \gamma_3 = -2i\frac{k}{C}\{\frac{\partial B_3}{\partial t_1} - \frac{\xi_0 C}{k}\frac{\partial B_3}{\partial x_1}\}\cos\eta_0(z+h) \tag{3.55a}$$

$$\frac{\partial \gamma_3}{\partial z} = 0 \qquad z = -h, \qquad \gamma_3 = \frac{\eta_0}{2}(D_2 B_1 + D_1 B_2) \qquad z = 0 \tag{3.55b-c}$$

The solvability condition of δ_3 yields

$$\frac{\partial B_3}{\partial t_1} - \frac{\xi_0 C}{k}\frac{\partial B_3}{\partial x_1} = \frac{i}{2}\frac{\eta_0^2 C}{kh}(D_2 B_1 + D_1 B_2) \tag{3.56}$$

Upon normalizing the spatial coordinates by k and time by ω, we obtain the following set of coupled partial differential equations:

$$\begin{cases} \frac{\partial A}{\partial t_1} + \nabla_1 \cdot (\vec{C}_{g_A} A) = i(\alpha_1 B_1 + \alpha_2 B_2), \\ \frac{\partial B_1}{\partial t_1} + \nabla_1 \cdot (\vec{C}_{g_{B_1}} B_1) = i(\alpha_1 A + \alpha_2 B_3), \\ \frac{\partial B_2}{\partial t_1} - \nabla_1 \cdot (\vec{C}_{g_A} B_2) = i(\alpha_2 A + \alpha_1 B_3), \\ \frac{\partial B_3}{\partial t_1} - \nabla_1 \cdot (\vec{C}_{g_{B_1}} B_3) = i(\alpha_2 B_1 + \alpha_1 B_2), \end{cases} \tag{3.57}$$

where the normalized group velocities are given by

$$\vec{C}_{g_A} = \Lambda \begin{pmatrix} 1 \\ 0 \end{pmatrix} \quad \& \quad \vec{C}_{g_{B_1}} = -\Lambda \begin{pmatrix} \cos\theta_1 \\ \sin\theta_1 \end{pmatrix} \tag{3.58a-b}$$

and $\alpha_{1,2}$ are defined in (3.19). Note the symmetry in (3.57). Each sound amplitude is forced by two of the four interacting waves, and each normalized surface wave-height α_1 and α_2 contributes equally to the forcing. There is no direct coupling between sound waves propagating in opposite directions (B_1 and B_2 or A and B_3).

3.2.3. *Case 3: One surface wave collinear to incident sound wave*

There are again four scattered sound waves whose phase functions read

$$\begin{cases} S = \xi_0 x - \omega t, & S_1 = (\xi_0 - m_1)x - n_1 y - \omega t, \\ S_2 = -\xi_0 x - \omega t, & S_3 = -(\xi_0 - m_1)x + n_1 y - \omega t. \end{cases} \tag{3.59}$$

We substitute (3.22) and (3.59) in (2.14$a-b$) to obtain at $\mathcal{O}(\epsilon)$

$$\nabla^2 \Phi_1 - \frac{1}{C^2}\frac{\partial^2 \Phi_1}{\partial t^2} = -2i\frac{k}{C}\Big[\{\frac{\partial A}{\partial t_1} + \frac{\xi_0 C}{k}\frac{\partial A}{\partial x_1}\}e^{iS} +$$

$$\{\frac{\partial B_1}{\partial t_1} - \frac{\xi_0 \cos\theta_1 C}{k}\frac{\partial B_1}{\partial x_1} - \frac{\xi_0 \sin\theta_1 C}{k}\frac{\partial B_1}{\partial y_1}\}e^{iS_1} +$$

$$\{\frac{\partial B_2}{\partial t_1} - \frac{\xi_0 C}{k}\frac{\partial B_2}{\partial x_1}\}e^{iS_2} +$$

$$\{\frac{\partial B_3}{\partial t_1} + \frac{\xi_0 \cos\theta_1 C}{k}\frac{\partial B_3}{\partial x_1} + \frac{\xi_0 \sin\theta_1 C}{k}\frac{\partial B_3}{\partial y_1}\}e^{iS_3}\Big]\cos\eta_0(z+h) \; + \; \text{NRT} \qquad (3.60)$$

$$\frac{\partial \Phi_1}{\partial z} = 0 \qquad z = -h \qquad (3.61)$$

and the free surface boundary condition (2.14c) reads

$$\Phi_1 = \frac{\eta_0}{2}\{(D_1 B_1 + D_2 B_2)e^{iS} + D_1 A e^{iS_1} +$$

$$(D_2 A + D_1 B_3)e^{iS_2} + D_1 B_2 e^{iS_3}\} \; + \; \text{NRT} \qquad z = 0 \qquad (3.62)$$

To satisfy $(3.60 - 62)$ and (3.88), we assume the following expression for Φ_1:

$$\Phi_1 = \gamma(z)e^{iS} + \gamma_1(z)e^{iS_1} + \gamma_2(z)e^{iS_2} + \gamma_3(z)e^{iS_3} + \text{NRT} \qquad (3.63)$$

Upon substitution and separation of the phases, we deduce the governing equations for $\gamma(z)$ and $\{\gamma_j(z)\}_{j=1,3}$ and the corresponding evolution equations:

e^{iS}:

$$\frac{\partial^2 \gamma}{\partial z^2} + \eta_0^2 \gamma = -2i\frac{k}{C}\{\frac{\partial A}{\partial t_1} + \frac{\xi_0 C}{k}\frac{\partial A}{\partial x_1}\}\cos\eta_0(z+h) \qquad (3.64a)$$

$$\frac{\partial \gamma}{\partial z} = 0 \qquad z = -h, \qquad \gamma = \frac{\eta_0}{2}(D_1 B_1 + D_2 B_2) \qquad z = 0 \qquad (3.64b-c)$$

The solvability condition for $\gamma(z)$ yields

$$\frac{\partial A}{\partial t_1} + \frac{\xi_0 C}{k}\frac{\partial A}{\partial x_1} = \frac{i}{2}\frac{\eta_0^2 C}{kh}(D_1 B_1 + D_2 B_2) \qquad (3.65)$$

e^{iS_1}:

$$\frac{\partial^2 \gamma_1}{\partial z^2} + \eta_0^2 \gamma_1 = -2i\frac{k}{C}\{\frac{\partial B_1}{\partial t_1} - \frac{\xi_0 \cos\theta_1 C}{k}\frac{\partial B_1}{\partial x_1} - \frac{\xi_0 \sin\theta_1 C}{k}\frac{\partial B_1}{\partial y_1}\}\cos\eta_0(z+h) \qquad (3.66a)$$

$$\frac{\partial \gamma_1}{\partial z} = 0 \qquad z = -h, \qquad \gamma_1 = \frac{\eta_0}{2}D_1 A \qquad z = 0 \qquad (3.66b-c)$$

The solvability condition for γ_1 yields

$$\frac{\partial B_1}{\partial t_1} - \frac{\xi_0 C}{k}\cos\theta_1\frac{\partial B_1}{\partial x_1} - \frac{\xi_0 C}{k}\sin\theta_1\frac{\partial B_1}{\partial y_1} = \frac{i}{2}\frac{\eta_0^2 C}{kh}D_1 A \qquad (3.67)$$

$e^{iS_2^-}$:

$$\frac{\partial^2\gamma_2}{\partial z^2}+\eta_0^2\gamma_2=-2i\frac{k}{C}\{\frac{\partial B_2}{\partial t_1}-\frac{\xi_0 C}{k}\frac{\partial B_2}{\partial x_1}\}\cos\eta_0(z+h) \qquad (3.68a)$$

$$\frac{\partial\gamma_2}{\partial z}=0 \qquad z=-h, \qquad \gamma_2=\frac{\eta_0}{2}(D_2A+D_1B_3) \qquad z=0 \qquad (3.68b-c)$$

and the solvability condition for γ_2 requires

$$\frac{\partial B_2}{\partial t_1}-\frac{\xi_0 C}{k}\frac{\partial B_2}{\partial x_1}=\frac{i}{2}\frac{\eta_0^2 C}{kh}(D_2A+D_1B_3) \qquad (3.69)$$

e^{iS_3}:

$$\frac{\partial^2\gamma_3}{\partial z^2}+\eta_0^2\gamma_3=-2i\frac{k}{C}\{\frac{\partial B_3}{\partial t_1}+\frac{\xi_0\cos\theta_1 C}{k}\frac{\partial B_3}{\partial x_1}+\frac{\xi_0\sin\theta_1 C}{k}\frac{\partial B_3}{\partial y_1}\}\cos\eta_0(z+h) \quad (3.70a)$$

$$\frac{\partial\gamma_3}{\partial z}=0 \qquad z=-h, \qquad \gamma_3=\frac{\eta_0}{2}D_1B_2 \qquad z=0 \qquad (3.70b-c)$$

The solvability condition for γ_3 requires

$$\frac{\partial B_3}{\partial t_1}+\frac{\xi_0\cos\theta_1 C}{k}\frac{\partial B_3}{\partial x_1}+\frac{\xi_0\sin\theta_1 C}{k}\frac{\partial B_3}{\partial y_1}=\frac{i}{2}\frac{\eta_0^2 C}{kh}D_1B_2 \qquad (3.71)$$

In conclusion, the evolution equations for the scattered sound are after normalization

$$\begin{cases} \frac{\partial A}{\partial t_1}+\nabla_1\cdot(\vec{C}_{g_A}A)=i(\alpha_1B_1+\alpha_2B_2), \\ \frac{\partial B_1}{\partial t_1}+\nabla_1\cdot(\vec{C}_{g_{B_1}}B_1)=i\alpha_1A, \\ \frac{\partial B_2}{\partial t_1}-\nabla_1\cdot(\vec{C}_{g_A}B_2)=i(\alpha_2A+\alpha_1B_3), \\ \frac{\partial B_3}{\partial t_1}-\nabla_1\cdot(\vec{C}_{g_{B_1}}B_3)=i\alpha_1B_2, \end{cases} \qquad (3.72)$$

where the group velocities are

$$\vec{C}_{g_A}=\Lambda\begin{pmatrix}1\\0\end{pmatrix} \quad \& \quad \vec{C}_{g_{B_1}}=-\Lambda\begin{pmatrix}\cos\theta_1\\\sin\theta_1\end{pmatrix} \qquad (3.73)$$

Note that the symmetry is different from that found in eqs. (3.57). Only the forward (A) and backscattering (B_2) sound amplitudes are forced by two other waves. Furthermore, they are directly forcing each other. While both surface waveheights are contributing equally to the forcing in *Case 2*, this is no longer true in *Case 3* where α_1 appears twice as often as α_2. This suggests that the two surface waves no longer play comparable roles.

4. DISPERSION OF ENVELOPES

4.1. Motivations

In Mei & Naciri(1991), the scatterer consisted of a single surface wave collinear to the incident sound. It was shown that the envelopes A and B of the forward and backscattered sound waves both satisfy the dispersive Klein-Gordon equation:

$$\{\frac{\partial^2}{\partial t_1^2} - C_g^2 \frac{\partial^2}{\partial x_1^2} + \alpha^2\} \begin{pmatrix} A \\ B \end{pmatrix} = 0 \tag{4.1}$$

Assuming a plane wave solution to (4.1)

$$\begin{pmatrix} A \\ B \end{pmatrix} (x_1, t_1) = \begin{pmatrix} T \\ R \end{pmatrix} e^{i(\mu x_1 - \sigma t_1)} \tag{4.2}$$

Existence of nontrivial solutions requires that

$$\sigma^2 = \alpha^2 + C_g^2 \mu^2 \tag{4.3}$$

Eq. (4.1) shows that different modulation wavenumbers (μ) propagate at different velocities. The sound amplitudes A and B are therefore dispersive due to the presence of the surface waves ($\alpha \neq 0$). The frequency σ may be referred to as the detuning frequency, *i.e.* a measure of the departure from resonance, $\sigma = 0$ meaning perfect tuning. The solution of this boundary value problem is found in terms of the eigenmodes of a spatial ($\frac{\partial}{\partial x_1}$) matrix differential operator. In particular, when the surface wave is uniform in amplitude, α is interpreted as a cutoff frequency since μ is imaginary when $\sigma < \alpha$ thus implying a monotonic spatial behavior and is real when $\sigma > \alpha$, therefore implying an oscillatory behavior.

Consider now the scattering of plane sound waves by uniform surface waves extending throughout space. We must therefore solve an initial value problem in terms of the eigenmodes of a temporal matrix differential operator ($\frac{\partial}{\partial t_1}$) . Wavenumber μ can therefore be viewed as a detuning ($\epsilon\mu$) from resonance since $e^{i\mu x_1} \equiv e^{i\epsilon\mu x}$. Moreover, perfect tuning will occur for $\mu = 0$. It is conjectured that envelope dispersion is the strongest at resonance. Therefore, the analysis of envelope dispersion for perfect tuning is likely to yield relevant information regarding the scatterer. Once the dispersion relation is obtained, the eigenvalue condition needed for the

numerical scheme in §5 is easily deduced. We nw seek the dispersion relations associated with partial differential equations (3.18), (3.57) and (3.72) respectively for *Cases 1, 2* and *3*.

4.2. Derivation of Envelope Dispersion Relations

The following dimensionless slow variables are introduced

$$(kx_1, ky_1, \omega t_1) = (x_1^\star, y_1^\star, t_1^\star) \tag{4.4}$$

where k and ω represent respectively the wavenumber and radian frequency of the incident sound wave. Upon subsituting (4.8) in (3.18), (3.57) and (3.72), and omitting the star superscripts, the three sets of equations are expressed in the following matrix form

$$\left\{ I \frac{\partial}{\partial t_1} + C_{g_x} \frac{\partial}{\partial x_1} + C_{g_y} \frac{\partial}{\partial y_1} - i\, N \right\} U \; = 0 \tag{4.5}$$

where N is a symmetric matrix describing the coupling between the scattered sound waves, C_{g_x} and C_{g_y} are diagonal matrices with entries respectively equal to the x- and y-components of the group velocity of each scattered sound wave, I designates the identity matrix and U is the sound amplitude column vector. The dimension of these square matrices is three for *Case 1* and four for *Cases 2* and *3*. To obtain the dispersion relations, we seek a solution of (4.5) in the form

$$U(x_1, y_1, t_1) = U_0 e^{i(\mu x_1 + \nu y_1 - \sigma t_1)} \tag{4.6}$$

where $\vec{\chi} \equiv (\mu, \nu)$ represents the horizontal modulational wavenumber vector and σ the modulational frequency of the sound envelopes. Upon substituting (4.6) into (4.5), we obtain the matrix equation

$$\big(P(\mu,\nu) + \sigma(\mu,\nu) I\big) U_0 = 0 \tag{4.7}$$

where the matrix P is defined by

$$P(\mu,\nu) = N - \left(\mu C_{g_x} + \nu C_{g_y}\right) \tag{4.8}$$

Eq. (4.7) admits non-trivial solutions provided that

$$\det\big[P(\mu,\nu) + \sigma(\mu,\nu) I\big] = 0 \tag{4.9}$$

Condition (4.9) can also be viewed as the characteristic equation associated with the matrix differential equation

$$\frac{\partial U}{\partial t_1} = iP(\mu,\nu)U \tag{4.10}$$

Solving (4.9) therefore not only provides the dispersion relation $\sigma(\mu,\nu)$, but also the eigenvalues to be used in the initial value problem considered in §5. Each of the three cases is now investigated separately.

4.2.1. *Case 1*

Since only three scattered sound waves are resonantly coupled together, the matrices introduced above will be 3×3. Matrices C_{g_x} and C_{g_y} read

$$C_{g_x} = \Lambda \begin{pmatrix} 1 & 0 & 0 \\ 0 & -\cos\theta_1 & 0 \\ 0 & 0 & -\cos\theta_2 \end{pmatrix} \qquad C_{g_y} = \Lambda \begin{pmatrix} 0 & 0 & 0 \\ 0 & -\sin\theta_1 & 0 \\ 0 & 0 & -\sin\theta_2 \end{pmatrix} \tag{4.11a-b}$$

where Λ stands for the directional cosine of the x-component of the incident sound as defined by (2.28a). Matrix N is defined by

$$N = \begin{pmatrix} 0 & \alpha_1 & \alpha_2 \\ \alpha_1 & 0 & 0 \\ \alpha_2 & 0 & 0 \end{pmatrix} \tag{4.12}$$

After substitution of (4.11) and (4.12) in (4.8) and (4.9), we obtain the following dispersion relation

$$\sigma^3 + a_2\sigma^2 + a_1\sigma + a_0 = 0 \tag{4.13}$$

with

$$a_2 = \Lambda\{(\cos\theta_1 + \cos\theta_2 - 1)\mu + (\sin\theta_1 + \sin\theta_2)\nu\} \tag{4.14a}$$

$$a_1 = -\Big[\alpha_1^2 + \alpha_2^2 + \Lambda^2\{(\cos\theta_1 + \cos\theta_2 - \cos\theta_1\cos\theta_2)\mu^2 + \\ +(\sin\theta_1 + \sin\theta_2 - \sin(\theta_1+\theta_2))\mu\nu - \sin\theta_1\sin\theta_2\nu^2\}\Big] \tag{4.14b}$$

and

$$a_0 = -\Big[\Lambda^3\{\cos\theta_1\cos\theta_2\mu^3 + \sin(\theta_1+\theta_2)\mu^2\nu + \sin\theta_1\sin\theta_2\mu\nu^2\} +$$

$$+\Lambda\left\{(\alpha_1^2\cos\theta_2+\alpha_2^2\cos\theta_1)\mu+(\alpha_1^2\sin\theta_2+\alpha_2^2\sin\theta_1)\nu\right\}\Big] \qquad (4.14c)$$

Solutions of (4.13) and $(4.14a-c)$ are found with Cardan's formulae (Korn & Korn, 1962). The discriminant is intractable analytically. However, our computations show that the three roots of (4.13) are always real. The dispersion relation therefore consists of three branches. There are two special cases where analytical expressions can be derived. First, when $\theta_1+\theta_2=0$, $\alpha_1=\alpha_2$ and $\nu=0$, the following three roots are found

$$\sigma_1=-\Lambda\mu\cos\theta_1 \qquad \sigma_{2,3}=\frac{\Lambda(1-\cos\theta_1)\mu\pm\sqrt{\Lambda^2(1+\cos\theta_1)^2\mu^2+8\alpha_1^2}}{2} \qquad (4.15a-c)$$

The first branch is a straight line, while the remaining two branches are hyperbolic. In particular, for large μ $\sigma_{2,3}$ approach the two straight lines $\sigma=\Lambda\mu$ and $\sigma=-\Lambda\mu\cos\theta_1$.

The second special case corresponds to perfect tuning *i.e.* $\mu=\nu=0$. In this case, the dispersion reduces to

$$\sigma\left\{\sigma^2-(\alpha_1^2+\alpha_2^2)\right\}=0 \qquad (4.16)$$

which immediately yields the three frequencies

$$\sigma_1=0, \quad \sigma_{2,3}=\pm\sqrt{\alpha_1^2+\alpha_2^2} \qquad (4.17a-c)$$

Therefore, the time behavior will consist of a DC component (σ_1) along with one pure tone ($\sigma_{2,3}$).

4.2.2. *Case 2*

The presence of two surface waves propagating at right angle causes four resonantly scattered sound waves. The matrices introduced in (4.5) are then 4×4 and read:

$$C_{g_x}=\Lambda\begin{pmatrix}1&0&0&0\\0&-\cos\theta_1&0&0\\0&0&\cos\theta_1&0\\0&0&0&-1\end{pmatrix} \qquad C_{g_y}=\Lambda\begin{pmatrix}0&0&0&0\\0&-\sin\theta_1&0&0\\0&0&\sin\theta_1&0\\0&0&0&0\end{pmatrix} \qquad (4.18a-b)$$

and

$$N = \begin{pmatrix} 0 & \alpha_1 & \alpha_2 & 0 \\ \alpha_1 & 0 & 0 & \alpha_2 \\ \alpha_2 & 0 & 0 & \alpha_1 \\ 0 & \alpha_2 & \alpha_1 & 0 \end{pmatrix} \tag{4.19}$$

The dispersion relation follows from (4.9)

$$\sigma^4 - b_2\sigma^2 + b_0 = 0 \tag{4.20}$$

where

$$b_2 = 2\alpha_1^2 + 2\alpha_2^2 + \Lambda^2\left[\mu^2 + (\mu\cos\theta_1 + \nu\sin\theta_1)^2\right] \tag{4.21a}$$

$$b_0 = \left[\alpha_1^2 - \alpha_2^2 + \Lambda^2\mu(\mu\cos\theta_1 + \nu\sin\theta_1)\right]^2 \tag{4.21b}$$

Dispersion relation (4.20) is in fact quadratic in σ^2. Its discriminant

$$\Delta \equiv b_2^2 - 4b_0 = \left[4\alpha_1^2 + \Lambda^2\left[\mu(1+\cos\theta_1) + \nu\sin\theta_1\right]^2\right] \times$$

$$\left[4\alpha_2^2 + \Lambda^2\left[\mu(1-\cos\theta_1) - \nu\sin\theta_1\right]^2\right] \tag{4.22}$$

is clearly positive thus ensuring the existence of two real roots for σ^2. Since the coefficients b_0 and b_2 are both positive, (4.20) admits two pairs of opposite real roots for σ (*i.e.* oscillatory behavior):

$$\sigma_{1,3}(\mu,\nu) = \pm\sqrt{\frac{b_2 + \sqrt{b_2^2 - 4b_0}}{2}} \qquad \sigma_{2,4}(\mu,\nu) = \pm\sqrt{\frac{b_2 - \sqrt{b_2^2 - 4b_0}}{2}} \tag{4.23a-b}$$

The frequencies $\{\sigma_j\}_{j=1,4}$ will be distinct except when b_0 vanishes in which case $\sigma = 0$ is a double root of (4.20). We conclude that the dispersion relation consists of two pairs of symmetric branches. In the absence of detuning *i.e.* $\mu = \nu = 0$, the frequencies are easily obtained

$$\sigma_{1,3} = \pm(\alpha_1 + \alpha_2), \qquad \sigma_{2,4} = \pm|\alpha_1 - \alpha_2| \tag{4.24}$$

4.2.3. *Case 3*

In *Case 3*, we again have four resonantly scattered sound waves. The matrices introduced in (4.5) now read

$$C_{g_x} = \Lambda \begin{pmatrix} 1 & 0 & 0 & 0 \\ 0 & -\cos\theta_1 & 0 & 0 \\ 0 & 0 & -1 & 0 \\ 0 & 0 & 0 & \cos\theta_1 \end{pmatrix} \qquad C_{g_y} = \Lambda \begin{pmatrix} 0 & 0 & 0 & 0 \\ 0 & -\sin\theta_1 & 0 & 0 \\ 0 & 0 & 0 & 0 \\ 0 & 0 & 0 & \sin\theta_1 \end{pmatrix} \tag{4.25}$$

and

$$N = \begin{pmatrix} 0 & \alpha_1 & \alpha_2 & 0 \\ \alpha_1 & 0 & 0 & 0 \\ \alpha_2 & 0 & 0 & \alpha_1 \\ 0 & 0 & \alpha_1 & 0 \end{pmatrix} \tag{4.26}$$

The corresponding dispersion relation is deduced

$$\sigma^4 - e_2\sigma^2 + e_0 = 0 \tag{4.27}$$

where

$$e_2 = 2\alpha_1^2 + \alpha_2^2 + \Lambda^2\left[\mu^2 + (\mu\cos\theta_1 + \nu\sin\theta_1)^2\right] \tag{4.28a}$$

and

$$e_0 = \Lambda^2\alpha_2^2(\mu\cos\theta_1 + \nu\sin\theta_1)^2 + \left[\alpha_1^2 + \Lambda^2\mu(\mu\cos\theta_1 + \nu\sin\theta_1)\right]^2 \tag{4.28b}$$

We again obtain a quadratic equation in σ^2. The discriminant is again evaluated numerically and is found to be positive. Moreover, the sign of e_0 and e_2 insures that the roots of (4.27 – 28) are all real. Furthermore, e_0 cannot vanish since both α_1 and α_2 are non-zero. Consequently, radian frequencies $\{\sigma_j\}_{j=1,4}$ are always distinct:

$$\sigma_{1,3}(\mu,\nu) = \pm\sqrt{\frac{e_2 + \sqrt{e_2^2 - 4e_0}}{2}} \qquad \sigma_{2,4}(\mu,\nu) = \pm\sqrt{\frac{e_2 - \sqrt{e_2^2 - 4e_0}}{2}} \tag{4.29a - b}$$

The dispersion relation of *Case 3* consists again of two pairs of symmetric branches. In the absence of detuning, equation (4.27) simplifies to

$$\sigma^4 - (2\alpha_1^2 + \alpha_2^2)\sigma^2 + \alpha_1^4 = 0 \tag{4.30}$$

and can be factorized to yield

$$\sigma_{1,3} = \pm\frac{\alpha_2 + \sqrt{\alpha_2^2 + 4\alpha_1^2}}{2} \tag{4.31a}$$

and

$$\sigma_{2,4} = \pm\frac{-\alpha_2 + \sqrt{\alpha_2^2 + 4\alpha_1^2}}{2} \qquad (4.31b)$$

4.3. Dependence of Envelope Dispersion on Surface Waves

The dispersion relation for *Cases 1*, *2* and *3* depend on four parameters; these are: the slopes ($k_{w_1}a_1$ and $k_{w_2}a_2$) and the directions (θ_1 and θ_2) of the two surface waves. We first, investigate the effect of θ_1 and θ_2 and then analyse the influence of $k_{w_1}a_1$.

In the absence of surface waves, the right hand sides of (3.18), (3.57) and (3.72) reduce to zero. The sound amplitudes are decoupled and thus non-dispersive. Their "dispersion relations" consist of straight lines listed here for completeness: $\sigma = \Lambda\mu$ and $\sigma = -\Lambda(\mu\cos\theta_{1,2} + \nu\sin\theta_{1,2})$ respectively for A, B_1 and B_2 in *Case 1*; $\pm\Lambda\mu$ for A and B_3, $\mp\Lambda(\mu\cos\theta_1 + \nu\sin\theta_1)$ for B_1 and B_2 in *Case 2* and finally in *Case 3*, $\pm\Lambda\mu$ for A and B_2 and $\mp\Lambda(\mu\cos\theta_1 + \nu\sin\theta_1)$ for B_1 and B_3. In the presence of surface waves, forcing terms will appear on the right hand side of the evolution equations. As a result, the corresponding dispersion relations will depart from the straight lines previously defined. This departure, for a given set of slopes $k_{w_1}a_1$, $k_{w_2}a_2$ and angles θ_1 and θ_2, depends on the modulational wavenumber $\vec{\chi}(\mu,\nu)$. Assuming for simplicity $\nu = 0$, we observe that the departure from the straight lines although significant for low $|\mu|$'s, becomes very small for large $|\mu|$'s. These straight lines are thus asymptotes to the dispersion branches.

Changing the values of θ_1 and (or) θ_2 clearly affects the position of the asymptote and consequently that of each dispersion branch.

Next, we analyse the influence of the surface slopes. In *Case 1*, we vary $k_{w_1}a_1$ within [0.05,0.15] while $\theta_1 = \pi/3$, $\theta_2 = -\pi/6$ and $k_{w_2}a_2 = 0.1$. Figure 4.1 shows that increasing slopes cause the dispersion branches (discontinuous lines) to depart further from their respective asymptotes (continuous lines), this is especially true for smaller $|\mu|$'s. The special case $\theta_1 = -\theta_2 = \pi/3$ is plotted in figure 4.2. Two asymptotes merge according to $(4.15a - c)$ and the corresponding dispersion branches approach each other as $|\mu|$ becomes large. The accuracy of the numerical scheme used in §5 hinges on the accurate determination of the σ's for large values

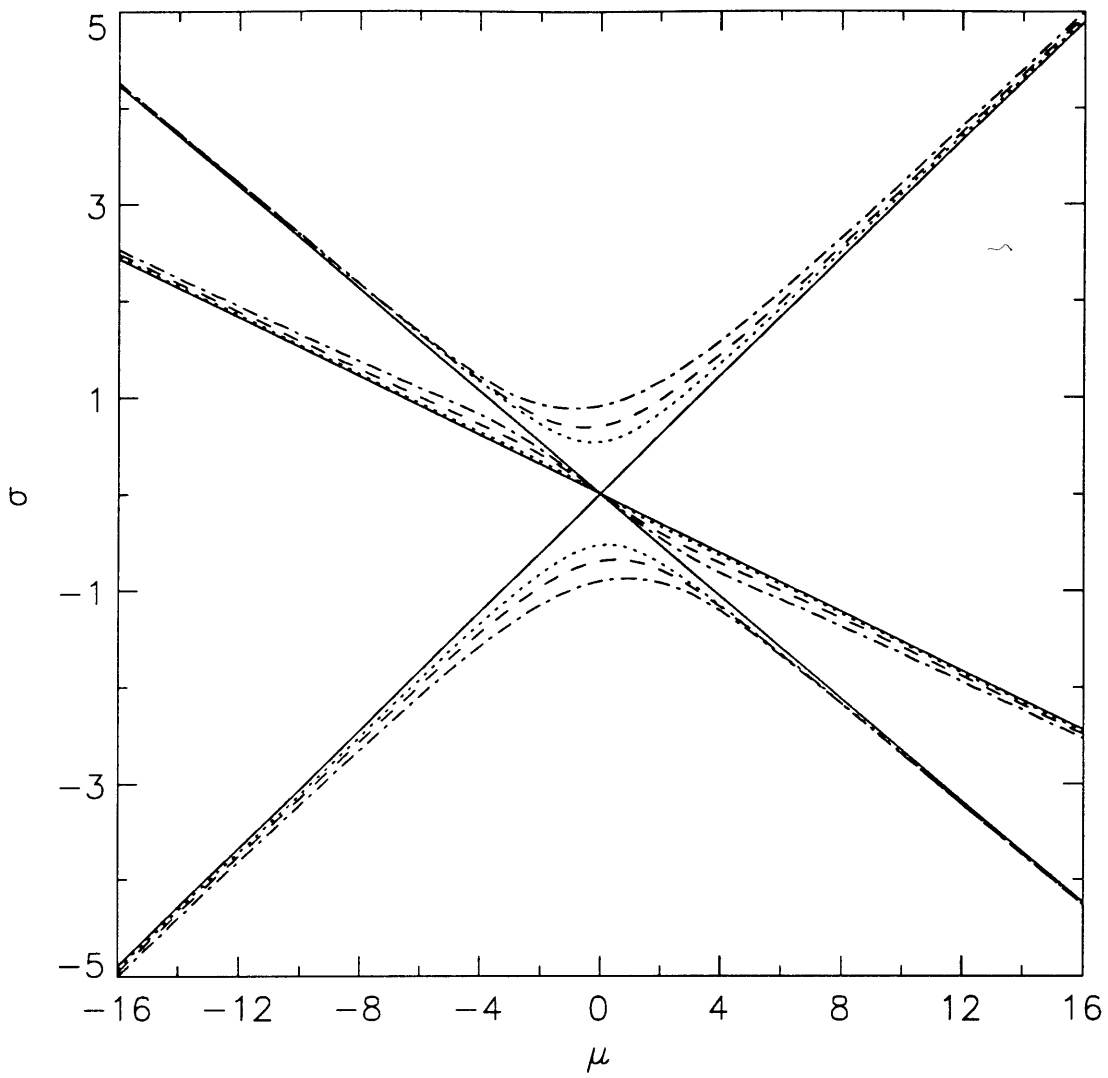

Figure 4.1: Dispersion relation for *Case 1* with $k_{w_2}a_2 = 0.1$, $\theta_1 = \pi/3$, $\theta_2 = -\pi/6$ and $k_{w_1}a_1 = 0.05$ $(\cdots\cdots)$, $k_{w_1}a_1 = 0.1$ $(- - -)$, $k_{w_1}a_1 = 0.15$ $(-\cdot-\cdot-\cdot)$.

of $|\mu|$.

Turning to *Cases 2* and *3* , we let $\theta_1 = \pi/3$. $k_{w_2}a_2 = 0.1$ while $k_{w_1}a_1$ varies within the same interval. Although the directions of scattering, *i.e.* the asymptotes, are identical in both figures 4.3 and figure 4.4, the position of the dispersion curves relative to their respective asymptotes is quite different in each case. The slopes control the departure of the dispersion branches from their asymptotes.

What are the implications of diagrams 4.1-4.4 concerning the propagation of an initial sound pulse. Consider for instance sound amplitude B_1 (the argument applies for any of the three or four sound amplitudes in *Cases 1*, *2* and *3*). Owing

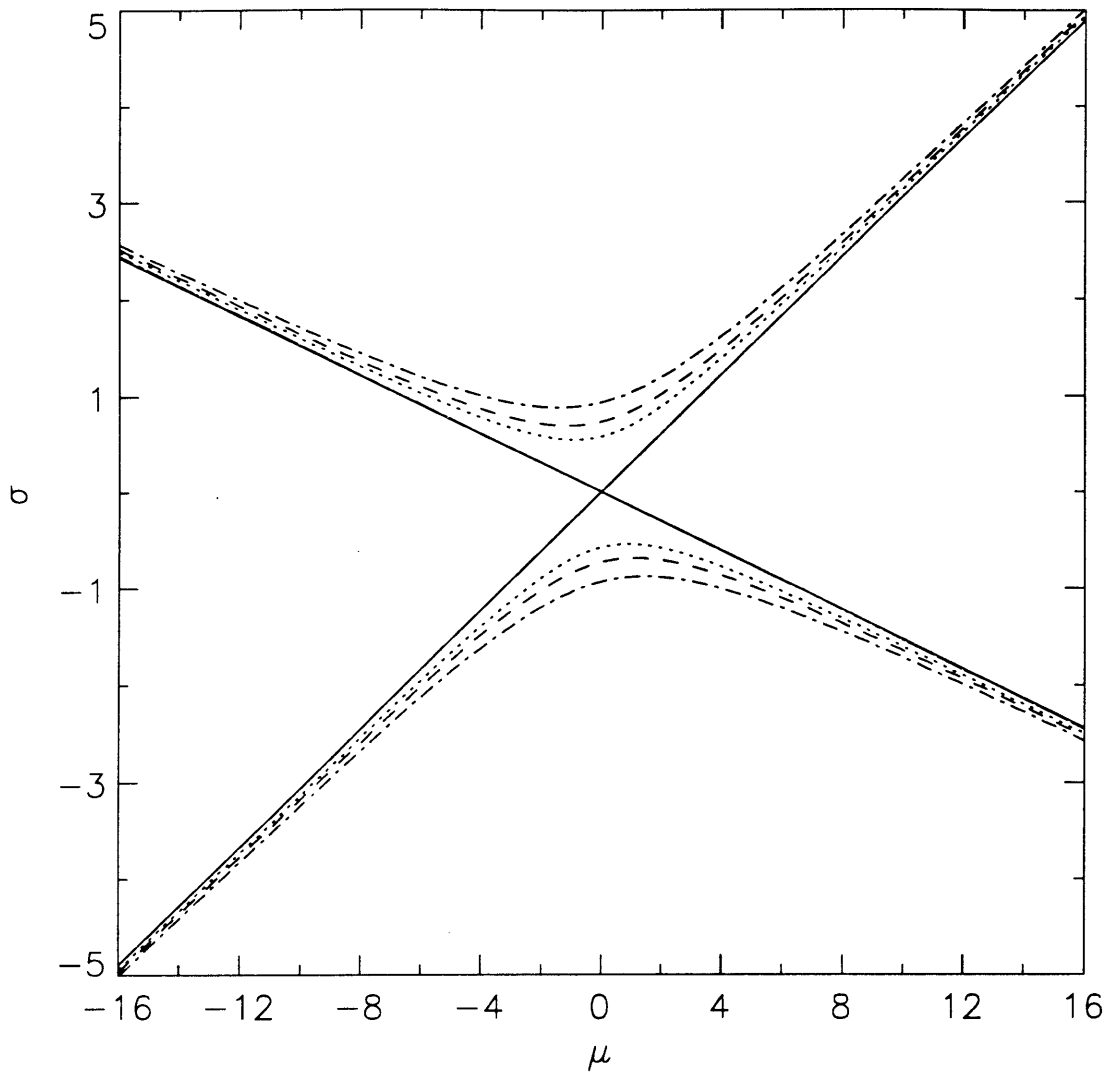

Figure 4.2: Dispersion relation for *Case 1* with $k_{w_2}a_2 = 0.1$, $\theta_1 = -\theta_2 = \pi/3$ and $k_{w_1}a_1 = 0.05$ $(\cdots\cdots)$, $k_{w_1}a_1 = 0.1$ $(- - -)$, $k_{w_1}a_1 = 0.15$ $(-\cdot-\cdot-)$.

to the linearity of (3.18), (3.57) and (3.72), it is sufficient to analyse a generic Fourier component (μ, ν). Through the coupling of the surface waves, this Fourier component will be expressed as linear combination of three or four eigenmodes corresponding to the solutions of the dispersion relation. From figure 4.1, it is clear that three directions of propagation appear for a given μ. By Fourier synthesis, we conclude that the envelope B_1 of a left-going sound wave (defined by (3.5*a*)) may propagate in as many as three directions in *Case 1* and four directions in *Cases 2* and *3*. Once again, we emphasize that the carrier wave and its envelope propagate in radically different directions.

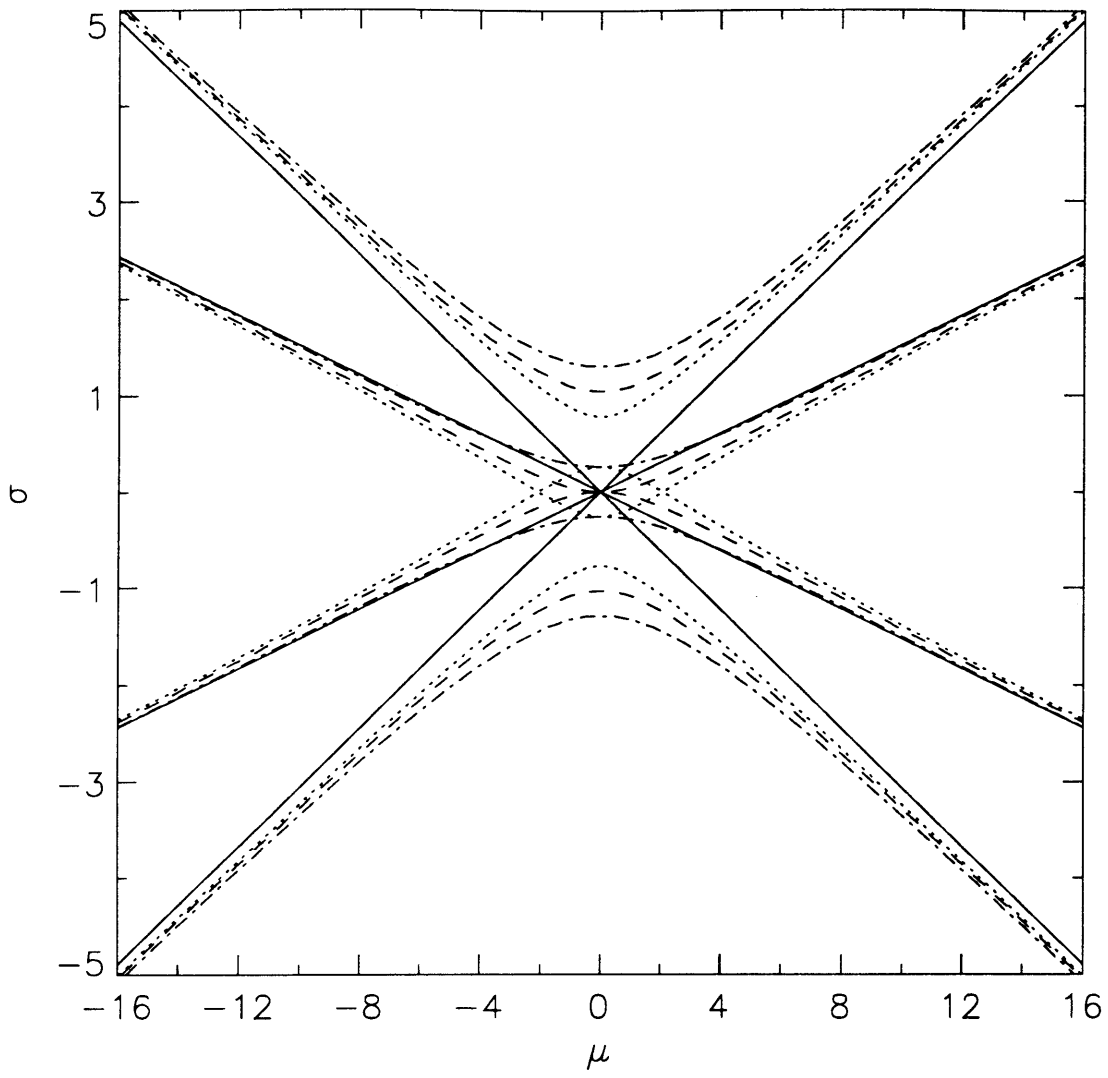

Figure 4.3: Dispersion relation for *Case 2* with $k_{w_2}a_2 = 0.1$, $\theta_1 = \pi/3$ and $k_{w_1}a_1 = 0.05$ $(\cdots\cdots)$, $k_{w_1}a_1 = 0.1$ $(---)$, $k_{w_1}a_1 = 0.15$ $(-\cdot-\cdot-\cdot)$.

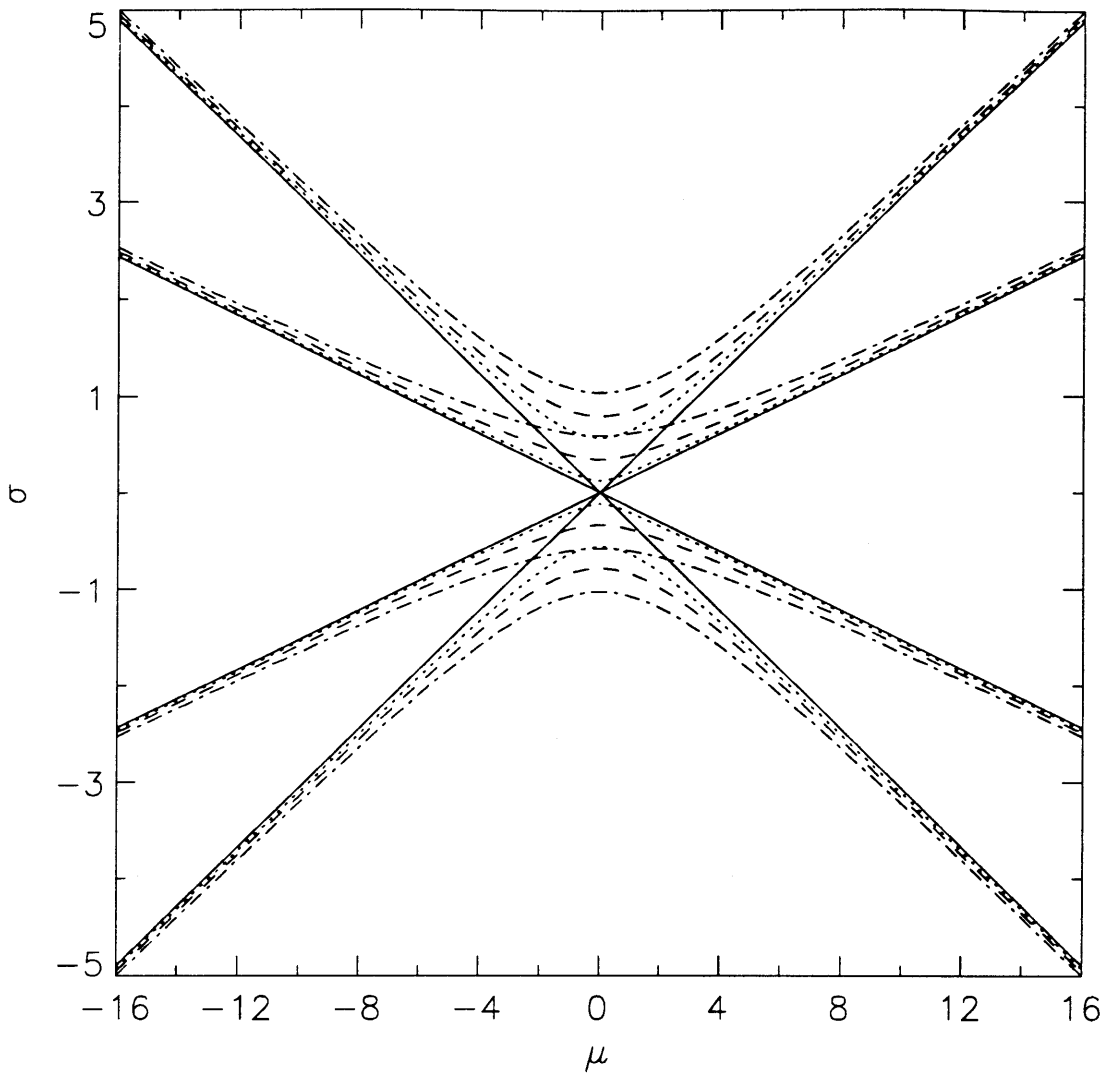

Figure 4.4: Dispersion relation for *Case 3* with $k_{w_2}a_2 = 0.1$, $\theta_1 = \pi/3$ and $k_{w_1}a_1 = 0.05$ $(\cdots\cdots)$, $k_{w_1}a_1 = 0.1$ $(- - -)$, $k_{w_1}a_1 = 0.15$ $(-\cdot-\cdot-\cdot)$.

5. ACOUSTIC FIELD OF A SOUND SOURCE IN THE PRESENCE OF TWO UNIFORM SURFACE WAVES

5.1. Description of the Problem

In §3, asymptotic equations were derived for the resonant scattering of a right going plane sound wave by two arbitrary surface waves. To generate such an incident plane sound wave, the acoustic field of a line source of infinite extent in the transverse direction is considered. Jump conditions are deduced for the sound envelopes across the discontinuity.

By virtue of linearity, it is possible to decompose the scattering problem into a "+" problem and a "-" problem corresponding to the outgoing sound wave component propagating respectively in the positive or negative x-directions. Since the "+" and "-" problems are mirror images of each other, we need only solve the former problem.

5.2. Near Field of a Slightly Oblique Line Source

A line source of infinite extent in the y-direction, is located at $(x, z) = (0, z_0)$. Its slowly varying envelope is in the form of a pulse (see (2.82)):

$$f(t_1) = \begin{cases} \sin^2\left(\frac{\pi}{2}t_1\right) & \text{if } 0 \le t_1 \le 2 \\ 0 & \text{if } t_1 > 2 \end{cases} \tag{5.1}$$

Note that f is C^1 on $[0, \infty[$. For a shallow enough waveguide † and large enough range ‡, the acoustic field of the line source consists of only one propagating mode and is well approximated by

$$\Psi_0(x, z, t_1) \approx i\, f(t_1) \cos\sqrt{k^2 - \xi_0^2}(z + h) e^{i\xi_0|x|} e^{-i\omega t} + (*) \quad \forall x \tag{5.2}$$

Assuming that the line array forms a small angle, $\epsilon\frac{\nu}{\xi_0}$, counterclockwise with the y-axis (cf. figure 5.1), the phase function of the right going wave becomes $S =$

† Provided the normalized water depth satisfies $\frac{\pi}{2} \le kh \le \frac{3\pi}{2}$, the waveguide sustains only one propagative mode.

‡ For ranges $kx = \mathcal{O}(1)$, the influence of the acoustic evanescent modes is negligible.

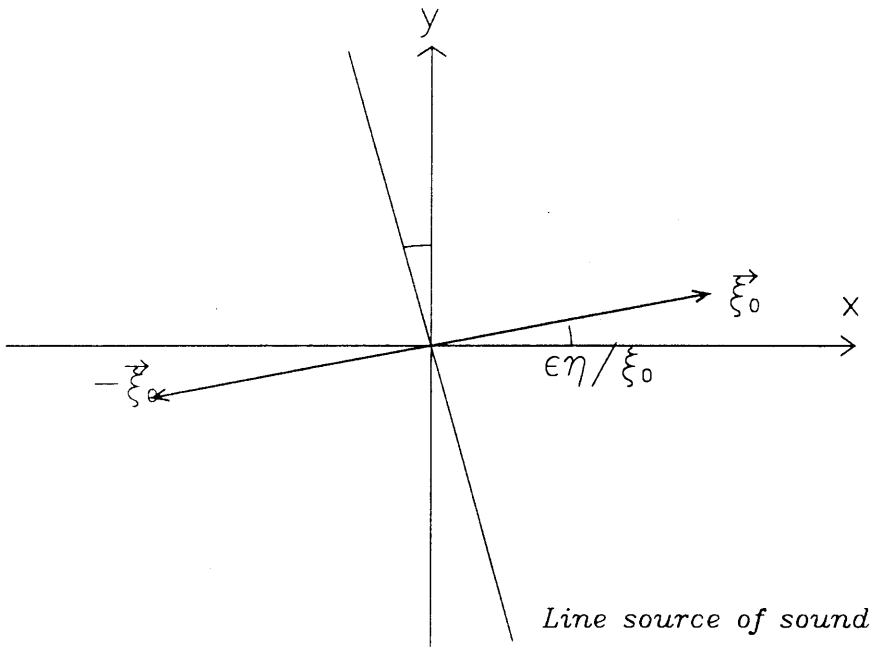

Figure 5.1: Geometry of slightly inclined line source.

$\xi_0 x + \epsilon\nu y - \omega t$. This phase function may alternately be written as $S = \xi_0 x - \omega t + \nu y_1$, thus corresponding to a sound wave propagating in the positive x-direction with an amplitude slowly varying in the transverse direction according to $e^{i\nu y_1}$. Similarly, the amplitude of the left going wave is modulated by $e^{-i\nu y_1}$. In summary, the potential Ψ_0 becomes:

$$\Psi_0(x, z, y_1, t_1) = i\ f(t_1) e^{i\ \mathrm{sign}(x)\nu y_1} \cos\sqrt{k^2 - \xi_0^2}(z+h) e^{i\xi_0|x|} e^{-i\omega t} + (*) \quad \forall x \quad (5.3)$$

The left and right going sound waves are both discontinuous at $x = 0$.

5.3. Asymptotic Matching of the Near and Far Fields

In order to account for the line source in the evolution equations of sound amplitudes, the inner approximation ($x_1 = \mathcal{O}(\epsilon)$) of the far field Φ_0 will be matched with the outer approximation ($x = \mathcal{O}(1)$) of the near field Ψ_0. The three cases are now treated separately.

5.3.1. *Case 1*

In *Case 1*, each of the two outgoing plane waves ($\pm\vec{\xi}_0$) yields its own set of two scattering directions ($\vec{k}^{\pm}_{1,2}$). In total, the acoustic field consists of six distinct sound waves whose directions are easily deduced once the surface waves are specified, see

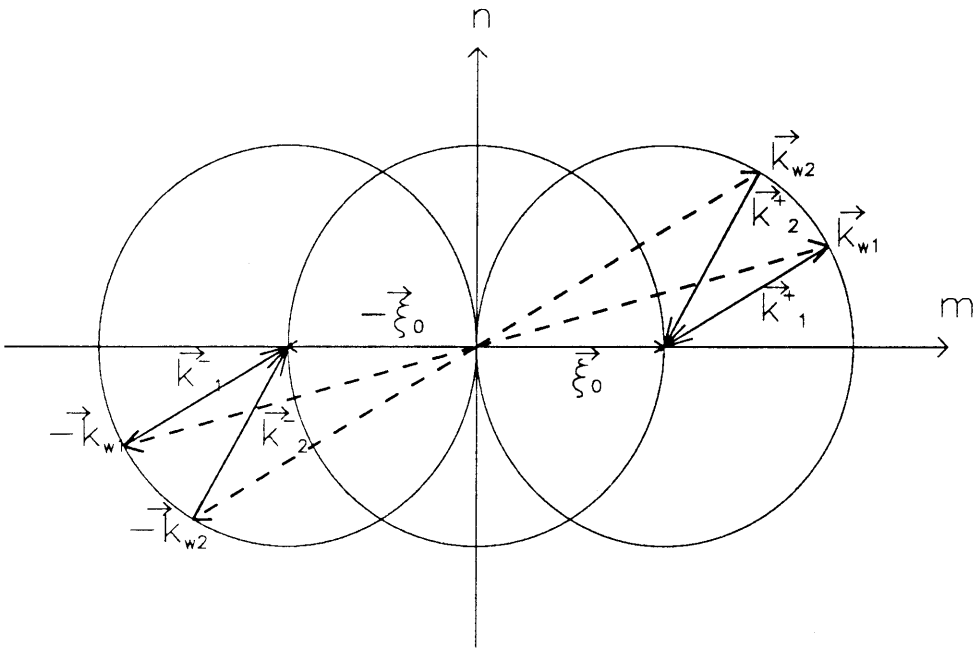

Figure 5.2: Scattering geometry for *Case 1* in the presence of two outgoing plane sound waves.

figure 5.2.

By a straightforward asymptotic matching, the discontinuity of the forward scattered sound wave A^+ accross $x_1 = 0$ is found to be

$$A^+(x_1 = 0^+, y_1, t_1) - A^+(x_1 = 0^-, y_1, t_1) = if(t_1)e^{i\nu y_1} \qquad (5.4a)$$

Similarly, we obtain

$$\left[B^+_{1,2}\right]^{0^+}_{0^-} = 0 \qquad (5.4b-c)$$

Away from the source, *i.e.* for $x_1 \neq 0$, the amplitudes A^+ and $B^+_{1,2}$ are governed by

$$\frac{\partial A^+}{\partial t_1} + \Lambda \frac{\partial A^+}{\partial x_1} = i\alpha_1 B^+_1 + i\alpha_2 B^+_2 \qquad (5.5a)$$

$$\frac{\partial B^+_{1,2}}{\partial t_1} - \Lambda \cos\theta_{1,2} \frac{\partial B^+_{1,2}}{\partial x_1} - \Lambda \sin\theta_{1,2} \frac{\partial B^+_{1,2}}{\partial y_1} = i\alpha_{1,2} A^+ \qquad (5.5b-c)$$

Taking the difference of $(5.5a)$ on both sides of the source and using $(5.4a-c)$, we obtain

$$\left[\frac{\partial A^+}{\partial x_1}\right]^{0^+}_{0^-} = -\frac{i}{\Lambda}\frac{df}{dt_1} e^{i\nu y_1} \qquad (5.6a)$$

Similarly, by taking the difference of $(5.5b-c)$ on both sides of the source, we obtain

$$\left[\frac{\partial B^+_{1,2}}{\partial x_1}\right]^{0^+}_{0^-} = \frac{\alpha_{1,2}}{\Lambda \cos\theta_{1,2}} f(t_1) e^{i\nu y_1} \qquad (5.6b-c)$$

As observed in figure 5.2, the scattered sound waves of the "-" problem propagate in directions opposite to those in the "+" problem. This implies that

$$A^-(x_1,y_1,t_1) = A^+(-x_1,-y_1,t_1) \qquad B^-_{1,2}(x_1,y_1,t_1) = B^+_{1,2}(-x_1,-y_1,t_1) \quad (5.7)$$

After solving for $A^\pm$ and $B^\pm_{1,2}$, the acoustic far field due to the line source radiating equally in both directions is then described by the following velocity potential

$$\begin{aligned}\Phi_0(x,y,z,x_1,y_1,t_1) = \big\{ & A^+ e^{i\xi_0 x} + A^- e^{-i\xi_0 x} + B^+_1 e^{i(\xi_0-m_1)x-in_1 y} \quad + \\ & + \quad B^-_1 e^{-i(\xi_0-m_1)x+in_1 y} + B^+_2 e^{i(\xi_0-m_2)x-in_2 y} \quad + \\ & + \quad B^-_2 e^{-i(\xi_0-m_2)x+in_2 y}\big\} e^{-i\omega t} \cos\sqrt{k^2-\xi_0^2}(z+h) + (*) \end{aligned} \quad (5.8)$$

where all six sound amplitudes are functions of x_1, y_1 and t_1. In summary (5.4a) and (5.6a) are two boundary conditions for A^+ while (5.4b,c) and (5.6b,c) are two boundary conditions for $B^+_{1,2}$.

5.3.2. *Case 2*

In *Case 2*, the right going plane wave in (5.3) yields two pairs of scattered sound waves propagating in opposite directions. Likewise, the left going wave is scattered, as seen in figure 5.3, in the same pairs of directions. In summary, the acoustic field of the line source is scattered in four directions only. By a straightforward asymptotic matching, we deduce the jumps in the sound amplitudes

$$\left[A^+\right]^{0^+}_{0^-} = if(t_1)\frac{\sin\sqrt{k^2-\xi_0^2}z_0}{\xi_0 h}e^{i\nu y_1} \qquad \left[B^+_j\right]^{0^+}_{0^-} = 0 \quad j=1,3 \qquad (5.9a-d)$$

Away from the the line source, the governing equations for A^+ and $B^+_{1,2,3}$ are simply

$$\frac{\partial A^+}{\partial t_1} + \Lambda\frac{\partial A^+}{\partial x_1} = i\alpha_1 B^+_1 + i\alpha_2 B^+_2 \qquad (5.10a)$$

$$\frac{\partial B^+_1}{\partial t_1} - \Lambda\cos\theta_1\frac{\partial B^+_1}{\partial x_1} - \Lambda\sin\theta_1\frac{\partial B^+_1}{\partial y_1} = i\alpha_1 A^+ + i\alpha_2 B^+_3 \qquad (5.10b)$$

$$\frac{\partial B^+_2}{\partial t_1} + \Lambda\cos\theta_1\frac{\partial B^+_2}{\partial x_1} + \Lambda\sin\theta_1\frac{\partial B^+_2}{\partial y_1} = i\alpha_2 A^+ + i\alpha_1 B^+_3 \qquad (5.10c)$$

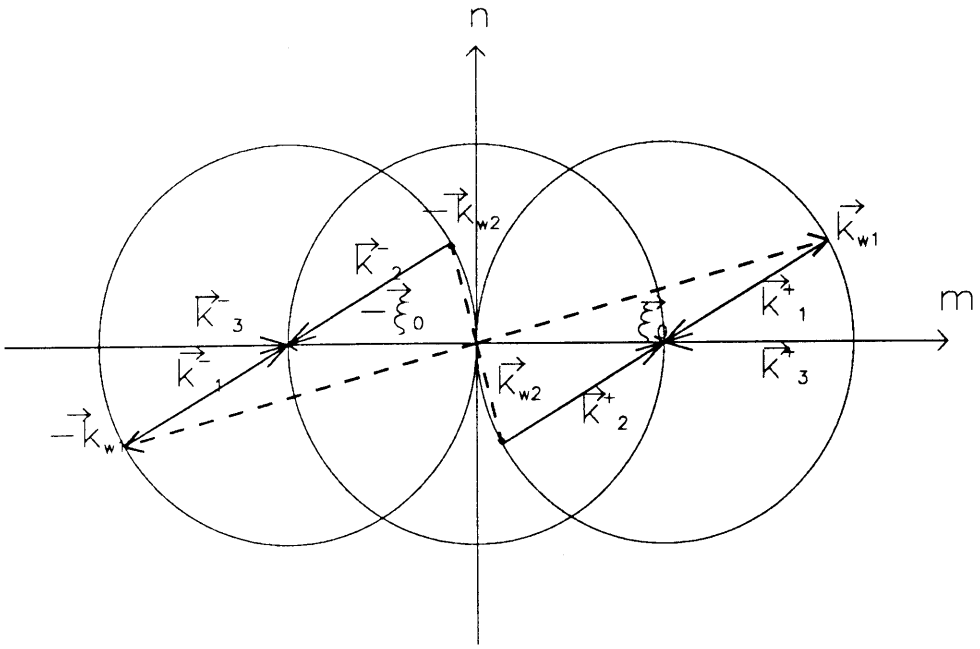

Figure 5.3: Scattering geometry for *Case 2* in the presence of two outgoing plane sound waves.

$$\frac{\partial B_3^+}{\partial t_1} - \Lambda \frac{\partial B_3^+}{\partial x_1} = i\alpha_1 B_2^+ + i\alpha_2 B_1^+ \qquad (5.10d)$$

Upon subtracting from $(5.10a)$ at $x_1 = 0^+$ eq. $(5.10a)$ at $x_1 = 0^-$, we deduce the jump in the gradient of A^+

$$\left[\frac{\partial A}{\partial x_1}\right]_{0^-}^{0^+} = -\frac{i}{\Lambda}\frac{df}{dt_1} e^{i\nu y_1} \qquad (5.11a)$$

Likewise, we obtain for the remaining three amplitudes

$$\left[\frac{\partial B_{1,2}^+}{\partial x_1}\right]_{0^-}^{0^+} = \frac{\alpha_{1,2}}{\Lambda \cos\theta_{1,2}} f(t_1) e^{i\nu y_1} \qquad \left[\frac{\partial B_3^+}{\partial x_1}\right]_{0^-}^{0^+} = 0 \qquad (5.11b-d)$$

Turning to the solution of the "-" problem, the symmetry in figure 5.3 implies the following relationships

$$A^-(x_1, y_1, t_1) = A^+(-x_1, -y_1, t_1) \qquad B_j^-(x_1, y_1, t_1) = B_j^+(-x_1, -y_1, t_1) \quad j = 1, 3 \qquad (5.12)$$

The scattered acoustic field is therefore described by

$$\Phi_0(x, y, z, t, x_1, y_1, t_1) = \left\{ A e^{i\xi_0 x} + B_1 e^{i(\xi_0 - m_1)x - in_1 y} + B_2 e^{i(\xi_0 - m_2)x - in_2 y} + \right.$$

$$\left. + \quad B_3 e^{-i\xi_0 x} \right\} e^{-i\omega t} \cos\sqrt{k^2 - \xi_0^2}(z + h) + \text{c.c.} \qquad (5.13)$$

where A and the B_j's may be deduced $\forall x_1, y_1, t_1$ from figure 5.3

$$\begin{cases} A = A^+ + B_3^- \\ B_1 = B_1^+ + B_2^- \\ B_2 = B_2^+ + B_1^- \\ B_3 = B_3^+ + A^- \end{cases} \tag{5.14}$$

i.e. after recalling (5.12)

$$\begin{cases} A(x_1, y_1) = A^+(x_1, y_1) + B_3^+(-x_1, -y_1) \\ B_1(x_1, y_1) = B_1^+(x_1, y_1) + B_2^+(-x_1, -y_1) \\ B_2(x_1, y_1) = B_2^+(x_1, y_1) + B_1^+(-x_1, -y_1) \\ B_3(x_1, y_1) = B_3^+(x_1, y_1) + A^+(-x_1, -y_1) \end{cases} \tag{5.15}$$

Note that the amplitudes in (5.15) are defined here in terms of the solution to the "+" problem only. The scattered acoustic field in the presence of the sound is now entirely specified by (5.13) and (5.15). In summary (5.9a) and (5.11a) are the boundary conditions for A^+ while (5.9$b-d$) and (5.11$b-d$) are the boundary conditions for $B_{1,2,3}^+$.

5.3.3. *Case 3*

In *Case 3*, the two outgoing sound waves in (5.3) yield the same sets of opposite scattering directions as observed in figure 5.4. By matching with the near field, the discontinuities in the sound amplitudes of the "+" problem are found to be the same as those for *Case 2*, *i.e.* given by (5.9). The evolution equations satisfied by A^+ and $B_{1,2,3}^+$ away from the source are

$$\frac{\partial A^+}{\partial t_1} + \Lambda \frac{\partial A^+}{\partial x_1} = i\alpha_1 B_1^+ + i\alpha_2 B_2^+ \tag{5.16a}$$

$$\frac{\partial B_1^+}{\partial t_1} - \Lambda \cos\theta_1 \frac{\partial B_1^+}{\partial x_1} - \Lambda \sin\theta_1 \frac{\partial B_1^+}{\partial y_1} = i\alpha_1 A^+ \tag{5.16b}$$

$$\frac{\partial B_2^+}{\partial t_1} - \Lambda \frac{\partial B_2^+}{\partial x_1} = i\alpha_2 A^+ + i\alpha_1 B_3^+ \tag{5.16c}$$

$$\frac{\partial B_3^+}{\partial t_1} + \Lambda \cos\theta_1 \frac{\partial B_3^+}{\partial x_1} + \Lambda \sin\theta_1 \frac{\partial B_3^+}{\partial y_1} = i\alpha_1 B_2^+ \tag{5.16d}$$

The jumps in the x_1 derivatives are deduced from (5.9$a-d$) and (5.16$a-d$)

$$\left[\frac{\partial A^+}{\partial x_1}\right]_{0^-}^{0^+} = \frac{i}{\Lambda}\frac{df}{dt_1} e^{i\nu y_1} \tag{5.17a}$$

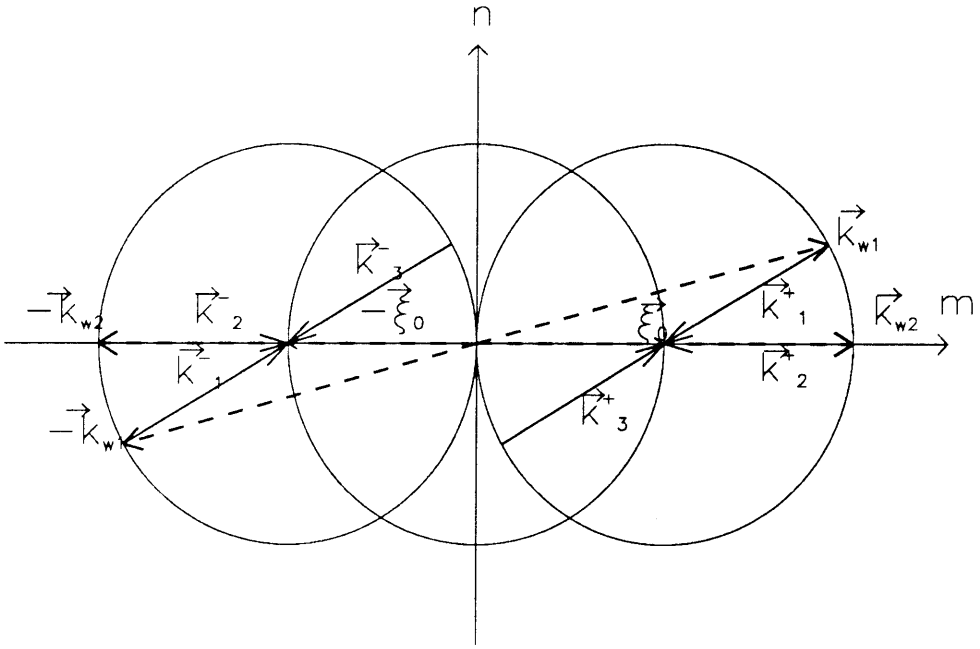

Figure 5.4: Scattering geometry for *Case 3* in the presence of two outgoing plane sound waves.

$$\left[\frac{\partial B_1^+}{\partial x_1}\right]_{0-}^{0+} = \frac{\alpha_1}{\Lambda \cos\theta_1} f(t_1) e^{i\nu y_1} \tag{5.17b}$$

and

$$\left[\frac{\partial B_2^+}{\partial x_1}\right]_{0-}^{0+} = \frac{\alpha_2}{\Lambda} f(t_1) e^{i\nu y_1} \tag{5.17c}$$

and

$$\left[\frac{\partial B_3^+}{\partial x_1}\right]_{0-}^{0+} = 0 \tag{5.17d}$$

The scattered acoustic far field is described by

$$\Phi_0(x,y,z,t,x_1,y_1,t_1) = \left\{ A e^{i\xi_0 x} + B_1 e^{i(\xi_0 - m_1)x - i n_1 y} \quad + \right.$$

$$\left. + \quad B_2 e^{-i\xi_0 x} + B_3 e^{-i(\xi_0 - m_1)x + i n_1 y} \right\} e^{-i\omega t} \cos\sqrt{k^2 - \xi_0^2}(z+h) + (*) \tag{5.18}$$

where A and the B_j's are obtained by superposition in agreement with figure 5.4

$$\begin{cases} A = A^+ + B_2^- \\ B_1 = B_1^+ + B_3^- \\ B_2 = B_2^+ + A^- \\ B_3 = B_3^+ + B_1^- \end{cases} \qquad \forall x_1, y_1, t_1 \tag{5.19}$$

Upon making use of (5.12), one obtains for all times t_1:

$$\begin{cases} A(x_1,y_1) = A^+(x_1,y_1) + B_2^+(-x_1,-y_1) \\ B_1(x_1,y_1) = B_1^+(x_1,y_1) + B_3^+(-x_1,-y_1) \\ B_2(x_1,y_1) = B_2^+(x_1,y_1) + A^+(-x_1,-y_1) \\ B_3(x_1,y_1) = B_3^+(x_1,y_1) + B_1^+(-x_1,-y_1) \end{cases} . \tag{5.20}$$

Again the combined amplitudes are expressed in terms of the amplitudes of the "+" problem only. The acoustic field due to the line source is characterized by (5.18) and (5.20). In summary (5.9a) and (5.17a) are the boundary conditions for A^+ while (5.9$b-d$) and (5.17$b-d$) are the boundary conditions for $B^+_{1,2,3}$.

5.4 Numerical Solution for the Far Field

We need only solve the "+" problem, for the "-" problem is easily deduced afterwards by symmetry. Since the coefficients of the governing equations are independent of x_1, a Fourier method, whereby each Fourier component satisfies a matrix ordinary differential equation, may be used. We thus solve an eigen problem for each Fourier mode. In contrast with the situation described in §2, the characteristic polynomial is cubic in *Case 1* and quartic otherwise. As a result, the eigenvalues and thus the inverse Fourier transform cannot be evaluated analytically. A discrete Fourier transform method must be used instead. For brevity, we replace x_1, y_1 and t_1 by x, y and t.

It is convenient to separate the problem into the initial phase during which the source is operating and the steady phase after the source has been turned off. Given our definition (5.1) of $f(t)$, the initial phase lasts for time $t = 2$. We recall that the slight steering of the line array results in an $e^{i\nu y_1}$ dependence of all sound amplitudes. We may therefore let

$$\begin{pmatrix} A \\ B_1 \\ \vdots \\ B_l \end{pmatrix}(x,y,t) = U(x,t)e^{i\nu y} \tag{5.21}$$

where $l = 2$ for *Case 1* and 3 for *Cases 2* and *3* and U is a column vector with $l+1$ components.

5.4.1. *Numerical solution for small times*

Let us divide the (x-y) space into two half planes and solve *simultaneously* a '<' left-plane problem ($U^<$ is defined in the left hand half-plane $x < 0$) and a '>' right plane problem ($U^>$ is defined in the right hand half-plane $x > 0$). The two problems

are coupled together through the jump conditions derived earlier at x=0. Consider a spatial domain $[-L, L]$ large enough to contain the fronts of all sound amplitudes for $t \in [0, 2]$. We discretize this domain in $2N$ grid points at intervals of $\Delta x = \frac{L}{N}$. We shall seek a solution at discrete times $t = n\Delta t$. Under the previous assumptions, the governing equations for the $\overset{>}{<}$ problems are summarized, in a matrix form, by

$$\{I\frac{\partial}{\partial t} + C_{g_x}\frac{\partial}{\partial x} + i\nu C_{g_y} - iN\}U^{\overset{>}{<}} = 0 \tag{5.22}$$

where again C_{g_x}, C_{g_y} and N are the square matrices defined in §4 for *Cases 1,2* and *3*. The spatial derivative operator is discretized by a second order accurate centered difference approximation, and the marching in time done with the 3^{rd} order Adams-Bashforth scheme. The discretized version of (5.22) thus reads

$$\begin{aligned} U^{\overset{>}{<}}_{n+1,j} = U^{\overset{>}{<}}_{n,j} + \Delta t\Big[\frac{23}{12}\{\mp C_{g_x}\frac{U^{\overset{>}{<}}_{n,j+1} - U^{\overset{>}{<}}_{n,j-1}}{2\Delta x} - i\nu\, C_{g_y}U^{\overset{>}{<}}_{n,j} + iNU^{\overset{>}{<}}_{n,j}\} \quad + \\ - \quad \frac{16}{12}\{\mp C_{g_x}\frac{U^{\overset{>}{<}}_{n-1,j+1} - U^{\overset{>}{<}}_{n-1,j-1}}{2\Delta x} - i\nu\, C_{g_y}U^{\overset{>}{<}}_{n-1,j} + iNU^{\overset{>}{<}}_{n-1,j}\} + \\ + \quad \frac{5}{12}\{\mp C_{g_x}\frac{U^{\overset{>}{<}}_{n-2,j+1} - U^{\overset{>}{<}}_{n-2,j-1}}{2\Delta x} - i\nu\, C_{g_y}U^{\overset{>}{<}}_{n-2,j} + iNU^{\overset{>}{<}}_{n-2,j}\}\Big] \\ \forall n \geq 2 \quad \forall j \in [1, N-1] \end{aligned} \tag{5.23}$$

where

$$U^{\overset{>}{<}}_{n,j} = U^{\overset{>}{<}}(x = \pm j\Delta x, t = n\Delta t) \qquad \forall n \geq 0 \quad \forall j \in [0, n] \tag{5.24}$$

Also define for later use

$$f_n = f(t = n\Delta t) \qquad \frac{df}{dt}_n = \frac{df}{dt}(t = n\Delta t) \qquad \forall n \geq 0 \tag{5.25}$$

Eq. (5 23) implicitly assumes the knowledge of three steps. Since the source is still turned off at $t = 0$, the initial data is simply

$$U^{\overset{>}{<}}_{0,j} = 0 \qquad \forall j = 0, \ldots, N \tag{5.26}$$

The second time step is obtained with the Euler-Forward scheme:

$$U^{\overset{>}{<}}_{1,j} = U^{\overset{>}{<}}_{0,j} + \Delta t\left[\mp C_{g_x}\frac{U^{\overset{>}{<}}_{0,j+1} - U^{\overset{>}{<}}_{0,j-1}}{2\Delta x} - i\nu\, C_{g_y}U^{\overset{>}{<}}_{0,j} + iNU^{\overset{>}{<}}_{0,j}\right] \tag{5.27}$$

and the third step using the 2^{nd} order Adams-Bashforth scheme:

$$U^{\gtrless}_{2,j} = U^{\gtrless}_{1,j} + \Delta t \left[\frac{3}{2}\{\mp C_{g_x}\frac{U^{\gtrless}_{1,j+1} - U^{\gtrless}_{1,j-1}}{2\Delta x} - i\nu\, C_{g_y} U^{\gtrless}_{1,j} + iNU^{\gtrless}_{1,j}\} \quad + \right.$$

$$\left. - \quad \frac{1}{2}\{\mp C_{g_x}\frac{U^{\gtrless}_{0,j+1} - U^{\gtrless}_{0,j-1}}{2\Delta x} - i\nu\, C_{g_y} U^{\gtrless}_{0,j} + iNU^{\gtrless}_{0,j}\}\right] \tag{5.28}$$

We specify the boundary condition at $\pm L$ by

$$U^{\gtrless}_{n,N} = 0 \qquad \forall n \tag{5.29}$$

In order to determine $U^{\gtrless}_{n,0}$, we use the jump conditions derived earlier for the sound amplitudes and their x-derivatives accross x=0. Each case is considered separately.

5.4.1.1. Derivation of $U^{\gtrless}_{n,0}$ in *Case 1*

Let $U^{\gtrless}_{n,j}$ be defined by

$$U^{\gtrless}_{n,j} = \left[\mathcal{A}^{\gtrless}_{n,j}, \mathcal{B}_1{}^{\gtrless}_{n,j}, \mathcal{B}_2{}^{\gtrless}_{n,j}\right]^{\mathrm{T}} \tag{5.30}$$

The discontinuity (5.8a) is discretized by

$$\mathcal{A}^{>}_{n,0} - \mathcal{A}^{<}_{n,0} = i\, f_n \tag{5.31a}$$

and the continuity of $B_{1,2}$ respectively translates into

$$\mathcal{B}_1{}^{>}_{n,0} = \mathcal{B}_1{}^{<}_{n,0} \qquad \mathcal{B}_2{}^{>}_{n,0} = \mathcal{B}_2{}^{<}_{n,0} \tag{5.31$b-c$}$$

From (5.31$a-c$), we obtain three equations for six unknowns. The additional three equations are obtained from the discretization of (5.6$a-c$) with a one sided second order finite difference approximation of the x-derivative. In particular, (5.6a) yields

$$\frac{-3\mathcal{A}^{>}_{n,0} + 4\mathcal{A}^{>}_{n,1} - \mathcal{A}^{>}_{n,2}}{2\Delta x} - \frac{3\mathcal{A}^{<}_{n,0} - 4\mathcal{A}^{<}_{n,1} + \mathcal{A}^{<}_{n,2}}{2\Delta x} = -\frac{i}{\Lambda}\frac{df}{dt}_n \tag{5.32a}$$

Note that (5.32a) involves $\mathcal{A}^{\gtrless}_{n,1}$ and $\mathcal{A}^{\gtrless}_{n,2}$, these are first evaluated from (5.23). Combining then (5.31a) with (5.32a), we obtain $\mathcal{A}^{\gtrless}_{n,0}$. Similarly, discretization of (5.6$b-c$) yields

$$\frac{-3\mathcal{B}_{1,2}{}^{>}_{n,0} + 4\mathcal{B}_{1,2}{}^{>}_{n,1} - \mathcal{B}_{1,2}{}^{>}_{n,2}}{2\Delta x} - \frac{3\mathcal{B}_{1,2}{}^{<}_{n,0} - 4\mathcal{B}_{1,2}{}^{<}_{n,1} + \mathcal{B}_{1,2}{}^{<}_{n,2}}{2\Delta x} = \frac{\alpha_{1,2}}{\Lambda\cos\theta_{1,2}} f_n \tag{5.32$b-c$}$$

Combining $(5.31b-c)$ and $(5.32b-c)$, we may solve for $\mathcal{B}_{1,2}{}^{>}_{<}{}_{n,0}$.

5.4.1.2. Derivation of $U^{>}_{<}{}_{n,0}$ in *Case 2*

In *Case 2*, $U^{>}_{<}{}_{n,j}$ refers to

$$U^{>}_{<}{}_{n,j} = \left[\mathcal{A}^{>}_{<}{}_{n,j}\ ,\ \mathcal{B}_1{}^{>}_{<}{}_{n,j}, \mathcal{B}_2{}^{>}_{<}{}_{n,j}\ ,\ \mathcal{B}_3{}^{>}_{<}{}_{n,j}\right]^{\mathrm{T}} \tag{5.33}$$

and the discontinuity $(5.16a)$ is discretized straightforwardly

$$\mathcal{A}^{>}_{n,0} - \mathcal{A}^{<}_{n,0} = i\ f_n \tag{5.34a}$$

while the continuity of $B_{1,2,3}$ accross $x = 0$ yields

$$\mathcal{B}_1{}^{>}_{n,0} = \mathcal{B}_1{}^{<}_{n,0} \qquad \mathcal{B}_2{}^{>}_{n,0} = \mathcal{B}_2{}^{<}_{n,0} \qquad \mathcal{B}_3{}^{>}_{n,0} = \mathcal{B}_3{}^{<}_{n,0} \tag{5.34b-d}$$

Four additional equations are obtained by discretizing $(5.11a-d)$ with a one sided second order finite difference approximation of the x-derivative:

$$\frac{-3\mathcal{A}^{>}_{n,0} + 4\mathcal{A}^{>}_{n,1} - \mathcal{A}^{>}_{n,2}}{2\Delta x} - \frac{3\mathcal{A}^{<}_{n,0} - 4\mathcal{A}^{<}_{n,1} + \mathcal{A}^{<}_{n,2}}{2\Delta x} = -\frac{i}{\Lambda}\frac{df}{dt}_n \tag{5.35a}$$

$$\frac{-3\mathcal{B}_{1,2}{}^{>}_{n,0} + 4\mathcal{B}_{1,2}{}^{>}_{n,1} - \mathcal{B}_{1,2}{}^{>}_{n,2}}{2\Delta x} - \frac{3\mathcal{B}_{1,2}{}^{<}_{n,0} - 4\mathcal{B}_{1,2}{}^{<}_{n,1} + \mathcal{B}_{1,2}{}^{<}_{n,2}}{2\Delta x} = \frac{\alpha_{1,2}}{\Lambda\cos\theta_{1,2}} f_n \tag{5.35b-c}$$

and

$$\frac{-3\mathcal{B}_3{}^{>}_{n,0} + 4\mathcal{B}_3{}^{>}_{n,1} - \mathcal{B}_3{}^{>}_{n,2}}{2\Delta x} - \frac{3\mathcal{B}_3{}^{<}_{n,0} - 4\mathcal{B}_3{}^{<}_{n,1} + \mathcal{B}_3{}^{<}_{n,2}}{2\Delta x} = 0 \tag{5.35d}$$

Upon combining (5.34) and (5.35), we may solve for $U^{>}_{<}{}_{n,0}$.

5.4.1.3. Derivation of $U^{>}_{<}{}_{n,0}$ in *Case 3*

In *Case 3*, $U^{>}_{<}{}_{n,0}$ is also defined by (5.33) and its components satisfy (5.34). The additional equations are obtained from the discretization of (5.17):

$$\frac{-3\mathcal{A}^{>}_{n,0} + 4\mathcal{A}^{>}_{n,1} - \mathcal{A}^{>}_{n,2}}{2\Delta x} - \frac{3\mathcal{A}^{<}_{n,0} - 4\mathcal{A}^{<}_{n,1} + \mathcal{A}^{<}_{n,2}}{2\Delta x} = -\frac{i}{\Lambda}\frac{df}{dt}_n \tag{5.36a}$$

$$\frac{-3\mathcal{B}1^{>}_{n,0} + 4\mathcal{B}1^{>}_{n,1} - \mathcal{B}1^{>}_{n,2}}{2\Delta x} - \frac{3\mathcal{B}1^{<}_{n,0} - 4\mathcal{B}1^{<}_{n,1} + \mathcal{B}1^{<}_{n,2}}{2\Delta x} = \frac{\alpha_1}{\Lambda \cos\theta_1} f_n \qquad (5.36b)$$

$$\frac{-3\mathcal{B}2^{>}_{n,0} + 4\mathcal{B}2^{>}_{n,1} - \mathcal{B}2^{>}_{n,2}}{2\Delta x} - \frac{3\mathcal{B}2^{<}_{n,0} - 4\mathcal{B}2^{<}_{n,1} + \mathcal{B}2^{<}_{n,2}}{2\Delta x} = \frac{\alpha_2}{\Lambda} f_n \qquad (5.36c)$$

and

$$\frac{-3\mathcal{B}3^{>}_{n,0} + 4\mathcal{B}3^{>}_{n,1} - \mathcal{B}3^{>}_{n,2}}{2\Delta x} - \frac{3\mathcal{B}3^{<}_{n,0} - 4\mathcal{B}3^{<}_{n,1} + \mathcal{B}3^{<}_{n,2}}{2\Delta x} = 0 \qquad (5.36d)$$

From (5.34) and (5.36), we deduce $U^{>}_{<\,n,0}$.

The sound field obtained at $t = 2$ *i.e.* for $n = \frac{2}{\Delta t}$ consists of three or four plane sound waves. Their envelopes are viewed as the initial data when solving the evolution equations (3.18), (3.57) and (3.72) for $t > 2$.

5.4.1.4. *Stability of numerical scheme*

Let us analyse the stability of the numerical scheme, and rewrite (5.22) as

$$\frac{\partial U^{>}_{<}}{\partial t} = \left\{-C_{g_x}\frac{\partial}{\partial x} - i\nu C_{g_y} + iN\right\} U^{>}_{<} \qquad (5.37)$$

The stability requirement is expressed in terms of the eigenmodes of operator

$$\mathcal{L} = -C_{g_x}\frac{\partial}{\partial x} - i\nu C_{g_y} + iN \qquad (5.38)$$

Operator $\mathcal{L}$ clearly admits $U = e^{i\mu x}U_0$ as eigenvector. If the corresponding eigenvalue is λ, we must have by definition

$$\mathcal{L}U = \lambda U \qquad (5.39)$$

U_0 will exist provided that λ is a solution of the characteristic equation

$$\det\left[\lambda I + i(\mu C_{g_x} + \nu C_{g_y} - N)\right] = 0 \qquad (5.40)$$

Comparison of (5.40) with (4.8)-(4.9) implies that $\lambda = -i\sigma(\mu,\nu)$. Eigenvalue λ is therefore purely imaginary. The stability condition follows from the requirement that $\lambda\Delta t$ be inside the region of stability for the 3^{rd} order Adams-Bashforth scheme, *i.e.*

$$|\sigma(\mu,\nu)|\Delta t < 0.723 \qquad (5.46)$$

for all relevant μ. Condition (5.41) must be satisfied for all wavenumber μ supported by the grid. The time step Δt will be dictated by the maximum value $|\sigma|$ can take. Since $|\sigma|$ is an increasing function of μ, for a fixed ν, this value corresponds to $\mu_{max} = \frac{\pi}{\Delta x}$. The stability condition becomes

$$\Delta t < \frac{0.723}{|\sigma(\mu_{max}, \nu)|} \tag{5.42a}$$

Since μ_{max} is in general large, we can approximate locally $\sigma(\mu_{max}, \nu)$ by its asymptote. The asymptote with the largest ordinate for a given μ is $\sigma = \Lambda\mu$. We thus obtain the following stability requirement

$$\Delta t \leq \frac{0.723}{\Lambda \mu_{\max}} = 0.723 \frac{\Delta x}{\Lambda \pi} \tag{5.42b}$$

Given a grid size Δx, (5.42b) yields the required time step for stability.

5.4.2. *Analytical solution for longer times*

For $t > 2$, a solution of

$$\frac{\partial U}{\partial t}^{\geq}_{<} = \left\{ -C_{g_x} \frac{\partial}{\partial x} - i\nu C_{g_y} + iN \right\} U \tag{5.43}$$

is sought in the Fourier domain. The Fourier transform of U with respect to x is defined as

$$\tilde{U}(\mu, \nu, t) = \int_{-\infty}^{\infty} U(x, \nu, t) e^{-i\mu x} dx \tag{5.44}$$

Transformation of (5.43) yields the following matrix ordinary differential equation:

$$\left\{ I \frac{\partial}{\partial t} + i(C_{g_x}\mu + C_{g_y}\nu - N) \right\} \tilde{U}(\mu, \nu, t) = 0 \tag{5.45}$$

Recalling the definition (4.8) of matrix P, (5.45) is rewritten as

$$\frac{\partial \tilde{U}}{\partial t} = i\ P(\mu, \nu)\tilde{U} \tag{5.46}$$

The solution of (5.46) is clearly a linear combination of the eigenmodes of matrix P. The corresponding eigenvalues are simply $-\sigma(\xi, \nu)$, where $\sigma(\xi, \nu)$ is a solution of the dispersion relation (4.9). In principle, we need to solve an eigenvalue problem

for all $|\mu| < \infty$ and then use the inverse Fourier transform to obtain the scattered sound field

$$U(x,\nu,t) = \frac{1}{2\pi} \int_{-\infty}^{\infty} \tilde{U}(\mu,\nu,t) e^{i\mu x} d\mu \tag{5.47}$$

However, if we are only interested in the scattering during a finite time $t = \mathcal{O}(1)$, the sound field is localized in space *i.e.* the sound amplitudes are periodic over a sufficiently large x-interval [-L,L]. As a result, they can be decomposed in terms of a *finite* number, $2N$, of integer Fourier modes $\mu \in \{-N, \ldots, N-1\}$. Thus we need only solve $2N$ eigen problems.

The discrete set of Fourier modes corresponds in the physical domain to a set of regularly spaced grid points $\{x_k\}_{k=1,2N}$ defined by

$$x_k = -L + (k-1)\Delta x \quad \text{with } k = 1, 2N \tag{5.48a}$$

where

$$\Delta x = \frac{L}{N} \tag{5.48b}$$

Next, we use instead of (5.47), the discrete inverse Fourier transform to obtain the scattered sound field on the grid:

$$U(x_k,\nu,t) = \frac{1}{2N} \sum_{\mu=-N}^{N-1} \tilde{U}(\mu,\nu,t) e^{i\mu x_k} \qquad k = 1, \ldots, 2N \tag{5.49}$$

This step is efficiently performed with an FFT routine. Provided the periodicity assumption is satisfied *i.e.* as long as the sound amplitude fronts have not reached $|x| = L$, we obtain very accurate results. Details pertaining to the eigenvalues and eigenvectors in each of the tree cases are presented in Appendix B.

5.5. Conservation Laws

Conservation laws are a necessary, though not always sufficient condition insuring the validity and accuracy of numerical schemes. In this section we derive the conservation laws in the physical and the Fourier domain characterizing the resonant scattering after the source has ceased to radiate. When $f(t) = 0$, the governing equations for sound amplitudes read in matrix form

$$\{I\frac{\partial}{\partial t} + C_{g_x}\frac{\partial}{\partial x} + i\nu C_{g_y} - iN\}U = 0 \tag{5.50}$$

where U is the column vector of scattered amplitudes and C_{g_x}, C_{g_y} are the diagonal matrices defined for each of the three cases in §4.2.

We left-multiply the conjugate of (5.50) by U^T and add to the conjugate of the result to obtain:

$$\frac{\partial |U|^2}{\partial t} + \frac{\partial}{\partial x}\{U^T C_{g_x} U^*\} = iU^T(N^T - N)U^* \tag{5.51}$$

Since N is symmetric we have, simply:

$$\frac{\partial |U|^2}{\partial t} + \frac{\partial}{\partial x}\{U^T C_{g_x} U^*\} = 0 \tag{5.52}$$

Next, we integrate (5.52) from $x = -\infty$ to ∞, and obtain by Green's theorem:

$$\frac{\partial}{\partial t}\{\int_{-\infty}^{\infty} |U(x,\nu,t)|^2 \, dx\} + \left[U^T \, C_{g_x} \, U^*\right]_{-\infty}^{\infty} = 0 \tag{5.53}$$

For a localized initial data, U is zero at $\pm\infty$ implying therefore that the second term in (5.53) drops out. The first conservation law is then

$$\frac{\partial}{\partial t}\{\int_{-\infty}^{\infty} |U(x,\nu,t)|^2 \, dx\} = 0 \tag{5.54}$$

Eq. (5.54) means that the L^2 norm of U is t-independent. For a localized initial condition, the scattered sound field is localized in space and may be discretized on a grid. We need only replace the L^2 norm by its discrete equivalent:

$$\frac{\partial}{\partial t}\left\{\sum_{k=-N}^{N-1} |U(x_k,\nu,t)|^2\right\} = 0 \tag{5.55}$$

where N is the number of grid points and thus the number of fourier modes. The (x_k)'s denote the location of grid points and, implicit in (5.55), $U(x_{-N})$ should be zero, *i.e.* the numerical domain should be large enough to encompass all sound wave fronts. By Parceval theorem, we deduce from (5.55) that

$$\frac{\partial}{\partial t}\left\{\sum_{\mu=-N}^{N-1} |\tilde{U}(\mu,\nu,t)|^2\right\} = 0 \tag{5.56}$$

There is yet a corresponding conservation relationship in the Fourier domain. Recall the matrix ordinary differential equation satisfied independently by each Fourier modes $\mu \in [-N, N-1]$:

$$\frac{\partial \tilde{U}}{\partial t} = iP(\mu,\nu)\tilde{U} \tag{5.57}$$

A simple manipulation of (5.57) yields the time variations of $|\tilde{U}(\mu,\nu,t)|^2$:

$$\frac{\partial}{\partial t}|\tilde{U}(\mu,\nu,t)|^2 = i\tilde{U}^T(\mu,\nu,t)(P^T - P)\tilde{U}^*(\mu,\nu,t) \tag{5.58}$$

Since P is symmetric, we obtain

$$\frac{\partial}{\partial t}|\tilde{U}(\mu,\nu,t)|^2 = 0 \tag{5.59}$$

As mentioned earlier, no energy is exchanged between different Fourier modes. Thus the energy contained initially in one Fourier mode is conserved throughout all times t. For *Case 1*, we obtain

$$\frac{d}{dt}\left\{|\tilde{A}(\mu,\nu)|^2 + |\tilde{B}_1(\mu,\nu)|^2 + |\tilde{B}_2(\mu,\nu)|^2\right\} = 0 \tag{5.60}$$

and for *Cases 2* and *3*:

$$\frac{d}{dt}\left\{|\tilde{A}(\mu,\nu)|^2 + |\tilde{B}_1(\mu,\nu)|^2 + |\tilde{B}_2(\mu,\nu)|^2 + |\tilde{B}_3(\mu,\nu)|^2\right\} = 0 \tag{5.62}$$

Therefore, exchange of energy can only occur between the scattered sound amplitudes for the same Fourier mode. We shall use both (5.55) and (5.59) to check the validity of our results.

6. NUMERICAL RESULTS

6.1 General Comments

The normalized water depth of the waveguide analysed in §2 and §3 is assumed to be $kh = 1.65$ so that only one propagating acoustic mode is sustained. The line source is exactly parallel to the y-axis ($\nu = 0$) and radiates monochromatic soud waves at frequency 30Hz. The normalized group velocity is then deduced $\Lambda \simeq 0.306$. The spatial interval $[-\pi, \pi]$ in the normalized coordinates (4.4) has been discretized into 512 grid points. The time step chosen, $\Delta t = 0.005$, satisfies the stability criteria (5.42*b*). For each of the three cases considered here, we will present profiles of the sound envelopes at $t = 2$, *i.e.* when the sound source ceases to radiate. The Fourier spectrum of each complex amplitude is also shown to ensure that the Fourier decomposition adequately describes the scattered sound envelopes for $t > 2$. We have chosen to use 256 Fourier modes to for the early stages of the scattering until the envelope fronts reach $\pm\pi$. The computational domain is then doubled keeping the grid size constant. Calculations can then be performed until $t \simeq 18$. Solution of an eigenvalue problem is sought for each Fourier mode. In *Case 1*, Cardan's formulae yield the eigenvalues to 10^{-5} accuracy. In *Cases 2* and *3*, the accuracy is that associated with the single precision arithmetic used in our programs. Conservation of the sound intensity (5.54) is checked favorably to 10^{-5} accuracy.

For each computer run, the time history of selected Fourier modes is shown to display the energy partition between each component of the scattered sound field. Next, space-time diagrams describe the evolution of each scattered sound amplitude. The space and time intervals considered here and in §2 are comparable.

6.2. Case 1

Let us first assume that the two surface waves, of equal slope $k_{w_1} a_1 = k_{w_2} a_2 = 0.1$, are symmetrically directed along $\theta_1 = -\theta_2 = \frac{\pi}{3}$. The corresponding values of the dimensionless coupling frequencies are $\alpha_1 = \alpha_2 = 0.518$. With these parameters, it is clear from the governing equations (3.18) that B_1 and B_2 are identical.

The sound amplitude profiles at $t = 2$ are shown in figures 6.1a-c. Dispersion

causes a trailing pulse to appear in figure 6.1a while the reflected amplitudes $|B_1|$ and $|B_2|$ rise to more than a third of the amplitude $|A|$ of the forward scattered wave owing to resonance.

The Fourier spectra $|\tilde{A}|, |\tilde{B}|$ and $|\tilde{B}_2|$ at $t = 2$ in figures 6.1d-f clearly indicate that 256 grid points are sufficient to insure that the amplitude of the first discarded Fourier mode is no larger than 10^{-3} that of the zeroth Fourier mode.

In figures 6.2a-f, we describe how the energy or sound intensity associated with a given Fourier mode μ is broken down between the resonant components of the acoustic field. The solid line corresponds to $|\tilde{A}(\mu,t)|^2$, the dotted line to $|\tilde{A}(\mu,t)|^2 + |\tilde{B}_1(\mu,t)|^2$. The dashed line is the grand total $|\tilde{A}|^2 + |\tilde{B}_1|^2 + |\tilde{B}_2|^2$. Thus, the vertical distance between the first two curves is simply $|\tilde{B}_1(\mu,t)|^2$. Likewise, the distance between the dotted curve and the dashed curve is exactly $|\tilde{B}_2(\mu,t)|^2$. All energies are normalized by that of the first mode ($\mu = 0$) at the initial time $t = 2$. In *Case 1*, a constant dashed line simply means the conservation of sound intensity for a Fourier mode *i.e.* (5.60). As the mode number increases, the ordinate of this line decreases in accordance with the decay observed in the previous figure. Focusing on figure 6.2a, we observe that the variation of all three Fourier mode amplitudes are in phase and periodic in time according to (4.17). The period is $\frac{2\pi}{2\sigma_1} = \frac{\pi}{\sqrt{2}\alpha_1} \simeq 4.3$. Note that the cumulative contributions of $|\tilde{B}_1|^2$ and $|\tilde{B}_2|^2$ oscillations between 0 and 100% of the initial intensity contained in the Fourier mode $\mu = 0$. The fact that the incident $|\tilde{A}|$ and the scattered $|\tilde{B}_{1,2}|$ sound amplitudes play comparable roles is typical of resonant phenomena. As the Fourier mode number μ is increased, a decreasing proportion of the initial energy is exchanged between $|\tilde{A}|$ and $|\tilde{B}_{1,2}|$. This is expected; indeed a Fourier mode $e^{i\mu x_1}$ can be interpreted as $e^{i\epsilon\mu x}$, thus implying that the x-component of the horizontal acoustic wavenumber vector must be corrected by $\epsilon\mu$. We have shown in §3 that resonance can be expressed as a vector identity involving the wavenumber vectors of the incident sound wave, the surface wave and of the scattered sound wave. Therefore, $\mu \neq 0$ can be viewed as a departure from the exact satisfaction of this vector identity, *i.e.*, a detuning from the resonance condition. Conversaly, $\mu = 0$ corresponds to perfect tuning. These observations are consistent with the dispersion branches deduced in §4 for *Case 1*. For low values of $|\mu|$, the dispersion branches depart significantly from

their asymptotes, as a result of the coupling of surface waves. For large $|\mu|$ on the other hand, they are almost straight signifying the absence of coupling and thus of dispersion.

The time evolution of $|A|$ and $|B_2|$ is plotted in figures 6.3a-b. In the top figure, the initial pulse propagates to the right at speed Λ and decays rapidly while dispersing in a train of trailing pulses. We also observe a front propagating to the left at speed $-\Lambda\cos\theta_1 = -\frac{\Lambda}{2}$ and whose amplitude is small. Note again the appearance of the crescent-like structures observed in §2. The scattered amplitude $|B_1|$ in figure 6.3b is no longer even in x. The left propagating front also decays while large trailing pulses appear.

Keeping the same parameters except for $\theta_2 = -\frac{\pi}{4}$ (i.e., $\alpha_2 = 0.486$), we observe in figures 6.4b-c that the scattering in direction $\vec{k}_1$ is prefered over direction $\vec{k}_2$. The Fourier spectra in figures 6.4d-f show a decay of at least three orders of magnitude. The time evolution of the scattered sound intensities in Fourier mode # 1 ($\mu = 0$) again suggest perfect tuning. It is, however, worth mentioning the uneven partition between the two scattered waves B_1 and B_2 in figure 6.5a. For higher Fourier mode numbers, the variations of each scattered energy are neither in phase nor periodic anymore as observed in figures 6.5b-f. A slow modulation is, however, observed. Nevertheless, the same trend of decreasing energy exchange between A, on the one hand, and B_1 and B_2 on the other, is noticeable.

Consider next the time evolution of the three scattered sound amplitudes in figures 6.6a-c. The right going pulse decays and disperses as described earlier. An additional front propagates now to the left at speed $\Lambda\cos\theta_2 = \frac{\Lambda}{\sqrt{2}}$. The scattered sound amplitude B_1, in figure 6.6b, shows more clearly the presence of two left propagating fronts (in addition to the front propagating to the right at speed $\simeq \Lambda$). As expected for B_1, the scattering direction $\vec{k}_1$ is prefered with the propagation of a large pulse while a smaller pulse propagates faster in the direction $\vec{k}_2$. The nodes of the amplitude modulation still yield crescent-like structures. Figures 6.6c for B_2, is quite different from figure 6.6b. In particular, the predominance of direction $\vec{k}_1$ is absent.

Finally, we consider yet another inclination $\theta_2 = -\frac{\pi}{6}$ (keeping $\theta_1 = \frac{\pi}{3}$) which

corresponds to $\alpha_2 = 0.464$. Upon recalling that $\alpha_1 = 0.518$, the predominance of B_1 over B_2 in figures 6.7b-c is understandable. Fourier spectra in figures 6.7d-f show a satisfactory decay.

The time history of several Fourier modes is summarized in Figures 6.8a-f. With the decrease in α_2, the period of the in-phase oscillations ($\frac{\pi}{\sqrt{\alpha_1^2+\alpha_2^2}}$) increases and the proportion of the scattered sound intensity due to B_2 decreases. For larger Fourier modes the variations are again o ıt of phase and slowly modulated.

The evolution of $|A|$ in figure 6.9a clearly indicates the presence of two left propagating fronts with respective speeds $-\frac{2\Lambda}{\sqrt{3}}$ and $-\frac{\Lambda}{2}$. The separation between these two fronts is even clearer in figures 6.9b-c for $|B_1|$ and may be compared to that observed in figures 6.6b-c.

The analysis of the scattering patterns for *Case 1* has confirmed several conjectures stated earlier. First, we have observed for each of the 3 sound wave amplitudes, the presence of as many propagating fronts. This is yet another instance where the carrier wave and its amplitude are not propagating in the same direction owing to a non-uniform boundary condition. The relative imbalance of B_1 and B_2 is primarily dictated by the dimensionless coupling frequencies α_1 and α_2. In the examples analysed earlier, these two parameters were assigned different though comparable values. This will not be true in general for Case 2. It is therefore expected that the balance between B_1 and B_2 will be lost in that case. Second, we have observed that perfect tuning ($\mu = 0$) corresponds indeed to the strongest possible interactions and yet to the simplest behavior (periodic, in phase variations). The analysis of the zeroth mode of the scattered sound is by far the most amenable and thus a likely avenue to investigate experimentally the characteristics of the scatterer.

6.3. Case 2

The scattering of sound by two surface waves propagating in perpendicular directions is now considered. Let θ_1 be $\frac{\pi}{3}$ (*i.e.* $\theta_2 = -\frac{2\pi}{3}$). The values of the coupling frequencies are $\alpha_1 = 0.518$ and $\alpha_2 = 0.897$. Sound is scattered in two pairs of opposite directions. In *Case 2*, the amplitudes have been plotted until $t = 8$ only to allow a better resolution in space and time. The spatial domain required is only

$[-\pi, \pi]$.

The sound amplitudes at $t = 2$, *i.e.* when the source is turned off, are presented in figures 6.10a-d. In contrast with *Case 1*, the highest energy is no longer associated with $|A|$, but rather with $|B_2|$ (the amplitude of a right going sound wave). The remaining two amplitudes, $|B_1|$ and $|B_3|$, are smaller than $|A|$. Note that the amplitude $|B_3|$ of the backscattered sound wave appears to be even in x. The Fourier diagrams in figures 6.10e-h show a decay of no less than three order magnitude for all four sound envelopes. Next, we plot the cumulative energy for several Fourier modes in figures 6.11a-f with the following convention: the solid line represents $|\tilde{A}(\mu,t)|^2$, the dotted line the cumulative contribution of $|\tilde{A}(\mu,t)|^2 + |\tilde{B}_2(\mu,t)|^2$, the dashed line the cumulative contribution of the $|\tilde{A}(\mu,t)|^2 + |\tilde{B}_2(\mu,t)|^2 + |\tilde{B}_1(\mu,t)|^2$ and finally, the dot-dash line the sum of all four squared Fourier amplitudes. We observe that the variations are out of phase. However, the total right propagating energy $|\tilde{A}(\mu,t)|^2 + |\tilde{B}_2(\mu,t)|^2$ represented by the dotted line is clearly periodic and again varies from 0 to 1 for $\mu = 0$. For perfect tuning, left and right propagation of the energy alternate. As μ is increased, the proportion of the initial energy that may propagate to the left decreases drastically. Note that the right propagating energy is evenly shared by $\tilde{A}$ and $\tilde{B}_2$.

The evolution of the four sound amplitudes is displayed in figures 6.12a-d. In contrast with *Case 1*, the dispersion curves of §4 suggest just two opposite propagation directions. The amplitude modulation observed in figure 6.12a is more complicated than its counterpart for *Case 1*. The succession of pulse growth, dispersion and decay is quite clear in the right propagating front. There is also a front with a mild amplitude propagating to the left. The amplitude $|B_1|$ is dominated by a left propagating front with speed $-\frac{\Lambda}{2}$, which disperses yielding trains of pulses inclined at $-\Lambda$. The amplitude $|B_2|$ of the right going scattered sound wave is qualitatively similar to $|A|$, although twice as large, and is dominated by a right going pulse at speed $\frac{\Lambda}{2}$, small pulses propagate ahead of this front at speed Λ. Finally, we observe that the amplitude $|B_3|$ resulting from multiple scattering is even in x as suggested by figure 6.10d and is otherwise qualitatively similar to the amplitude $|B_1|$ of the other left going sound wave.

In the next example we assume $\theta_1 = \frac{\pi}{6}$ $(i.e.\ \theta_2 = -\frac{5\pi}{6})$. The values of the dimensionless coupling frequencies are deduced $\alpha_1 = 0.464$ and $\alpha_2 = 1.733$. The large ratio $\frac{\alpha_2}{\alpha_1} \simeq 4$ suggests that the surface have $\vec{k}_{w2}$ will play a leading role in the scattering. This is confirmed in figure 6.13c where the amplitude $|B_2|$ reaches unity. Note also the enhanced dispersion in figures 6.13a-b in comparison with figures 6.10a-b. $|A|$ is now split into two pulses of almost equal amplitude and $|B_2|$ is double peaked. The decay in the Fourier spectrum is appropriate.

Next, the energy decomposition is shown for several Fourier modes in figures 6.14a-f. The same characteristics observed earlier for $\theta_1 = \frac{\pi}{3}$ are seen again. However, $|B_2|$ accounts for more energy than $|A|$ for large values of μ as observed in figures 6.14e-f.

The amplitude of the right going sound waves A and B_2 bear qualitative resemblance and so do the amplitudes B_1 and B_3 of the left going sound waves. It is therefore sufficient to comment on A and B_1 alone. One clearly observes recurring patterns for both amplitudes. Regarding A, the rear peak in the initial data overtakes the front peak to form a higher pulse which itself disperses with the appearance of trailing waves at its foot. The amplitude $|A|$ then decreases sharply while the relative importance of the trailing pulse increases. The same scenario is repeated again. Turning to figure 6.15b, it is worth pointing out that $|B_1|$ is large when and where $|A|$ is (as suggested by the governing equation of B_1). The twinpeaked initial pulse propagates in the positive and negative directions with a slight depression between the two fronts. The almost flat resulting peak then decreases in amplitude with the appearance of small leading waves. These leading waves are then overtaken yielding again a twinpeaked pulse with a noticeable depression.

6.4. Case 3

When one of the two surface waves involved in the scattering is colinear to the incident sound wave $i.e.\ \theta_2 = 0$ sound is scattered in two sets of opposite directions. With the above parameters we deduce $\alpha_1 = 0.518$ and $\alpha_2 = 0.449$. We shall again consider two geometries $\theta_1 = \frac{\pi}{3}$ and $\theta_1 = \frac{\pi}{6}$. The corresponding directions of scattering are identical to those in *Case 2.*

Consider first $\theta_1 = \frac{\pi}{3}$. The coupling frequency α_1 is of the same order of magnitude as α_2. The sound amplitudes at $t = 2$ are plotted in figures 6.16a-d. The amplitude $|A|$ is clearly dominant in contrast with *Case 2.* The backscattered wave amplitude (B_2) is even in x. The Fourier spectra in figures 6.16e-h confirm that enough modes have been used in the Fourier decomposition. The break up of the Fourier energy among the four components of the scattered sound field is described in figures 6.17a-f. The same plotting convention is adopted here. The dotted line now represents the energy propagating along the positive and negative x-axis. This curve is clearly periodic in figure 6.17a for $\mu = 0$. For larger values of μ, all variations are out of phase and do not show any periodicity on the time scale considered. The time evolution of the four sound amplitudes is described in figures 6.18a-d until $t \approx 17$. The initial pulse in $|A|$ decays rapidly while dispersing giving rise to a series of trailing pulses. Meanwhile, two weak fronts propagating to the left at speed $-\frac{\Lambda}{2}$ and $-\Lambda$ are also observed. The amplitude $|B_1|$ consists primarily of a left going pulse at speed $-\frac{\Lambda}{2}$. Two more fronts are also identified, one also propagating to the left at speed $-\Lambda$ and the other to the right at speed Λ. The nodes of the amplitude modulation have again a crescent-like shape. As expected the amplitude of the backscattered sound wave is even in x. The evolution of amplitude $|B_3|$ is more complex. The main front propagates to the right at speed $\Lambda \cos\theta_1 = \frac{\Lambda}{2}$ and disperses. Two symmetric fronts propagate at speed $\pm\Lambda$.

In the next example $\theta_1 = \frac{\pi}{6}$. The corresponding coupling frequency, $\alpha_1 = 0.464$, is smaller than its previous value and closer to α_2, The snapshots of the sound amplitudes when the source ceases to emit are qualitatively similar to the $\theta_1 = \frac{\pi}{3}$ case, with the expected exception of a reduced peak for B_1. The decomposition of the Fourier energy in figure 6.20b-f for $\mu > 0$ is slowly varying in time. The time evolution of the sound amplitudes is shown in figures 6.21a-d. Strong similarities with the previous case ($\theta_1 = \frac{\pi}{3}$) appear. It is clear however that $|B_1|$ is generally weaker as a result of the smaller value of the coupling frequency α_1 and that the amplitude $|B_3|$ is less dispersive.

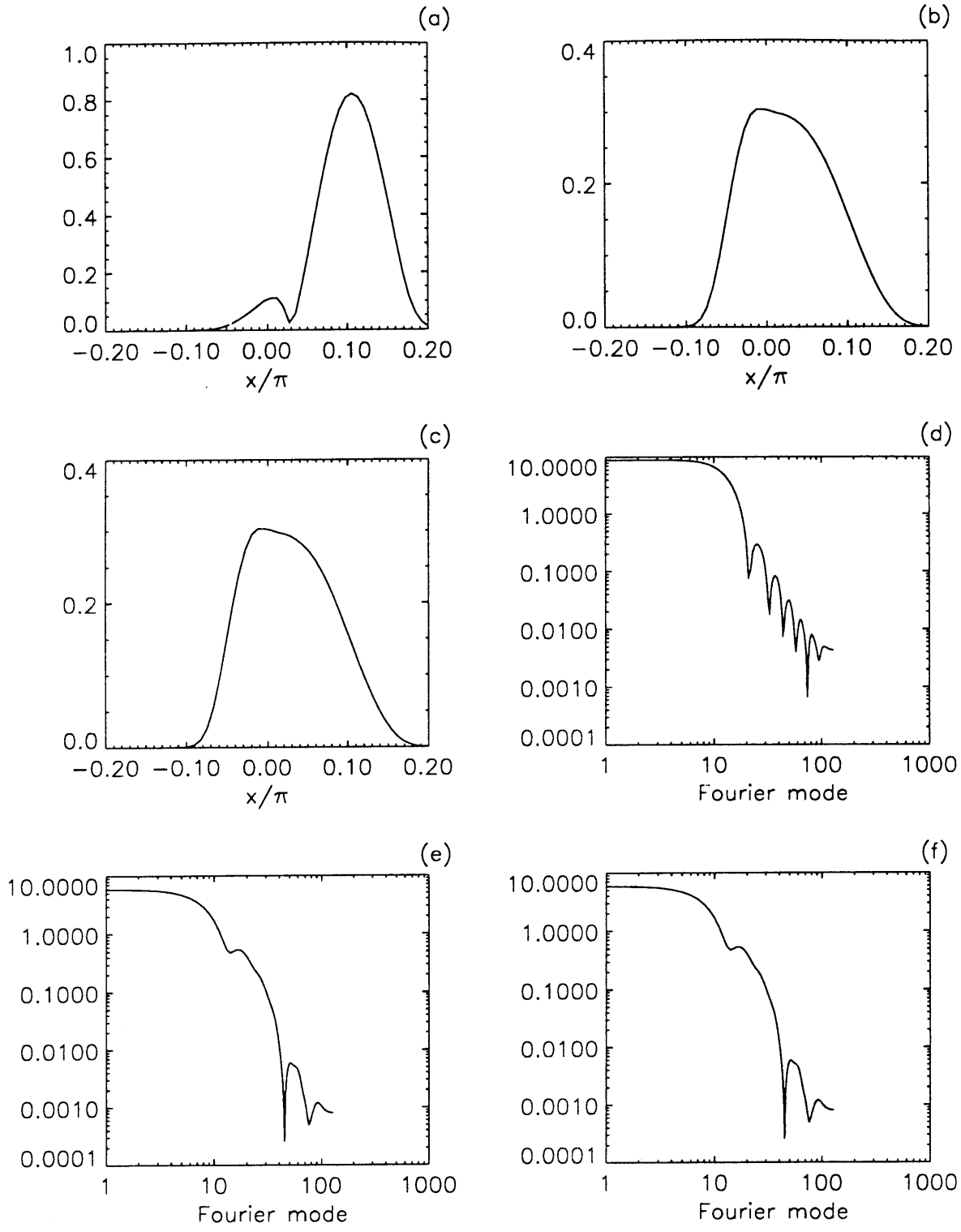

Figures 6.1a-f: Scattered sound at $t = 2$ for *Case 1* and $\theta_1 = -\theta_2 = 60°$ and $\alpha_1 = \alpha_2 = 0.518$; Physical sound envelopes (a) $|A|$, (b) $|B_1|$ and (c) $|B_2|$; Fourier sound envelopes (d) $|\tilde{A}|$, (e) $|\tilde{B}_1|$ and (f) $|\tilde{B}_2|$.

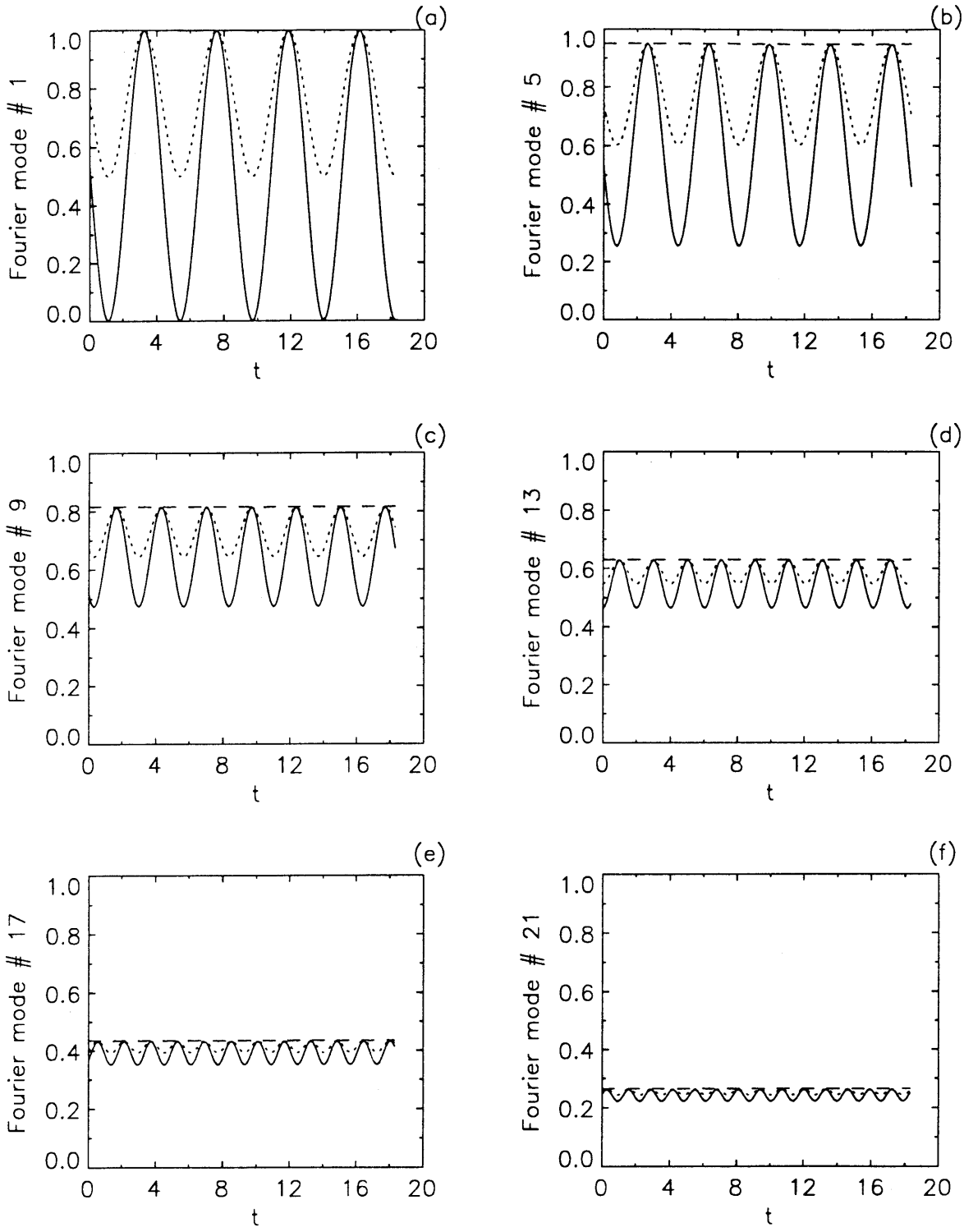

Figures 6.2a-f: Partition of Fourier energy in *Case 1* for modes 1, 5, 9, 13, 17 and 21, with $\theta_1 = -\theta_2 = 60°$ and $\alpha_1 = \alpha_2 = 0.518$; $|\tilde{A}|^2$ (——), $|\tilde{A}|^2 + |\tilde{B}_1|^2$ (· · ··) and $|\tilde{A}|^2 + |\tilde{B}_1|^2 + |\tilde{B}_2|^2$ (- - - - -).

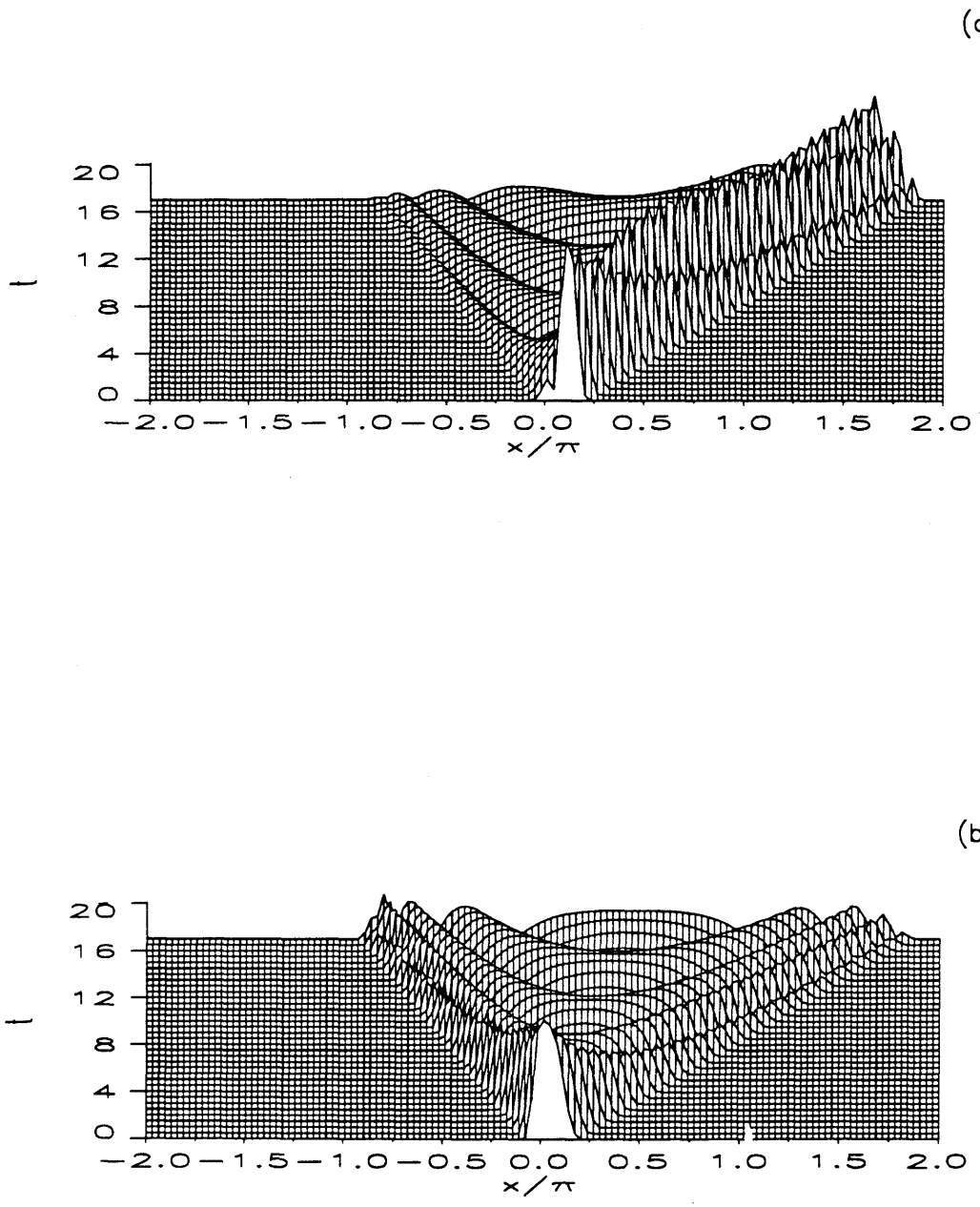

Figures 6.3a-b: Evolution of sound envelopes in *Case 1* with $\theta_1 = -\theta_2 = 60°$ and $\alpha_1 = \alpha_2 = 0.518$; (a) $|A|$ and (b) $|B_1|$.

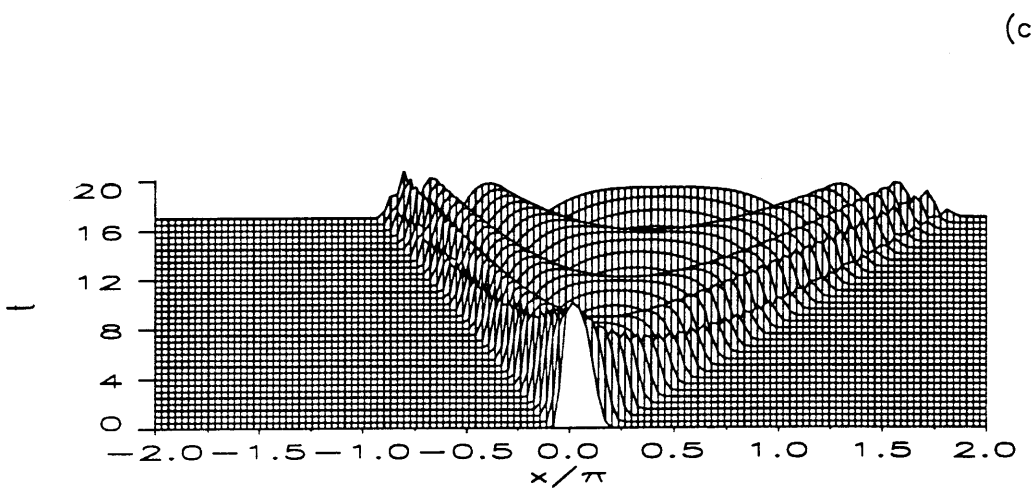

Figure 6.3c: Evolution of sound envelope $|B_2|$ in *Case 1* with $\theta_1 = -\theta_2 = 60°$ and $\alpha_1 = \alpha_2 = 0.518$.

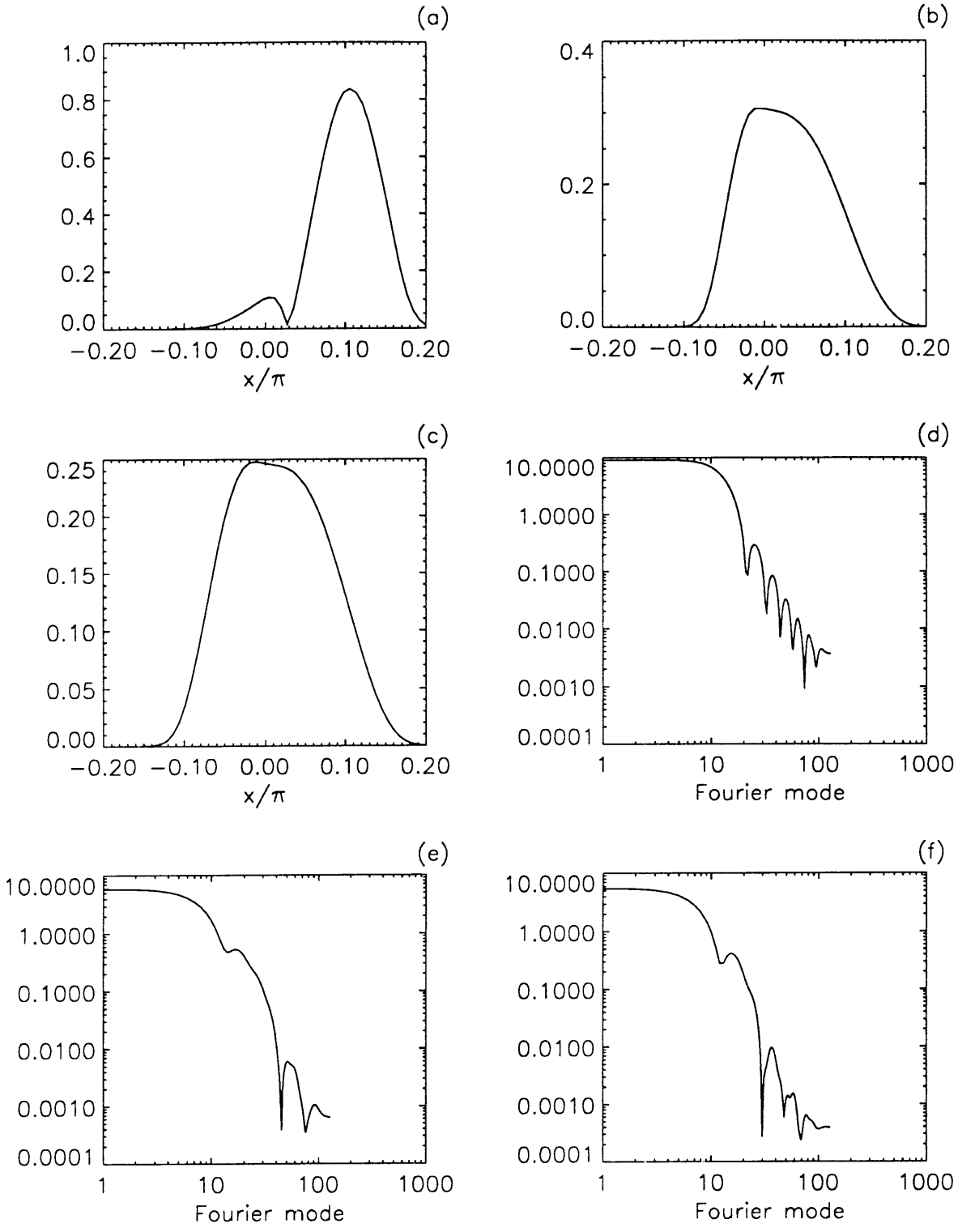

Figures 6.4a-f: Scattered sound at $t = 2$ for *Case 1*, $\theta_1 = 60°$ and $\theta_2 = 45°$, $\alpha_1 = 0.518$ and $\alpha_2 = 0.486$; Physical sound envelopes (a) $|A|$, (b) $|B_1|$ and (c) $|B_2|$; Fourier sound envelopes (d) $|\tilde{A}|$, (e) $|\tilde{B}_1|$ and (f) $|\tilde{B}_2|$.

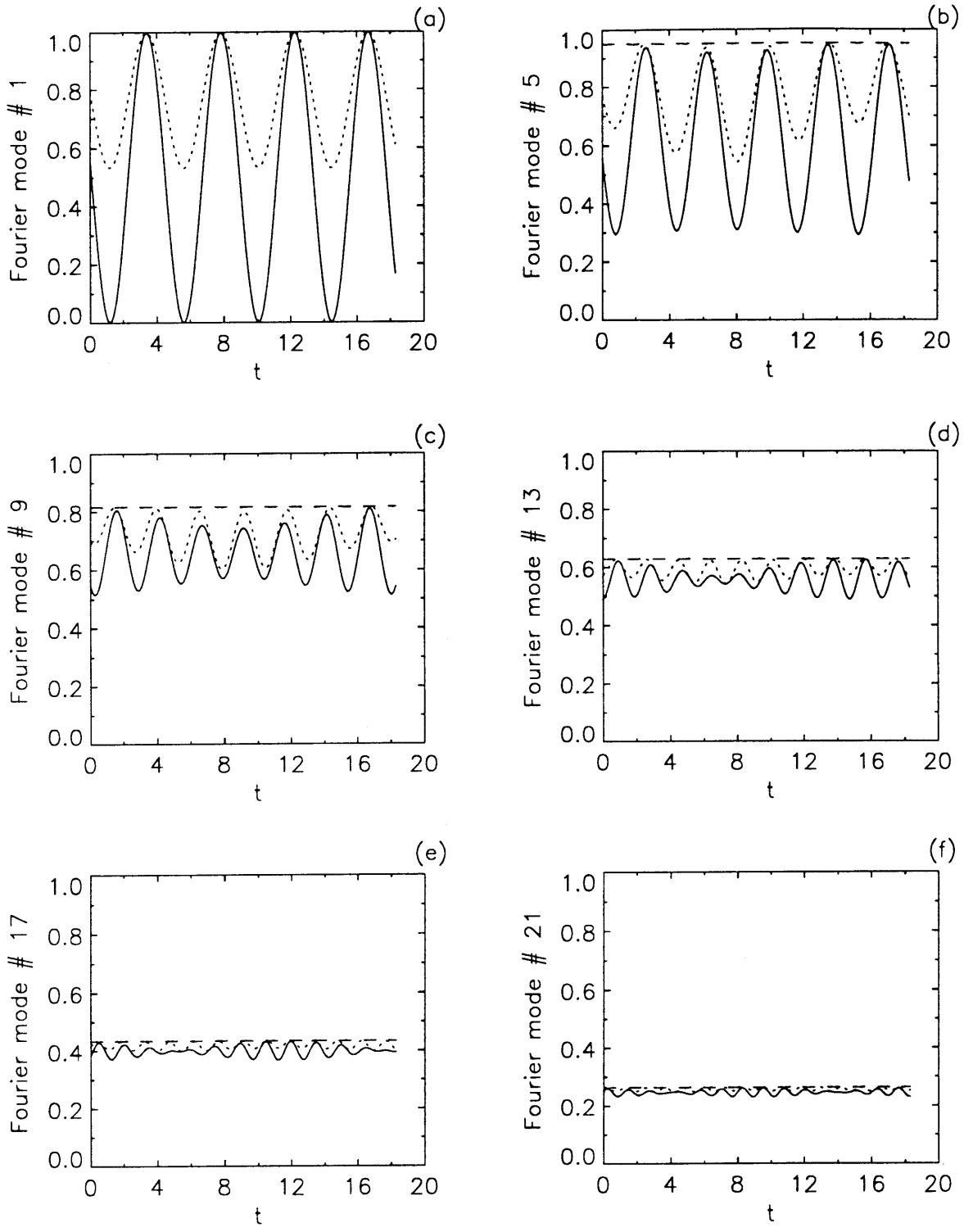

Figures 6.5a-f: Partition of Fourier energy in *Case 1* for modes 1, 5, 9, 13, 17 and 21, with $\theta_1 = 60°, \theta_2 = 45°$, $\alpha_1 = 0.518$ and $\alpha_2 = 0.486$; $|\tilde{A}|^2$ (——), $|\tilde{A}|^2 + |\tilde{B}_1|^2$ $(\cdots)$ and $|\tilde{A}|^2 + |\tilde{B}_1|^2 + |\tilde{B}_2|^2$ (- - - - -).

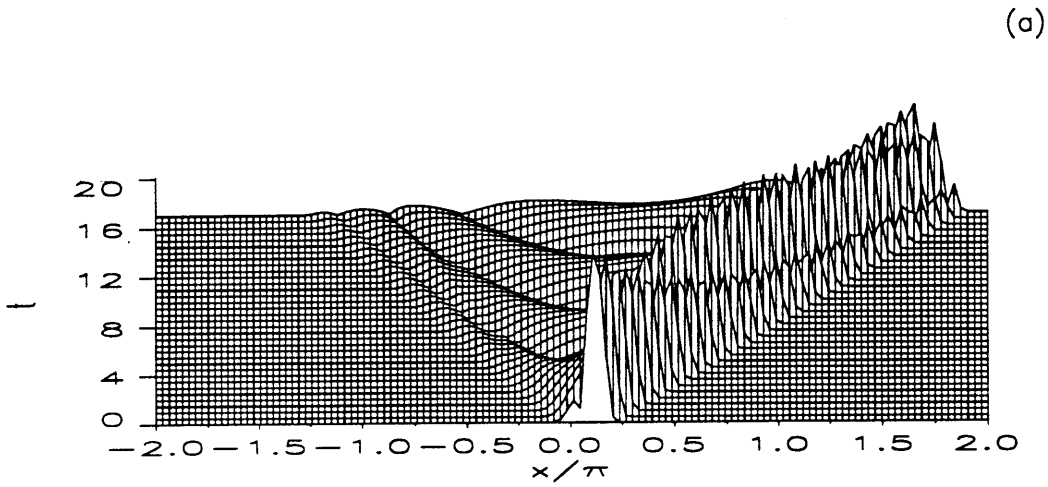

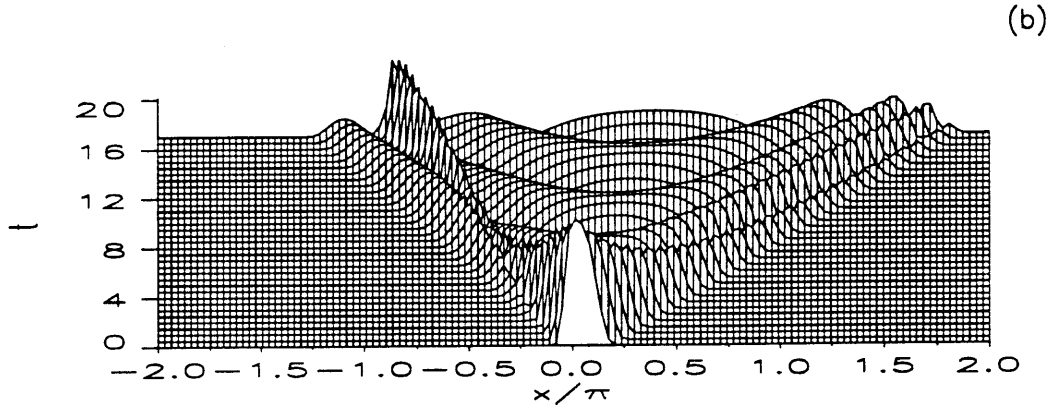

Figures 6.6a-b: Evolution of sound envelopes in *Case 1* with $\theta_1 = 60°$, $\theta_2 = 45°$ $\alpha_1 = 0.518$ and $\alpha_2 = 0.486$; (a) $|A|$ and (b) $|B_1|$.

(c)

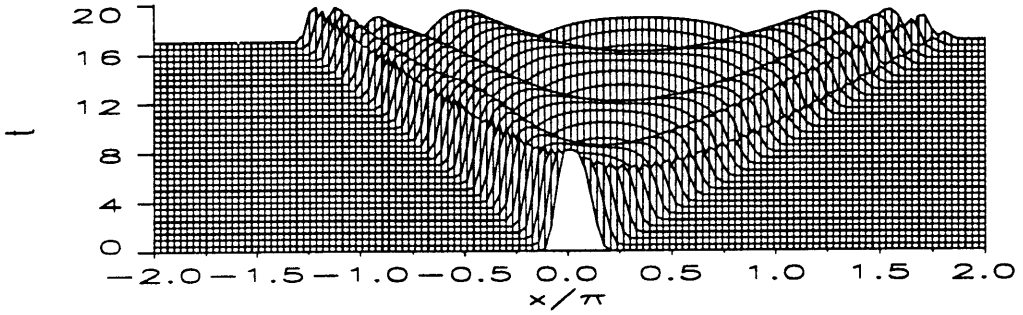

Figure 6.6c: Evolution of sound envelope $|B_2|$ *Case 1* with $\theta_1 = 60°$, $\theta_2 = 45°$, $\alpha_1 = 0.518$ and $\alpha_2 = 0.486$.

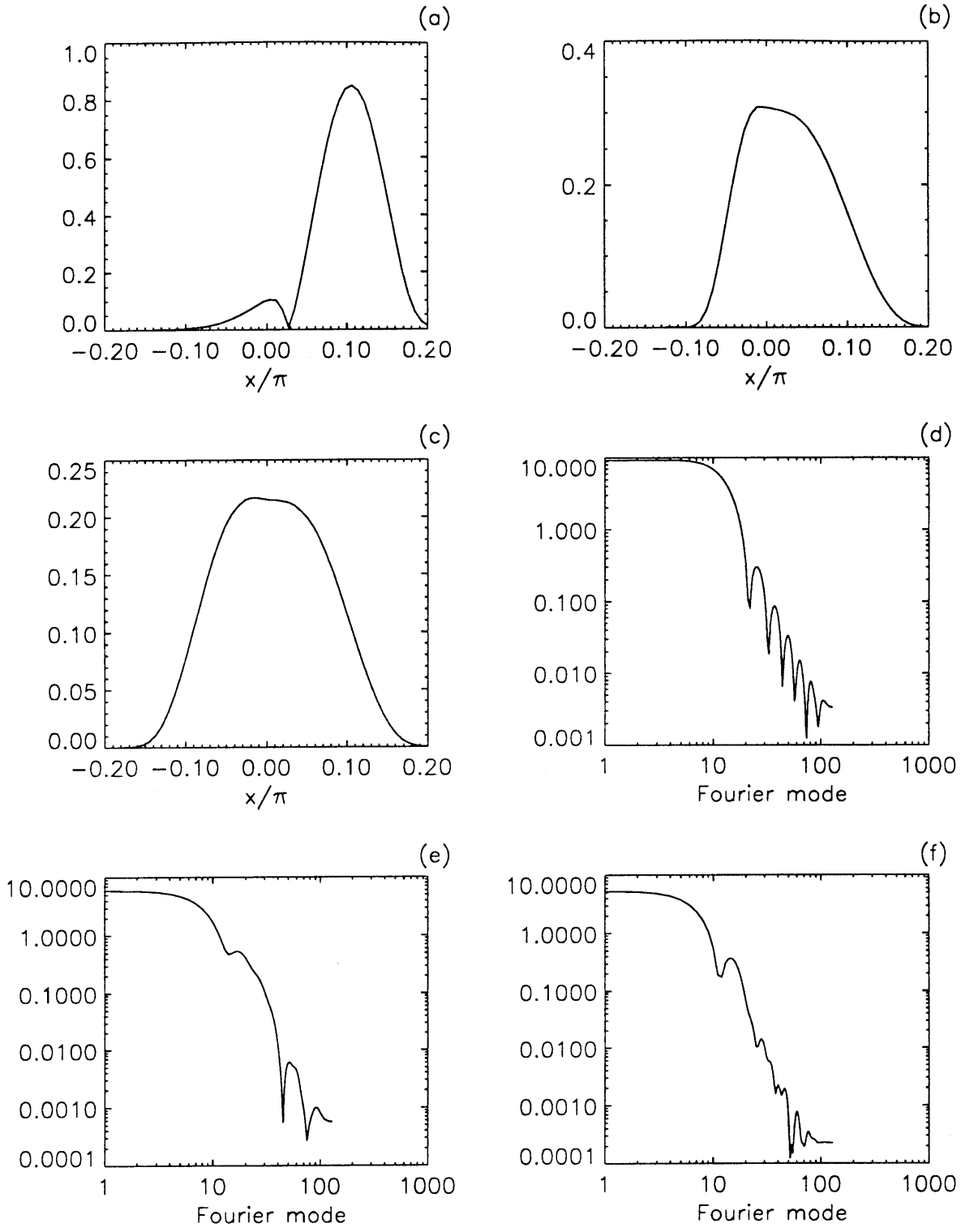

Figures 6.7a-f: Scattered sound at $t = 2$ for *Case 1*, $\theta_1 = 60°$ and $\theta_2 = -30°$, $\alpha_1 = 0.518$ and $\alpha_2 = 0.464$; Physical sound envelopes (a) $|A|$, (b) $|B_1|$ and (c) $|B_2|$; Fourier sound envelopes (d) $|\tilde{A}|$, (e) $|\tilde{B}_1|$ and (f) $|\tilde{B}_2|$.

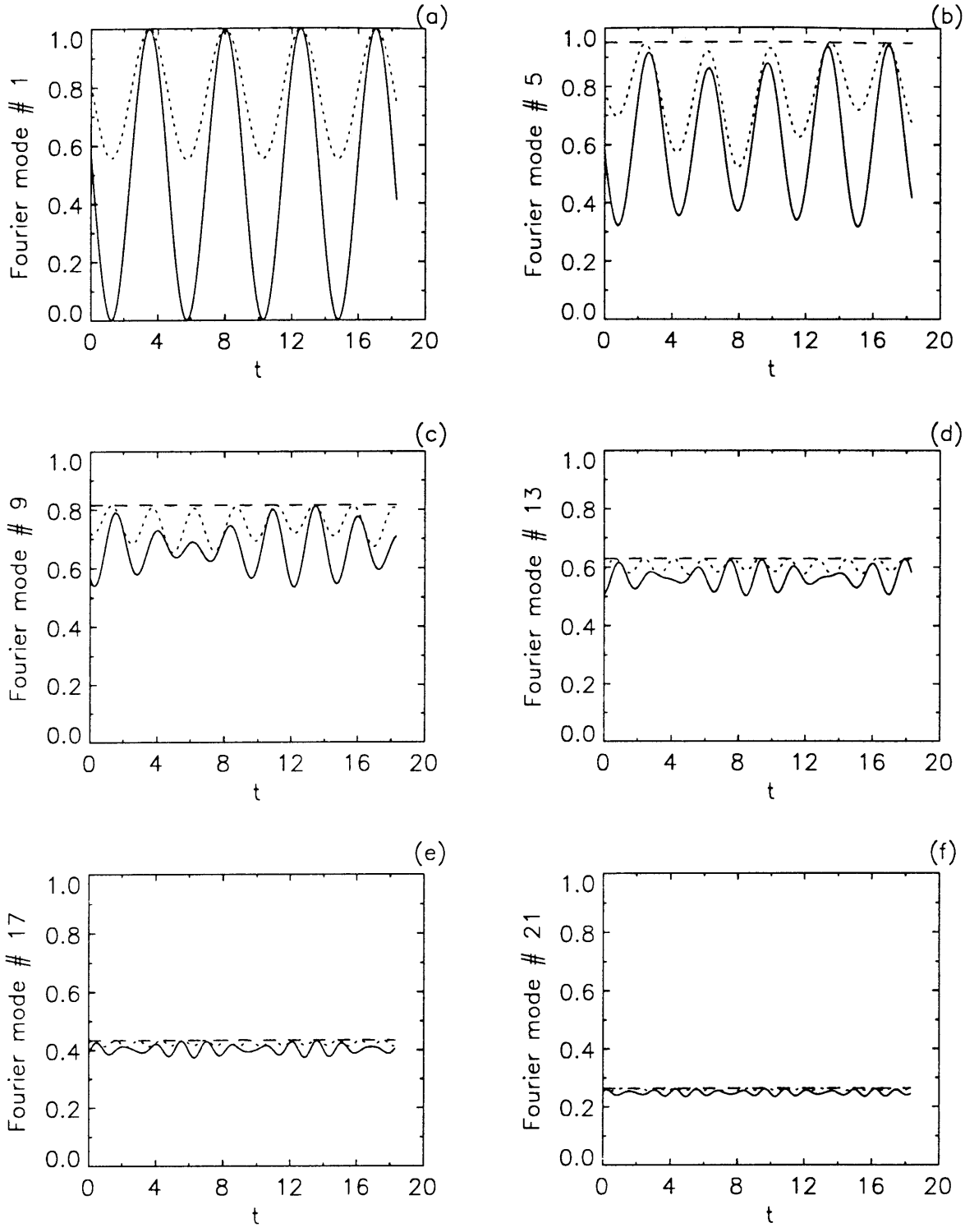

Figures 6.8a-f: Partition of Fourier energy in *Case 1* for modes 1, 5, 9, 13, 17 and 21, with $\theta_1 = 60°, \theta_2 = -30°$, $\alpha_1 = 0.518$ and $\alpha_2 = 0.464$; $|\tilde{A}|^2$ (——), $|\tilde{A}|^2 + |\tilde{B}_1|^2$ ($\cdots$) and $|\tilde{A}|^2 + |\tilde{B}_1|^2 + |\tilde{B}_2|^2$ (- - - - -).

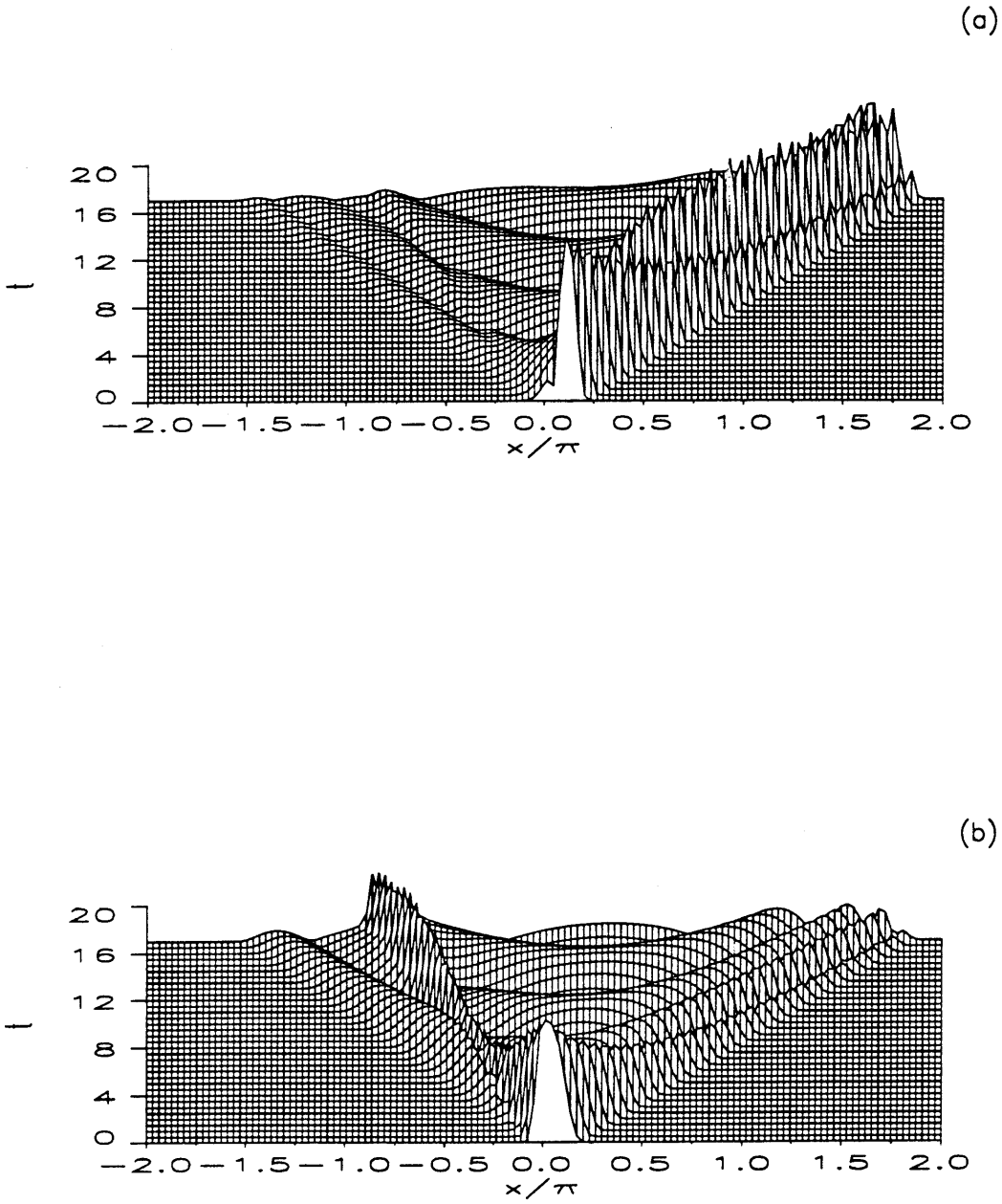

Figures 6.9a-b: Evolution of sound envelopes in *Case 1* with $\theta_1 = 60°$, $\theta_2 = -30°$, $\alpha_1 = 0.518$ and $\alpha_2 = 0.464$; (a) $|A|$ and (b) $|B_1|$.

(c)

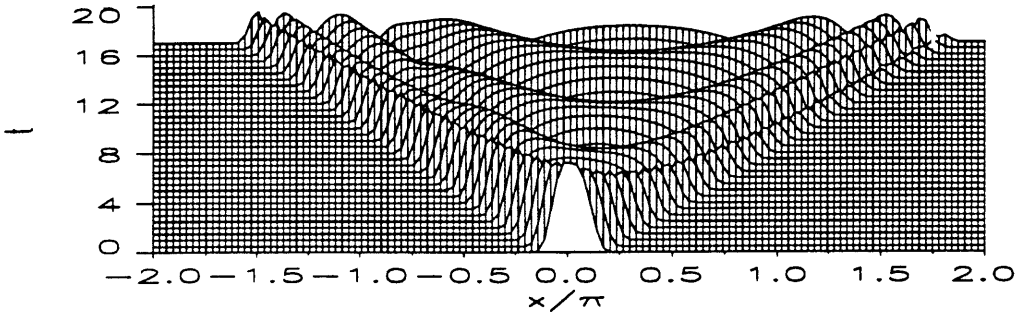

Figure 6.9c: Evolution of sound envelope $|B_2|$ in *Case 1* with $\theta_1 = 60°$, $\theta_2 = -30°$ $\alpha_1 = 0.518$ and $\alpha_2 = 0.464$.

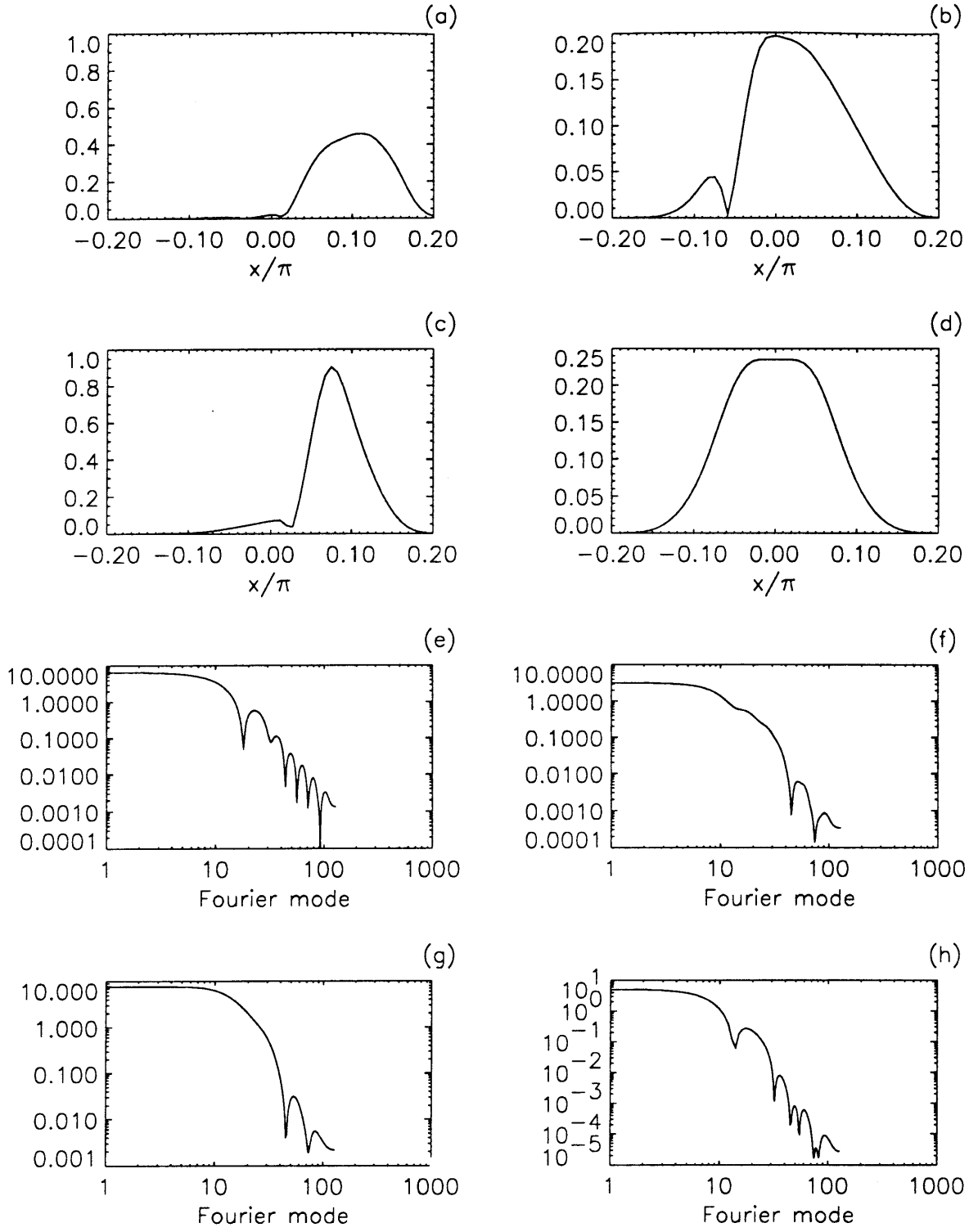

Figures 6.10a-h: Scattered sound at $t = 2$ for *Case 2*, $\theta_1 = 60°$, $\alpha_1 = 0.518$ and $\alpha_2 = 0.897$; Physical sound envelopes (a) $|A|$, (b) $|B_1|$, (c) $|B_2|$ and (d) $|B_3|$; Fourier sound envelopes (e) $|\tilde{A}|$, (f) $|\tilde{B}_1|$, (g) $|\tilde{B}_2|$ and (h) $|\tilde{B}_3|$.

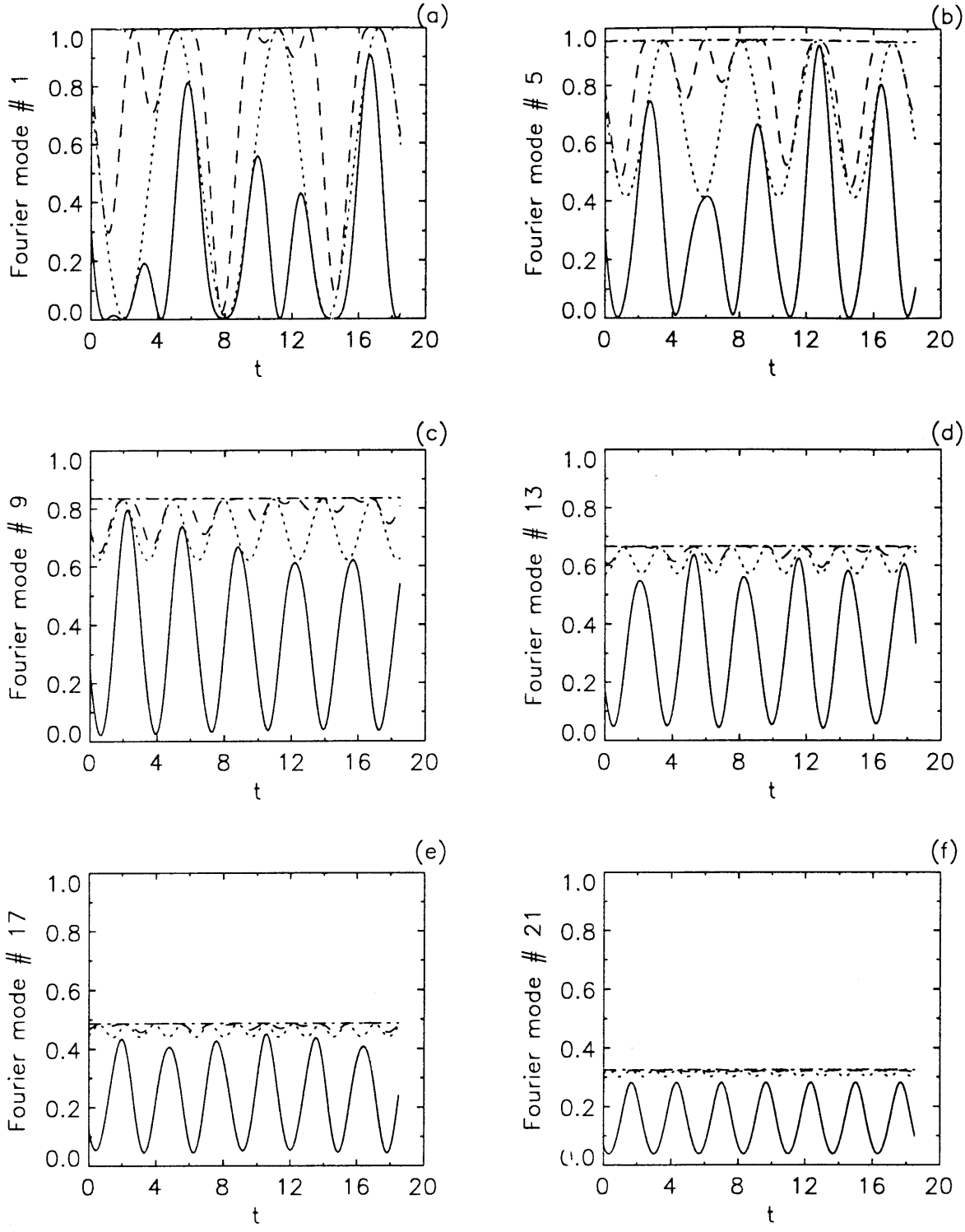

Figures 6.11a-f: Partition of Fourier energy in *Case 2* for modes 1, 5, 9, 13, 17 and 21, with $\theta_1 = 60°$, $\alpha_1 = 0.518$ and $\alpha_2 = 0.897$; $|\tilde{A}|^2$ (——), $|\tilde{A}|^2 + |\tilde{B}_2|^2$ (· · ·), $|\tilde{A}|^2 + |\tilde{B}_1|^2 + |\tilde{B}_2|^2$ (- - - - -) and $|\tilde{A}|^2 + |\tilde{B}_1|^2 + |\tilde{B}_2|^2 + |\tilde{B}_3|^2$ (--------).

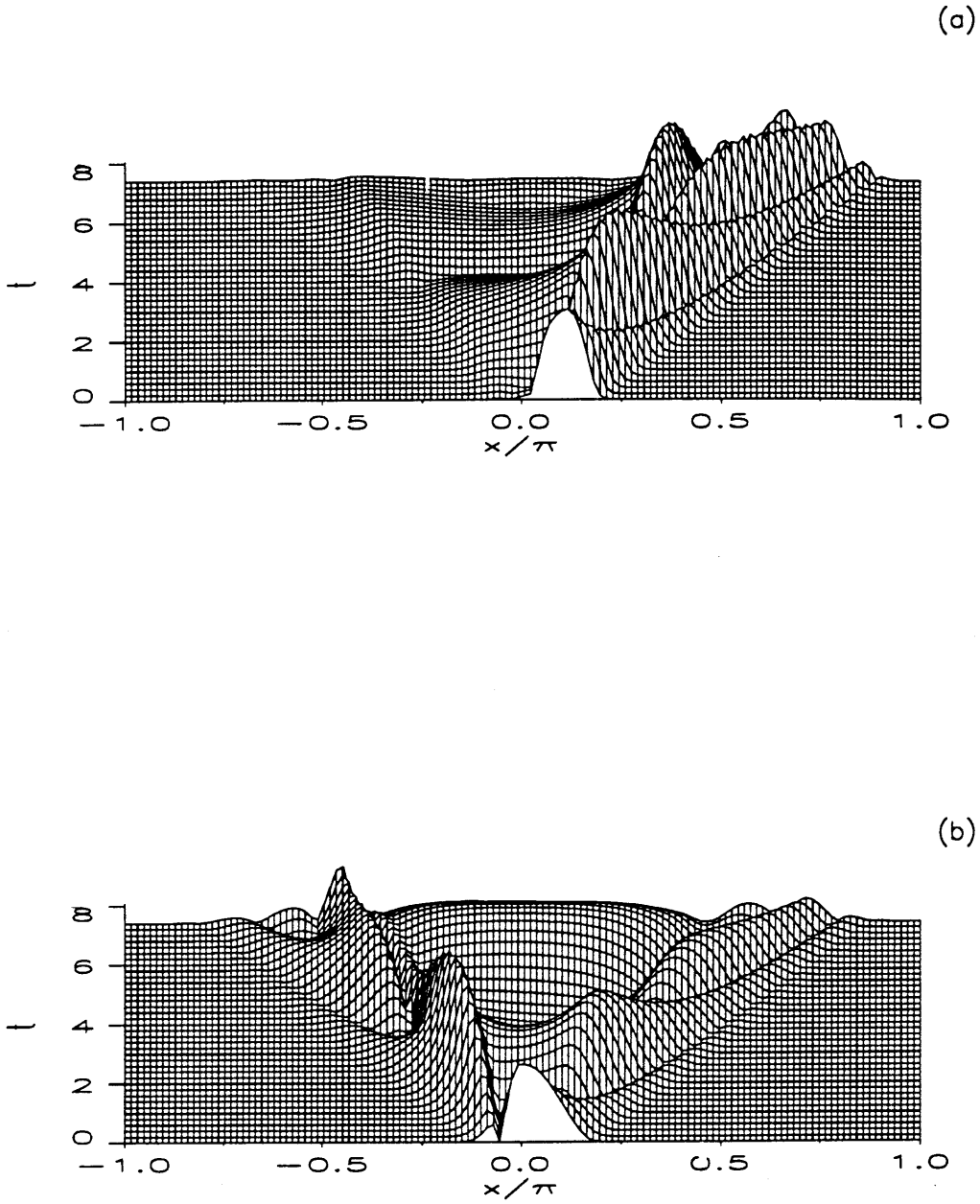

Figures 6.12a-b: Evolution of sound envelopes in *Case 2* with $\theta_1 = 60°$, $\alpha_1 = 0.518$ and $\alpha_2 = 0.897$; (a) $|A|$ and (b) $|B_1|$.

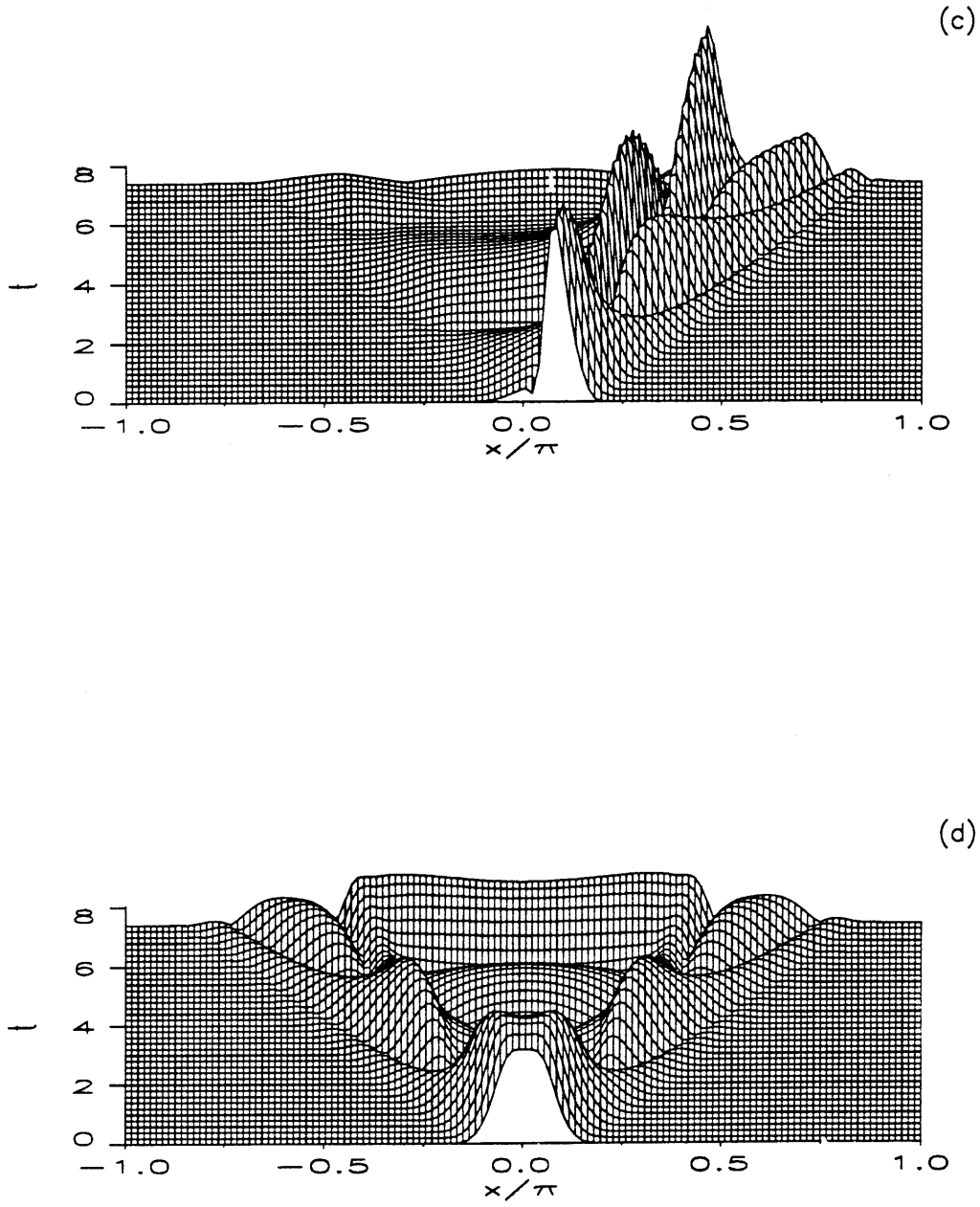

Figures 6.12c-d: Evolution of sound envelopes in *Case 2* with $\theta_1 = 60°$, $\alpha_1 = 0.518$ and $\alpha_2 = 0.897$; (c) $|B_2|$ and (d) $|B_3|$.

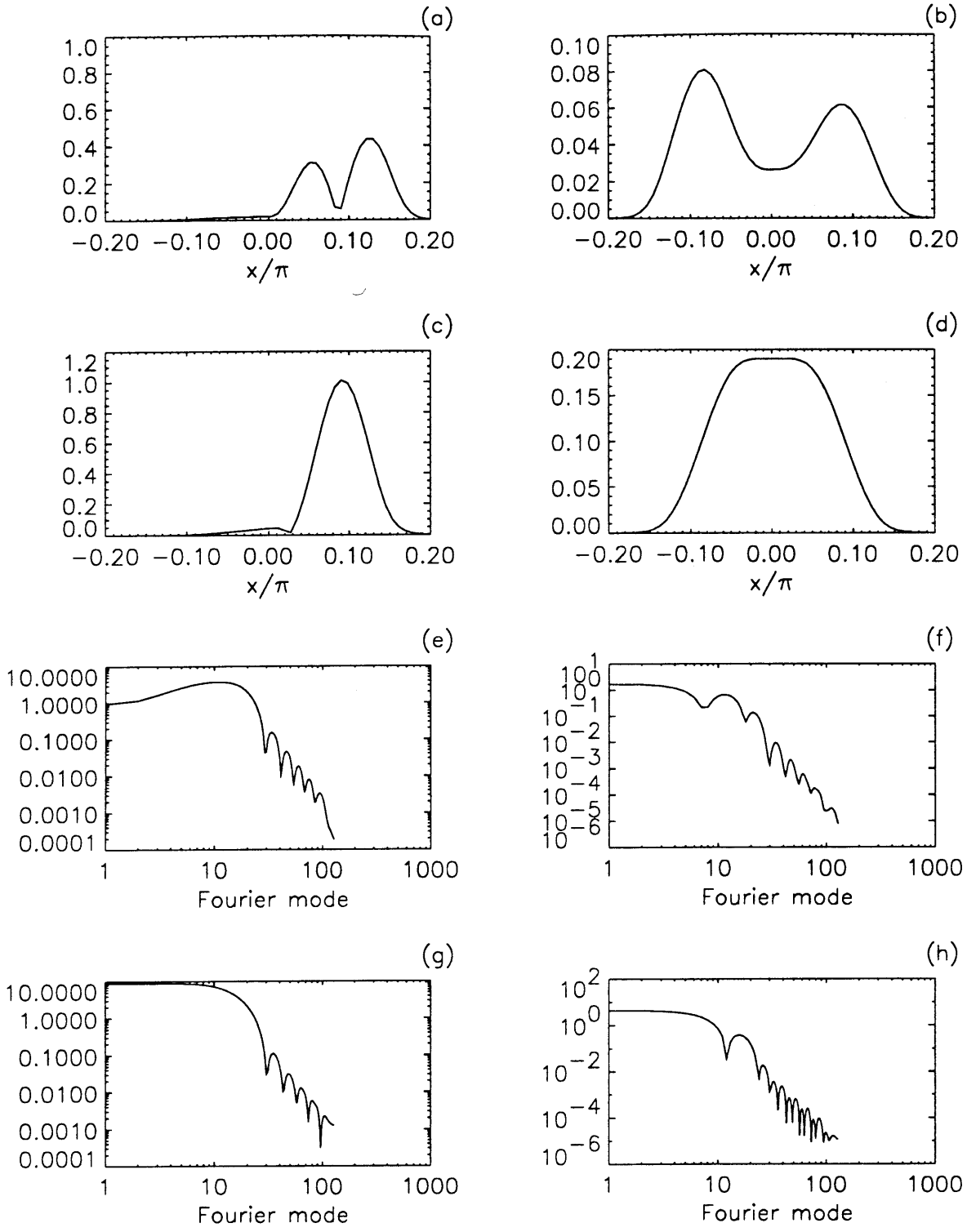

Figures 6.13a-h: Scattered sound at $t = 2$ for *Case 2*, $\theta_1 = 30°$, $\alpha_1 = 0.464$ and $\alpha_2 = 1.733$; Physical sound envelopes (a) $|A|$, (b) $|B_1|$, (c) $|B_2|$ and (d) $|B_3|$; Fourier sound envelopes (e) $|\tilde{A}|$, (f) $|\tilde{B}_1|$, (g) $|\tilde{B}_2|$ and (h) $|\tilde{B}_3|$.

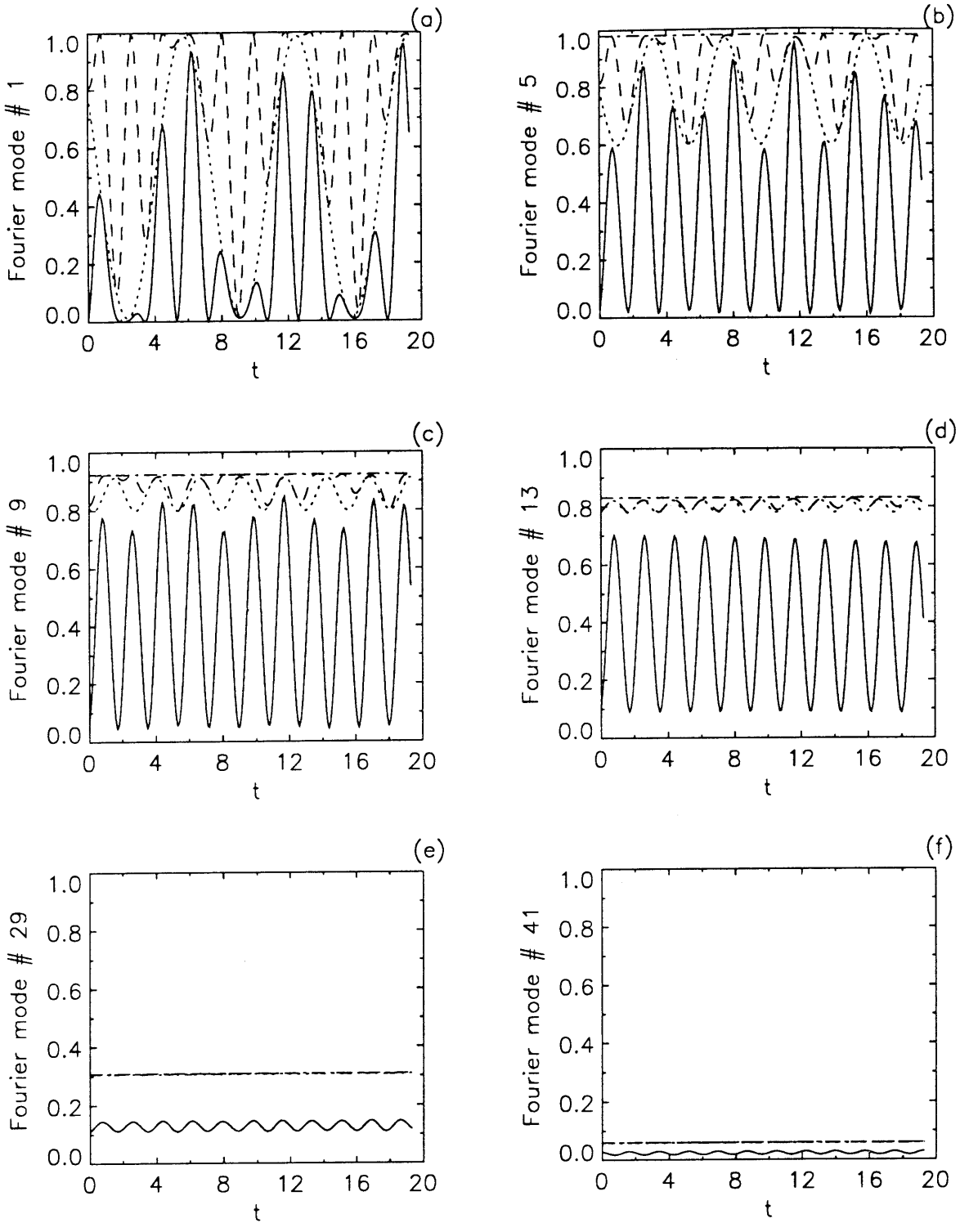

Figures 6.14a-f: Partition of Fourier energy in *Case 2* for modes 1, 5, 9, 13, 17 and 21, with $\theta_1 = 30°$, $\alpha_1 = 0.464$ and $\alpha_2 = 1.733$; $|\tilde{A}|^2$ (——), $|\tilde{A}|^2 + |\tilde{B}_2|^2$ (· · ·), $|\tilde{A}|^2 + |\tilde{B}_1|^2 + |\tilde{B}_2|^2$ (- - - - -) and $|\tilde{A}|^2 + |\tilde{B}_1|^2 + |\tilde{B}_2|^2 + |\tilde{B}_3|^2$ (·····).

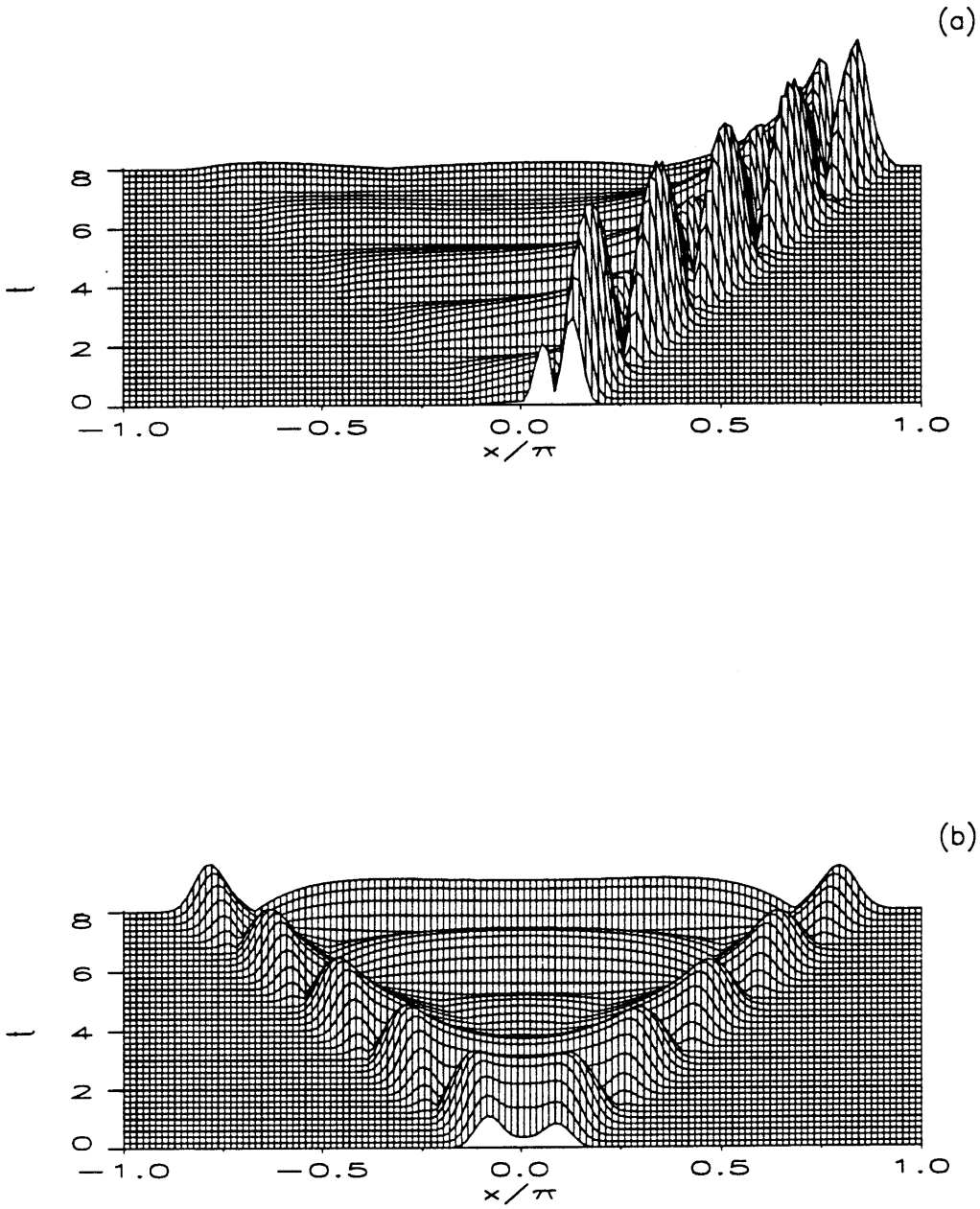

Figures 6.15a-b: Evolution of sound envelopes in *Case 2* with $\theta_1 = 30°$, $\alpha_1 = 0.464$ and $\alpha_2 = 1.733$; (a) $|A|$ and (b) $|B_1|$.

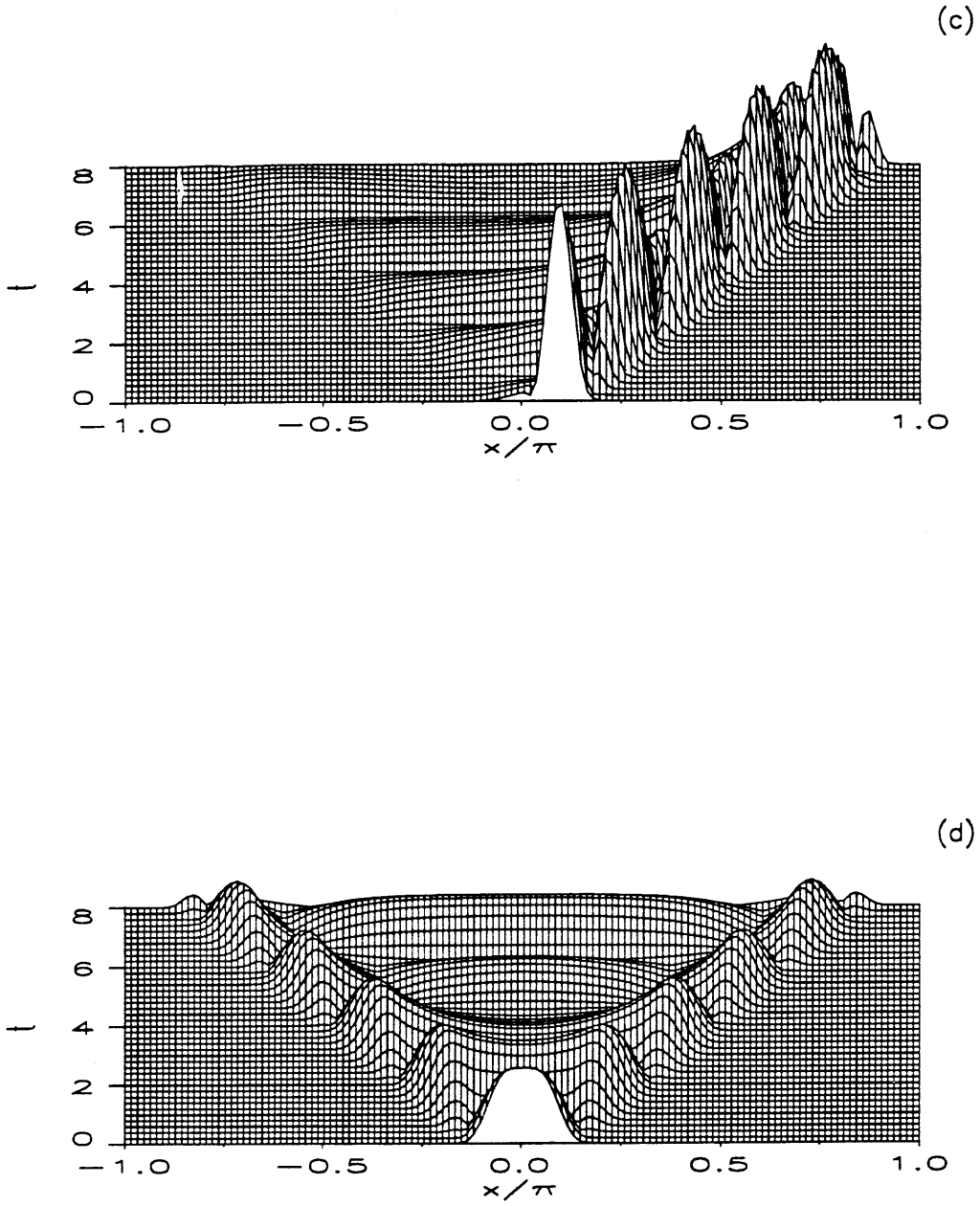

Figure 6.15c-d: Evolution of sound envelopes in *Case 2* with $\theta_1 = 30°$; $\alpha_1 = 0.464$ and $\alpha_2 = 1.733$ (c) $|B_2|$ and (d) $|B_3|$.

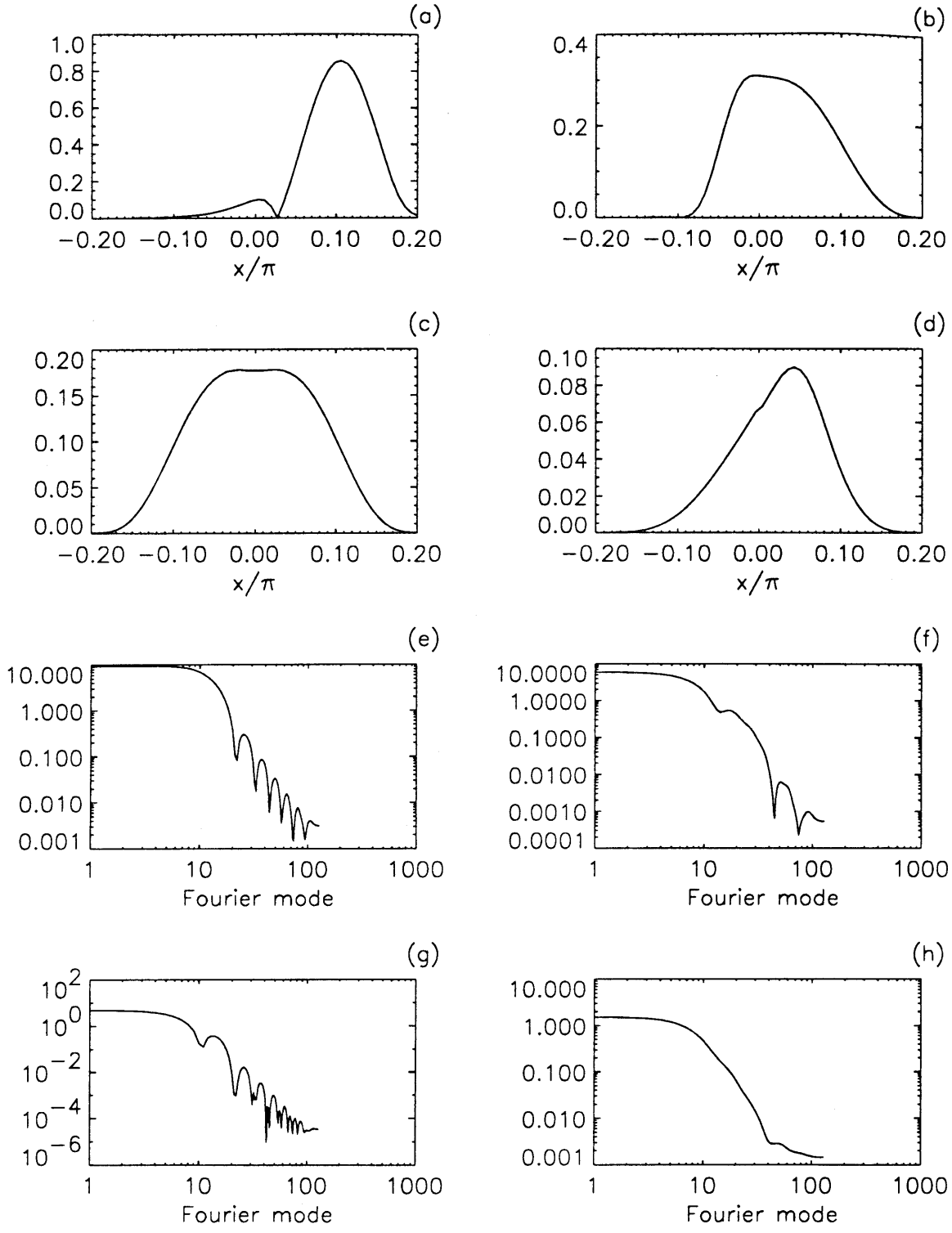

Figures 6.16a-h: Scattered sound at $t = 2$ for *Case 3*, $\theta_1 = 60°$, $\alpha_1 = 0.518$ and $\alpha_2 = 0.449$; Physical sound envelopes (a) $|A|$, (b) $|B_1|$, (c) $|B_2|$ and (d) $|B_3|$; Fourier sound envelopes (e) $|\tilde{A}|$, (f) $|\tilde{B}_1|$, (g) $|\tilde{B}_2|$ and (h) $|\tilde{B}_3|$.

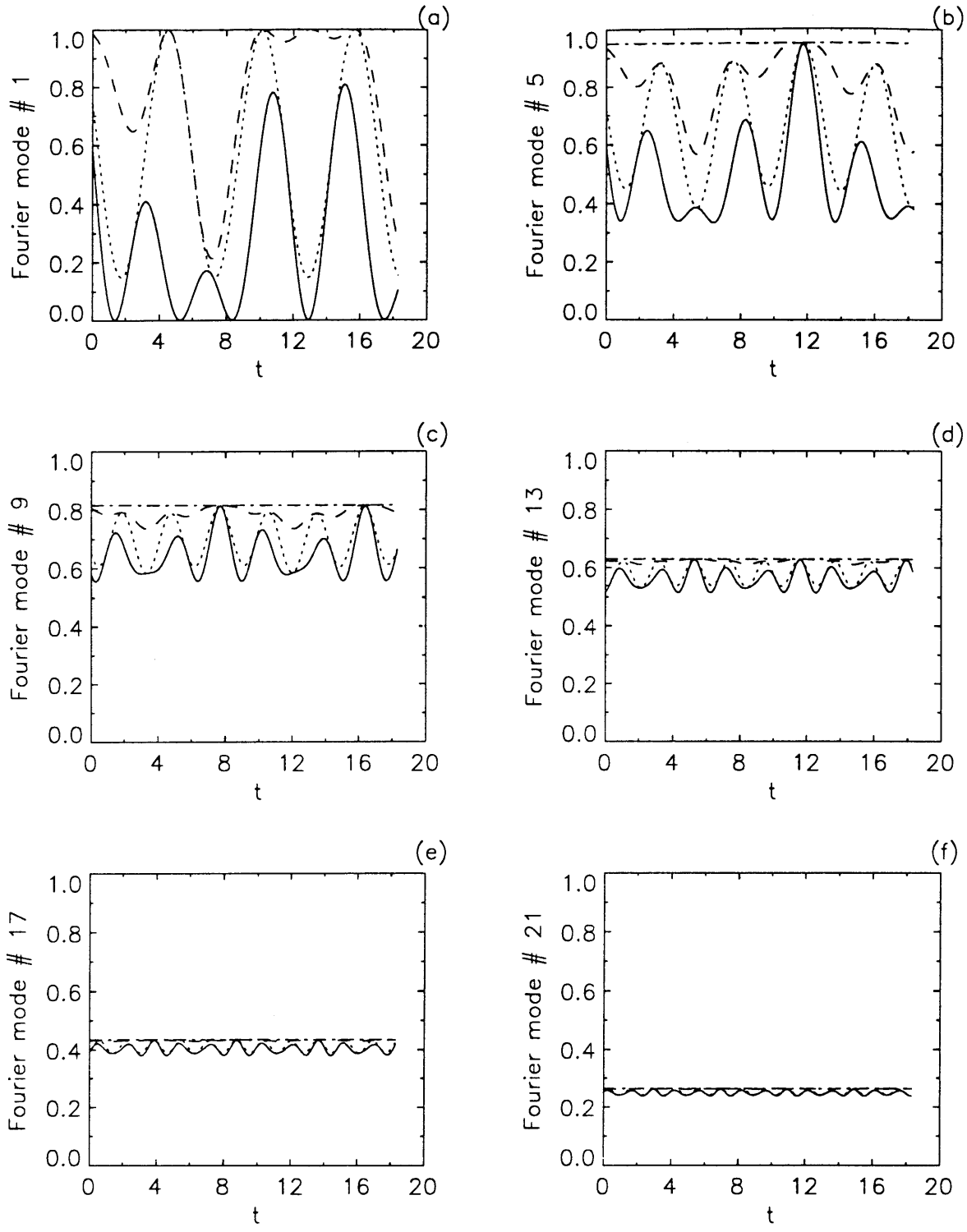

Figures 6.17a-f: Partition of Fourier energy in *Case 3* for modes 1, 5, 9, 13, 17 and 21, with $\theta_1 = 60°$, $\alpha_1 = 0.518$ and $\alpha_2 = 0.449$; $|\tilde{A}|^2$ (——), $|\tilde{A}|^2 + |\tilde{B}_2|^2$ (· · ··), $|\tilde{A}|^2 + |\tilde{B}_1|^2 + |\tilde{B}_2|^2$ (- - - - -) and $|\tilde{A}|^2 + |\tilde{B}_1|^2 + |\tilde{B}_2|^2 + |\tilde{B}_3|^2$ (·····).

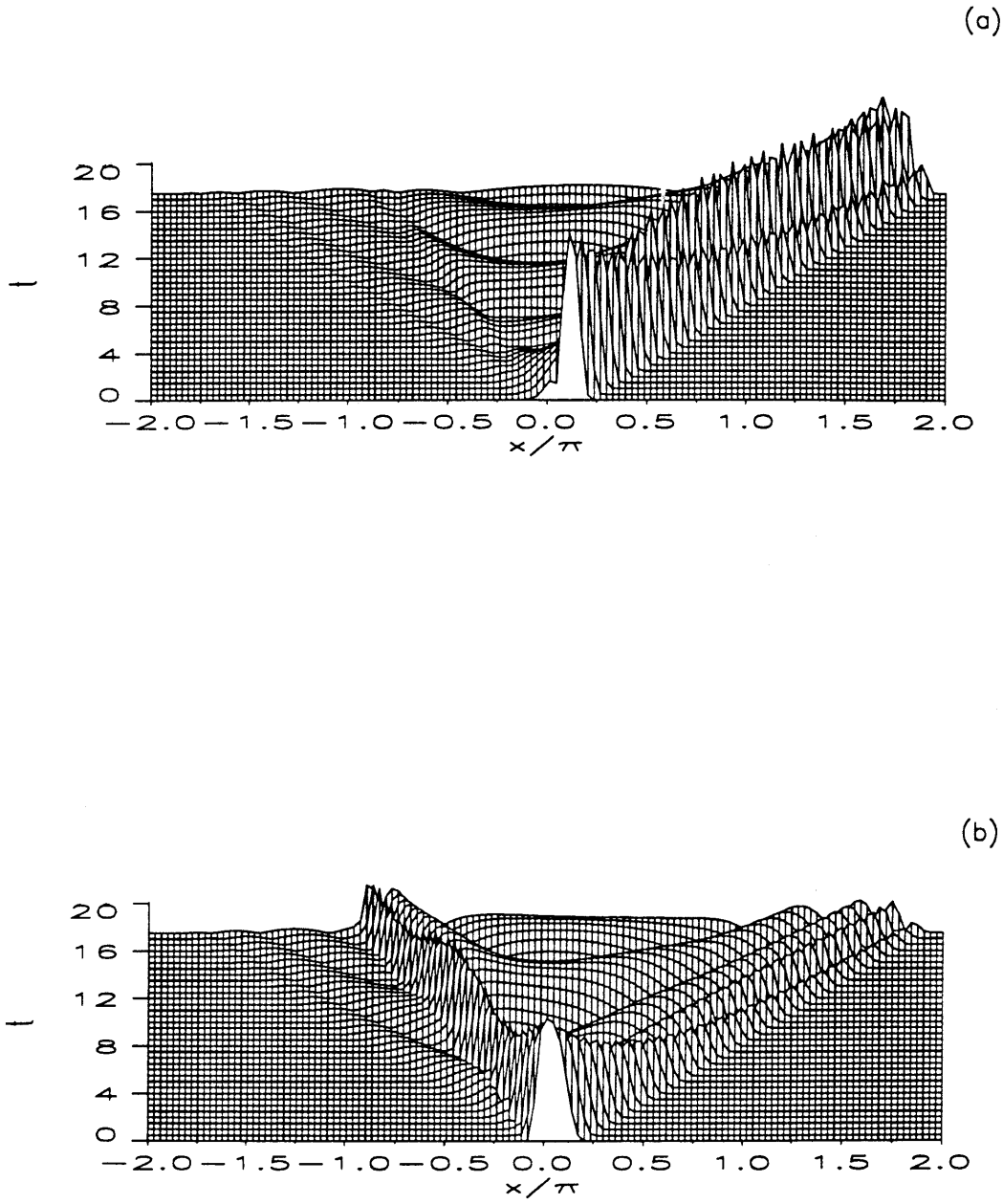

Figures 6.18a-b: Evolution of sound envelopes in *Case 3* with $\theta_1 = 60°$, $\alpha_1 = 0.518$ and $\alpha_2 = 0.449$; (a) $|A|$ and (b) $|B_1|$.

(c)

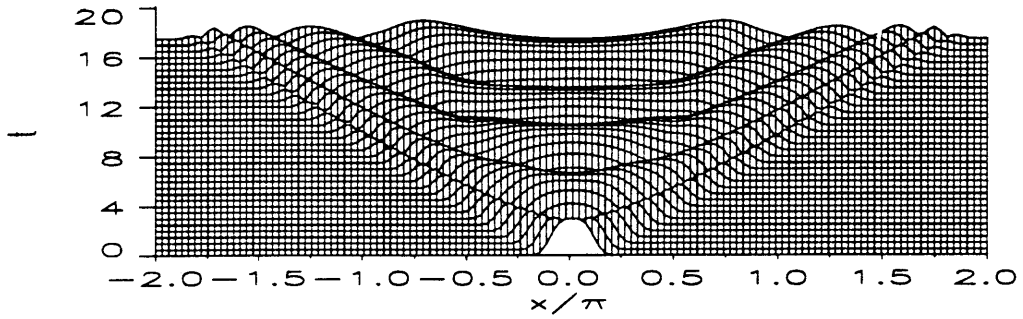

(d)

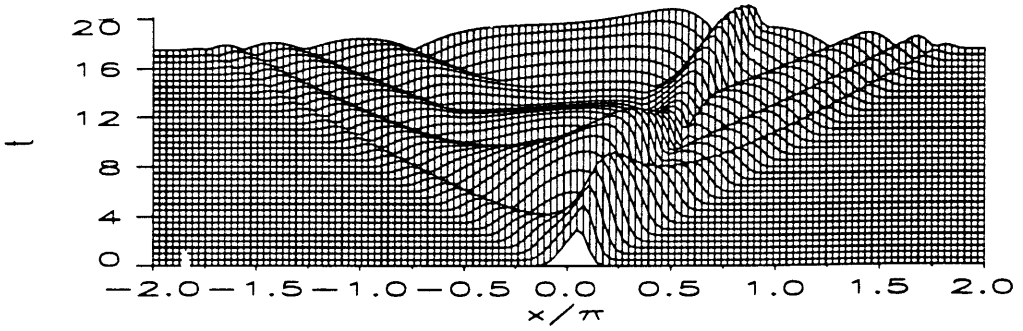

Figures 6.18c-d: Evolution of sound envelopes in *Case 3* with $\theta_1 = 60°$ $\alpha_1 = 0.518$ and $\alpha_2 = 0.449$; (c) $|B_2|$ and (d) $|B_3|$.

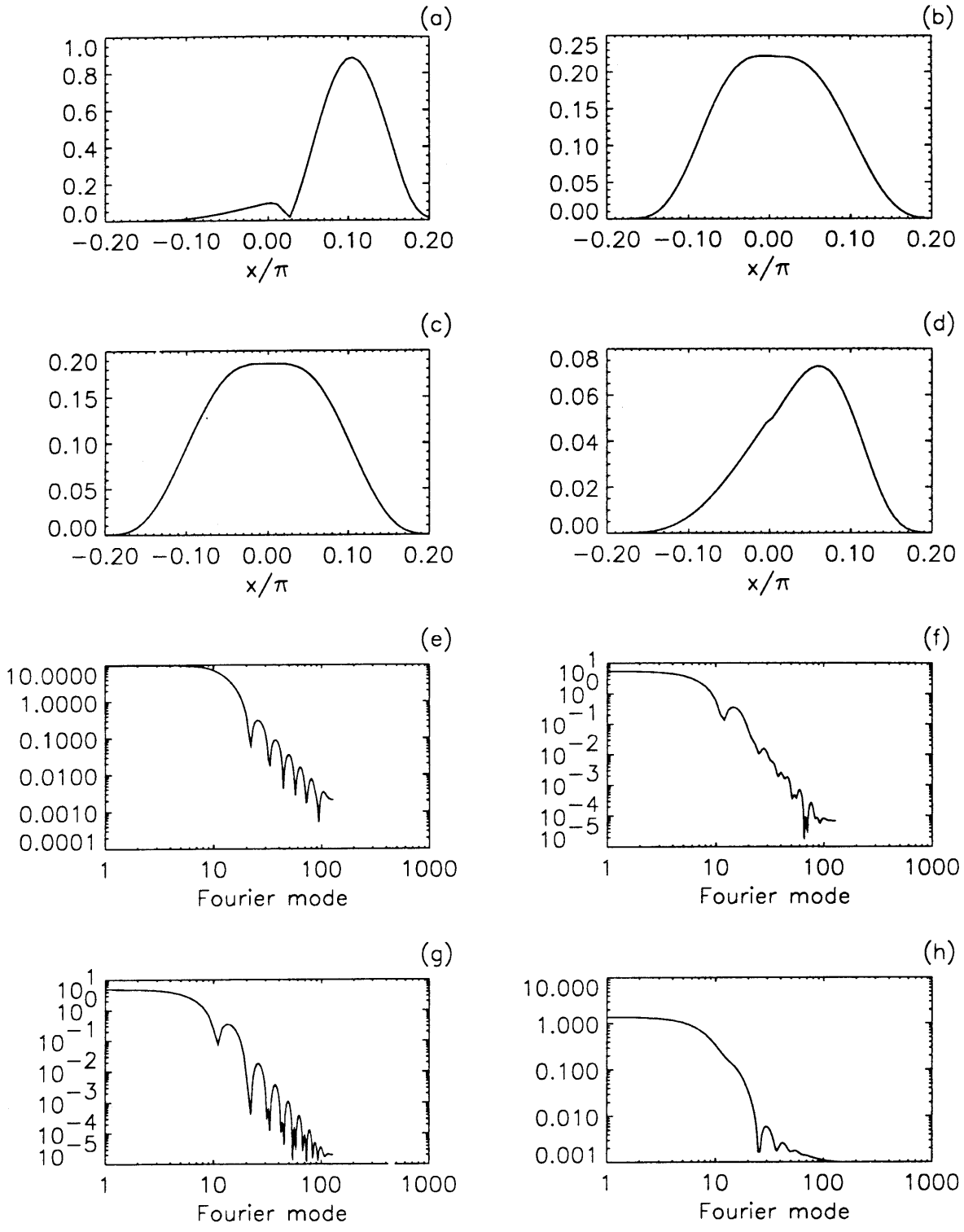

Figures 6.19a-h: Scattered sound at $t = 2$ for *Case 3*, $\theta_1 = 30°$, $\alpha_1 = 0.464$ and $\alpha_2 = 0.449$; Physical sound envelopes (a) $|A|$, (b) $|B_1|$, (c) $|B_2|$ and (d) $|B_3|$; Fourier sound envelopes (e) $|\tilde{A}|$, (f) $|\tilde{B}_1|$, (g) $|\tilde{B}_2|$ and (h) $|\tilde{B}_3|$.

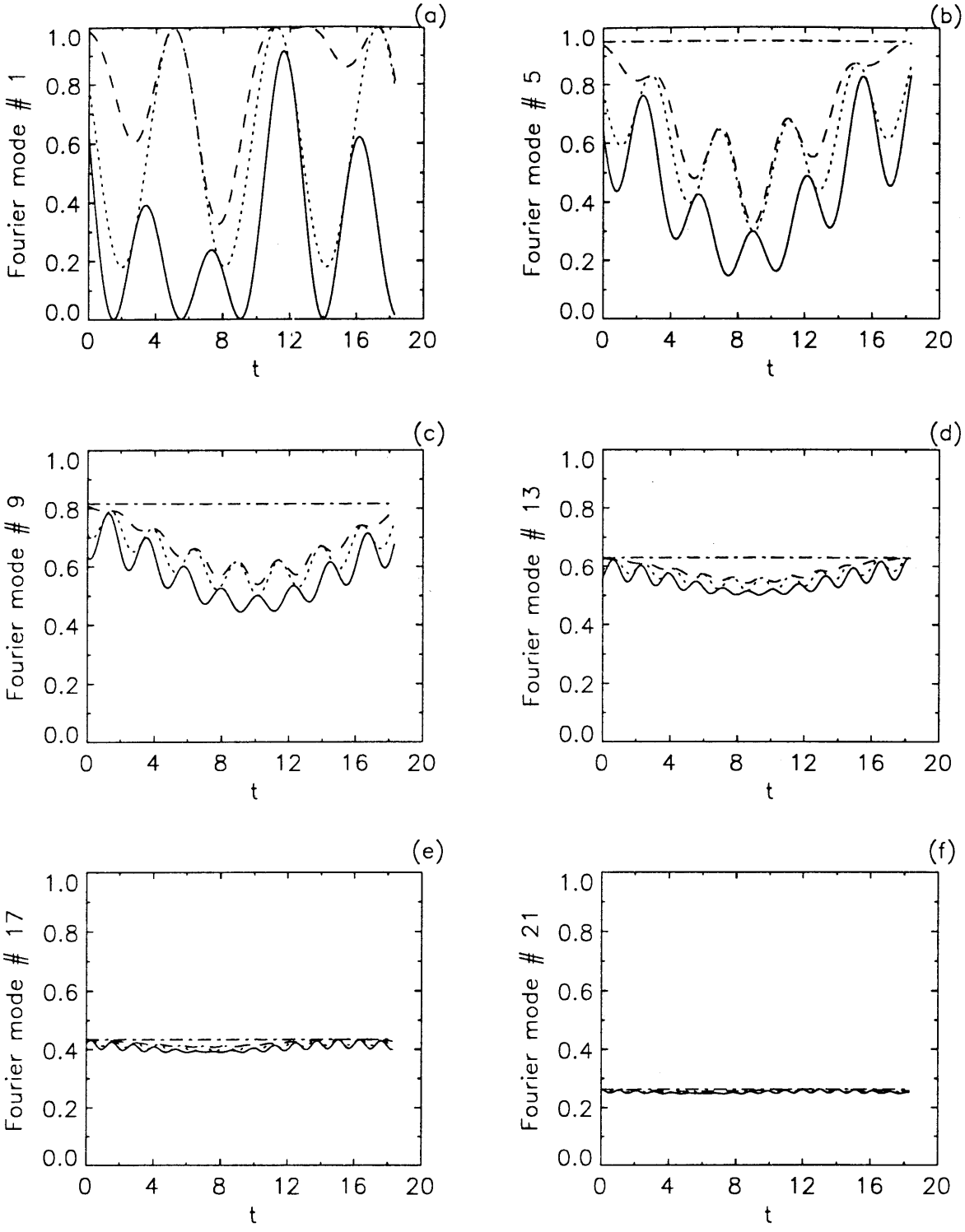

Figures 6.20a-f: Partition of Fourier energy in *Case 3* for modes 1, 5, 9, 13, 17 and 21, with $\theta_1 = 30°$, $\alpha_1 = 0.464$ and $\alpha_2 = 0.449$; $|\tilde{A}|^2$ (——), $|\tilde{A}|^2 + |\tilde{B}_2|^2$ (· · ·), $|\tilde{A}|^2 + |\tilde{B}_1|^2 + |\tilde{B}_2|^2$ (- - - - -) and $|\tilde{A}|^2 + |\tilde{B}_1|^2 + |\tilde{B}_2|^2 + |\tilde{B}_3|^2$ (·-·-·-·-·).

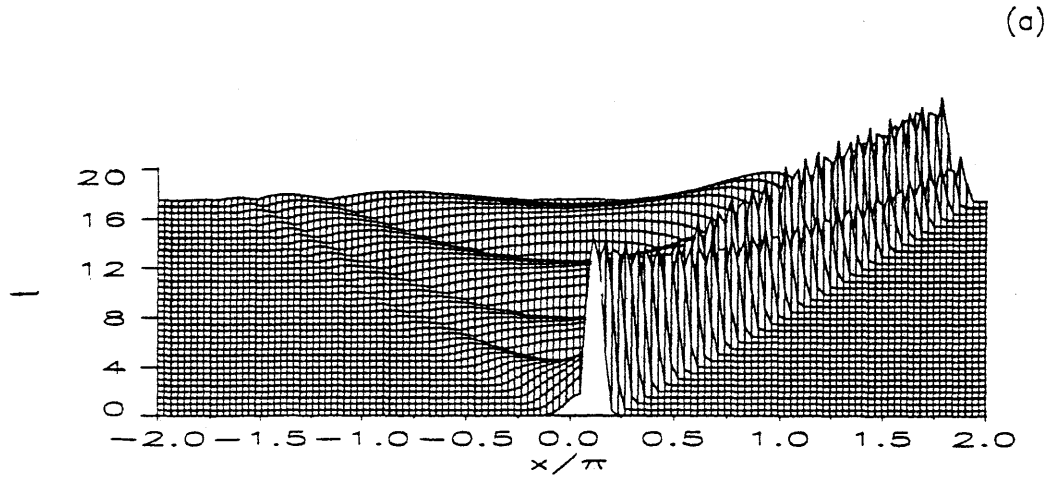

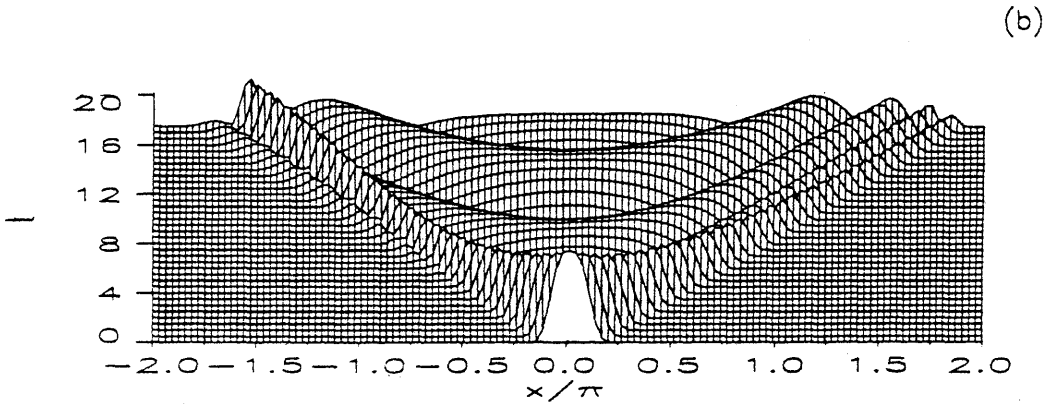

Figures 6.21a-b: Evolution of sound envelopes in *Case 3* with $\theta_1 = 30°$, $\alpha_1 = 0.464$ and $\alpha_2 = 0.449$; (a) $|A|$ and (b) $|B_1|$.

(c)

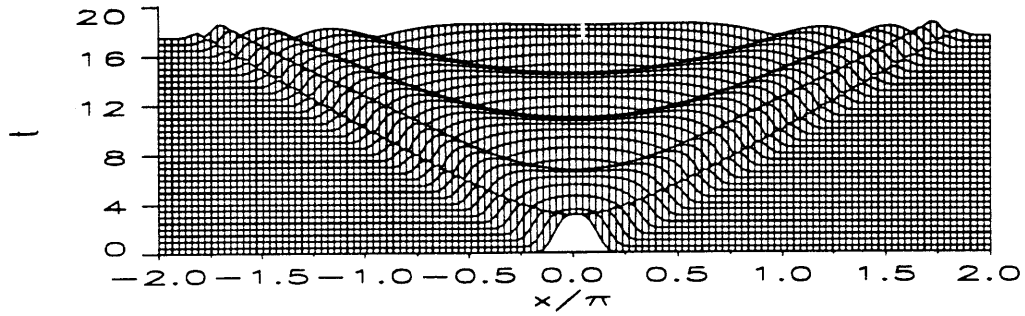

(d)

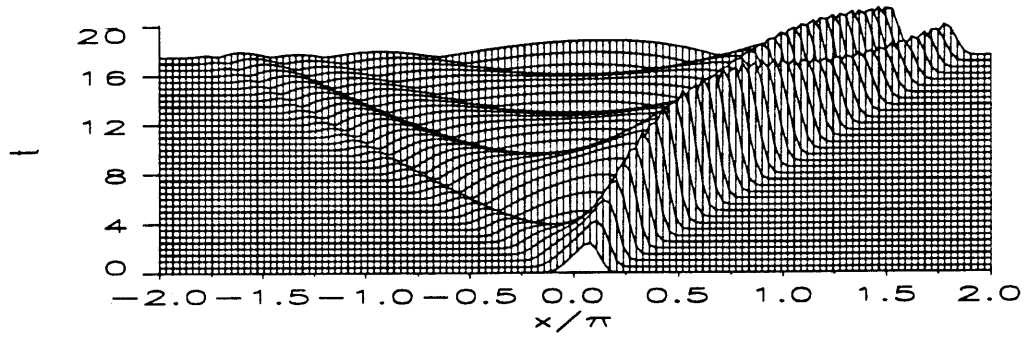

Figures 6.21c-d: Evolution of sound envelopes in *Case 3* with $\theta_1 = 30°$, $\alpha_1 = 0.464$ and $\alpha_2 = 0.449$; (c) $|B_2|$ and (d) $|B_3|$.

7. SUMMARY

We have investigated the Bragg scattering of plane sound waves in a shallow water waveguide by one or two uniform surface waves over the entire sea surface. A soft boundary condition is applied at the free surface and a hard boundary condition at the bottom. A line source generates cylindrical sound waves which are eventually transformed to a single outgoing plane sound wave far to the right and far to the left of the source, provided that the waveguide be shallow enough. The two sound waves interact resonantly with the corrugated free surface and yield strong scattered sound waves. Geometrically, the resonance condition is described in the wavenumber domain by a vector relation involving the wavenumber vectors of the incident and scattered sound waves and the wavenumber of the surface wave. In order to describe the slow modulation of the sound field at and near resonance, multiple time and space scales are introduced.

In the first example, we assume the presence of one surface wave only. The outgoing sound waves are inclined at angles θ and $\pi - \theta$ relative to the x-axis. A uniform surface wave propagating along this axis will resonate either of these two sound waves provided that its wavenumber be $m = 2\xi_0 \cos\theta$ (see figure 2.2 P27), where ξ_0 is the magnitude of the horizontal wavenumber. If the outgoing wave is inclined at angle θ with respect to the x-axis, the scattered sound wave is inclined at angle $\pi - \theta$ and vice-versa. In total, there are only two sound waves.

Owing to linearity, the scattering problem can be decomposed into a "+" problem and a "-" problem corresponding respectively to the right and left radiated sound waves from the source. Since these problems are mirror images of each other, we need only solve the "+" problem. This solution is found analytically by Fourier transform (§2.4, PP36-39). Either sound envelope may propagate both to the left and to the right (see figure 2.4a-b, P42). This phenomenon is also known to happen for surface waves propagating over a variable current or topography (Mei, 1989).

In the second example, we assume that two surface waves (with wavenumbers

$\vec{k}_{w_1}$ and $\vec{k}_{w_2}$) are inclined at an arbitrary angle. The line source radiates sound in the $\pm$ x-directions. Its envelope is slowly varying in the form of a pulse and is tapered off after a finite time. As shown in figure 3.1b, a surface wave interacts resonantly with a plane sound wave, provided that the tip of its wavenumber falls on a circle of radius ξ_0 and centered at $(\xi_0, 0)$ in the wavenumber domain (m, n). The direction of scattering is simply obtained geometrically by the vector difference $\vec{k}_{1,2} = \vec{\xi}_0 - \vec{k}_{1,2}$. In general (*Case 1*) each surface wave scatters the incident sound wave in the above manner. Therefore, there is a total of six sound waves (see figure 5.2 P79). Two special cases arise when the two surface waves satisfy certain geometrical criteria. In the first criterium, the two surface waves are crossing at right angle ($\vec{k}_{w_1} \cdot \vec{k}_{w_2} = 0$ as described in figure 3.2a, P56 *Case 2*). In addition to the two directions $\vec{k}_{1,2}$, sound is backscattered in the third direction $\vec{k}_3$ (see figure 3.2b, P57). The conjecture of Holford(1981a) is confirmed. This new scattering direction can be understood geometrically by considering the successive reflection of an incident sound ray on the crest of the first and then second surface wave (see figure 3.4, P60). Alternately, this scattering direction may be attributed to the forced surface wave $\vec{k}_1 + \vec{k}_2 = 2\vec{\xi}_0$ as suggested by Barrick(1972). Note however the important difference. This scattered sound wave is comparable in amplitude to the incident sound wave. In the second special case (*Case 3*), one surface wave is collinear to an outgoing sound wave from the source and further satisfies $\vec{k}_{w_2} = 2\xi_0$ (see figure 3.3a, P58). The third scattering direction is due to the forced surface wave $\vec{k}_{w_2} - \vec{k}_{w_1}$ and can again be deduced by considering the successive reflections on the crest of the first and then second surface wave (see figure 3.5, P61).

In both special cases, we have a quartet resonance involving two sets of two sound waves propagating in opposite directions and whose envelopes are all comparable in magnitude owing to resonance. A set of three (four) coupled linear evolution equations is derived for the sound envelopes in *Case 1* (*Cases 2* and *3*).

Next we analyse the dispersion in the sound envelopes. To this end, we postulate a solution in the form $\exp\{i(\mu x_1 + \nu y_1 - \sigma t_1)\}$ and seek a dispersion relation between σ and (μ, ν). Three (four) branches are found for *Case 1* (*Cases 2* and *3*). In the absence of surface waves, these branches reduce to straight lines and the sound envelopes are decoupled and thus non-dispersive. In the presence of surface

waves, the dispersion branches depart from these straight lines significantly only for low modulational wavenumbers ($|\mu|, |\nu| < 10$). Since μ and ν can be interpreted as corrections to the horizontal component of the acoustic wavenumber vector, we conclude that only for near perfect resonance is the coupling between the sound and surface waves strong and dispersion effects important in the sound envelopes. When μ, ν are large, resonance is weak and the scattered sound waves are small compared to the incident sound wave.

By matching the near and far fields, connection conditions are deduced for each far field amplitude and its spatial derivative, across the line source. The evolution of the sound envelopes is then computed by finite differences while the source of sound is active, and by a Fourier decomposition method for later times. The conservation of sound intensity during the latter phase is used to check the accuracy (eqs. (5.54) and (5.55) P91). The time history of the intensity in each Fourier mode is analysed. Referring to figures 6.2a-c, the distance below (above) the solid line is proportional to the sound intensity of the incident (scattered) waves. For small value of (μ, ν), the intensity of the scattered sound waves represents a large proportion (up to 100% for $\mu = 0$, see figure 6.2a) of the total sound intensity alloted initially to the Fourier mode (μ, ν). For larger values of (μ, ν), the sound intensity in the scattered waves represents only a small fraction of its initial value (see figure 6.2f on P87). The linear evolution of the sound envelopes is then investigated for long times. Again, the envelope of a unidirectional plane sound wave may propagate both to the left and to the right.

The scattering and evolution patterns are more complex for *Cases 2* and *3* than for *Case 1* due to the presence of an extra propagating front (see figures 6.6a-c, 6.12a-d and 6.18a-d).

Although the directions of scattering are identical in *Case 2* and *Case 3* once θ_1 is fixed, the evolution of the sound envelopes is determined by the relative importance of the coupling frequencies α_1 and α_2. Scattering occurs more favorably in one direction if the corresponding coupling frequency clearly dominates.

We emphasize once more that the present work is about a resonance mechanism which leads to a strong scattered sound field. Although in nature all scattered

sound waves are diminished by dissipation at the bottom, strongly scattered waves should still be more easily detected than weakly scattered waves by non-resonant mechanisms.

Before contemplating any field studies, confirmation of the theory must be undertaken in a laboratory where the reflective bottom boundary condition can be more easily modelled. Experimental confirmation of a similar theory for surface wave scattering by bottom bars has already been obtained (Hara & Mei, 1989).

Extensions to a deeper waveguide is worthwhile. More propagating acoustic modes are then possible. A surface wave may be coupled with two or more distinct acoustic modes. Possibilities for resonance are greater.

Extensions to the radiation from a point source is also desirable since such devices are more easily implemented in the field.

We have seen that an oblique plane sound wave resonates only one component ($m = 2\xi_0 \cos\theta$) of the spectrum of long crested surface waves. Thus, by varying the angle θ, we may resonate any component within $[0, 2\xi_0]$. In this way, one may infer from the scattered sound field the properties of the resonant surface wave, and obtain relevant information about the frequency spectrum.

Bibliography for Part 1

Anand G.V. and M.K. George, 1986. Normal Mode Sound Propagation in an Ocean with Sinusoidal Surface Waves *J. Acoust. Soc. Am.* **80**(1) 238-243.

Barrick D.E., Remote Sensing of Sea State by Radar in *Remote Sensing of the Troposphere* . Edited by V.E. Derr, US Government Printing Office, Washington, DC 1972.

Bass F.G., I.M. Fuks, A.E. Kalmykov, I.E. Ostrovsky and A.D. Rosenberg, 1968. Very High Frequency Radiowave Scattering by a Disturbed Sea Surface *IEEE Trans.* **AP-16** 554-568.

Bass F.G. and I.M. Fuks, *Wave Scattering from Statistically Rough Surfaces*, Pergamon New York, 1978.

Bender C.M. and Orszag S.A., 1978. *Advanced Mathematical Methods for Scientists and Engineers.* McGraw Hill.

Brekhovskikh L. and Y. Lysanov. *Fundamentals of Ocean Acoustics* Springer-Verlag, Berlin Heidelberg New York, 1982.

Chuang S.L. and J.A. Kong, 1981. Wave Scattering from Periodic Surfaces *Procceding of the IEEE*, **69** No 9 1,132-1,144.

Crombie D.D., 1955. Doppler Spectrum of Sea Echo at 13.56 MKc/s *Nature* **175** 681-682.

DeSanto J.A., 1981. Scattering from A Perfectly Reflecting Arbitrary Periodic Surface: An Exact Solution *Radio Science* **16** 1,315-1,326.

Erdélyi A. ed., Magnus, W., Berhettinger, F.O. & Tricomi, F.G. 1953. *Bateman Manuscript Project.* California Institute of Technology.

Feinberg E.L. *Propagation of Radiowaves Along the Earth's Surface*, Izd. Akad. Nauk SSSR, Moscow, 1961.

Fortuin L., 1970. "Survey of Literature on Reflection and Scattering of Sound Waves at the Sea Surface" *J. Acoust. Soc. Am.* **47** 1,209-1,228.

Hasselmann K., 1966. Feynman Diagrams and Interaction Rules for Wave-Wave Scattering *Rev. Geophys.* **4** 1-32.

Holford R.L., 1981a. Scattering of Sound Waves at the Ocean Surface: A diffraction Theory *J. Acoust. Soc. Am.* **70**(4) 1,103-,1,115.

Holford R.L., 1981b. "Scattering of Sound Waves at a Periodic Pressure Release Surface: An Exact Solution" *J. Acoust. Soc. Am.* **70**(4) 1,116-,1,128.

Korn G.A. and Korn T.M., 1968. *Mathematical Handbook for Scientists and Engineers*, second edition. McGraw-Hill.

Lakhtakia A., V.K. Varadan and V.V. Varadan, 1985. Scattering by a Partially Illuminated, Doubly Periodic, Doubly Infinite Surface. *J. Acoust. Soc. Am.* **77**(6) 1,999-2,004.

Mc Daniel S.T. and A.D. Gorman, 1983. An Examination of the Composite-Roughness Scattering Model *J. Acoust. Soc. Am.* **73**(5) 1,476-1486.

Medwin H. and G.L. D'Spain, 1986. Near Grazing Low Frequency Propagation over Randomly Rough, Rigid Surfaces *J. Acoust. Soc. Am.* **79** 657-665.

Mei C.C. *The Applied Dysnamics of Ocean Surface Waves*, Second Edition, World Scientific, 1989.

Mei C.C. and Naciri M., 1991. "Bragg Scattering of Sound by Surface Waves in Shallow Water" *Wave Motion* **13** 353-368.

Naciri M., 1987. *Bragg Scattering by Periodic Boundaries*, Master Thesis, MIT.

Naciri M. and Mei C.C., 1988."Bragg Scattering of Surface Waves on a Doubly Periodic Seabed" *J. Fluid Mechanics* **192** 51-74.

Nayfeh, A.H., 1974. Sound Waves in Two-Dimensional Ducts with Sinusoidal Walls *J. Acoust. Soc. Am.* **56** 768-770.

Nayfeh, A.H. and O.R. Asfar, 1974. Parallel-Plate wave guide with Sinusoidally Perturbed Boundaries *J. Appl. Phys.* **45** 4,794-4,800.

Nayfeh, A.H. and O.A. Kandil, 1978. Propagation of Waves in Cylindrical Hard-Walled Ducts with Generally Weak Undulation *AIAA J.* **16** 1,041-1,045.

Phillips O.M., *The Dynamics of the Upper Ocean*, Cambridge University Press, Second Edition, 1977.

Rice S.O., 1951. Reflection of Electromagnetic Waves from Slightly Rough Surfaces *Comm. Pure Appl. Math.* **4** 351-378.

Salant R.F., 1973. Acoustic Propagation in Waveguides with Sinusoidal Walls *J. Acoust. Soc. Am.* **53**(2) 504-507.

Samuels J.C., 1959. On Propagation of Waves in Slightly Rough Ducts *J. Acoust. Soc. Am.* **31**(3) 319-325.

Strutt J.W. (Lord Rayleigh), *Scientific Papers* Vol. V-VI, Dover, 1964.

Uretsky J.L., 1954. The Scattering of Plane Waves from Periodic Surfaces *Ann. Phys.* **1** 400-427.

Wright J.W., 1968. A New Model of Sea Clutter *IEEE Trans.* **AP-16** 217-223.

Figure Captions for Part 1

Figure 2.1: Geometry of the acoustic waveguide.

Figure 2.2: Geometrical interpretation of the resonance condition for the scattered sound wave in the (m,n) wavenumber domain. $\vec{\xi}_0$ and $\vec{k}_1$ are respectively the horizontal wavenumber vectors of the incident and scattered sound waves.

Figure 2.3: Contour in the complex ξ plane used to perform the integration of (2.37).

Figures 2.4a-b: Evolution of sound envelopes in the right-radiation problem with $\theta = 0$; (a) $|A^+|$, (b) $|B^+|$.

Figures 2.5a-b: Evolution of sound envelopes in the left-radiation problem with $\theta = 0$; (a) $|A^-|$, (b) $|B^-|$.

Figures 2.6a-b: Evolution of sound envelopes in the two-way radiation problem with $\theta = 0$; (a) $|A|$, (b) $|B|$.

Figures 2.7a-b: Evolution of sound envelopes in the right-radiation problem with $\theta = 30°$; (a) $|A^+|$, (b) $|B^+|$.

Figures 2.7c-d: Evolution of sound envelopes in the two-way radiation problem with $\theta = 30°$; (c) $|A|$, (d) $|B|$.

Figures 2.8a-b: Evolution of sound envelopes in the right-radiation problem with $\theta = 45°$; (a) $|A^+|$, (b) $|B^+|$.

Figures 2.8c-d: Evolution of sound envelopes in the two-way radiation problem with $\theta = 45°$; (c) $|A|$, (d) $|B|$.

Figures 2.9a-b: Evolution of sound envelopes in the right-radiation problem with $\theta = 60°$; (a) $|A^+|$, (b) $|B^+|$.

Figures 2.9c-d: Evolution of sound envelopes in the two-way radiation problem with $\theta = 60°$; (c) $|A|$, (d) $|B|$.

Figure 3.1a: Geometry of the sound and surface waves for *Case 1.* $\vec{\xi}_0$ represents the horizontal component of the sound wavenumber for the acoustic mode $\ell = 0$.

Figure 3.1b: Resonance condition for *Case 1.*

Figure 3.2a: Geometry of the sound and surface waves for *Case 2.*

Figure 3.2b: Resonance condition for *Case 2.*

Figure 3.3a: Geometry of the sound and surface waves for *Case 3.*

Figure 3.3b: Resonance condition for *Case 3.*

Figure 3.4: Schematic of multiple scattering for *Case 2*.

Figure 3.5: Schematic of multiple scattering for *Case 3*.

Figure 4.1: Dispersion relation for *Case 1* with $k_{w_2}a_2 = 0.1$, $\theta_1 = \pi/3$, $\theta_2 = -\pi/6$ and $k_{w_1}a_1 = 0.05$ ($\cdots\cdots$), $k_{w_1}a_1 = 0.1$ (- - - - -), $k_{w_1}a_1 = 0.15$ (-·-·-·).

Figure 4.2: Dispersion relation for *Case 1* with $k_{w_2}a_2 = 0.1$, $\theta_1 = -\theta_2 = \pi/3$ and $k_{w_1}a_1 = 0.05$ ($\cdots\cdots$), $k_{w_1}a_1 = 0.1$ (- - - - -), $k_{w_1}a_1 = 0.15$ (-·-·-·).

Figure 4.3: Dispersion relation for *Case 2* with $k_{w_2}a_2 = 0.1$, $\theta_1 = \pi/3$ and $k_{w_1}a_1 = 0.05$ ($\cdots\cdots$), $k_{w_1}a_1 = 0.1$ (- - - - -), $k_{w_1}a_1 = 0.15$ (-·-·-·).

Figure 4.4: Dispersion relation for *Case 3* with $k_{w_2}a_2 = 0.1$, $\theta_1 = \pi/3$ and $k_{w_1}a_1 = 0.05$ ($\cdots\cdots$), $k_{w_1}a_1 = 0.1$ (- - - - -), $k_{w_1}a_1 = 0.15$ (-·-·-·).

Figure 5.1: Geometry of slightly inclined line source.

Figure 5.2: Scattering geometry for *Case 1* in the presence of two outgoing plane sound waves.

Figure 5.3: Scattering geometry for *Case 2* in the presence of two outgoing plane sound waves.

Figure 5.4: Scattering geometry for *Case 3* in the presence of two outgoing plane sound waves.

Figures 6.1a-f: Scattered sound at $t = 2$ for *Case 1* and $\theta_1 = -\theta_2 = 60°$ and $\alpha_1 = \alpha_2 = 0.518$; Physical sound envelopes (a) $|A|$, (b) $|B_1|$ and (c) $|B_2|$; Fourier sound envelopes (d) $|\tilde{A}|$, (e) $|\tilde{B}_1|$ and (f) $|\tilde{B}_2|$.

Figures 6.2a-f: Partition of Fourier energy in *Case 1* for modes 1, 5, 9, 13, 17 and 21, with $\theta_1 = -\theta_2 = 60°$ and $\alpha_1 = \alpha_2 = 0.518$; $|\tilde{A}|^2$ (——), $|\tilde{A}|^2 + |\tilde{B}_1|^2$ ($\cdots$) and $|\tilde{A}|^2 + |\tilde{B}_1|^2 + |\tilde{B}_2|^2$ (- - - - -).

Figures 6.3a-b: Evolution of sound envelopes in *Case 1* with $\theta_1 = -\theta_2 = 60°$ and $\alpha_1 = \alpha_2 = 0.518$; (a) $|A|$ and (b) $|B_1|$.

Figure 6.3c: Evolution of sound envelope $|B_2|$ in *Case 1* with $\theta_1 = -\theta_2 = 60°$ and $\alpha_1 = \alpha_2 = 0.518$.

Figures 6.4a-f: Scattered sound at $t = 2$ for *Case 1*, $\theta_1 = 60°$ and $\theta_2 = 45°$, $\alpha_1 = 0.518$ and $\alpha_2 = 0.486$; Physical sound envelopes (a) $|A|$, (b) $|B_1|$ and (c) $|B_2|$; Fourier sound envelopes (c) $|\dot{A}|$, (d) $|\tilde{B}_1|$ and (e) $|\tilde{B}_2|$.

Figures 6.5a-f: Partition of Fourier energy in *Case 1* for modes 1, 5, 9, 13, 17 and 21, with $\theta_1 = 60°, \theta_2 = 45°$, $\alpha_1 = 0.518$ and $\alpha_2 = 0.486$; $|\tilde{A}|^2$ (——), $|\tilde{A}|^2 + |\tilde{B}_1|^2$ ($\cdots$) and $|\tilde{A}|^2 + |\tilde{B}_1|^2 + |\tilde{B}_2|^2$ (- - - - -).

Figures 6.6a-b: Evolution of sound envelopes in *Case 1* with $\theta_1 = 60°$, $\theta_2 = 45°$ $\alpha_1 = 0.518$ and $\alpha_2 = 0.486$; (a) $|A|$ and (b) $|B_1|$.

Figure 6.6c: Evolution of sound envelope $|B_2|$ *Case 1* with $\theta_1 = 60°$, $\theta_2 = 45°$, $\alpha_1 = 0.518$ and $\alpha_2 = 0.486$.

Figures 6.7a-f: Scattered sound at $t = 2$ for *Case 1*, $\theta_1 = 60°$ and $\theta_2 = -30°$, $\alpha_1 = 0.518$ and $\alpha_2 = 0.464$; Physical sound envelopes (a) $|A|$, (b) $|B_1|$ and (c) $|B_2|$; Fourier sound envelopes (c) $|\tilde{A}|$, (d) $|\tilde{B}_1|$ and (e) $|\tilde{B}_2|$.

Figures 6.8a-f: Partition of Fourier energy in *Case 1* for modes 1, 5, 9, 13, 17 and 21, with $\theta_1 = 60°, \theta_2 = -30°$, $\alpha_1 = 0.518$ and $\alpha_2 = 0.464$; $|\tilde{A}|^2$ (——), $|\tilde{A}|^2 + |\tilde{B}_1|^2$ ($\cdots$) and $|\tilde{A}|^2 + |\tilde{B}_1|^2 + |\tilde{B}_2|^2$ (- - - - -).

Figures 6.9a-b: Evolution of sound envelopes in *Case 1* with $\theta_1 = 60°$, $\theta_2 = -30°$, $\alpha_1 = 0.518$ and $\alpha_2 = 0.464$; (a) $|A|$ and (b) $|B_1|$.

Figure 6.9c: Evolution of sound envelope $|B_2|$ in *Case 1* with $\theta_1 = 60°$, $\theta_2 = -30°$ $\alpha_1 = 0.518$ and $\alpha_2 = 0.464$.

Figures 6.10a-h: Scattered sound at $t = 2$ for *Case 2*, $\theta_1 = 60°$, $\alpha_1 = 0.518$ and $\alpha_2 = 0.897$; Physical sound envelopes (a) $|A|$, (b) $|B_1|$, (c) $|B_2|$ and (d) $|B_3|$; Fourier sound envelopes (e) $|\tilde{A}|$, (f) $|\tilde{B}_1|$, (g) $|\tilde{B}_2|$ and (h) $|\tilde{B}_3|$.

Figures 6.11a-f: Partition of Fourier energy in *Case 2* for modes 1, 5, 9, 13, 17 and 21, with $\theta_1 = 60°$, $\alpha_1 = 0.518$ and $\alpha_2 = 0.897$; $|\tilde{A}|^2$ (——), $|\tilde{A}|^2 + |\tilde{B}_2|^2$ ($\cdots$), $|\tilde{A}|^2 + |\tilde{B}_1|^2 + |\tilde{B}_2|^2$ (- - - - -) and $|\tilde{A}|^2 + |\tilde{B}_1|^2 + |\tilde{B}_2|^2 + |\tilde{B}_3|^2$ (--------).

Figures 6.12a-b: Evolution of sound envelopes in *Case 2* with $\theta_1 = 60°$, $\alpha_1 = 0.518$ and $\alpha_2 = 0.897$; (a) $|A|$ and (b) $|B_1|$.

Figures 6.12c-d: Evolution of sound envelopes in *Case 2* with $\theta_1 = 60°$, $\alpha_1 = 0.518$ and $\alpha_2 = 0.897$; (a) $|B_2|$ and (b) $|B_3|$.

Figures 6.13a-h: Scattered sound at $t = 2$ for *Case 2*, $\theta_1 = 30°$, $\alpha_1 = 0.464$ and $\alpha_2 = 1.733$; Physical sound envelopes (a) $|A|$, (b) $|B_1|$, (c) $|B_2|$ and (d) $|B_3|$; Fourier sound envelopes (e) $|\tilde{A}|$, (f) $|\tilde{B}_1|$, (g) $|\tilde{B}_2|$ and (h) $|\tilde{B}_3|$.

Figures 6.14a-f: Partition of Fourier energy in *Case 2* for modes 1, 5, 9, 13, 17 and 21, with $\theta_1 = 30°$, $\alpha_1 = 0.464$ and $\alpha_2 = 1.733$; $|\tilde{A}|^2$ (——), $|\tilde{A}|^2 + |\tilde{B}_2|^2$ ($\cdots$), $|\tilde{A}|^2 + |\tilde{B}_1|^2 + |\tilde{B}_2|^2$ (- - - - -) and $|\tilde{A}|^2 + |\tilde{B}_1|^2 + |\tilde{B}_2|^2 + |\tilde{B}_3|^2$ (--------).

Figures 6.15a-b: Evolution of sound envelopes in *Case 2* with $\theta_1 = 30°$, $\alpha_1 = 0.464$ and $\alpha_2 = 1.733$; (a) $|A|$ and (b) $|B_1|$.

Figures 6.15c-d: Evolution of sound envelopes in *Case 2* with $\theta_1 = 30°$; $\alpha_1 = 0.464$ and $\alpha_2 = 1.733$ (a) $|B_2|$ and (b) $|B_3|$.

Figures 6.16a-h: Scattered sound at $t = 2$ for *Case 3*, $\theta_1 = 60°$, $\alpha_1 = 0.518$ and $\alpha_2 = 0.449$; Physical sound envelopes (a) $|A|$, (b) $|B_1|$, (c) $|B_2|$ and (d) $|B_3|$; Fourier sound envelopes (e) $|\tilde{A}|$, (f) $|\tilde{B}_1|$, (g) $|\tilde{B}_2|$ and (h) $|\tilde{B}_3|$.

Figures 6.17a-f: Partition of Fourier energy in *Case 3* for modes 1, 5, 9, 13, 17 and 21, with $\theta_1 = 60°$, $\alpha_1 = 0.518$ and $\alpha_2 = 0.449$; $|\tilde{A}|^2$ (——), $|\tilde{A}|^2 + |\tilde{B}_2|^2$ ($\cdots$), $|\tilde{A}|^2 + |\tilde{B}_1|^2 + |\tilde{B}_2|^2$ (- - - - -) and $|\tilde{A}|^2 + |\tilde{B}_1|^2 + |\tilde{B}_2|^2 + |\tilde{B}_3|^2$ (--------).

Figures 6.18a-b: Evolution of sound envelopes in *Case 3* with $\theta_1 = 60°$, $\alpha_1 = 0.518$ and $\alpha_2 = 0.449$; (a) $|A|$ and (b) $|B_1|$.

Figures 6.18c-d: Evolution of sound envelopes in *Case 3* with $\theta_1 = 60°$ $\alpha_1 = 0.518$ and $\alpha_2 = 0.449$; (a) $|B_2|$ and (b) $|B_3|$.

Figures 6.19a-h: Scattered sound at $t = 2$ for *Case 3*, $\theta_1 = 30°$, $\alpha_1 = 0.464$ and $\alpha_2 = 0.449$; Physical sound envelopes (a) $|A|$, (b) $|B_1|$, (c) $|B_2|$ and (d) $|B_3|$; Fourier sound envelopes (e) $|\tilde{A}|$, (f) $|\tilde{B}_1|$, (g) $|\tilde{B}_2|$ and (h) $|\tilde{B}_3|$.

Figures 6.20a-f: Partition of Fourier energy in *Case 3* for modes 1, 5, 9, 13, 17 and 21, with $\theta_1 = 30°$, $\alpha_1 = 0.464$ and $\alpha_2 = 0.449$; $|\tilde{A}|^2$ (——), $|\tilde{A}|^2 + |\tilde{B}_2|^2$ ($\cdots$), $|\tilde{A}|^2 + |\tilde{B}_1|^2 + |\tilde{B}_2|^2$ (- - - - -) and $|\tilde{A}|^2 + |\tilde{B}_1|^2 + |\tilde{B}_2|^2 + |\tilde{B}_3|^2$ (·-·-·-·-·).

Figures 6.21a-b: Evolution of sound envelopes in *Case 3* with $\theta_1 = 30°$, $\alpha_1 = 0.464$ and $\alpha_2 = 0.449$; (a) $|A|$ and (b) $|B_1|$.

Figures 6.21c-d: Evolution of sound envelopes in *Case 3* with $\theta_1 = 30°$, $\alpha_1 = 0.464$ and $\alpha_2 = 0.449$; (a) $|B_2|$ and (b) $|B_3|$.

Appendix A: Estimate of Time Scales

The contrast between the time scales of the sound and surface waves can be estimated from their respective dispersion relations $\omega = Ck$ and $\omega_w = \sqrt{gk_w}$ (in deep water). The frequency ratio is therefore

$$\frac{\omega_w}{\omega} = \frac{k_w}{k}\sqrt{\frac{g}{k_w}}\frac{1}{C} = \frac{k_w}{k}\frac{c_w}{C} \tag{A.1}$$

where c_w is the phase velocity of the surface wave. For Bragg resonance $\frac{k_w}{k} = \mathcal{O}(1)$ so that

$$\mathcal{O}(\frac{\omega_w}{\omega}) = \frac{c_w}{C} \tag{A.2}$$

The ratio of frequency is therefore well approximated by the ratio of the surface wave to sound wave phase velocities. Typical values of the sound and surface wave characteristics are given in Table A.1 in both the laboratory and field environments.

		Sound Waves	Water Waves
Lab	λ(m)	5	8.17
	$\omega/2\pi$ (Hz)	300	0.38
	T(s)	$3.33\ 10^{-3}$	2.62
Field	λ(m)	50	81.7
	$\omega/2\pi$ (Hz)	30	0.12
	T(s)	$3.33\ 10^{-2}$	8.27

Table A.1: Typical scales for Bragg scattering for a normalized water depth $kh = 1.65$.

Appendix B: Derivation of Eigenvectors

B.1.*Eigenvectors for Case 1*

In *Case 1*, matrix $P(\mu,\nu)$ reads

$$P(\mu,\nu) = \begin{pmatrix} -\Lambda\mu & \alpha_1 & \alpha_2 \\ \alpha_1 & \Lambda(\mu\cos\theta_1 + \nu\sin\theta_1) & 0 \\ \alpha_2 & 0 & \Lambda(\mu\cos\theta_2 + \nu\sin\theta_2) \end{pmatrix} \qquad (A.1)$$

The eigenvalues of P, -$\sigma(\mu,\nu)$, have been found in §4. The eigenvector of P associated with eigenvalue $-\sigma_j$, $\tilde{X}_j(\mu,\nu) = [x_{1j}^{(1)}, x_{2j}^{(1)}, x_{3j}^{(1)}]^T$, satisfies by definition

$$\big(P(\mu,\nu) + \sigma(\mu,\nu)I\big)\ \tilde{X}_j(\mu,\nu) = 0 \qquad (A.2)$$

where I is the order 3×3 identity matrix. For a given (μ,ν), the solution is found by substitution:

$$\begin{cases} x_{1j}^{(1)} = \alpha_2\big\{\Lambda(\mu\cos\theta_1 + \nu\sin\theta_1) + \sigma_j\big\} \\ x_{2j}^{(1)} = -\alpha_1\alpha_2 \qquad\qquad j = 1,2,3 \\ x_{3j}^{(1)} = \alpha_1^2 + (\Lambda\mu - \sigma_j)\big\{\Lambda(\mu\cos\theta_1 + \nu\sin\theta_1) + \sigma_j\big\} \end{cases} \qquad (A.3)$$

The general solution of the matrix differential equation follows:

$$\begin{pmatrix} \tilde{\mathcal{A}} \\ \tilde{\mathcal{B}}_1 \\ \tilde{\mathcal{B}}_2 \end{pmatrix}(\mu,\nu,t) = \sum_{j=1}^{3} p_j \tilde{X}_j(\mu,\nu)\ e^{-i\sigma(\mu,\nu)t} \qquad (A.4)$$

where the $\{p_j\}_{j=1,3}$ are determined from the initial conditions obtained numerically

$$\begin{pmatrix} \tilde{\mathcal{A}} \\ \tilde{\mathcal{B}}_1 \\ \tilde{\mathcal{B}}_2 \end{pmatrix}(\mu,\nu,t=2) \qquad (A.5)$$

B.2. *Eigenvectors for Case 2*

Matrix P now reads

$$P(\mu,\nu) = \begin{pmatrix} -\Lambda\mu & \alpha_1 & \alpha_2 & 0 \\ \alpha_1 & \Lambda(\mu\cos\theta_1 + \nu\sin\theta_1) & 0 & \alpha_2 \\ \alpha_2 & 0 & -\Lambda(\mu\cos\theta_1 + \nu\sin\theta_1) & \alpha_1 \\ 0 & \alpha_2 & \alpha_1 & \Lambda\mu \end{pmatrix} \qquad (A.6)$$

Assume $\tilde{X}_j(\mu,\nu) = [x_{1j}^{(2)}, x_{2j}^{(2)}, x_{3j}^{(2)}, x_{4j}^{(2)}]^T$ to be an eigenvector of P, it is then required that

$$(P(\mu,\nu) + \sigma_j(\mu,\nu)I)\ \tilde{X}_j(\mu,\nu) = 0 \tag{A.7}$$

where I is the 4×4 identity matrix. A solution to $(A.7)$ is straightforwardly found:

$$\begin{cases} x_{1j}^{(2)} = \alpha_1\alpha_2(\tau_j + \rho_j) \\ x_{2j}^{(2)} = -\alpha_2(\beta_j\rho_j + \alpha_1^2 - \alpha_2^2) \\ x_{3j}^{(2)} = -\alpha_1(\beta_j\tau_j + \alpha_2^2 - \alpha_1^2) \\ x_{4j}^{(2)} = \beta_j\tau_j\rho_j - \rho_j\alpha_1^2 - \tau_j\alpha_2^2 \end{cases} \tag{A.8}$$

where for brevity we have defined

$$\begin{cases} \beta_j = -\Lambda\mu + \sigma_j \\ \tau_j = \Lambda(\mu\cos\theta_1 + \nu\sin\theta_1) + \sigma_j \\ \rho_j = -\Lambda(\mu\cos\theta_1 + \nu\sin\theta_1) + \sigma_j \end{cases} \tag{A.9}$$

the general solution for *Case 2* is then

$$\begin{pmatrix} \tilde{\mathcal{A}} \\ \tilde{\mathcal{B}}_1 \\ \tilde{\mathcal{B}}_2 \\ \tilde{\mathcal{B}}_3 \end{pmatrix}(\mu,\nu,t) = \sum_{j=1}^{4} p_j\tilde{X}_j(\mu,\nu)\ e^{-i\sigma_j(\mu,\nu)t} \tag{A.10}$$

where the $\{p_j\}_{j=1,..,4}$ are determined by the initial condition

$$\begin{pmatrix} \tilde{\mathcal{A}} \\ \tilde{\mathcal{B}}_1 \\ \tilde{\mathcal{B}}_2 \\ \tilde{\mathcal{B}}_3 \end{pmatrix}(\mu,\nu,t=2) \tag{A.11}$$

computed with the finite difference scheme.

B.3.*Eigenvectors for Case 3*

Matrix $P(\mu,\nu)$ reads

$$P(\mu,\nu) = \begin{pmatrix} -\Lambda\mu & \alpha_1 & \alpha_2 & 0 \\ \alpha_1 & \Lambda(\mu\cos\theta_1 + \nu\sin\theta_1) & 0 & 0 \\ \alpha_2 & 0 & \Lambda\mu & \alpha_1 \\ 0 & 0 & \alpha_1 & -\Lambda(\mu\cos\theta_1 + \nu\sin\theta_1) \end{pmatrix} \tag{A.12}$$

Its eigenvectors $\tilde{X}_j(\mu,\nu) = [x_{1j}^{(3)}, x_{2j}^{(3)}, x_{3j}^{(3)}, x_{4j}^{(3)}]^T$ must satisfy

$$(P(\mu,\nu) + \sigma_j(\mu,\nu)I)\ \tilde{X}_j(\mu,\nu) = 0 \tag{A.13}$$

A solution of which is obtained by substitution:

$$\begin{cases} x_{1j}^{(3)} = \alpha_1 \alpha_2 \tau_j \\ x_{2j}^{(3)} = -\alpha_1^2 \alpha_2 \\ x_{3j}^{(3)} = -\alpha_1 (\beta_j \tau_j - \alpha_1^2) \\ x_{4j}^{(3)} = \beta_j \tau_j \rho_j - \rho_j \alpha_1^2 - \tau_j \alpha_2^2 \end{cases} \tag{A.14}$$

where for brevity we have defined

$$\begin{cases} \beta_j = -\Lambda\mu + \sigma_j \\ \tau_j = \Lambda(\mu \cos\theta_2 + \nu \sin\theta_2) + \sigma_j \\ \rho_j = \Lambda\mu + \sigma_j \end{cases} \tag{A.15}$$

the general solution for *Case 3* is then

$$\begin{pmatrix} \tilde{\mathcal{A}} \\ \tilde{\mathcal{B}}_1 \\ \tilde{\mathcal{B}}_2 \\ \tilde{\mathcal{B}}_3 \end{pmatrix} (\mu, \nu, t) = \sum_{j=1}^{4} p_j \tilde{X}_j(\mu, \nu)\ e^{-i\sigma_j(\mu,\nu)t} \tag{A.16}$$

where the $\{p_j\}_{j=1,..,4}$ are determined by the initial condition

$$\begin{pmatrix} \tilde{\mathcal{A}} \\ \tilde{\mathcal{B}}_1 \\ \tilde{\mathcal{B}}_2 \\ \tilde{\mathcal{B}}_3 \end{pmatrix} (\mu, \nu, t = 2) \tag{A.17}$$

obtained from earlier computations.

Part 2
INTERACTIONS OF SHORT AND LONG WAVES ON THE SEA SURFACE

Notations for Part 2

a	Horizontal Lagrangian independent variable.
a_j	Stretched horizontal Lagrangian independent variables.
A	Short wave amplitude.
$\overline{A}$	Reference short wave amplitude for normalization.
A'	Short wave amplitude A after integration of linear phase terms.
$\mathcal{A}$	Short wave amplitude A' after normalization by $\overline{A}$.
$\mathcal{A}_s$	Stokes wave complex amplitude.
$\tilde{\mathcal{A}}$	Short wave amplitude $\mathcal{A}$ after integration of linear amplitude terms.
$\tilde{\mathcal{A}}^n$	Discretized values of $\tilde{\mathcal{A}}$ at $n\Delta\phi$.
b	Horizontal transverse Lagrangian independent variable.
b_j	Stretched horizontal transverse Lagrangian independent variables.
B	Long wave amplitude.
$\tilde{\mathcal{B}}_0$	Zeroth Fourier mode amplitude (Stokes wave) in the decomposition of $\tilde{\mathcal{A}}$.
$\tilde{\mathcal{B}}_1$	First Fourier mode amplitudes (Symmetric sidebands) in the decomposition of $\tilde{\mathcal{A}}$.
$\tilde{\mathcal{B}}_j$	The j-th Fourier mode amplitude in the decomposition of $\tilde{\mathcal{A}}$.
c	Vertical Lagrangian independent variable.
c_j	Stretched vertical Lagrangian independent variables.
C_g	Group velocity of short waves in a fixed reference frame.
C_{gx}	X-component of the group velocity C_g for oblique short waves.
C_{gY}	Y-component of the group velocity C_g for oblique short waves.
d	Short wave real amplitude in Floquet stability analysis.
d'	Disturbance in the real amplitude of short wave in Floquet Theory.
$\tilde{d}$	Amplitude of sinusoidal disturbance in Floquet theory.
$\tilde{d}^{(j)}$	Amplitude of sinusoidal disturbance for eigenvector j.
D	Linear time dependent amplitude term in Schrödinger equation for $\mathcal{A}$.
D_r	Real part of the coefficient of the linear term in linear evolution equation (in Chapter III).
D_i	Imaginary part of the coefficient of the linear term in linear evolution equation (in Chapter III).
$E_{j\ell}$	Forcing term in continuity equation at $\mathcal{O}(\epsilon^j)$ for the harmonic ℓ of short waves.
$\tilde{E}_{jm}$	Forcing term in the continuity equation for the m-th harmonic of the long wave displacement at $\mathcal{O}(\epsilon^j)$.
F	Generating function defining contact transformation.
$F_{j\ell}$	Forcing term in first vorticity equation at $\mathcal{O}(\epsilon^j)$ for the harmonic ℓ of short waves.
$\mathcal{F}$	Fourier transform operator.
$\mathcal{F}^{-1}$	Inverse Fourier transform operator.
g	Gravitational acceleration.
$\vec{g}$	Gravitational acceleration vector.
$\vec{g}_{\text{Gerstner}}$	Gravitational acceleration due to the Gerstner wave.

g_{eff}	Effective gravitational acceleration.
$\vec{g}_{\text{eff}}$	Effective gravitational acceleration vector.
g_r	Growth rate in Floquet theory.
G	Coefficient of cubic term in Schrödinger equation for $\tilde{A}$.
$G_{j\ell}$	Forcing term in the second vorticity equation at $\mathcal{O}(\epsilon^j)$ for the harmonic ℓ of short waves.
$\tilde{G}_{jm}$	Forcing term in second vorticity equation for the m-th harmonic of the long wave displacements at $\mathcal{O}(\epsilon^j)$.
h	Spacial discretization in numerical scheme.
$H_{j\ell}$	Forcing term in third vorticity equation at $\mathcal{O}(\epsilon^j)$ for the harmonic ℓ of short waves.
$\mathcal{H}$	Hamiltonian.
i	Square root of -1.
I_0	Action of Stokes mode.
I_1	Action of disturbance mode.
$I_{j\ell}$	Forcing term in first dynamic free surface boundary condition at $\mathcal{O}(\epsilon^j)$ for harmonic ℓ of short waves .
$\tilde{I}_{jm}$	Forcing term in dynamic free surface boundary condition for the m-th harmonic of the long wave displacements at $\mathcal{O}(\epsilon^j)$.
J	Jacobian of transformation from Lagrangian to Eulerian.
J_0	Action variable derived from canonical contact transformation.
J_1	Action variable derived from canonical contact transformation.
$J_{j\ell}$	Forcing term in second dynamic free surface boundary condition for harmonic ℓ of short wave displacements at $\mathcal{O}(\epsilon^j)$.
k	Short wave Lagrangian horizontal wavenumber.
k^e	Short wave Eulerian wavenumber.
$\vec{k}^e$	Short wave Eulerian wavenumber vector.
k_x^e	Short wave Eulerian horizontal wavenumber.
k_z^e	Short wave Eulerian vertical wavenumber.
K	Long wave Lagrangian horizontal wavenumber.
L	Transposed of the Jacobian matrix.
L_j	Contribution at $\mathcal{O}(\epsilon^j)$ of L.
m	Fourier mode in nonlinear evolution computations.
M	(2×2) coefficient matrix of a system of ODE for first harmonic short wave displacements.
$\mathcal{M}$	Nonlinear amplitude modulation.
n_{jl}	Entries of matrix N.
N	(2×2) matrix of forcing in system of ODE for first harmonic short wave displacements.
$\mathcal{O}(\cdot)$	Order of $(\cdot)$.
p_n	Geometrical points in the complex μ-plane.
P	Pressure field.
P_j	Polynomials defining the phase change of A at $\mathcal{O}(\epsilon^2)$.
Q	Correction term in the Eulerian dispersion relation.
R	Correction term in the dispersion relation of short waves

	for oblique incidence.
S	Phase function of short wave.
$\tilde{S}$	Short wave phase function including contribution of linear evolution equation.
$\tilde{S}_j$	Contribution of $\tilde{S}$ at $\mathcal{O}(\epsilon^j)$.
$\mathcal{S}_x$	Multiplication factor in the amplitude of the x-component of the short wave displacement at $\mathcal{O}(\epsilon)$.
$\mathcal{S}_y$	Multiplication factor in the amplitude of the y-component of the short wave displacement at $\mathcal{O}(\epsilon)$.
t	Time variable.
t_j	Stretched time variables.
T	Long wave period.
U	Vector whose components are the displacements for a given harmonic
$U^{\pm}$	Eigenvectors associated with the eigenvalues $\kappa^{\pm}$.
$\mathbf{U}$	Eulerian velocity vector.
$\mathcal{U}$	x-component of vector Λ.
$\mathcal{V}$	y-component of vector Λ.
W	Phase of short wave complex amplitude in Floquet theory.
W'	Disturbance in the phase of the short wave complex amplitude.
$\tilde{W}$	Amplitude of sinusoidal disturbance in the short wave phase.
$\tilde{W}^{(j)}$	Amplitude of sinusoidal disturbance in the short wave phase along eigenvector j.
$\mathcal{W}$	z-component of vector Λ.
x	Lagrangian horizontal displacement.
x_j	Contribution to Lagrangian displacement x at $\mathcal{O}(\epsilon^j)$.
$x_{j\ell}$	Contribution to x_j along harmonic ℓ.
X	Eulerian horizontal coordinate of particles.
X_j	Stretched Eulerian horizontal coordinates of particules.
X_0	X-component of a particle at a given initial time.
y	Lagrangian horizontal transverse displacement.
y_j	Contribution to Lagrangian displacement y at $\mathcal{O}(\epsilon^j)$.
$y_{j\ell}$	Contribution to y_j along harmonic ℓ.
Y	Eulerian horizontal transverse coordinate of particles.
Y_j	Stretched Eulerian horizontal transverse coordinates of particules.
z	Lagrangian vertical displacement.
z_j	Contribution to Lagrangian displacement z at $\mathcal{O}(\epsilon^j)$.
$z_{j\ell}$	Contribution to z_j along harmonic ℓ.
Z	Eulerian vertical coordinate of particles.
Z_j	Stretched Eulerian vertical coordinates of particules.
Z_0	Z-component of a particle at a given initial time.
α	Coefficient of dispersion and nonlinearity in Schrödinger equation for $\mathcal{A}$.
β	Stokes wave phase.
γ	Phase change derived from the linear evolution equation for A.
Γ	Phase change derived from the nonlinear Schrödinger equation for A.
δ	$(1 - \frac{\epsilon}{2}\frac{\Omega}{\sigma})$.

Δ	Coefficient in the Mathieu equation.
Δk	Change in wavenumber for the uniform short wave solution.
$\Delta\sigma$	Change in intrinsic frequency for the uniform short wave solution.
$\Delta\phi$	"Time" step in numerical scheme.
ϵ	Small parameter scaling as the short wave slope.
ϵ_1	Initial amplitude of sideband disturbance.
η	Transverse normalized coordinate for oblique short waves.
η_j	Phase of Floquet multiplier μ_j.
θ	Incidence angle of short waves relative to long waves.
θ_0	Argument of complex amplitude of Stokes mode.
θ_1	Argument of complex amplitude of sideband mode.
Θ	Obliqueness of short waves absolute group velocity relative to long waves.
ϑ	Inclination of the Eulerian wavenumber vector relative to the horizontal.
κ	Vertical Lagrangian complex wavenumber.
$\kappa^{\pm}$	Eigenvalues for the short wave differential operator.
κ_r	Real part of κ.
κ_i	Imaginary part of κ.
λ_j	Floquet exponents.
Λ	Vector related to the vorticity in three dimensions.
μ_j	Floquet multiplier j.
ν	Disturbance wavenumber.
$\vec{\nu}$	Disturbance wavenumber vector.
ν_x	x-component of the disturbance wavenumber vector.
ν_y	y-component of the disturbance wavenumber vector.
ξ	Normalized group velocity coordinate.
ξ'	Group velocity coordinate $(a_1 - \frac{\omega}{2k}t_1)$.
$\tilde{\xi}$	Group velocity coordinate after second normalization by ν.
$\tilde{\xi}^j$	Discretized value of $\tilde{\xi}$ at jh.
Ξ	Twice the real part of $\mathcal{S}_x$.
π	3.14159265 ...
ϖ	Vorticity transverse component for planar interactions.
ϖ_j	Contribution to ϖ at $\mathcal{O}(\epsilon^j)$.
ϖ^g	Vorticity transverse component due to Gerstner's wave.
ϖ^X	X-component of ϖ in three dimensions.
ϖ^Y	Y-component of ϖ in three dimensions.
ϖ^Z	Z-component of ϖ in three dimensions.
ρ	Density of water.
ρ_j	Modulus of Floquet multiplier μ_j.
σ	Short wave intrinsic frequency.
σ_0	Short wave intrinsic frequency at $\theta = 0$ in Chapter III.
τ	Normalized time $(\Omega t_1 - \epsilon K a_1)$.
ϕ	Lagrangian phase of long Gerstner waves.
ϕ_0	Reference Lagrangian phase.

$\Phi_{j,l}$	Basis solution of Floquet linear equations.
χ	Inclination of the free surface of the Gertsner wave relative to the horizontal.
ψ_0	Angle variable conjugate to J_0 from canonic contact transformation.
ψ_1	Angle variable conjugate to J_1 from canonic contact transformation.
ω	Short wave absolute frequency in a fixed frame.
Ω	Long wave intrinsic frequency.
∇	Eulerian gradient with respect to fast variables (X, Z) or (X, Y, Z).
∇_j	Eulerian gradient with respect to slow variables (X_j, Z_j) or (X_j, Y_j, Z_j).
Υ	Coefficient in the Mathieu equation.
$\Re$	Real part of argument.
$\Im$	Imaginary part of argument.

GENERAL INTRODUCTION
Literature Review

The dynamical processes on the ocean surface have long been a subject of scientific interest. In particular, the transfer of energy from wind to the short capillary waves down to the gravity waves is still not fully understood. During the last decade, the study of these dynamical processes has been tremendously stimulated by the remote sensing of the ocean surface from high altitude planes and satellites. For example, synthetic aperture radar (SAR) images of the English channel have shown, unexpectedly at first, the contours of its bathymetry. This and other observations have led to the conclusion that a better understanding of the interactions between the short gravity capillary waves and the longer waves, swells and currents is a prerequisite for the fruitful and successful interpretation of SAR imagery.

We owe the first rigorous analysis of long wave-short wave interactions to Longuet-Higgins & Stewart(1960), who demonstrated that short waves become steeper near the long wave crest and milder at its trough. The same authors investigated the effect of non-uniform currents on short waves using a similar approach, and introduced the concept of radiation stress to account for the energy flux from the long waves to the short waves (Longuet-Higgins & Stewart (1961)). Bretherton & Garrett(1969) have shown that short wavetrains propagating on a slowly varying medium satisfy the law of conservation of action which is defined as the ratio of the energy to the intrinsic frequency. From this conservation principle, the slow modulation of the wavetrain amplitude is deduced.

More recently, Phillips(1981) has considered the interactions between a train of linear short waves riding on a finite amplitude Stokes wave. He postulates that the short wave is steady relative to the long wave. In a reference frame moving at the phase speed of the long wave, the absolute frequency ω is related to the intrinsic frequency σ by the Doppler shift relation $\omega = \sigma + \mathbf{k} \cdot \mathbf{u}$. Under the steadyness assumption, the short wave wavenumber vector $\mathbf{k}$ is not a function of

time and therefore ω is uniform. The modulation of the intrinsic frequency can then be deduced provided that the velocity field $\mathbf{u}$ is known. Once the variation of the intrinsic frequency is derived, the amplitude modulation is deduced from the conservation of wave action. Phillips did not give quantitative estimates of the modulation, except for weakly nonlinear waves.

With recent advances in computing steep Stokes waves up to the maximum height (Longuet-Higgins, 1985), quantitative estimates of the modulation of short waves have become available. Longuet-Higgins(1987) has shown, under the steadiness assumption, that the modulation of linear short waves by steep irrotational Stokes waves is much stronger than suggested by the classical weakly nonlinear theory.

Henyey *et al.*(1988) have analysed the linearized evolution of short gravity-capillary waves on a steep two-dimensional irrotational long wave field. The principle of action conservation is rederived from a Hamiltonian formulation. Dysthe *et al*(1988) established an analogy between short and long interacting gravity waves and the orbiting double pendulum. The action of this simple system is derived using a Hamiltonian theory and is shown numerically to be nearly constant. More recently, Kharif(1990) generalized the ray theory and wave action conservation of Bretherton & Garrett by accounting for capillarity effects in the short wave and nonlinear effects in the long wave. His numerical results agree with Longuet-Higgins'.

Zhang & Melville(1990) extended Longuet-Higgins' theory and proved that the slow modulation of weakly nonlinear short waves on a steep irrotational Stokes wave is governed by a Schrödinger equation. With the short waves assumed to be steady relative to the numerically obtained long waves, they studied the amplitude, wavenumber and frequency modulations.

It is well known that a wavetrain propagating on an otherwise calm sea is unstable to sideband disturbances (Benjamin & Feir(1967)), and that the long time evolution past the initial stage may involve a complex interplay between nonlinear and dispersive effects. In particular, Fermi-Pasta-Ulam recurrence may happen whereby energy is periodically exchanged between the uniform Stokes wave and its sideband disturbances leading to the almost exact reconstruction of the initial

data (see Yuen & Ferguson, 1978). The linear stability of deep water waves to sideband disturbances has also been investigated by Crawford *et al*(1981) using the Zakharov formulation. For two-dimensional disturbances, restabilization is observed for large enough wave slope. With the narrow band assumption, the Benjamin & Feir instability diagram is recovered. For three dimensional disturbances, the instability region is finite and has the shape of a hook. In the limit of narrow banded waves, the infinite instability strip of Benney & Roskes(1969) is recovered. Based on the results of Crawford *et al*, Caponi *et al*(1982) used Zakharov theory to compute the nonlinear stability of gravity waves to two-dimensional sideband disturbances for several wave slopes. For sufficiently small slopes, the symmetric sidebands alone are unstable and an FPU recurrence is found. As the wave slope increases, harmonics of the unstable sideband become unstable. The evolution of the lowest Fourier amplitudes is found to be chaotic. Such situations are termed "confined chaos" in reference to the narrowness of the Fourier spectrum. For yet larger slopes (≈ 0.5) restabilization occurs and the evolution is periodic. With the narrow band asumption, similar computations are performed based on the nonlinear Schrödinger equation. Calculations for a slope equal to 0.5 which is outside the realm of validity suggest a chaotic evolution. The results are of course questionable.

Very recently, Yoshinaga *et al*(1991) have considered a set of two nonlinear coupled equations modelling, in a variety of physical contexts, the interactions of a short and a long wave when the group velocity of the former wave matches the phase velocity of the latter wave. A similar situation is known to occur in gravity-capillary waves. The scaling assumptions chosen by the authors are such that the long wave is very weak. A linearized instability analysis is performed around a basic solution consisting solely of a uniform short wave. The short wave envelope and the long wave are then expanded in Fourier series and a set of co ıpled nonlinear ordinary differential equations are derived for the time dependent Fourier amplitudes. The initial data includes only the uniform short wave disturbed by two symmetric unstable sidebands. Integration of these equations is performed for times much longer than customary for Schrödinger and KdV equations. Depending on the strength of dispersion, recurrence or chaotic motions are observed. In the latter case, only a small number of Fourier modes concentrated in the lower range of the spectrum

evolve chaotically.

Scope of Present Work

Instead of the classical approach, we shall formulate the problem in Lagrangian variables so that the location of the free surface is known at all times. We begin in Chapter I with an irrotational theory by assuming that both short and long waves have comparably small steepness, but the length contrast is very large. An evolution equation is derived for the short wave envelope. The result can be simply given as the product of two factors representing respectively the modulation due to long wave and nonlinearity in the short wave itself as seen by a fluid particle.

In order to simplify the analysis for finite amplitude long waves we shall model in Chapter II the steep long wave by the simple and exact solution of Gerstner(1802) in Lagrangian variables. In contrast to the Stokes wave, Gerstner's wave has a finite time-independent vorticity which decays exponentially with depth. The vorticity is the greatest on the free surface and is proportional to the square of the long wave steepness KB. For the range of long wave slopes to be considered here ($KB \leq 0.3$), the difference in vorticity is only moderate. The simplicity of Gerstner's solution greatly facilitates the analytical and numerical examinations of new aspects of the nonlinear interactions. This is one of the main features of Chapters II & III.

In Chapter II, analytical results are first deduced for the modulation of the amplitude, wavenumber and slope of a linearized short wave riding on a long Gerstner wave. These results are then compared with Longuet-Higgins(1987). Despite differences in the profiles of Gerstner's and Stokes' waves, the agreement is good for the slope and wavenumber modulation. Comparison with Henyey *et al*(1988) is consistent with the $\mathcal{O}(K^2B^2)$ difference in vorticity between the two theories. An asymptotic equation giving the long-time evolution of the short wave amplitude is derived with explicit time-dependent coefficients. Floquet theory is invoked to analyse the linearized sideband instability of a uniform solution. Secondary bands of sideband instability are found in addition to the classical Benjamin & Feir(1967) band. The importance of the parameter α - which is proportional to the square of the short wave slope, $\epsilon k\overline{A}$ and inversely proportional to the long to short wave

frequency ratio, $\epsilon\frac{\Omega}{\sigma}$ - is pointed out. The nonlinear evolution of the short wave amplitude disturbed by its most unstable sideband is then investigated for a large range of α. For moderately large values of α, evidence of chaos is found. To gain more insight on the tendency to chaos, a truncated two-term expansion, involving solely the uniform carrier wave and its symmetric sidebands, is analyzed. Numerical integration of the resulting dynamical system confirms the tendency to chaos. Thus, long wave-short wave interactions appear to be a powerful deterministic mechanism contributing to the chaotic appearance of the sea surface.

In Chapter III, the short waves are assumed to be inclined at an angle θ relative to the long Gerstner wave. The modulation of the amplitude and wavenumber of the linearized oblique short wave is first deduced analytically. In contrast to the well-known result for a steady current, short waves propagating perpendicularly to the long waves are still modulated in amplitude owing to the time dependent gravity field. An asymptotic equation describing the nonlinear evolution of the amplitude of a slightly oblique short wave ($\theta \ll 1$) is then derived. The result is a nonlinear two-dimensional Schrödinger equation with time-periodic coefficients. By Floquet theory, the stability to two-dimensional sideband disturbances of a uniform short wave riding on a steep long wave is investigated. It is found that additional instability bands appear next to the known strip of Benney & Roskes(1969).

CHAPTER I: TWO-DIMENSIONAL INTERACTIONS OF WEAK SHORT AND LONG WAVES

1. INTRODUCTION

In this Chapter, the evolution of short waves riding on a mild irrotational long wave is investigated. The characteristic scales of both waves are such that the particle velocity, ΩB, of the long wave (where Ω and B represent respectively its frequency and amplitude), is comparable to the intrinsic group velocity, $\frac{\sigma}{2k}$, of the short waves (where σ and k refer respectively to its intrinsic frequency and wavenumber). It is well known in wave-current interactions that blockage occurs when the current velocity equals the group velocity of the waves. Since the long waves are equivalent, as far as the short waves are concerned, to an oscillatory current, it is worthwhile to analyse to what extent blockage may also happen here.

We shall investigate here how weakly nonlinear and slowly modulated long waves affect the nonlinear evolution of comparably weak and modulated short waves ($kA \approx KB \ll 1$). In particular, we analyse in §5 how a solitary short wave in Lagrangian coordinates is perceived by a fixed observer as a soliton whose peak location varies as the long wave passes.

In principle the Lagrangian coordinates can be employed for slightly steep long waves $kA \ll KB \ll 1$; but the algebra becomes very cumbersome. We shall instead examine in the last two chapters a rotational and uniform long wave $KB \leq \mathcal{O}(1)$ whose solution is known exactly.

2. FORMULATION OF THE PROBLEM

2.1. Governing Equations

In the Lagrangian frame, the equations governing the fluid motion are expressed in terms of the coordinates (X,Z) of a particle. These coordinates depend on some characteristic parameters of the particle (a,c), such as the position of the particle at a given initial time. For completeness, the governing equations in Lagrangian coordinates are rederived, following Stoker (1968, pp514-515).

First, continuity requires that :

$$\frac{D(X,Z)}{D(a,c)} \equiv \frac{\partial X}{\partial a}\frac{\partial Z}{\partial c} - \frac{\partial X}{\partial c}\frac{\partial Z}{\partial a} = \frac{D(X_0,Z_0)}{D(a,c)} = J(a,c) \qquad (I.2.1)$$

where (X_0, Z_0) is the initial position of the particle, and the Jacobian J is independent of time. The two components of the momentum equation read

$$\frac{\partial^2 X}{\partial t^2} = -\frac{1}{\rho}\frac{\partial P}{\partial X} \qquad \frac{\partial^2 Z}{\partial t^2} + g = -\frac{1}{\rho}\frac{\partial P}{\partial Z} \qquad (I.2.2a-b)$$

where ρ is the density of water, P the pressure field and g the gravitational acceleration. When $(I.2.2a)$ is multiplied throughout by $\frac{\partial X}{\partial a}$ and $(I.2.2b)$ by $\frac{\partial Z}{\partial a}$, and the resulting equations are added together, we obtain

$$\frac{\partial X}{\partial a}\frac{\partial^2 X}{\partial t^2} + \frac{\partial Z}{\partial a}\left(\frac{\partial^2 Z}{\partial t^2} + g\right) = -\frac{1}{\rho}\left[\frac{\partial P}{\partial X}\frac{\partial X}{\partial a} + \frac{\partial P}{\partial Z}\frac{\partial Z}{\partial a}\right] = -\frac{1}{\rho}\frac{\partial P}{\partial a} \qquad (I.2.3a)$$

Likewise,

$$\frac{\partial X}{\partial c}\frac{\partial^2 X}{\partial t^2} + \frac{\partial Z}{\partial c}\left(\frac{\partial^2 Z}{\partial t^2} + g\right) = -\frac{1}{\rho}\left[\frac{\partial P}{\partial X}\frac{\partial X}{\partial c} + \frac{\partial P}{\partial Z}\frac{\partial Z}{\partial c}\right] = -\frac{1}{\rho}\frac{\partial P}{\partial c} \qquad (I.2.3b)$$

Eqs. $(I.2.3a-b)$ represent the two components of the momentum equation in Lagrangian coordinates.

In the Lagrangian formulation (cf. Appendix A), the vorticity is expressed as

$$\varpi = \frac{1}{J}\left\{\frac{\partial X}{\partial a}\frac{\partial^2 X}{\partial c \partial t} - \frac{\partial X}{\partial c}\frac{\partial^2 X}{\partial a \partial t} + \frac{\partial Z}{\partial a}\frac{\partial^2 Z}{\partial c \partial t} - \frac{\partial Z}{\partial c}\frac{\partial^2 Z}{\partial a \partial t}\right\} \qquad (I.2.4)$$

Eliminating the pressure P by cross-differentiation of $(I.2.3a)$ and $(I.2.3b)$ yields the following conservation relation

$$\frac{\partial}{\partial t}\{J\varpi\} = 0 \qquad (I.2.5)$$

Since J is independent of time, $(I.2.5)$ implies that the vorticity ϖ is conserved. If the vorticity is absent in the initial state, it will remain so for all times.

At the free surface, the pressure gradient vanishes. The following dynamic boundary condition is thus satisfied

$$\frac{\partial X}{\partial a}\frac{\partial^2 X}{\partial t^2} + \frac{\partial Z}{\partial a}\left(g + \frac{\partial^2 Z}{\partial t^2}\right) = 0 \qquad c = 0 \tag{$I.2.6$}$$

From now on, it is assumed that (a, c) represents the initial position. As a result, J reduces to unity.

It is more convenient to express the governing equations in terms of the Lagrangian particle displacements $x(a, c, t)$ and $z(a, c, t)$ defined by

$$X(a, c, t) = a + x(a, c, t) \qquad Z(a, c, t) = c + z(a, c, t) \tag{$I.2.7$}$$

The law of mass conservation becomes

$$\frac{\partial x}{\partial a} + \frac{\partial z}{\partial c} + \frac{\partial x}{\partial a}\frac{\partial z}{\partial c} - \frac{\partial x}{\partial c}\frac{\partial z}{\partial a} = 0 \tag{$I.2.8$}$$

The irrotationality equation $(I.2.5)$ reduces to

$$\frac{\partial^3 x}{\partial c \partial t^2} - \frac{\partial^3 z}{\partial a \partial t^2} + \frac{\partial^3 x}{\partial c \partial t^2}\frac{\partial x}{\partial a} - \frac{\partial^3 z}{\partial a \partial t^2}\frac{\partial z}{\partial c} - \frac{\partial^3 x}{\partial a \partial t^2}\frac{\partial x}{\partial c} + \frac{\partial^3 z}{\partial c \partial t^2}\frac{\partial z}{\partial a} = 0 \tag{$I.2.9$}$$

Finally, the free surface dynamic boundary condition yields

$$\frac{\partial^2 x}{\partial t^2} + g\frac{\partial z}{\partial a} + \frac{\partial x}{\partial a}\frac{\partial^2 x}{\partial t^2} + \frac{\partial z}{\partial a}\frac{\partial^2 z}{\partial t^2} = 0 \qquad c = 0 \tag{$I.2.10$}$$

Note that the continuity equation is now nonlinear, in contrast to its expression in the Eulerian formulation. On the other hand a significant advantage of this formulation is that the position of the free surface is known *a priori*. Furthermore, only one free surface boundary condition is needed since, by definition, the particles that are initially at the free surface remain at the free surface for all times. Lastly, we require that the displacements decay when c goes to $-\infty$.

2.2. Multiple Scale Analysis

Consider two trains of deep water gravity waves characterised by a large scale contrast. More specifically, the ratios of the long to short wave wavenumbers, $\frac{K}{k}$, and frequencies, $\frac{\Omega}{\sigma}$, scale respectively as $\mathcal{O}(\epsilon^2)$ and $\mathcal{O}(\epsilon)$ where $\epsilon \ll 1$ is a measure of the short wave slope kA. In Chapter I, the long wave slope is small $KB = \mathcal{O}(\epsilon)$. The following relations among the parameters are then deduced

$$kB = \frac{k}{K} KB = \mathcal{O}(\epsilon^{-1}) \qquad \frac{A}{B} = \frac{kA}{KB}\frac{K}{k} = \mathcal{O}(\epsilon^2) \qquad (I.2.11a-b)$$

The ratio of the short wave group velocity to the long wave particle velocity is easily evaluated

$$\frac{\frac{\sigma}{k}}{\Omega B} = \mathcal{O}(1) \qquad (I.2.11c)$$

which suggests that blockage of short waves may happen.

The short wave is slowly modulated not only through self-interaction but also due to the straining by the non-uniform long wave. The long wave two may be modulated over large spatial and time scales. Accordingly, we introduce the following cascade of length and time scales:

$$(a_j, c_j, t_j) = \epsilon^j (a, c, t) \qquad j = 1, 2, 3, \ldots \qquad (I.2.12)$$

The long wave displacements will depend on (a_2, c_2, t_1) as well as longer scales, whereas short wave displacements may depend on all scales. In the subsequent analysis, the small parameter ϵ is the sole indicator of order while all physical variables are regarded as being $\mathcal{O}(1)$. After the asymptotic analysis is complete, ϵ can be dropped and $(I.2.11a-c)$ are restored.

2.3. Perturbation Analysis

The solution for Lagrangian displacements is sought in perturbation series in the small parameter ϵ. Since particle orbits in deep water scale as the amplitude of the motion, $(I.2.11b)$ suggests that the ratio of the leading order short to long wave displacements be $\mathcal{O}(\epsilon^2)$. Accordingly, we introduce the following expansions:

$$x = \epsilon^{-1}x_{-1} + x_0 + \epsilon x_1 + \epsilon^2 x_2 + \epsilon^3 x_3 + \mathcal{O}(\epsilon^4) \qquad (I.2.13a)$$

$$z = \epsilon^{-1}z_{-1} + z_0 + \epsilon z_1 + \epsilon^2 z_2 + \epsilon^3 z_3 + \mathcal{O}(\epsilon^4) \qquad (I.2.13b)$$

In equations $(I.2.13a-b)$, displacements (x_{-1}, z_{-1}) and (x_0, z_0) are solely associated with long waves. On the other hand, (x_1, z_1), (x_2, z_2) *etc* ... correspond primarily to the leading order short wave displacements and their corrections. Note, however, that if the evolution of long waves is sought for long enough times, (x_1, z_1) and higher order displacements may also include correction terms for the long waves.

Equations $(I.2.7)$ and $(I.2.13)$ may be combined resulting in two series expansions of the Eulerian coordinates (X, Z) of a particle:

$$X = a + \epsilon^{-1}x_{-1} + x_0 + \epsilon x_1 + \epsilon^2 x_2 + \epsilon^3 x_3 + \mathcal{O}(\epsilon^4) \qquad (I.2.14a)$$

$$Z = c + \epsilon^{-1}z_{-1} + z_0 + \epsilon z_1 + \epsilon^2 z_2 + \epsilon^3 z_3 + \mathcal{O}(\epsilon^4) \qquad (I.2.14b)$$

Upon substituting $(I.2.13)$ in $(I.2.8)$-$(I.2.10)$, and collecting terms of similar order in ϵ , we obtain a sequence of governing equations. Since we intend to derive an equation describing the evolution of the short wave amplitude over a range $ka_2 = \mathcal{O}(1)$ and for times $\omega t_2 = \mathcal{O}(1)$, governing equations up to $\mathcal{O}(\epsilon^3)$ will be needed for short waves. We present below the $\mathcal{O}(\epsilon)$ and $\mathcal{O}(\epsilon^2)$ equations.

<u>At $\mathcal{O}(\epsilon)$:</u>

Continuity:

$$\frac{\partial x_1}{\partial a} + \frac{\partial z_1}{\partial c} + \frac{\partial x_{-1}}{\partial a_2} + \frac{\partial z_{-1}}{\partial c_2} = 0 \qquad (I.2.15a)$$

Irrotationality:

$$\frac{\partial^3 x_1}{\partial c \partial t^2} - \frac{\partial^3 z_1}{\partial a \partial t^2} = 0 \qquad (I.2.15b)$$

Free surface boundary condition:

$$\frac{\partial^2 x_1}{\partial t^2} + g\frac{\partial z_1}{\partial a} + \frac{\partial^2 x_{-1}}{\partial t_1^2} + g\frac{\partial z_{-1}}{\partial a_2} = 0 \qquad c = 0 \qquad (I.2.15c)$$

<u>At $\mathcal{O}(\epsilon^2)$:</u>

Continuity:

$$\frac{\partial x_2}{\partial a} + \frac{\partial z_2}{\partial c} + \frac{\partial x_1}{\partial a_1} + \frac{\partial z_1}{\partial c_1} + \frac{\partial x_0}{\partial a_2} + \frac{\partial z_0}{\partial c_2} + \frac{\partial x_{-1}}{\partial a_3} + \frac{\partial z_{-1}}{\partial c_3} +$$

$$+\frac{\partial x_1}{\partial a}\frac{\partial z_1}{\partial c}-\frac{\partial x_1}{\partial c}\frac{\partial z_1}{\partial a}+\frac{\partial x_1}{\partial a}\frac{\partial z_{-1}}{\partial c_2}-\frac{\partial x_1}{\partial c}\frac{\partial z_{-1}}{\partial a_2}+$$

$$+\frac{\partial x_{-1}}{\partial a_2}\frac{\partial z_1}{\partial c}-\frac{\partial x_{-1}}{\partial c_2}\frac{\partial z_1}{\partial a}+\frac{\partial x_{-1}}{\partial a_2}\frac{\partial z_{-1}}{\partial c_2}-\frac{\partial x_{-1}}{\partial c_2}\frac{\partial z_{-1}}{\partial a_2}=0 \qquad (I.2.16a)$$

Irrotationality:

$$\frac{\partial^3 x_2}{\partial c\partial t^2}-\frac{\partial^3 z_2}{\partial a\partial t^2}+\frac{\partial^3 x_1}{\partial c_1\partial t^2}-\frac{\partial^3 z_1}{\partial a_1\partial t^2}+2\frac{\partial^3 x_1}{\partial c\partial t\partial t_1}-2\frac{\partial^3 z_1}{\partial a\partial t\partial t_1}+$$

$$+\frac{\partial x_1}{\partial a}\frac{\partial^3 x_1}{\partial c\partial t^2}-\frac{\partial^3 x_1}{\partial a\partial t^2}\frac{\partial x_1}{\partial c}+\frac{\partial z_1}{\partial a}\frac{\partial^3 z_1}{\partial c\partial t^2}-\frac{\partial^3 z_1}{\partial a\partial t^2}\frac{\partial z_1}{\partial c}+$$

$$+\frac{\partial^3 x_1}{\partial c\partial t^2}\frac{\partial x_{-1}}{\partial a_2}-\frac{\partial^3 x_1}{\partial a\partial t^2}\frac{\partial x_{-1}}{\partial c_2}+\frac{\partial^3 z_1}{\partial c\partial t^2}\frac{\partial z_{-1}}{\partial a_2}-\frac{\partial^3 z_1}{\partial a\partial t^2}\frac{\partial z_{-1}}{\partial c_2}=0 \qquad (I.2.16b)$$

Free surface boundary condition:

$$\frac{\partial^2 x_2}{\partial t^2}+g\frac{\partial z_2}{\partial a}+2\frac{\partial^2 x_1}{\partial t\partial t_1}+g\frac{\partial z_1}{\partial a_1}+\frac{\partial^2 x_0}{\partial {t_1}^2}+g\frac{\partial z_0}{\partial a_2}+2\frac{\partial^2 x_{-1}}{\partial t_1\partial t_2}+g\frac{\partial z_{-1}}{\partial a_3}+$$

$$+\frac{\partial x_1}{\partial a}\frac{\partial^2 x_1}{\partial t^2}+\frac{\partial z_1}{\partial a}\frac{\partial^2 z_1}{\partial t^2}+\frac{\partial x_1}{\partial a}\frac{\partial^2 x_{-1}}{\partial {t_1}^2}+\frac{\partial^2 x_1}{\partial t^2}\frac{\partial x_{-1}}{\partial a_2}+$$

$$+\frac{\partial z_1}{\partial a}\frac{\partial^2 z_{-1}}{\partial {t_1}^2}+\frac{\partial^2 z_1}{\partial t^2}\frac{\partial z_{-1}}{\partial a_2}+\frac{\partial x_{-1}}{\partial a_2}\frac{\partial^2 x_{-1}}{\partial {t_1}^2}+\frac{\partial z_{-1}}{\partial a_2}\frac{\partial^2 z_{-1}}{\partial {t_1}^2}=0 \qquad c=0 \quad (I.2.16c)$$

The $\mathcal{O}(\epsilon^3)$ governing equations are lengthy and listed for reference in Appendix B.

3. EVOLUTION EQUATIONS FOR SHORT AND LONG WAVES

3.1. Solutions for Displacements at the Leading Order

The solutions for the long wave displacements (x_{-1}, z_{-1}) and the short wave displacements (x_1, z_1) are sought in this paragraph. The continuity equation and free surface boundary condition $(I.2.15a, c)$ both involve short and long wave displacements, while the irrotationality $(I.2.15b)$ is expressed solely in terms of short wave displacements. The deep water short waves become exponentially small for depths greater than a few wavelengths $(\frac{2\pi}{k})$. The thin layer, where short waves are significant, is therefore extremely small compared to the region where long waves prevail, *i.e.* for depths of the order of a few long wavelenghs, $\frac{2\pi}{\epsilon^2 K}$. As a result, it is expected that the long waves are not affected at the leading order by the short waves. Eqs. $(I.2.15a)$ can therefore be separated as

$$\frac{\partial x_1}{\partial a} + \frac{\partial z_1}{\partial c} = 0 \qquad \frac{\partial x_{-1}}{\partial a_2} + \frac{\partial z_{-1}}{\partial c_2} = 0 \qquad (I.3.1a-b)$$

and likewise for $(I.2.15c)$

$$\frac{\partial^2 x_1}{\partial t^2} + g\frac{\partial z_1}{\partial a} = 0 \quad c = 0, \qquad \frac{\partial^2 x_{-1}}{\partial t_1^2} + g\frac{\partial z_{-1}}{\partial a_2} = 0 \quad c_2 = 0 \qquad (I.3.2a-b)$$

By a similar argument, we deduce from the $\mathcal{O}(\epsilon^3)$ irrotationality equation, the missing governing equation for (x_{-1}, z_{-1}):

$$\frac{\partial^3 x_{-1}}{\partial c_2 \partial t_1^2} - \frac{\partial^3 z_{-1}}{\partial a_2 \partial t_1^2} = 0 \qquad (I.3.3)$$

At the leading order, the short wave displacements are then governed by $(I.3.1a)$, $(I.2.15b)$ and $(I.3.2a)$, and the long wave displacements by $(I.3.1b)$, $(I.3.3)$ and $(I.3.2b)$. Solutions for the leading order short and long waves are now sought.

3.1.1. *The short wave*

Consider the Lagrangian potential defined by

$$\frac{\partial \Phi_L}{\partial a} = \frac{\partial x_1}{\partial t} \qquad \frac{\partial \Phi_L}{\partial c} = \frac{\partial z_1}{\partial t} \qquad (I.3.4a-b)$$

Potential Φ_L is clearly irrotational. Substitution of $(I.3.4a-b)$ in the continuity equation $(I.3.1a)$ yields

$$\nabla^2 \Phi_L \equiv \frac{\partial^2 \Phi_L}{\partial a^2} + \frac{\partial^2 \Phi_L}{\partial c^2} = 0 \qquad (I.3.5)$$

which admits the solution

$$\Phi_{\mathrm{L}}(a,c,t) = -\frac{ig}{\sigma} A e^{kc} e^{i(ka-\sigma t)} + (*) \qquad (I.3.6)$$

where $A(a_1,t_1,a_2,t_2,\ldots)$ is the slowly varying amplitude and k is the Lagrangian wavenumber of the short waves. The frequency σ is termed the *intrinsic* frequency since it describes the oscillatory time behavior in a moving coordinate system. Upon taking the time derivative of $(I.3.2a)$, $(I.3.4a-b)$ may be substituted in to give

$$\frac{\partial}{\partial a}\left[\frac{\partial^2 \Phi_{\mathrm{L}}}{\partial t^2} + g\frac{\partial \Phi_{\mathrm{L}}}{\partial c}\right] = 0 \qquad c = 0 \qquad (I.3.7)$$

When $(I.3.7)$ is evaluated with $(I.3.6)$, we obtain

$$\sigma^2 = gk \qquad (I.3.8)$$

The short waves satisfy the deep water dispersion relation.

The expression of (x_1, z_1) is deduced from $(I.3.4a-b)$ with the help of $(I.3.6)$

$$x_1 = x_{10} + \frac{i}{2} A\ \epsilon^{kc} e^{i(ka-\sigma t)} + (*) \qquad z_1 = z_{10} + \frac{1}{2} A\ e^{kc} e^{i(ka-\sigma t)} + (*) \quad (I.3.9a-b)$$

where $x_{10}(c,a_1,c_1,t_1)$ and $z_{10}(c,a_1,c_1,t_1)$ correspond to slowly varying Lagrangian displacements arising from quadratic nonlinearities. From the $\mathcal{O}(\epsilon)$ continuity equation and the $\mathcal{O}(\epsilon^2)$ free surface boundary condition, we deduce

$$\frac{\partial z_{10}}{\partial c} = 0 \qquad \frac{\partial z_{10}}{\partial a_1} = 0 \quad c = 0 \qquad (I.3.10a-b)$$

The mean vertical drift z_{10} satisfies a set of homogeneous equations and therefore may be dropped from $(I.3.9b)$ without loss of generality. Finally, the governing equation for x_{10} is deduced from the approximate irrotationality equation at $\mathcal{O}(\epsilon^3)$:

$$\frac{\partial^3 x_{10}}{\partial c \partial t_1^2} = 2\sigma k^2 e^{2kc} \frac{\partial}{\partial t_1} |A|^2 \qquad (I.3.11a)$$

which is easily integrated twice

$$\frac{\partial x_{10}}{\partial t_1} = \sigma k e^{2kc} |A|^2 \qquad (I.3.11b)$$

yielding the Stokes drift velocity. A further time integration of $(I.3.11b)$ gives the Stokes drift itself

$$x_{10}(c, a_1, t_1, \ldots) = \sigma k e^{2kc} \int_0^{t_1} |A|^2 dt_1 \qquad (I.3.12)$$

Eqs. $(I.3.9a - b)$, $(I.3.12)$ and $(I.3.8)$ define the particle displacements caused by the short waves at the leading order.

3.1.2. *The long wave*

The derivation of the leading order displacements for long waves follows the steps of §I.3.1.1. and is not repeated here. The results are

$$x_{-1} = \tilde{x}_{-10} + \frac{i}{2} B e^{Kc_2} e^{-i\phi} + (*) \qquad z_{-1} = \frac{1}{2} B e^{Kc_2} e^{-i\phi} + (*) \qquad (I.3.13a - b)$$

where the phase of the long wave

$$\phi \equiv \Omega t_1 - K a_2 \qquad (I.3.13c)$$

is introduced for brevity. In $(I.3.13c)$, K and Ω stand respectively for the Lagrangian wavenumber and intrinsic frequency of the long wave, and in $(I.3.13a - b)$, $\tilde{x}_{-10}(c_2, a_3, c_3, t_2, \ldots)$ is the mean horizontal displacement and $B(a_3, t_2, \ldots)$ the slowly varying amplitude of long waves. Note that $\tilde{z}_{-10}$ has been omitted for the same reason discussed for z_{10}. The equation governing $\tilde{x}_{-10}$ is deduced from the irrotationality at $\mathcal{O}(\epsilon^5)$ and reads

$$\frac{\partial^3 \tilde{x}_{-10}}{\partial c_2 \partial t_2^2} = 2\Omega K^2 e^{2Kc_2} \frac{\partial}{\partial t_2} |B|^2 \qquad (I.3.14)$$

which is easily integrated as

$$\tilde{x}_{-10}(c_2, a_3, t_2, \ldots) = \Omega K e^{2Kc_2} \int_0^{t_2} |B|^2 dt_2 \qquad (I.3.15)$$

Finally, substitution of $(I.3.13a - b)$ in the free surface boundary condition $(I.3.2a)$ yields the dispersion relation

$$\Omega^2 = gK \qquad (I.3.16)$$

The long wave is determined at the leading order by $(I.3.13a - c)$, $(I.3.15)$ and $(I.3.16)$. Both long and short waves satisfy the deep water dispersion relation.

3.2. Governing Equations at Arbitrary Orders

Based on the expressions of the leading order displacements for the short and long waves, the following general expansion for the Lagrangian displacements at $\mathcal{O}(\epsilon^j)$ is postulated

$$x_j = \tilde{x}_{j0}(c_2, a_3, t_2) + \frac{i}{2}\sum_{m>0} \tilde{x}_{jm}(c_2, a_3, t_2)e^{-im\phi} + (*) \qquad j = -1, 0 \qquad (I.3.17a)$$

and

$$z_j = \tilde{z}_{j0}(c_2, a_3, t_2) + \frac{1}{2}\sum_{m>0} \tilde{z}_{jm}(c_2, a_3, t_2)e^{-im\phi} + (*) \qquad j = -1, 0 \qquad (I.3.17b)$$

The maximum value taken by m corresponds to the highest harmonic of $\exp(-i\varphi)$ present at $\mathcal{O}(\epsilon^j)$. We have seen earlier that $\tilde{z}_{-10}$ is not a function of c_2 and may be dropped. However, this is not true at higher orders.

For $j \geq 1$, the expansion involves both short and long waves

$$x_j = \tilde{x}_{j0}(c_2, a_3, t_2) + \frac{i}{2}\sum_{m>0} \tilde{x}_{jm}(c_2, a_3, t_2)e^{-im\phi} +$$

$$+ x_{j0}(c, a_1, t_1) + \frac{i}{2}\sum_{\ell>0} x_{j\ell}(c, a_1, t_1)e^{i\ell(ka-\sigma t)} + (*) \qquad (I.3.18a)$$

and likewise for the vertical displacement

$$z_j = \tilde{z}_{j0}(c_2, a_3, t_2) + \frac{1}{2}\sum_{m} \tilde{z}_{jm}(c_2, a_3, t_2)e^{-im\phi} +$$

$$+ z_{j0}(c, a_1, t_1) + \frac{1}{2}\sum_{\ell>0} z_{j\ell}(c, a_1, t_1)e^{i\ell(ka-\sigma t)} + (*) \qquad (I.3.18b)$$

The "~" symbol has been introduced to distinguish the short from the long wave at $\mathcal{O}(\epsilon^j)$ in $(I.3.18a-b)$ for $j \geq 1$. For consistency, the long waves at lower orders are also identified by the "~" sign.

In the two governing equations obtained at $\mathcal{O}(\epsilon^j)$ and valid in the bulk of the fluid, short wave terms are distinguished by their dependence on the vertical spatial variables c and c_1. A harmonic decomposition yields two governing equations for the short wave displacements $(x_{j\ell}, z_{j\ell})_{\ell=0,1,2,\ldots}$. Long wave terms, on the other

hand, are independent of c and c_1. Again, through harmonic decomposition, the equations governing $(\tilde{x}_{jm}, \tilde{z}_{jm})_{m=0,1,2}$ are deduced. In the boundary condition at the free surface, short wave terms depend on a_1 while long wave terms do not.

The equations governing the m^{th} harmonic of the long wave displacements at $\mathcal{O}(\epsilon^j)$ are summarized for $j = -1, 0, \ldots$ by

$$\frac{\partial \tilde{z}_{jm}}{\partial c_2} - mK\tilde{x}_{jm} = \tilde{E}_{jm} \qquad m = 1, 2, \ldots \tag{$I.3.19a$}$$

$$\frac{\partial \tilde{x}_{jm}}{\partial c_2} - mK\tilde{z}_{jm} = \tilde{G}_{jm} \qquad m = 1, 2, \ldots \tag{$I.3.19b$}$$

respectively for the continuity and irrotationality equations. The free surface boundary condition simplifies to

$$m\tilde{x}_{jm} - \tilde{z}_{jm} = \tilde{I}_{jm} \qquad c_2 = 0 \qquad m = 1, 2, \ldots \tag{$I.3.19c$}$$

Eqs. ($I.3.19a - c$) arise respectively at $\mathcal{O}(\epsilon^{j+2})$, $\mathcal{O}(\epsilon^{j+4})$ and $\mathcal{O}(\epsilon^{j+2})$ owing to the dependence upon slow scales only. The mean displacements $\tilde{x}_{j0}$ and $\tilde{z}_{j0}$ are governed by the new set of equations

$$\frac{\partial \tilde{z}_{j0}}{\partial c_2} = \tilde{E}_{j0} \qquad \frac{\partial^3 \tilde{x}_{j0}}{\partial c_2 \partial t_2^2} = \tilde{G}_{j0} \qquad \frac{\partial \tilde{z}_{j0}}{\partial a_3} = \tilde{I}_{j0} \quad c_2 = 0 \tag{$I.3.20a - c$}$$

deduced respectively at $\mathcal{O}(\epsilon^{j+2})$, $\mathcal{O}(\epsilon^{j+6})$ and $\mathcal{O}(\epsilon^{j+3})$.

Similarly, for $j \geq 1$, the equation governing the ℓ^{th} harmonic of the short wave displacements at $\mathcal{O}(\epsilon^j)$ are

$$\frac{\partial z_{j\ell}}{\partial c} - \ell k x_{j\ell} = E_{j\ell} \qquad \ell = 1, 2, \ldots \tag{$I.3.21a$}$$

$$\frac{\partial x_{j\ell}}{\partial c} - \ell k z_{j\ell} = G_{j\ell} \qquad \ell = 1, 2, \ldots \tag{$I.3.21b$}$$

along with the free surface boundary condition

$$\ell x_{j\ell} - z_{j\ell} = I_{j\ell} \qquad c = 0 \qquad \ell = 1, 2, \ldots \tag{$I.3.21c$}$$

The above equations have all been deduced at $\mathcal{O}(\epsilon^j)$. The mean displacements satisfy again a different set of equations

$$\frac{\partial z_{j0}}{\partial c} = E_{j0} \qquad \frac{\partial^3 x_{j0}}{\partial c \partial t_1^2} = G_{j0} \qquad \frac{\partial z_{j0}}{\partial a_1} = I_{j0} \quad c = 0 \tag{$I.3.22a - c$}$$

Equations $(I.3.22a-c)$ have been obtained respectively at $\mathcal{O}(\epsilon^j)$, $\mathcal{O}(\epsilon^{j+2})$ and $\mathcal{O}(\epsilon^{j+1})$. In particular, when $j=1$, the forcing terms are

$$E_{10}=0 \qquad G_{10}=2\sigma k^2 e^{2kc}|A|^2 \qquad I_{10}=0 \qquad (I.3.23a-c)$$

which were used earlier to derive the expression of x_{10}.

Owing to the diversity of slow scales in this problem, the three approximate equations governing the displacements at $\mathcal{O}(\epsilon^j)$ can arise at much higher orders. Approximate governing must therefore be deduced at a very high order. In practice, however, the irrotationality equation primarily suffers from this drawback, owing to the presence of third order derivatives.

Our objective is to analyse the effect of the long waves on the evolution of the short wave amplitude A over long spatial and time scales so that $ka_2=\mathcal{O}(1)$ and $\sigma t_2=\mathcal{O}(1)$. During this time span, the long waves themselves may be modulated. The corresponding spatial modulation scale is $ka_3=\mathcal{O}(1)$ as will be confirmed later. Establishing the evolution equation for A requires, as far as short waves are concerned, the derivation of approximate governing equations up to $\mathcal{O}(\epsilon^3)$. Approximate irrotationality equations will be needed up to $\mathcal{O}(\epsilon^5)$ in order to solve for various long wave displacements contributing to the nonlinear evolution of A.

3.3. Linear Evolution Equations

3.3.1. *The short wave*

The equations governing the first harmonic displacements at $\mathcal{O}(\epsilon^2)$ are given by $(I.3.21a-c)$ with $(j,\ell)=(2,1)$ along with the forcing terms

$$E_{21}=G_{21}=i\left\{k\left(\frac{\partial x_{10}}{\partial c}+\frac{\partial \tilde{x}_{-10}}{\partial c_2}-iKB^*e^{i\phi}\right)A-\frac{\partial A}{\partial t_1}\right\}e^{kc} \qquad (I.3.24a-b)$$

and

$$I_{21}=-\frac{2i}{\sigma}\left\{\frac{\partial A}{\partial t_1}+\frac{g}{2\sigma}\frac{\partial A}{\partial a_1}\right\} \qquad (I.3.24c)$$

The factor e^{kc}, which appears in the forcing terms $(I.3.24a-b)$, is also a solution of the homogeneous equations. To insure the existence of a solution to the inhomogeneous problem, a solvability condition must be enforced. We prove in Appendix

C, that the familiar Green formula for the Laplacian operator is equivalent to the following condition

$$\int_{-\infty}^{0} [G_{21} - E_{21}] e^{kc} dc = I_{21} \qquad (I.3.25)$$

Substitution of $(I.3.24a - c)$ in $(I.3.25)$ yields

$$\frac{\partial A}{\partial t_1} + \frac{\sigma}{2k} \frac{\partial A}{\partial a_1} = 0 \qquad (I.3.26)$$

Eq. $(I.3.26)$ describes the evolution of the short wave amplitude A for spatial scales $ka_1 = \mathcal{O}(1)$, and times $\sigma t_1 = \mathcal{O}(1)$ and can also be put in the form

$$\frac{\partial}{\partial t_1} \left(\frac{|A|^2}{\sigma} \right) + \frac{\sigma}{2k} \frac{\partial}{\partial a_1} \left(\frac{|A|^2}{\sigma} \right) = 0 \qquad (I.3.27)$$

The wave action is therefore conserved. It is important to point out that neither the expression of x_{10} nor that of $\tilde{x}_{-10}$ is needed to deduce $(I.3.26)$.

3.3.2. *The long wave*

The equations governing $(\tilde{x}_{01}, \tilde{z}_{01})$ are deduced from $(I.3.19a - b)$ with the following forcing terms

$$\tilde{E}_{21} = \tilde{G}_{21} = i \left\{ K \frac{\partial \tilde{x}_{-10}}{\partial c_2} B - \frac{\partial B}{\partial t_2} \right\} e^{Kc_2} \qquad (I.3.28a - b)$$

and

$$\tilde{I}_{21} = -\frac{2i}{\Omega} \left\{ \frac{\partial B}{\partial t_2} + \frac{g}{2\Omega} \frac{\partial B}{\partial a_3} \right\} \qquad (I.3.28c)$$

Again, the presence of e^{Kc_2} terms in $(I.3.28a - b)$ requires that the solvability condition

$$\int_{-\infty}^{0} [\tilde{G}_{21} - \tilde{E}_{21}] e^{Kc_2} dc_2 = \tilde{I}_{21} \qquad (I.3.29)$$

be met. This implies after use is made of $(I.3.28a - c)$

$$\frac{\partial B}{\partial t_2} + \frac{\Omega}{2K} \frac{\partial B}{\partial a_3} = 0 \qquad (I.3.30)$$

Eq. $(I.3.31)$ describes the evolution of the long wave for scales $ka_3 = \mathcal{O}(1)$ and $\sigma t_2 = \mathcal{O}(1)$ and can also be put in the form of a conservation law

$$\frac{\partial}{\partial t_2} \left(\frac{|B|^2}{\Omega} \right) + \frac{\Omega}{2K} \frac{\partial}{\partial a_3} \left(\frac{|B|^2}{\Omega} \right) = 0 \qquad (I.3.31)$$

For the present purpose, it is sufficient and consistent to describe the evolution of the long wave by the linear equation ($I.3.30$) only.

3.4. Corrections to Leading Order Displacements

3.4.1. *The short wave*

Once the solvability condition ($I.3.26$) is met, it is possible to solve for the first harmonic displacements at $\mathcal{O}(\epsilon^2)$. By straightforward elimination of one of the two variables, a linear non-homogeneous second order differential equation is obtained and solved with the method of variation of parameters. The result is

$$x_{21}(c, a_1, t_1, \ldots) = z_{21}(c, a_1, t_1, \ldots) =$$

$$i\left\{k\left[\sigma k \epsilon^{2kc}\int_0^{t_1}|A|^2 dt_1 + 2K\sigma c\int_0^{t_2}|B|^2 dt_2 - iKB^* c e^{i\phi}\right]A - c\frac{\partial A}{\partial a_1}\right\}e^{kc} \qquad (I.3.32a-b)$$

The short wave displacements at $\mathcal{O}(\epsilon^2)$ are again identical in magnitude. The second harmonic displacements (x_{22}, z_{22}) are governed by ($I.3.21a-c$) along with the forcing terms $E_{22} = G_{22} = I_{22} = 0$. Therefore, no second harmonics are generated at this order. This result is also true in the Eulerian formulation.

It has been pointed out that the linear evolution equation ($I.3.26$) was derived without the knowledge of x_{10}. It is therefore expected that the nonlinear evolution equation deduced at $\mathcal{O}(\epsilon^3)$ can likewise be derived without solving explicitly for (x_{20}, z_{20}).

3.4.2. *The long wave*

With the solvability condition ($I.3.31$), it is now possible to derive the long wave displacements, $(\tilde{x}_{01}, \tilde{z}_{01})$, at $\mathcal{O}(1)$ by solving again a linear non-homogeneous second order differential equation. The solution is straightforwardly found

$$\tilde{x}_{01}(c_2, a_3, t_2, \ldots) = \tilde{z}_{01}(c_2, a_3, t_2, \ldots) = i\left\{\Omega K^2 B e^{2Kc_2}\int_0^{t_2}|B|^2 dt_2 - c_2\frac{\partial B}{\partial a_3}\right\}e^{Kc_2} \qquad (I.3.33a-b)$$

The vertical and horizontal displacements are again identical. The second harmonics satisfy a set of homogeneous equations and thus are absent at $\mathcal{O}(1)$.

The zeroth harmonic displacements $(\tilde{x}_{00}, \tilde{z}_{00})$ are not needed to evaluate the solvability condition for the short wave first harmonic at $\mathcal{O}(\epsilon^3)$ and are therefore omitted here.

3.5. Nonlinear Evolution Equation for Short Waves

The solvability condition for (x_{31}, z_{31}) at $\mathcal{O}(\epsilon^3)$ reads

$$\int_{-\infty}^{0} [G_{31} - E_{31}] e^{kc} dc = I_{31} \qquad (I.3.34)$$

where the integrand is given in terms of the lower order long and short wave displacements by

$$G_{31} - E_{31} = \left\{ i \left(\frac{\partial x_{21}}{\partial a_1} - \frac{\partial z_{21}}{\partial a_1} \right) + KB \left(\frac{\partial x_{21}}{\partial c} - \frac{\partial z_{21}}{\partial c} \right) e^{-i\phi} + \right.$$

$$- \frac{2i}{\sigma} \frac{\partial^2 x_{21}}{\partial c \partial t_1} + \frac{2ik}{\sigma} \frac{\partial z_{21}}{\partial t_1} + ik(x_{21} - z_{21}) \left[\frac{\partial x_{10}}{\partial c} + \frac{\partial \tilde{x}_{-10}}{\partial c_2} - iKBe^{-i\phi} \right] +$$

$$\left. + \frac{2}{\sigma} \frac{\partial^2 A}{\partial a_1 \partial t_1} - \frac{2k}{\sigma} \left[\frac{\partial x_{10}}{\partial c} + \frac{\partial \tilde{x}_{-10}}{\partial c_2} - 4iKB^* e^{i\phi} \right] \frac{\partial A}{\partial t_1} \right\} e^{kc} \qquad (I.3.35)$$

and the right hand side by

$$I_{31} = - \frac{2i}{\sigma} \frac{\partial x_{21}}{\partial t_1} - \frac{i}{k} \frac{\partial z_{21}}{\partial a_1} + KBe^{-i\phi}(x_{21} - z_{21}) +$$

$$+ \frac{2i}{\sigma} KB^* e^{i\phi} \frac{\partial A}{\partial t_1} - \frac{2i}{\sigma} \frac{\partial A}{\partial t_2} - \frac{i}{k} \frac{\partial A}{\partial a_2} + \frac{1}{\sigma^2} \frac{\partial^2 A}{\partial t_1^2} + \frac{i}{k} KB^* \frac{\partial A}{\partial a_1} e^{i\phi} +$$

$$\left\{ K(\tilde{x}_{01} - \tilde{z}_{01}) e^{-i\phi} - \frac{\partial x_{10}}{\partial c} - \frac{\partial \tilde{x}_{-10}}{\partial c_2} \right\} A \qquad c = 0 \qquad (I.3.36)$$

Note that all displacements appearing in $(I.3.35)$ and $(I.3.36)$ are known. Substituting the adequate equations in $(I.3.35)$ and $(I.3.36)$ first and then the results in the solvability condition $(I.3.34)$ yields after simplifications

$$\frac{\partial A}{\partial t_2} + \frac{\sigma}{2k} \frac{\partial A}{\partial a_2} + \frac{i\sigma}{8k^2} \frac{\partial^2 A}{\partial a_1^2} + \frac{i}{2} \sigma k^2 |A|^2 A + i\sigma K^2 |B|^2 A - i\Omega KB^* e^{i\phi} = 0 \qquad (I.3.37)$$

Eq. $(I.3.37)$ is a nonlinear cubic Schrödinger equation describing the evolution of the short wave amplitude A over scales $ka_2 = \mathcal{O}(1)$ and $\sigma t_2 = \mathcal{O}(1)$. The first four terms in $(I.3.37)$ are the usual Schrödinger terms. The fifth term corresponds to a

phase change and, finally, the sixth term describes changes in both the amplitude and the phase of A.

Next, the linear and nonlinear evolution equations are combined

$$\frac{\partial A}{\partial t_1} + \frac{\sigma}{2k}\frac{\partial A}{\partial a_1} + i\epsilon\left\{\frac{\sigma}{8k^2}\frac{\partial^2 A}{\partial a_1^2} + \frac{1}{2}\sigma k^2|A|^2 A + \sigma K^2|B|^2 A - \Omega K B^* e^{i\phi} A\right\} = \mathcal{O}(\epsilon^2) \tag{I.3.38}$$

The following variables are now introduced

$$\xi = a_1 - \frac{\sigma}{2k}t_1 \qquad \phi = \Omega t_1 - \epsilon K a_1 \tag{I.3.39a-b}$$

with the corresponding differentiation rules

$$\frac{\partial}{\partial t_1} = \Omega\frac{\partial}{\partial \tau} - \frac{\sigma}{2k}\frac{\partial}{\partial \xi} \qquad \frac{\partial}{\partial a_1} = \frac{\partial}{\partial \xi} - \epsilon K\frac{\partial}{\partial \tau} \qquad \frac{\partial^2}{\partial a_1^2} = \frac{\partial^2}{\partial \xi^2} + \mathcal{O}(\epsilon) \tag{I.3.40a-c}$$

The evolution equations becomes

$$\frac{\partial A}{\partial \phi} + \frac{i\epsilon}{\delta\Omega}\left\{\frac{\sigma}{8k^2}\frac{\partial^2 A}{\partial \xi^2} + \frac{1}{2}\sigma k^2|A|^2 A + \sigma K^2|B|^2 A - \Omega K B^* e^{i\phi} A\right\} = \mathcal{O}(\epsilon^2) \tag{I.3.41}$$

where

$$\delta \equiv 1 - \epsilon\frac{\Omega}{2\sigma} \tag{I.3.42}$$

Note that the ϵ factor has not been absorbed in the new time variable because ϕ appears explicitly in the governing equation (I.3.38). The analysis of (I.3.41) and its implications regarding the modulation due to long waves are carried out in §I.4.

With a view to eliminating the phase terms in (I.3.41), we introduce a new complex amplitude A'

$$A(\xi,\phi) = A'(\xi,\phi)e^{i\Gamma(\phi)} \tag{I.3.43}$$

where $\Gamma(\phi)$ is easily found to be

$$\Gamma(\phi, \epsilon K B, \epsilon\frac{\Omega}{\sigma}) = -\frac{\epsilon\sigma}{\delta\Omega}K^2|B|^2\phi + \lambda\sin\phi + \mathcal{O}(\epsilon^2) \tag{I.3.44}$$

and the parameter λ is defined by

$$\lambda \equiv \frac{\epsilon K B^*}{\delta} = \mathcal{O}(\epsilon) \tag{I.3.45}$$

The governing equation for A' is deduced after substituting $(I.3.43)$ in $(I.3.41)$:

$$\frac{\partial A'}{\partial \phi} + \frac{i\epsilon}{\delta\Omega}\left\{\frac{\sigma}{8k^2}\frac{\partial^2 A'}{\partial \xi^2} + \frac{1}{2}\sigma k^2 |A'|^2 A'\right\} + \lambda \sin\phi \; A' = \mathcal{O}(\epsilon^2) \qquad (I.3.46)$$

Next, the following dimensionless variables are introduced

$$\mathcal{A} = \frac{A'}{\overline{A}} \qquad \xi' = k^2 \overline{A} \xi \qquad (I.3.47a - b)$$

If use is made of $(I.3.47a - b)$ in $(I.3.46)$, we obtain the evolution equation for $\mathcal{A}$

$$\frac{\partial \mathcal{A}}{\partial \phi} + \frac{i\alpha}{4}\frac{\partial^2 \mathcal{A}}{\partial \xi'^2} + i\alpha |\mathcal{A}|^2 \mathcal{A} + \lambda \sin\phi \; \mathcal{A} = \mathcal{O}(\epsilon^2) \qquad (I.3.48)$$

where

$$\alpha \equiv \frac{\epsilon}{2\delta}\frac{(k\overline{A})^2}{\frac{\Omega}{\sigma}} \qquad (I.3.49)$$

is an $\mathcal{O}(\epsilon)$ parameter describing the common magnitude of the nonlinear and dispersion terms.

In summary, the long waves are governed by $(I.3.31)$ up to the time scale $t_2 = \epsilon^2 t = \mathcal{O}(1)$, and are not affected by the short waves. The short waves, however, are affected by the long waves through $(I.3.48)$. Feedback effect on the long waves can be expected at the next order, but the analysis is dauntingly complex and is not pursued here.

4. MODULATION OF SHORT WAVES RIDING ON A LONG WAVE

In the following section, the modulation of the short wave amplitude and wavenumber is sought and the relationship between intrinsic and absolute frequencies investigated.

4.1. Modulation of the Short Wave Amplitude

The linear term in the Schrödinger equation (I.3.48) can be removed by introducing the a new variable $\tilde{\mathcal{A}}$ according to

$$\mathcal{A}(\xi,\phi) = \tilde{\mathcal{A}}(\xi,\phi)\exp(\lambda\cos\phi) \tag{I.4.1}$$

Then, $\tilde{\mathcal{A}}$ satisfies

$$\frac{\partial\tilde{\mathcal{A}}}{\partial\phi} + \frac{i\alpha}{4}\frac{\partial^2\tilde{\mathcal{A}}}{\partial\xi^2} + i\alpha|\tilde{\mathcal{A}}|^2\tilde{\mathcal{A}} = \mathcal{O}(\epsilon^2) \tag{I.4.2}$$

We conclude that, within $\mathcal{O}(\epsilon^2)$ errors, the amplitude $\mathcal{A}$ is the product of a solution of the classic Schrödinger equation (I.4.2) by a modulation factor $\mathcal{M}$

$$\mathcal{M} = \exp(\lambda\cos\phi) \tag{I.4.3a}$$

Expansion for small ϵ yields

$$\mathcal{M} = 1 + \epsilon KB\cos\phi + \mathcal{O}(\epsilon^2) \tag{I.4.3b}$$

which is the same as the results derived by Longuet-Higgins & Stewart(1960).

4.2. Modulation of the Short Wave Wavenumber

In view of (I.3.43), the Lagrangian phase function S must be corrected to account for the phase term (I.3.44)

$$\tilde{S} = S + \Gamma(\phi, KB, \epsilon\frac{\Omega}{\sigma}) = ka - \sigma t + \Gamma(\phi, KB, \epsilon\frac{\Omega}{\sigma}) \tag{I.4.4}$$

Recalling the series expansion (I.2.14a) for the horizontal coordinate X of a particle, we deduce

$$a = X - \frac{1}{\epsilon}x_{-1} - x_0 - \epsilon x_1 + \mathcal{O}(\epsilon^2) \tag{I.4.5}$$

Substitution of $(I.4.5)$ in $(I.4.4)$ yields

$$\tilde{S} = \frac{1}{\epsilon}\tilde{S}_{-1} + \tilde{S}_0 + \epsilon\tilde{S}_1 + \mathcal{O}(\epsilon^2) \qquad (I.4.6a)$$

where

$$\tilde{S}_{-1} = -kx_{-1} \qquad \tilde{S}_0 = k(X - x_0) - \sigma t \qquad \tilde{S}_1 = \Gamma(\phi, KB, \epsilon\frac{\Omega}{\sigma}) - k\overline{x}_1 \quad (I.4.6b-d)$$

where $\overline{x}_1$ designates the component of x_1 that is independent of the phase function S. On the other hand, the harmonic term in x_1 is expanded as an amplitude correction. The Eulerian wavenumber is obtained as the Eulerian gradient of $(I.4.6a)$ according to the chain rule

$$\vec{k}^e = \nabla\tilde{S} + \epsilon\nabla_1\tilde{S} + \epsilon^2\nabla_2\tilde{S} + \mathcal{O}(\epsilon^2) \qquad (I.4.7)$$

where ∇ and ∇_i stand respectively for (∂_X, ∂_Z) and $(\partial_{X_i}, \partial_{Z_i})$. Substitution of $(I.4.6a)$ in $(I.4.7)$ yields

$$\vec{k}^e = \nabla\tilde{S}_0 + \epsilon\nabla_2\tilde{S}_{-1} + \mathcal{O}(\epsilon^2) \qquad (I.4.8a)$$

Since $\tilde{S}_{-1}$ is a function of a_2 (through ϕ) and of c_2, $(I.4.8a)$ can be simplified to

$$\vec{k}^e = \nabla\tilde{S}_0 + \epsilon\Big[\frac{\partial\tilde{S}_{-2}}{\partial a_2}\nabla_2 a_2 + \frac{\partial\tilde{S}_{-2}}{\partial c_2}\nabla_2 c_2\Big] \qquad (I.4.8b)$$

To evaluate the slow gradient in $(I.4.8b)$, we first multiply $(I.2.12a-b)$ throughout by ϵ^2

$$X_2 = a_2 + \epsilon x_{-1} + \mathcal{O}(\epsilon^2) \qquad Z_2 = c_2 + \epsilon z_{-1} + \mathcal{O}(\epsilon^2) \qquad (I.4.9a-b)$$

and evaluate $\nabla_2 a_2$ to leading order only

$$\nabla_2 a_2 = \left(\frac{\partial Z_2}{\partial c_2}, -\frac{\partial X_2}{\partial c_2}\right) = (1 + \mathcal{O}(\epsilon), \mathcal{O}(\epsilon)) \qquad (I.4.10a)$$

and likewise for $\nabla_2 c_2$

$$\nabla_2 c_2 = \left(-\frac{\partial Z_2}{\partial a_2}, \frac{\partial X_2}{\partial a_2}\right) = (\mathcal{O}(\epsilon), 1 + \mathcal{O}(\epsilon)) \qquad (I.4.10b)$$

The horizontal component, k_x^e, of $\vec{k}^e$ is then

$$k_x^e = k + \epsilon \frac{\partial \tilde{S}_{-1}}{\partial a_2} + \mathcal{O}(\epsilon^2) \qquad (I.4.11a)$$

When $(I.4.6b)$ is substituted in $(I.4.11a)$ with the help of $(I.3.13a)$, the wavenumber modulation is deduced

$$\frac{k_x^e}{k} = 1 + \epsilon K B \cos\phi + \mathcal{O}(\epsilon^2) \qquad (I.4.11b)$$

assuming that B is real. The wavenumber modulation of Longuet-Higgins & Stewart(1960) is again recovered.

Next, the vertical component, k_z^e, is evaluated as

$$k_z^e = \epsilon \frac{\partial \tilde{S}_{-1}}{\partial c_2} + \mathcal{O}(\epsilon^2) \qquad (I.4.12a)$$

therefore, after the obvious substitutions

$$\frac{k_z^e}{k} = -\epsilon \frac{\partial x_{-1}}{\partial c_2} = -\epsilon \left\{ K B \sin\phi + 2\Omega K^2 \int_0^{t_2} |B|^2 dt_2 \right\} + \mathcal{O}(\epsilon^2) \qquad (I.4.12b)$$

which is valid for times $\sigma t_2 = \mathcal{O}(1)$. Owing to the presence of the long waves, the short wave wavenumber has an $\mathcal{O}(\epsilon)$ vertical component.

4.3. Absolute and Intrinsic Frequencies

The absolute frequency, ω, or the frequency of the short waves in a fixed frame of reference is defined in terms of the phase function $\tilde{S}$ and at the leading order

$$\omega = -\frac{\partial \tilde{S}}{\partial t}\bigg|_{X,X_1} - \epsilon \frac{\partial \tilde{S}}{\partial t_1}\bigg|_{X,X_1} + \mathcal{O}(\epsilon) \qquad (I.4.13)$$

where the time derivative must be taken while keeping X and X_1 constant. Substitution of $(I.4.6a)$ in $(I.4.13)$ results in

$$\omega = -\frac{\partial \tilde{S}_0}{\partial t}\bigg|_{X,X_1} - \frac{\partial \tilde{S}_{-1}}{\partial t_1}\bigg|_{X,X_1} + \mathcal{O}(\epsilon) = \sigma - \frac{\partial \tilde{S}_{-1}}{\partial \phi}\frac{\partial \phi}{\partial t_1}\bigg|_{X,X_1} + \mathcal{O}(\epsilon) \qquad (I.4.14)$$

Before evaluating $(I.4.14)$, a relation between ϕ and $\phi_E \equiv \Omega t_1 - K X_2$ is sought first. Upon multiplying $(I.4.9a)$ by K and subtracting from both sides Ωt_1, we clearly obtain

$$\phi_E = \phi - \epsilon K x_{-1} + \mathcal{O}(\epsilon^2) \qquad (I.4.15a)$$

Substitution of $(I.3.13a)$ yields at the free surface $c_2 = 0$

$$\phi_{\mathrm{E}} = \phi - \epsilon KB \sin\phi - \epsilon K \tilde{x}_{-10} + \mathcal{O}(\epsilon^2) \qquad (I.4.15b)$$

Upon taking the Eulerian t_1-derivative of $(I.4.15b)$ we deduce

$$\left.\frac{\partial \phi}{\partial t_1}\right|_{X,X_1} = \left.\frac{\partial \phi_{\mathrm{E}}}{\partial t_1}\right|_{X,X_1} (1 - \epsilon KB\cos\phi)^{-1} + \mathcal{O}(\epsilon^2) = \frac{\Omega}{1 - \epsilon KB\cos\phi} + \mathcal{O}(\epsilon^2) \quad (I.4.16)$$

With the definitions $(I.4.6b-c)$ of $\tilde{S}_{-1}$ and $(I.4.16)$, we deduce at the leading order

$$\frac{\omega}{\sigma} = 1 + \frac{\Omega}{\sigma} k \frac{\partial x_{-1}}{\partial \phi} + \mathcal{O}(\epsilon) = 1 + \frac{\Omega}{\sigma} kB\cos\phi + \mathcal{O}(\epsilon) \qquad (I.4.17)$$

after making use of the dispersion relations $(I.3.8)$ and $(I.3.16)$.

Two special cases are noteworthy. Firstly, when the absolute and intrinsic frequencies are identical, *i.e.* when $\cos\phi = 0$. From $(I.4.15a)$, it is clear that the Lagrangian and Eulerian phases ϕ and ϕ_{E} differ only by an $\mathcal{O}(\epsilon KB)$ quantity. The solutions of the previous equation are therefore at the leading order

$$\phi_{\mathrm{E}} = \frac{\pi}{2} + \mathcal{O}(\epsilon KB) \qquad \phi_{\mathrm{E}} = \frac{3\pi}{2} + \mathcal{O}(\epsilon KB) \qquad (I.4.18a-b)$$

More interesting is the situation where the short waves appear to be steady *i.e.* when $\frac{\omega}{\sigma} = 0$. This situation occurs provided that $\epsilon KB \geq \epsilon\frac{\Omega}{\sigma}$. There are then two symmetric solutions

$$\phi_{\mathrm{E}} = \arccos\Big[-\frac{\epsilon\frac{\Omega}{\sigma}}{\epsilon KB}\Big] + \mathcal{O}(\epsilon KB) \qquad \phi_{\mathrm{E}} = 2\pi - \arccos\Big[-\frac{\epsilon\frac{\Omega}{\sigma}}{\epsilon KB}\Big] + \mathcal{O}(\epsilon KB) \qquad (I.4.19a-b)$$

In figure 4.1 we have superimposed, in the $(\phi_{\mathrm{E}}, \epsilon KB)$ plane, the branches representing $(I.4.18a-b)$ and $(I.4.19a-b)$ for $\epsilon\frac{\Omega}{\sigma}$=0.05, 0.075, 0.1 and 0.125. In the vicinity of the crest, the absolute frequency ω is greater than the intrinsic frequency σ. This is expected since the long wave particle velocity vector at the free surface and the short wavenumber vector both point to the right. Elsewhere, we observe that $\omega < \sigma$. For a given value of $\epsilon\frac{\Omega}{\sigma}$, the short waves appear, to a fixed observer, to propagate to the left near the trough of steep enough long waves $(\epsilon KB \geq \epsilon\frac{\Omega}{\sigma})$.

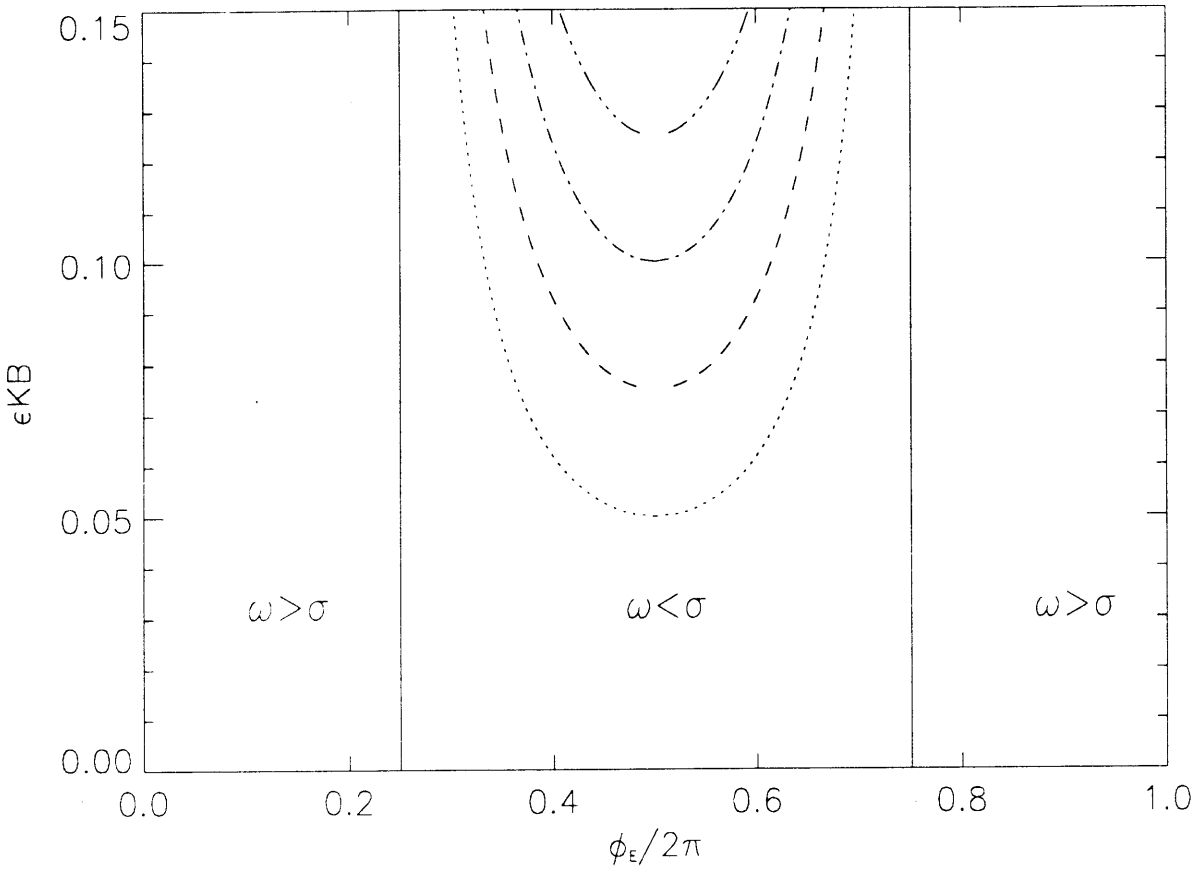

Figure I.4.1: Contours of $\frac{\omega}{\sigma}(\phi_E, \epsilon KB)$, $\frac{\omega}{\sigma} = 1$ (——); $\frac{\omega}{\sigma} = 0$ with $\epsilon\frac{\Omega}{\sigma} = 0.05$ (· · · · ·), 0.075 (- - - - -), 0.1 (—·—·—) and 0.125 (—· · ·—· · ·—· · ·—).

In the presence of a variable current or topography, it is well known that a gravity wave and its amplitude may propagate in different directions. In the next section, we investigate the direction of propagation of the short wave energy.

4.4. Group Velocity and Blockage

The linear evolution of the short wave amplitude A is described by (I.3.26)

$$\frac{\partial A}{\partial t_1} + \frac{\sigma}{2k}\frac{\partial A}{\partial a_1} = 0 \qquad (I.4.20)$$

where the first term is a Lagrangian or particle time derivative and the second term a Lagrangian gradient. Since $A = A(a_1(X_1, t_1), t_1)$, the Lagrangian time derivative

is decomposed as follows

$$\left.\frac{\partial A}{\partial t_1}\right|_{a_1} = \left.\frac{\partial A}{\partial t_1}\right|_{X_1} + \frac{\partial A}{\partial X_1}\frac{\partial X_1}{\partial t_1} \qquad (I.4.21)$$

where X_1 is obtained by multiplying $(I.2.14a)$ throughout by ϵ, *i.e.*

$$X_1 = a_1 + \tilde{x}_{-10}(c_2, a_3, t_2) + B(a_3, t_2)\sin\phi e^{Kc_2} + \mathcal{O}(\epsilon) \qquad (I.4.22)$$

after assuming for simplicity that B is real. Eq. $(I.4.21)$ becomes after substitution of $(I.4.22)$

$$\left.\frac{\partial A}{\partial t_1}\right|_{a_1} = \left.\frac{\partial A}{\partial t_1}\right|_{X_1} + \Omega B\cos\phi\frac{\partial A}{\partial X_1} \qquad (I.4.23)$$

The relationship between the Eulerian and Lagrangian gradients is deduced from $(I.4.22)$:

$$\frac{\partial}{\partial a_1} = \frac{\partial}{\partial X_1} + \mathcal{O}(\epsilon^2) \qquad (I.4.24)$$

With $(I.4.23)$ and $(I.4.24)$, the linear evolution equation for A can be rewritten as

$$\left.\frac{\partial A}{\partial t_1}\right|_{X_1} + C_g\frac{\partial A}{\partial X_1} = \mathcal{O}(\epsilon) \qquad (I.4.25a)$$

where

$$C_g = \frac{\sigma}{2k} + \Omega B\cos\phi + \mathcal{O}(\epsilon KB) \qquad (I.4.25b)$$

is the absolute group velocity of the short waves. In the vicinity of the crest ($\phi = \phi_E = 0$), C_g is positive and the short wave energy propagates to the right. If the long wave particle velocity is large enough ($\Omega B > \frac{\sigma}{2k}$), the group velocity becomes negative near the trough ($\phi = \phi_E = \pi$). The phase location where C_g changes of sign is a reflection or blockage point and is defined by

$$\phi_E = \arccos\Big[-\frac{1}{2}\frac{\epsilon\frac{\Omega}{\sigma}}{\epsilon KB}\Big] + \mathcal{O}(\epsilon KB) \qquad \phi_E = 2\pi - \arccos\Big[-\frac{1}{2}\frac{\epsilon\frac{\Omega}{\sigma}}{\epsilon KB}\Big] + \mathcal{O}(\epsilon KB) \qquad (I.4.26a-b)$$

We have plotted in figure 4.2 the three contours $\omega = \sigma$, $\omega = 0$ and $C_g = 0$ in the $(\phi_E, \epsilon KB)$ plane. For intermediate values of KB, energy may propagate to the left while the carrier wave is still propagating to the right, in agreement with $(I.4.19a-b)$ and $(I.4.26a-b)$. Note however that when the short carrier wave is left going so is its energy.

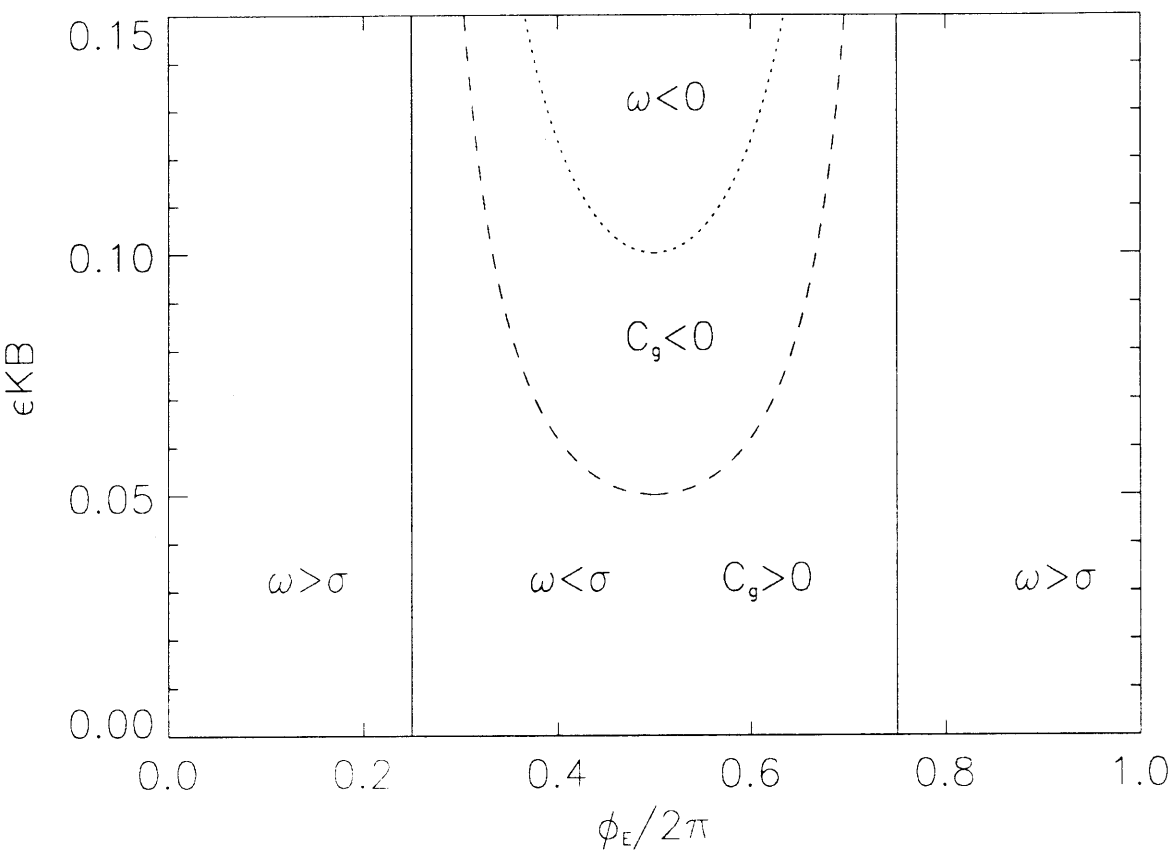

Figure I.4.2: Absolute frequency and group velocity. $\frac{\omega}{\sigma} = 1$ (——-), $\frac{\omega}{\sigma} = 0$ (·····), and $C_g = 0$ (- - - -) with $\epsilon\frac{\Omega}{\sigma} = 0.1$.

5. NONLINEAR EVOLUTION OF SHORT WAVES ON A LONG WAVE

5.1. A Solitary Solution for Short Wave

The short wave complex amplitude $\tilde{A}$ satisfies the nonlinear Schrödinger equation (I.4.2). There is an exact solution (see Mei, 1989) corresponding to the solitary wave

$$\tilde{A}(\xi,\phi) = \operatorname{sech}\sqrt{2}\xi \; e^{-i(\alpha\frac{\phi}{2}+\varphi)} \tag{I.5.1a}$$

where ξ is the coordinate in the frame moving at the group velocity of the short waves

$$\xi = k^2\overline{A}(a_1 - \frac{\sigma}{2k}t_1) \tag{I.5.1b}$$

and φ is an arbitrary phase angle. The Lagrangian variable a_1 which may be replaced in terms of X_1 and Lagrangian displacements according to (I.4.22):

$$a_1 = X_1 - \tilde{x}_{-10}(c_2,a_3,t_2) - B(a_3 - \frac{\Omega}{2K}t_2)\sin\phi + \mathcal{O}(\epsilon) \tag{I.5.2}$$

on the free surface ($c_2 = 0$). Substitution of (I.5.2) in (I.5.1b) yields

$$\xi = \xi_{\mathrm{E}} - k^2\overline{A}\big(\Omega K\int_0^{t_2}|B|^2dt_2 + B\sin\phi + \mathcal{O}(\epsilon)\big) \tag{I.5.3a}$$

where the Eulerian counterpart, ξ_{E}, of ξ is defined by

$$\xi_{\mathrm{E}} = k^2\overline{A}(X_1 - \frac{\sigma}{2k}t_1) \tag{I.5.3b}$$

The real amplitude of $\tilde{A}$ can then be rewritten as

$$|\tilde{A}| = \operatorname{sech}\sqrt{2}\xi = \operatorname{sech}\sqrt{2}\big[\xi_{\mathrm{E}} - (\xi_{\mathrm{E}} - \xi)\big] \tag{I.5.4}$$

Thus, $\xi_{\mathrm{E}} - \xi$ represents the displacement of the soliton peak due to the presence of the long wave. The variations of $\xi_{\mathrm{E}} - \xi$ are analysed next for three choices of the modulated long wave amplitude B. For the spatial and time scales of interest here ($ka_2 = \mathcal{O}(1)$ and $\sigma t_2 = \mathcal{O}(1)$), the modulation in the long wave amplitude is felt with the passage of time and not so much with the propagation over ranges $ka_3 = \mathcal{O}(1)$. Thus, within $\mathcal{O}(\epsilon)$ error, B is a function of $\epsilon\phi$ only. We then adopt ϕ as the integration variable in (I.5.3a) and obtain

$$\xi_{\mathrm{E}} - \xi = k^2\overline{A}\Big\{K\int_0^{\phi}|B(\epsilon\phi')|^2d\phi' + B\sin\phi + \mathcal{O}(\epsilon)\Big\} \tag{I.5.5}$$

which can be rewritten as

$$\xi_E - \xi = \epsilon k\overline{A} \int_0^{\phi} \left(\frac{\epsilon K |B(\epsilon\phi')|}{\epsilon\frac{\Omega}{\sigma}} \right)^2 d\phi' + \frac{\epsilon k\overline{A}\epsilon KB}{(\epsilon\frac{\Omega}{\sigma})^2} \sin\phi + \mathcal{O}(\epsilon) \qquad (I.5.6)$$

where the magnitude of each parameter in $(I.5.6)$ is indicated only by the the small parameter ϵ. The integral represents Stokes' drift in the long wave.

The amplitude B of the long wave is alternately assumed to be uniform, sinusoidally modulated and Gaussian,

(a) $B = \overline{B}$

(b) $B = \overline{B}\cos(\frac{\phi}{\chi})$

(c) $B = \overline{B}\exp\left[-\frac{1}{2}\left\{\frac{(\phi-\phi_0)}{\chi}\right\}^2\right]$

where $\overline{B}$ is the peak amplitude of the modulated long wave, χ is a modulation wavelength much longer than 2π.

5.2. Numerical Results

All computations are performed for $\epsilon k\overline{A} = \epsilon K\overline{B} = \epsilon\frac{\Omega}{\sigma} = 0.1$. When the long wave amplitude is uniform (case (a), see figure 5.1), the Stokes drift increases monotonically with ϕ_E. As a result, the position of the soliton peak is slowly shifted to the right while oscillating rapidly as the troughs and crests of the long wave pass by.

When the long wave amplitude is sinusoidal with period χ chosen to be 8π here, the Stokes drift is 2χ-periodic and can vanish, as seen for $\phi_E/2\pi \simeq 6$ in figure 5.2. Likewise, the soliton peak oscillates rapidly due to the passage of crests and troughs.

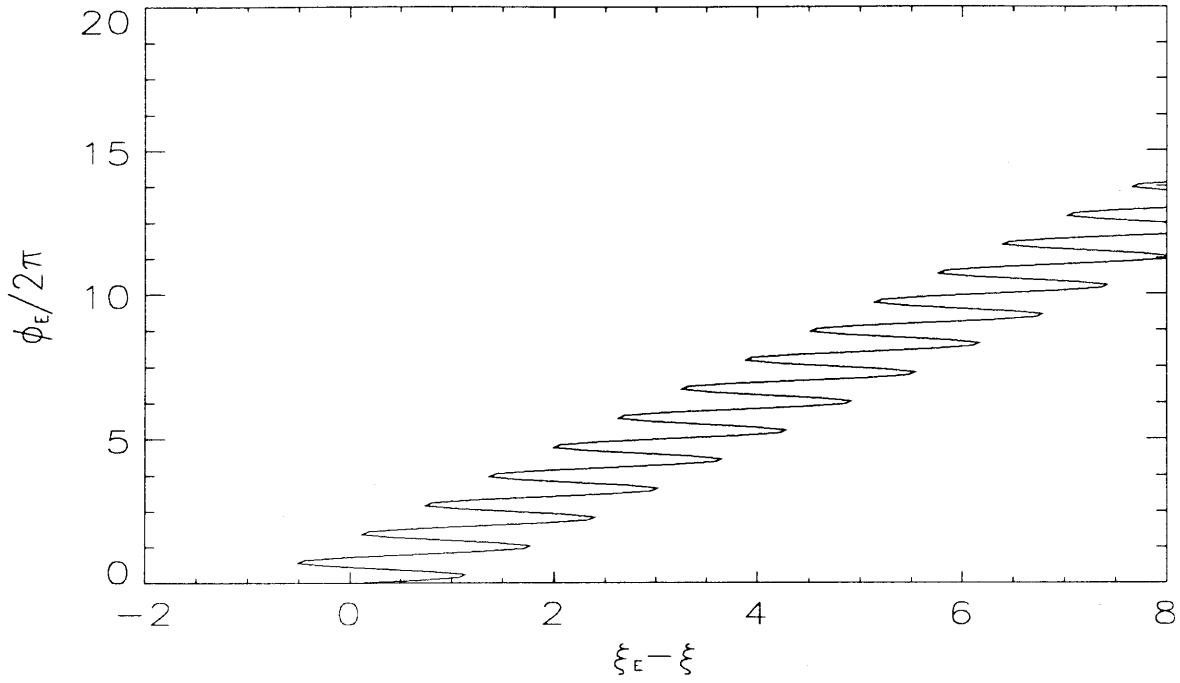

Figure I.5.1: Displacement of the peak of a short wave soliton riding on a long wave with uniform amplitude (case (a)) with $\epsilon k\overline{A} = 0.1$, $\epsilon K\overline{B} = 0.1$ and $\epsilon\frac{\Omega}{\sigma} = 0.1$.

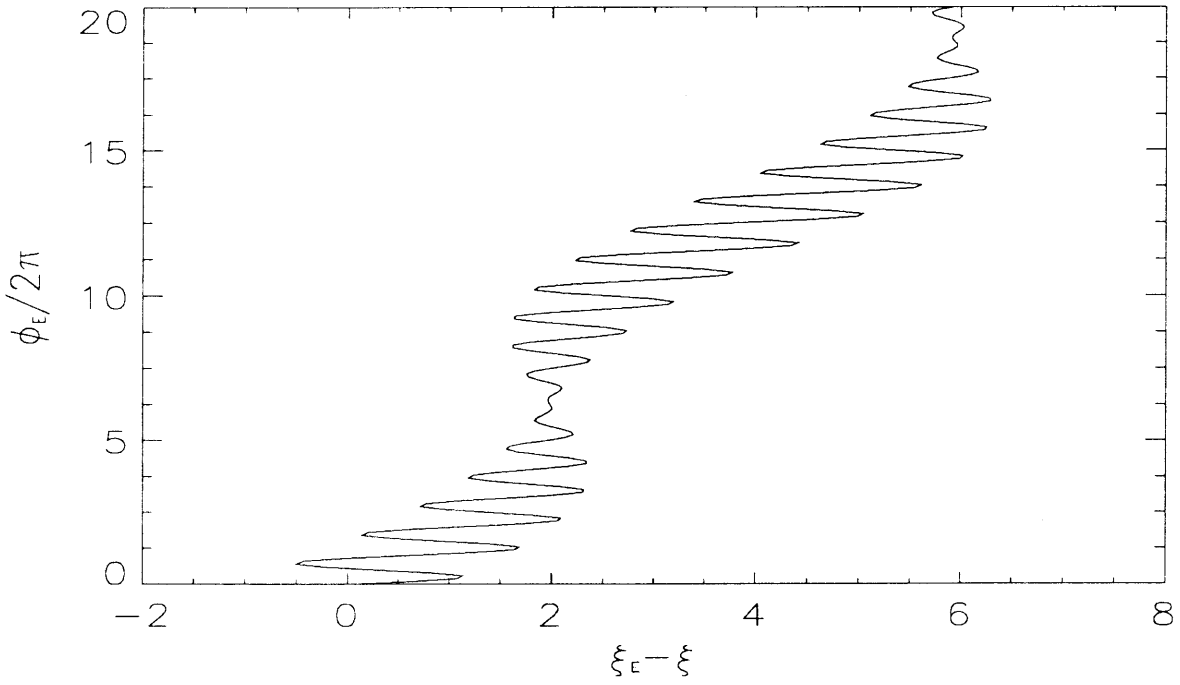

Figure I.5.2: Displacement of the peak of a short wave soliton riding on a long wave with sinusoidally modulated amplitude (case (b)) with $\chi = 8\pi$, $\epsilon k\overline{A} = 0.1$, $\epsilon K\overline{B} = 0.1$ and $\epsilon\frac{\Omega}{\sigma} = 0.1$.

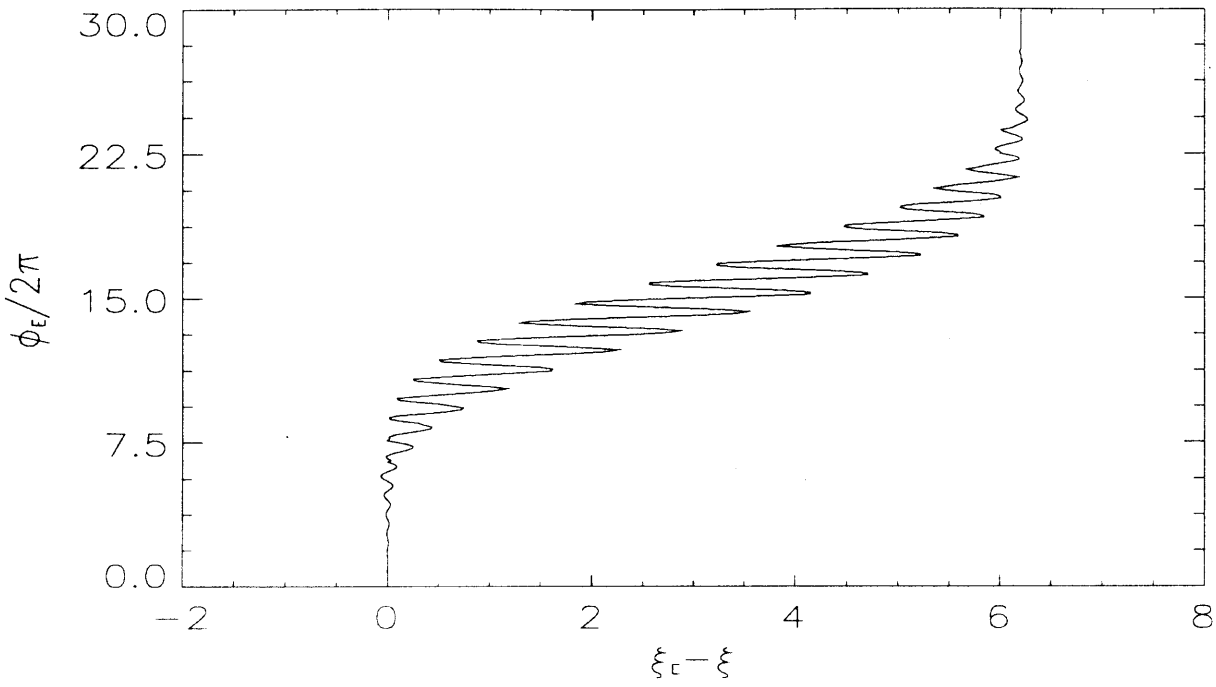

Figure I.5.3: Displacement of the peak of a short wave soliton riding on a long wave with a Gaussian amplitude (case (c)) with $\chi = 8\pi$, $\phi_0 = 30\pi$, $\epsilon k\overline{A} = 0.1$, $\epsilon K\overline{B} = 0.1$ and $\epsilon\frac{\Omega}{\sigma} = 0.1$.

Finally, for a Gaussian long wave amplitude (case (c) see figure 5.3), the short wave soliton is initially propagating on an otherwise calm sea surface and $\xi_E - \xi$ is identically zero. As the front of the long wave packet approaches, the amplitude of the fast oscillations grows and reaches a maximum at $\phi_0 = 30\pi$ before decreasing monotonically as the tail of the packet disappears. The Stokes drift, initially absent, increases monotonically and then reaches a plateau near $\xi_E - \xi = 6$. Thus, the long wave group pushes the short wave group forward by the distance $\xi_E - \xi = 6$.

6. CONCLUSIONS

We have analysed the evolution of a train of short gravity waves riding on a weak irrotational long wave. The particle velocity of the long wave and the group velocity of the short wave are assumed to have comparable magnitudes.

Although the Lagrangian formulation may appear at first more complicated than its Eulerian counterpart, it has eliminated the need to introduce a moving coordinate system and has produced compact results.

Under our scaling assumptions it is shown that the wavenumber modulation of the short wave is still adequately given by the theory of Longuet-Higgins & Stewart(1960). However, the amplitude modulation is described by the product of two factors, one corresponding to the theory of Longuet-Higgins & Stewart and the other obeying the nonlinear Schrödinger equation.

The relationship between absolute and intrinsic frequencies is established. In particular, for relatively steep long waves, the short carrier waves may appear to propagate to the left in a fixed frame of reference. For intermediate long wave slopes ϵKB, the short carrier wave may propagate to the right while its energy propagates to the left. Thus energy may be reflected !

Upon factoring out the Stokes solution, the evolution equation (I.3.48) reduces to the Schrödinger equation (I.4.2). The linearized stability of sideband disturbances is then adequately described by the theory of Benjamin & Feir(1967), as seen by a fluid particle. Next, a solitary wave solution in Lagrangian variables is assumed for the short wave. After translation to Eulerian coordinates, it is found that the position of the soliton peak, in a fixed frame of reference, varies slowly as a result of the mean Stokes drift while oscillating rapidly as the soliton is overtaken by the successive crests and troughs of the long wave.

The theory suggests that if the evolution is sought for larger KB, ϕ-periodic coefficients will then appear in the reduced evolution equation (I.4.2). Hence, we shall consider in the following two chapters finite amplitude long waves.

CHAPTER II: TWO-DIMENSIONAL INTERACTIONS OF WEAK SHORT WAVES AND A FINITE AMPLITUDE LONG WAVE

1. INTRODUCTION

After having described the interactions of a train of short waves with weakly nonlinear long waves, we now assume a long wave of finite amplitude. Extension to an irrotational Stokes waves with a slope $0.1 < KB$ is in principle possible, but has proved to be excessively complicated. We therefore resort to the much simpler solution of Gerstner(1802) which is strictly periodic and is known to have an exponentially decaying time-independent vorticity.

The governing equations in Lagrangian variables are deduced in §2. In particular, it is confirmed that the vorticity field in Lagrangian form is conserved in time. If the short waves are initially irrotational they will remain so for all times. The time independent vorticity field is therefore solely due to the long Gerstner wave.

The Gerstner and Stokes wave profiles are compared in §3 for different values of the long wave slope KB. Quantitative discrepancies in the profiles increase with KB and are largest near the mean sea level crossing.

Asymptotic equations describing the long time evolution of the short wave amplitude are derived in §4. We obtain a nonlinear Schrödinger equation whose coefficients are explicit periodic functions of time.

In §5, the modulation of the short waves at the crest and trough of the long wave is compared with the numerical theory of Longuet-Higgins(1987). Since the difference in vorticity between the two waves scales as $\mathcal{O}(K^2B^2)$, our results for $KB \leq 0.3$ should be consistent with his at the leading order. Our results are also checked against the theory of Henyey *et al*(1988).

The linear stage of the Benjamin and Feir instability of a uniform short wave to sideband disturbances is analysed with Floquet theory in §6. Owing to the periodic

then proved theoretically. With Floquet's estimate of the most unstable sideband disturbance, nonlinear calculations are performed. For small values of α, recurrence is observed. When α becomes moderately large, the short wave envelope appears chaotic.

Can chaos happen in the absence of the (stable or unstable) higher harmonics of the unstable sideband ? To answer this question, the short wave amplitude is decomposed as a two-term Fourier series involving the uniform short wave and its sideband disturbance. A one degree of freedom dynamical system is then deduced in §8 using Hamiltonian theory. Integration of this system confirms that the higher harmonics of the sideband do not play a key role in triggering chaos for moderately large α.

2. FORMULATION OF THE PROBLEM

2.1. Governing Equations

For completeness, the equations governing the coordinates (X, Z) of a particle in terms of the Lagrangian independent variables (a, c, t) are quoted again from Chapter I. The continuity equation is

$$\frac{D(X,Z)}{D(a,c)} \equiv \frac{\partial X}{\partial a}\frac{\partial Z}{\partial c} - \frac{\partial X}{\partial c}\frac{\partial Z}{\partial a} = \frac{D(X_0,Z_0)}{D(a,c)} = J(a,c) \qquad (II.2.1)$$

where (X_0, Z_0) represents the initial position of the particle and where J is independent of time. The conservation of vorticity reads

$$\frac{\partial}{\partial t}\{J\varpi\} = 0 \qquad (II.2.2)$$

which becomes after substituting the expression $(I.2.4)$ of ϖ,

$$\frac{\partial X}{\partial a}\frac{\partial^3 X}{\partial c \partial t^2} - \frac{\partial Z}{\partial c}\frac{\partial^3 Z}{\partial a \partial t^2} - \frac{\partial X}{\partial c}\frac{\partial^3 X}{\partial a \partial t^2} + \frac{\partial Z}{\partial a}\frac{\partial^3 Z}{\partial c \partial t^2} = 0 \qquad (II.2.3)$$

Finally, the dynamic boundary condition at the free surface yields

$$\frac{\partial X}{\partial a}\frac{\partial^2 X}{\partial t^2} + \frac{\partial Z}{\partial a}\left(g + \frac{\partial^2 Z}{\partial t^2}\right) = 0 \qquad c = 0 \qquad (II.2.4)$$

where g is the gravitational acceleration.

Let us now introduce the Lagrangian displacements † $x(a, c, t)$ and $z(a, c, t)$ by

$$X(a,c,t) = a + x(a,c,t) \qquad Z(a,c,t) = c + z(a,c,t) \qquad (II.2.5)$$

The law of mass conservation becomes

$$1 + \frac{\partial x}{\partial a} + \frac{\partial z}{\partial c} + \frac{\partial x}{\partial a}\frac{\partial z}{\partial c} - \frac{\partial x}{\partial c}\frac{\partial z}{\partial a} = J \qquad (II.2.6)$$

The vorticity equation $(II.2.3)$ reduces to

$$\frac{\partial^3 x}{\partial c \partial t^2} - \frac{\partial^3 z}{\partial a \partial t^2} + \frac{\partial^3 x}{\partial c \partial t^2}\frac{\partial x}{\partial a} - \frac{\partial^3 z}{\partial a \partial t^2}\frac{\partial z}{\partial c} - \frac{\partial^3 x}{\partial a \partial t^2}\frac{\partial x}{\partial c} + \frac{\partial^3 z}{\partial c \partial t^2}\frac{\partial z}{\partial a} = 0 \qquad (II.2.7)$$

† Note that (x, z) represents the displacement vector of a particle only if (a, c) refers to its initial position.

Finally, the free surface boundary condition yields

$$\frac{\partial^2 x}{\partial t^2} + g\frac{\partial z}{\partial a} + \frac{\partial x}{\partial a}\frac{\partial^2 x}{\partial t^2} + \frac{\partial z}{\partial a}\frac{\partial^2 z}{\partial t^2} = 0 \qquad c = 0 \qquad (II.2.8)$$

Eqs. $(II.2.6)$-$(II.2.8)$ are the basis of subsequent analyses.

2.2. Multiple Scale Analysis

We consider two trains of deep water waves and a situation where the scale contrast between the long wave and the short wave is large. More specifically, the wavenumber and frequency ratios are respectively $\frac{K}{k} = \mathcal{O}(\epsilon^2)$ and $\frac{\Omega}{\sigma} = \mathcal{O}(\epsilon)$. The short waves are weakly nonlinear while the long waves have a finite amplitude. Their respective slopes are $kA = \mathcal{O}(\epsilon)$ and $KB = \mathcal{O}(1)$. From the assumed orders of magnitude, it follows that

$$kB = \frac{k}{K}KB = \mathcal{O}(\epsilon^{-2}) \qquad \frac{A}{B} = \frac{kA}{KB}\frac{K}{k} = \mathcal{O}(\epsilon^3) \qquad (II.2.9a-b)$$

Short waves may be slowly modulated either through self-modulation or due to the straining by the non-uniform background (long wave). The long waves, however, are assumed to be uniform in space and time. We thus introduce the following cascade of length and time scales:

$$(a_j, c_j, t_j) = \epsilon^j (a, c, t) \qquad j = 1, 2, 3, \ldots \qquad (II.2.10)$$

The long wave displacements will depend solely on (a_2, c_2, t_1). whereas short wave displacements may depend on all scales. From now on, the small parameter ϵ is the sole indicator of order, while all physical variables are regarded as being $\mathcal{O}(1)$. After the asymptotic analysis is complete, ϵ can be dropped and $(II.2.9a-b)$ will be restored.

2.3. Perturbation Analysis

The solution for Lagrangian displacements is sought in perturbation series in the small parameter ϵ. Since, in deep water, particle orbits scale as the amplitude of the motion, $(II.2.9b)$ suggests that the ratio of the leading order short wave displacement to the long wave displacement be of the order of $\frac{A}{B} = \mathcal{O}(\epsilon^3)$. Accordingly, we

introduce the following expansion:

$$x = \epsilon^{-2}x_{-2} + \epsilon x_1 + \epsilon^2 x_2 + \epsilon^3 x_3 + \mathcal{O}(\epsilon^4) \qquad (II.2.11a)$$

$$z = \epsilon^{-2}z_{-2} + \epsilon z_1 + \epsilon^2 z_2 + \epsilon^3 z_3 + \mathcal{O}(\epsilon^4) \qquad (II.2.11b)$$

We shall adopt Gerstner's wave as the solution for x_{-2} and z_{-2}. The absence of the $\mathcal{O}(\epsilon^{-1})$ and $\mathcal{O}(1)$ displacements in $(II.2.11a-b)$ is a consequence of the exactness of Gerstner's solution.

Eqs. $(II.2.5)$ and $(II.2.11)$ may be combined to obtain series expansions for the Eulerian coordinates (X, Z) of a particle:

$$X = a + \epsilon^{-2}x_{-2} + \epsilon x_1 + \epsilon^2 x_2 + \epsilon^3 x_3 + \mathcal{O}(\epsilon^4) \qquad (II.2.12a)$$

$$Z = c + \epsilon^{-2}z_{-2} + \epsilon z_1 + \epsilon^2 z_2 + \epsilon^3 z_3 + \mathcal{O}(\epsilon^4) \qquad (II.2.12b)$$

Upon substituting $(II.2.11)$ in $(II.2.6)$-$(II.2.8)$, and collecting terms of similar order in ϵ , we obtain a sequence of governing equations. Our objective being the derivation of an equation describing the evolution of the short wave amplitude over a range $ka_2 = \mathcal{O}(1)$ and for times $\omega t_2 = \mathcal{O}(1)$, governing equations up to $\mathcal{O}(\epsilon^3)$ will be needed.

At $\mathcal{O}(1)$:

Continuity:

$$1 + \frac{\partial x_{-2}}{\partial a_2} + \frac{\partial z_{-2}}{\partial c_2} + \frac{\partial x_{-2}}{\partial a_2}\frac{\partial z_{-2}}{\partial c_2} - \frac{\partial x_{-2}}{\partial c_2}\frac{\partial z_{-2}}{\partial a_2} = J \qquad (II.2.13a)$$

The vorticity equation yields no contribution at this order.

Free surface boundary condition:

$$\frac{\partial^2 x_{-2}}{\partial t_1^2} + g\frac{\partial z_{-2}}{\partial a_2} + \frac{\partial x_{-2}}{\partial a_2}\frac{\partial^2 x_{-2}}{\partial t_1^2} + \frac{\partial z_{-2}}{\partial a_2}\frac{\partial^2 z_{-2}}{\partial t_1^2} = 0 \qquad c = 0 \qquad (II.2.13b)$$

Note that $(II.2.13a-b)$ involve only long wave displacements.

At $\mathcal{O}(\epsilon)$:

Continuity:

$$\frac{\partial x_1}{\partial a} + \frac{\partial z_1}{\partial c} + \frac{\partial x_{-2}}{\partial a_2}\frac{\partial z_1}{\partial c} - \frac{\partial x_{-2}}{\partial c_2}\frac{\partial z_1}{\partial a} - \frac{\partial z_{-2}}{\partial a_2}\frac{\partial x_1}{\partial c} + \frac{\partial z_{-2}}{\partial c_2}\frac{\partial x_1}{\partial a} = 0 \qquad (II.2.14a)$$

Vorticity:

$$\frac{\partial^3 x_1}{\partial c \partial t^2} - \frac{\partial^3 z_1}{\partial a \partial t^2} + \frac{\partial z_{-2}}{\partial a_2}\frac{\partial^3 z_1}{\partial c \partial t^2} - \frac{\partial z_{-2}}{\partial c_2}\frac{\partial^3 z_1}{\partial a \partial t^2} + \frac{\partial x_{-2}}{\partial a_2}\frac{\partial^3 x_1}{\partial c \partial t^2} - \frac{\partial x_{-2}}{\partial c_2}\frac{\partial^3 x_1}{\partial a \partial t^2} = 0 \qquad (II.2.14b)$$

Free surface boundary condition:

$$\frac{\partial^2 x_1}{\partial t^2} + g\frac{\partial z_1}{\partial a} +$$

$$+\frac{\partial z_{-2}}{\partial a_2}\frac{\partial^2 z_1}{\partial t^2} + \frac{\partial^2 z_{-2}}{\partial t_1^2}\frac{\partial z_1}{\partial a} + \frac{\partial x_{-2}}{\partial a_2}\frac{\partial^2 x_1}{\partial t^2} + \frac{\partial^2 x_{-2}}{\partial t_1^2}\frac{\partial x_1}{\partial a} = 0 \qquad c = 0 \quad (II.2.14c)$$

At $\mathcal{O}(\epsilon^2)$

Continuity:

$$\frac{\partial x_2}{\partial a} + \frac{\partial z_2}{\partial c} + \frac{\partial x_1}{\partial a_1} + \frac{\partial z_1}{\partial c_1} +$$

$$+\frac{\partial x_{-2}}{\partial a_2}\frac{\partial z_2}{\partial c} - \frac{\partial x_{-2}}{\partial c_2}\frac{\partial z_2}{\partial a} - \frac{\partial z_{-2}}{\partial a_2}\frac{\partial x_2}{\partial c} + \frac{\partial z_{-2}}{\partial c_2}\frac{\partial x_2}{\partial a} +$$

$$+\frac{\partial x_1}{\partial a}\frac{\partial z_1}{\partial c} - \frac{\partial x_1}{\partial c}\frac{\partial z_1}{\partial a} + \frac{\partial x_{-2}}{\partial a_2}\frac{\partial z_1}{\partial c_1} - \frac{\partial x_{-2}}{\partial c_2}\frac{\partial z_1}{\partial a_1} - \frac{\partial z_{-2}}{\partial a_2}\frac{\partial x_1}{\partial c_1} + \frac{\partial z_{-2}}{\partial c_2}\frac{\partial x_1}{\partial a_1} = 0 \qquad (II.2.15a)$$

Vorticity:

$$\frac{\partial^3 x_{-2}}{\partial t_1^2 \partial c_2} - \frac{\partial^3 z_{-2}}{\partial t_1^2 \partial a_2} + \frac{\partial^3 x_{-2}}{\partial t_1^2 \partial c_2}\frac{\partial x_{-2}}{\partial a_2} - \frac{\partial^3 z_{-2}}{\partial t_1^2 \partial a_2}\frac{\partial z_{-2}}{\partial c_2} - \frac{\partial^3 x_{-2}}{\partial t_1^2 \partial a_2}\frac{\partial x_{-2}}{\partial c_2} + \frac{\partial^3 z_{-2}}{\partial t_1^2 \partial c_2}\frac{\partial z_{-2}}{\partial a_2} +$$

$$+\frac{\partial^3 x_2}{\partial c \partial t^2} - \frac{\partial^3 z_2}{\partial a \partial t^2} + 2\frac{\partial^3 x_1}{\partial t_1 \partial c \partial t} - 2\frac{\partial^3 z_1}{\partial t_1 \partial a \partial t} + \frac{\partial^3 x_1}{\partial c_1 \partial t^2} - \frac{\partial^3 z_1}{\partial a_1 \partial t^2} +$$

$$+\frac{\partial x_{-2}}{\partial a_2}\frac{\partial^3 x_2}{\partial c \partial t^2} - \frac{\partial x_{-2}}{\partial c_2}\frac{\partial^3 x_2}{\partial a \partial t^2} + \frac{\partial x_1}{\partial a}\frac{\partial^3 x_1}{\partial c \partial t^2} - \frac{\partial^3 x_1}{\partial a \partial t^2}\frac{\partial x_1}{\partial c} + 2\frac{\partial x_{-2}}{\partial a_2}\frac{\partial^3 x_1}{\partial t_1 \partial c \partial t} +$$

$$-2\frac{\partial x_{-2}}{\partial c_2}\frac{\partial^3 x_1}{\partial t_1 \partial a \partial t} + \frac{\partial x_{-2}}{\partial a_2}\frac{\partial^3 x_1}{\partial c_1 \partial t^2} - \frac{\partial x_{-2}}{\partial c_2}\frac{\partial^3 x_1}{\partial a_1 \partial t^2} + \frac{\partial z_{-2}}{\partial a_2}\frac{\partial^3 z_2}{\partial c \partial t^2} - \frac{\partial z_{-2}}{\partial c_2}\frac{\partial^3 z_2}{\partial a \partial t^2} +$$

$$+\frac{\partial z_1}{\partial a}\frac{\partial^3 z_1}{\partial c \partial t^2} - \frac{\partial^3 z_1}{\partial a \partial t^2}\frac{\partial z_1}{\partial c} + 2\frac{\partial z_{-2}}{\partial a_2}\frac{\partial^3 z_1}{\partial t_1 \partial c \partial t} - 2\frac{\partial z_{-2}}{\partial c_2}\frac{\partial^3 z_1}{\partial t_1 \partial a \partial t} +$$

$$+\frac{\partial z_{-2}}{\partial a_2}\frac{\partial^3 z_1}{\partial c_1 \partial t^2} - \frac{\partial z_{-2}}{\partial c_2}\frac{\partial^3 z_1}{\partial a_1 \partial t^2} = 0 \qquad (II.2.15b)$$

Free surface boundary condition:

$$\frac{\partial^2 x_2}{\partial t^2} + g\frac{\partial z_2}{\partial a} + 2\frac{\partial^2 x_1}{\partial t_1 \partial t} + g\frac{\partial z_1}{\partial a_1} +$$

$$+\frac{\partial x_{-2}}{\partial a_2}\frac{\partial^2 x_2}{\partial t^2}+\frac{\partial^2 x_{-2}}{\partial t_1^2}\frac{\partial x_2}{\partial a}+\frac{\partial x_1}{\partial a}\frac{\partial^2 x_1}{\partial t^2}+2\frac{\partial x_{-2}}{\partial a_2}\frac{\partial^2 x_1}{\partial t_1 \partial t}+\frac{\partial^2 x_{-2}}{\partial t_1^2}\frac{\partial x_1}{\partial a_1}+$$

$$+\frac{\partial z_{-2}}{\partial a_2}\frac{\partial^2 z_2}{\partial t^2}+\frac{\partial^2 z_{-2}}{\partial t_1^2}\frac{\partial z_2}{\partial a}+\frac{\partial z_1}{\partial a}\frac{\partial^2 z_1}{\partial t^2}+2\frac{\partial z_{-2}}{\partial a_2}\frac{\partial^2 z_1}{\partial t_1 \partial t}+\frac{\partial^2 z_{-2}}{\partial t_1^2}\frac{\partial z_1}{\partial a_1}=0 \qquad c=0$$

$$(II.2.15c)$$

The $\mathcal{O}(\epsilon^3)$ equations needed to derive the long time evaluation of the short wave amplitude are not presented here for brevity and may be found in Appendix D.

3. GERSTNER'S TROCHOIDAL WAVE

3.1. Governing Equations and Solution

Two equations governing the long waves - $(II.2.13a-b)$ - are already obtained from the continuity equation and dynamic free surface boundary condition at $\mathcal{O}(1)$. For the third equation, we turn to the $\mathcal{O}(\epsilon^2)$ vorticity equation, $(II.2.15b)$. In the first line, the linear and nonlinear terms involve solely long wave displacements while the four remaining lines contain only short wave terms and interaction terms. We choose to set the first line to zero, expecting that the short waves, being so small $(\frac{A}{B} = \mathcal{O}(\epsilon^3))$, cannot affect the long waves at the leading order. Consequently, the equations governing the long wave are:

$$1 + \frac{\partial x_{-2}}{\partial a_2} + \frac{\partial z_{-2}}{\partial c_2} + \frac{\partial x_{-2}}{\partial a_2}\frac{\partial z_{-2}}{\partial c_2} - \frac{\partial x_{-2}}{\partial c_2}\frac{\partial z_{-2}}{\partial a_2} = J \qquad (II.3.1a)$$

$$\frac{\partial^3 x_{-2}}{\partial c_2 \partial t_1^2} - \frac{\partial^3 z_{-2}}{\partial a_2 \partial t_1^2} + \frac{\partial^3 x_{-2}}{\partial c_2 \partial t_1^2}\frac{\partial x_{-2}}{\partial a_2} - \frac{\partial^3 z_{-2}}{\partial a_2 \partial t_1^2}\frac{\partial z_{-2}}{\partial c_2} + \frac{\partial z_{-2}}{\partial a_2}\frac{\partial^3 z_{-2}}{\partial c_2 \partial t_1^2} - \frac{\partial x_{-2}}{\partial c_2}\frac{\partial^3 x_{-2}}{\partial a_2 \partial t_1^2} = 0 \qquad (II.3.1b)$$

both for $c < 0$ and

$$\frac{\partial^2 x_{-2}}{\partial t_1^2} + g\,\frac{\partial z_{-2}}{\partial a_2} + \frac{\partial^2 x_{-2}}{\partial t_1^2}\frac{\partial x_{-2}}{\partial a_2} + \frac{\partial z_{-2}}{\partial a_2}\frac{\partial^2 z_{-2}}{\partial t_1^2} = 0 \qquad c = 0 \qquad (II.3.1c)$$

The exact solution of Gerstner (1802) is chosen

$$x_{-2} = Be^{Kc_2}\sin\phi \qquad z_{-2} = Be^{Kc_2}\cos\phi \qquad (II.3.2a-b)$$

where the phase ϕ is defined by

$$\phi \equiv \Omega t_1 - Ka_2 \qquad (II.3.2c)$$

and B, K and Ω are respectively the uniform amplitude, the Lagrangian wavenumber and frequency of Gerstner's wave. Upon multiplying $(II.2.12a-b)$ throughout by ϵ^2 and neglecting terms of $\mathcal{O}(\epsilon^3)$ and higher, we may express (X_2, Z_2) in terms of (a_2, c_2):

$$X_2 = a_2 + Be^{Kc_2}\sin\phi + \mathcal{O}(\epsilon^3) \qquad Z_2 = c_2 + Be^{Kc_2}\cos\phi + \mathcal{O}(\epsilon^3) \quad (II.3.3a-b)$$

Substitution of $(II.3.2a-b)$ into $(II.3.1a)$ yields

$$J = 1 - K^2B^2e^{2Kc_2} = \frac{D(X_2, Z_2)}{D(a_2, c_2)} \qquad (II.3.4)$$

where use has been made of $(II.3.3a-b)$. Note that J does not depend on time. It is easily verified that $(II.3.2a-b)$ satisfy the vorticity equation $(II.3.1b)$. Finally, we substitute $(II.3.3a-b)$ into the dynamic boundary condition $(II.3.1c)$ on the free surface to find the dispersion relation

$$\Omega^2 = gK \qquad (II.3.5)$$

Eq. $(II.3.5)$ is identical to the dispersion relation for deep water gravity waves in the Eulerian formulation.

3.2. The Vorticity Field

Before introducing multiple scales, the expression of the vorticity is obtained in terms of the Lagrangian displacements (x,z)

$$\varpi = \frac{(1+\frac{\partial x}{\partial a})\frac{\partial^2 x}{\partial c \partial t} - (1+\frac{\partial z}{\partial c})\frac{\partial^2 z}{\partial a \partial t} + \frac{\partial z}{\partial a}\frac{\partial^2 z}{\partial c \partial t} - \frac{\partial x}{\partial c}\frac{\partial^2 x}{\partial a \partial t}}{1+\frac{\partial x}{\partial a}+\frac{\partial z}{\partial c}+\frac{\partial x}{\partial a}\frac{\partial z}{\partial c}-\frac{\partial x}{\partial c}+\frac{\partial z}{\partial a}} \qquad (II.3.6)$$

In the absence of short waves, the vorticity of Gerstner's wave is obtained

$$\varpi^g = \epsilon\frac{(1+\frac{\partial x_{-2}}{\partial a_2})\frac{\partial^2 x_{-2}}{\partial c_2 \partial t_1} - (1+\frac{\partial z_{-2}}{\partial c_2})\frac{\partial^2 z_{-2}}{\partial a_2 \partial t_1} + \frac{\partial z_{-2}}{\partial a_2}\frac{\partial^2 z_{-2}}{\partial c_2 \partial t_1} - \frac{\partial x_{-2}}{\partial c_2}\frac{\partial^2 x_{-2}}{\partial a_2 \partial t_1}}{1+\frac{\partial x_{-2}}{\partial a_2}+\frac{\partial z_{-2}}{\partial c_2}+\frac{\partial x_{-2}}{\partial a_2}\frac{\partial z_{-2}}{\partial c_2}-\frac{\partial x_{-2}}{\partial c_2}\frac{\partial z_{-2}}{\partial a_2}} \qquad (II.3.7)$$

After substituting in $(II.3.2a-b)$ and a little algebra, we get

$$\varpi^g = \epsilon\frac{-2\Omega K^2 B^2 e^{2Kc_2}}{1-K^2B^2e^{2Kc_2}} \qquad (II.3.8)$$

The above result was derived by Kochin *et al*(1965). Gerstner's wave field is therefore rotational and its vorticity decays exponentially fast with depth. Its magnitude at the free surface is $\mathcal{O}(K^2B^2)$.

3.3. Interpretation of Lagrangian Coordinates

We have mentioned earlier that the Jacobian J is different from unity therefore implying that (a_2,c_2) does not correspond to (X_2,Z_2) at some initial time t_0. Let us then find a physical interpretation of the Lagrangian coordinates. Most of the

following analysis can be found in Kochin *et al*(1965). Consider a line of constant c_2 described by $(II.3.2b)$. The mean excursion $Z_2^{(0)}$ of this profile from $Z_2 = c_2$ is

$$Z_2^{(0)} - c_2 = \frac{K}{2\pi}\int_0^{\frac{2\pi}{K}} (Z_2 - c_2)dX_2 = \frac{K}{2\pi}\int_0^{\frac{2\pi}{K}} Be^{Kc_2}\cos\phi\, dX_2 \qquad (II.3.9)$$

Upon differentiating $(II.3.2a)$ while keeping c_2 constant and substituting the result in $(II.3.9)$, we may integrate to obtain the mean excursion

$$Z_2^{(0)} = c_2 - \frac{KB^2}{2}e^{2Kc_2} \qquad (II.3.10)$$

From $(II.3.10)$ it is clear that c_2 corresponds to the elevation at rest increased by a small correction decaying exponentially fast with depth. Next, we must relate a_2 to $X_2^{(0)}$. To this end, consider an infinitesimal surface element da_2dc_2. The corresponding small surface element in the (X_2, Z_2) plane is

$$Jda_2dc_2 = (1 - K^2B^2e^{2Kc_2})da_2dc_2 = dX_2^{(0)}dZ_2^{(0)} \qquad (II.3.11)$$

Upon differentiating $(II.3.10)$ with respect to c_2 and substituting the result in $(II.3.11)$, we obtain the simple relation

$$dX_2^{(0)} = da_2 \qquad (II.3.12)$$

Except for a constant translation, a_2 represents the Eulerian horizontal coordinate of a given particle when the fluid is at rest.

3.4. Comparison of Gerstner and Stokes Waves

Existing studies of long wave/short wave interactions assume a Stokes long wave of infinitesimal or finite amplitude. It is therefore worthwhile to assess to what extent the profile of a Gerstner wave departs from that of a Stokes wave. The free surface elevation for Gerstner's wave is obtained by setting $c_2 = 0$ in $(II.3.3b)$:

$$Z_2 = B\cos\phi \qquad (II.3.13)$$

and must be expressed as a function of Eulerian phase $\phi_E \equiv \Omega t_1 - Ka_2$ to allow comparison. The relationship between ϕ and ϕ_E is described in Appendix E. The

profile of a Stokes wave is first computed from the Taylor expansion solution derived by Schwartz(1974) (cf. Appendix F) and then compared with Gerstner's profile in figures 3.1a-c for KB=0.1, 0.2 and 0.3. The agreement for $KB = 0.1$ is excellent. The departure between the two profiles is largest in the vicinity of the calm sea level crossing and increases with the long wave slope KB. It is therefore interesting to investigate the details of both waves near their crossing with the mean sea level. First, we recall that the mean excursion of Gerstner's wave is given by $(II.3.10)$. In particular, for $c_2 = 0$, we obtain the calm sea level *i.e.*

$$Z_2^{(0)}(c_2 = 0) = -\frac{KB^2}{2} = B\cos\phi \qquad (II.3.14)$$

From $(II.3.14)$, we deduce the Lagrangian phase at the zero crossing ϕ^g_{crossing} as

$$\cos\phi^g_{\text{crossing}} = -\frac{KB}{2} \qquad (II.3.15)$$

For small KB, ϕ^g_{crossing} is either slightly greater than $\pi/2$ or less than $3\pi/2$. We concentrate herein on the solution near $\pi/2$. From $(E.5a)$, we easily deduce that

$$\phi_{\text{E}_{\text{crossing}}} = \phi_{\text{crossing}} - KB\sin\phi_{\text{crossing}} \qquad (II.3.16)$$

For small KB, a straightforward Taylor expansion yields the Eulerian phase at the crossing

$$\phi^g_{\text{E}_{\text{crossing}}} = \frac{\pi}{2} - \frac{1}{2}KB + \frac{7}{48}K^3B^3 + \frac{13}{1280}K^5B^5 + \mathcal{O}(K^7B^7) \qquad (II.3.17a)$$

and

$$\cos\phi^g_{\text{E}_{\text{crossing}}} = \frac{1}{2}KB - \frac{1}{6}K^3B^3 + \frac{1}{120}K^5B^5 + \mathcal{O}(K^7B^7) \qquad (II.3.17b)$$

Next, we derive the corresponding results for the Stokes wave. From Schwartz's expansions, we solve for the phase (his χ) for which the free surface elevation equals the mean sea level (cf. Appendix F). We obtain the Eulerian phase at the crossing

$$\phi^s_{\text{E}_{\text{crossing}}} = \frac{\pi}{2} - \frac{3}{2}KB + \frac{29}{48}K^3B^3 + \frac{5743}{11520}K^5B^5 + \mathcal{O}(K^7B^7) \qquad (II.3.18a)$$

therefore

$$\cos\phi^s_{\text{E}_{\text{crossing}}} = \frac{3}{2}KB - \frac{7}{6}K^3B^3 + \frac{11}{45}K^5B^5 + \mathcal{O}(K^7B^7) \qquad (II.3.18b)$$

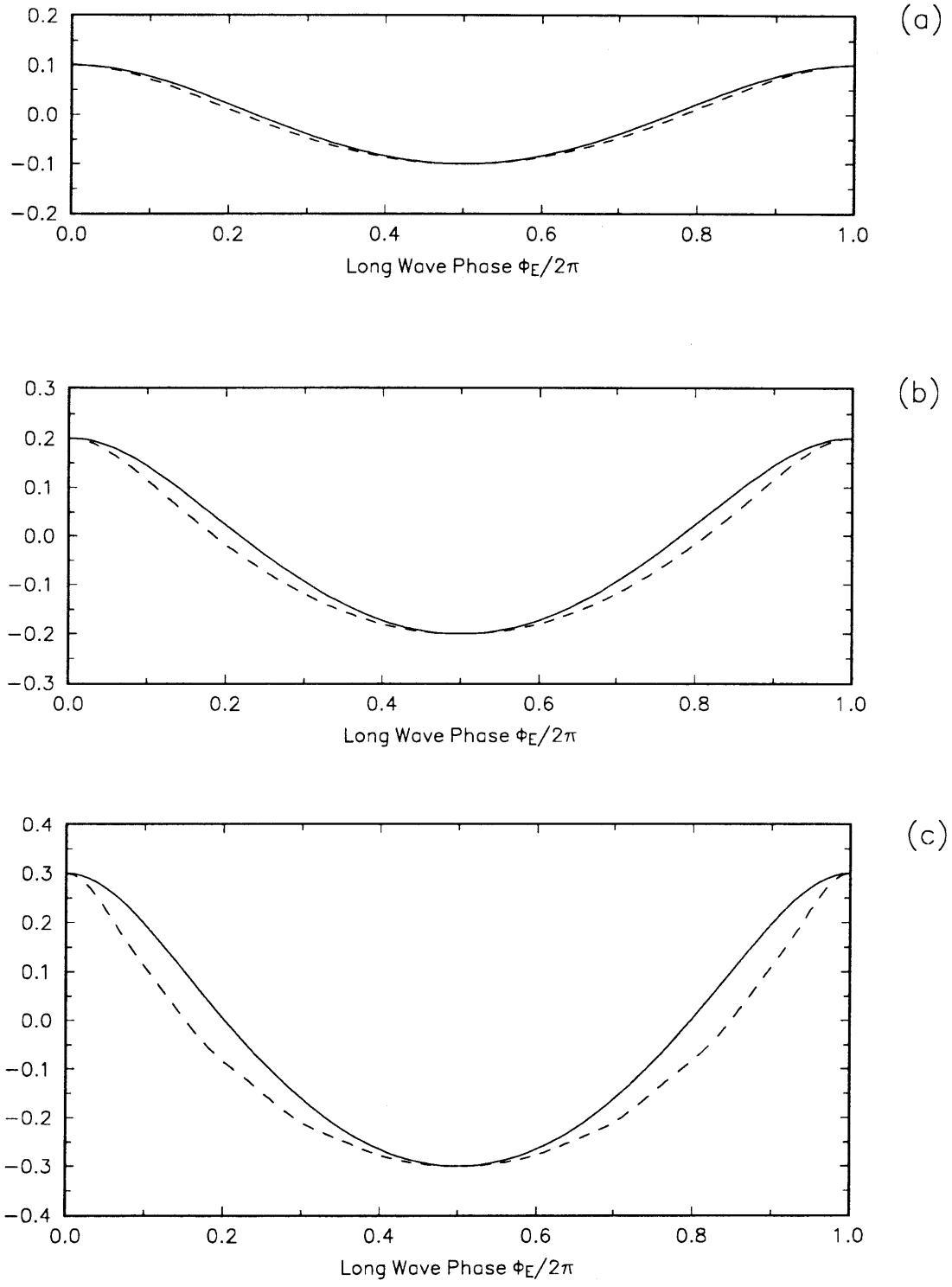

Figure II.3.1: Comparison of Gerstner wave (——) and Stokes wave(- - -) profiles for (a) $KB = 0.1$, (b) $KB = 0.2$ and (c) $KB = 0.3$.

Upon using ($II.3.16$), we easily deduce the Lagrangian phase at the crossing ϕ^s_{crossing}

$$\phi^s_{\text{crossing}} = \frac{\pi}{2} - \frac{1}{2}KB + \frac{23}{48}K^3B^3 + \frac{8533}{11520}K^5B^5 + \mathcal{O}(K^7B^7) \qquad (II.3.19a)$$

and its cosine

$$\cos\phi^s_{\text{crossing}} = \frac{1}{2}KB - \frac{1}{2}K^3B^3 - \frac{49}{72}K^5B^5 + \mathcal{O}(K^7B^7) \qquad (II.3.19b)$$

Whether the phase of the crossing points of the Stokes and Gerstner waves are expressed in Lagrangian or Eulerian coordinates, their cosines differ exactly by KB at the leading order (see figure 3.2).

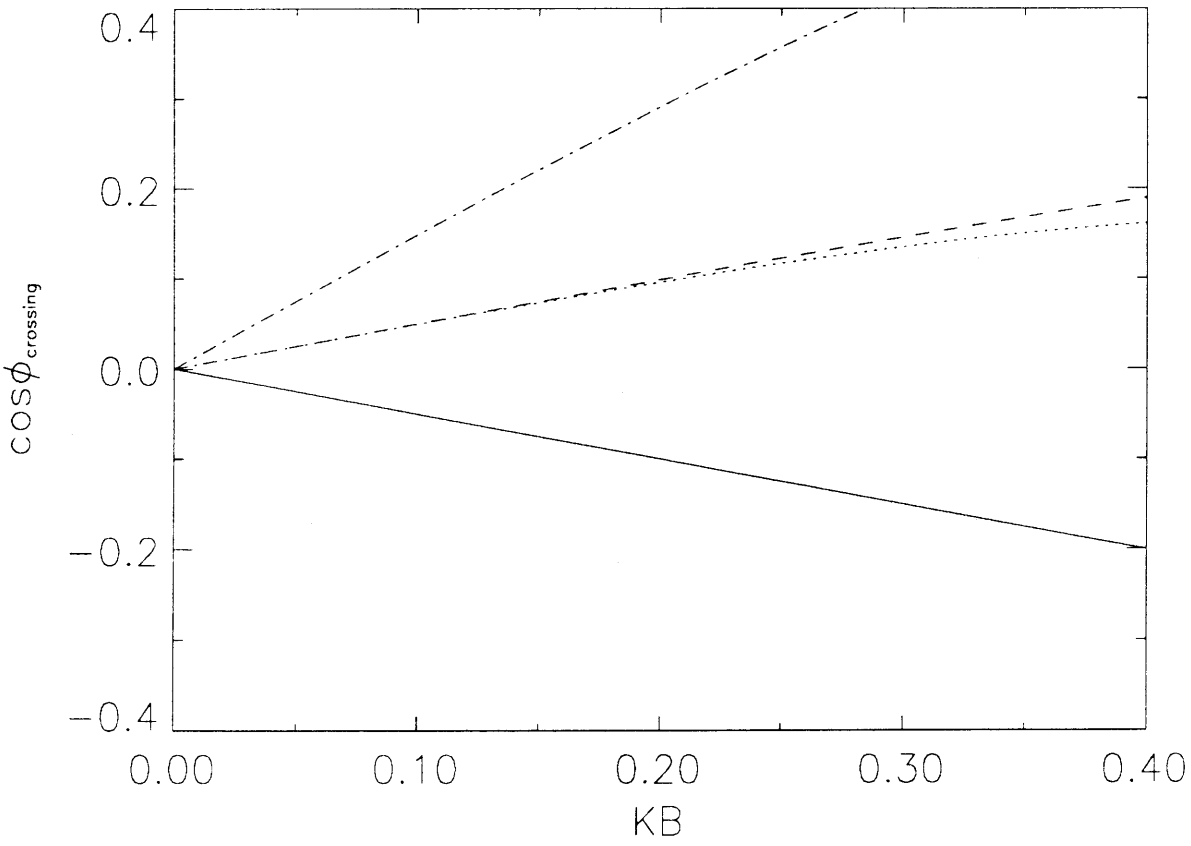

Figure II.3.2: Comparison of mean sea level crossing locations. In the Lagrangian frame: Gerstner (——), Stokes (·····); In the Eulerian frame: Gerstner (– – –), Stokes (–·–·–).

4. EVOLUTION EQUATIONS FOR NARROW BANDED SHORT WAVES

While the long wave has a time-independent vorticity, the short waves are assumed to be irrotational at some initial time. Solutions for the short waves at the leading order are sought before formalizing the governing equations at higher orders.

4.1. Short Waves at the Leading Order

Upon using the expression (II.3.2) for Gerstner's wave displacements in (II.2.13$a-b$) we obtain from the continuity equation

$$(1+KB\cos\phi)\frac{\partial x_1}{\partial a}+(1-KB\cos\phi)\frac{\partial z_1}{\partial c}-KB\sin\phi\left[\frac{\partial x_1}{\partial c}+\frac{\partial z_1}{\partial a}\right]=0 \quad (II.4.1a)$$

The vorticity equation results in

$$(1-KB\cos\phi)\frac{\partial^3 x_1}{\partial c\partial t^2}-(1+KB\cos\phi)\frac{\partial^3 z_1}{\partial a\partial t^2}-KB\sin\phi\left[\frac{\partial^3 x_1}{\partial a\partial t^2}-\frac{\partial^3 z_1}{\partial c\partial t^2}\right]=0 \quad (II.4.1b)$$

and the dynamic free surface boundary condition (II.2.13c) yields

$$(1-KB\cos\phi)\left[\frac{\partial^2 x_1}{\partial t^2}+g\frac{\partial z_1}{\partial a}\right]+KB\sin\phi\left[\frac{\partial^2 z_1}{\partial t^2}-g\frac{\partial x_1}{\partial a}\right]=0 \qquad c=0 \quad (II.4.1c)$$

Use has been made in (II.4.1c) of the dispersion relation (II.3.5) along with the definition of the Lagrangian phase of the long wave

$$\phi \equiv \Omega t_1 - Ka_2 \quad (II.4.1d)$$

Because $KB = O(1)$ the short waves are affected at the leading order by the long waves. We postulate the following solution for short wave displacements:

$$\begin{pmatrix} x_1 \\ z_1 \end{pmatrix} = \begin{pmatrix} ix_{11} \\ x_{11} \end{pmatrix} e^{iS} \qquad S \equiv ka - \sigma t \quad (II.4.2a-b)$$

where $x_{11}(c)$ and $z_{11}(c)$ are yet to be found. Upon substituting (II.4.2) in (II.4.1$a-b$), we obtain the following matrix ordinary differential equation:

$$M\,\frac{\partial U}{\partial c} = k\,N\,U \quad (II.4.3a)$$

where $U = (x_{11}, z_{11})^T$ and the 2×2 matrices M and N are given by

$$M = \begin{pmatrix} -iKB\sin\phi & 1 - KB\cos\phi \\ 1 - KB\cos\phi & -iKB\sin\phi \end{pmatrix} \qquad N = \begin{pmatrix} 1 + KB\cos\phi & iKB\sin\phi \\ iKB\sin\phi & 1 + KB\cos\phi \end{pmatrix} \tag{II.4.3b-c}$$

Left multiplication by the non-singular matrix M^{-1} yields

$$\frac{\partial U}{\partial c} = \frac{k}{1 - 2KB\cos\phi + K^2B^2} \begin{pmatrix} 2iKB\sin\phi & 1 - K^2B^2 \\ 1 - K^2B^2 & 2iKB\sin\phi \end{pmatrix} U \tag{II.4.4}$$

We must now solve an eigenvalue problem for matrix $M^{-1}N$. The eigenvalues, $\kappa^{\pm}$ are readily obtained

$$\kappa^{\pm} = k\frac{\pm(1 - K^2B^2) + 2iKB\sin\phi}{1 - 2KB\cos\phi + K^2B^2} \tag{II.4.5a-b}$$

The corresponding eigenvectors are easily found to be

$$U^{\pm} = \begin{pmatrix} 1 \\ \pm 1 \end{pmatrix} \tag{II.4.5c-d}$$

Since the values of c range from $-\infty$ to 0 and $KB < 1$, we must discard κ^- to insure boundedness. Let us introduce for brevity the real and imaginary parts of $\kappa = \kappa^+$:

$$\kappa_r = \frac{k(1 - K^2B^2)}{1 - 2KB\cos\phi + K^2B^2} \qquad \kappa_i = \frac{2kKB\sin\phi}{1 - 2KB\cos\phi + K^2B^2} \tag{II.4.6a-b}$$

note that κ_r and κ_i depend on a_2 and t_1 through ϕ. The imaginary part κ_i of κ may be interpreted as the vertical component of a Lagrangian wavenumber associated with the phase function $\tilde{S}$

$$\tilde{S} = S + \kappa_i c = ka + \kappa_i c - \sigma t \tag{II.4.7}$$

Since both components of U^+ are equal, so are the amplitudes of the horizontal and vertical displacements, as is well known for linearized deep water waves in potential theory. The common amplitude of x_{11} and z_{11} will be refered to as A. The solution we have postulated for the $\mathcal{O}(\epsilon)$ short wave displacement involves only the first harmonic. In anticipation of nonlinear effects, the full expression of the short waves at the leading order is

$$\begin{pmatrix} x_1 \\ z_1 \end{pmatrix} = \begin{pmatrix} x_{10} \\ z_{10} \end{pmatrix} + \frac{1}{2}\begin{pmatrix} i \\ 1 \end{pmatrix} Ae^{iS}e^{\kappa c} + (*) \tag{II.4.8}$$

where $x_{10}(a_1, c, t_1)$ and $z_{10}(a_1, c, t_1)$ correspond to mean drifts and $A(a_1, t_1)$ is the slowly varying amplitude of the short wave. Finally, we enforce the dynamic boundary condition $(II.4.1c)$ and obtain after simple algebra

$$\sigma^2 = gk \tag{II.4.9}$$

In Lagrangian coordinates, the dispersion relation of short waves does not depend *explicitly* on long wave quantities. However, $(II.4.9)$ is reexamined in §II.5 after the introduction of the effective gravity and the Eulerian short wave wavenumber $\vec{k}^e$.

The slowly varying displacements x_{10} and z_{10} remain to be solved. From the contribution of the zeroth harmonic in the $\mathcal{O}(\epsilon)$ continuity equation and the $\mathcal{O}(\epsilon^3)$ vorticity equation, we deduce respectively

$$-KB\sin\phi\frac{\partial x_{10}}{\partial c} + (1 - KB\cos\phi)\frac{\partial z_{10}}{\partial c} = 0 \tag{II.4.10a}$$

$$(1 - KB\cos\phi)\frac{\partial^3 x_{10}}{\partial c \partial t_1^2} + KB\sin\phi\frac{\partial^3 z_{10}}{\partial c \partial t_1^2} +$$

$$-\Omega^2 KB\left[\cos\phi\frac{\partial x_{10}}{\partial c} - \sin\phi\frac{\partial z_{10}}{\partial c}\right] = \frac{\partial}{\partial t_1}\left[2\sigma k\kappa_r |A|^2 e^{2\kappa_r c}\right] \tag{II.4.10b}$$

Likewise, from the zeroth order contribution of the $\mathcal{O}(\epsilon^2)$ free surface boundary condition, we obtain

$$-KB\sin\phi\frac{\partial x_{10}}{\partial a_1} + (1 - KB\cos\phi)\frac{\partial z_{10}}{\partial a_1} = 0 \qquad c = 0 \tag{II.4.10c}$$

We then integrate $(II.4.10b)$ by parts with respect to t_1, keeping in mind the definition $(II.3.2b)$ of ϕ:

$$\frac{\partial}{\partial t_1}\Bigg\{(1 - KB\cos\phi)\frac{\partial^2 x_{10}}{\partial c \partial t_1} + KB\sin\phi\frac{\partial^2 z_{10}}{\partial c \partial t_1} +$$

$$-\Omega KB\left[\sin\phi\frac{\partial x_{10}}{\partial c} + \cos\phi\frac{\partial z_{10}}{\partial c}\right] - 2\sigma k\kappa_r |A|^2 e^{2\kappa_r c}\Bigg\} = 0 \tag{II.4.11}$$

The quantity within curly brackets is equal to the Jacobian J times the slowly varying vorticity due to the $\mathcal{O}(\epsilon)$ short waves. Since, vorticity is assumed to be zero at initial time $t_1 = 0$, we deduce that the expression within curly brackets in $(II.4.11)$ is identically zero

$$(1 - KB\cos\phi)\frac{\partial^2 x_{10}}{\partial c \partial t_1} + KB\sin\phi\frac{\partial^2 z_{10}}{\partial c \partial t_1} +$$

$$-\Omega KB\left[\sin\phi\frac{\partial x_{10}}{\partial c}+\cos\phi\frac{\partial z_{10}}{\partial c}\right]=2\sigma k\kappa_r|A|^2e^{2\kappa_r c} \qquad (II.4.12)$$

On the other hand, it follows from the continuity equation $(II.4.10a)$ that

$$\frac{\partial z_{10}}{\partial c}=\frac{KB\sin\phi}{1-KB\cos\phi}\frac{\partial x_{10}}{\partial c} \qquad (II.4.13)$$

where the denominator never vanishes since $KB<1$. If $(II.4.13)$ is substituted in $(II.4.12)$, we obtain after a c-integration and a few simplifications

$$\left(\frac{\partial}{\partial t_1}-\frac{\Omega KB\sin\phi}{1-KB\cos\phi}\right)x_{10}=\frac{1-KB\cos\phi}{1-2KB\cos\phi+K^2B^2}\sigma k|A|^2e^{2\kappa_r c} \qquad (II.4.14)$$

which is straightforwardly solved to yield

$$\begin{pmatrix}x_{10}\\ z_{10}\end{pmatrix}=\sigma k\int_0^{t_1}\frac{|A|^2e^{2\kappa_r c}}{1-2KB\cos\phi+K^2B^2}dt_1\begin{pmatrix}1-KB\cos\phi\\ KB\sin\phi\end{pmatrix} \qquad (II.4.15)$$

One can verify easily that $(II.4.15)$ satisfies the dynamic free surface boundary condition $(II.4.10c)$. The first order short wave displacement is now entirely determined by:

$$\begin{pmatrix}x_1\\ z_1\end{pmatrix}=\sigma k\int_0^{t_1}\frac{|A|^2e^{2\kappa_r c}}{1-2KB\cos\phi+K^2B^2}dt_1\begin{pmatrix}1-KB\cos\phi\\ KB\sin\phi\end{pmatrix}$$
$$+\frac{1}{2}\begin{pmatrix}i\\ 1\end{pmatrix}Ae^{iS}e^{\kappa c}+(*) \qquad (II.4.16)$$

where κ, κ_r and S are given respectively by $(II.4.5a)$, $(II.4.6a)$ and $(II.4.2b)$.

4.2. Governing Equations at Arbitrary Orders $\mathcal{O}(\epsilon^j)$

We may now generalize $(II.4.16)$ of the leading order short wave displacement to the displacements at any order $\mathcal{O}(\epsilon^j)$ as follows

$$x_j=x_{j0}(a_1,c,t_1)+\frac{i}{2}\sum_{\ell=1}^{n_j}x_{j\ell}(a_1,c,t_1)\,e^{i\ell(ka-\sigma t)}+(*) \qquad j=1,2,3 \quad (II.4.17a)$$

$$z_j=z_{j0}(a_1,c,t_1)+\frac{1}{2}\sum_{\ell=1}^{n_j}z_{j\ell}(a_1,c,t_1)\,e^{i\ell(ka-\sigma t)}+(*) \qquad j=1,2,3 \quad (II.4.17b)$$

where the displacements $x_{j\ell}$ and $z_{j\ell}$ depend on c as well as on modulation and long wave scales and n_j is the highest harmonic at a given order. Upon substituting

$(II.4.17a-b)$ in the $\mathcal{O}(\epsilon^j)$ governing equations, we obtain governing equations for each pair of displacements. In particular, the continuity and vorticity equations can be combined to yield a non-homogeneous matrix ordinary differential equation:

$$M\frac{\partial U}{\partial c} = \ell k N U + \begin{pmatrix} E_{j\ell} \\ G_{j\ell} \end{pmatrix} \qquad j=1,2,3 \qquad \ell = 1,\ldots,n_j \qquad (II.4.18a)$$

where $U = (x_{j\ell}, z_{j\ell})^T$. If use is made of the dispersion relations for both short and long waves, the free surface boundary condition takes the simple form

$$(1 - KB\cos\phi)\left[\ell x_{j\ell} - z_{j\ell}\right] + iKB\sin\phi\left[x_{j\ell} - \ell z_{j\ell}\right] = I_{j\ell} \quad c = 0$$

$$j = 1,2,3 \qquad \ell = 1,\ldots,n_j \qquad (II.4.18b)$$

In particular, comparison of $(II.4.1a-c)$ and $(II.4.18a,b)$ shows that $F_{11} = G_{11} = I_{11} = 0$.

Next we consider the zeroth harmonics x_{j0} and z_{j0} of the jth order displacements whose governing equations can be put in a general form

$$-KB\sin\phi\frac{\partial x_{j0}}{\partial c} + (1 - KB\cos\phi)\frac{\partial z_{j0}}{\partial c} = E_{j0} \qquad j=1,2,3 \qquad (II.4.19a)$$

$$(1 - KB\cos\phi)\frac{\partial^3 x_{j0}}{\partial c \partial t_1^2} + KB\sin\phi\frac{\partial^3 z_{j0}}{\partial c \partial t_1^2} +$$

$$-\Omega^2 KB\left[\cos\phi\frac{\partial x_{j0}}{\partial c} - \sin\phi\frac{\partial z_{j0}}{\partial c}\right] = G_{j0} \qquad j=1,2,3 \qquad (II.4.19b)$$

$$-KB\sin\phi\frac{\partial x_{j0}}{\partial a_1} + (1 - KB\cos\phi)\frac{\partial z_{j0}}{\partial a_1} = I_{j0} \qquad c=0 \qquad j=1,2,3 \quad (II.4.19c)$$

Note that $(II.4.12a-c)$ are obtained respectively at $\mathcal{O}(\epsilon^j)$, $\mathcal{O}(\epsilon^{j+2})$ and $\mathcal{O}(\epsilon^{j+1})$.

4.3. Linear Evolution of a Short Wave on a Long Gerstner Wave

The governing equations for the first harmonic short wave displacements at $\mathcal{O}(\epsilon^2)$ are described by $(II.4.18a,b)$ along with

$$E_{21} = i\left\{k\left(\frac{\partial x_{10}}{\partial c} - i\frac{\partial z_{10}}{\partial c}\right)A - (1 + KB\cos\phi + iKB\sin\phi)\frac{\partial A}{\partial a_1}\right\}e^{\kappa c} \qquad (II.4.20a)$$

$$G_{21} = i\left\{k\left(\frac{\partial x_{10}}{\partial c} - i\frac{\partial z_{10}}{\partial c}\right)A - (1 + KB\cos\phi + iKB\sin\phi)\frac{\partial A}{\partial a_1} +\right.$$

$$-\frac{2\Omega}{\sigma}(1 - KB\cos\phi - iKB\sin\phi)\frac{\partial\kappa}{\partial\phi}A\Big\}e^{\kappa c} \qquad (II.4.20b)$$

and

$$I_{21} = -\frac{2i}{\sigma}(1 - KB\cos\phi - iKB\sin\phi)\{\frac{\partial A}{\partial t_1} + \frac{\omega}{2k}\frac{\partial A}{\partial a_1}\} \qquad (II.4.20c)$$

Left multiplication of $(II.4.18a)$ by M^{-1} yields

$$\frac{\partial U}{\partial c} = kM^{-1}NU + M^{-1}\begin{pmatrix} E_{21} \\ G_{21} \end{pmatrix} \qquad (II.4.21)$$

The homogeneous problem is identical to $(II.4.3a)$ and therefore admits the following general solution

$$U = \mu^+ U^+ e^{\kappa_r c + i\kappa_i c} + \mu^- U^- e^{-\kappa_r c + i\kappa_i c} \qquad (II.4.22)$$

where $\mu^\pm$ are yet unknown. For the inhomogenous solution we now apply the method of variation of parameters, and assume that $\mu^\pm = \mu^\pm(c)$. Substitution of $(II.4.22)$ into $(II.4.21)$ then yields:

$$\frac{\partial\mu^+}{\partial c}U^+ e^{\kappa_r c + i\kappa_i c} + \frac{\partial\mu^-}{\partial c}U^- e^{-\kappa_r c + i\kappa_i c} =$$

$$\frac{1}{1 - 2KB\cos\phi + K^2B^2}\begin{pmatrix} iKB\sin\phi\ E_{21} + (1 - KB\cos\phi)\ G_{21} \\ (1 - KB\cos\phi)\ E_{21} + iKB\sin\phi\ G_{21} \end{pmatrix} \qquad (II.4.23)$$

This linear system of two equations with the two unknowns $\frac{\partial\mu^\pm}{\partial c}$ is easily solved. We then perform two c-integrations and obtain

$$\mu^+ = \frac{1}{2}\frac{1 - KB\cos\phi + iKB\sin\phi}{1 - 2KB\cos\phi + K^2B^2}\int^c \left[G_{21} + E_{21}\right]e^{-\kappa_r c'}e^{-i\kappa_i c'}dc' \qquad (II.4.24a)$$

where a full evaluation awaits the substitution of $G_{21}(c)$ and $E_{21}(c)$. Note that $\mu^+(c)e^{\kappa_r c}$ decays to zero as c goes to $-\infty$. Similarly, we obtain for μ^-

$$\mu^- = \frac{1}{2}\frac{1 - KB\cos\phi - iKB\sin\phi}{1 - 2KB\cos\phi + K^2B^2}\int^c \left[G_{21} - E_{21}\right]e^{\kappa_r c'}e^{-i\kappa_i c'}dc' \qquad (II.4.24b)$$

Since the integrand is well behaved near $-\infty$, the lower bound in $(II.4.24b)$ may be set to $-\infty$ provided that an integration constant h_{21}^- be introduced. Boundedness then requires that $\mu^-(c)e^{-\kappa_r c}$ decay to zero as c approaches $-\infty$, this implies that h_{21}^- must be zero. The lower band in $(II.4.24a)$ will be determined in §4.4 when

carrying out the integration. We may then substitute $(II.4.24a-b)$ into $(II.4.22)$ to find

$$U = \frac{1/2}{1 - KB\cos\phi - iKB\sin\phi}\int^{c}[G_{21}+E_{21}]e^{-\kappa_r c' - i\kappa_i c'}dc'\begin{pmatrix}1\\1\end{pmatrix}e^{\kappa_r c + i\kappa_i c} +$$

$$+\frac{1/2}{1 - KB\cos\phi + iKB\sin\phi}\int_{-\infty}^{c}[G_{21}-E_{21}]e^{\kappa_r c' - i\kappa_i c'}dc'\begin{pmatrix}1\\-1\end{pmatrix}e^{-\kappa_r c + i\kappa_i c} \qquad (II.4.25)$$

The dynamic boundary condition on the free surface must now be satisfied. Recalling $(II.4.11b)$ with $j=2$ and $\ell=1$:

$$(1 - KB\cos\phi + iKB\sin\phi)(x_{21} - z_{21}) = I_{21} \qquad c = 0 \qquad (II.4.26)$$

Only the second term in $(II.4.25)$ will contribute to $x_{21} - z_{21}$, and

$$(x_{21} - z_{21})\Big|_{c=0} = \frac{1}{1 - KB\cos\phi + iKB\sin\phi}\int_{-\infty}^{0}[G_{21}-E_{21}]e^{\kappa_r c - i\kappa_i c}dc \quad (II.4.27)$$

Upon combining $(II.4.26)$ and $(II.4.27)$, we obtain the solvability condition:

$$\int_{-\infty}^{0}[G_{21}-E_{21}]e^{\kappa_r c - i\kappa_i c}dc = I_{21} \qquad (II.4.28)$$

This is a compact and general form for the solvability condition for a pair of first harmonic displacements at *any order*. We have seen in Chapter I (for $KB \ll 1$) that E_{21} and G_{21} are identical. Consequently, the left hand side of $(II.4.28)$ vanishes and the solvability condition reduces to $I_{21} = 0$ which leads to the familiar law of wave action conservation. However, for a finite KB, E_{21} and G_{21} are no longer identical and their difference is evaluated from $(II.4.20a-b)$

$$G_{21} - E_{21} = -\frac{2i\Omega}{\sigma}(1 - KB\cos\phi - iKB\sin\phi)\frac{\partial\kappa}{\partial\phi}Ae^{\kappa_r c}e^{i\kappa_i c} \qquad (II.4.29)$$

The left hand side of $(II.4.28)$ is then evaluated

$$\int_{-\infty}^{0}[G_{21}-E_{21}]e^{\kappa_r c - i\kappa_i c}dc = -\frac{i\Omega}{\sigma\kappa_r}(1 - KB\cos\phi - iKB\sin\phi)\frac{\partial\kappa}{\partial\phi}A \quad (II.4.30)$$

Upon combining $(II.4.30)$ and $(II.4.20c)$, we obtain the evolution equation over long scales a_1 and t_1

$$\frac{\partial A}{\partial t_1} + \frac{\sigma}{2k}\frac{\partial A}{\partial a_1} - \frac{\Omega}{2\kappa_r}\frac{\partial\kappa}{\partial\phi}A = 0 \qquad (II.4.31a)$$

or

$$\frac{\partial A}{\partial t_1}+\frac{\sigma}{2k}\frac{\partial A}{\partial a_1}-\frac{\Omega}{2\kappa_r}\frac{\partial \kappa_r}{\partial \phi}A-\frac{i\Omega}{2\kappa_r}\frac{\partial \kappa_i}{\partial \phi}A=0 \qquad (II.4.31b)$$

For infinitesimal KB, κ does not depend on ϕ; the familiar law of wave action conservation of Chapter I is recovered. For finite KB however, we associate the third and fourth terms in $(II.4.31b)$ respectively to amplitude and phase modulation. Upon making use of $(II.4.6a-b)$, we may evaluate the time derivatives of κ_r and κ_i to obtain

$$\frac{\partial A}{\partial t_1}+\frac{\sigma}{2k}\frac{\partial A}{\partial a_1}+\frac{\Omega KB\sin\phi}{1-2KB\cos\phi+K^2B^2}A+$$

$$-i\frac{\Omega KB}{1-K^2B^2}\frac{(1+K^2B^2)\cos\phi-2KB}{1-2KB\cos\phi+K^2B^2}A=0 \qquad (II.4.32)$$

Eq. $(II.4.32)$ will be examined in §5.

4.4. Short Wave Displacements at the Second Order

4.4.1. *First harmonic:*

We first complete the derivation of x_{21} and z_{21}, by evaluating the two integrals in $(II.4.25)$ for arbitrary c. The second integral yields

$$\int_{-\infty}^{c}\left[G_{21}-E_{21}\right]e^{\kappa_r c'}e^{-i\kappa_i c'}dc'=-\frac{i\Omega}{\sigma\kappa_r}(1-KB\cos\phi-iKB\sin\phi)\frac{\partial\kappa}{\partial\phi}Ae^{2\kappa_r c} \qquad (II.4.33)$$

The integrand of the first integral is

$$\left[G_{21}+E_{21}\right]e^{-\kappa_r c}e^{-i\kappa_i c}=2i\Big\{k\Big(\frac{\partial x_{10}}{\partial c}-i\frac{\partial z_{10}}{\partial c}\Big)A-(1+KB\cos\phi+iKB\sin\phi)\frac{\partial A}{\partial a_1}+$$

$$-\frac{\Omega}{\sigma}(1-KB\cos\phi-iKB\sin\phi)\frac{\partial\kappa}{\partial\phi}A\Big\} \qquad (II.4.34)$$

It is clear that $(II.4.34)$ cannot be integrated from $-\infty$ to c. Let us first compute the indefinite integral:

$$\int^{c}\left[G_{21}+E_{21}\right]e^{-\kappa_r c'-i\kappa_i c'}dc'=2i\Big\{k(x_{10}-iz_{10})A+$$

$$-c(1+KB\cos\phi+iKB\sin\phi)\frac{\partial A}{\partial a_1}-\frac{c\Omega}{\sigma}(1-KB\cos\phi-iKB\sin\phi)\frac{\partial\kappa}{\partial\phi}A\Big\}+h_{21}^{+} \qquad (II.4.35)$$

where h_{21}^{+} corresponds to a homogeneous solution. If use is made of $(II.4.18)$ for x_{10} and z_{10}, $(II.4.35)$ reduces to

$$\int^{c} \left[G_{21} + E_{21}\right] e^{-\kappa_r c' - i\kappa_i c'} dc' =$$

$$2i\Big\{\sigma k^2(1 - KB\cos\phi - iKB\sin\phi)\int_0^{t_1} \frac{|A|^2 e^{2\kappa_r c} dt_1}{1 - 2KB\cos\phi + K^2B^2} +$$

$$-c(1 + KB\cos\phi + iKB\sin\phi)\frac{\partial A}{\partial a_1} - \frac{c\Omega}{\sigma}(1 - KB\cos\phi - iKB\sin\phi)\frac{\partial \kappa}{\partial \phi}A\Big\} + h_{21}^{+} \qquad (II.4.36)$$

The solution for x_{21} and z_{21} is deduced after combining eqs. $(II.4.22)$, $(II.4.33)$ and $(II.4.36)$:

$$\begin{pmatrix} x_{21} \\ z_{21} \end{pmatrix} = \Big\{i\sigma k^2 \int_0^{t_1} \frac{|A|^2 e^{2\kappa_r c} dt_1}{1 - 2KB\cos\phi + K^2B^2} - ic\frac{\kappa}{k}\frac{\partial A}{\partial a_1} - \frac{ic}{\omega}\frac{\partial \kappa}{\partial t_1}A\Big\}\begin{pmatrix} 1 \\ 1 \end{pmatrix} e^{\kappa_r c} e^{i\kappa_i c} +$$

$$-\frac{i\Omega}{2\sigma\kappa_r}\frac{1 - KB\cos\phi - iKB\sin\phi}{1 - KB\cos\phi + iKB\sin\phi}\frac{\partial \kappa}{\partial \phi}A\begin{pmatrix} 1 \\ -1 \end{pmatrix} e^{\kappa_r c} e^{i\kappa_i c} + h_{21}^{+}\begin{pmatrix} 1 \\ 1 \end{pmatrix} e^{\kappa_r c} e^{i\kappa_i c} \qquad (II.4.37)$$

Whereas the vertical and horizontal displacements are identical at $\mathcal{O}(\epsilon)$, the dependence of κ on ϕ causes them to differ at $\mathcal{O}(\epsilon^2)$. If use is made of $(II.4.5)$, the above equation simplifies to the explicit expression

$$\begin{pmatrix} x_{21} \\ z_{21} \end{pmatrix} = \Big\{i\sigma k^2 \int_0^{t_1} \frac{|A|^2 e^{2\kappa_r c} dt_1}{1 - 2KB\cos\phi + K^2B^2} - ic\frac{1 + KB\cos\phi + iKB\sin\phi}{1 - KB\cos\phi - iKB\sin\phi}\frac{\partial A}{\partial a_1} +$$

$$-\frac{2kc\Omega KB(KB - \cos\phi - i\sin\phi)}{(1 - KB\cos\phi - iKB\sin\phi)(1 - 2KB\cos\phi + K^2B^2)}A\Big\}\begin{pmatrix} 1 \\ 1 \end{pmatrix} e^{\kappa_r c} e^{i\kappa_i c} +$$

$$-\frac{\Omega KB(\cos\phi + i\sin\phi)}{\sigma(1 - K^2B^2)}A\begin{pmatrix} 1 \\ -1 \end{pmatrix} e^{\kappa_r c} e^{i\kappa_i c} + h_{21}^{+}\begin{pmatrix} 1 \\ 1 \end{pmatrix} e^{\kappa_r c} e^{i\kappa_i c} \qquad (II.4.38)$$

The homogenous solution h_{21}^{+} may now be set to zero.

4.4.2. *Second harmonic*

The equations governing $U = (x_{22}, z_{22})^T$ are described by $(II.4.18a,b)$ along with the following forcing terms:

$$E_{22} = G_{22} = I_{22} = 0 \qquad (II.4.39)$$

The absence of forcing terms in $(II.4.18a-b)$ implies that no second harmonic displacements are present.

We have seen in §II.3 that the linear evolution of short waves is independent of the drifts x_{10} and z_{10}, these mean displacements affecting only x_{21} and z_{21}. Similarly, x_{20} and z_{20} are needed only to solve for x_{31} and z_{31}.

4.5. Nonlinear Evolution of Short Wave Amplitude

The solvability condition governing the long time evolution of the short waves amplitude is deduced from E_{31}, G_{31} and I_{31}

$$\int_{-\infty}^{0}\left[G_{31}-E_{31}\right]e^{\kappa_r c-i\kappa_i c}dc=I_{31} \qquad (II.4.40)$$

Omitting the lengthy expressions of G_{31} and E_{31}, we give however the expression of their difference:

$$\begin{aligned}
G_{31}-E_{31}&=i(1+KB\cos\phi-iKB\sin\phi)\Big\{\frac{\partial x_{21}}{\partial a_1}-\frac{\partial z_{21}}{\partial a_1}\Big\}-\frac{2kKB\sin\phi}{\sigma}\frac{\partial x_{21}}{\partial t_1}+\\
&-\frac{2i}{\sigma}(1-KB\cos\phi)\frac{\partial^2 x_{21}}{\partial c\partial t_1}-\frac{2KB\sin\phi}{\sigma}\frac{\partial^2 z_{21}}{\partial c\partial t_1}+\frac{2ik}{\sigma}(1+KB\cos\phi)\frac{\partial z_{21}}{\partial t_1}+\\
&+ik(x_{21}-z_{21})\Big\{\frac{\partial x_{10}}{\partial c}+i\frac{\partial z_{10}}{\partial c}\Big\}-\frac{2k}{\sigma}\Big(\frac{\partial x_{10}}{\partial c}-i\frac{\partial z_{10}}{\partial c}\Big)\Big(\frac{\partial A}{\partial t_1}+c\Omega\frac{\partial\kappa}{\partial\phi}A\Big)e^{\kappa_r c}e^{i\kappa_i c}+\\
&+\Bigg\{\frac{2c\Omega}{\sigma}(1+KB\cos\phi+iKB\sin\phi)\frac{\partial\kappa}{\partial\phi}\frac{\partial A}{\partial a_1}+\frac{2}{\sigma}(1+KB\cos\phi+iKB\sin\phi)\frac{\partial^2 A}{\partial a_1\partial t_1}+\\
&+\frac{\Omega}{\sigma^2}(1-KB\cos\phi-iKB\sin\phi)\Big(\Omega\frac{\partial^2\kappa}{\partial\phi^2}A+2\Omega c\Big(\frac{\partial\kappa}{\partial\phi}\Big)^2A+2\frac{\partial\kappa}{\partial\phi}\frac{\partial A}{\partial t_1}\Big)+\\
&-\frac{2k\Omega^2KB(\cos\phi+i\sin\phi)}{\sigma^2(1-KB\cos\phi+iKB\sin\phi)}A\Bigg\}e^{\kappa_r c}e^{i\kappa_i c} \qquad (II.4.41)
\end{aligned}$$

The right hand side of $(II.4.40)$ is given by

$$\begin{aligned}
I_{31}&=-\frac{2i}{\sigma}(1-KB\cos\phi)\frac{\partial x_{21}}{\partial t_1}-\frac{2KB\sin\phi}{\sigma}\frac{\partial z_{21}}{\partial t_1}+\\
&-\frac{KB\sin\phi}{k}\frac{\partial x_{21}}{\partial a_1}-\frac{i}{k}(1-KB\cos\phi)\frac{\partial z_{21}}{\partial a_1}-\Big(\frac{\partial x_{10}}{\partial a_1}-i\frac{\partial z_{10}}{\partial a_1}\Big)A+\\
&-\frac{2i}{\sigma}(1-KB\cos\phi-iKB\sin\phi)\Big(\frac{\partial A}{\partial t_2}+\frac{\sigma}{2k}\frac{\partial A}{\partial t_2}+\frac{i}{2\sigma}\frac{\partial^2 A}{\partial t_1^2}\Big) \qquad c=0 \qquad (II.4.42)
\end{aligned}$$

Let the solutions $(II.4.15)$ for x_{10} and z_{10}, and $(II.4.38)$ for x_{21} and z_{21} be substituted in $(II.4.41)$ and $(II.4.42)$. For the sake of brevity, all detailed algebraic manipulations are omitted and only the result is given:

$$\frac{\partial A}{\partial t_2}+\frac{\sigma}{2k}\frac{\partial A}{\partial a_2}+\frac{i\sigma}{8k^2}\frac{\partial^2 A}{\partial a_1^2}+\frac{i\sigma k^2|A|^2A}{2(1-2KB\cos\phi+K^2B^2)}+$$

$$+\frac{\Omega^2}{2\sigma}\{\frac{1}{\kappa_r^2}\frac{\partial\kappa_r}{\partial\phi}\frac{\partial\kappa_i}{\partial\phi}-\frac{1}{\kappa_r}\frac{\partial^2\kappa_i}{\partial\phi^2}-\frac{\kappa_i}{2k}\}A+\frac{i\Omega^2}{2\sigma\kappa_r}\{\frac{\partial^2\kappa_r}{\partial\phi^2}+$$

$$-\frac{3}{4\kappa_r}(\frac{\partial\kappa_r}{\partial\phi})^2+\frac{1}{4\kappa_r}(\frac{\partial\kappa_i}{\partial\phi})^2+\frac{\Omega^2BKk(-2KB+(1+K^2B^2)\cos\phi)}{(1-2KB\cos\phi+K^2B^2)^2}\}A=0 \qquad (II.4.43)$$

Note that the fifth and sixth terms in $(II.4.43)$ correspond respectively to changes in amplitude and phase of the complex amplitude A. Furthermore, if KB is very small, κ no longer depends on ϕ and $(II.4.43)$ reduces to the familar nonlinear Schrödinger equation. If use is made of $(II.4.6a-b)$ for κ_r and κ_i, $(II.4.43)$ can be simplified to

$$\frac{\partial A}{\partial t_2}+\frac{\sigma}{2k}\frac{\partial A}{\partial a_2}+\frac{i\sigma}{8k^2}\frac{\partial^2 A}{\partial a_1^2}+\frac{i\sigma k^2|A|^2A}{2(1-2KB\cos\phi+K^2B^2)}+$$

$$+\frac{\Omega^2}{2\sigma}\frac{KB\sin\phi(1+2KB\cos\phi-3K^2B^2)}{(1-2KB\cos\phi+K^2B^2)^2}A+$$

$$+\frac{i\Omega^2KB}{2\sigma(1-K^2B^2)^2}\frac{P_2(KB)\cos^2\phi+P_1(KB)\cos\phi+P_0(KB)}{(1-2KB\cos\phi+K^2B^2)^2}A=0 \qquad (II.4.44)$$

where $P_j(KB)$ are the following polynomials

$$P_2(KB)\equiv 2(KB)^5+4(KB)^3-2KB \qquad (II.4.45a)$$

$$P_1(KB)\equiv -3(KB)^6-7(KB)^4+3(KB)^2-1 \qquad (II.4.45b)$$

and

$$P_0(KB)\equiv 7(KB)^5-6(KB)^3+3KB \qquad (II.4.45c)$$

Next, we add ϵ times $(II.4.44)$ to the linear evolution equation $(II.4.32)$ for the short wave amplitude, and use the multiple scale relations

$$\frac{\partial}{\partial a_1}+\epsilon\frac{\partial}{\partial a_2}\longrightarrow\frac{\partial}{\partial a_1} \qquad (II.4.46a)$$

$$\frac{\partial}{\partial t_1}+\epsilon\frac{\partial}{\partial t_2}\longrightarrow\frac{\partial}{\partial t_1} \qquad (II.4.46b)$$

to obtain

$$\frac{\partial A}{\partial t_1}+\frac{\sigma}{2k}\frac{\partial A}{\partial a_1}+\frac{\Omega KB\sin\phi}{1-2KB\cos\phi+K^2B^2}A-i\frac{\Omega KB}{1-K^2B^2}\frac{(1+K^2B^2)\cos\phi-2KB}{1-2KB\cos\phi+K^2B^2}A+$$

$$+\frac{i\epsilon\sigma}{8k^2}\frac{\partial^2 A}{\partial a_1^2}+\frac{i\epsilon\sigma k^2|A|^2A}{2(1-2KB\cos\phi+K^2B^2)}+$$

$$+\frac{\epsilon\Omega^2}{2\sigma}\frac{KB\sin\phi(1+2KB\cos\phi-3K^2B^2)}{(1-2KB\cos\phi+K^2B^2)^2}A+$$

$$+\frac{i\epsilon\Omega^2KB}{2\sigma(1-K^2B^2)^2}\frac{P_2(KB)\cos^2\phi+P_1(KB)\cos\phi+P_0(KB)}{(1-2KB\cos\phi+K^2B^2)^2}A=\mathcal{O}(\epsilon^2) \quad (II.4.47)$$

In summary, the short wave amplitude A satisfies a cubic nonlinear Schrödinger equation whose coefficients are ϕ-periodic with the long Gerstner wave.

Next, we introduce the following change of variables

$$\xi'=a_1-\frac{\sigma}{2k}t_1 \qquad \phi=\Omega t_1-\epsilon Ka_1 \qquad (II.4.48a-b)$$

then

$$\frac{\partial}{\partial t_1}=\Omega\frac{\partial}{\partial\phi}-\frac{\sigma}{2k}\frac{\partial}{\partial\xi'} \qquad \frac{\partial}{\partial a_1}=\frac{\partial}{\partial\xi'}-\epsilon K\frac{\partial}{\partial\phi} \qquad \frac{\partial^2}{\partial a_1^2}=\frac{\partial^2}{\partial\xi'^2}+\mathcal{O}(\epsilon) \quad (II.4.49a-c)$$

It follows from $(II.4.47)$ that

$$\frac{\partial A}{\partial\phi}=-\frac{1}{\delta}\frac{KB\sin\phi}{1-2KB\cos\phi+K^2B^2}A+i\frac{KB}{\delta(1-K^2B^2)}\frac{(1+K^2B^2)\cos\phi-2KB}{1-2KB\cos\phi+K^2B^2}A+$$

$$-\frac{i\epsilon\sigma}{8\delta\Omega k^2}\frac{\partial^2 A}{\partial\xi'^2}-i\frac{\epsilon\sigma k^2}{2\delta\Omega}\frac{|A|^2A}{(1-2KB\cos\phi+K^2B^2)}+$$

$$-\frac{\epsilon\Omega}{2\delta\sigma}\frac{KB\sin\phi(1+2KB\cos\phi-3K^2B^2)}{(1-2KB\cos\phi+K^2B^2)^2}A+$$

$$-\frac{i\epsilon\Omega KB}{2\delta\sigma(1-K^2B^2)^2}\frac{P_2(KB)\cos^2\phi+P_1(KB)\cos\phi+P_0(KB)}{(1-2KB\cos\phi+K^2B^2)^2}A+\mathcal{O}(\epsilon^2) \quad (II.4.50)$$

where

$$\delta\equiv 1-\epsilon\frac{\Omega}{2\sigma} \qquad (II.4.51)$$

The ϕ-dependent coefficients in $(II.4.50)$ are now periodic with period 2π. With a view to eliminating the phase terms proportional to iA, we introduce the following change of variable:

$$A(\xi', \phi) = A'(\xi', \phi) e^{i\Gamma(\phi)} \qquad (II.4.52)$$

where A' is still a complex quantity. The expression of $\Gamma(\phi)$ is easily found to be

$$\Gamma(\phi, KB, \epsilon\frac{\Omega}{\sigma}) = \frac{1}{\delta}\left[\arctan\Big\{\frac{1+KB}{1-KB}\frac{\sin\phi}{1+\cos\phi}\Big\} - \frac{1+K^2B^2}{1-K^2B^2}\arctan\Big\{\frac{\sin\phi}{1+\cos\phi}\Big\}\right] +$$

$$+\frac{\epsilon\Omega}{2\sigma\delta}\left[\frac{2KB\sin\phi}{1-2KB\cos\phi+K^2B^2} - \arctan\Big\{\frac{1+KB}{1-KB}\frac{\sin\phi}{1+\cos\phi}\Big\} + \right.$$

$$\left. -\frac{B^4K^4+2B^2K^2-1}{(1-B^2K^2)^2}\arctan\Big\{\frac{\sin\phi}{1+\cos\phi}\Big\}\right] \qquad (II.4.53)$$

Substitution of $(II.4.52)$ in $(II.4.50)$ yields the governing equation for A'

$$\frac{\partial A'}{\partial\phi} = -\frac{1}{\delta}\frac{KB\sin\phi}{1-2KB\cos\phi+K^2B^2}\left[1+\frac{\epsilon}{2}\frac{\Omega}{\omega}\frac{1+2KB\cos\phi-3K^2B^2}{1-2KB\cos\phi+K^2B^2)^2}\right]A' +$$

$$-\frac{i\epsilon\sigma}{8\delta\Omega k^2}\frac{\partial^2 A'}{\partial\xi'^2} - \frac{i\epsilon\sigma k^2}{2\delta\Omega}\frac{|A'|^2A'}{1-2KB\cos\phi+K^2B^2} + \mathcal{O}(\epsilon^2) \qquad (II.4.54)$$

Finally, we normalize the short wave amplitude A' and coordinate ξ' as

$$\mathcal{A} = \frac{A'}{\overline{A}} \qquad \xi = \xi' k^2 \overline{A} \qquad (II.4.55a-b)$$

and combine $(II.4.55a-b)$ with $(II.4.54)$ to obtain

$$\frac{\partial\mathcal{A}}{\partial\phi} = -\frac{1}{\delta}\frac{KB\sin\phi}{1-2KB\cos\phi+K^2B^2}\left[1+\frac{\epsilon}{2}\frac{\Omega}{\sigma}\frac{1+2KB\cos\phi-3K^2B^2}{1-2KB\cos\phi+K^2B^2}\right]\mathcal{A} +$$

$$-\frac{i\alpha}{4}\frac{\partial^2\mathcal{A}}{\partial\xi^2} - i\alpha\frac{|\mathcal{A}|^2\mathcal{A}}{1-2KB\cos\phi+K^2B^2} + \mathcal{O}(\epsilon^2) \qquad (II.4.56)$$

where the parameter α is defined by

$$\alpha = \frac{\epsilon}{2\delta}\frac{(k\overline{A})^2}{\frac{\Omega}{\sigma}} \qquad (II.4.57)$$

Recall that $k\overline{A}$, $\frac{\Omega}{\sigma}$ and δ are $\mathcal{O}(1)$, hence α is $\mathcal{O}(\epsilon)$.

Equation $(II.4.56)$ describes the nonlinear evolution of short waves riding on finite amplitude long waves.

5. LEADING ORDER MODULATION OF SHORT WAVES RIDING ON A LONG GERSTNER WAVE

We first investigate the modulation of the short wave amplitude, wavenumber at the leading order and also the relationship between intrinsic and absolute frequencies over the time scale $\phi = \mathcal{O}(1)$. To allow comparison with the quantitative study by Longuet-Higgins (1987) for short waves on steep irrotational Stokes waves, our results will be expressed in terms of Eulerian variables. A brief description of this transformation is given in Appendix E.

5.1. Modulation of the Short Wave Amplitude

We recall the linear evolution equation $(II.4.32)$ for the complex amplitude, A, of the short waves:

$$\frac{\partial A}{\partial t_1} + \frac{\sigma}{2k}\frac{\partial A}{\partial a_1} + \frac{\Omega KB\sin\phi}{1-2KB\cos\phi+K^2B^2}A+$$

$$-i\frac{\Omega KB}{1-K^2B^2}\frac{(1+K^2B^2)\cos\phi-2KB}{1-2KB\cos\phi+K^2B^2}A = 0 \qquad (II.5.1)$$

The frame moving at the group velocity is described by

$$\xi = a_1 - \frac{\sigma}{2k}t_1 \qquad \phi = \Omega t_1 - \epsilon K a_1 \qquad (II.5.2a-b)$$

$(II.5.1)$ can be simplified to leading order

$$\frac{\partial A}{\partial \phi} + \frac{KB\sin\phi}{1-2KB\cos\phi+K^2B^2}A - i\frac{KB}{1-K^2B^2}\frac{(1-K^2B^2)\cos\phi-2KB}{1-2KB\cos\phi+K^2B^2}A = 0 \qquad (II.5.3)$$

It is clear from $(II.5.3)$ that both the amplitude $|A|$ and the phase γ of A are functions of ϕ. The amplitude $|A|$ satisfies

$$\frac{\partial |A|}{\partial \phi} = -\frac{KB\sin\phi}{1-2KB\cos\phi+K^2B^2}|A| \qquad (II.5.4)$$

which can be rewritten as

$$\frac{\partial}{\partial \phi}\left[|A|(1-2KB\cos\phi+K^2B^2)^{\frac{1}{2}}\right] = 0 \qquad (II.5.5a)$$

and is integrated as

$$\frac{|A|}{\overline{A}} = (1 - 2KB\cos\phi + K^2B^2)^{-\frac{1}{2}} \qquad (II.5.5b)$$

where $\overline{A}$ refers to the amplitude of the short wave in the absence of long waves †. When the slope of Gerstner's wave is small, $KB \ll 1$, the well known result of Longuet-Higgins and Stewart(1960) is recovered

$$\frac{|A|}{\overline{A}} = 1 + KB\cos\phi + O(K^2B^2) \qquad (II.5.6)$$

For arbitrarily large KB, we may now examine the normalized short wave amplitude at the crest ($\phi = 0$) and trough ($\phi = \pi$):

$$\frac{|A|_{\text{crest}}}{\overline{A}} = \frac{1}{1 - KB} \qquad \frac{|A|_{\text{trough}}}{\overline{A}} = \frac{1}{1 + KB} \qquad (II.5.7a - b)$$

We have shown in §II.3 that Gerstner's free surface crosses the mean sea level at the location characterized by $\cos\phi = -\frac{KB}{2}$. Consequently, the amplitude at that location is

$$\frac{|A|_{\text{crossing}}}{\overline{A}} = (1 + 2K^2B^2)^{-\frac{1}{2}} \qquad (II.5.7c)$$

In contrast with existing numerical studies by Longuet-Higgins(1987) and Zhang & Melville(1990), the modulation of the short wave amplitude is now obtained analytically.

5.2. Effective Gravity

Short waves propagating on the free surface of Gerstner's wave are subjected to both the gravitational acceleration $\vec{g}$ and the acceleration $\vec{g}_{\text{Gerstner}}$ due to the time varying long wave velocity field at that location. The resultant of these two accelerations may be called the effective gravity $\vec{g}_{\text{eff}}$

$$\vec{g}_{\text{eff}} = \vec{g} - \vec{g}_{\text{Gerstner}} \qquad (II.5.8)$$

Upon introducing a parametric description of the free surface

$$X_2 = a_2 + B\sin\phi \qquad Z_2 = B\cos\phi \qquad (II.5.9a - b)$$

† Note that $\overline{A}$ also corresponds to the amplitude of the short wave at the specific phase of the long wave $\cos\phi = \frac{KB}{2}$.

we may deduce the components of $\vec{g}_{\text{Gerstner}}$ as

$$\vec{g}_{\text{Gerstner}} = \begin{pmatrix} \frac{\partial^2 X_2}{\partial t_1^2} \\ \frac{\partial^2 Z_2}{\partial t_1^2} \end{pmatrix} = -gKB \begin{pmatrix} \sin\phi \\ \cos\phi \end{pmatrix} \qquad (II.5.10a-b)$$

after making use of the dispersion relation (II.3.5). It follows that

$$\frac{\vec{g}_{\text{eff}}}{g} = \begin{pmatrix} KB\sin\phi \\ -1 + KB\cos\phi \end{pmatrix} \qquad (II.5.11)$$

whose magnitude g_{eff} is

$$\frac{g_{\text{eff}}}{g} = \sqrt{1 + K^2B^2 - 2KB\cos\phi} \qquad (II.5.12)$$

At the crest ($\phi = 0$) and at the trough ($\phi = \pi$), the effective gravity takes on the simpler form

$$\frac{g_{\text{eff}_{\text{crest}}}}{g} = 1 - KB \qquad \frac{g_{\text{eff}_{\text{trough}}}}{g} = 1 + KB \qquad (II.5.13a-b)$$

We have shown in §II.3 that the free surface of Gerstner's wave crosses the mean sea level at $\cos\phi = -\frac{KB}{2}$, where the effective gravity is

$$\frac{g_{\text{eff}_{\text{crossing}}}}{g} = \sqrt{1 + 2K^2B^2} \qquad (II.5.13c)$$

The variations of $\frac{g_{\text{eff}}}{g}$ against ϕ_{E} are plotted in figure 5.1 for $KB = 0.1$, 0.2 and 0.3 along with the results of Longuet-Higgins (1987). The agreement is excellent for $KB = 0.1$ and fair for larger slopes.

In light of (II.5.12), eq. (II.5.4) may be reinterpreted as the following conservation equation along the long wave profile

$$\frac{\partial}{\partial\phi}(|A|g_{\text{eff}}) = 0 \qquad (II.5.14)$$

Alternately, let us substitute $|A|e^{i\gamma}$ for A in (II.5.1)

$$\frac{\partial|A|}{\partial t_1} + \frac{\sigma}{2k}\frac{\partial|A|}{\partial a_1} + \frac{\Omega KB\sin\phi}{1 - 2KB\cos\phi + K^2B^2}|A| = 0 \qquad (II.5.15a)$$

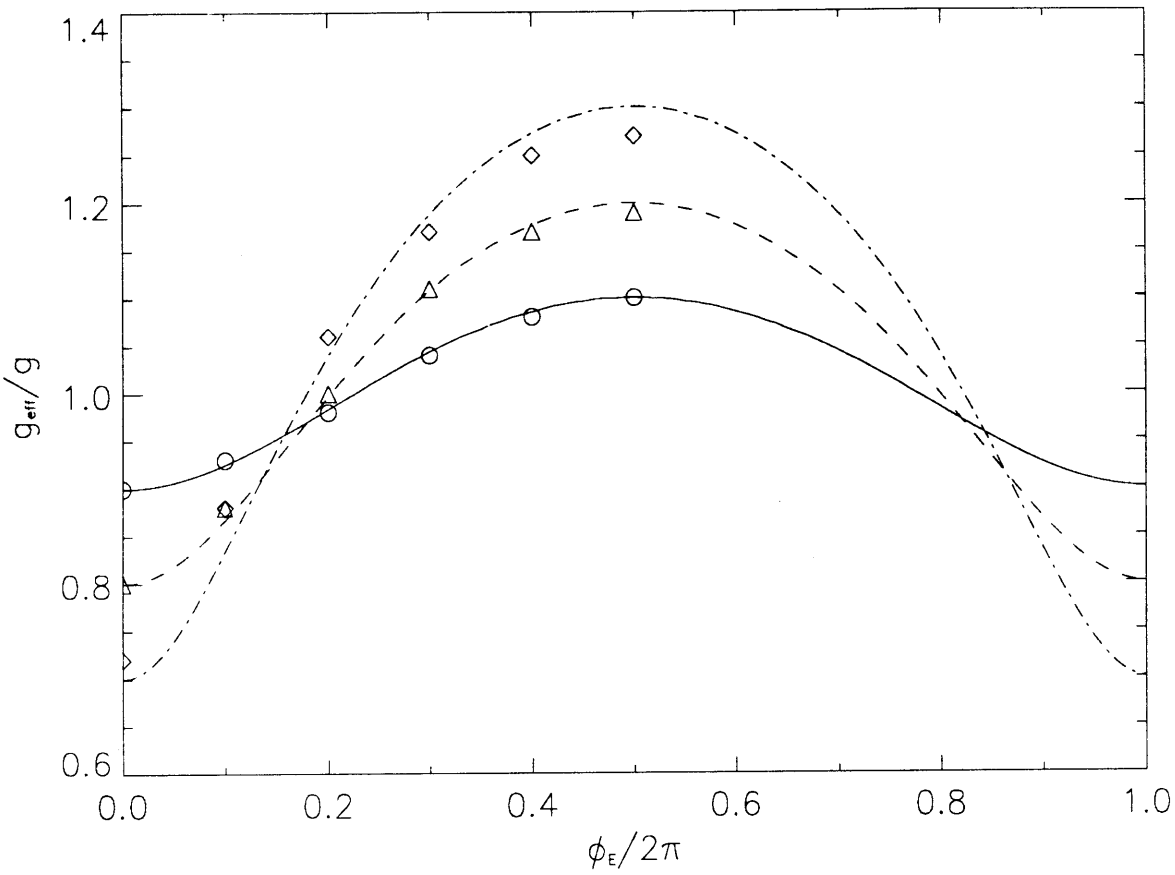

Figure II.5.1: Effective gravity for Gerstner wave: $KB = 0.1$ (——), $KB = 0.2$ (– – –), and $KB = 0.3$ (-·-·-·-); Stokes wave (from Longuet-Higgins, 1987): $KB = 0.1$ (○), $KB = 0.2$ (△) and $KB = 0.3$ (◇).

Upon multiplying $(II.5.15a)$ throughout by g_{eff}, it may be rewritten as

$$\frac{\partial}{\partial t_1}\left[g_{\text{eff}}|A|\right] + \frac{\sigma}{2k}\frac{\partial}{\partial a_1}\left[g_{\text{eff}}|A|\right] = 0 \qquad (II.5.15b)$$

which plays the role of the law of conservation of wave action in the Lagrangian frame.

5.3. Modulation of the Short Wave Wavenumber

The Lagrangian wavenumber, defined as $(\partial_a \tilde{S}, \partial_c \tilde{S})$, has been shown in §II.4 to be modulated by the presence of Gerstner's wave. In order to compare the results of our theory to existing results in Eulerian frame, the modulation of the Eulerian wavenumber is needed. In view of $(II.4.32)$, the phase function $\tilde{S}$ must be corrected

to incorporate the slowly varying phase variations of A. The expression of $\gamma(\phi, KB)$ is deduced by setting ϵ to zero in the expression $(II.4.53)$ of $\Gamma(\phi, KB)$:

$$\gamma(\phi, KB) = \arctan\left[\frac{1+KB}{1-KB}\frac{\sin\phi}{1+\cos\phi}\right] - \frac{1+K^2B^2}{1-K^2B^2}\arctan\left[\frac{\sin\phi}{1+\cos\phi}\right] \quad (II.5.16)$$

In summary, the phase function reads:

$$\tilde{S} = k\big[a - \frac{2KB\sin\phi}{1-2KB\cos\phi+K^2B^2}c\big] - \sigma t + \gamma(\phi, KB) + \mathcal{O}(\epsilon) \quad (II.5.17)$$

where the independent Lagrangian variables must be replaced by their Eulerian counterparts and ϕ stands for $\Omega t_1 - Ka_2$. Given the order of approximation in $(II.5.17)$, it is sufficient to consider the leading order expansion of (a, c) in terms of Eulerian coordinates:

$$a = X - \frac{B}{\epsilon^2}\sin\phi\ e^{Kc_2} + \mathcal{O}(\epsilon) \qquad c = Z - \frac{B}{\epsilon^2}\cos\phi\ e^{Kc_2} + \mathcal{O}(\epsilon) \quad (II.5.18)$$

Upon substituting $(II.5.18)$ into $(II.5.17)$, we obtain

$$\tilde{S} = \frac{1}{\epsilon^2}\tilde{S}_{-2} + \tilde{S}_0 + \mathcal{O}(\epsilon) \quad (II.5.19a)$$

where

$$\tilde{S}_{-2} = -\frac{k(1+K^2B^2)\ B\sin\phi}{1-2KB\cos\phi+K^2B^2}e^{Kc_2} \quad (II.5.19b)$$

and

$$\tilde{S}_0 = k\big[X + \frac{2KB\sin\phi}{1-2KB\cos\phi+K^2B^2}Z\big] - \sigma t + \gamma(\phi, KB) \quad (II.5.19c)$$

Note that both $\tilde{S}_{-2}$ and γ depend on ϕ *i.e.* on X_2 and t_1, whereas $\tilde{S}_0$ depends on the fast Eulerian scales (X, Z, t). In order to obtain the Eulerian wavenumber, we need to take the Eulerian gradient of the phase function $\tilde{S}$ as described by $(II.5.19a)$, accounting for the presence of multiple scales. This yields

$$\vec{k}^e = \nabla\tilde{S} + \epsilon\nabla_1\tilde{S} + \epsilon^2\nabla_2\tilde{S} + \mathcal{O}(\epsilon) \quad (II.5.20)$$

where ∇ and ∇_i stand respectively for (∂_X, ∂_Z) and $(\partial_{X_i}, \partial_{Z_i})$. Owing to the finite slope of the long wave, the short wave wavenumber is no longer horizontal. After substituting $(II.5.19a)$ in $(II.5.20)$, we obtain

$$\vec{k}^e = \nabla\tilde{S}_0 + \nabla_2\tilde{S}_{-2} + \mathcal{O}(\epsilon) \quad (II.5.21)$$

Due to its scale dependence, γ will not contribute to the modulation of the wavenumber at the leading order. Since $\tilde{S}_{-2}$ is a function of both ϕ (thus of a_2 and t_1) and c_2, we may rewrite $(II.5.21)$ as

$$\vec{k}^e = \nabla\tilde{S}_0 + \frac{\partial\tilde{S}_{-2}}{\partial a_2}\nabla_2 a_2 + \frac{\partial\tilde{S}_{-2}}{\partial c_2}\nabla_2 c_2 \qquad (II.5.22a)$$

i.e. after recalling the definition $(II.4.1d)$ of ϕ and $(II.5.19b)$

$$\vec{k}^e = \nabla\tilde{S}_0 + K\left[\tilde{S}_{-2}\nabla_2 c_2 - \frac{\partial\tilde{S}_{-2}}{\partial\phi}\nabla_2 a_2\right] \qquad (II.5.22b)$$

The gradients $\nabla_2 a_2$ and $\nabla_2 c_2$ can be calculated from $(II.3.3)$

$$X_2 = a_2 + B\sin\phi\ e^{Kc_2} \qquad Z_2 = c_2 + B\cos\phi\ e^{Kc_2} \qquad (II.5.23a-b)$$

where $\mathcal{O}(\epsilon^3)$ terms have been omitted. Leaving the details to Appendix A, we cite the results

$$\frac{\partial a_2}{\partial X_2} = \frac{1}{J}\frac{\partial Z_2}{\partial c_2} = \frac{1+KB\sin\phi\ e^{Kc_2}}{1-K^2B^2e^{2Kc_2}} \qquad \frac{\partial a_2}{\partial Z_2} = -\frac{1}{J}\frac{\partial X_2}{\partial c_2} = -\frac{KB\sin\phi\ e^{Kc_2}}{1-K^2B^2e^{2Kc_2}} \qquad (II.5.24a-b)$$

$$\frac{\partial c_2}{\partial X_2} = -\frac{1}{J}\frac{\partial Z_2}{\partial a_2} = -\frac{KB\cos\phi\ e^{Kc_2}}{1-K^2B^2e^{2Kc_2}} \qquad \frac{\partial c_2}{\partial Z_2} = \frac{1}{J}\frac{\partial X_2}{\partial a_2} = \frac{1-KB\cos\phi\ e^{Kc_2}}{1-K^2B^2e^{2Kc_2}} \qquad (II.5.25a-b)$$

The horizontal component of $\vec{k}^e$ may now be evaluated

$$\frac{k_x^e}{k} = \frac{1-3KB\cos\phi+4K^2B^2\cos^2\phi-2K^3B^3\cos\phi\sin^2\phi}{(1-K^2B^2)(1-2KB\cos\phi+K^2B^2)^2} +$$

$$+\frac{-K^4B^4(1+4\cos^2\phi)+K^5B^5\cos\phi(1+2\cos^2\phi)}{(1-K^2B^2)(1-2KB\cos\phi+K^2B^2)^2}+\mathcal{O}(\epsilon) \qquad (II.5.26)$$

For small long wave slope KB, $(II.5.26)$ may be expanded

$$\frac{k_x^e}{k} = 1+KB\cos\phi+K^2B^2(4\cos^2\phi-1)+\mathcal{O}(\epsilon,K^3B^3) \qquad (II.5.27)$$

The leading order term in $(II.5.27)$ is identical to the classical result of Longuet-Higgins & Stewart(1960). From $(II.5.26)$, we deduce the x-component of the wavenumber at the crest and trough for arbitrary KB

$$\frac{k^e_{x\,\mathrm{crest}}}{k} = \frac{1-2KB+3K^2B^2}{(1-KB)^3} \qquad \frac{k^e_{x\,\mathrm{trough}}}{k} = \frac{1+2KB+3K^2B^2}{(1+KB)^3} \qquad (II.5.28a-b)$$

and at the mean sea level crossing ($\cos\phi = -\frac{KB}{2}$)

$$\frac{k^e_{x\,\text{crossing}}}{k} = \frac{1 + \frac{3}{2}K^2B^2 + K^4B^4 - \frac{7}{4}K^6B^6 - \frac{1}{4}K^8B^8}{(1-K^2B^2)(1+2K^2B^2)^2} \qquad (II.5.28c)$$

For small slopes KB, $(II.5.28c)$ may be expanded as

$$\frac{k^e_{x\,\text{crossing}}}{k} = 1 - \frac{3}{2}K^2B^2 + \mathcal{O}(K^4B^4) \qquad (II.5.29)$$

Note that k^e_x is always positive at the crest, trough and free surface crossing. This result will be important when assessing the direction of propagation of the short waves as seen by a fixed observer.

Next, we evaluate the vertical component of the wavenumber k^e_z

$$\frac{k^e_z}{k} = \frac{KB\sin\phi}{(1-K^2B^2)(1-2KB\cos\phi+K^2B^2)^2}\times$$

$$\left[1-2KB\cos\phi-2K^2B^2\cos^2\phi+6K^3B^3\cos\phi-K^4B^4(1+2\cos^2\phi)\right]+\mathcal{O}(\epsilon) \quad (II.5.30)$$

When the long wave slope is mild, $(II.5.30)$ may be expanded as

$$\frac{k^e_z}{k} = KB\sin\phi + K^2B^2\sin 2\phi + \mathcal{O}(K^3B^3,\epsilon) \qquad (II.5.31)$$

For arbitrary KB, the modulations at the crest and trough are

$$\frac{k^e_{z\,\text{crest}}}{k} = \frac{k^e_{z\,\text{trough}}}{k} = 0 \qquad (II.5.32a-b)$$

as expected. The location of the mean sea level has been characterized in §II.3 by $\cos\phi = -\frac{KB}{2}$. This equation admits two solutions in the interval $[0,2\pi]$, whose sine is $\pm\sqrt{1-\frac{K^2B^2}{4}}$ respectively for the crossing near $\frac{\pi}{2}$ and $\frac{3\pi}{2}$. The expression of k^e_z at the two crossing points is then

$$\frac{k^e_{z\,\text{crossing}}}{k} = \frac{\pm KB(1+K^2B^2-\frac{9}{2}K^4B^4-\frac{1}{2}K^6B^6)\sqrt{1-\frac{1}{4}K^2B^2}}{(1-K^2B^2)(1+2K^2B^2)^2} \qquad (II.5.32c)$$

For small KB, $(II.5.32c)$ yields

$$\frac{k^e_{z\,\text{crossing}}}{k} = \pm KB + \mathcal{O}(K^3B^3) \qquad (II.5.33)$$

The inclination ϑ of $\vec{k}^e$ is

$$\tan\vartheta = \frac{k_z^e}{k_x^e} \qquad (II.5.34)$$

The slope of the long wave free surface, on the other hand is by definition

$$\tan\chi_{\text{Gerstner}} = \left.\frac{\frac{\partial Z_2}{\partial a_2}}{\frac{\partial X_2}{\partial a_2}}\right|_{c_2=0} = \frac{KB\sin\phi}{1-KB\cos\phi} \qquad (II.5.35)$$

after using the parametric representation $(II.5.9a-b)$. Straightforward manipulations show that $|\tan\vartheta - \tan\chi_{\text{Gertsner}}|$ is an $\mathcal{O}(K^3B^3)$ quantity. We have plotted in figure 5.2 $\tan\vartheta$ and $\tan\chi_{\text{Gerstner}}$ against the long wave phase ϕ_{E}. For $KB = 0.1$ the two curves are undistinguishable. As KB increases small discrepancies arise.

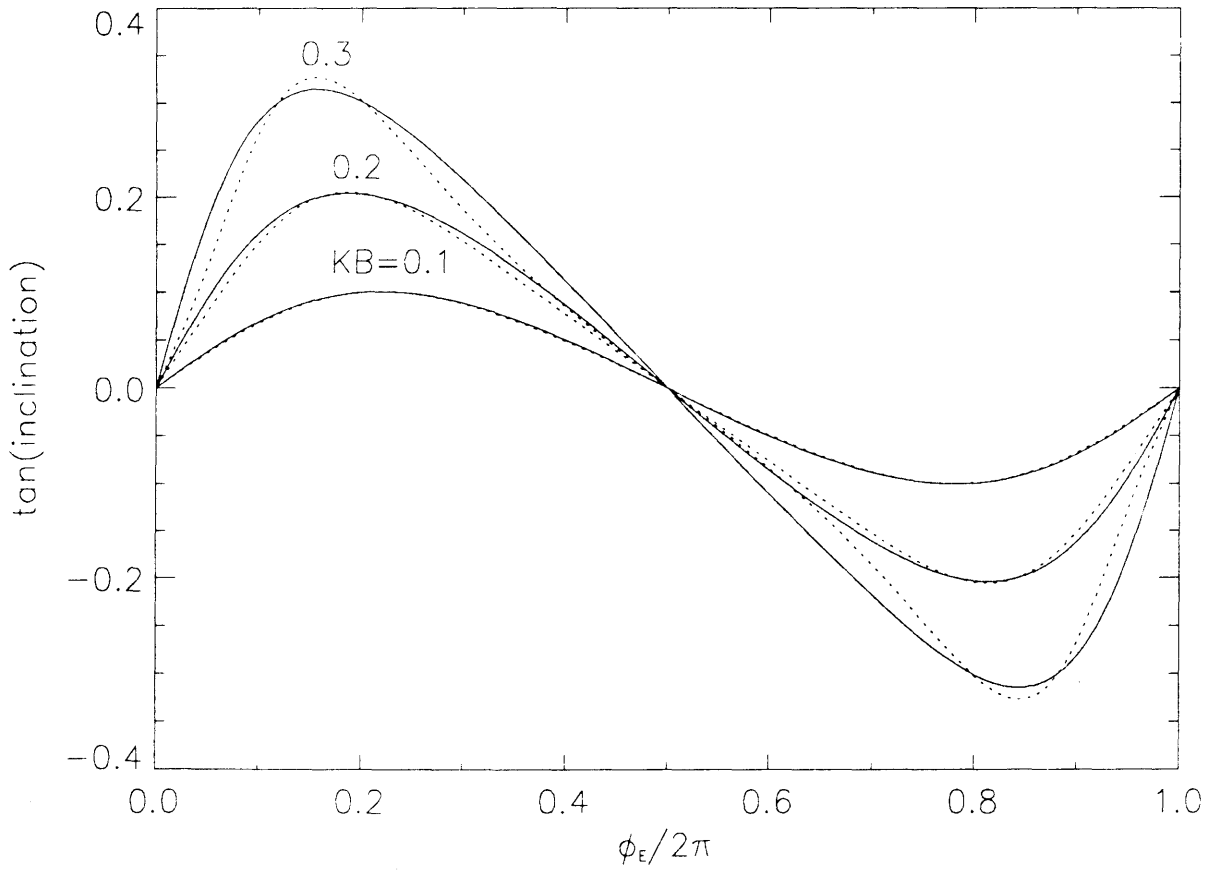

Figure II.5.2: Comparison of inclination of the free surface of Gerstner's wave (——) with the inclination of $\vec{k}^e$ (· · · · ·).

Next our results on the wavenumber and wave steepness modulation are compared with those of Longuet-Higgins(1987). His wavenumber k and amplitude A of the short waves are normalized by their values at the crossing of the long Stokes wave. Since the location of the zero-crossing for the Gerstner and Stokes waves are quite different (see §II.3), two normalizations have been adopted. The first one assumes the Gerstner zero-crossing. The corresponding amplitude is given by $(II.5.7c)$ and the wavenumber k^e_{crossing} is readily deduced from $(II.5.28c)$ and $(II.5.32c)$. Changes of wavenumber at the crest and at the trough, denoted by Longuet-Higgins as $\frac{k_1}{k}$ and $\frac{k_2}{k}$ respectively, are plotted versus the long wave slope in figure 5.3a. The agreement is good at the trough, while our theory predicts a significantly larger modulation at the crest for intermediate wave slopes KB.

Following Longuet-Higgins, the steepening ratios r_1 and r_2 are defined as the ratio of the slope respectively at the crest and at the trough to the slope at the free surface crossing. The comparison is presented in figure 5.3b. Our theory still overestimates - though to a lesser extent - the short wave steepness at the crest. The agreement at the trough is fair. Finally, we present in figure 5.3c the variations of the steepening ratio r against the long wave Eulerian phase ϕ_E for three values of the long wave slope $KB = 0.1$, 0.2 and 0.3. The agreement is fair for all three slopes.

Next, we assume the normalizing amplitude and wavenumber to be evaluated at the zero-crossing of the Stokes wave. The agreement between our theory and Longuet-Higgins' is very good (see figures 5.4a-c) despite the presence of the $\mathcal{O}(K^2B^2)$ vorticity field associated with the Gerstner wave.

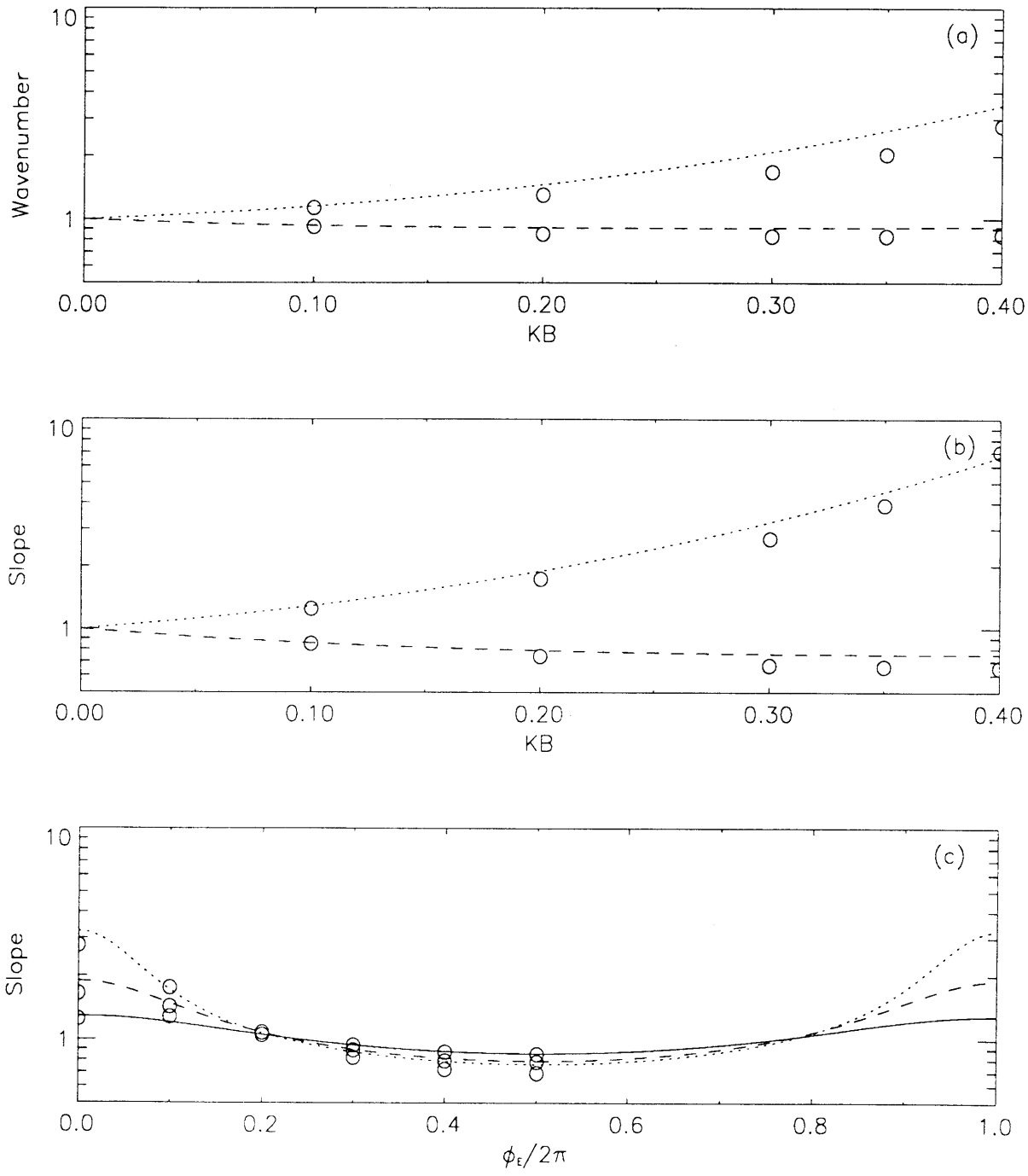

Figure II.5.3: Modulation of linearized short waves riding on a Gerstner wave and a Stokes wave (○, from Longuet-Higgins, 1987). (a) Wavenumber modulation at the crest (· · · · ·) and at the trough (– – –); (b) likewise for the wave steepness; (c) Wave steepness for $KB = 0.1$ (——), $KB = 0.2$ (– – –) and $KB = 0.3$ (· · · · ·). Normalization based on zero-crossing of the Gerstner wave.

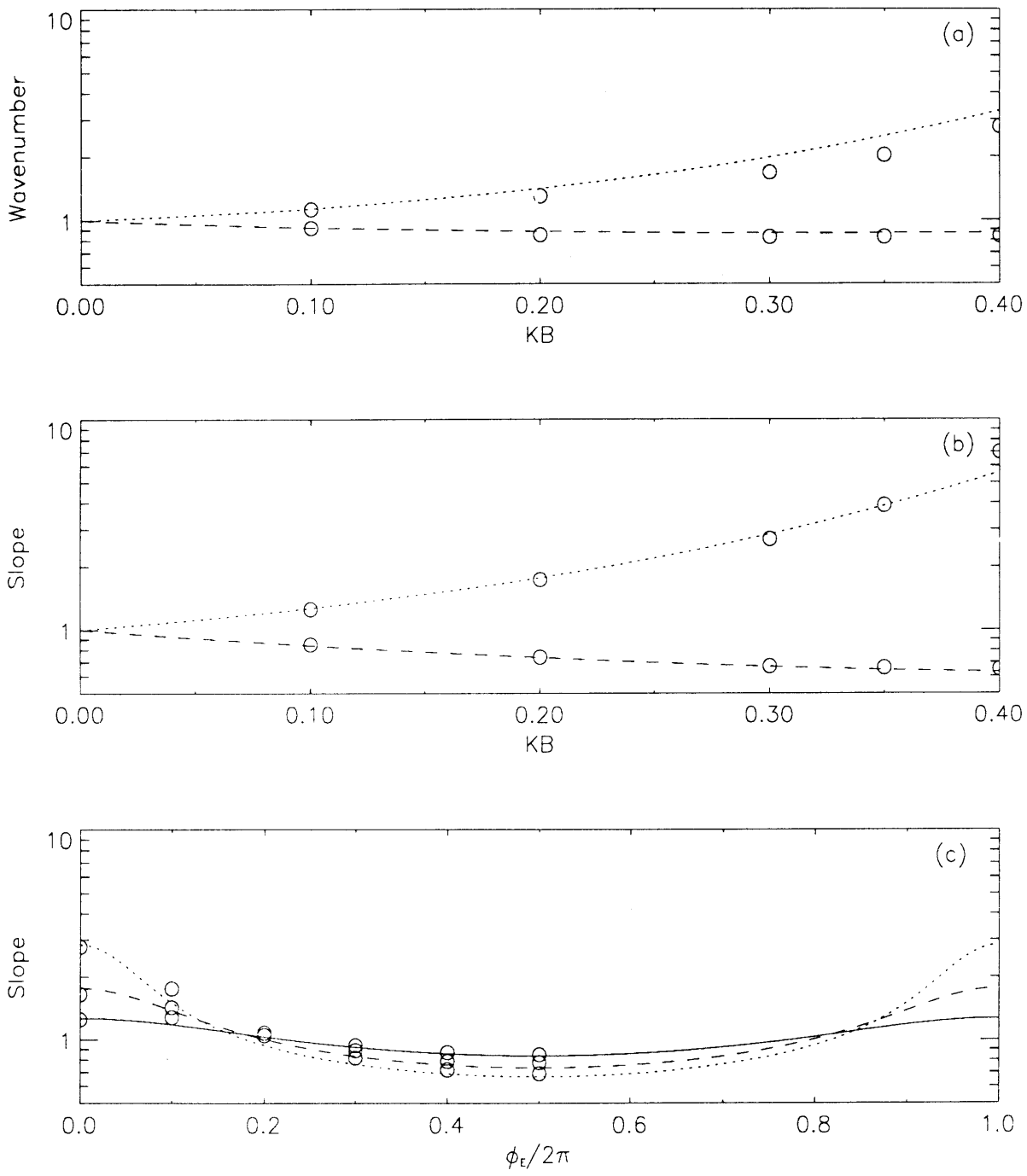

Figure II.5.4: Modulation of linearized short waves riding on a Gerstner wave and a Stokes wave (○, from Longuet-Higgins, 1987). (a) Wavenumber modulation at the crest (· · · · ·) and at the trough (– – –); (b) likewise for the wave steepness; (c) Wave steepness for $KB = 0.1$ (——), $KB = 0.2$ (– – –) and $KB = 0.3$ (· · · · ·). Normalization based on zero-crossing of the Stokes wave.

5.4. Dispersion Relation in the Eulerian Frame

The dispersion relation $(II.4.9)$ can be rewritten in terms of the Eulerian short wave wavenumber k^e and the effective gravity g_{eff} as follows

$$\sigma^2 = g_{\text{eff}} k^e Q(KB, \phi) \qquad (II.5.36)$$

where Q is given by

$$Q(KB, \phi) = \frac{g}{g_{\text{eff}}} \frac{k}{k^e} \qquad (II.5.37)$$

Substitution of $(II.5.12)$, $(II.5.26)$ $(II.5.30)$ in $(II.5.37)$ yields the explicit expression of Q

$$Q(KB,\phi) = (1 - K^2B^2)(1 - 2KB\cos\phi + K^2B^2)^{\frac{3}{2}} \times$$

$$\big[1 - 6KB\cos\phi + K^2B^2(1 + 16\cos^2\phi) +$$

$$- 8K^3B^3\cos\phi(1 + 2\cos^2\phi) + 2K^4B^4(-1 + 2\cos^2\phi + 2\cos^4\phi) +$$

$$+ 4K^5B^5\cos\phi(5 + 2\cos^2\phi + 2\cos^4\phi) - 2K^6B^6(1 + 18\cos^2\phi + 10\cos^4\phi) +$$

$$+ 8K^7B^7\cos\phi(1 + 2\cos^4\phi) + K^8B^8(1 + 44\cos^2\phi - 20\cos^4\phi) +$$

$$- 2K^9B^9\cos\phi(7 + 12\cos^2\phi - 4\cos^4\phi) + K^{10}B^{10}(1 + 4\cos^2\phi + 4\cos^4\phi)\big]^{-1} \qquad (II.5.38)$$

For small slopes KB, Q may be expanded

$$Q(KB, \cos\phi) = 1 - 2K^2B^2\cos^2\phi + 4K^3B^3\cos\phi(1 - 2\cos^2\phi) + \mathcal{O}(K^4B^4) \quad (II.5.39)$$

In existing works where the long wave is an irrotational Stokes wave (Henyey *et al*(1988)), the corresponding dispersion relation for the short wave is $\sigma^2 = g_{\text{eff}} k^e$, the difference between this and $(II.5.36)$ is of the same order as the vorticity difference in the long waves.

5.5. Absolute and Intrinsic Frequencies

We seek now the frequency of the short waves in a fixed Eulerian frame of reference. This frequency is called the *absolute* frequency ω, as distinguished from the *intrinsic*

frequency σ seen in the Lagrangian frame attached to a particle. By definition, we have

$$\omega = -\frac{\partial \tilde{S}}{\partial t}\bigg|_{X,X_1} - \epsilon \frac{\partial \tilde{S}}{\partial t_1}\bigg|_{X,X_1} + \mathcal{O}(\epsilon) \qquad (II.5.40)$$

Upon substituting $(II.5.11a)$ in $(II.5.40)$ in accordance with the chain rule, we obtain straightforwardly

$$\omega = \sigma - \frac{1}{\epsilon}\frac{\partial \tilde{S}_{-2}}{\partial \phi}\frac{\partial \phi}{\partial t_1}\bigg|_{X,X_1} + \mathcal{O}(\epsilon) \qquad (II.5.41)$$

where the time derivative in the right hand side awaits evaluation. To this end, we recall the relationship $(E.5a)$ between ϕ and ϕ_{E}

$$\phi_{\mathrm{E}} = \phi - KB\sin\phi \qquad (II.5.42)$$

and take the t_1-derivative, thus obtaining

$$\frac{\partial \phi}{\partial t_1}\bigg|_{X,X_1} = \frac{\partial \phi_{\mathrm{E}}}{\partial t_1}\bigg|_{X,X_1} (1 - KB\cos\phi)^{-1} + \mathcal{O}(\epsilon^2) = \frac{\Omega}{1 - KB\cos\phi} + \mathcal{O}(\epsilon^2) \qquad (II.5.43)$$

Upon substituting $(II.5.19b)$ into $(II.5.43)$, we obtain

$$\omega = \sigma + \frac{1}{\epsilon} k\Omega B \frac{1 + K^2B^2}{1 - KB\cos\phi}\frac{-2KB + (1 + K^2B^2)\cos\phi}{(1 - 2KB\cos\phi + K^2B^2)^2} + \mathcal{O}(\epsilon) \qquad (II.5.44)$$

After making use of the dispersion relations, the relative change in frequencies is obtained

$$\frac{\omega}{\sigma} = 1 + \frac{KB}{\epsilon\frac{\Omega}{\sigma}}\frac{1 + K^2B^2}{1 - KB\cos\phi}\frac{-2KB + (1 + K^2B^2)\cos\phi}{(1 - 2KB\cos\phi + K^2B^2)^2} + \mathcal{O}(\epsilon) \qquad (II.5.45)$$

Note that the presence of the small parameter $\epsilon\frac{\Omega}{\sigma}$ in the denominator of $(II.5.45)$ implies that the ratio $\frac{\omega}{\sigma}$ may be large. From $(II.5.45)$, the absolute frequency, ω, of the short wave (*i.e.* the frequency as seen by a stationary observer) may be equal to the intrinsic frequency σ provided that

$$\cos\phi = \frac{2KB}{1 + K^2B^2} \qquad (II.5.46)$$

For a given KB, eq. $(II.5.46)$ admits two solutions for ϕ. The corresponding Eulerian phases ϕ_{E} is then deduced from $(II.5.42)$ and plotted in the (ϕ_{E}, KB)

plane in figure 5.5. More interesting is the special case $\omega = 0$ corresponding to stationary short waves in the fixed frame of reference. Depending on the value of KB, this equation may or may not have solutions for a given $\epsilon\frac{\Omega}{\sigma}$. We have superimposed on figure 5.5 the contours $\omega = 0$ obtained for $\epsilon\frac{\Omega}{\sigma} = 0.05$, 0.075, 0.1, 0.125 and 0.15. The absolute frequency ω is positive (negative) below (above) a given contour. For small enough long wave slope *i.e.* for $KB < KB_{\min}$, short waves are always propagating to the right ($\omega > 0$) whereas for larger values of KB, short waves propagate to the left while in the trough of the long wave ($\omega < 0$). Note that $KB_{\min}$ decreases with $\epsilon\frac{\Omega}{\sigma}$ *i.e.* with the scale contrast between the long and short waves.

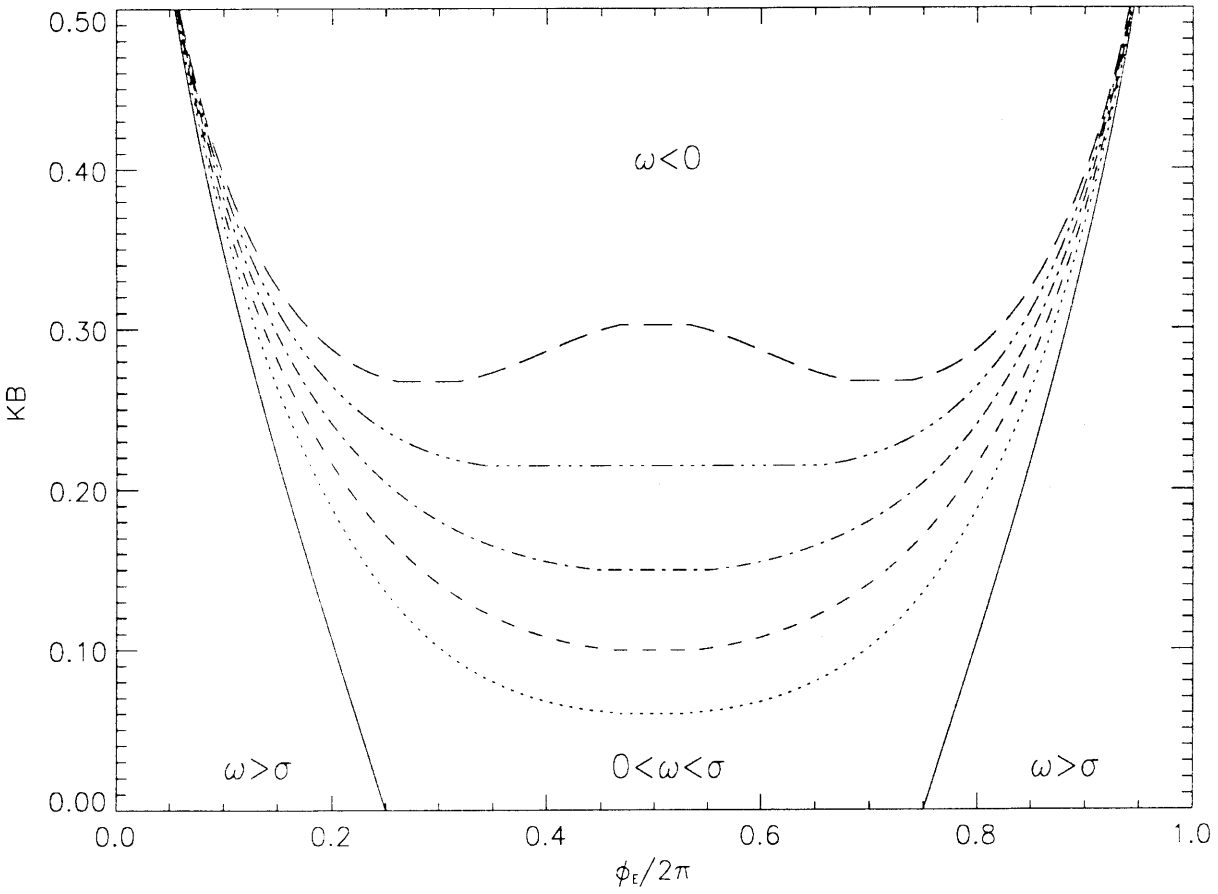

Figure II.5.5: Contours of $\frac{\omega}{\sigma}(\phi_E, KB, \epsilon\frac{\Omega}{\sigma})$, $\frac{\omega}{\sigma} = 1$ (solid lines); $\frac{\omega}{\sigma} = 0$ with $\epsilon\frac{\Omega}{\sigma} = 0.05$ (· · · · ·), $\epsilon\frac{\Omega}{\sigma} = 0.075$ (- - -), $\epsilon\frac{\Omega}{\sigma} = 0.1$ (-·-·-), $\epsilon\frac{\Omega}{\sigma} = 0.125$ (—· · ·—· · ·—) and $\epsilon\frac{\Omega}{\sigma_0} = 0.15$ (— — —).

6. LINEARIZED SIDEBAND INSTABILITY OF A SHORT STOKES WAVE

As in the classical case (without long waves), the first step towards the study of the nonlinear evolution is to examine the linearized instability of a periodic modulation of a Stokes wave train. We first seek a solution uniform in ξ. Owing to the presence of periodic coefficients in the linearized evolution equations, Floquet theory is invoked to study the instability. For convenience, certain results of this theory are quoted in Appendix G. We shall then investigate the influence of the disturbance wavenumber ν, KB and α on its stability.

6.1. The Stokes Wave

We recall the nonlinear Schrödinger equation $(II.4.56)$ satisfied by $\mathcal{A}$:

$$\frac{\partial \mathcal{A}}{\partial \phi} = -D(\phi, KB, \epsilon\frac{\Omega}{\sigma})\mathcal{A} - \frac{i\alpha}{4}\frac{\partial^2 \mathcal{A}}{\partial \xi^2} - i\alpha\frac{|\mathcal{A}|^2\mathcal{A}}{1 - 2KB\cos\phi + K^2B^2} \qquad (II.6.1a)$$

where

$$D(\phi, KB, \frac{\epsilon\Omega}{\sigma}) = \frac{1}{\delta}\frac{KB\sin\phi}{1 - 2KB\cos\phi + K^2B^2}\left[1 + \frac{\epsilon}{2}\frac{\Omega}{\sigma}\frac{1 + 2KB\cos\phi - 3K^2B^2}{1 - 2KB\cos\phi + K^2B^2}\right] \qquad (II.6.1b)$$

and α is defined by $(II.4.57)$. The uniform wave solution is sought in the form:

$$\mathcal{A}_s(\phi) = |\mathcal{A}_s(\phi)|e^{i\beta(\phi)} \qquad (II.6.2)$$

where $\beta(\phi)$ is real. Substitution of $(II.6.2)$ into $(II.6.1a)$ yields two equations:

$$\frac{\partial|\mathcal{A}_s|}{\partial\phi} = -D(\phi, KB, \epsilon\frac{\Omega}{\sigma})\,|\mathcal{A}_s| \qquad \frac{\partial\beta}{\partial\phi} = -\alpha\frac{|\mathcal{A}_s|^2}{1 - 2KB\cos\phi + K^2B^2} \quad (II.6.3a - b)$$

Integration of $(II.6.3a)$ with the help of $(II.6.1b)$ yields straighforwardly

$$|\mathcal{A}_s(\phi)| = \sqrt{\frac{N(\phi_0)}{N(\phi)}}\exp\{\frac{\epsilon}{2\delta}\frac{\Omega}{\sigma}(1 - K^2B^2)(\frac{1}{N(\phi)} - \frac{1}{N(\phi_0)})\} \qquad (II.6.4a)$$

where

$$N(\phi) = 1 - 2KB\cos\phi + K^2B^2 \qquad (II.6.4b)$$

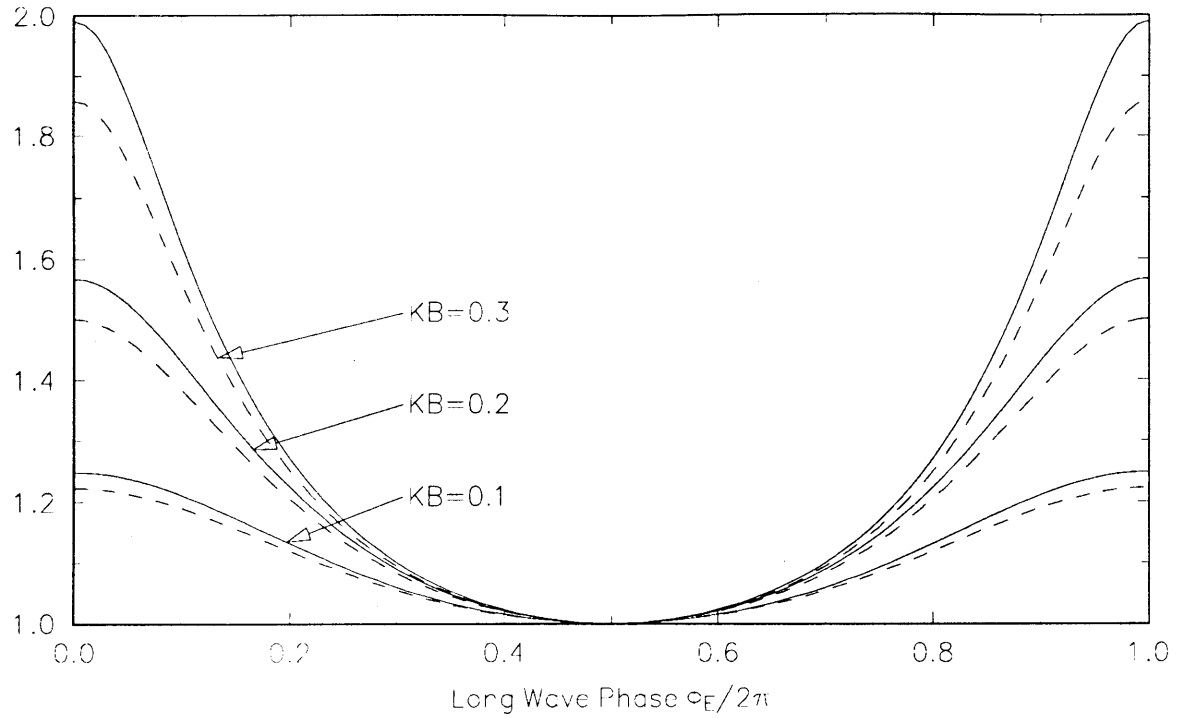

Figure II.6.1: Amplitude of uniform Stokes wave (——) and amplitude modulation according to the linear evolution equation (- - - -).

Note that the leading order amplitude term in $(II.6.4a)$ is identical to the amplitude modulation $(II.5.5b)$. This modulation is enhanced at $\mathcal{O}(\epsilon)$ by the presence of the exponential factor. We plot in figure 6.1 the variations of $|\mathcal{A}_s|$, normalized by its value at the trough, against the Eulerian phase ϕ_{E} of the long wave. Note also that if the long waves become infinitely long *i.e.* $KB \rightarrow 0$ and $\epsilon\frac{\Omega}{\sigma} \rightarrow 0$, $(II.6.4a)$ reduces to the classic result $|\mathcal{A}_s|$=const.

Substitution of $(II.6.4a)$ into $(II.6.3b)$ yields

$$\beta(\phi) = -\alpha \int_{\phi_0}^{\phi} G(\phi')d\phi' \qquad (II.6.5a)$$

where

$$G(\phi) = \frac{|\mathcal{A}_s(\phi)|^2}{N(\phi)} \qquad (II.6.5b)$$

The phase $\beta(\phi)$ cannot be integrated analytically. Instead, we investigate the changes in Lagrangian wavenumber and intrinsic frequency due to $\beta(\phi)$:

$$\Delta k = (\frac{\partial}{\partial a} + \epsilon\frac{\partial}{\partial a_1} + \epsilon^2\frac{\partial}{\partial a_2})\beta(\phi) \qquad \Delta\sigma = -(\frac{\partial}{\partial t} + \epsilon\frac{\partial}{\partial t_1})\beta(\phi) \qquad (II.6.6a-b)$$

Consider first Δk to which only the a_2-derivative contributes. We deduce from the chain rule of differentiation

$$\Delta k = \epsilon^2 \frac{\partial \phi}{\partial a_2} \frac{\partial \beta}{\partial \phi} = \alpha \epsilon^2 K G(\phi) \qquad (II.6.7)$$

where use is made of $\phi = \Omega t_1 - K a_2$. The normalized change in the wavenumber is of $\mathcal{O}(\epsilon^3)$ and therefore is too small to be included here. Note that this result in consistent with the known property of the Stokes waves in the absence of long waves. Next, we turn to $(II.6.6b)$ and evaluate the t_1-derivative by using the chain rule of differentiation

$$\Delta \sigma = -\epsilon \frac{\partial \phi}{\partial t_1} \frac{\partial \beta}{\partial \phi} = \epsilon \alpha \Omega G(\phi) + \mathcal{O}(\epsilon^3) \qquad (II.6.8)$$

The relative change in frequency is thus

$$\frac{\Delta \sigma}{\sigma} = \epsilon \alpha \frac{\Omega}{\sigma} G(\phi) = \frac{1}{2} \epsilon^2 (k\overline{A})^2 G(\phi) + \mathcal{O}(\epsilon^3) \qquad (II.6.9)$$

provided use is made of the definition $(II.4.57)$ of α. Again, if the long wave is infinitely long, we have $G(\phi) = 1$ and the classical second order frequency shift is recovered

$$\frac{\Delta \sigma}{\sigma} = \frac{1}{2} \epsilon^2 (k\overline{A})^2 + \mathcal{O}(\epsilon^3) \qquad (II.6.10)$$

We need not plot the variations of $\frac{\Delta \sigma}{\sigma}$ with ϕ since they merely correspond to the square of these plotted in figure 6.1. for the uniform wave amplitude. In summary, the uniform Stokes wave solution of $(II.6.1a-b)$ is characterized by $(II.6.4a-b)$ and $(II.6.5a-b)$. We may now investigate its linear instability.

6.2. Linearized Instability of a Uniform Wave Train

We first let

$$\mathcal{A}(\xi, \phi) = \mathcal{A}_s(\phi) \tilde{\mathcal{A}}(\xi, \phi) \qquad (II.6.11)$$

and substitute it in $(II.6.1a)$ to deduce the governing equation for $\tilde{\mathcal{A}}$:

$$\frac{\partial \tilde{\mathcal{A}}}{\partial \phi} = -\frac{i\alpha}{4} \frac{\partial^2 \tilde{\mathcal{A}}}{\partial \xi^2} - i\alpha G(\phi) |\tilde{\mathcal{A}}|^2 \tilde{\mathcal{A}} \qquad (II.6.12)$$

Next, we introduce the amplitude d and phase $\int^{\xi} W d\xi$ of $\tilde{\mathcal{A}}$

$$\tilde{\mathcal{A}} = de^{i\int^{\xi} W d\xi} \qquad (II.6.13)$$

where both $d(\xi,\phi)$ and $W(\xi,\phi)$ are real. Substitution of $(II.6.13)$ into $(II.6.12)$ yields two governing equations:

$$\frac{\partial d}{\partial \phi} = \frac{\alpha}{4}\Big[\frac{\partial (dW)}{\partial \xi} + W\frac{\partial d}{\partial \xi}\Big] \qquad (II.6.14a)$$

and

$$\frac{\partial W}{\partial \phi} = -\alpha\frac{\partial}{\partial \xi}\left\{\frac{1}{4}\Big[\frac{1}{d}\frac{\partial^2 d}{\partial \xi^2} - W^2\Big] + G(\phi)d^2\right\} \qquad (II.6.14b)$$

In view of $(II.6.11)$, the uniform Stokes wave solution derived in §II.6 has amplitude $d_0 = 1$ and phase $W_0 = 0$. We then allow for small perturbations around this solution:

$$d = 1 + d' \qquad W = W' \qquad (II.6.15a-b)$$

Upon substituting $(II.6.15a-b)$ into $(II.6.14a-b)$, and ignoring the nonlinear terms in the perturbations, we obtain

$$\frac{\partial d'}{\partial \phi} = \frac{\alpha}{4}\frac{\partial W'}{\partial \xi} \qquad (II.6.16a)$$

and

$$\frac{\partial W'}{\partial \phi} = -\alpha\frac{\partial}{\partial \xi}\left\{\frac{1}{4}\frac{\partial^2 d'}{\partial \xi^2} + G(\phi)(1+2d')\right\} \qquad (II.6.16b)$$

Consider spatially sinusoidal disturbances

$$d' = \tilde{d}e^{i\nu\xi} \qquad W' = \tilde{W}e^{i\nu\xi} \qquad (II.6.17a-b)$$

where $\nu = \mathcal{O}(1)$ designates the disturbance wavenumber. Eqs. $(II.6.16a-b)$ then become

$$\frac{\partial \tilde{d}}{\partial \phi} = i\frac{\alpha\nu}{4}\tilde{W} \qquad (II.6.18a)$$

and

$$\frac{\partial \tilde{W}}{\partial \phi} = -2i\alpha\nu\Big[G(\phi) - \frac{\nu^2}{8}\Big]\tilde{d} \qquad (II.6.18b)$$

Furthermore $(II.6.18a-b)$ can be combined to give a Hill equation

$$\frac{\partial^2 \tilde{d}}{\partial \phi^2} + \frac{1}{2}\alpha^2\nu^2\Big[\frac{\nu^2}{8} - G(\phi)\Big]\tilde{d} = 0 \qquad (II.6.19)$$

since $G(\phi)$ is a periodic function of ϕ. Eq. $(II.6.19)$ reduces to a Mathieu equation in the limit of small KB and will be used to shed some light on the general stability analysis based on $(II.6.18a-b)$.

6.3. Results of Instability Analysis

The stability of a Stokes wave to a sideband disturbance depends on 4 parameters: (i) the wavenumber ν of the sideband disturbance, (ii) the long wave slope KB, (iii) the short wave slope ϵkA and (iv) the ratio of long to short wave frequencies $\epsilon\frac{\Omega}{\sigma}$.

It is clear that the parameter space is quite large, thus precluding an exhaustive analysis of the entire 4-dimension space. For the sake of simplicity, we shall analyse the changes occuring as only one parameter is varied at a time.

It is convenient to define the Floquet exponents λ_1 and λ_2 as

$$\lambda_j = \frac{\ln \mu_j}{T} \qquad j = 1,2 \tag{$II.6.20$}$$

where μ_1 and μ_2 are the two Floquet multipliers defined in Appendix G and $T = 2\pi$. With the definition of μ, we may express $\tilde{d}$ one period later as

$$\tilde{d}(\phi + T) = \mu\tilde{d}(\phi) = e^{\lambda T}\tilde{d}(\phi) \tag{$II.6.21$}$$

Thus a non-autonomous T-periodic system sampled at intervals of T bears some resemblance to an autonomous system with exponential time dependence λ (this is one of the reasons to introduce the Floquet exponent). For our non-autonomous system, the stability of the disturbance depends on the sign of $\Re(\lambda)$. Alternately, if one introduces the moduli and phases of μ_1 and μ_2:

$$\mu_j = \rho_j e^{i\eta_j} \qquad j = 1,2 \tag{$II.6.22$}$$

the stability then depends on the sign of $\rho_j - 1$. The two Floquet multipliers are shown in Appendix G to satisfy the following simple relationship:

$$\mu_1\mu_2 = 1 \tag{$II.6.23$}$$

i.e. if $(II.6.22)$ is used

$$\rho_1\rho_2 = 1 \qquad \eta_1 + \eta_2 = 0\ [2\pi] \tag{$II.6.24$}$$

Since both ρ_1 and ρ_2 are positive, only two scenarios may arise:

Neutral stability:

When $\rho_1 = \rho_2 = 1$, the growth rate *i.e.* the real part of the Floquet exponents ($II.6.20$) reduces to zero. Consequently, if $(\tilde{d}, \tilde{W})^T$is parallel to the first eigenvector, $\tilde{d}(\phi + T)$ differs from $\tilde{d}(\phi)$ only by a phase factor equal to $e^{i\eta_1}$. Moreover, in the complex plane, the family of points $\left\{\tilde{d}(\phi + nT)\right\}_{n=1,\ldots}$ is located on a circle C of radius $|\tilde{d}(\phi)|$. Two situations arise depending on the commensurability of the ratio $\frac{\eta_1}{2\pi}$. If $\frac{\eta_1}{2\pi}$ is a rational number $\frac{p}{q}$ then there are only q points on C visited by the iterates of $\left\{\tilde{d}(\phi+nT)\right\}_{n=1,\ldots}$ as seen in figure 6.2a. However, if $\frac{\eta_1}{2\pi}$ is irrational, any point on the circle C will eventually be visited by the iterates of $\left\{\tilde{d}(\phi+nT)\right\}_{n=1,\ldots}$ as seen in figure 6.2b.

Instability:

When $\rho_1 \neq 1$, assuming $\rho_1 > 1$, the growth rate $\Re(\lambda_1) = \frac{\ln\rho_1}{T}$ is strictly positive, causing $\tilde{d}(\phi+T)$ to be greater than $\tilde{d}(\phi)$, and $\tilde{d}(\phi+2T)$ to be greater than $\tilde{d}(\phi+T)$ and so on, this leads to instability, cf. figure 6.2c.

6.3.1. *Influence of the disturbance wavenumber ν*

Let us fix the following parameters $KB = 0.3$, $\epsilon k\overline{A} = 0.13$ and $\alpha = 0.125$ (this implies $\epsilon\frac{\Omega}{\sigma} = 0.07$). We analyse the influence of the wavenumber ν on the stability of the disturbance. In order not to stray far from the narrow banded assumption, the values of ν must remain $\mathcal{O}(1)$. Solution for μ_1 and μ_2 are sought when ν varies from 0 to 5. We have plotted in figure 6.3a the locus of μ_1 in the complex plane as ν changes. We also present in figure 6.3b the variations of the real and imaginary parts of $\ln\mu_1$. Similar plots are given for μ_2 in figures 6.3c-d.

When $\nu = 0$, $\mu_1 = 1$ and is identified by p_0 in the complex μ plane. increasing ν, μ_1 leaves the unit circle *i.e.* $\ln\rho_1 \neq 0$ and the disturbance becomes unstable. When ν reaches 1.65, μ_1 corresponds to the most unstable disturbance (point p_1 in figures 6.3a-b). A further increase of ν brings μ_1 to neutral stability (point p_2) for $\nu \simeq 2.3$. If ν is further increased, μ_1 bifurcates to the unit circle, its argument η_1 then varies from 0 at p_2 to π at p_3 where μ_1 undergoes a second bifurcation at $\nu \simeq 3.8$. For ν past the above bifurcation value, $\eta_1 = \pi$ and $\ln\rho_1$ becomes negative

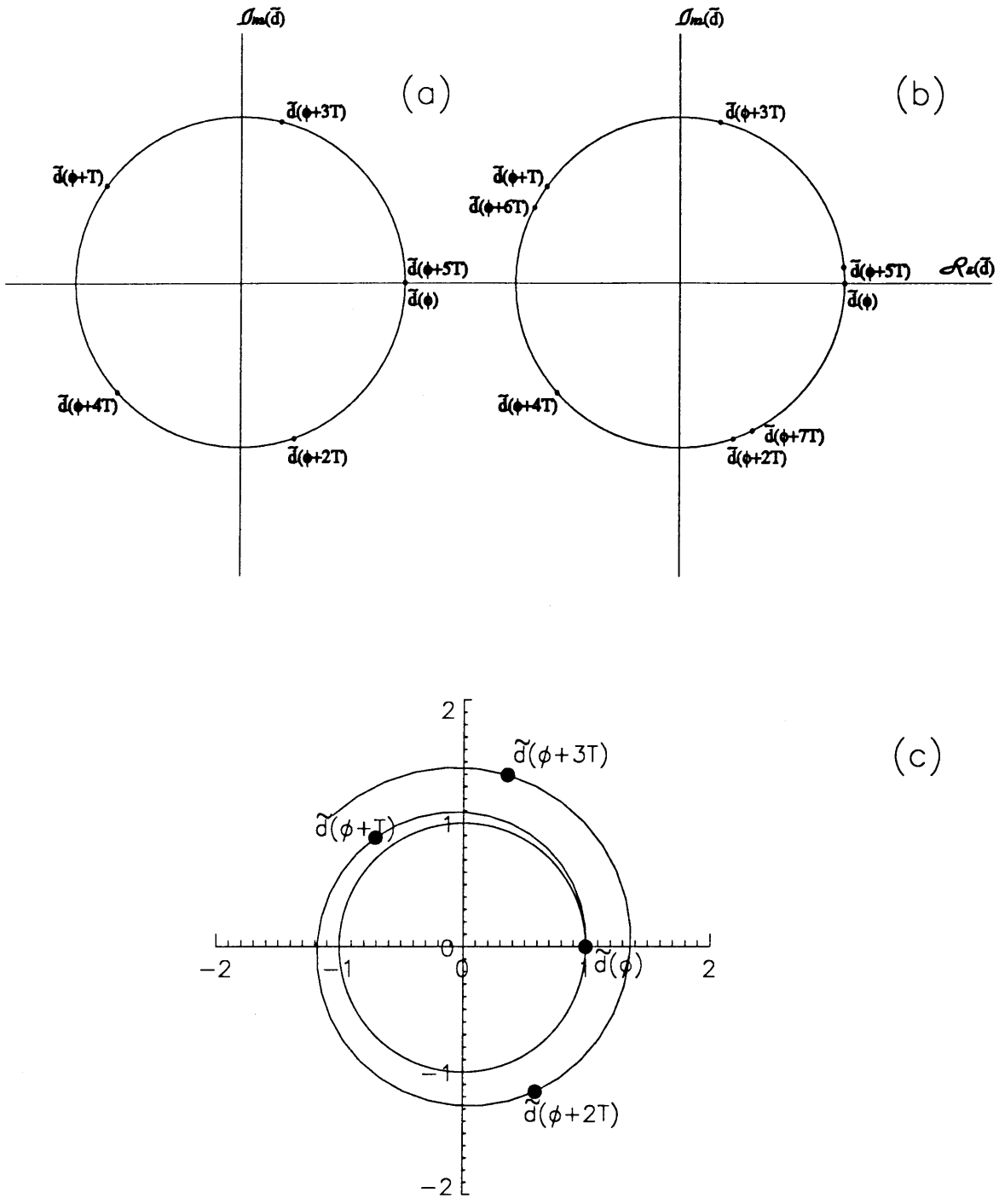

Figure II.6.2: Floquet multipliers and Poincaré map iterates, (a) Neutral stability: phase locking, (b) Neutral stability: quasiperiodicity, (c) Instability.

i.e. $\ln \rho_2 > 0$ (cf. figures 6.3b and 6.3d). The disturbance is therefore unstable. It is most unstable at p_4 and neutrally stable at p_5 for $\nu \simeq 4.25$. We conclude from this example that the transition from neutral instability to instability and vice versa occurs only on the real axis in the complex μ-plane and at $\mu = \pm 1$.

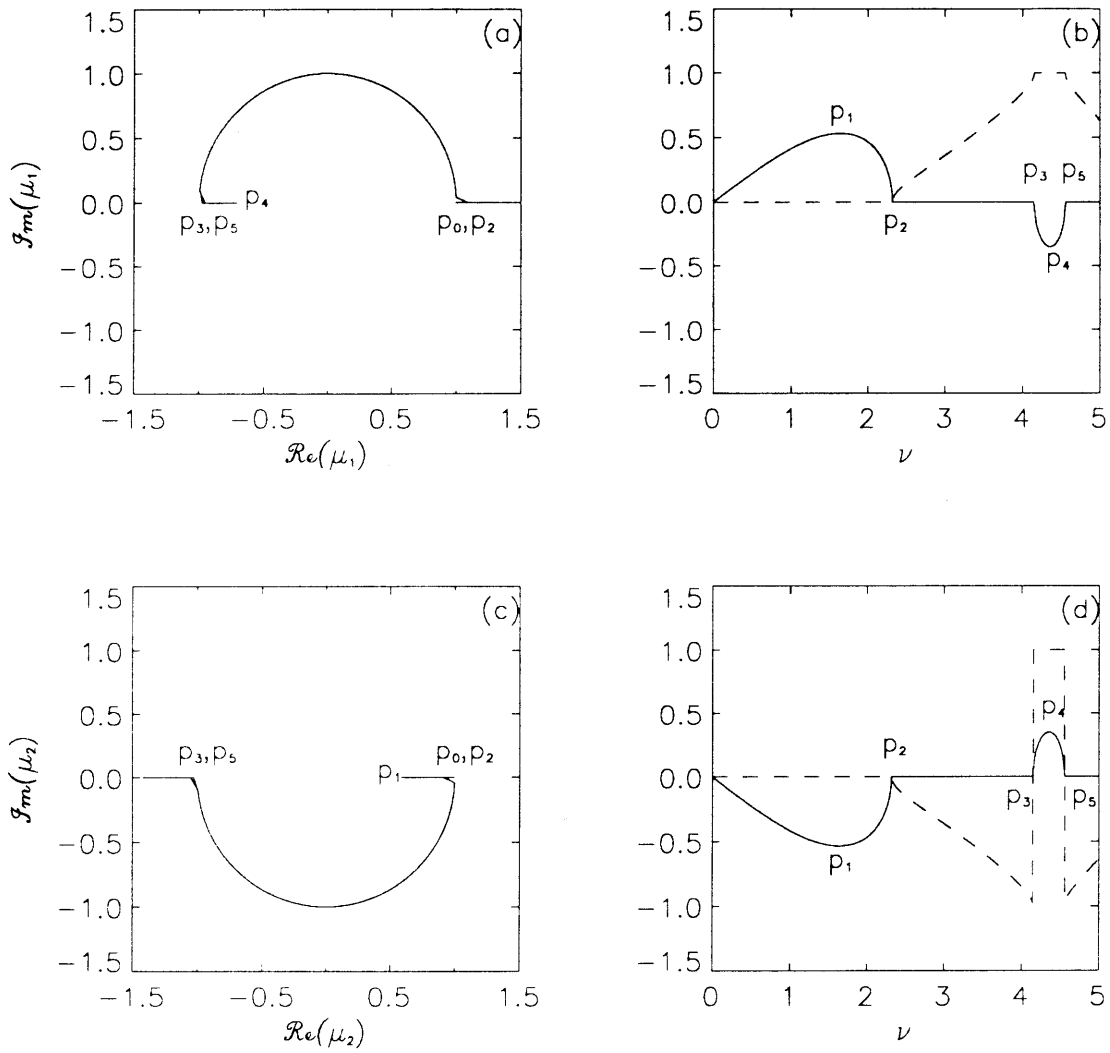

Figure II.6.3: Floquet multipliers, (a) locus of μ_1 in the complex μ plane, (b) $\ln(\rho_1)$ (——) and $\frac{\eta_1}{2\pi}$ (- - -), (c) locus of μ_2 in the complex μ plane, (d) $\ln(\rho_2)$ (——) and $\frac{\eta_2}{2\pi}$ (- - -).

In the following analysis, the growth rate defined by

$$g_r = \mathrm{Max}(\ln \rho_1, \ln \rho_2) \qquad (II.6.25)$$

will be plotted against $\nu \in [0, 6]$ and the parameter of interest.

6.3.2. *Influence of the long wave slope KB*

We fix the parameters $\epsilon k\overline{A} = 0.13$, $\alpha = 0.125$ (*i.e.* $\epsilon\frac{\Omega}{\sigma} = 0.07$) and compute the growth rate for long wave slopes $KB \in [0, 0.5]$. The results are shown in figure 6.4a. Accurate estimates of the width of each instability lobe may be read from figure 6.4b, where the the contour $g_r = 0^+$ is plotted in the (ν, KB) plane.

For large values of KB, the growth rate first decreases and then levels off. The bandwidth defined as the smallest non-zero stable disturbance, decreases with KB and increases again when $KB > 0.4$. Note the presence of two additional bands of instability whose peak position is not affected significantly by KB but whose width increases monotonically with KB.

6.3.3. *Influence of α*

The two parameters $\epsilon k\overline{A}$ and $\epsilon\frac{\Omega}{\sigma}$ appear in $(II.6.18a - b)$ through α as defined by $(II.4.57)$. It is therefore convenient to investigate the influence of α instead. To this end, the growth rates are evaluated for $KB = 0.3$ and $\epsilon k\overline{A} = 0.13$ when $\alpha \in [0.05, 0.15]$ †. The results are plotted in figures 6.5a-b. The bandwidth of the first lobe is only slightly affected by changes in α. Note however, that with increasing α, the number of secondary instability bands increases and their positions are shifted towards smaller values of ν. As a result, it becomes more likely that higher (2nd or 3rd ...) harmonics of an unstable disturbance may also be unstable and that higher harmonics of a stable disturbance may be unstable.

† Since $\epsilon k\overline{A} = 0.13$, the corresponding range for $\epsilon\frac{\Omega}{\sigma}$ is $[0.058, 0.186]$ with the upper bound corresponding to $\alpha = 0.05$.

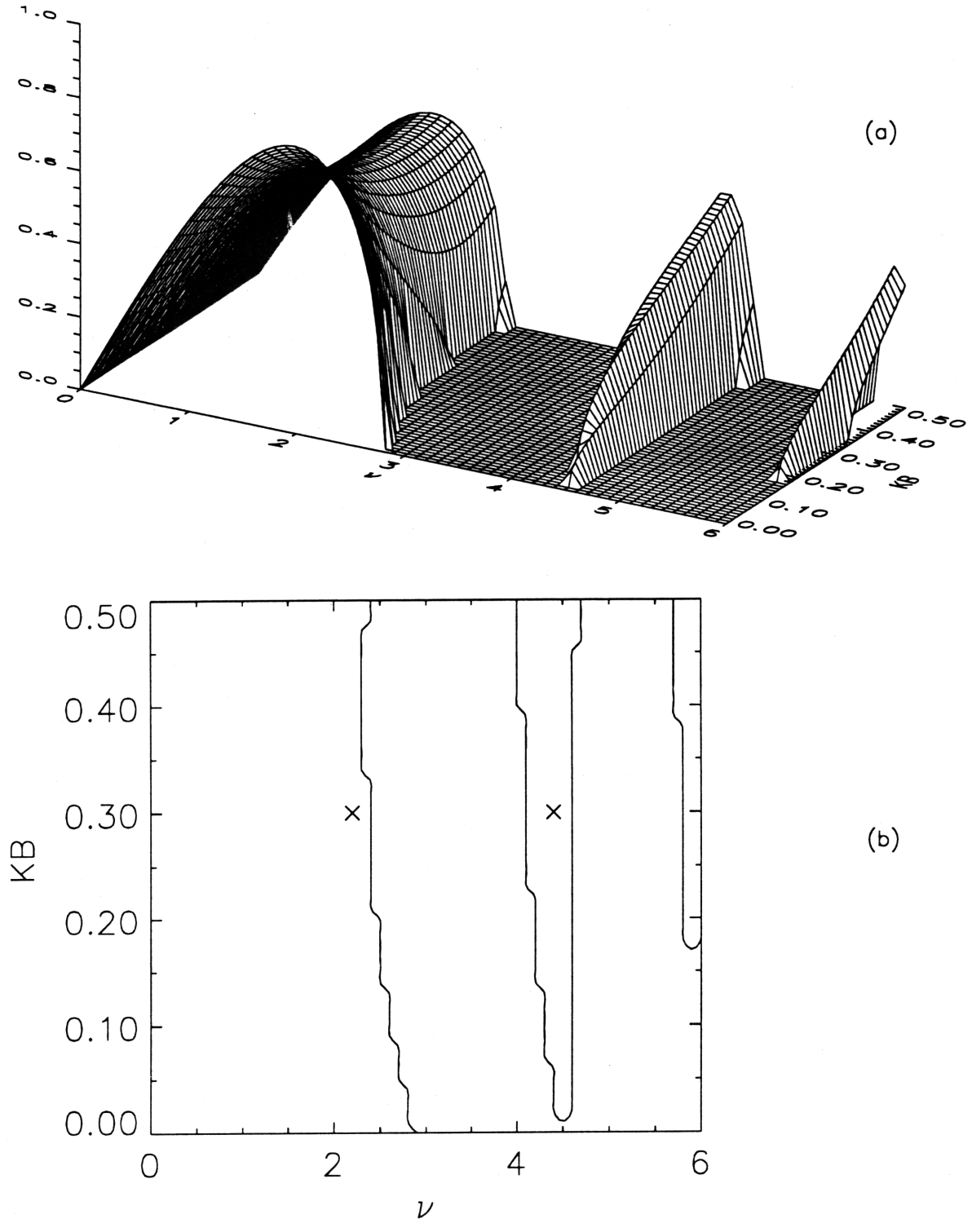

Figure II.6.4: Growth rate as a function of ν and KB, with $\epsilon k\overline{A} = 0.13$ and $\alpha = 0.125$. (a) Three dimensional view, (b) Stability boundaries, ($\times$) symbol refers to $\nu = 2.2$ and its second harmonic $2\nu = 4.4$.

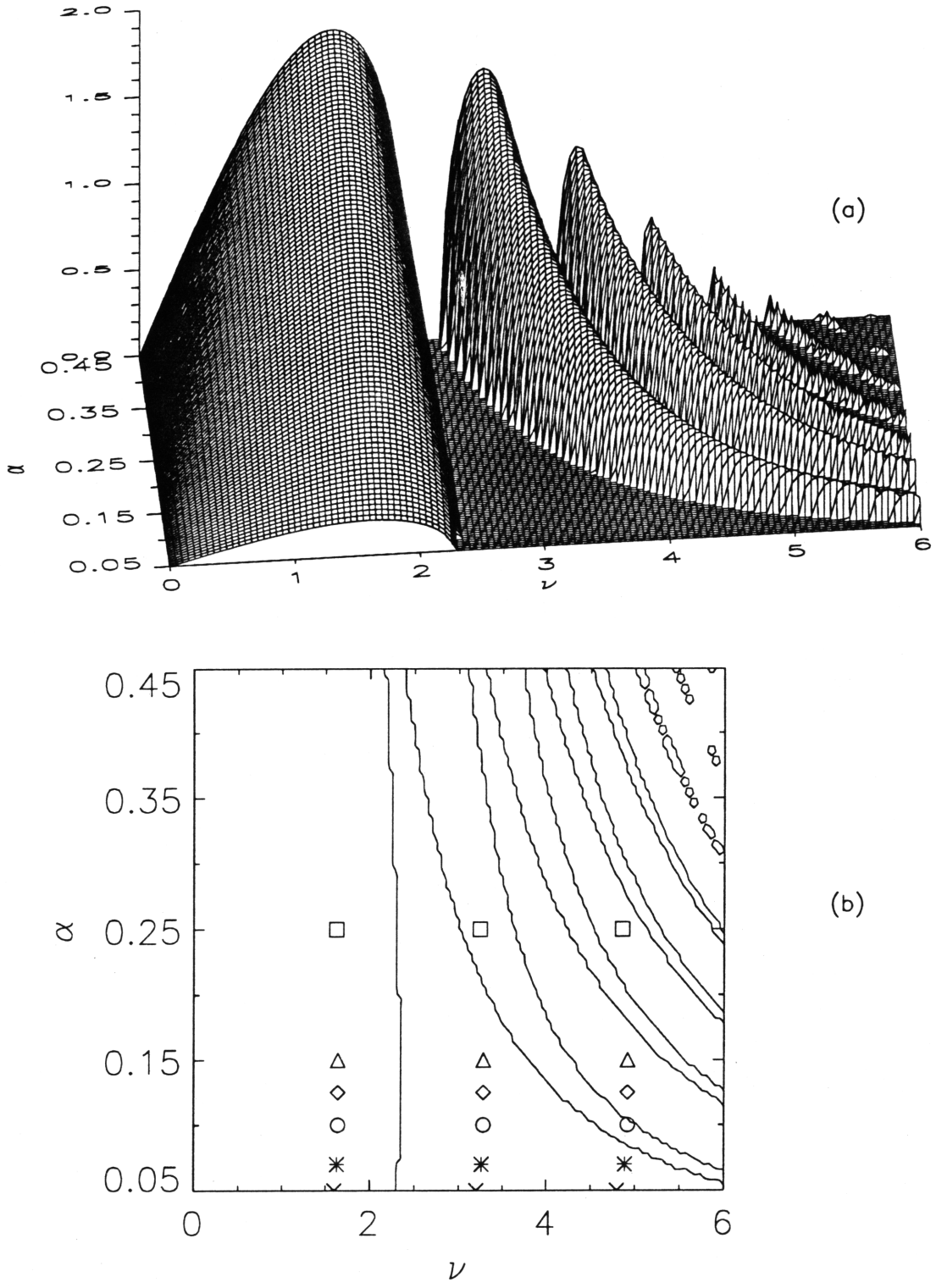

Figure II.6.5: Growth rate as a function of ν and α, with $KB = 0.3$ and $\epsilon k\overline{A} = 0.13$. (a) Three dimensional view, (b) Stability boundaries, symbols refer, for a given α, to the most unstable disturbance and its second and third harmonics.

6.4. Limiting Case of a Milder Long Wave

The long wave slope is assumed to be $KB = \mathcal{O}(\epsilon^{\frac{1}{2}})$. In this case, new insights can be gained about the secondary instability bands observed earlier if $G(\phi)$ is expanded as

$$G(\phi) = 1 - 2KB + 4KB\cos\phi + \mathcal{O}(\epsilon, K^2B^2) \qquad (II.6.26)$$

Substitution of $(II.6.26)$ in $(II.6.19)$ yields the Mathieu equation

$$\tilde{d}_{\phi\phi} + (\Upsilon + \Delta\cos\phi)\tilde{d} = 0 \qquad (II.6.27)$$

where Υ and Δ are two functions of ν, KB and α:

$$\Upsilon(\nu, KB, \alpha) = \frac{1}{2}\alpha^2\nu^2\left[\frac{\nu^2}{8} + 2KB - 1\right] \qquad \Delta(\nu, KB, \alpha) = -2\alpha^2\nu^2 KB$$
$$(II.6.28a - b)$$

The well known stability diagram of Strutt(1928) in the (Υ, Δ) plane can be used as a check of our calculations. For instance, when the long waves are absent, $KB = \Delta = 0$ and $(II.6.27)$ admits harmonic - thus stable - solutions when $\nu^2 > 8$ *i.e.* when $\nu > 2\sqrt{2}$. This is just the classical result of Benjamin and Feir(1967).

For non-zero values of KB and α, $(II.6.28a - b)$ define parametrically a curve $\mathcal{C}$ in the (Υ, Δ) plane which is superimposed on the Strutt diagram. In order to relate the instability observed in the (Υ, Δ) plane to the disturbance wavenumber ν, we also plot ν against Υ according to $(II.6.28a)$.

We have plotted in figures 6.6a-b, $\mathcal{C}$ for $\alpha = 0.125$ and two values of the long wave slope $KB = 0.1$ and $KB = 0.2$. For both values of KB, $\mathcal{C}$ crosses three instability regions in the Strutt diagram. The first region corresponds to the main instability lobe of Benjamin & Feir(1967); upon extending a vertical line down from the intersection of either discontinuous lines with the left-most solid line, the bandwidth is obtained. The next intersection of $\mathcal{C}$ with an instability region happens for ν in the vicinity of 4.5. The third and last intersection occurs near $\nu = 6$.

Increasing the value of KB causes $\mathcal{C}$ to depart further from the Υ-axis, and thus to intercept a larger instability zone in the (Υ, Δ) plane. Consequently, the range of unstable ν's is also increased in agreement with figure 6.4a-b. Similarly, upon increasing α, $\mathcal{C}$ will span a longer Υ interval, therefore intersecting more instability zones. This confirms the results shown in figure 6.5a-b.

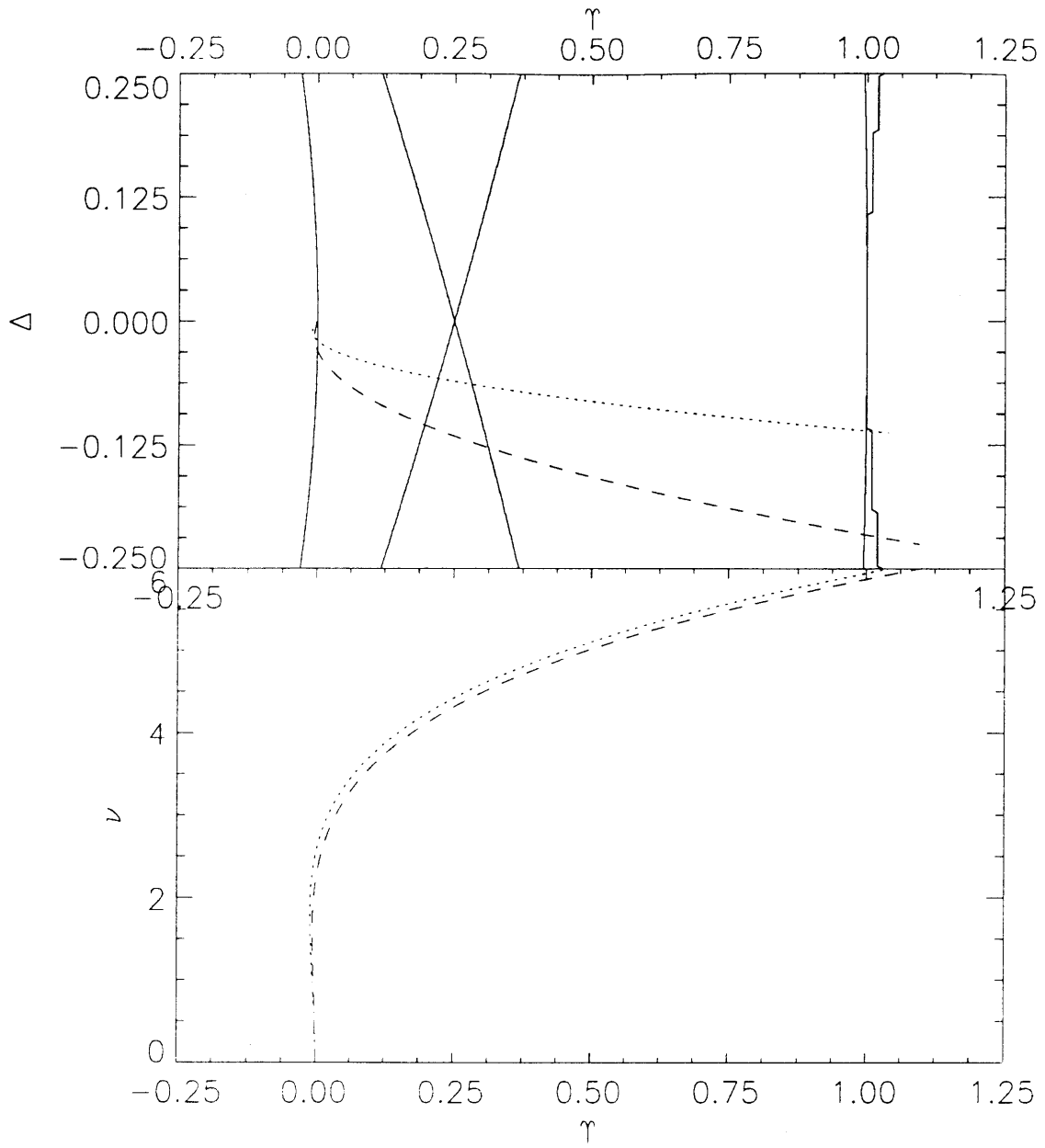

Figure II.6.6: Linearized stability and Strutt diagram. (Top) Strutt stability boundaries (——), C with $KB = 0.1$ (·····), with $KB = 0.2$ (– – –), with $\nu \in [0, 6]$ and $\alpha = 0.125$; (Bottom) Disturbance wavenumber ν vs. Υ, with the same conventions.

Upon further reducing the order of magnitude of the long wave slope to $KB = \mathcal{O}(\epsilon)$, expansion of $G(\phi)$ now reduces to

$$G(\phi) = 1 + \mathcal{O}(\epsilon, KB) \qquad (II.6.29)$$

and the stability diagram reduces to that of Benjamin and Feir's. This agrees

with the conclusions reached in Chapter I where the long waves are assumed to be infinitesimal.

6.5. Concluding remarks

We have demonstrated that a short Stokes wave propagating on a steep Gerstner wave may also be unstable to sideband disturbances. We have however shown that, unlike the situation in the absence of long waves, there exists several lobes of instability. This allows FPU recurrence described by Yuen & Ferguson(1978) to occur not only when a disturbance and some of its harmonics all belong to the main instability lobe but also, as described above, when higher harmonics of a disturbance fall on secondary instability lobes.

J. Zhang and W.K. Melville(private communication, 1991) have reported similar results when studying the linearized instability of a steady short wave on a finite amplitude irrotational long wave. In particular, they too observe, as α is increased, that the number of secondary instability lobes increases as these lobes are shifted towards the main instability lobe.

It is worth pointing out that, with the excitation of unstable high harmonics, thermalization may occur to invalidate the narrow band assumption. These issues will be addressed in §II.7 when integrating the partial differential equation (*II*.6.12) and in §II.8 when analysing a simpler model of that equation.

7. NONLINEAR STABILITY OF SIDEBANDS: A NUMERICAL SOLUTION OF THE EVOLUTION EQUATION

The linear stability of a short Stokes wave to sideband disturbances has been investigated in §II.6 using Floquet theory. The fully nonlinear evolution of these unstable sidebands is now pursued by solving the partial differential equation ($II.6.12$). In this context, the implications of the existence of additional bands of instability are analysed.

The split-step Fourier method used by Tappert(1974) and Lo & Mei (1985) is adopted here. The numerical scheme and the results are described respectively in §II.7.2 and §II.7.3.

7.1. Numerical Scheme

7.1.1. *The initial data*

The Stokes wave and its sidebands can be expressed at the initial stage by :

$$\tilde{A}(\xi, \phi = 0) = 1 + d' + i \int^{\xi} W' d\xi + \mathcal{O}(d'^2, d'W', W'^2) \qquad (II.7.1)$$

(cf ($II.6.13$) and ($II.6.15a-b$)). For spacially sinusoidal disturbance ($II.6.17a-b$), it becomes

$$\begin{aligned} \tilde{A}(\xi, \phi = 0) &\approx 1 + \frac{1}{2}(\tilde{d}e^{i\nu\xi} + *) + \frac{i}{2}\int(\tilde{W}e^{i\nu\xi} + *)d\xi \\ &= 1 + \frac{1}{2}\tilde{d}\left[1 + \frac{\tilde{W}}{\nu\tilde{d}}\right]e^{i\nu\xi} + \frac{1}{2}\tilde{d}^*\left[1 + \frac{\tilde{W}^*}{\nu\tilde{d}^*}\right]e^{-i\nu\xi} \end{aligned} \qquad (II.7.2)$$

We have shown, according to Floquet theory, that an unstable disturbance (with wavenumber ν) is characterized by two real Floquet multipliers which are the inverse of each other. Let μ_1 be the one satisfying $|\mu_1| > 1$, and $U^{(1)}$ the corresponding eigenvector. Then, the growth is likely to be greatest when $(\tilde{d}, \tilde{W})$ is proportional to $U^{(1)}$. By definition, $U^{(1)}$ is solution of a homogeneous system with coefficient matrix $N - \mu_1 I$ (cf. Appendix D for the definition of $N = (n_{ij})$). As a result

$$\frac{\tilde{W}^{(1)}}{\tilde{d}^{(1)}} = -\frac{n_{1,1} - \mu_1}{n_{1,2}} \qquad (II.7.3)$$

It is easy to prove that $n_{1,1}$ is real while $n_{1,2}$ is purely imaginary. Consequently, the above ratio is also purely imaginary and the two square brackets in ($II.7.2$) are

identical. Eq. $(II.7.2)$ may be rewritten as

$$\tilde{A}(\xi, \phi = 0) = 1 + \frac{1}{2}\tilde{d}^{(1)}\left[1 + \frac{\tilde{W}^{(1)}}{\nu \tilde{d}^{(1)}}\right]\left(e^{i\nu\xi} + e^{-i\nu\xi}\right) \qquad (II.7.4)$$

where $\tilde{d}^{(1)}$ is chosen to be real.

The initial data therefore consists of the superposition of a uniform Stokes wave with unit amplitude and two symmetric sideband disturbances

$$\tilde{A}(\phi = 0, \xi) = 1 + \epsilon_1 e^{i\theta_1} \cos \nu\xi \qquad (II.7.5)$$

where ϵ_1 and θ_1 are respectively the sideband disturbance initial amplitude and phase. Since the disturbances are initially small, we have chosen $\epsilon_1 = 0.1$ in all computations. It is clear that θ_1 corresponds to the phase of the quantity within square brackets in $(II.7.4)$. For a given disturbance wavenumber ν, θ_1^u is defined as the value of that phase after one long wave period *i.e.* at $\phi = 2\pi$. In the following nonlinear computations, the initial phase of the sideband disturbance is initially θ_1^u.

7.1.2. *Discrete Fourier transform*

The following rescaling is introduced

$$\tilde{\xi} = \nu\xi \qquad (II.7.6)$$

Eq. $(II.6.11b)$ then becomes

$$\frac{\partial \tilde{A}}{\partial \phi} = -\frac{i\alpha\nu^2}{4}\frac{\partial^2 \tilde{A}}{\partial \tilde{\xi}^2} - i\alpha G(\phi)|\tilde{A}|^2\tilde{A} \qquad (II.7.7)$$

$\tilde{A}$ is now periodic with period 2π. We may then consider its restriction to interval $[-\pi, \pi]$, and discretize this interval in N (a power of 2) grid points:

$$\tilde{\xi}_{-\frac{N}{2}} = -\pi, \ldots, \tilde{\xi}_0 = 0, \ldots, \tilde{\xi}_{\frac{N}{2}-1} = \pi - h \qquad (II.7.8a)$$

where the grid size h is defined by

$$h = \frac{2\pi}{N} \qquad (II.7.8b)$$

The discrete Fourier transform, $\tilde{\mathcal{B}}$, of $\tilde{\mathcal{A}}$ may be defined as

$$\tilde{\mathcal{B}}_m = \left\{\mathcal{F}(\tilde{\mathcal{A}})\right\}_m = h \sum_{j=-\frac{N}{2}}^{\frac{N}{2}-1} e^{-imjh} \tilde{\mathcal{A}}_j \qquad (II.7.9a)$$

where the wavenumber m takes the following values

$$m = -\frac{N}{2}, \ldots, 0, \ldots, \frac{N}{2} - 1 \qquad (II.7.9b)$$

and

$$\tilde{\mathcal{A}}_j = \tilde{\mathcal{A}}(\tilde{\xi}_j) \qquad j = -\frac{N}{2}, \ldots, 0, \ldots, \frac{N}{2} - 1 \qquad (II.7.9c)$$

Once the Fourier amplitudes $\left\{\tilde{\mathcal{B}}_m\right\}_{m=-\frac{N}{2},\frac{N}{2}-1}$ are computed, we may recover $\tilde{\mathcal{A}}_j$ by inverse discrete Fourier transform:

$$\tilde{\mathcal{A}}_j = \left\{\mathcal{F}^{-1}(\tilde{\mathcal{B}})\right\}_j = \frac{1}{2\pi} \sum_{m=-\frac{N}{2}}^{\frac{N}{2}-1} e^{imjh} \tilde{\mathcal{B}}_m \qquad (II.7.10)$$

Let $\Delta\phi$ be the time step and

$$\tilde{\mathcal{A}}^n \equiv \tilde{\mathcal{A}}(\phi = n\Delta\phi) \quad \tilde{\mathcal{B}}^n \equiv \tilde{\mathcal{B}}(\phi = n\Delta\phi) \quad G^n \equiv G(\phi = n\Delta\phi) \qquad (II.7.11)$$

7.1.3. *The split-step numerical scheme*

In accordance with the split-step method, we integrate the linear term in the right hand side of $(II.6.12)$ exactly in the Fourier domain, and the nonlinear term numerically with the modified Euler scheme (2^{nd} order Runge-Kutta). We thus take advantage of the accurate evaluation of the spatial derivative associated with Fourier methods without having to evaluate convolution integrals for nonlinear terms.

Consider the nonlinear part of $(II.7.7)$

$$\frac{\partial \tilde{\mathcal{A}}}{\partial \phi} = -i\alpha G(\phi) |\tilde{\mathcal{A}}|^2 \tilde{\mathcal{A}} \qquad (II.7.12a)$$

A predictor step estimates the solution half a time step ahead:

$$\bar{\tilde{\mathcal{A}}}^{n+\frac{1}{2}} = \tilde{\mathcal{A}}^n - \frac{i}{2} \Delta\phi \alpha G^n |\tilde{\mathcal{A}}^n|^2 \tilde{\mathcal{A}}^n \qquad (II.7.12b)$$

A corrector step then yields the solution of $(II.7.12a)$ at $n+1$:

$$\bar{\tilde{\mathcal{A}}}^{n+1} = \tilde{\mathcal{A}}^n - i\Delta\phi\alpha G^{n+\frac{1}{2}} |\bar{\tilde{\mathcal{A}}}^{n+\frac{1}{2}}|^2 \bar{\tilde{\mathcal{A}}}^{n+\frac{1}{2}} \qquad (II.7.12c)$$

Next, we turn to the linear part of $(II.7.7)$:

$$\frac{\partial \tilde{\mathcal{A}}}{\partial \phi} = -\frac{i\alpha\nu^2}{4} \frac{\partial^2 \tilde{\mathcal{A}}}{\partial \tilde{\xi}^2} \qquad (II.7.13a)$$

The Fourier transform, $\tilde{\mathcal{B}}_m$, of $\tilde{\mathcal{A}}$ can be solved exactly as

$$\tilde{\mathcal{B}}_m(\phi) = \tilde{\mathcal{B}}_m(0) \exp\left(i\frac{\alpha}{4}\nu^2 m^2 \phi\right) \qquad (II.7.13b)$$

The estimate of $\tilde{\mathcal{A}}$ at $n+1$ is then obtained from $(II.7.13b)$ and the Fourier transform of the estimate, $\bar{\tilde{\mathcal{A}}}$, of the solution of the nonlinear problem at time $n+1$, *i.e.*

$$\tilde{\mathcal{A}}^{n+1} = \mathcal{F}^{-1}\left\{ \mathcal{F}(\bar{\tilde{\mathcal{A}}}^{n+1})_m \exp\left(i\frac{\alpha}{4}\Delta\phi\nu^2 m^2\right) \right\} \qquad (II.7.13c)$$

In the next step the linear term is integrated first and the nonlinear term second. This procedure ensures a second-order accurate scheme stable for adequate choices of $\Delta\phi$ once N is chosen. The accuracy of the computations has been checked by monitoring the changes in the total energy $\mathcal{E}$:

$$\mathcal{E} = h \sum_{j=-\frac{N}{2}}^{\frac{N}{2}-1} |\tilde{\mathcal{A}}_j|^2 \qquad (II.7.14)$$

which was found to deviate from its initial value by no more than 1.0e-5. The Fourier spectrum $\tilde{\mathcal{B}}_m$ at the last time step is also checked against aliasing errors.

7.2. Discussion of Results

Computations have been performed to investigate the importance of the disturbance wavenumber ν, α and KB in the nonlinear evolution. The evolution of the amplitude $\tilde{\mathcal{A}}$ of the short wave is computed for 50 long wave periods, *i.e.* for $\phi \leq 100\pi$. All calculations were performed using a 64 Fourier mode decomposition. We present for each run, the time evolution of the normalized Fourier spectrum † $|\mathcal{F}(\tilde{\mathcal{A}})|$ and the time evolution of the amplitude $|\tilde{\mathcal{A}}|$.

† The Fourier components are all normalized by the value of the Stokes wave component at the initial time. Note also that only positive wavenumbers need to be plotted, since both the initial data and the order of differentiation in $(II.7.7)$ are even.

7.2.1 *Influence of the sideband disturbance wavenumber* ν

We investigate to what extent the presence of secondary lobes may modify the Fermi-Pasta-Ulam recurrence ‡. Consider first the following parameters $KB = 0.3$, $\epsilon k\overline{A} = 0.13$ and $\alpha = 0.125$ (*i.e.* $\epsilon\frac{\Omega}{\sigma} \simeq 0.07$). The resulting Floquet stability diagram can be viewed as a section of figure 6.4a. In particular, if the sideband disturbance has a wavenumber $\nu = 2.2$, its second harmonic falls in the second instability band (cf. figure 6.4b). Furthermore, the growth rate of $2\nu = 4.4$ is greater than that of $\nu = 2.2$. Assuming the phase of the sideband disturbance to be θ_1^u initially, how are these facts reflected in the fully nonlinear equations?

We show in figure 7.1a the evolution of the Fourier spectrum. At first, the sideband disturbance grows to about one fourth of the original uniform Stokes wave amplitude after approximately 8 long wave periods, then, the amplitude of this disturbance recedes while its second harmonic increases to almost half of the original uniform Stokes wave amplitude. The time evolution of amplitude $|\tilde{A}|$ in figure 7.1b clearly shows the alternating predominance of the sideband disturbance and its second harmonic. Thus, the secondary instability lobes may participate in the nonlinear interactions and yield an FPU recurrence.

7.2.2. *Influence of* α

Calculations have been performed for $\alpha = 0.05$, 0.07, 0.1, 0.125, 0.15 and 0.25. In each case, we consider the most unstable disturbance with $\theta_1(0) = \theta_1^u$ both deduced from Floquet theory. The remaining parameters are $KB = 0.3$, $\epsilon k\overline{A} = 0.13$ and $\epsilon\frac{\Omega}{\sigma}$ is deduced from $(II.4.57)$ for each value of α. To illustrate the stability of higher harmonics (2^{nd}, 3^{rd} etc ...) of the disturbance, for a given α, we have identified these harmonics in the (ν, α) plane in figure 6.6b.

For $\alpha = 0.05$ (*i.e.* $\epsilon\frac{\Omega}{\sigma} = 0.186$), figure 7.2a shows a classic Fermi-Pasta-Ulam recurrence. The amplitude in figure 7.2b is alternately dominated by the Stokes

‡ The FPU recurrence refers to the periodic exchange of energy between a Stokes wave propagating on a calm sea and its disturbance, leading to the almost exact reconstruction of the initial data after every recurrence period.

wave and its sideband disturbance in accordance with the time evolution of the Fourier amplitudes.

For $\alpha = 0.07$ ($i.e.$ $\epsilon\frac{\Omega}{\sigma} = 0.130$), an almost periodic recurrence behavior is observed in figure 7.3a. Note that the period is now shortened. The amplitude evolves almost periodically and displays oscillations due to the growth of higher harmonic components in the Fourier spectrum.

For $\alpha = 0.1$ ($i.e.$ $\epsilon\frac{\Omega}{\sigma} = 0.084$), the third and fourth harmonics of the disturbance are also unstable and take an active role in the nonlinear interactions, as seen in figure 7.4a. As a result, the amplitude evolution in figure 7.4b is now more complex.

When α is increased to 0.125 ($i.e.$ $\epsilon\frac{\Omega}{\sigma} = 0.07$), the envelope evolution in figure 7.5b becomes very irregular, reflecting the increasing role played by higher spatial harmonics. Note however, that the amplitudes of these harmonics remain small compared to the amplitude of the zeroth mode. The narrow band assumption is not seriously violated.

For $\alpha = 0.15$, energy is exchanged chaotically, but now more evenly among the low harmonics, within a somewhat broader band (see figures 7.6a-b).

Finally, when $\alpha = 0.25$ ($i.e.$ $\epsilon\frac{\Omega}{\sigma} = 0.034$) which is somewhat outside the realm of validity of our theory, the amplitude evolution appears chaotic. Indeed, the amplitude at a fixed location ξ is an irregular function of ϕ as seen in figure 7.7b. Figure 7.7a shows that the carrier wave amplitude (zeroth harmonic) no longer dominates and that the Fourier spectrum becomes broad-banded.

7.2.3. *Influence of the long wave slope KB*

All previous computations were performed with the large value $KB = 0.3$. It is worthwhile to investigate whether the trends identified earlier are still relevant when the slope KB is decreased to 0.2 and then 0.1. The remaining parameters are $\epsilon k\overline{A} = 0.13$, $\epsilon\frac{\Omega}{\sigma} = 0.058$, ($i.e.$ $\alpha = 0.15$).

For $KB = 0.2$, the amplitude of the Stokes wave ($m = 0$ in figure 7.8a) and that of the disturbance ($m = 1$) remain large for all times, though higher harmonics

are still significant. The evolution of $|\tilde{\mathcal{A}}|$ in figure 7.8b is less disordered as a result.

As KB is further decreased to 0.1, the first two modes oscillate in phase almost periodically, while all harmonics, except the third, remain small. The evolution of the amplitude is now more regular (see figure 7.9b).

7.3. Conclusions

We have first confirmed that the presence of secondary instability bands may give rise to Fermi-Pasta-Ulam recurrence patterns whereby an unstable disturbance and one of its unstable harmonics exchange energy periodically. Since an increasing number of instability bands appear at the lower range of wavenumbers ν when α increases (see figures 6.5a-b), a cascade of unstable harmonics may arise to the point where the initial energy is no longer contained in a narrow band of modulational wavenumbers. The narrow band assumption is then jeopardized. Except for $\alpha = 0.25$, this assumption has not been violated in our computations.

When α is small, our computations have shown periodic or almost periodic evolution patterns reminiscent of the well known results in the absence of long waves. However, when α is increased, apparently chaotic evolutions are observed.

Finally, when the long wave slope is reduced to 0.2 and then to 0.1, the predominance of the the Stokes wave and its sideband disturbance is enhanced at the expense of higher harmonics. Oscillations between the $m = 0$ and $m = 1$ modes are now almost periodic thus bringing more regularity to the amplitude evolution. As expected, our theory therefore agrees well with the limiting case of infinitesimal irrotational long waves.

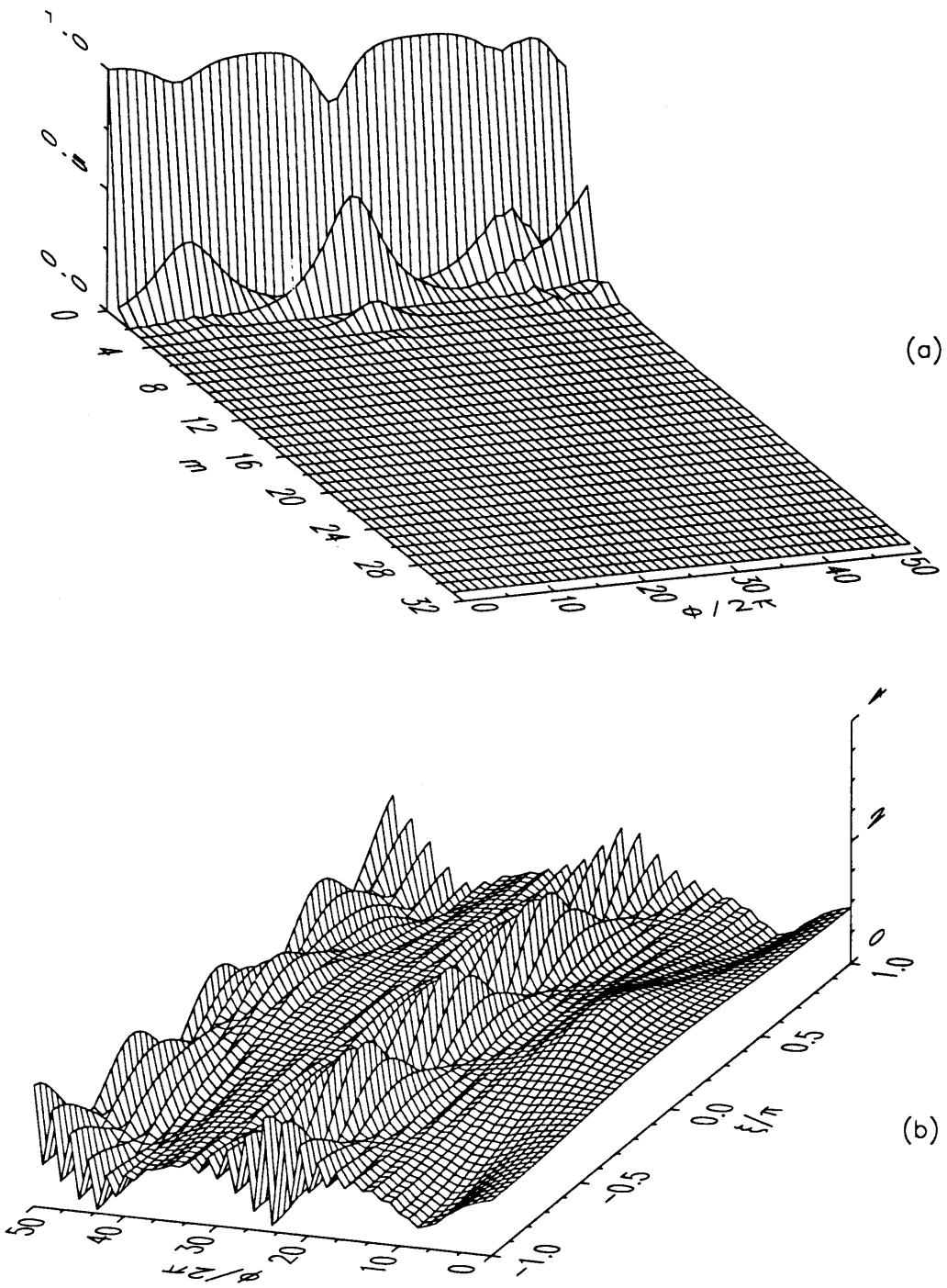

Figure II.7.1: Nonlinear evolution of short wave amplitudes in (a) the Fourier domain (b) the physical domain with $KB = 0.3$, $\epsilon k\bar{A} = 0.13$, $\alpha = 0.125$, $\nu = 2.2$ and $\theta_1(0) = -0.344$.

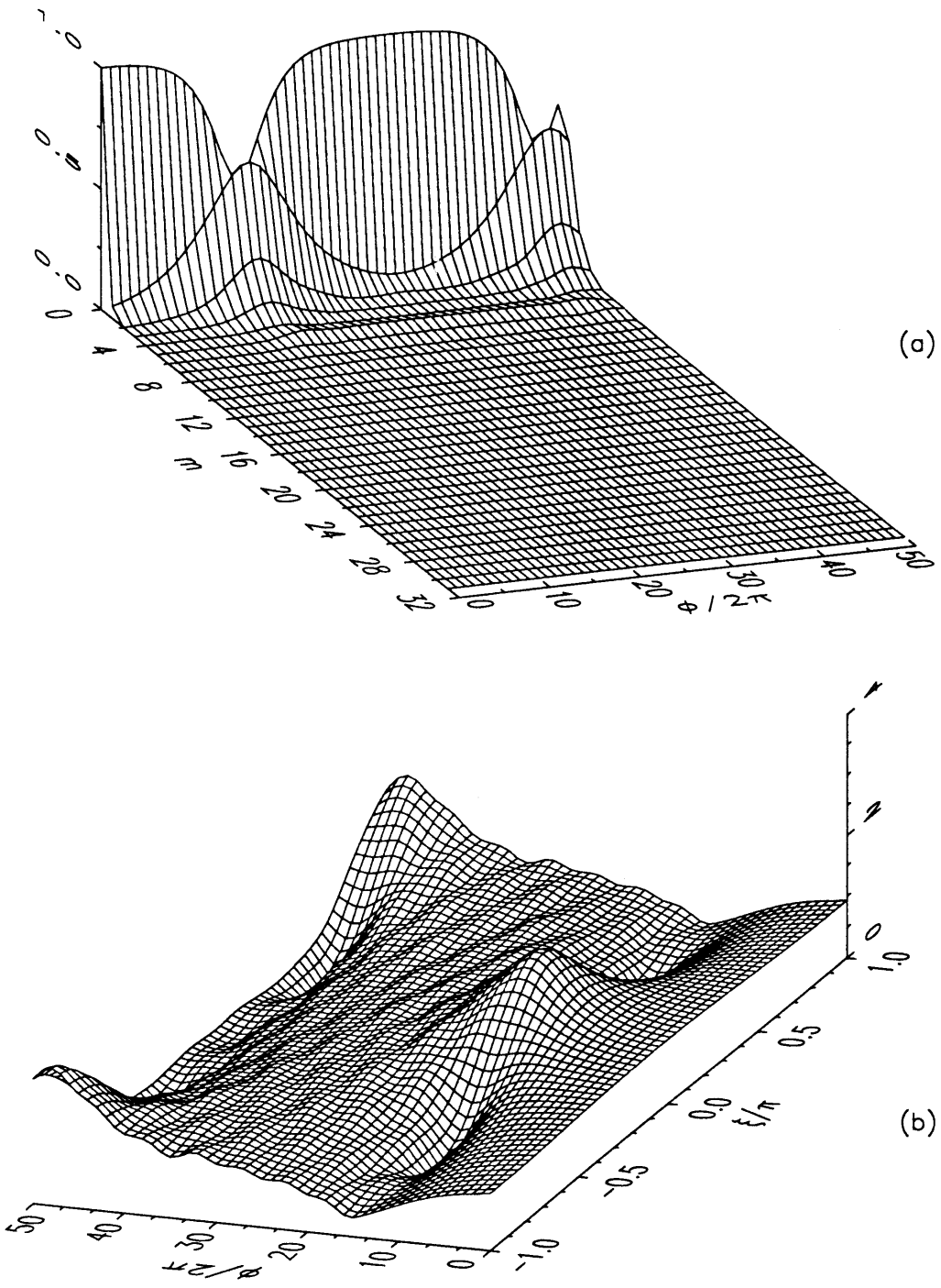

Figure II.7.2: Nonlinear evolution of short wave amplitudes in (a) the Fourier domain (b) the physical domain with $KB = 0.3$, $\epsilon k\bar{A} = 0.13$, $\alpha = 0.05$, $\nu = 1.60$ and $\theta_1(0) = -0.789$.

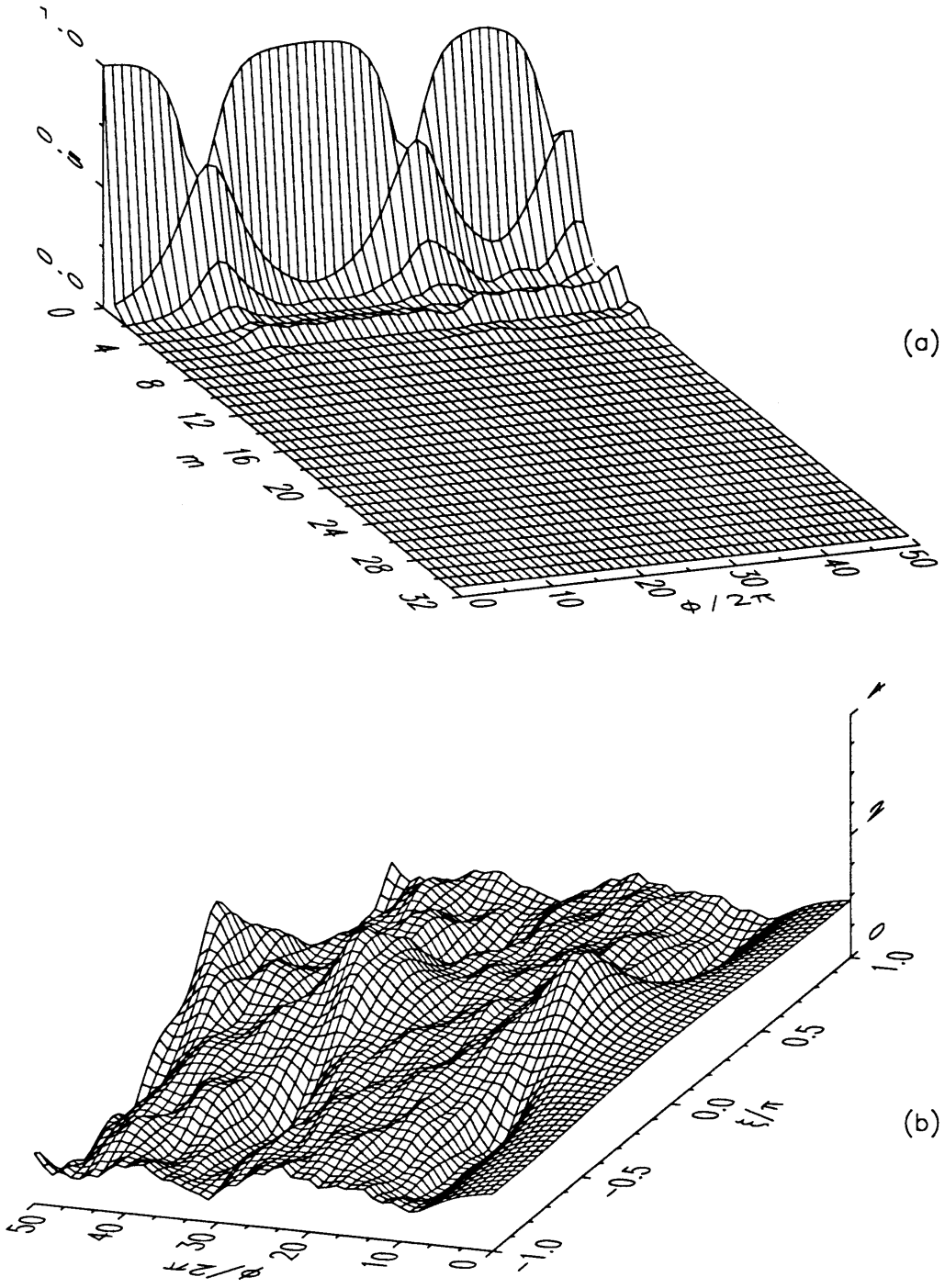

Figure II.7.3: Nonlinear evolution of short wave amplitudes in (a) the Fourier domain (b) the physical domain with $KB = 0.3$, $\epsilon k\bar{A} = 0.13$, $\alpha = 0.07$, $\nu = 1.63$ and $\theta_1(0) = -0.792$.

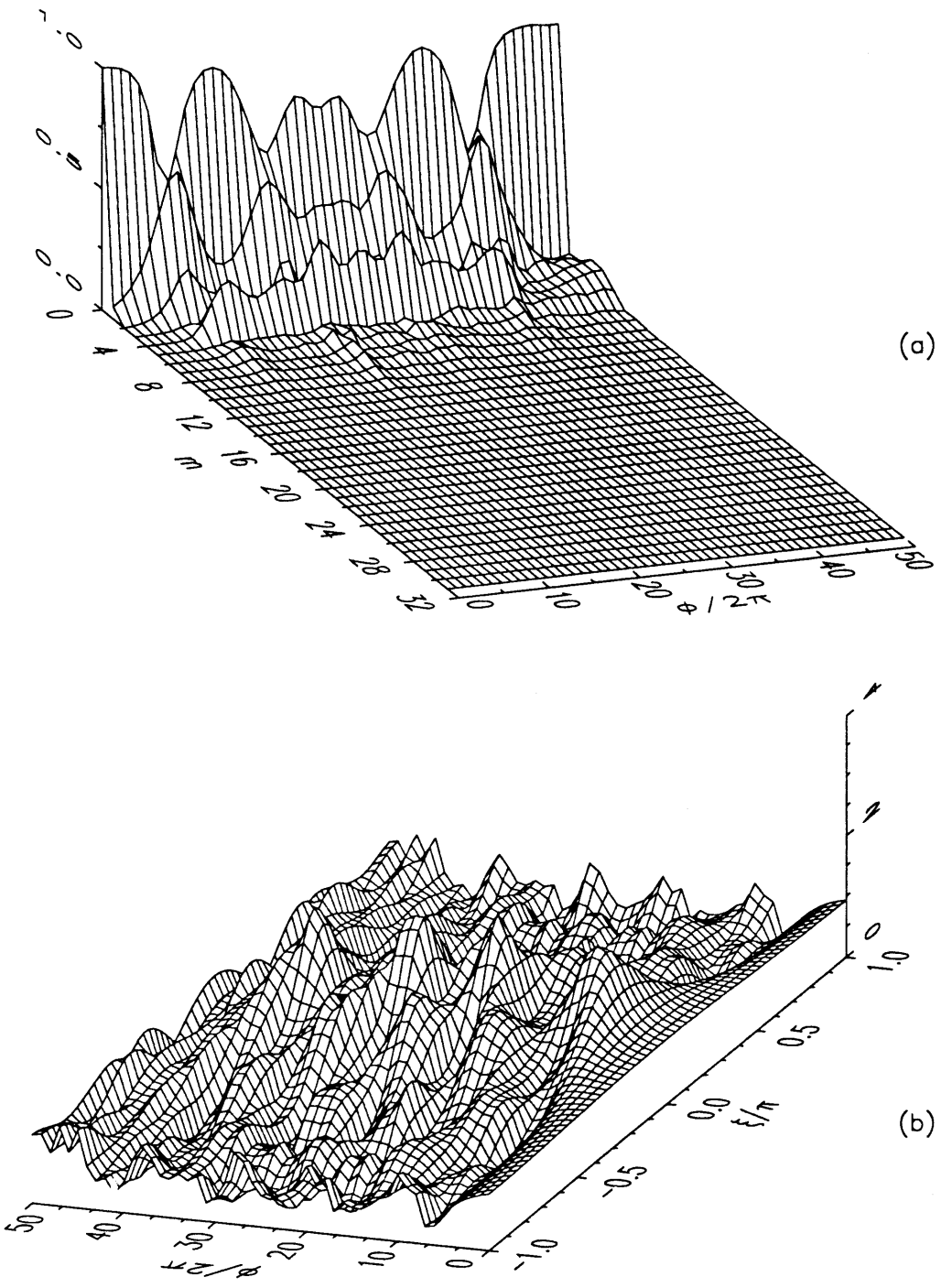

Figure II.7.4: Nonlinear evolution of short wave amplitudes in (a) the Fourier domain (b) the physical domain with $KB = 0.3$, $\epsilon k\bar{A} = 0.13$, $\alpha = 0.1$, $\nu = 1.64$ and $\theta_1(0) = -0.80$.

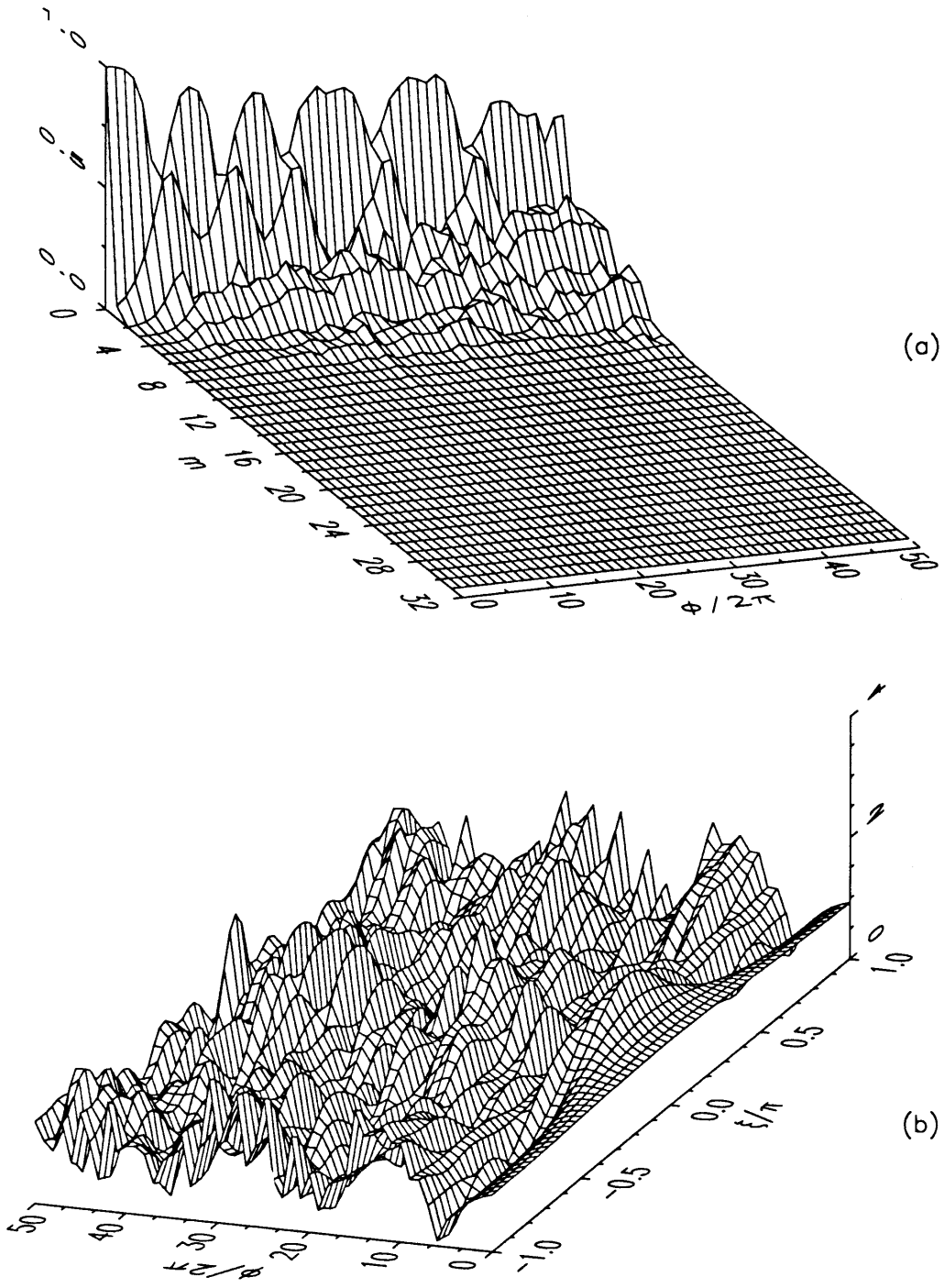

Figure II.7.5: Nonlinear evolution of short wave amplitudes in (a) the Fourier domain (b) the physical domain with $KB = 0.3$, $\epsilon k\bar{A} = 0.13$, $\alpha = 0.125$, $\nu = 1.64$ and $\theta_1(0) = -0.8089$.

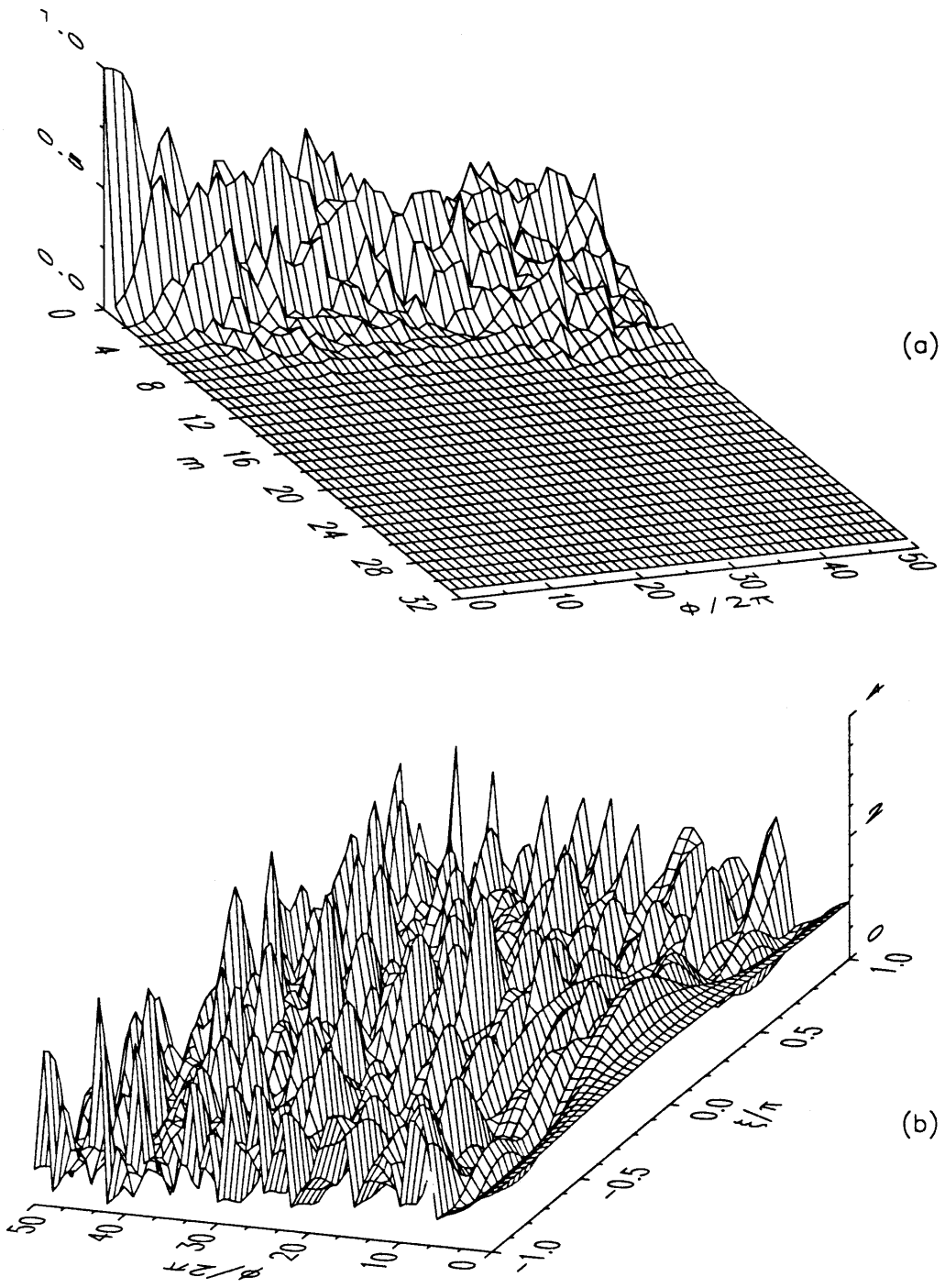

Figure II.7.6: Nonlinear evolution of short wave amplitudes in (a) the Fourier domain (b) the physical domain with $KB = 0.3$, $\epsilon k\bar{A} = 0.13$, $\alpha = 0.15$, $\nu = 1.64$ and $\theta_1(0) = -0.817$.

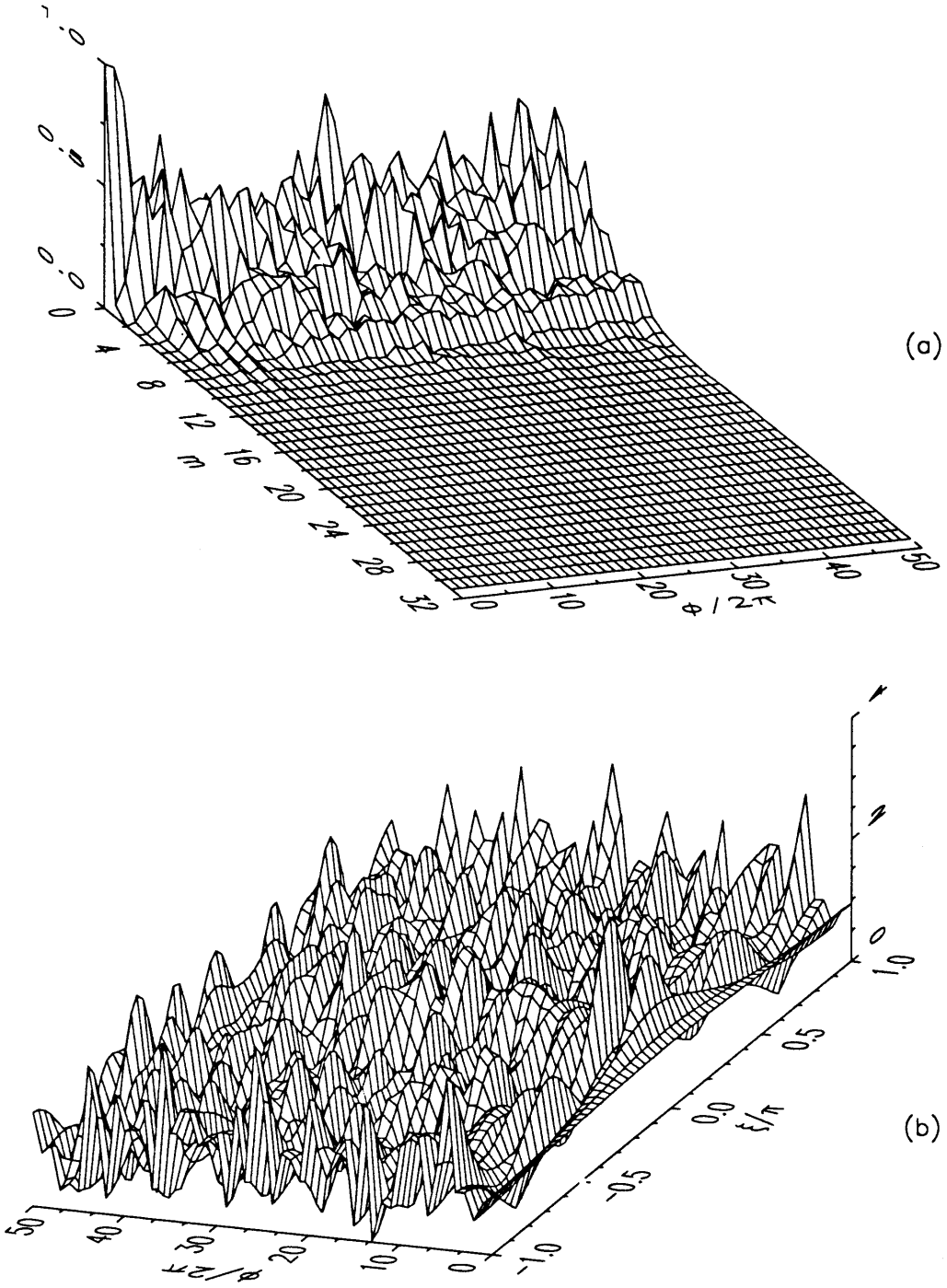

Figure II.7.7: Nonlinear evolution of short wave amplitudes in (a) the Fourier domain (b) the physical domain with $KB = 0.3$, $\epsilon k\bar{A} = 0.13$, $\alpha = 0.25$, $\nu = 1.62$ and $\theta_1(0) = -0.865$.

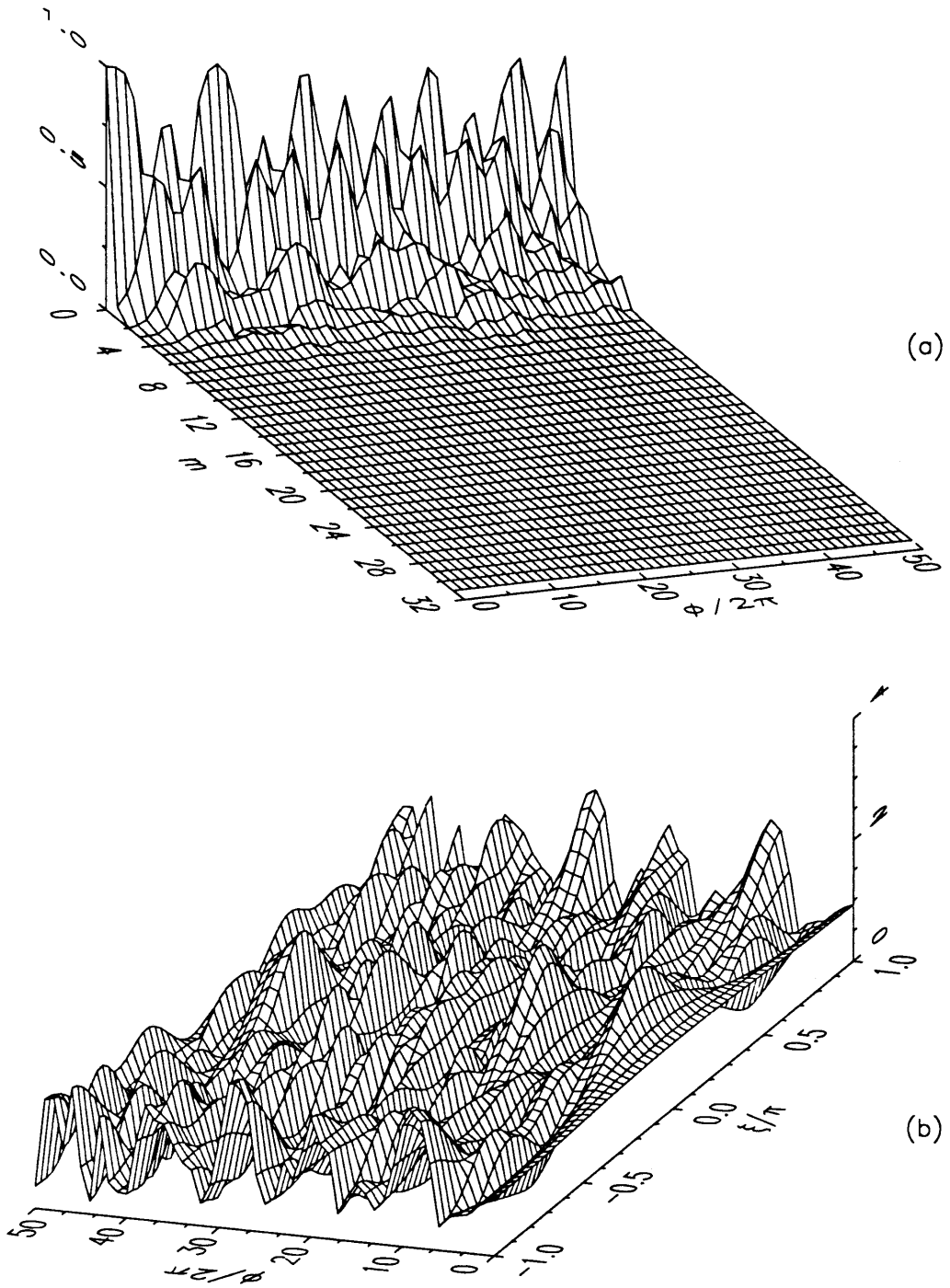

Figure II.7.8: Nonlinear evolution of short wave amplitudes in (a) the Fourier domain (b) the physical domain with $KB = 0.2$, $\epsilon k\bar{A} = 0.13$, $\alpha = 0.15$, $\nu = 1.70$ and $\theta_1(0) = -0.811$.

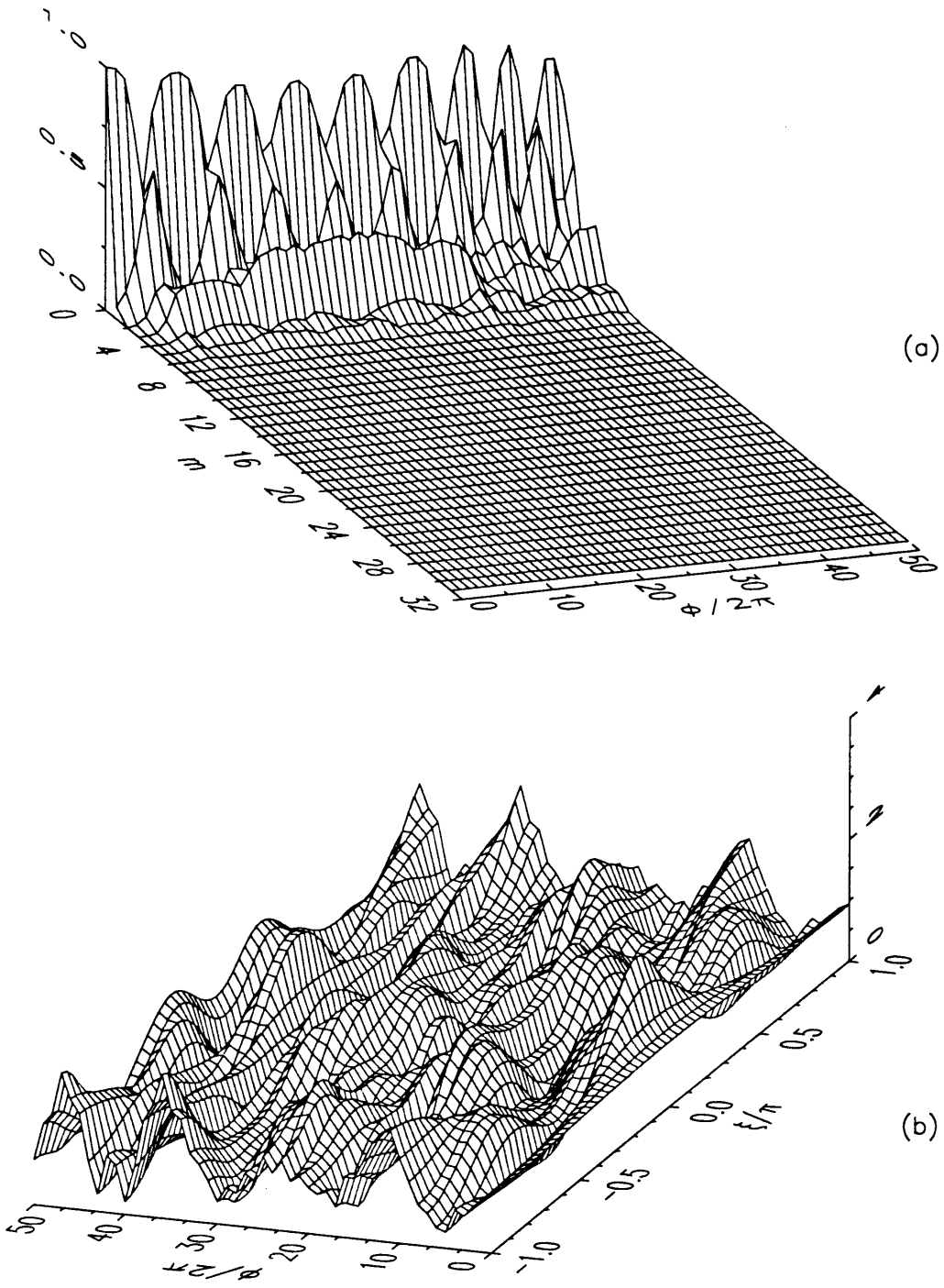

Figure II.7.9: Nonlinear evolution of short wave amplitudes in (a) the Fourier domain (b) the physical domain with $KB = 0.1$, $\epsilon k\bar{A} = 0.13$, $\alpha = 0.15$, $\nu = 1.80$ and $\theta_1(0) = -0.811$.

8. NONLINEAR STABILITY OF SIDEBANDS: A TWO-MODE APPROXIMATION

Calculations of the nonlinear evolution of a short Stokes wave and its sideband disturbance have emphasized the importance of secondary instability bands. If higher harmonics of an unstable disturbance are also unstable, the resulting nonlinear interactions become very complex. Apparently chaotic evolutions have been observed for moderate to relatively large values of α for which multiple instability bands are known to arise. It is therefore worthwhile to investigate whether the presence of these bands is essential to triggering chaotic behaviors.

To gain further insight, we examine a simpler (and thus cruder) version of the nonlinear Schrödinger equation by considering a truncated Fourier expansion for $\tilde{A}$ with two modes only, corresponding to the carrier wave and its symmetric sideband disturbances $e^{\pm i\nu\xi}$. Similar truncations have often been successfull in the past. As early as 1963, Lorentz analysed the Rayleigh-Bénard convection in the atmosphere by adopting a one-term eigenfunction expansion for the streamfunction and a two-term eigenfunction expansion for the temperature field. He then derived the well known Lorenz dynamical system. In shallow water theory, Mei & Ünlüata(1973) and Bryant(1973) have analysed the second harmonic generation by reducing the KdV equation to two differential equations coupling the first and second harmonics. The recurrence of the second harmonic is then predicted by the renowned solution of Armstrong *et al* (1962) in nonlinear optics, and agrees well with experiments. For deep water waves on an otherwise calm sea level, Infeld(1981) and Stiassnie & Kroszynski(1982) have reduced the classic constant coefficient nonlinear Schrödinger equation to two ordinary differential equations coupling the amplitudes of the Stokes wave and its sideband disturbance. The well known results of the full Schrödinger equations were then essentially recovered analytically. By following a similar approach we aim to see whether the calculated features of the full PDE can be seen through the truncated system.

Our investigations will be guided by the information gathered in §II.6 from the linearized stability analysis.

8.1. Derivation of a Lower Order System

From the analysis carried out in §II.7 for small times, we postulate a solution of $(II.6.12)$ in the form

$$\tilde{\mathcal{A}}(\xi,\phi) = \tilde{\mathcal{B}}_0(\phi) + \frac{1}{\sqrt{2}}\tilde{\mathcal{B}}_1(\phi)\big(e^{i\nu\xi} + e^{-i\nu\xi}\big) \qquad (II.8.1)$$

where $\tilde{\mathcal{B}}_{0,1}(\phi)$ are in effect two complex Fourier amplitudes satisfying respectively

$$\tilde{\mathcal{B}}_0(\phi = 0) = 1 \qquad (II.8.2a)$$

and

$$\frac{1}{\sqrt{2}}\tilde{\mathcal{B}}_1(\phi = 0) = \frac{1}{2}\tilde{d}^{(1)}\big[1 + \frac{\tilde{W}^{(1)}}{\nu\tilde{d}^{(1)}}\big] \qquad (II.8.2b)$$

The $\sqrt{2}$ factor in $(II.8.1)$ is introduced to make the total energy proportional to $|\tilde{\mathcal{B}}_0|^2 + |\tilde{\mathcal{B}}_1|^2$. The modulus of $\tilde{\mathcal{B}}_1(\phi = 0)$ is assigned a small value while its phase is chosen to be that of $1 + \frac{\tilde{W}^{(1)}}{\nu\tilde{d}^{(1)}}$. Expansion $(II.8.1)$ can be regarded as the two-mode truncation of the Fourier series

$$\tilde{\mathcal{A}}(\xi,\phi) = \tilde{\mathcal{B}}_0(\phi) + \frac{1}{\sqrt{2}}\sum_{m=-\infty}^{\infty}\tilde{\mathcal{B}}_m(\phi)e^{im\nu\xi} \qquad (II.8.3)$$

used in §II.7, in a slightly different form. By nonlinear self-interaction of the first harmonics $(\pm\nu)$, second and higher harmonics are, in principle, to be expected. Recall that our two-mode approximation is meaningful only if the second, third and higher harmonics are not unstable. This will be carefully monitored in our numerical examples.

We now substitute $(II.8.1)$ in $(II.6.12)$. In particular, the cubic term $|\tilde{\mathcal{A}}|^2\tilde{\mathcal{A}}$ yields

$$|\tilde{\mathcal{B}}_0|^2\tilde{\mathcal{B}}_0 + \tilde{\mathcal{B}}_0^*\tilde{\mathcal{B}}_1^2 + 2|\tilde{\mathcal{B}}_1|^2\tilde{\mathcal{B}}_0 +$$

$$+\frac{1}{\sqrt{2}}\big\{\tilde{\mathcal{B}}_1^*\tilde{\mathcal{B}}_0^2 + 2|\tilde{\mathcal{B}}_0|^2\tilde{\mathcal{B}}_1 + \frac{3}{2}|\tilde{\mathcal{B}}_1|^2\tilde{\mathcal{B}}_1\big\}\big\{e^{-i\nu\xi} + e^{i\nu\xi}\big\} + \text{higher harmonics} \qquad (II.8.4)$$

where the superscript "*" represents the complex conjugate. The contribution of the linear terms in $(II.6.12)$ is quite evident. In order to derive governing equations for the Fourier complex amplitudes $\tilde{\mathcal{B}}_j(\phi)$, we use the orthogonality of the Fourier modes. For $\tilde{\mathcal{B}}_0$, $(II.8.1)$ is integrated over the domain $\xi = [0, \frac{2\pi}{\nu}]$, to give

$$\frac{\partial\tilde{\mathcal{B}}_0}{\partial\phi} = -i\alpha G(\phi)\big\{|\tilde{\mathcal{B}}_0|^2\tilde{\mathcal{B}}_0 + \tilde{\mathcal{B}}_0^*\tilde{\mathcal{B}}_1^2 + 2|\tilde{\mathcal{B}}_1|^2\tilde{\mathcal{B}}_0\big\} \qquad (II.8.5a)$$

Similarly, for $\tilde{\mathcal{B}}_1$, we multiply the equation by $e^{-i\nu\xi}$ and integrate over the same domain. The result is

$$\frac{\partial\tilde{\mathcal{B}}_1}{\partial\phi} = \frac{i\alpha\nu^2}{4}\tilde{\mathcal{B}}_1 - i\alpha G(\phi)\{\tilde{\mathcal{B}}_1^*\tilde{\mathcal{B}}_0^2 + 2|\tilde{\mathcal{B}}_0|^2\tilde{\mathcal{B}}_1 + \frac{3}{2}|\tilde{\mathcal{B}}_1|^2\tilde{\mathcal{B}}_1\} \qquad (II.8.5b)$$

The action-angle variables are introduced

$$\tilde{\mathcal{B}}_0 = \sqrt{2I_0}e^{i\theta_0} \qquad \tilde{\mathcal{B}}_1 = \sqrt{2I_1}e^{i\theta_1} \qquad (II.8.6a-b)$$

Upon separating the real and imaginary parts of $(II.8.5a-b)$, we obtain the following 4-dimensional dynamical system:

$$\frac{dI_0}{d\phi} = 4\alpha G(\phi)I_0I_1\sin 2(\theta_1-\theta_0) \qquad (II.8.7a)$$

$$\frac{d\theta_0}{d\phi} = -\alpha G(\phi)\{2I_0 + 4I_1 + 2I_1\cos 2(\theta_1-\theta_0)\} \qquad (II.8.7b)$$

$$\frac{dI_1}{d\phi} = -4\alpha G(\phi)I_0I_1\sin 2(\theta_1-\theta_0) \qquad (II.8.7c)$$

$$\frac{d\theta_1}{d\phi} = \frac{\alpha\nu^2}{4} - \alpha G(\phi)\{4I_0 + 3I_1 + 2I_0\cos 2(\theta_1-\theta_0)\} \qquad (II.8.7d)$$

A Hamiltonian $\mathcal{H}$ may be derived such that

$$\frac{dI_0}{d\phi} = -\frac{\partial\mathcal{H}}{\partial\theta_0} \qquad \frac{d\theta_0}{d\phi} = \frac{\partial\mathcal{H}}{\partial I_0} \qquad \frac{dI_1}{d\phi} = -\frac{\partial\mathcal{H}}{\partial\theta_1} \qquad \frac{d\theta_1}{d\phi} = \frac{\partial\mathcal{H}}{\partial I_1} \qquad (II.8.8a-d)$$

where

$$\mathcal{H}(I_0,\theta_0,I_1,\theta_1,\phi) = \frac{\alpha\nu^2}{4}I_1 - \alpha G(\phi)\left\{I_0^2 + \frac{3}{2}I_1^2 + 4I_0I_1 + 2I_0I_1\cos 2(\theta_0-\theta_1)\right\} \qquad (II.8.9)$$

Since the angles $\theta_{0,1}$ appear only in the form of their difference, we introduce the following *contact transformation*

$$\psi_0 = \theta_0 - \theta_1 \qquad \psi_1 = \theta_0 + \theta_1 \qquad (II.8.10a-b)$$

and the corresponding *generating function* F

$$F = (\theta_0-\theta_1)J_0 + (\theta_0+\theta_1)J_1 \qquad (II.8.10c)$$

It follows that

$$I_0 = \frac{\partial F}{\partial \theta_0} = J_1 + J_0 \qquad I_1 = \frac{\partial F}{\partial \theta_1} = J_1 - J_0 \qquad (II.8.11a-b)$$

Since the generating function does not depend explicitly on time, we may simply replace in $(II.8.9)$ the old variables by the new ones

$$\mathcal{H}(J_0, \psi_0, J_1, \psi_1, \phi) = \frac{\alpha\nu^2}{4}(J_1 - J_0) +$$

$$+\alpha G(\phi)\left\{\frac{3}{2}J_0^2 + J_0 J_1 - \frac{13}{2}J_1^2 + 2(J_0^2 - J_1^2)\cos 2\psi_0\right\} \qquad (II.8.12)$$

Hamiltonian $\mathcal{H}$ is cyclic in ψ_1, *i.e.* is independent of ψ_1. Since the transformation is canonical, the rate of change of J_1 is simply

$$\frac{dJ_1}{d\phi} = -\frac{\partial \mathcal{H}}{\partial \psi_1} = 0 \qquad (II.8.13)$$

implying that the action variable J_1 is a constant of motion. From $(II.8.11a-b)$, we deduce

$$J_0 = \frac{1}{2}(I_0 - I_1) \qquad J_1 = \frac{1}{2}(I_0 + I_1) \;=\; \text{const} \qquad (II.8.14a-b)$$

The constancy of J_1 corresponds physically to the conservation of energy $I_0 + I_1$. This integral of motion in effect reduces the total number of degrees of freedom by two. We may write the new set of Hamilton's equations as

$$\frac{dJ_0}{d\phi} = \dot{J}_0 = -\frac{\partial \mathcal{H}}{\partial \psi_0} = 4\alpha G(\phi)(J_0^2 - J_1^2)\sin 2\psi_0 \qquad (II.8.15a)$$

$$\frac{d\psi_0}{d\phi} = \dot{\psi}_0 = \frac{\partial \mathcal{H}}{\partial J_0} = -\frac{\alpha\nu^2}{4} + \alpha G(\phi)\{3J_0 + J_1 + 4J_0\cos 2\psi_0\} \qquad (II.8.15b)$$

For a given set of parameters and two initial conditions, this non-autonomous set can be integrated numerically.

To verify whether $\mathcal{H}$ is also a constant of motion, we evaluate its rate of change

$$\frac{d\mathcal{H}}{d\phi} = \frac{\partial \mathcal{H}}{\partial J_0}\frac{\partial J_0}{\partial \phi} + \frac{\partial \mathcal{H}}{\partial \psi_0}\frac{\partial \psi_0}{\partial \phi} + \frac{\partial \mathcal{H}}{\partial \phi} \qquad (II.8.16)$$

If use is made of Hamilton's equations, the first two terms on the right hand side of $(II.8.16)$ cancel, so that

$$\frac{d\mathcal{H}}{d\phi} = \frac{\partial \mathcal{H}}{\partial \phi} = \alpha\frac{dG(\phi)}{d\phi}\left\{\frac{3}{2}J_0^2 + J_0 J_1 - \frac{13}{2}J_1^2 + 2(J_0^2 - J_1^2)\cos 2\psi_0\right\} \qquad (II.8.17)$$

Therefore, the Hamiltonian $\mathcal{H}$ is not an integral of motion.

Finally, the relative rate of change of a volume $\mathcal{V}$ in the phase space is

$$\frac{1}{\mathcal{V}}\frac{\partial \mathcal{V}}{\partial \dot{\phi}} = \frac{\partial \dot{J}_0}{\partial J_0} + \frac{\partial \dot{\psi}_0}{\partial \psi_0} \qquad (II.8.18)$$

Because of $(II.8.15a-b)$ the right hand side clearly vanishes, meaning that volumes are preserved in the phase space, as is expected for a Hamiltonian system.

8.2. Methods of Integration

To integrate the system of ordinary differential equations $(II.8.15a-b)$, we have taken advantage of the commercial package Dynamical Software. The integrator used is a variable step, variable order Adams-Bashforth scheme (Shampine & Gordon, 1975). The accuracy is monitored, as in most integration packages, by the local error committed at each step †. The tolerance, *i.e.* the largest local error allowed during the course of the integration, must be specified. This parameter has to be greater than the smallest non-zero real recognized by the machine which, for the PS/2 50Z/386 used in our computations, is of the order of 10^{-19}.

Chaotic dynamical systems are characterized by a very strong sensitivity to initial conditions, *i.e.* the trajectories derived from two slightly different initial conditions may diverge exponentially with time under adequate circumstances. The presence of truncation errors suggests that the integration of chaotic dynamical systems would be bound to fail. In this context, classical tests of convergence clearly cannot apply. Instead, a numerical trajectory will be accepted provided that a further decrease of the tolerance does not change the trajectory *qualitatively.*

8.3. Poincaré Maps

Trajectories for an autonomous dynamical system with two unknowns are often represented in the phase plane *i.e.* the (ψ_0, J_0) plane or in any of the two state planes $(\psi_0, \dot{\psi}_0)$, $(J_0, \dot{J}_0)$. For our non-autonomous dynamical system with time-periodic

† This error is defined as the difference between the current numerical approximation and the true value of a solution curve based at the previous time step.

coefficients, we use the Poincaré map which displays the sequence of points p_0, p_1, ..., p_n with $p_n = \{J_0(\phi + nT), \psi_0(\phi + nT)\}$ where $T = 2\pi$ is the period of the long wave. Alternately, each of the above points can be viewed as the intersection of the trajectory $(J_0(\phi), \psi_0(\phi))$ in the above three-dimensional space with the plane $\phi = nT$. The sequence of points thus defines a discrete mapping $\mathcal{M}$ characterized by a point p_0 and the recurrence relation $p_{n+1} = \mathcal{M}[p_n]$. It is known that the qualitative properties of the flow (*i.e.* the trajectory) in the phase space are *preserved* in the map.

We shall present Poincaré maps both in the $(\psi_0, \dot{\psi}_0)$ and $(J_0, \dot{J}_0)$ planes. Since J_0 is proportional to the energy difference between the Stokes wave and its side-band disturbance - cf. $(II.8.14a)$ - Poincaré maps in the $(J_0, \dot{J}_0)$ plane yield direct information about the strength of the interactions. However, if we seek information about the phase difference between the two wave components or are interested in the influence of the initial phase $\psi_0(0)$, Poincaré maps in the $(\psi_0, \dot{\psi}_0)$ plane are more convenient.

8.4. Spectral Analysis

To complement the Poincaré maps, we also compute the frequency spectrum of J_0 †. For consistency, the sampling rate is chosen to be $\frac{1}{\Delta\phi} = \frac{1}{2\pi}$. The record length is set to $2^{11}\Delta\phi = 2^{12}\pi$. After the mean is subtracted from the time series, it is tapered with a Blackman window ‡. Given the sampling rate and record length chosen, the Nyquist frequency is $\frac{1}{2\Delta\phi} = \frac{1}{4\pi} \simeq 0.08$ and the resolution is $\Delta f = \frac{1}{2^{12}\pi} \simeq 7.77E-5$. The results are plotted in logarithmic scale.

The dynamical system $(II.8.15a-c)$ is integrated for times much longer than allowed by Schrödinger theory. This is nevertheless necessary to be able to identify the nature and characteristics of the motion in order to make qualitative comparisons with the results of §II.7.

---

† We are in fact plotting power spectra since J_0 is proportional to the difference of energy between the Stokes wave and its disturbance.

‡ The Blackman window was chosen for its very low side lobe level.

8.5. Discussion of Results

In the following, the influence of the disturbance wavenumber ν, the initial phase $\psi_0(\phi = 0)$ and the effect of parameter α is analysed. Finally, the effects of smaller long wave slope KB are investigated.

The uniform Stokes wave is assumed to have initially a unit amplitude according to $(II.8.2a)$. Consequently, $I_0 = \frac{1}{2}$ and $\theta_0 = 0$ at $\phi = 0$. The initial amplitude, $\sqrt{2I_1}$, and the phase, θ_1, of $\tilde{\mathcal{B}}_1$ at $\phi = 0$ therefore dictate the initial conditions for (J_0, ψ_0). Let ϵ_1 be the maximum amplitude of the disturbance, then we deduce from $(II.8.6b)$ and $(II.8.2b)$ that $|\tilde{\mathcal{B}}_1| = \sqrt{2I_1} = \frac{\epsilon_1}{\sqrt{2}}$, the value of J_0 and J_1 is then implied by $(II.8.14)$:

$$J_0(\phi = 0) = \frac{2 - \epsilon_1^2}{8} \qquad J_1(\phi = 0) = \frac{2 + \epsilon_1^2}{8} \qquad (II.8.19a - b)$$

The initial value of ψ_0 is deduced from $(II.8.10a)$

$$\psi_0(\phi = 0) = -\theta_1(\phi = 0) \qquad (II.8.19c)$$

The initial amplitude ϵ_1 of the disturbance is kept constant and equal to 0.1. To analyse the dependence on initial conditions, we perform computations for various choices of the phase $\psi_0(\phi = 0)$. The Poincaré maps are listed at the end of §II.8.

8.5.1. *Influence of the sideband disturbance wavenumber ν*

To investigate the influence of ν, we fix all other parameters as follows: $KB = 0.3$, $\epsilon k\overline{A} = 0.13$ and $\alpha = 0.125$ $(i.e.\ \epsilon\frac{\Omega}{\sigma} = 0.07)$. Guided by the initial growth rates plotted in figures 6.4a-b for $KB = 0.3$. The nonlinear evolution according to $(II.8.15)$ is then computed for several values of the wavenumber ν. One of our objectives is to investigate to what extent the predictions of Floquet theory are consistent with and confirmed by the behavior of the truncated dynamical system.

The admissible disturbance wavenumbers:

In choosing the values of ν, it is necessary to bear in mind that the truncated dynamical system yields meaningful results only when the second, third and higher

harmonics of ν do not become large. Let us focus on the lowest two bands present in figure 6.4a-b. The first and larger band corresponds to $\nu \in [0, 2.32]$. If ν is less than half the width of this band, recurrence patterns may arise as shown by Yuen & Ferguson(1978) for Stokes waves propagating on an otherwise calm sea. On the other hand, provided that ν is larger than half the width of this band, no second or higher harmonic of ν will fall in the same band and thus be unstable. Moreover, we must insure that higher harmonics of $\nu \in [\frac{2.32}{2}, 2.32]$ do not fall in the second instability band $[4.15, 4.55]$. In particular, second harmonic instability will be averted if $\nu \notin [\frac{4.15}{2}, \frac{4.55}{2}]$, third harmonic instability is avoided if $\nu \notin [\frac{4.15}{3}, \frac{4.55}{3}]$ etc ...

After straightforward calculations, we conclude that the unstable disturbance ν must belong to the following set: $[1.16, 1.38] \cup [1.52, 2.07] \cup [2.27, 2.32]$ if reliable information about the nonlinear stability according to $(II.6.12)$ is expected from the truncated dynamical system. If the fundamental disturbance is stable, no requirement is made regarding its harmonics since the disturbance itself remains small at all times. In this section, the initial phase $\psi_0(\phi = 0)$ is set to zero.

The stable and unstable regimes:

We first choose a stable disturbance $\nu = 2.5$ and then an unstable disturbance, $\nu = 1.65$, in the vicinity of the most unstable disturbance, $\nu_{\max} = 1.639$. The Poincaré maps in the $(J_0, \dot{J}_0)$ plane are shown in figure 8.1a-b. For $\nu = 2.5$, the disturbance remains small at all times. The variations of J_0 - and by the same token of $\dot{J}_0$ - are consequently small too. However, for $\nu = 1.65$ the disturbance is unstable and its amplitude may become comparable to the Stokes wave amplitude $(J_0 = 0)$ as seen in figure 8.1a. Poincaré maps in the $(J_0, \dot{J}_0)$ plane thus provide an efficient tool for detecting instability.

Alternately, the Poincaré maps in the $(\psi_0, \dot{\psi}_0)$ plane shown in figures 8.1c-d consist of a periodic *open* curve for $\nu = 2.5$ and of two half branches which can be connected - if use is made of periodicity - to form a *closed* curve for $\nu = 1.65$. Note that in the unstable regime, only a small range of ψ_0 is covered by the Poincaré map.

We also show in figures 8.2a-b the power spectrum of J_0 for $\nu = 2.5$ and $\nu = 1.65$. When $\nu = 2.5$, the spectrum is clearly periodic with a fundamental frequency $f \simeq 0.0238$. For this value of ν, Floquet theory predicts two complex conjugate multipliers $\mu_{1,2} = e^{\pm i\eta}$, with $\eta \simeq 0.465$. According to the definition of Floquet exponents ($II.6.19$), the equivalent radian frequency is $\frac{\eta}{2\pi}$, *i.e.* the equivalent frequency is $\frac{\eta}{(2\pi)^2} \simeq 0.0118$. Since J_0 is quadratic in the amplitudes, its variations occur at twice that frequency, that is $\frac{\eta}{2\pi^2} \simeq 0.0236$ which gives $\eta \simeq 0.4658$ and is in excellent agreement with the results of the nonlinear dynamical system. Secondary peaks in figure 8.2a correspond to second and third harmonics of f. Note also the very low background level. When $\nu = 1.65$ (unstable case), we again observe in figure 8.2b a periodic spectrum with higher harmonics of the fundamental frequency f. Note however that both the fundamental frequency spectrum and the background spectral levels have increased from those in figure 8.2a by one logarithmic unit. This increase, although not drastic, is a prelude to the onset of chaos.

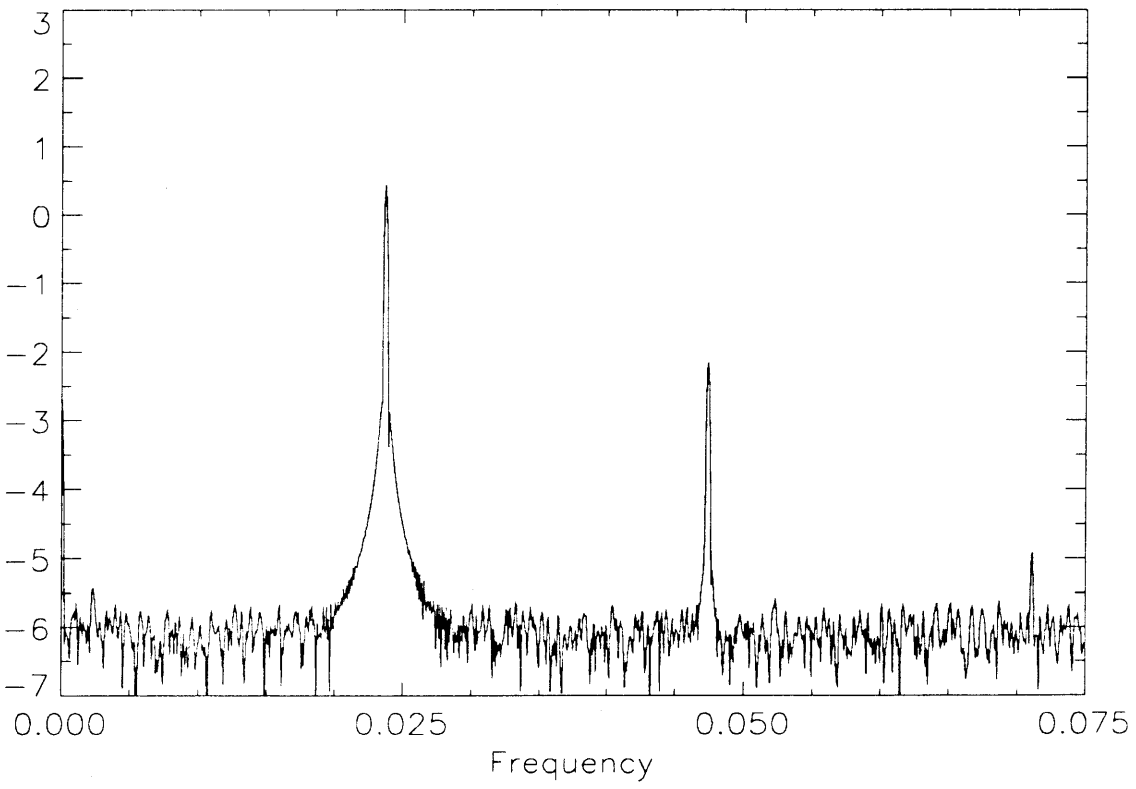

Figure II.8.2a: Frequency spectra of J_0 with $KB = 0.3$, $\epsilon k\overline{A} = 0.13$, $\alpha = 0.125$ and $\nu = 2.5$ (stable).

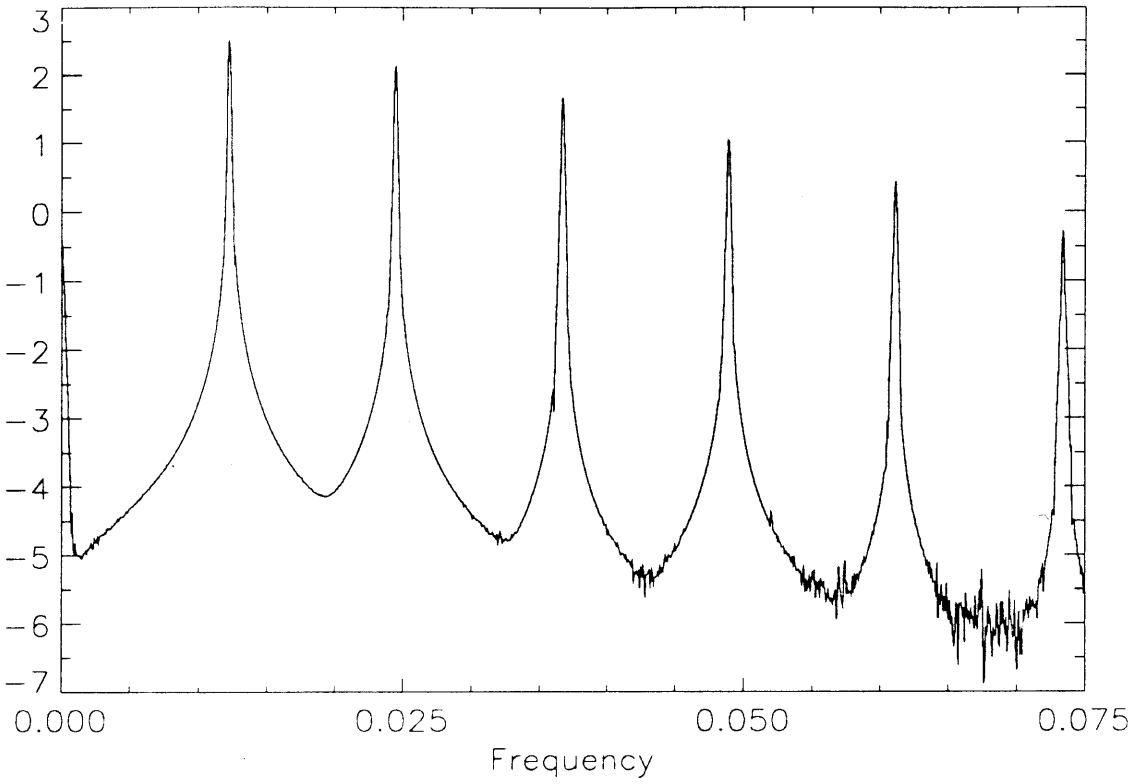

Figure II.8.2b: Frequency spectra of J_0 with $KB = 0.3$, $\epsilon k\overline{A} = 0.13$, $\alpha = 0.125$ and $\nu = 1.65$ (unstable).

Next, we investigate how ν affects the shape of the Poincaré maps in the unstable case. To this end, calculations are made for three admissible values of the disturbance wavenumber corresponding to decreasing growth rates, $\nu = 1.65$, 1.85 and 2.05. The Poincaré map in the $(J_0, \dot{J}_0)$ plane is presented in figure 8.3. Note that the enclosed areas, *i.e.* the range of variation for both variables, J_0 and $\dot{J}_0$, decreases with the growth rate. This is expected since the resonant interactions between the sidebands and the Stokes wave are weaker. In the limit of zero growth rate these areas shrink to zero as was observed in figure 8.1a.

The threshold of stability:

According to Floquet theory, the threshold between zero and non-zero growth rate belongs to the neighborhood [2.3181, 2.3182]. For very small growth rates, it is difficult to distinguish between a stable and an unstable disturbance from a $(J_0, \dot{J}_0)$ Poincaré map. In the $(\psi_0, \dot{\psi}_0)$ plane, however, stable and unstable maps are qualitatively different. Specifically, stable and unstable states are associated with

closed and open orbits respectively (cf. figures 8.1c-d). We have computed many trajectories for values of ν between 2.31 and 2.32, and have located the transition to 10^{-4} accuracy. Figure 8.4a shows two Poincaré maps for $\nu = 2.3185$ and $\nu = 2.3186$. The corresponding orbits are closed and open respectively. For a detailed view of the transition, we have magnified the neighborhood of $\psi_0 = 0$ in figure 8.4b. Floquet theory therefore predicts extremely accurately the transition between two nonlinear regimes of the approximate dynamical system.

The vicinity of the maximum growth rate:

In nature, the sideband disturbance with the largest growth rate is the most likely to be observed. We therefore compute accurately the corresponding wavenumber and find $\nu_{\max} \simeq 1.639$. The Poincaré maps obtained are almost identical to those obtained in figure 8.1a-b for $\nu = 1.65$. Upon magnification, any section of the Poincaré map remains a one-dimensional curve. We have performed calculations for several values of ν in the vicinity of $\nu_{\max}$ and have found no qualitative changes.

8.5.2. *Influence of the initial phase* $\psi_0(\phi = 0)$

It is well known that a strong sensitivity to initial conditions (SIC) is a symptom of chaos. We shall therefore investigate to what extent the initial phase of the disturbance, $\psi_0(\phi = 0)$, determines the regularity of trajectories. The fixed parameters are $KB = 0.3$, $\epsilon k\overline{A}$, $\alpha = 0.125$, $\nu = 1.639 = \nu_{\max}$.

Physical interpretation of $\psi_0(\phi = 0)$*:*

We concentrate our efforts on the influence of the initial phase in the unstable regime. As seen in §II.7, this regime is characterized by two real Floquet multipliers μ_1 and μ_2 satisfying the relationship $\mu_1\mu_2 = 1$. If both are real, one of them - μ_1 say - is greater than unity in absolute value. Let U_1 and U_2 be the eigenvector associated with μ_1 and μ_2. An initial disturbance is characterized by a vector U in the $(\tilde{d}, \tilde{W})$ plane (cf. figure 8.5). It is expected that the growth of the disturbance will be the greatest if U and U_1 are colinear. This requirement defines an optimal phase θ_1^u for the complex amplitude, $\tilde{\mathcal{B}}_1$, of the sideband disturbance. From $(II.8.19c)$, we

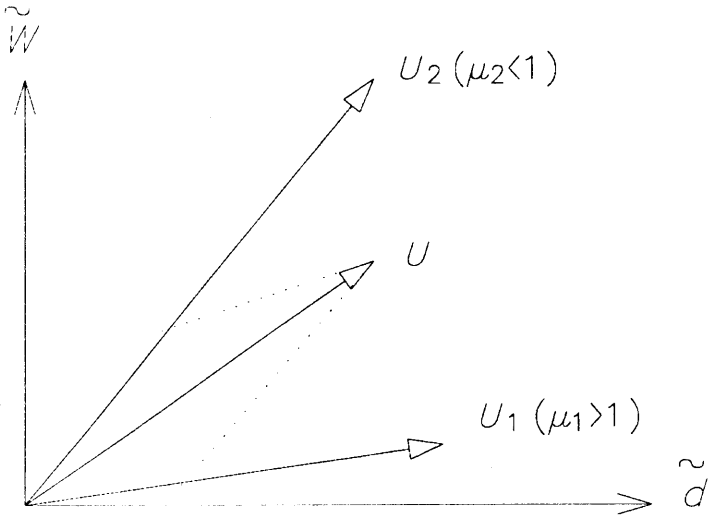

Figure II.8.5: Directions of growth and decay in Floquet theory (unstable and stable manifolds) in the $(\tilde{d}, \tilde{W})$ plane.

deduce the corresponding optimal initial value of ψ_0:

$$\psi_0^u(\phi = 0) = -\theta_0^u \qquad (II.8.20)$$

With the above parameters, the colinearity condition yields $\psi_0^u(0) \simeq 0.808$.

On Poincaré maps:

In this analysis, it is more convenient to consider Poincaré maps in the $(\psi_0, \dot{\psi}_0)$ plane. To see the influence of $\psi_0(\phi = 0)$, we superimpose, in figures 8.6a, three maps for $\psi_0(0) = \frac{\pi}{6}$, $\frac{\pi}{2}$ and π. Note that all three maps correspond to the same energy J_1. For $\psi_0(0) = \frac{\pi}{6}$ the map consists of two half-branches and is similar to those described in figure 8.1d. These maps are called type I. For $\psi_0(0) = \frac{\pi}{2}$, we observe an open periodic curve. Similar maps will be referred to as type II. Finally, for $\psi_0(0) = \pi$, the map is a closed orbit centered at $\psi_0 = \pi$, similar maps will be referred to as type I', which is the same as type I except for a phase shift.

To ascertain that any Poincaré map does fall into one of the above 3 types, we superimpose the Poincaré maps of 63 trajectories characterized by $\psi_0(\phi = 0) = 0.1 \times (j - 1)$ for $j = 1, 2, \ldots, 63$. The map in figure 8.6b is not symmetrical with

respect to the horizontal axis in contrast with the Poincaré map for the classical pendulum. This figure is clearly composed of several maps of types I, II and I'.

In order to identify the range of $\psi_0(0)$ corresponding to each type of map, we have first made use of the previous computations and established on the above coarse grid the location of each transition. For instance, the transition from I to II was found near $\psi_0(0) = 0.8$. After refining the grid in that vicinity, the transition can be pin-pointed to the interval $[0.8075, 0.8097]$. We then perform 23 calculations for $\psi_0(0) = 0.8075, 0.8076, \ldots, 0.8097$ and conclude the existence of an interval of values of $\psi_0(0)$, $[\psi_0^-(0), \psi_0^+(0)]$, such that any $\psi_0(0) < \psi_0^-(0)$ $(> \psi_0^+(0))$ yields a Poincaré map of type I (II), while $\psi_0(0) \in [\psi_0^-(0), \psi_0^+(0)]$ gives rise to a map combining the essential features of types I, II and I'.

		$\psi_0(0)$	$<$	0.8084	Type I
0.8084	$<$	$\psi_0(0)$	$<$	0.8094	Types I, II or I'
0.8094	$<$	$\psi_0(0)$	$<$	2.332	Type II
2.332	$<$	$\psi_0(0)$	$<$	2.333	Types I, II or I'
2.333	$<$	$\psi_0(0)$	$<$	π	Type I'

Table II.8.1: Geometry of Poincaré maps for various values of the initial phase $\psi_0(0) \in [0, \pi]$.

It is found that $\psi_0^-(0) = 0.8084$ and $\psi_0^+(0) = 0.8094$. Within this range, there is a very strong sensitivity to the initial phase $\psi_0(0)$. We perform the same analysis for the transition between map types II and I' and find that the new thresholds are $\psi_0^-(0) = 2.332$ and $\psi_0^+(0) = 2.333$. For any value of $\psi_0(0)$ within this window, any of the three types can happen. Because ψ_0 appears at the argument of the sine and cosine functions in $(II.8.15a-b)$, if $[\psi_0^-(0), \psi_0^+(0)]$ is a window of sensitivity to initial conditions so is the window $[\psi_0^-(0) + \pi, \psi_0^+(0) + \pi]$. It is therefore sufficient to analyse the interval $[0, \pi]$ only. The types of Poincaré maps are summarized in Table 8.1.

The vicinity of the most unstable disturbance:

We present in figure 8.7a, the Poincaré map in the $(\psi_0, \dot{\psi}_0)$ plane associated

with the mid-range value $\psi_0(0) = 0.8089$ which is close to $\psi_0^u(0) = 0.8080$. It indeed consists of the superposition of all three map types. Note the sparseness of the points except near the intersection of the branches in the neighborhood of $\dot{\psi}_0 \simeq 0.16$. To elucidate the structure of these intersections, we magnify a small neighborhood of one of them as in figure 8.7b. What appeared to be a continuous line actually consists of a chaotic cloud of points (also called a *chaotic zone*).

Recall that for an arbitrary value of $\psi_0(0)$ far from 0.8089, the Poincaré map consists of a one dimensional curve. This is clearly no longer true. In figures 8.7c-d, we have included for reference the Poincaré maps in the $(J_0, \dot{J}_0)$ plane where the right corner turns, upon magnification, into a chaotic zone.

The Fourier spectrum of J_0, in figure 8.7e, shows the absence of any fundamental frequency and the drastic rise of the spectral background level. These features clearly confirm the onset of chaos. It is therefore appropriate to conclude that Floquet theory and the truncated dynamical system corroborate each other well.

To further illustrate the effect of $\psi_0(0)$ near the transition zone, two Poincaré maps are shown for $\psi_0(0) < 0.8084$. In figure 8.8a, for $\psi_0(0) = 0.8081$, the map is shaped as a broken loop. Magnification of the corner reveals islands which are also called *tori*. These structures arise for dynamical systems whose temporal behavior is characterized by a small number of independent frequencies. In the present case, one frequency dictates how each island is formed, while the second frequency describes the motion between islands. For the slightly different value $\psi_0(0) = 0.8080$, the Poincaré map in figure 8.9a is qualitatively the same. However, upon magnification of the corner, the tori observed earlier are on the verge of breaking up.

8.5.3. *Influence of* α

We first recall the expression of δ and α

$$\delta = 1 - \frac{\epsilon}{2}\frac{\Omega}{\sigma} \qquad \alpha \equiv \frac{\epsilon}{2\delta}\frac{(kA)^2}{\frac{\Omega}{\sigma}} \qquad (II.8.21a-b)$$

Parameter α is $\mathcal{O}(\epsilon)$ and increases with increasing short wave slopes, $\epsilon k\overline{A}$, and with decreasing frequency ratios $\epsilon\frac{\Omega}{\sigma}$, *i.e.* with larger scale contrast. Having performed in §II.8.5.2 an extensive analysis of all types of Poincaré map for $\alpha = 0.125$, we

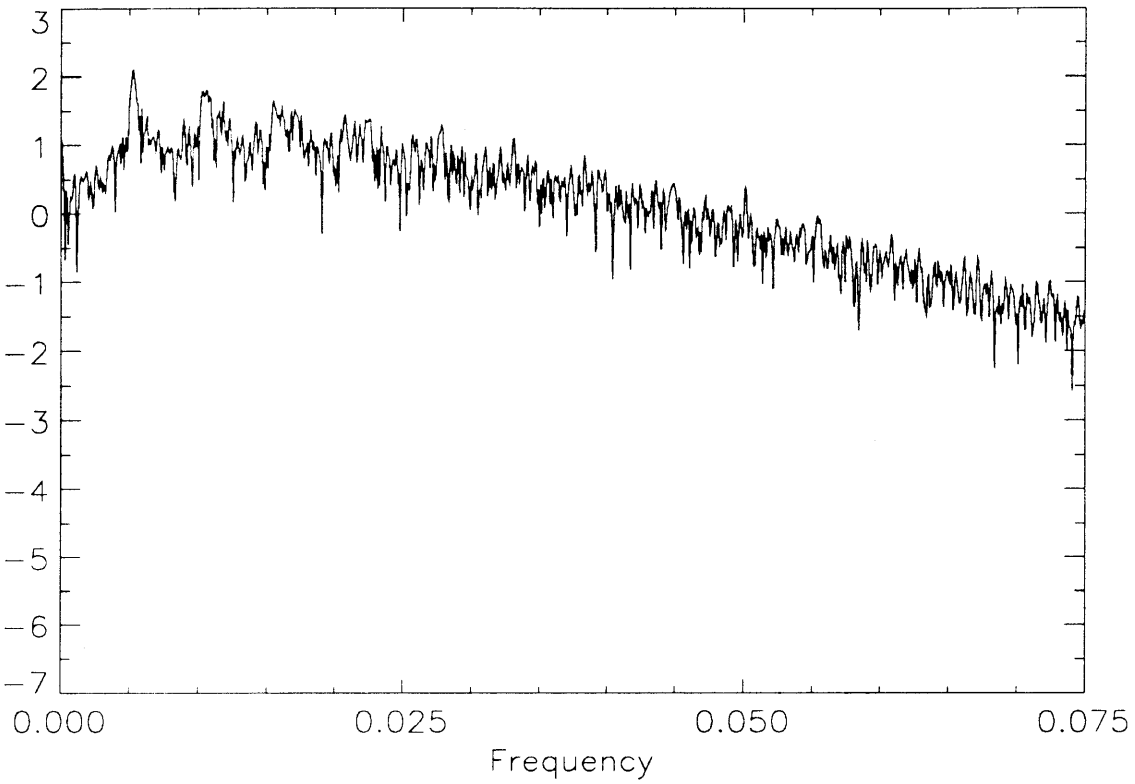

Figure II.8.7e: Frequency spectrum of J_0 with $KB = 0.3$, $\epsilon k\overline{A} = 0.13$, $\alpha = 0.125$, $\nu = 1.639$ and $\psi_0(0) = 0.8084$

consider now two more values $\alpha = 0.05$ and $\alpha = 0.15$. For the sake of simplicity, we assume the short wave slope to be constant $\epsilon k\overline{A} = 0.13$, and vary the frequency ratio $\epsilon\frac{\Omega}{\sigma}$.

In the rest of the section, ν will be chosen as $\nu_{\max}$, the most unstable disturbance in the main lobe. The Floquet stability diagrams in figure 6.5a-b may be used to check the stability of harmonics of $\nu_{\max}$.

For $\alpha = 0.05$ (*i.e.* $\epsilon\frac{\Omega}{\sigma} \simeq 0.1864$) the maximum growth rate occurs at $\nu_{\max} = 1.604$. The disturbance $\nu_{\max}$ and two of its harmonics are represented by the symbol "$\vee$" in figure 6.5b. Only the fourth harmonic of $\nu_{\max}$ is unstable with a 5% growth rate (*i.e.* $|\mu_1| = 1.05$). Since neither its second nor its third harmonic is unstable, the growth of the fourth harmonic should not be significant. The initial phase is chosen to be the most unstable value suggested by Floquet analysis $\psi_0^u(0) = 0.789$. The Poincaré map in the $(J_0, \dot{J}_0)$ plane is shown in figure 8.10a. Upon magnifying

the neighborhood of the corner, we obtain in figure 8.10b a one-dimensional curve. The Fourier spectrum of J_0 in figure 8.10c suggests a periodic motion with frequency $f \simeq$2.23e-3.

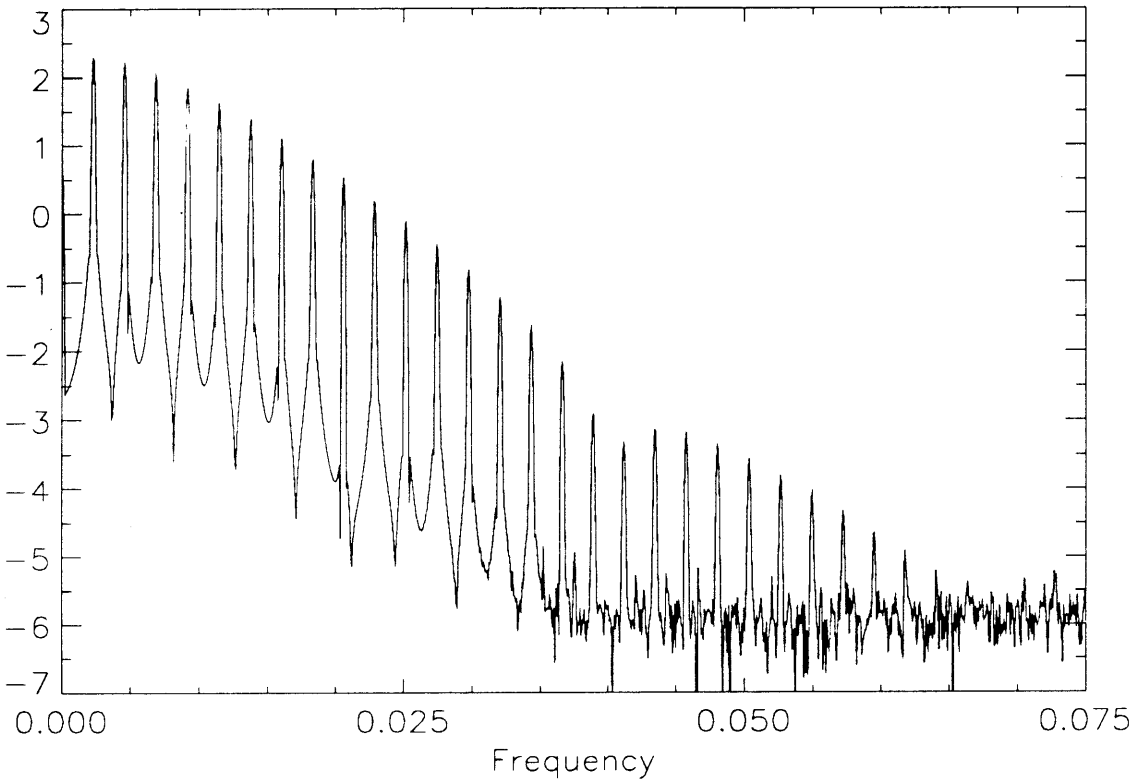

Figure II.8.10c: Frequency spectrum of J_0 with $KB = 0.3$, $\epsilon k\bar{A} = 0.13$, $\alpha = 0.05$, $\nu_{\max} = 1.604$ and $\psi_0(0) = 0.789$.

For $\alpha = 0.15$ ($i.e.$ $\epsilon\frac{\Omega}{\sigma} \simeq 0.058$), $\nu_{\max} = 1.638$ and the associated value of the phase is $\psi_0^u(0) = 0.817$ (see the "$\triangle$" symbols in figure 6.5b). Again, only the fourth harmonic of $\nu_{\max}$ is unstable with an 11% growth rate. The Poincaré map in the $(J_0, \dot{J}_0)$ plane is shown in figure 8.11a. Figure 8.11b shows that the neighborhood of the corner is a chaotic zone. The Fourier spectrum of J_0 is strikingly different from that for $\alpha = 0.05$, and marked by a rise of the background level and the disappearance of the dominant frequency.

So far the parameters have been chosen within the legitimate bounds of our theory. To speculate what might happen for steep short waves or greater scale contrast, we have also performed calculations for rather large values of α. Figures

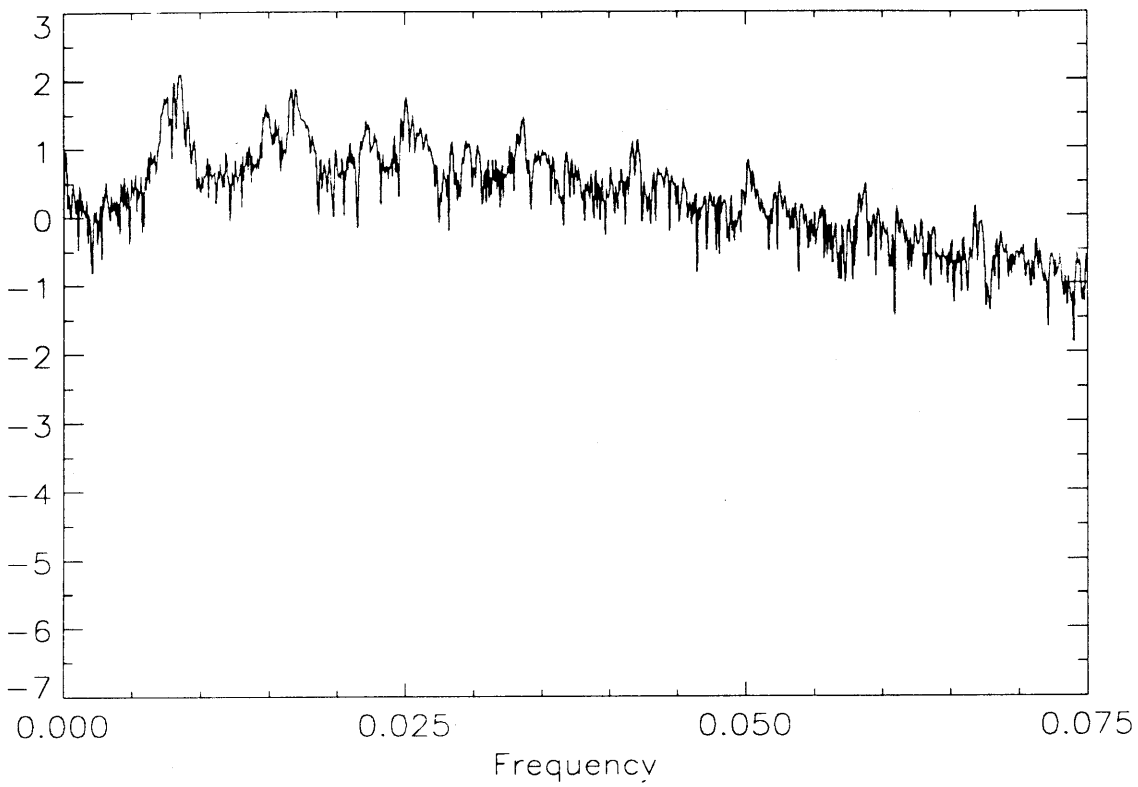

Figure II.8.11c: Frequency spectrum of J_0 with $KB = 0.3$, $\epsilon k\bar{A} = 0.13$, $\alpha = 0.15$, $\nu_{\max} = 1.638$ and $\psi_0(0) = 0.817$.

8.12a-b, 8.13a-b and 8.14a-b show Poincaré maps respectively for $\alpha = 0.25$, 0.30 and 0.45. The corresponding most unstable disturbances are $\nu_{\max} = 1.62$, 1.60 and 1.55. The stability of their second and third harmonics is summarized in figure 6.5b respectively by the symbols "◯", "△" and "⊔". The second harmonic is stable only for $\alpha = 0.45$. The third harmonic is stable only for $\alpha = 0.25$, and the fourth harmonic is always stable. With larger α, the range of variation of all four variables J_0, $\dot{J}_0$, ψ_0 and $\dot{\psi}_0$ increases and chaotic zones become larger and larger.

We have seen earlier that chaotic zones arise when the initial phase $\psi_0(0)$ belongs to specific intervals characterized by a high sensitivity to initial conditions (cf. Table 8.1 for $\alpha = 0.125$). If $\Delta\psi_0(0)$ represents the union of of all these intervals, the size of $\Delta\psi_0(0)$ is clearly a measure of the likelyhood of chaotic motions. Upon performing a classification such as that of Table 8.1 for $\alpha = 0.15$, 0.2 and 0.45, we plot in figure 8.15 $\Delta\psi_0(0)/2\pi$ versus α. A ratio of unity means that chaotic zones

appear for all value of $\psi_0(0)$ in the interval $[0, 2\pi]$. As α increases, *i.e.* when the short waves become steeper and (or) the scale ratio smaller, $\Delta\psi_0(0)/2\pi$ approaches unity, thus implying that chaos is widespread.

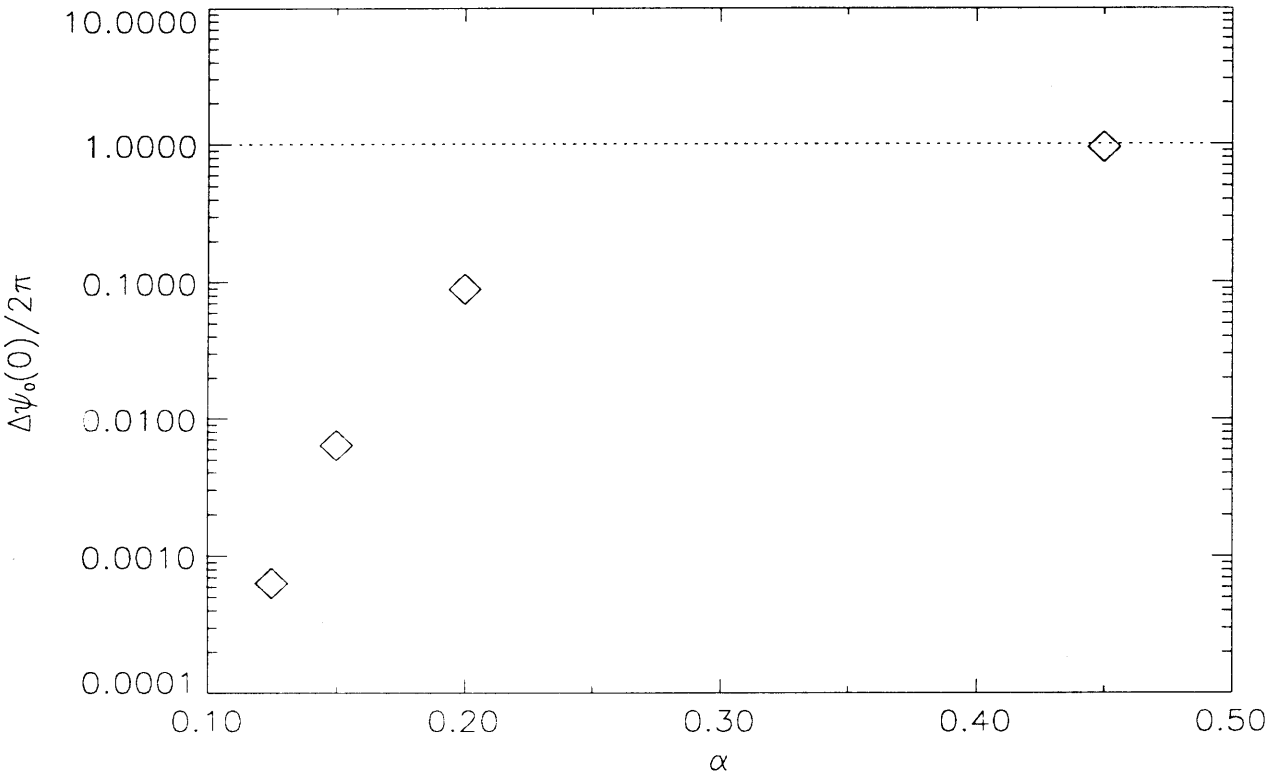

Figure II.8.15: Basin of chaos for various parameters α.

8.5.4. *Influence of the long wave slope KB*

All the results presented so far were obtained with a relatively steep Gerstner wave ($KB = 0.3$). Although this slope is much smaller than the critical slope of a Stokes wave ($KB \approx 0.443$), it may still be somewhat too large to be a model of steep waves in nature since breaking may be present owing to instability of the long wave itself. It is therefore important to examine to what extent the above results are preserved when $KB = 0.2$ and $KB = 0.1$. The parameters chosen for comparison are $\epsilon k\overline{A} = 0.13$, $\alpha = 0.15$, $\nu = \nu_{\max}$ and $\psi_0(0) = \psi_0^u$. Since the scale contrast, $\epsilon\frac{\Omega}{\sigma}$ is kept constant, the amplitude B of Gerstner's wave changes.

The $(J_0, \dot{J}_0)$ Poincaré maps for $KB = 0.3$, 0.2 and 0.1 are superimposed in figure 8.16. All three maps are shaped like a tear drop whose contour is discontinuous. When KB decreases, so does the range of variations of $\dot{J}_0$. Next, we have magnified † the vicinity of the corner for $KB = 0.2$ and $KB = 0.1$ in figures 8.17b and 8.18b which show that the chaotic zone near the corner diminishes with KB.

† The area magnified is much larger than that shown before for $KB = 0.3$.

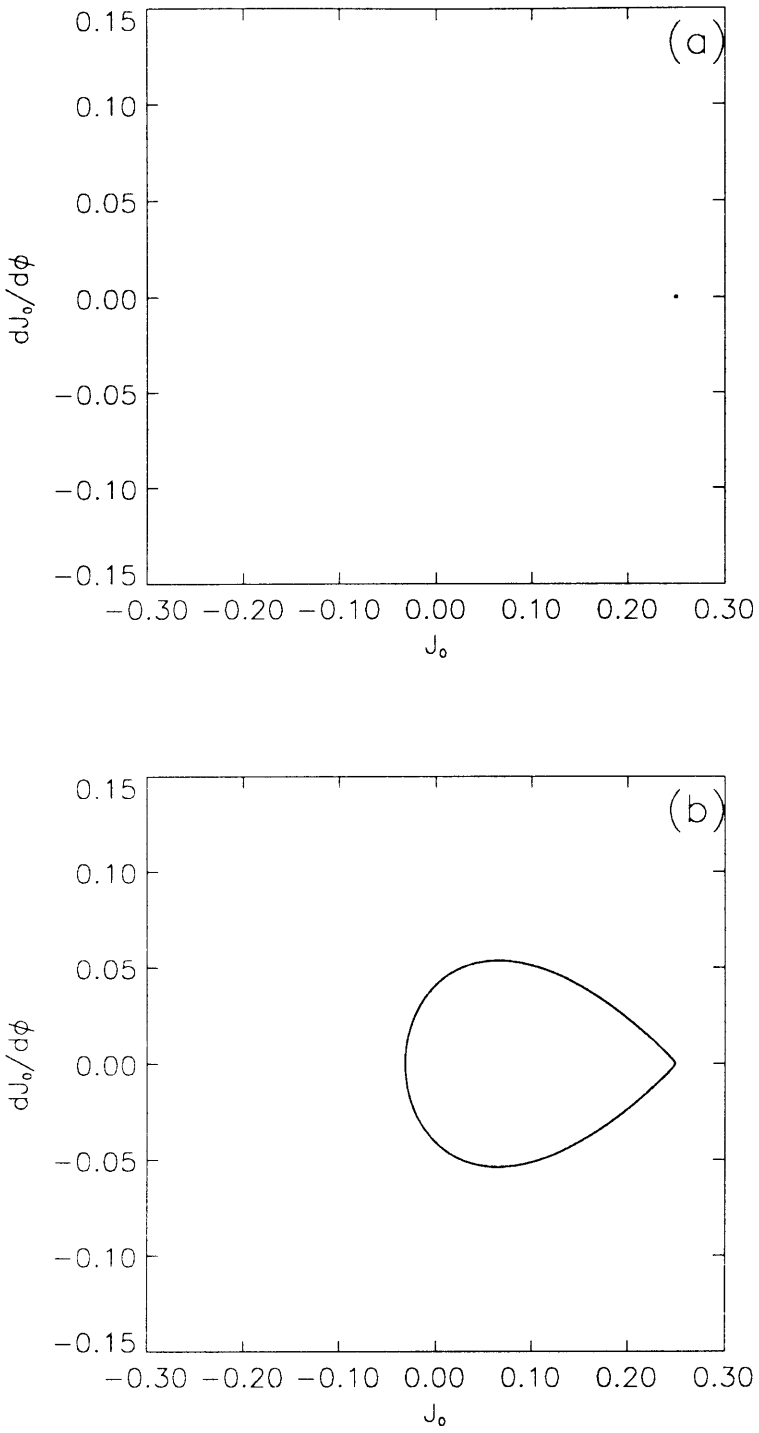

Figures II.8.1a-b: Poincaré maps in the $(J_0, \dot{J}_0)$ plane with $KB = 0.3$, $\epsilon k\overline{A} = 0.13$, $\alpha = 0.125$; (a) $\nu = 2.5$ (stable), (b) $\nu = 1.65$ (unstable).

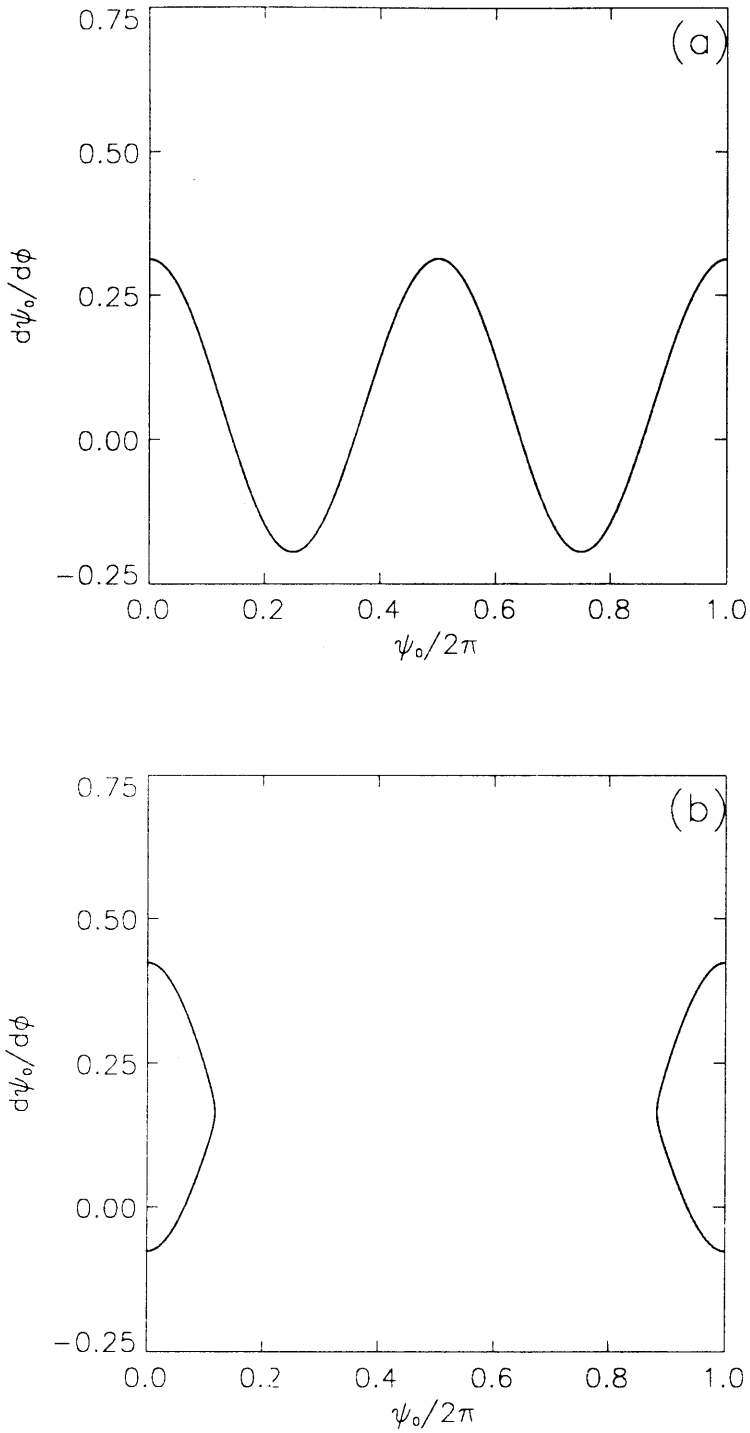

Figures II.8.1c-d: Poincaré maps in the $(\psi_0, \dot{\psi}_0)$ plane with $KB = 0.3$, $\epsilon k \overline{A} = 0.13$, $\alpha = 0.125$; (c) $\nu = 2.5$ (stable), (d) $\nu = 1.65$ (unstable).

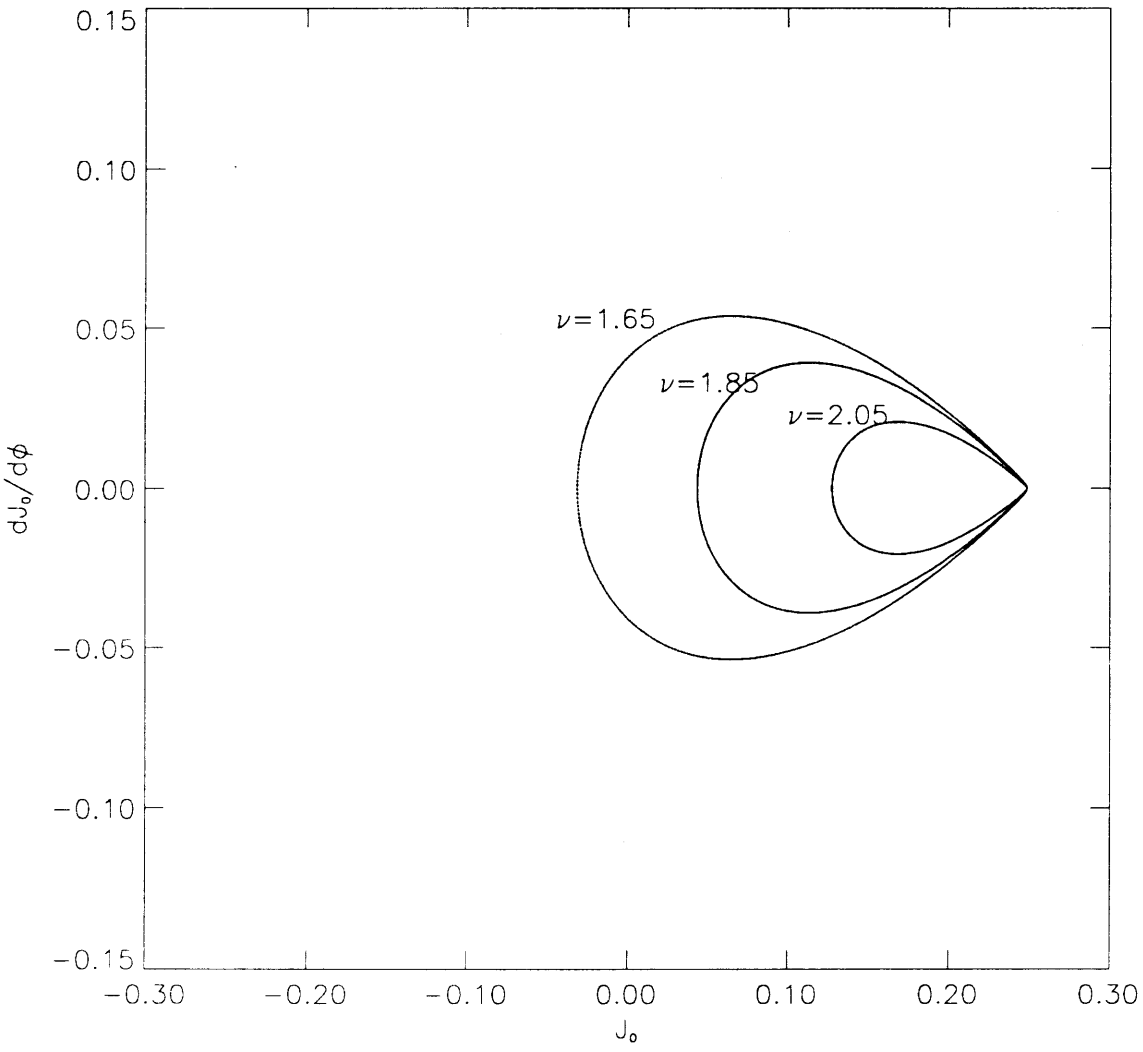

Figure II.8.3: Superposition of three Poincaré maps in the $(J_0, \dot{J}_0)$ plane with $KB = 0.3$, $\epsilon k\overline{A} = 0.13$, $\alpha = 0.125$ for three unstable disturbances $\nu = 1.65$, 1.85 and 2.05.

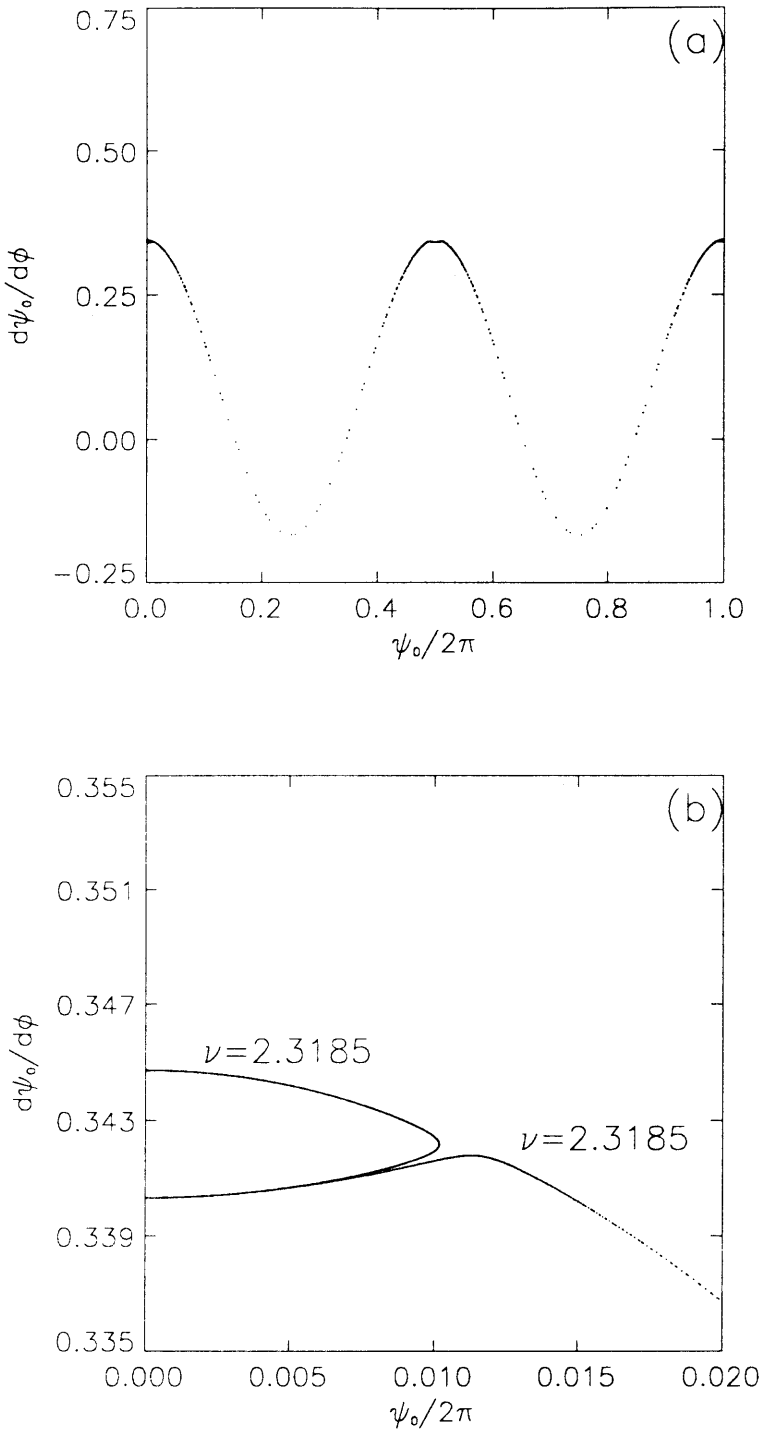

Figures II.8.4a-b: Poincaré maps in the $(\psi_0, \dot{\psi}_0)$ plane at the transition between instability ($\nu = 2.3185$) and stability ($\nu = 2.3186$). Parameters are $KB = 0.3$, $\epsilon k \overline{A} = 0.13$ and $\alpha = 0.125$; (a) global view, (b) detail.

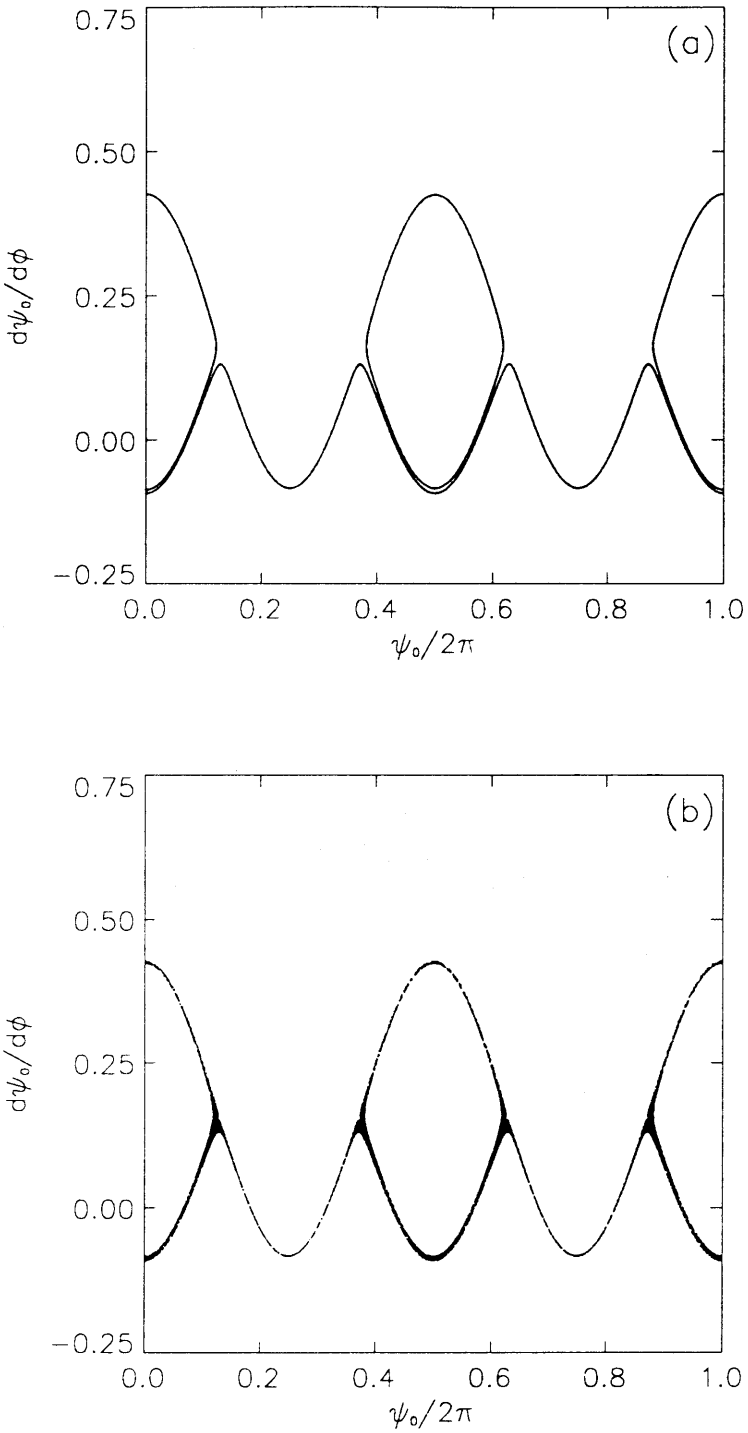

Figures II.8.6a-b: Poincaré maps in the $(\psi_0, \dot{\psi}_0)$ plane and the effect of the intial phase. (a) superposition of three maps for $\psi_0(0) = \frac{\pi}{6}, \frac{\pi}{2}$ and π, (b) superposition of 63 values of the initial phase: $\psi_0(0) = 0., 0.1, \ldots, 6.2$.

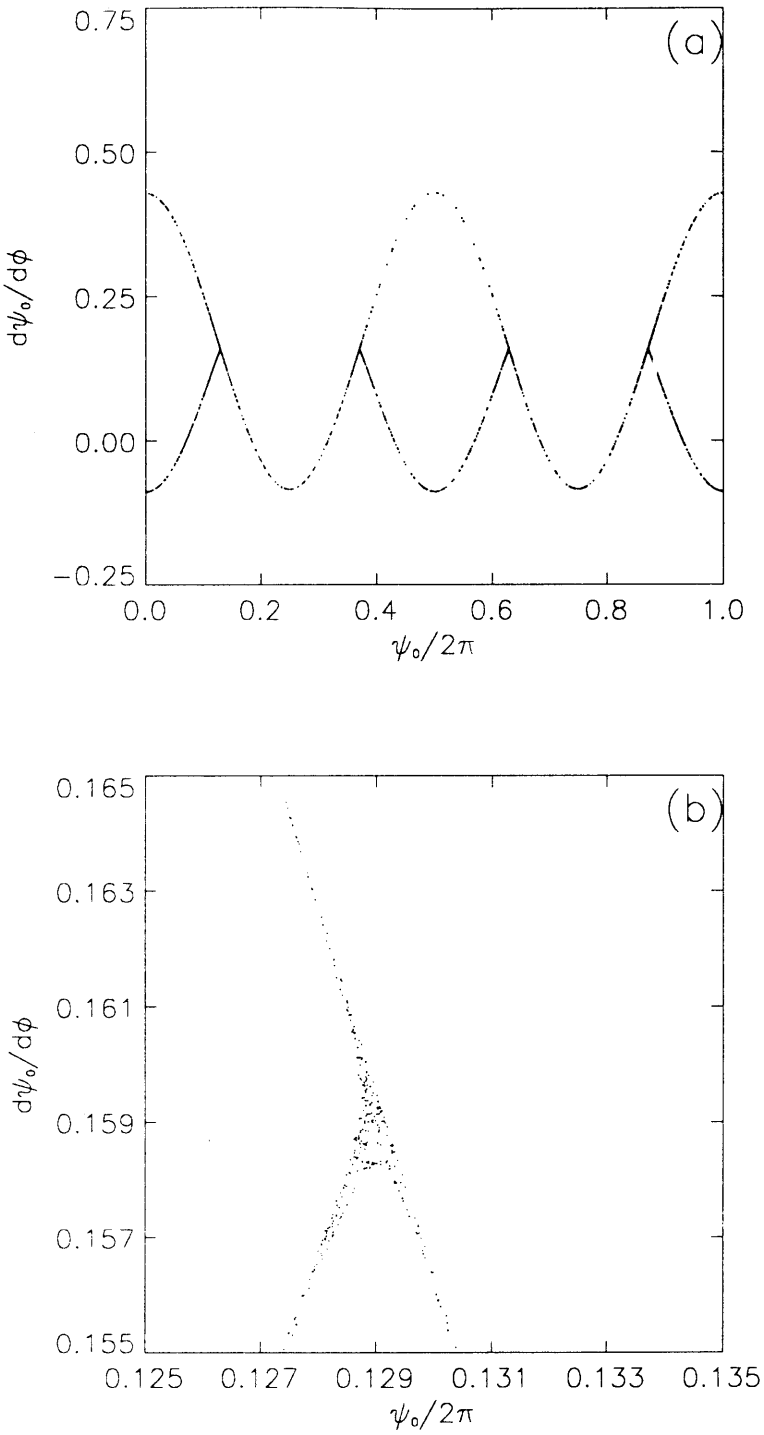

Figures II.8.7a-b: Poincaré maps in the $(\psi_0, \dot{\psi}_0)$ plane with $KB = 0.3$, $\epsilon k\overline{A} = 0.13$, $\alpha = 0.125$, $\nu = 1.639$ and $\psi_0(0) = 0.8084$; (a) global view, (b) detail of left-most intersection.

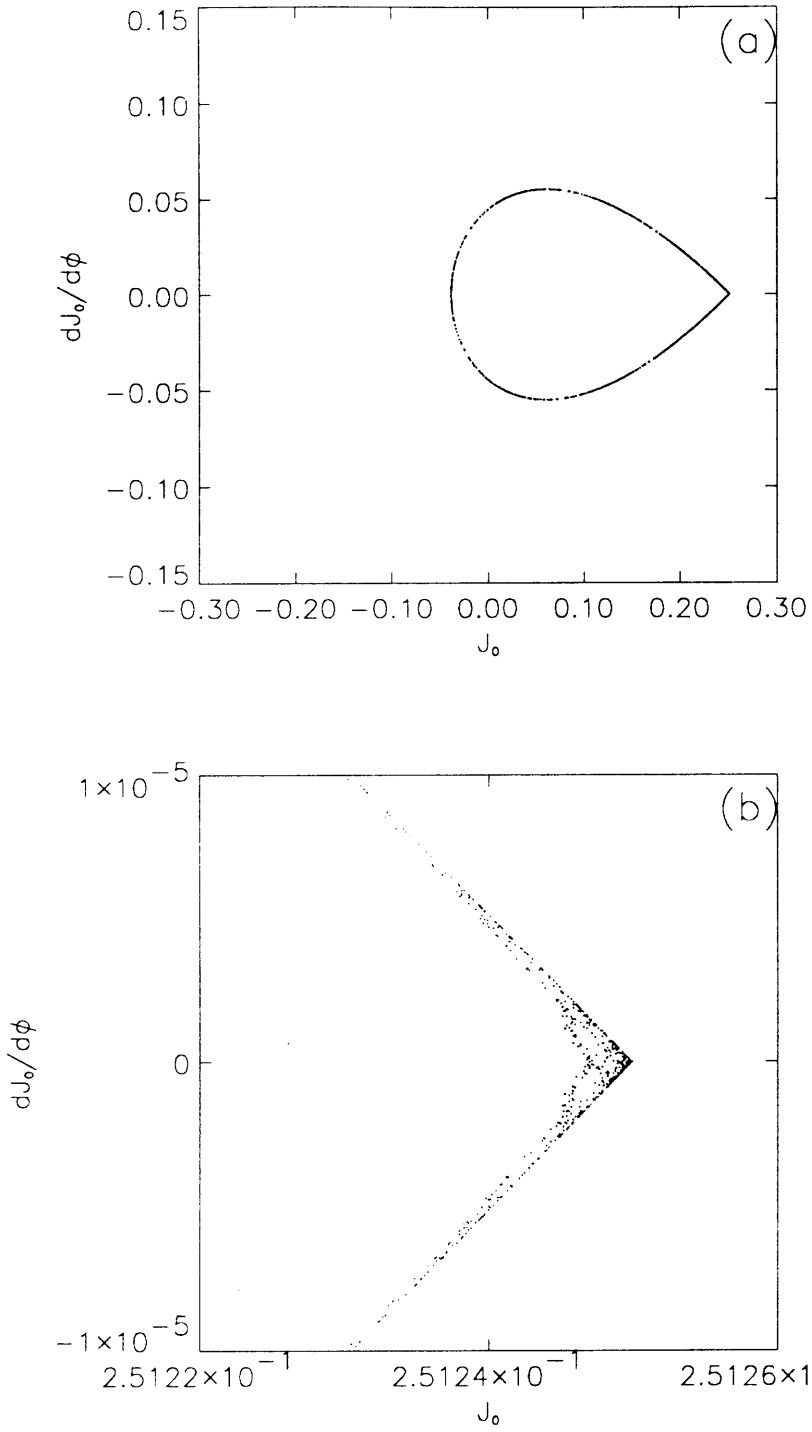

Figures II.8.7c-d: Poincaré maps in the $(J_0, \dot{J}_0)$ plane with $KB = 0.3$, $\epsilon k\overline{A} = 0.13$, $\alpha = 0.125$, $\nu = 1.639$ and $\psi_0(0) = 0.8084$; (a) global view, (b) detail of the corner.

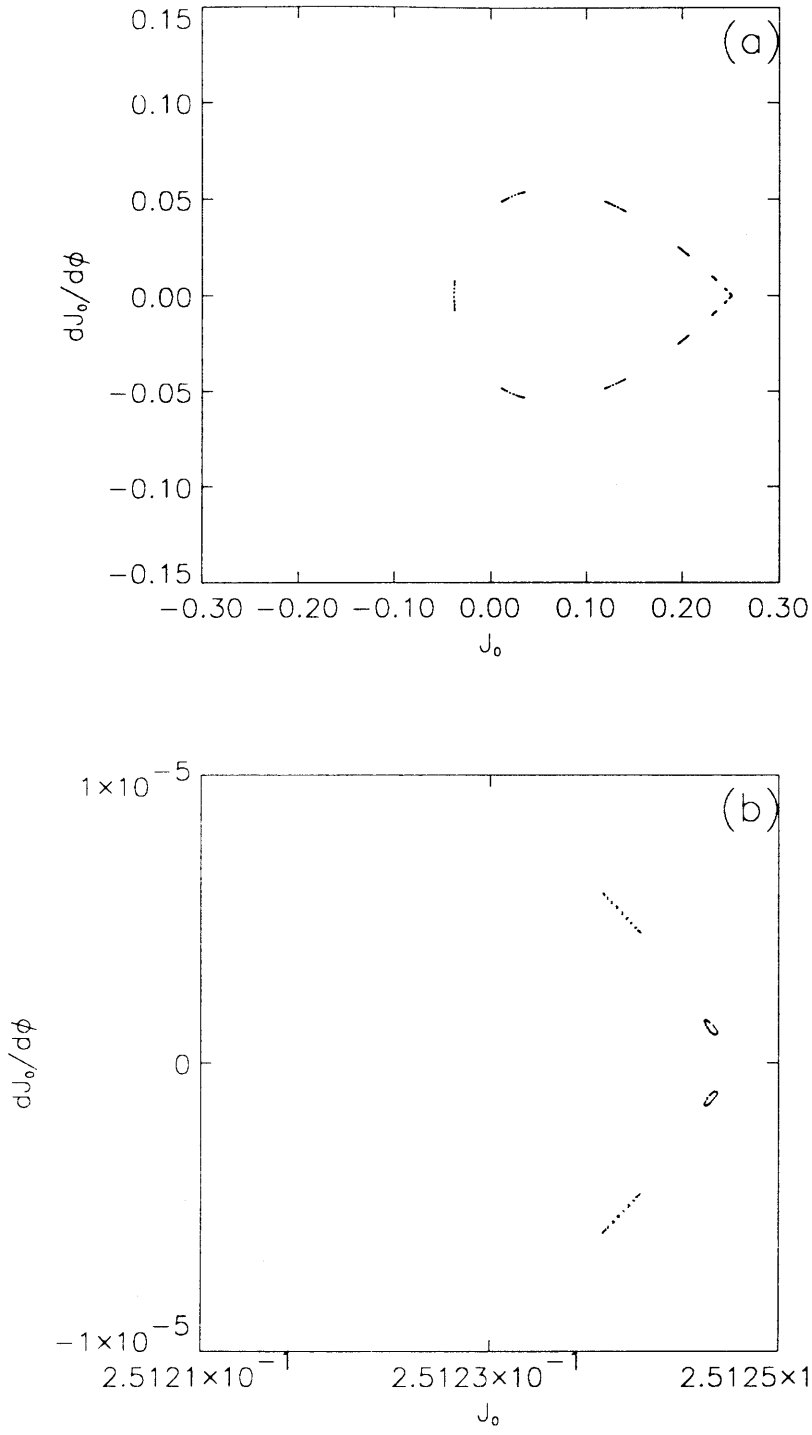

Figures II.8.8a-b: Poincaré map in the plane $(J_0, \dot{J}_0)$ with $KB = 0.3$, $\epsilon k \bar{A} = 0.13$, $\alpha = 0.125$, $\nu_{\max} = 1.639$ and $\psi_0(0) = 0.8081$; (a) global view, (b) detail of Poincaré map in the vicinity of corner.

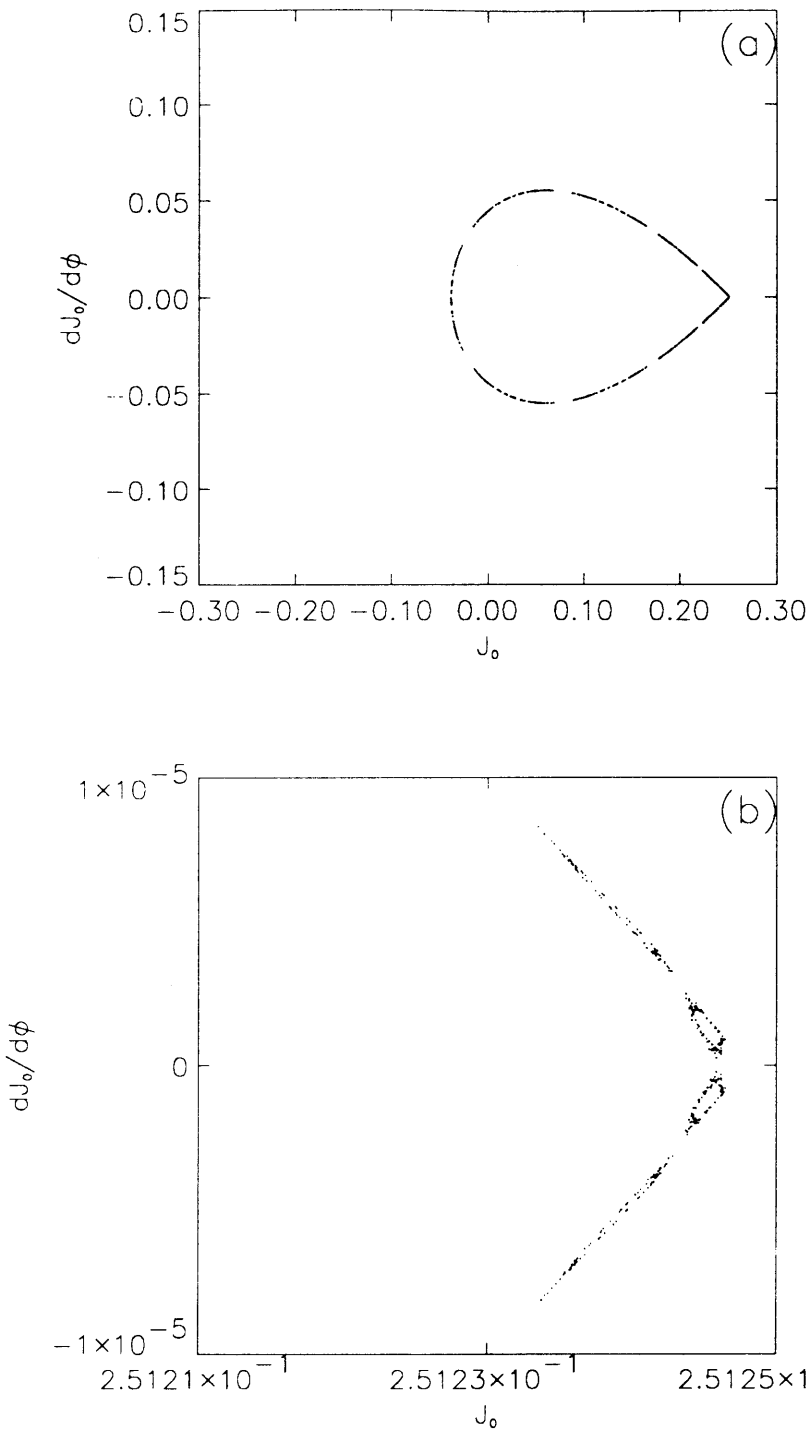

Figures II.8.9a-b: Poincaré map in the plane $(J_0, \dot{J}_0)$ with $KB = 0.3$, $\epsilon k\bar{A} = 0.13$, $\alpha = 0.125$, $\nu_{\max} = 1.639$ and $\psi_0(0) = 0.8080$; (a) global view, (b) detail of Poincaré map in the vicinity of corner.

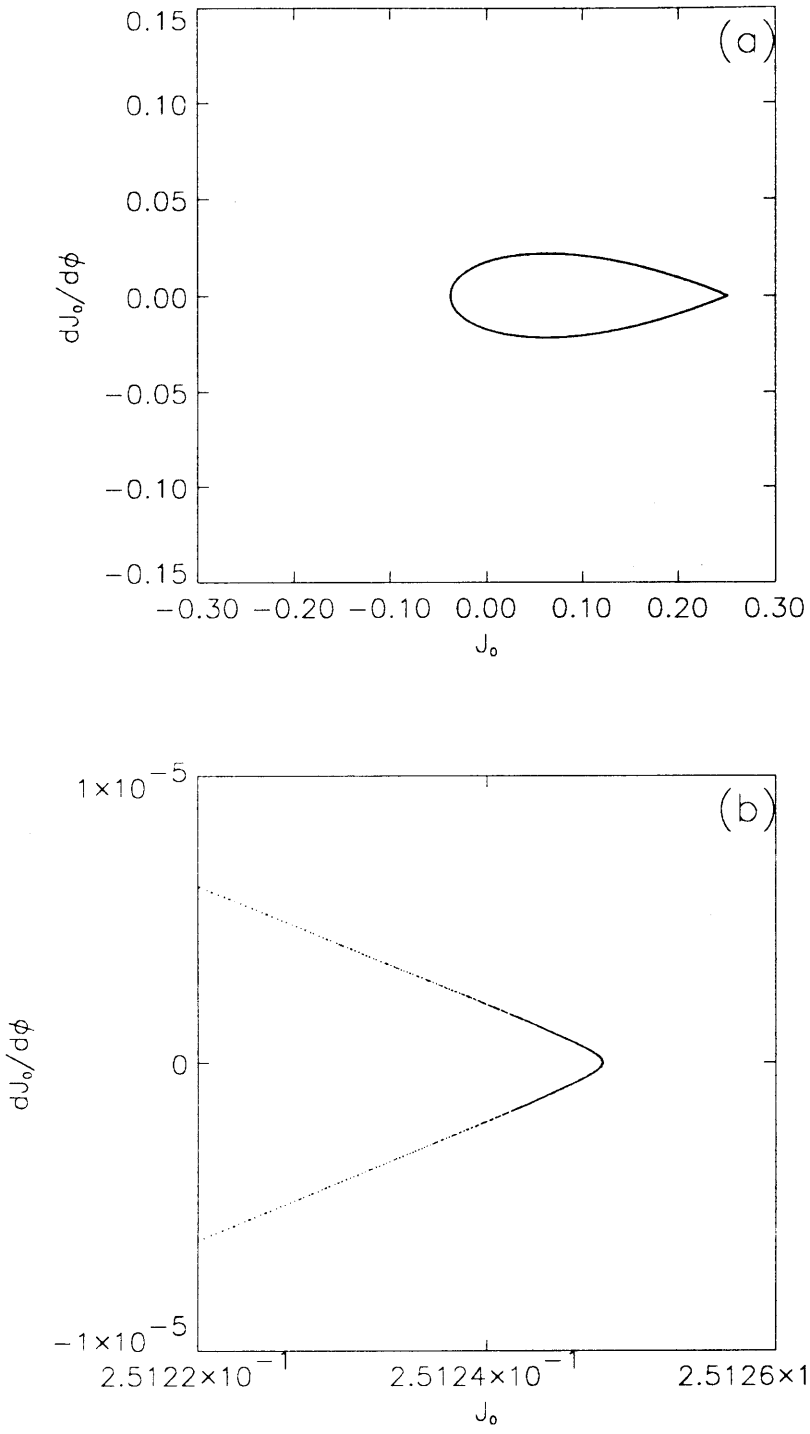

Figures II.8.10a-b: (a) Poincaré maps in the $(J_0, \dot{J}_0)$ plane (b) Detail of Poincaré map in the vicinity of corner with $KB = 0.3$, $\epsilon k \bar{A} = 0.13$, $\alpha = 0.05$, $\nu_{\max} = 1.604$ and $\psi_0(0) = 0.789$.

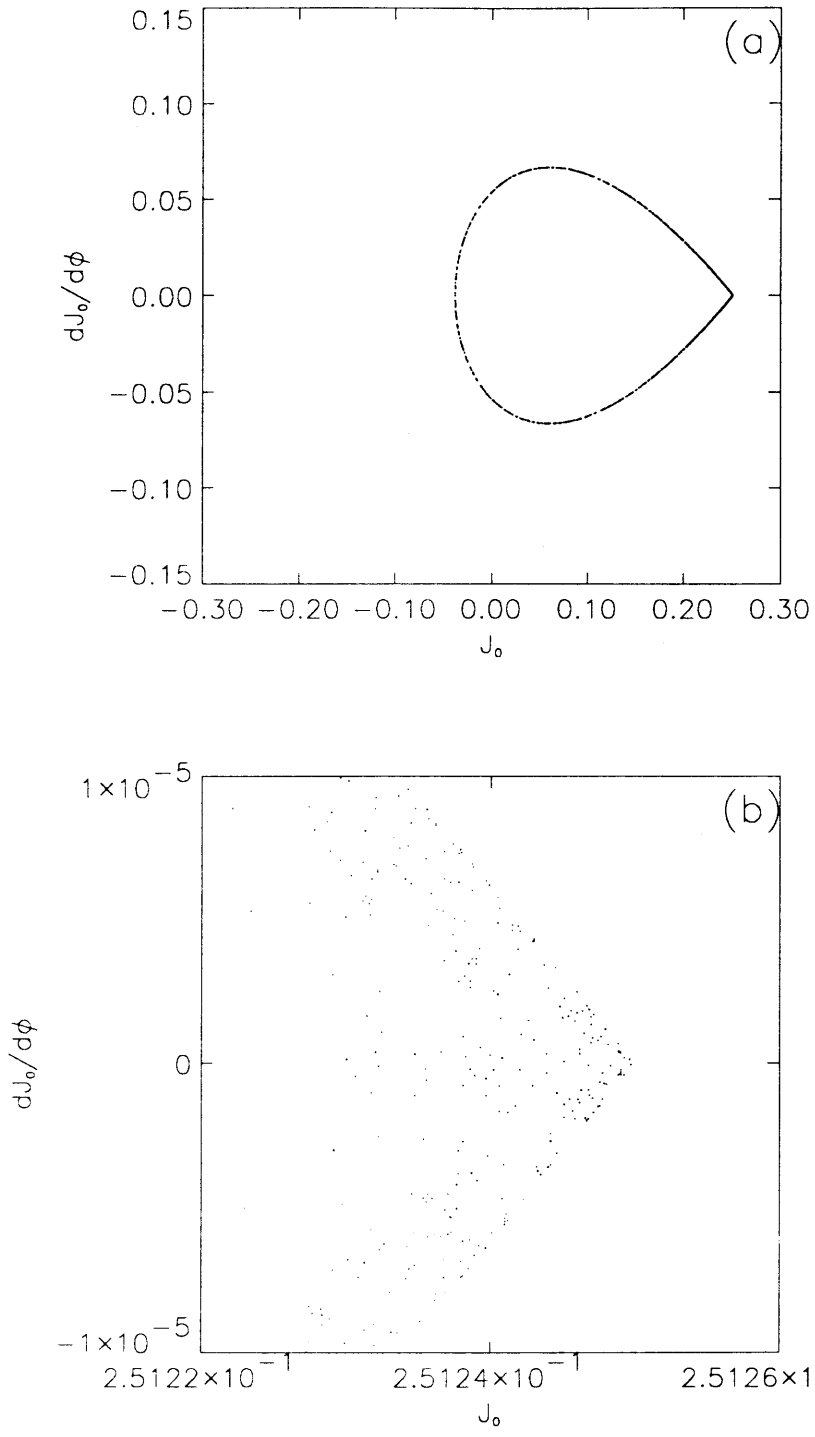

Figures II.8.11a-b: (a) Poincaré maps in the $(J_0, \dot{J}_0)$ plane (b) Detail of Poincaré map in the vicinity of corner with $KB = 0.3$, $\epsilon k\bar{A} = 0.13$, $\alpha = 0.15$, $\nu_{\max} = 1.638$ and $\psi_0(0) = 0.817$.

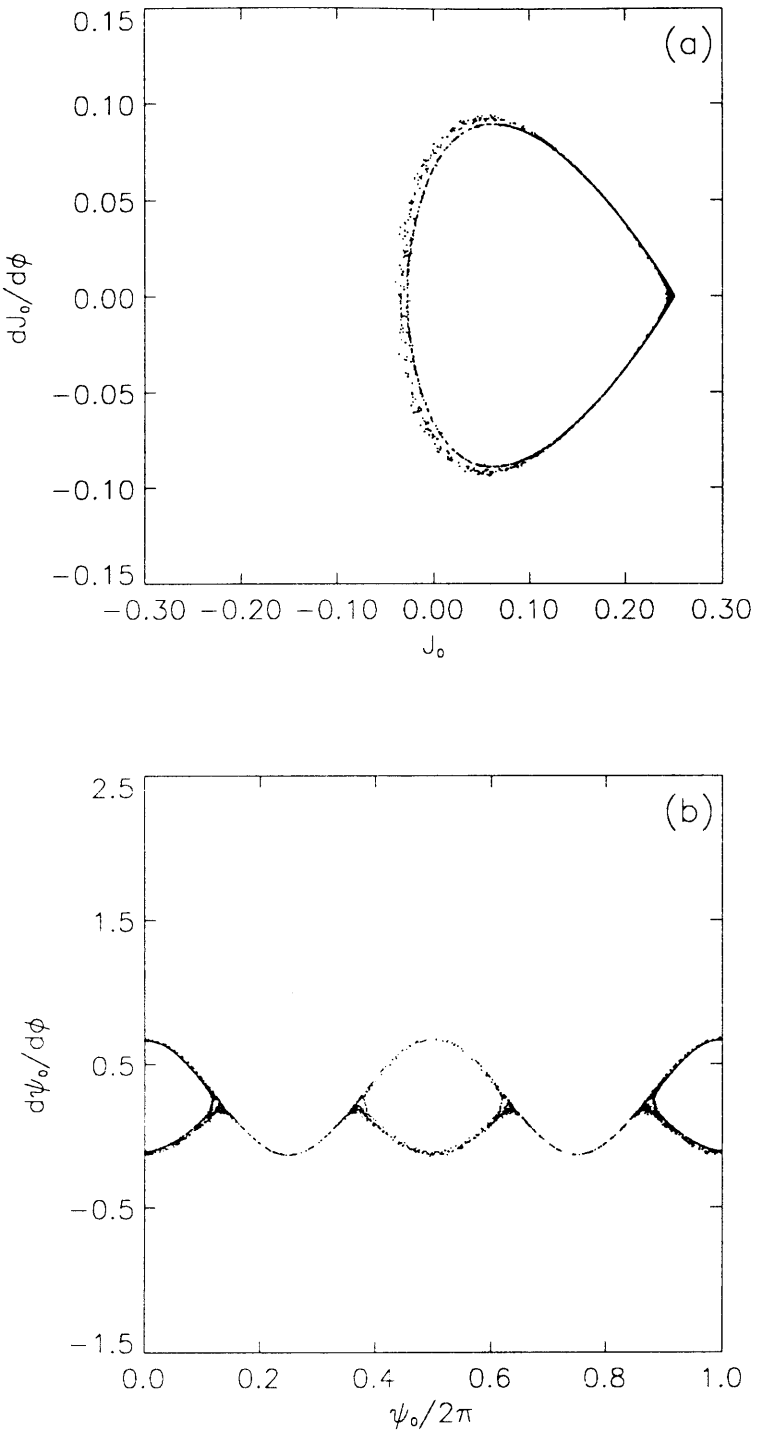

Figures II.8.12a-b: (a) Poincaré map in the $(J_0, \dot{J}_0)$ plane (b) Poincaré map in the $(\psi_0, \dot{\psi}_0)$ plane with $KB = 0.3$, $\epsilon k \bar{A} = 0.13$, $\alpha = 0.25$, $\nu_{\max} = 1.62$ and $\psi_0(0) = 0.865$.

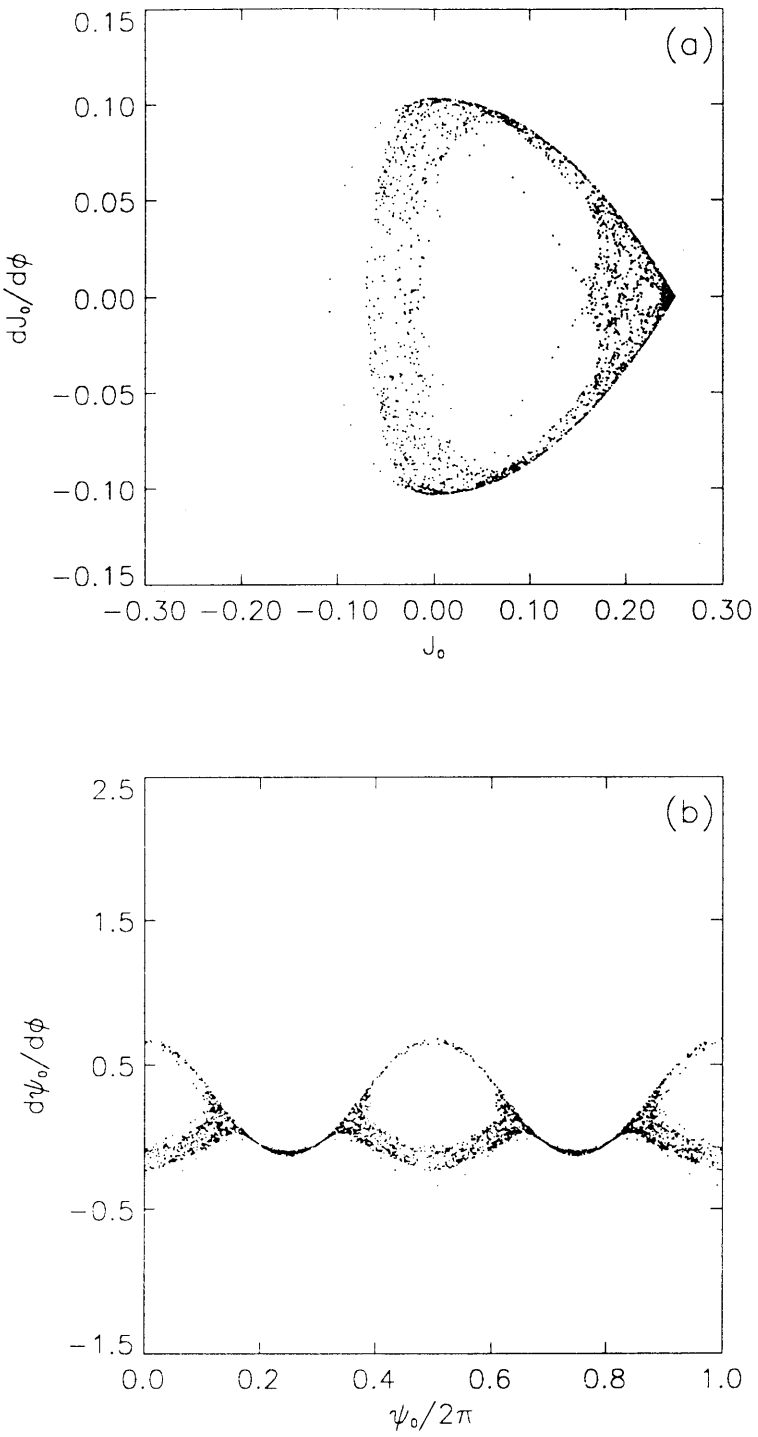

Figures II.8.13a-b: (a) Poincaré map in the $(J_0, \dot{J}_0)$ plane (b) Poincaré map in the $(\psi_0, \dot{\psi}_0)$ plane with $KB = 0.3$, $\epsilon k \bar{A} = 0.13$, $\alpha = 0.30$, $\nu_{\max} = 1.60$ and $\psi_0(0) = 0.892$.

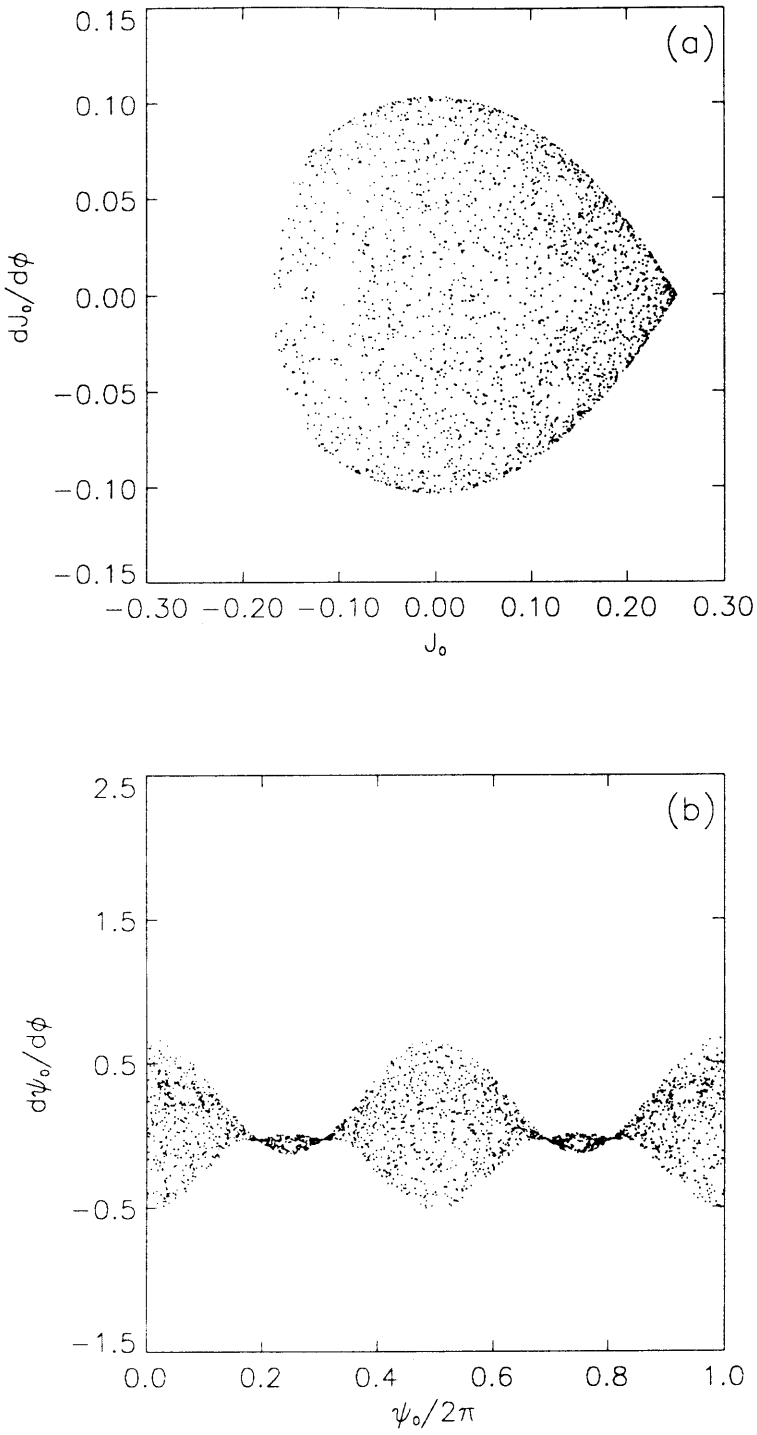

Figures II.8.14a-b: (a) Poincaré maps in the $(J_0, \dot{J}_0)$ plane (b) Poincaré map in the $(\psi_0, \dot{\psi}_0)$ plane with $KB = 0.3$, $\epsilon k \bar{A} = 0.13$, $\alpha = 0.45$, $\nu_{\max} = 1.55$ and $\psi_0(0) = 0.970$.

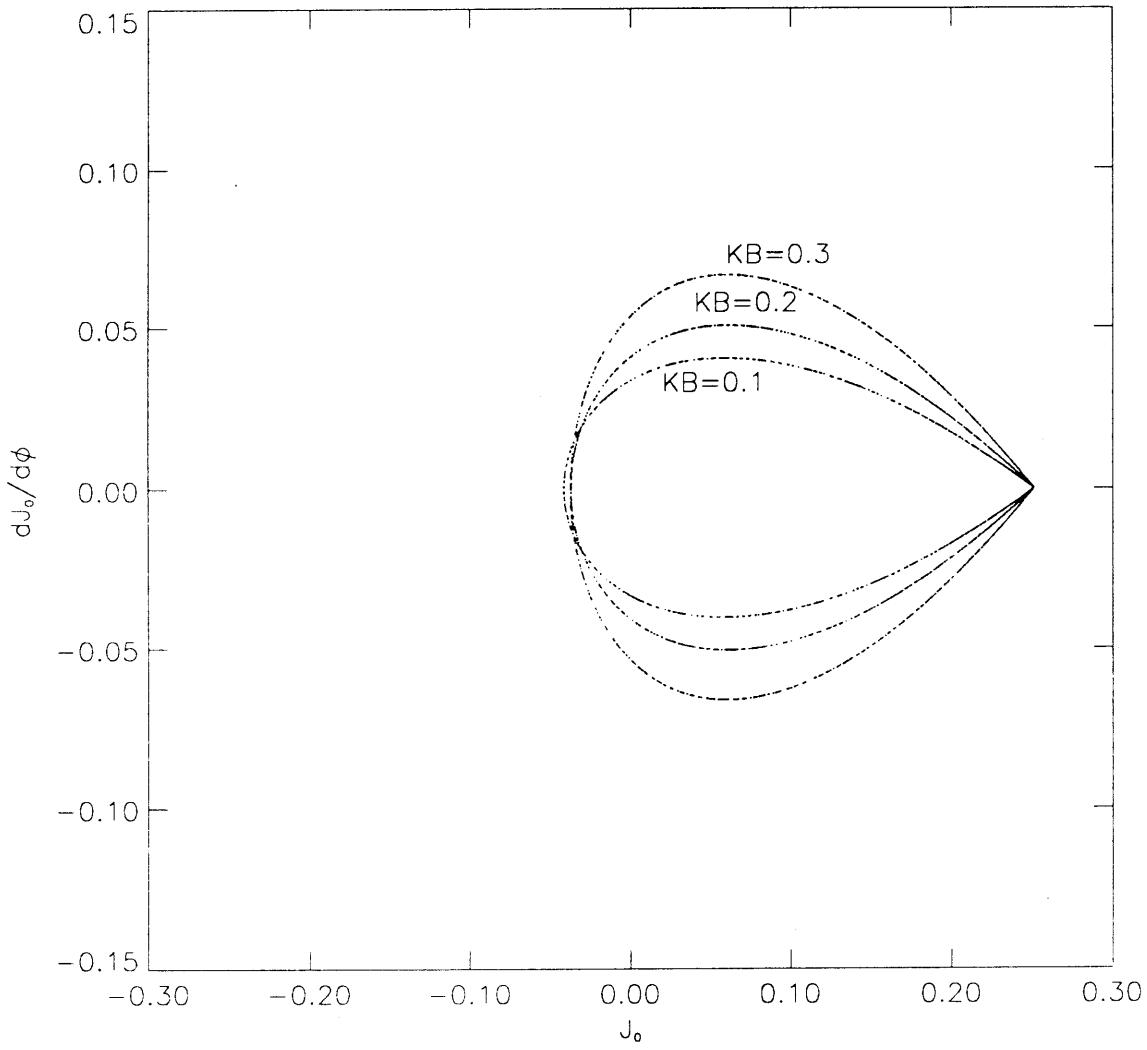

Figure II.8.16: Poincaré map in the $(J_0, \dot{J}_0)$ plane for $KB = 0.1$, 0.2 and 0.3, with $\epsilon k\overline{A} = 0.13$, $\alpha = 0.15$, $\nu = \nu_{\max}$ and $\psi_0(0) = \psi_0^u$.

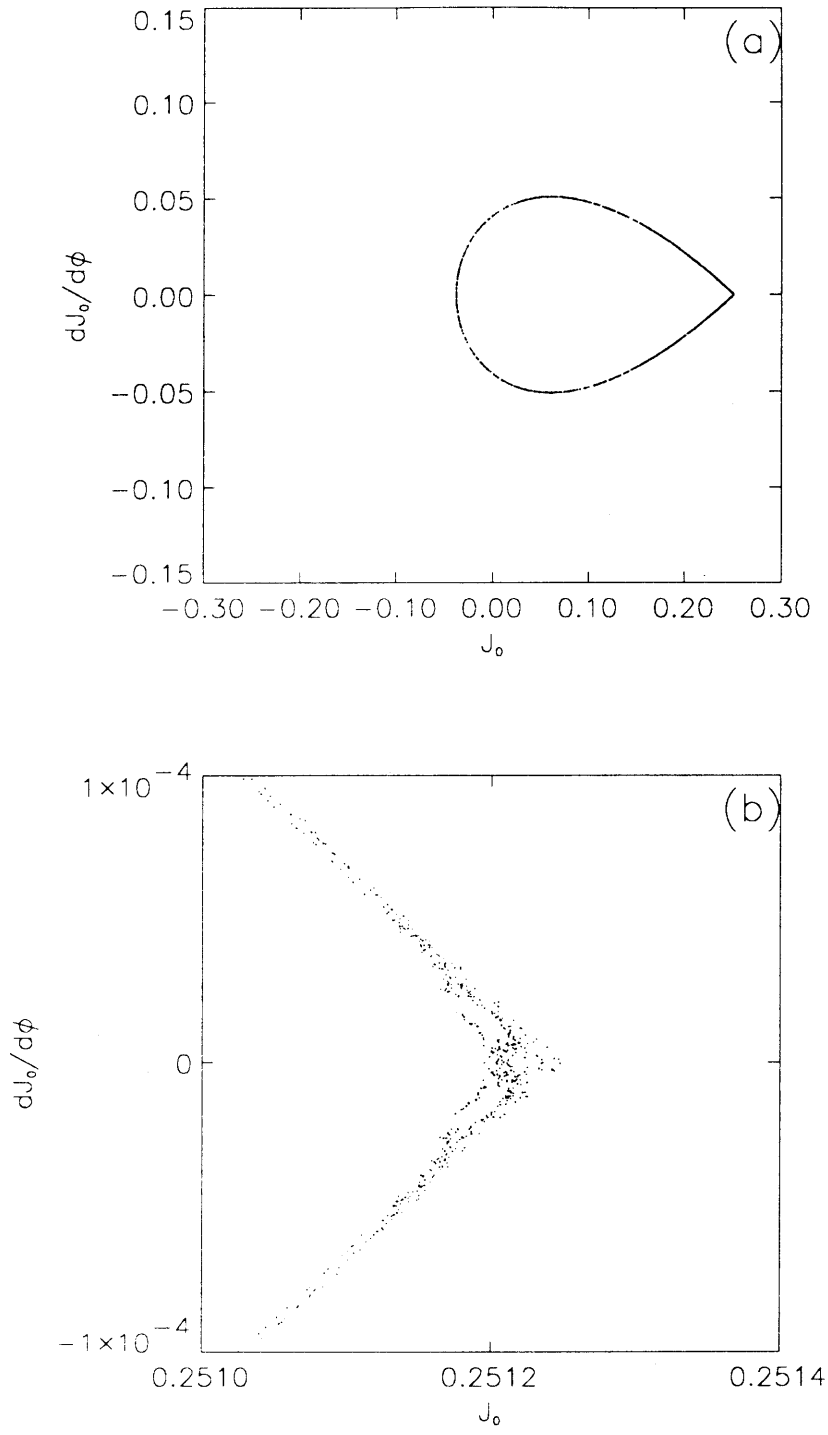

Figures II.8.17a-b: (a) Poincaré maps in the $(J_0, \dot{J}_0)$ plane (b) Detail of Poincaré map in the vicinity of corner with $K\bar{B} = 0.2$, $\epsilon k\bar{A} = 0.13$, $\alpha = 0.15$, $\nu_{\max} = 1.7$ and $\psi_0(0) = 0.811$.

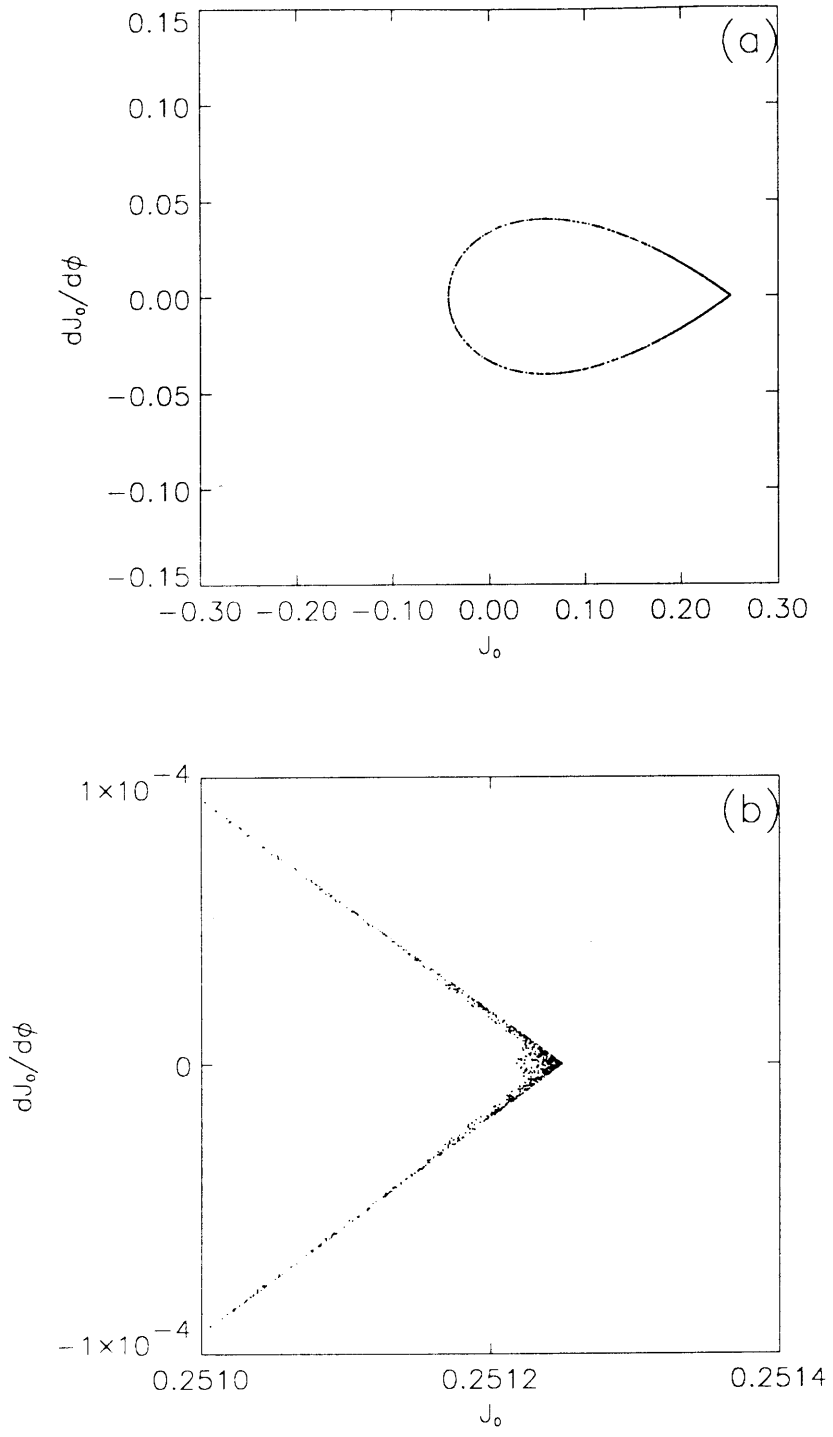

Figures II.8.18a-b: (a) Poincaré maps in the $(J_0, \dot{J}_0)$ plane (b) Detail of Poincaré map in the vicinity of corner with $KB = 0.1$, $\epsilon k\bar{A} = 0.13$, $\alpha = 0.15$, $\nu_{\max} = 1.8$ and $\psi_0(0) = 0.811$.

9. CONCLUSIONS

We have investigated the interactions of a weakly nonlinear short wave riding on a long wave of finite amplitude. The Lagrangian formulation is chosen in which the steep long waves are described by Gerstner's simple and exact solution. The evolution of the short wave amplitude is then governed by a nonlinear Schrödinger equation with time-periodic coefficients.

The linearized modulation of the short wave amplitude, wavenumber and slope is obtained analytically and compares well with the numerical theories of Longuet-Higgins(1987) and Zhang & Melville(1990). Owing to the presence of the steep long waves, the short wave train is subjected to an oscillatory gravity field $\bar{g}_{\text{eff}}$. The dispersion relation in the Eulerian frame reduces to $\sigma^2 = g_{\text{eff}} k^e$ within $\mathcal{O}(K^2 B^2)$ errors, which is consistent with the difference in vorticity between the Gerstner and Stokes wave. Examination of the absolute frequency ω shows that, for steep enough long waves, the short carrier wave and its amplitude may propagate in opposite directions. In particular, there exist blockage points where the short wave energy is reflected.

The linearized instability of a uniform short wave riding on the steep Gerstner wave is examined by Floquet theory. Owing to the oscillatory gravity field, additional bands of modulational instability arise. Their numbers, width and peak growth rate all increase with α while their position is shifted towards the main instability band. With the proliferation of instability bands, harmonics of a given sideband may become unstable. Thermalization is then possible in principle.

Owing to the nonlinearity of the short waves and to its nonlinear interactions with the long Gerstner wave, unstable disturbances interact with a uniform train of short waves regularly, with the appearance of Fermi-Pasta-Ulam recurrence for small α and, in the contrary, chaotically when α becomes moderately large. In order to assess the role played by the sideband higher harmonics, a two term Fourier series involving the uniform short wave and its sideband is adopted. Integration of the

corresponding dynamical system also shows evidence of chaos for moderately large α. We thus conclude that the presence of harmonics of the unstable sideband is not essential to triggering chaotic evolutions. We have also found that the initial phase of the disturbance is a key parameter in the long time evolution. Floquet's estimate of the initial phase leading to the most unstable situation is quite accurate. It is shown that, as α increases, so does the likelyhood of chaotic motions.

In conclusion, the periodic forcing of short waves by the uniform Gerstner wave provides a deterministic route to chaos, which may partly explain the irregular appearance of the ocean surface.

CHAPTER III: THREE-DIMENSIONAL INTERACTIONS OF WEAK SHORT WAVES AND A FINITE AMPLITUDE LONG WAVE

1. INTRODUCTION

Realistic ocean waves are rarely long crested. Instead, they usually consist of many wave components propagating in different directions. It is therefore worthwhile to investigate to what extent the conclusions of Chapter II are affected by the introduction of an angle θ of incidence. We begin in §2 by deriving the governing equations in Lagrangian variables starting from the basic principles. In particular, the equation for the evolution of vorticity is derived in Lagrangian form. A linear evolution equation for the short wave amplitude is deduced for arbitrary θ. For the nonlinear problem, the algebra is daunting. We have therefore assumed further the short waves to be slightly oblique relative to the long wave (*i.e.* $\theta \ll 1$). We then obtain in §3 a two-dimensional nonlinear Schrödinger equation with time-periodic coefficients.

The modulation of a train of linearized short waves is then examined in §4 for arbitrary θ. It is found that the amplitude is not affected significantly by the obliqueness and therefore is primarily a function of the position on the long wave profile. Both the absolute frequency and group velocity, defined respectively as the frequency and speed of propagation of the energy in a fixed frame of reference, can change sign thus implying the possibility of blocking.

In §5 the linear stability of a uniform train of short waves to two-dimensional sideband disturbances is studied. The presence of time-periodic coefficients again suggests the use of Floquet theory. The analysis of growth rates shows the proliferation of new bands of instability next to the single strip of Benney & Roskes(1969).

2. FORMULATION OF THE PROBLEM

2.1. Governing Equations

In the Lagrangian description, a particle in a three dimensional space is characterized by three parameters (a,b,c). The position of a given particle (X,Y,Z) is then a function of time only. The governing equations consist of the continuity equation

$$\frac{D(X,Y,Z)}{D(a,b,c)} \equiv \begin{vmatrix} \frac{\partial X}{\partial a} & \frac{\partial Y}{\partial a} & \frac{\partial Z}{\partial a} \\ \frac{\partial X}{\partial b} & \frac{\partial Y}{\partial b} & \frac{\partial Z}{\partial b} \\ \frac{\partial X}{\partial c} & \frac{\partial Y}{\partial c} & \frac{\partial Z}{\partial c} \end{vmatrix} = J(a,b,c) \qquad (III.2.1a)$$

and the three components of the momentum equation

$$\frac{\partial X}{\partial a}\frac{\partial^2 X}{\partial t^2} + \frac{\partial Y}{\partial a}\frac{\partial^2 Y}{\partial t^2} + \frac{\partial Z}{\partial a}(g + \frac{\partial^2 Z}{\partial t^2}) = -\frac{1}{\rho}\frac{\partial P}{\partial a} \qquad (III.2.1b)$$

$$\frac{\partial X}{\partial b}\frac{\partial^2 X}{\partial t^2} + \frac{\partial Y}{\partial b}\frac{\partial^2 Y}{\partial t^2} + \frac{\partial Z}{\partial b}(g + \frac{\partial^2 Z}{\partial t^2}) = -\frac{1}{\rho}\frac{\partial P}{\partial b} \qquad (III.2.1c)$$

and

$$\frac{\partial X}{\partial c}\frac{\partial^2 X}{\partial t^2} + \frac{\partial Y}{\partial c}\frac{\partial^2 Y}{\partial t^2} + \frac{\partial Z}{\partial c}(g + \frac{\partial^2 Z}{\partial t^2}) = -\frac{1}{\rho}\frac{\partial P}{\partial c} \qquad (III.2.1d)$$

Upon taking the curl of $(III.2.1b-d)$, the pressure P is eliminated leading to three conservation laws:

$$\frac{\partial \mathcal{U}}{\partial t} = \frac{\partial \mathcal{V}}{\partial t} = \frac{\partial \mathcal{W}}{\partial t} = 0 \qquad (III.2.2a-c)$$

where

$$\mathcal{U}(a,b,c) = \frac{\partial X}{\partial c}\frac{\partial^2 X}{\partial b \partial t} - \frac{\partial X}{\partial b}\frac{\partial^2 X}{\partial c \partial t} + \frac{\partial Y}{\partial c}\frac{\partial^2 Y}{\partial b \partial t} - \frac{\partial Y}{\partial b}\frac{\partial^2 Y}{\partial c \partial t} + \frac{\partial Z}{\partial c}\frac{\partial^2 Z}{\partial b \partial t} - \frac{\partial Z}{\partial b}\frac{\partial^2 Z}{\partial c \partial t} \qquad (III.2.3a)$$

$$\mathcal{V}(a,b,c) = \frac{\partial X}{\partial a}\frac{\partial^2 X}{\partial c \partial t} - \frac{\partial X}{\partial c}\frac{\partial^2 X}{\partial a \partial t} + \frac{\partial Y}{\partial a}\frac{\partial^2 Y}{\partial c \partial t} - \frac{\partial Y}{\partial c}\frac{\partial^2 Y}{\partial a \partial t} + \frac{\partial Z}{\partial a}\frac{\partial^2 Z}{\partial c \partial t} - \frac{\partial Z}{\partial c}\frac{\partial^2 Z}{\partial a \partial t} \qquad (III.2.3b)$$

and

$$\mathcal{W}(a,b,c) = \frac{\partial X}{\partial b}\frac{\partial^2 X}{\partial a \partial t} - \frac{\partial X}{\partial a}\frac{\partial^2 X}{\partial b \partial t} + \frac{\partial Y}{\partial b}\frac{\partial^2 Y}{\partial a \partial t} - \frac{\partial Y}{\partial a}\frac{\partial^2 Y}{\partial b \partial t} + \frac{\partial Z}{\partial b}\frac{\partial^2 Z}{\partial a \partial t} - \frac{\partial Z}{\partial a}\frac{\partial^2 Z}{\partial b \partial t} \qquad (III.2.3c)$$

and should not be confused with Eulerian velocities. It will be shown later that $(\mathcal{U},\mathcal{V},\mathcal{W})$ are related to the vorticity components.

Instead of $(III.2.1a-d)$ for (X,Y,Z,P), we adopt the following three governing equations: $(III.2.1a)$, $(III.2.2b)$ and $(III.2.2c)$ with the two definitions $(III.2.3b)$ and $(III.2.3c)$.

Since the pressure is constant on the free surface, $c = 0$, the horizontal momentum equations $(III.2.1b,c)$ yield two dynamic boundary conditions:

$$\frac{\partial X}{\partial a}\frac{\partial^2 X}{\partial t^2} + \frac{\partial Y}{\partial a}\frac{\partial^2 Y}{\partial t^2} + \frac{\partial Z}{\partial a}(g + \frac{\partial^2 Z}{\partial t^2}) = 0 \qquad c = 0 \qquad (III.2.4a)$$

$$\frac{\partial X}{\partial b}\frac{\partial^2 X}{\partial t^2} + \frac{\partial Y}{\partial b}\frac{\partial^2 Y}{\partial t^2} + \frac{\partial Z}{\partial b}(g + \frac{\partial^2 Z}{\partial t^2}) = 0 \qquad c = 0 \qquad (III.2.4b)$$

Again the Lagrangian displacements (x, y, z) are introduced according to

$$X = a + x(a,b,c,t) \qquad Y = b + y(a,b,c,t) \qquad Z = c + z(a,b,c,t) \quad (III.2.5a-c)$$

The continuity equation yields in terms of x, y and z:

$$1 + \frac{\partial x}{\partial a} + \frac{\partial y}{\partial b} + \frac{\partial z}{\partial c} +$$

$$+\frac{\partial x}{\partial a}\frac{\partial y}{\partial b} - \frac{\partial x}{\partial b}\frac{\partial y}{\partial a} + \frac{\partial x}{\partial a}\frac{\partial z}{\partial c} - \frac{\partial x}{\partial c}\frac{\partial z}{\partial a} + \frac{\partial y}{\partial b}\frac{\partial z}{\partial c} - \frac{\partial y}{\partial c}\frac{\partial z}{\partial b} +$$

$$+(\frac{\partial x}{\partial b}\frac{\partial y}{\partial c} - \frac{\partial x}{\partial c}\frac{\partial y}{\partial b})\frac{\partial z}{\partial a} + (\frac{\partial x}{\partial c}\frac{\partial y}{\partial a} - \frac{\partial x}{\partial a}\frac{\partial y}{\partial c})\frac{\partial z}{\partial b} + + (\frac{\partial x}{\partial a}\frac{\partial y}{\partial b} - \frac{\partial x}{\partial b}\frac{\partial y}{\partial a})\frac{\partial z}{\partial c} = 0 \quad (III.2.6a)$$

and the two vorticity equations become

$$\frac{\partial^3 x}{\partial c \partial t^2} - \frac{\partial^3 z}{\partial a \partial t^2} +$$

$$+\frac{\partial^3 x}{\partial c \partial t^2}\frac{\partial x}{\partial a} - \frac{\partial^3 x}{\partial a \partial t^2}\frac{\partial x}{\partial c} + \frac{\partial^3 y}{\partial c \partial t^2}\frac{\partial y}{\partial a} - \frac{\partial^3 y}{\partial a \partial t^2}\frac{\partial y}{\partial c} + \frac{\partial^3 z}{\partial c \partial t^2}\frac{\partial z}{\partial a} - \frac{\partial^3 z}{\partial a \partial t^2}\frac{\partial z}{\partial c} = 0 \qquad (III.2.6b)$$

and

$$\frac{\partial^3 x}{\partial b \partial t^2} - \frac{\partial^3 y}{\partial a \partial t^2} +$$

$$+\frac{\partial^3 x}{\partial b \partial t^2}\frac{\partial x}{\partial a} - \frac{\partial^3 x}{\partial a \partial t^2}\frac{\partial x}{\partial b} + \frac{\partial^3 y}{\partial b \partial t^2}\frac{\partial y}{\partial a} - \frac{\partial^3 y}{\partial a \partial t^2}\frac{\partial y}{\partial b} + \frac{\partial^3 z}{\partial b \partial t^2}\frac{\partial z}{\partial a} - \frac{\partial^3 z}{\partial a \partial t^2}\frac{\partial z}{\partial b} = 0 \qquad (III.2.6c)$$

Similarly, the two dynamic boundary conditions at the free surface become

$$\frac{\partial^2 x}{\partial t^2} + g\frac{\partial z}{\partial a} + \frac{\partial x}{\partial a}\frac{\partial^2 x}{\partial t^2} + \frac{\partial y}{\partial a}\frac{\partial^2 y}{\partial t^2} + \frac{\partial z}{\partial a}\frac{\partial^2 z}{\partial t^2} = 0 \qquad c = 0 \qquad (III.2.7a)$$

and

$$\frac{\partial^2 y}{\partial t^2} + g\frac{\partial z}{\partial b} + \frac{\partial x}{\partial b}\frac{\partial^2 x}{\partial t^2} + \frac{\partial y}{\partial b}\frac{\partial^2 y}{\partial t^2} + \frac{\partial z}{\partial b}\frac{\partial^2 z}{\partial t^2} = 0 \qquad c = 0 \qquad (III.2.7b)$$

Note that in the limit of colinear waves, $y = 0$ and $\frac{\partial}{\partial b} = 0$ so that $(III.2.7a)$ is trivially satisfied. We finally require that all solutions of $(III.2.6a - c)$ and $(III.2.7a - b)$ be bounded as c goes to $-\infty$.

2.2. Multiple Scale Analysis

The long and short waves are still characterized by the same wavenumber, frequency and amplitude ratios $\epsilon^2 \frac{K}{k}$, $\epsilon \frac{\Omega}{\sigma}$ and $\epsilon^3 \frac{A}{B}$ respectively. Modulation of the oblique short wave train may now occur over large ranges in all directions in the horizontal plane. We must therefore introduce yet new stretched scales in the transverse direction *i.e.*

$$(a_i, b_i, c_i, t_1) = \epsilon^i (a, b, c, t) \qquad i = 1, 2, \ldots \tag{III.2.8}$$

As in Chapter II, the long waves depend only on (a_2, c_2, t_1), while the short waves depend on all scales.

Next, the Lagrangian displacements are each expanded in a Laurent series similar to $(II.2.11a - b)$:

$$x = \frac{x_{-2}}{\epsilon^2} + \epsilon x_1 + \epsilon^2 x_2 + \epsilon^3 x_3 + \mathcal{O}(\epsilon^4) \tag{III.2.9a}$$

$$y = \epsilon y_1 + \epsilon^2 y_2 + \epsilon^3 y_3 + \mathcal{O}(\epsilon^4) \tag{III.2.9b}$$

$$z = \frac{z_{-2}}{\epsilon^2} + \epsilon z_1 + \epsilon^2 z_2 + \epsilon^3 z_3 + \mathcal{O}(\epsilon^4) \tag{III.2.9c}$$

Note that Gerstner's wave is long crested and therefore does not contribute to the transverse displacement y. Eqs. $(III.2.5a - c)$ and $(III.2.9a - c)$ may be combined to give

$$X = a + \frac{x_{-2}}{\epsilon^2} + \epsilon x_1 + \epsilon^2 x_2 + \epsilon^3 x_3 + \mathcal{O}(\epsilon^4) \tag{III.2.10a}$$

$$Y = b + \epsilon y_1 + \epsilon^2 y_2 + \epsilon^3 y_3 + \mathcal{O}(\epsilon^4) \tag{III.2.10b}$$

$$Z = c + \frac{z_{-2}}{\epsilon^2} + \epsilon z_1 + \epsilon^2 z_2 + \epsilon^3 z_3 + \mathcal{O}(\epsilon^4) \tag{III.2.10c}$$

Eqs. $(III.2.10a - c)$ define a mapping between the Eulerian and Lagrangian variables. Upon substituting $(III.2.9a - c)$ in $(III.2.6a - c)$ and $(III.2.7a - b)$ and separating the contributions at each order of ϵ, we obtain the following cascade of governing equations:

At $\mathcal{O}(1)$:

Continuity:

$$1 + \frac{\partial x_{-2}}{\partial a_2} + \frac{\partial z_{-2}}{\partial c_2} + \frac{\partial x_{-2}}{\partial a_2}\frac{\partial z_{-2}}{\partial c_2} - \frac{\partial x_{-2}}{\partial c_2}\frac{\partial z_{-2}}{\partial a_2} = J \qquad (III.2.11a)$$

All three vorticity equations do not contribute at $\mathcal{O}(1)$.

Free surface boundary condition 1:

$$\frac{\partial^2 x_{-2}}{\partial t_1^2} + g\frac{\partial z_{-2}}{\partial a_2} + \frac{\partial x_{-2}}{\partial a_2}\frac{\partial^2 x_{-2}}{\partial t_1^2} + \frac{\partial z_{-2}}{\partial a_2}\frac{\partial^2 z_{-2}}{\partial t_1^2} = 0 \qquad c = 0 \qquad (III.2.11b)$$

The second free surface boundary condition does not contribute at this order either.

At $\mathcal{O}(\epsilon)$:

Continuity:

$$\frac{\partial x_1}{\partial a} + \frac{\partial y_1}{\partial b} + \frac{\partial z_1}{\partial c} +$$
$$+\frac{\partial z_{-2}}{\partial c_2}\frac{\partial x_1}{\partial a} + \frac{\partial x_{-2}}{\partial a_2}\frac{\partial y_1}{\partial b} + \frac{\partial z_{-2}}{\partial c_2}\frac{\partial y_1}{\partial b} + \frac{\partial x_{-2}}{\partial a_2}\frac{\partial z_1}{\partial c} - \frac{\partial z_{-2}}{\partial a_2}\frac{\partial x_1}{\partial c} - \frac{\partial x_{-2}}{\partial c_2}\frac{\partial z_1}{\partial a} +$$
$$+\frac{\partial x_{-2}}{\partial a_2}\frac{\partial z_{-2}}{\partial c_2}\frac{\partial y_1}{\partial b} - \frac{\partial x_{-2}}{\partial c_2}\frac{\partial z_{-2}}{\partial a_2}\frac{\partial y_1}{\partial b} = 0 \qquad (III.2.12a)$$

Y-vorticity equation:

$$\frac{\partial^3 x_1}{\partial c \partial t^2} - \frac{\partial^3 z_1}{\partial a \partial t^2} + \frac{\partial x_{-2}}{\partial a_2}\frac{\partial^3 x_1}{\partial c \partial t^2} - \frac{\partial x_{-2}}{\partial c_2}\frac{\partial^3 x_1}{\partial a \partial t^2} + \frac{\partial z_{-2}}{\partial a_2}\frac{\partial^3 z_1}{\partial c \partial t^2} - \frac{\partial z_{-2}}{\partial c_2}\frac{\partial^3 z_1}{\partial a \partial t^2} = 0 \qquad (III.2.12b)$$

Z-vorticity equation:

$$\frac{\partial^3 x_1}{\partial b \partial t^2} - \frac{\partial^3 y_1}{\partial a \partial t^2} + \frac{\partial x_{-2}}{\partial a_2}\frac{\partial^3 x_1}{\partial b \partial t^2} + \frac{\partial z_{-2}}{\partial a_2}\frac{\partial^3 z_1}{\partial b \partial t^2} = 0 \qquad (III.2.12c)$$

Free surface boundary condition 1:

$$\frac{\partial^2 x_1}{\partial t^2} + g\frac{\partial z_1}{\partial a} + \frac{\partial x_{-2}}{\partial a_2}\frac{\partial^2 x_1}{\partial t^2} + \frac{\partial^2 x_{-2}}{\partial {t_1}^2}\frac{\partial x_1}{\partial a} + \frac{\partial z_{-2}}{\partial a_2}\frac{\partial^2 z_1}{\partial t^2} + \frac{\partial^2 z_{-2}}{\partial {t_1}^2}\frac{\partial z_1}{\partial a} = 0 \quad c = 0 \qquad (III.2.13a)$$

Free surface boundary condition 2:

$$\frac{\partial^2 y_1}{\partial t^2} + g\frac{\partial z_1}{\partial b} + \frac{\partial^2 x_{-2}}{\partial {t_1}^2}\frac{\partial x_1}{\partial b} + \frac{\partial^2 z_{-2}}{\partial {t_1}^2}\frac{\partial z_1}{\partial b} = 0 \quad c = 0 \qquad (III.2.13b)$$

At $\mathcal{O}(\epsilon^2)$:

Continuity:

$$\frac{\partial x_2}{\partial a}+\frac{\partial y_2}{\partial b}+\frac{\partial z_2}{\partial c}+\frac{\partial x_1}{\partial a_1}+\frac{\partial y_1}{\partial b_1}+\frac{\partial z_1}{\partial c_1}+$$
$$+\frac{\partial z_{-2}}{\partial c_2}\frac{\partial x_2}{\partial a}-\frac{\partial z_{-2}}{\partial a_2}\frac{\partial x_2}{\partial c}+\frac{\partial z_{-2}}{\partial c_2}\frac{\partial y_2}{\partial b}+\frac{\partial x_{-2}}{\partial a_2}\frac{\partial y_2}{\partial b}+\frac{\partial x_{-2}}{\partial a_2}\frac{\partial z_2}{\partial c}-\frac{\partial x_{-2}}{\partial c_2}\frac{\partial z_2}{\partial a}+$$
$$+\frac{\partial z_{-2}}{\partial c_2}\frac{\partial x_1}{\partial a_1}-\frac{\partial z_{-2}}{\partial a_2}\frac{\partial x_1}{\partial c_1}+\frac{\partial z_{-2}}{\partial c_2}\frac{\partial y_1}{\partial b_1}+\frac{\partial x_{-2}}{\partial a_2}\frac{\partial y_1}{\partial b_1}+\frac{\partial x_{-2}}{\partial a_2}\frac{\partial z_1}{\partial c_1}-\frac{\partial x_{-2}}{\partial c_2}\frac{\partial z_1}{\partial a_1}+$$
$$+\frac{\partial x_1}{\partial a}\frac{\partial z_1}{\partial c}-\frac{\partial x_1}{\partial c}\frac{\partial z_1}{\partial a}+\frac{\partial x_1}{\partial a}\frac{\partial y_1}{\partial b}-\frac{\partial x_1}{\partial b}\frac{\partial y_1}{\partial a}+\frac{\partial y_1}{\partial b}\frac{\partial z_1}{\partial c}-\frac{\partial y_1}{\partial c}\frac{\partial z_1}{\partial b}+$$
$$+\frac{\partial x_{-2}}{\partial a_2}\frac{\partial z_{-2}}{\partial c_2}\frac{\partial y_2}{\partial b}-\frac{\partial x_{-2}}{\partial c_2}\frac{\partial z_{-2}}{\partial a_2}\frac{\partial y_2}{\partial b}+\frac{\partial x_{-2}}{\partial a_2}\frac{\partial z_{-2}}{\partial c_2}\frac{\partial y_1}{\partial b_1}-\frac{\partial x_{-2}}{\partial c_2}\frac{\partial z_{-2}}{\partial a_2}\frac{\partial y_1}{\partial b_1}+$$
$$+\frac{\partial z_{-2}}{\partial a_2}\frac{\partial x_1}{\partial b}\frac{\partial y_1}{\partial c}-\frac{\partial z_{-2}}{\partial a_2}\frac{\partial x_1}{\partial c}\frac{\partial y_1}{\partial b}+\frac{\partial z_{-2}}{\partial c_2}\frac{\partial x_1}{\partial a}\frac{\partial y_1}{\partial b}-\frac{\partial z_{-2}}{\partial c_2}\frac{\partial x_1}{\partial b}\frac{\partial y_1}{\partial a}+$$
$$+\frac{\partial x_{-2}}{\partial a_2}\frac{\partial y_1}{\partial b}\frac{\partial z_1}{\partial c}-\frac{\partial x_{-2}}{\partial a_2}\frac{\partial y_1}{\partial c}\frac{\partial z_1}{\partial b}+\frac{\partial x_{-2}}{\partial c_2}\frac{\partial y_1}{\partial a}\frac{\partial z_1}{\partial b}-\frac{\partial x_{-2}}{\partial c_2}\frac{\partial y_1}{\partial b}\frac{\partial z_1}{\partial a}=0 \quad (III.2.14a)$$

Y-vorticity equation:

$$\frac{\partial^3 x_2}{\partial c\partial t^2}-\frac{\partial^3 z_2}{\partial a\partial t^2}+\frac{\partial^3 x_1}{\partial c_1\partial t^2}+2\frac{\partial^3 x_1}{\partial c\partial t\partial t_1}-\frac{\partial^3 z_1}{\partial a_1\partial t^2}-2\frac{\partial^3 z_1}{\partial a\partial t\partial t_1}+$$
$$+\frac{\partial^3 x_{-2}}{\partial c_2\partial {t_1}^2}-\frac{\partial^3 z_{-2}}{\partial a_2\partial {t_1}^2}+\frac{\partial x_{-2}}{\partial a_2}\frac{\partial^3 x_{-2}}{\partial c_2\partial {t_1}^2}-\frac{\partial^3 x_{-2}}{\partial a_2\partial {t_1}^2}\frac{\partial x_{-2}}{\partial c_2}+\frac{\partial z_{-2}}{\partial a_2}\frac{\partial^3 z_{-2}}{\partial c_2\partial {t_1}^2}+$$
$$-\frac{\partial^3 z_{-2}}{\partial a_2\partial {t_1}^2}\frac{\partial z_{-2}}{\partial c_2}+\frac{\partial x_{-2}}{\partial a_2}\frac{\partial^3 x_2}{\partial c\partial t^2}-\frac{\partial x_{-2}}{\partial c_2}\frac{\partial^3 x_2}{\partial a\partial t^2}+\frac{\partial z_{-2}}{\partial a_2}\frac{\partial^3 z_2}{\partial c\partial t^2}-\frac{\partial z_{-2}}{\partial c_2}\frac{\partial^3 z_2}{\partial a\partial t^2}+$$
$$+\frac{\partial x_{-2}}{\partial a_2}\frac{\partial^3 x_1}{\partial c_1\partial t^2}+2\frac{\partial x_{-2}}{\partial a_2}\frac{\partial^3 x_1}{\partial c\partial t\partial t_1}-\frac{\partial x_{-2}}{\partial c_2}\frac{\partial^3 x_1}{\partial a_1\partial t^2}-2\frac{\partial x_{-2}}{\partial c_2}\frac{\partial^3 x_1}{\partial a\partial t\partial t_1}+$$
$$+\frac{\partial z_{-2}}{\partial a_2}\frac{\partial^3 z_1}{\partial c_1\partial t^2}+2\frac{\partial z_{-2}}{\partial a_2}\frac{\partial^3 z_1}{\partial c\partial t\partial t_1}-\frac{\partial z_{-2}}{\partial c_2}\frac{\partial^3 z_1}{\partial a_1\partial t^2}-2\frac{\partial z_{-2}}{\partial c_2}\frac{\partial^3 z_1}{\partial a\partial t\partial t_1}+$$
$$+\frac{\partial x_1}{\partial a}\frac{\partial^3 x_1}{\partial c\partial t^2}-\frac{\partial^3 x_1}{\partial a\partial t^2}\frac{\partial x_1}{\partial c}+\frac{\partial y_1}{\partial a}\frac{\partial^3 y_1}{\partial c\partial t^2}-\frac{\partial^3 y_1}{\partial a\partial t^2}\frac{\partial y_1}{\partial c}+\frac{\partial z_1}{\partial a}\frac{\partial^3 z_1}{\partial c\partial t^2}-\frac{\partial^3 z_1}{\partial a\partial t^2}\frac{\partial z_1}{\partial c}=0 \quad (III.2.14b)$$

Z-vorticity equation:

$$\frac{\partial^3 x_2}{\partial b\partial t^2}-\frac{\partial^3 y_2}{\partial a\partial t^2}+\frac{\partial^3 x_1}{\partial b_1\partial t^2}+2\frac{\partial^3 x_1}{\partial b\partial t\partial t_1}-\frac{\partial^3 y_1}{\partial a_1\partial t^2}-2\frac{\partial^3 y_1}{\partial a\partial t\partial t_1}+$$

$$+\frac{\partial x_{-2}}{\partial a_2}\frac{\partial^3 x_2}{\partial b\partial t^2}+\frac{\partial z_{-2}}{\partial a_2}\frac{\partial^3 z_2}{\partial b\partial t^2}+\frac{\partial x_{-2}}{\partial a_2}\frac{\partial^3 x_1}{\partial b_1\partial t^2}+2\frac{\partial x_{-2}}{\partial a_2}\frac{\partial^3 x_1}{\partial b\partial t\partial t_1}+$$

$$+\frac{\partial z_{-2}}{\partial a_2}\frac{\partial^3 z_1}{\partial b_1\partial t^2}+2\frac{\partial z_{-2}}{\partial a_2}\frac{\partial^3 z_1}{\partial b\partial t\partial t_1}+\frac{\partial x_1}{\partial a}\frac{\partial^3 x_1}{\partial b\partial t^2}-\frac{\partial^3 x_1}{\partial a\partial t^2}\frac{\partial x_1}{\partial b}+$$

$$+\frac{\partial y_1}{\partial a}\frac{\partial^3 y_1}{\partial b\partial t^2}-\frac{\partial^3 y_1}{\partial a\partial t^2}\frac{\partial y_1}{\partial b}+\frac{\partial z_1}{\partial a}\frac{\partial^3 z_1}{\partial b\partial t^2}-\frac{\partial^3 z_1}{\partial a\partial t^2}\frac{\partial z_1}{\partial b}=0 \qquad (III.2.14c)$$

Free surface boundary condition 1:

$$\frac{\partial^2 x_2}{\partial t^2}+g\frac{\partial z_2}{\partial a}+2\frac{\partial^2 x_1}{\partial t\partial t_1}+g\frac{\partial z_1}{\partial a_1}+$$

$$+\frac{\partial x_{-2}}{\partial a_2}\frac{\partial^2 x_2}{\partial t^2}+\frac{\partial^2 z_{-2}}{\partial {t_1}^2}\frac{\partial z_2}{\partial a}+\frac{\partial^2 x_{-2}}{\partial {t_1}^2}\frac{\partial x_2}{\partial a}+\frac{\partial z_{-2}}{\partial a_2}\frac{\partial^2 z_2}{\partial t^2}+$$

$$+2\frac{\partial x_{-2}}{\partial a_2}\frac{\partial^2 x_1}{\partial t\partial t_1}+\frac{\partial^2 x_{-2}}{\partial {t_1}^2}\frac{\partial x_1}{\partial a_1}+\frac{\partial^2 z_{-2}}{\partial {t_1}^2}\frac{\partial z_1}{\partial a_1}+2\frac{\partial z_{-2}}{\partial a_2}\frac{\partial^2 z_1}{\partial t\partial t_1}+$$

$$+\frac{\partial x_1}{\partial a}\frac{\partial^2 x_1}{\partial t^2}+\frac{\partial y_1}{\partial a}\frac{\partial^2 y_1}{\partial t^2}+\frac{\partial z_1}{\partial a}\frac{\partial^2 z_1}{\partial t^2}=0 \qquad c=0 \qquad (III.2.15a)$$

Free surface boundary condition 2:

$$\frac{\partial^2 y_2}{\partial t^2}+g\frac{\partial z_2}{\partial b}+2\frac{\partial^2 y_1}{\partial t\partial t_1}+g\frac{\partial z_1}{\partial b_1}+$$

$$+\frac{\partial^2 x_{-2}}{\partial {t_1}^2}\frac{\partial x_2}{\partial b}+\frac{\partial^2 z_{-2}}{\partial {t_1}^2}\frac{\partial z_2}{\partial b}+\frac{\partial^2 x_{-2}}{\partial {t_1}^2}\frac{\partial x_1}{\partial b_1}+\frac{\partial^2 z_{-2}}{\partial {t_1}^2}\frac{\partial z_1}{\partial b_1}+$$

$$+\frac{\partial x_1}{\partial b}\frac{\partial^2 x_1}{\partial t^2}+\frac{\partial y_1}{\partial b}\frac{\partial^2 y_1}{\partial t^2}+\frac{\partial z_1}{\partial b}\frac{\partial^2 z_1}{\partial t^2}=0 \qquad c=0 \qquad (III.2.15b)$$

We omit here the $\mathcal{O}(\epsilon^3)$ equations for brevity and list them in Appendix H.

2.3. Remarks on Vorticity

We have shown in Chapter II that the vorticity field, although non-uniform in space, was constant in time and associated solely with Gerstner's wave. To examine the status of a three-dimensional motion, we have derived the general expression of the vorticity vector ϖ in terms of Lagrangian coordinates (cf. Appendix I). Specifically, its components ϖ^X, ϖ^Y and ϖ^Z are related to $\mathcal{U}$, $\mathcal{V}$, $\mathcal{W}$ by

$$\varpi=\frac{1}{J}L\Lambda \qquad (III.2.16a)$$

where

$$\varpi = \begin{pmatrix} \varpi^X \\ \varpi^Y \\ \varpi^Z \end{pmatrix} \qquad L = \begin{pmatrix} \frac{\partial X}{\partial a} & \frac{\partial X}{\partial b} & \frac{\partial X}{\partial c} \\ \frac{\partial Y}{\partial a} & \frac{\partial Y}{\partial b} & \frac{\partial Y}{\partial c} \\ \frac{\partial Z}{\partial a} & \frac{\partial Z}{\partial b} & \frac{\partial Z}{\partial c} \end{pmatrix} \qquad \Lambda = \begin{pmatrix} \mathcal{U}(a,b,c) \\ \mathcal{V}(a,b,c) \\ \mathcal{W}(a,b,c) \end{pmatrix} \tag{III.2.16b-d}$$

Note that $J \neq 0$ is exactly the determinant of L. The conservation of Λ is thus equivalent to

$$\frac{\partial \mathcal{U}}{\partial t} = J\frac{\partial}{\partial t}\{\frac{\partial a}{\partial X}\varpi^X + \frac{\partial b}{\partial X}\varpi^Y + \frac{\partial c}{\partial X}\varpi^Z\} = 0 \tag{III.2.17a}$$

$$\frac{\partial \mathcal{V}}{\partial t} = J\frac{\partial}{\partial t}\{\frac{\partial a}{\partial Y}\varpi^X + \frac{\partial b}{\partial Y}\varpi^Y + \frac{\partial c}{\partial Y}\varpi^Z\} = 0 \tag{III.2.17b}$$

$$\frac{\partial \mathcal{W}}{\partial t} = J\frac{\partial}{\partial t}\{\frac{\partial a}{\partial Z}\varpi^X + \frac{\partial b}{\partial Z}\varpi^Y + \frac{\partial c}{\partial Z}\varpi^Z\} = 0 \tag{III.2.17c}$$

In the limit of a two-dimensional motion in the (X, Z) plane, $\varpi^X = \varpi^Z = 0$ and $\frac{\partial b}{\partial X} = \frac{\partial b}{\partial Z} = 0$, $(III.2.17a-c)$ reduce to

$$\frac{\partial v}{\partial t} = \frac{\partial}{\partial t}(J\frac{\partial b}{\partial Y}\varpi^Y) = \frac{\partial}{\partial t}(J\varpi^Y) = \frac{\partial}{\partial t}\left[(\frac{\partial X}{\partial a}\frac{\partial Z}{\partial c} - \frac{\partial X}{\partial c}\frac{\partial Z}{\partial a})\varpi^Y\right] = 0 \tag{III.2.18a}$$

after making use of eq. $(7b)$ in Appendix I. Since the Jacobian in a two-dimensional motion is independent of time, we get

$$\frac{\partial \varpi^Y}{\partial t} = 0 \tag{III.2.18b}$$

Thus, the vorticity field is conserved only for two-dimensional motions. In the three-dimensional case, we take the time derivative of $(III.2.16a)$ and obtain

$$\frac{\partial \varpi}{\partial t} = \frac{1}{J}\begin{pmatrix} \frac{\partial^2 X}{\partial a \partial t} & \frac{\partial^2 X}{\partial b \partial t} & \frac{\partial^2 X}{\partial c \partial t} \\ \frac{\partial^2 Y}{\partial a \partial t} & \frac{\partial^2 Y}{\partial b \partial t} & \frac{\partial^2 Y}{\partial c \partial t} \\ \frac{\partial^2 Z}{\partial a \partial t} & \frac{\partial^2 Z}{\partial b \partial t} & \frac{\partial^2 Z}{\partial c \partial t} \end{pmatrix} \Lambda \tag{III.2.19}$$

since both J and Λ are conserved. We prove in Appendix J that $(III.2.19)$ is equivalent to the well known vorticity evolution equation

$$\frac{\partial \varpi}{\partial t} = \varpi.\nabla \mathbf{U} \tag{III.2.20}$$

where $\frac{\partial}{\partial t}$ and $\mathbf{U}$ stand for the Lagrangian time derivative and the Eulerian velocity vector respectively. Therefore, in the presence of the steady vorticity field of the

long Gerstner wave, a non colinear train of short waves will generate an unsteady vorticity field.

To analyse the contributions to the vorticity at each order, we introduce perturbations series for ϖ, L and Λ:

$$\varpi = \epsilon\varpi_1 + \epsilon^2\varpi_2 + \epsilon^3\varpi_3 + \mathcal{O}(\epsilon^4) \qquad (III.2.21a)$$

$$L = L_0 + \epsilon L_1 + \epsilon L_2 + \mathcal{O}(\epsilon^3) \qquad (III.2.21b)$$

and

$$\Lambda = \epsilon\Lambda_1 + \epsilon^2\Lambda_2 + \epsilon^3\Lambda_3 + \mathcal{O}(\epsilon^4) \qquad (III.2.21c)$$

Note that the leading order vorticity is $\mathcal{O}(\epsilon)$. The conservation equations $(III.2.2a-c)$ lead to respectively at $\mathcal{O}(\epsilon)$, $\mathcal{O}(\epsilon^2)$ and $\mathcal{O}(\epsilon^3)$

$$\frac{\partial\Lambda_1}{\partial t} = 0 \qquad \frac{\partial\Lambda_2}{\partial t} + \frac{\partial\Lambda_1}{\partial t_1} = 0 \qquad \frac{\partial\Lambda_3}{\partial t} + \frac{\partial\Lambda_2}{\partial t_1} + \frac{\partial\Lambda_1}{\partial t_2} = 0 \qquad (III.2.22a-c)$$

at $\mathcal{O}(\epsilon)$, $\mathcal{O}(\epsilon^2)$ and $\mathcal{O}(\epsilon^3)$. Similarly, substitution of $(III.2.21a-c)$ in $(III.2.16a)$ yields at $\mathcal{O}(\epsilon)$, $\mathcal{O}(\epsilon^2)$ and $\mathcal{O}(\epsilon^3)$ the following sequence of definitions

$$J\varpi_1 = L_0\Lambda_1 \qquad J\varpi_2 = L_0\Lambda_2 + L_1\Lambda_1 \qquad (III.2.23a-b)$$

$$J\varpi_3 = L_0\Lambda_3 + L_1\Lambda_2 + L_2\Lambda_1 \qquad (III.2.23c)$$

From the definition $(III.2.16c)$ of L and $(III.2.10a-c)$, we deduce

$$L_0 = \begin{pmatrix} 1+\frac{\partial x_{-2}}{\partial a_2} & 0 & \frac{\partial x_{-2}}{\partial c_2} \\ 0 & 1 & 0 \\ \frac{\partial z_{-2}}{\partial a_2} & 0 & 1+\frac{\partial z_{-2}}{\partial c_2} \end{pmatrix} \qquad L_1 = \begin{pmatrix} \frac{\partial x_1}{\partial a} & \frac{\partial x_1}{\partial b} & \frac{\partial x_1}{\partial c} \\ \frac{\partial y_1}{\partial a} & \frac{\partial y_1}{\partial b} & \frac{\partial y_1}{\partial c} \\ \frac{\partial z_1}{\partial a} & \frac{\partial z_1}{\partial b} & \frac{\partial z_1}{\partial c} \end{pmatrix} \quad (III.2.24a-b)$$

These equations will be analysed in the next section once the solution for the first harmonic short wave displacements at $\mathcal{O}(\epsilon)$ is determined.

3. EVOLUTION EQUATIONS FOR NARROW BANDED OBLIQUELY INCIDENT SHORT WAVES

Let us recall for convenience the expression of Gerstner's wave

$$x_{-2} = Be^{Kc_2}\sin\phi \qquad z_{-2} = Be^{Kc_2}\cos\phi \qquad (III.3.1a-b)$$

where

$$\phi \equiv \Omega t_1 - Ka_2 \qquad \Omega^2 = gK \qquad (III.3.1c-d)$$

represent respectively the Lagrangian phase and dispersion relation.

3.1. Short Waves at the Leading Order

3.1.1. *The first harmonic*

The governing equations for the short waves at the leading order are given by $(III.2.12a-c)$ and $(III.2.13a-b)$. We seek a solution in the form:

$$\begin{pmatrix} x_1 \\ y_1 \\ z_1 \end{pmatrix} = \frac{1}{2}\begin{pmatrix} ix_{11} \\ iy_{11} \\ z_{11} \end{pmatrix} e^{iS} + (*) \qquad (III.3.2)$$

where x_{11}, y_{11} and z_{11} are functions of c and S is the Lagrangian phase function. As is customary in WKB theory, the wavenumber k and frequency σ are given in terms of S as

$$k\cos\theta = \frac{\partial S}{\partial a} \qquad k\sin\theta = \frac{\partial S}{\partial b} \qquad \sigma = -\frac{\partial S}{\partial t} \qquad (III.3.3a-c)$$

where θ is the incidence angle with respect to the direction of propagation of Gerstner's wave. Substitution of $(III.3.2)$ in $(III.2.12a-c)$ yields

$$-iKB\sin\phi\frac{\partial x_{11}}{\partial c} + (1 - KB\cos\phi)\frac{\partial z_{11}}{\partial c} = k(1 + KB\cos\phi)\cos\theta\ x_{11} +$$

$$+k(1 - K^2B^2)\sin\theta\ y_{11} + ikKB\sin\phi\cos\theta\ z_{11} \qquad (III.3.4a)$$

for continuity. The Y-vorticity equation yields

$$(1 - KB\cos\phi)\frac{\partial x_{11}}{\partial c} - iKB\sin\phi\frac{\partial z_{11}}{\partial c} = ikKB\sin\phi\cos\theta\ x_{11} +$$

$$+k(1 + KB\cos\phi)\cos\theta\ z_{11} \qquad (III.3.4b)$$

while the Z-vorticity equation becomes

$$-i(1 - KB\cos\phi)\sin\theta\ x_{11} + i\cos\theta\ y_{11} - KB\sin\phi\sin\theta\ z_{11} = 0 \qquad (III.3.4c)$$

From $(III.3.4c)$, y_{11} may be expressed in terms of x_{11} and z_{11} and then eliminated from $(III.3.4a)$ to yield the following matrix ordinary differential system:

$$M\frac{\partial U}{\partial c} = kNU \qquad (III.3.5)$$

where $U \equiv [x_{11}, z_{11}]^T$, M and N are two 2×2 matrices

$$M = \begin{pmatrix} -iKB\sin\phi & 1 - KB\cos\phi \\ 1 - KB\cos\phi & -iKB\sin\phi \end{pmatrix} \qquad (III.3.6)$$

and $N = (n_{ij})$ with

$$n_{11} = (1 + KB\cos\phi)\cos\theta + (1 - K^2B^2)(1 - KB\cos\phi)\frac{\sin^2\theta}{\cos\theta}$$

$$n_{12} = iKB\sin\phi\cos\theta - i(1 - K^2B^2)KB\sin\phi\frac{\sin^2\theta}{\cos\theta}$$

$$n_{21} = iKB\sin\phi\cos\theta \qquad n_{22} = (1 + KB\cos\phi)\cos\theta \qquad (III.3.7a - d)$$

To solve the homogeneous problem defined by $(III.3.5)$, we first seek the eigenvalues κ satisfying

$$\det(\kappa M - kN) = 0 \qquad (III.3.8)$$

The two solutions are readily found

$$\kappa^{\pm} = k\frac{\pm R(1 - K^2B^2) + 2iKB\sin\phi\cos\theta}{1 + K^2B^2 - 2KB\cos\phi} \equiv \pm\kappa_r + i\kappa_i \qquad (III.3.9a - b)$$

where

$$R = R(\phi, \theta) = \sqrt{1 + (K^2B^2 - 2KB\cos\phi)\sin^2\theta} \qquad (III.3.9c)$$

The two eigenvector, $U^{\pm}$, associated with $\kappa^{\pm}$ are

$$U^{+} = \begin{pmatrix} \mathcal{S}_x \\ 1 \end{pmatrix} \qquad U^{-} = \begin{pmatrix} \mathcal{S}_x^* \\ -1 \end{pmatrix} \qquad (III.3.10a - b)$$

where the superscript "$*$" refers to the complex conjugate and

$$\mathcal{S}_x = \frac{(1 - KB\cos\phi)\cos\theta + iRKB\sin\phi}{R(1 - KB\cos\phi) + iKB\sin\phi\cos\theta} \qquad (III.3.10c)$$

From $(III.3.4a)$, the transverse displacements corresponding to eigenmodes $U^{\pm}$ are found to be $\mathcal{S}_y$ and $\mathcal{S}_y^*$ respectively with

$$\mathcal{S}_y = \frac{(1 + K^2B^2 - 2KB\cos\phi)\sin\theta}{R(1 - KB\cos\phi) + iKB\sin\phi\cos\theta} \qquad (III.3.10d)$$

It is easily shown that $\mathcal{S}_x^2 + \mathcal{S}_y^2 = 1$. Note that in the limit of normal incidence, $\theta = 0$, $R = 1$; the eigenvalues $(III.3.9a - b)$ reduce to $(II.4.5)$ and the eigenvectors $U^{\pm}$ to $[1, \pm 1]^T$ in agreement with the results of Chapter II.

For boundedness at $c \to -\infty$, the eigenmode U^- must be discarded from the solution at this order.

3.1.2. *The dispersion relation*

We need now apply the two boundary conditions on the free surface

$$\Big[\frac{\sigma^2}{gk}(1 - KB\cos\phi) + iKB\sin\phi\cos\theta\Big]x_{11} +$$

$$-\big[(1 - KB\cos\phi)\cos\theta + i\frac{\sigma^2}{gk}KB\sin\phi\big]z_{11} = 0 \qquad c = 0 \qquad (III.3.11a)$$

and

$$iKB\sin\phi\sin\theta\ x_{11} + \frac{\sigma^2}{gk}y_{11} - (1 - KB\cos\phi)\sin\theta\ z_{11} = 0 \qquad c = 0 \quad (III.3.11b)$$

Upon substituting the solution U^+ and using $(III.3.10c - d)$, both boundary conditions yield the same dispersion relation:

$$\sigma^2 = Rgk \qquad (III.3.12)$$

Since σ is the frequency of the wave motion in a reference frame attached to a fluid particle, we shall refer to it as the intrinsic frequency. Eq. $(III.3.12)$ suggests that the oblique short waves propagate in an oscillatory gravity field $R(\phi, \theta)g$. It is therefore expected that k and/or σ are also functions of ϕ. In order to determine the scale dependence of k and σ, we shall examine the kinematic relations implied by their definitions $(III.3.3a - c)$.

The phase function S can be eliminated from $(III.3.3a-b)$ by cross-differentiation to give

$$\frac{\partial k}{\partial b}\cos\theta - \frac{\partial k}{\partial a}\sin\theta = 0 \qquad (III.3.13a)$$

Eq. $(III.3.13a)$ corresponds to the c-component of the general relation $\nabla_{\mathrm{L}} \times \vec{k} = 0$. Similarly, elimination of S between $(III.3.3a)$ and $(III.3.3c)$ and between $(III.3.3b)$ and $(III.3.3c)$ yields two more relations

$$\frac{\partial k}{\partial t}\cos\theta + \frac{\partial \sigma}{\partial a} = 0 \qquad \frac{\partial k}{\partial t}\sin\theta + \frac{\partial \sigma}{\partial b} = 0 \qquad (III.3.13b-c)$$

which are just the two components of the vector law of conservation of crests. The wavenumber k and frequency σ are slowly varying and may depend only on the long wave scales, *i.e.* on a_2 and t_1. Upon expanding $(III.3.13a-c)$ according to the rules of multiple scales, the first non-zero contribution of $(III.3.13a)$ occurs at $\mathcal{O}(\epsilon^2)$

$$\frac{\partial k}{\partial a_2}\sin\theta = 0 \qquad (III.3.14a)$$

Therefore, k is independent of a_2. Similarly, the first non-zero contribution of $(III.3.13b)$ and $(III.3.13c)$ arises at $\mathcal{O}(\epsilon)$ yielding

$$\frac{\partial k}{\partial t_1} = 0 \qquad (III.3.14b)$$

Thus, k is independent of both a_2 and t_1, *i.e.* of ϕ. It follows from $(III.3.12)$ that $\sigma = \sigma(\phi, \theta)$. In figure 3.1, we plot the variations of $\sigma^2(\phi, \theta)$ normalized by its constant values σ_0^2 at $\theta = 0$, as a function of both ϕ and θ. For oblique incidence, we observe that σ is greater that σ_0 in the trough and smaller than σ_0 at the crest of the long waves.

3.1.3. *The vorticity field revisited*

Having solved for the first harmonic of the short waves at $\mathcal{O}(\epsilon)$, we may evaluate Λ_1 from the $\mathcal{O}(\epsilon)$ contribution of $(III.2.3.a-c)$ and find

$$\Lambda_1 = [0, -2\Omega K^2 B^2 e^{2Kc_2}, 0]^T \qquad (III.3.15)$$

which is independent of t on all scales. The leading order vorticity field may be evaluated from $(III.2.23a)$ and $(III.2.24a)$

$$J\varpi_1 = L_0\Lambda_1 = \Lambda_1 \qquad (III.3.16)$$

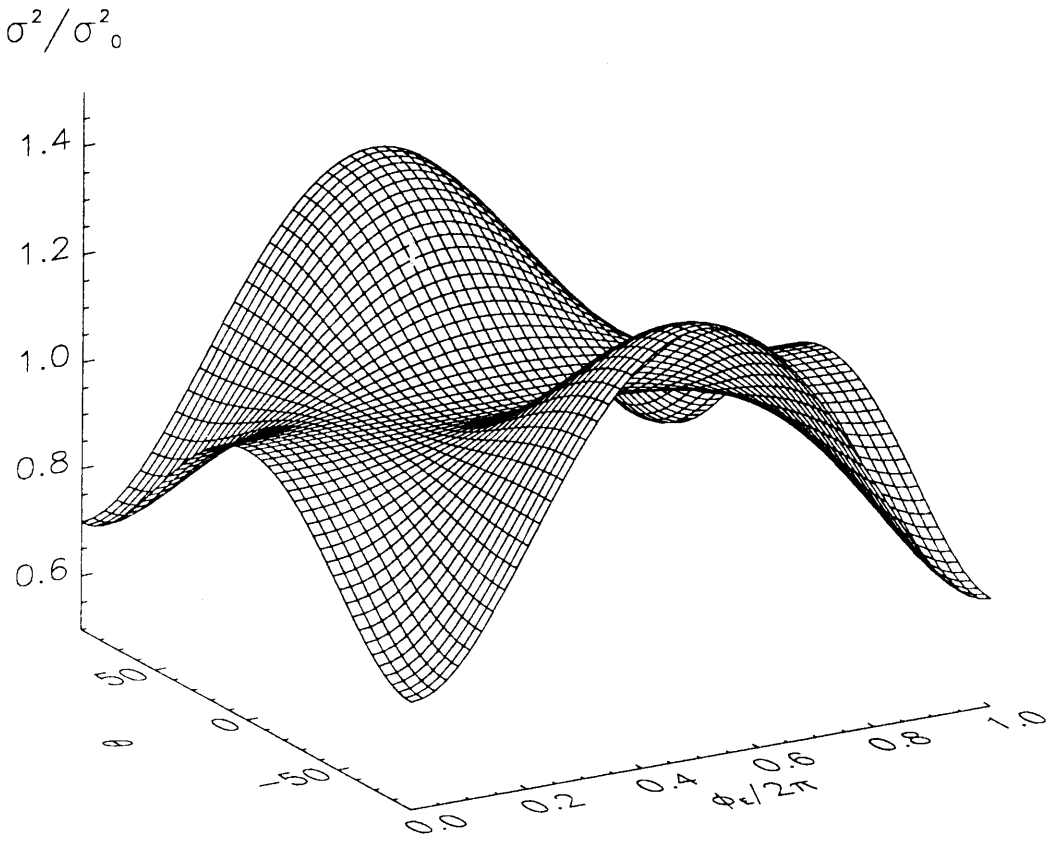

Figure III.3.1: Variations of the intrinsic frequency with the long wave phase ϕ and the incidence angle θ with $KB = 0.3$.

This simply states that the Y-axis vorticity is solely due to Gerstner's wave, and that the short waves are irrotational at the leading order.

At $\mathcal{O}(\epsilon^2)$, the vorticity is given by $(III.2.23b)$, *i.e.*

$$J\varpi_2 = \begin{pmatrix} 1 - KB\cos\phi & 0 & KB\sin\phi \\ 0 & 1 & 0 \\ KB\sin\phi & 0 & 1 + KB\cos\phi \end{pmatrix} \Lambda_2 \; - \; 2\Omega K^2 B^2 \begin{pmatrix} \frac{\partial x_1}{\partial b} \\ \frac{\partial y_1}{\partial b} \\ \frac{\partial z_1}{\partial b} \end{pmatrix} \quad (III.3.17)$$

where c_2 is approximately zero for the water layer of interest. From $(III.2.22b)$ and the expression $(III.3.15)$ of Λ_1, it is clear that Λ_2 is independent of fast time t. Furthermore, $(III.2.22c)$ becomes

$$\frac{\partial \Lambda_3}{\partial t} + \frac{\partial \Lambda_2}{\partial t_1} = 0 \qquad (III.3.18a)$$

where the first term clearly consists of non-zeroth harmonics while the second is independent of fast time. Consequently, the two terms must vanish independently:

$$\frac{\partial \Lambda_3}{\partial t} = 0 \qquad \frac{\partial \Lambda_2}{\partial t_1} = 0 \qquad (III.3.18b-c)$$

Upon assuming Λ_2 to be zero at $t_1 = 0$, we then conclude that it is true for all t_1. By implication, the only component of the vorticity field at $\mathcal{O}(\epsilon^2)$ is an oscillatory one.

3.1.4. *The zeroth harmonic*

As observed in Chapter II, the full solution for the short waves at the leading order also includes a slowly varying component resulting from quadratic interactions. The mean displacements x_{10}, y_{10} and z_{10} may now be solved. The continuity and two vorticity equations yield respectively

$$-KB\sin\phi\frac{\partial x_{10}}{\partial c} + (1 - KB\cos\phi)\frac{\partial z_{10}}{\partial c} = 0 \qquad (III.3.19a)$$

$$\frac{\partial^3 y_{10}}{\partial c \partial t_1^2} = \frac{\partial}{\partial t_1}\left\{\sigma k \kappa_r \sin\theta(1 + |\mathcal{S}_x|^2 + |\mathcal{S}_y|^2)|A|^2 e^{2\kappa_r c}\right\} \qquad (III.3.19b)$$

$$(1 - KB\cos\phi)\frac{\partial^3 x_{10}}{\partial c \partial t_1^2} + KB\sin\phi\frac{\partial^3 z_{10}}{\partial c \partial t_1^2} - \Omega^2 KB\left(\cos\phi\frac{\partial x_{10}}{\partial c} - \sin\phi\frac{\partial z_{10}}{\partial c}\right) =$$

$$\frac{\partial}{\partial t_1}\left\{\sigma k \kappa_r \cos\theta(1 + |\mathcal{S}_x|^2 + |\mathcal{S}_y|^2)|A|^2 e^{2\kappa_r c}\right\} \qquad (III.3.19c)$$

The two dynamic boundary conditions on the free surface yield

$$-KB\sin\phi\frac{\partial x_{10}}{\partial a_1} + (1 - KB\cos\phi)\frac{\partial z_{10}}{\partial a_1} = 0 \qquad c = 0 \qquad (III.3.20a)$$

$$-KB\sin\phi\frac{\partial x_{10}}{\partial b_1} + (1 - KB\cos\phi)\frac{\partial z_{10}}{\partial b_1} = 0 \qquad c = 0 \qquad (III.3.20b)$$

In particular $(III.3.19b-c)$ can be written as

$$\frac{\partial}{\partial t_1}\left\{-\frac{\partial^2 y_{10}}{\partial c \partial t_1} + \sigma k \kappa_r \sin\theta(1 + |\mathcal{S}_x|^2 + |\mathcal{S}_y|^2)|A|^2 e^{2\kappa_r c}\right\} = 0 \qquad (III.3.21a)$$

and

$$\frac{\partial}{\partial t_1}\left\{(1 - KB\cos\phi)\frac{\partial^2 x_{j0}}{\partial c \partial t_1} + KB\sin\phi\frac{\partial^2 z_{j0}}{\partial c \partial t_1} +\right.$$

$$-\Omega^2 KB\left(\sin\phi\frac{\partial x_{j0}}{\partial c}+\cos\phi\frac{\partial z_{j0}}{\partial c}\right)-\sigma k\kappa_r\cos\theta(1+|\mathcal{S}_x|^2+|\mathcal{S}_y|^2)|A|^2e^{2\kappa_r c}\Big\}=0 \qquad (III.3.21b)$$

Note that $(III.3.21b)$ bears a close resemblance and reduces to $(II.4.14)$ when $\theta = 0$. In Chapter II, we identified the quantity within the curly bracket as the vorticity, assumed it to be zero at $t_1 = 0$ and deduced that is was zero at all times. The expressions within the curly brackets in $(III.3.21a-b)$ are exactly the a- and b-components of Λ_2. From $(III.2.3c)$, it is clear that the c-component reduces to zero. Upon assuming $\Lambda_2 = 0$ at $t_1 = 0$, we deduce in view of $(III.3.18c)$ that this is true for all times, *i.e.*

$$\frac{\partial^2 y_{10}}{\partial c\partial t_1}=\sigma k\kappa_r\sin\theta(1+|\mathcal{S}_x|^2+|\mathcal{S}_y|^2)|A|^2e^{2\kappa_r c} \qquad (III.3.22a)$$

and

$$(1-KB\cos\phi)\frac{\partial^2 x_{j0}}{\partial c\partial t_1}+KB\sin\phi\frac{\partial^2 z_{j0}}{\partial c\partial t_1}+$$

$$-\Omega^2 KB\left(\sin\phi\frac{\partial x_{j0}}{\partial c}+\cos\phi\frac{\partial z_{j0}}{\partial c}\right)-\sigma k\kappa_r\cos\theta(1+|\mathcal{S}_x|^2+|\mathcal{S}_y|^2)|A|^2e^{2\kappa_r c}=0 \qquad (III.3.22b)$$

This implies the absence of slowly varying terms in the vorticity ϖ_2. Note in particular, in the limit of colinear long and short waves, that $\frac{\partial}{\partial b}=0$ and we recover the irrotationality of short waves at $\mathcal{O}(\epsilon^2)$.

Straightforward integration of $(III.3.22a)$, $(III.3.19a)$ and $(III.3.22b)$ yields respectively the expressions of y_{10}, x_{10} and z_{10}:

$$y_{10}=\frac{1}{2}\sigma k\sin\theta\int_0^{t_1}(1+|\mathcal{S}_x|^2+|\mathcal{S}_y|^2)|A|^2e^{2\kappa_r c}dt_1 \qquad (III.3.23a)$$

$$\begin{pmatrix}x_{10}\\ z_{10}\end{pmatrix}=\frac{1}{2}\sigma k\cos\theta\int_0^{t_1}(1+|\mathcal{S}_x|^2+|\mathcal{S}_y|^2)|A|^2e^{2\kappa_r c}dt_1\begin{pmatrix}1-KB\cos\phi\\ KB\sin\phi\end{pmatrix} \qquad (III.3.23b-c)$$

In summary, short wave displacements at the leading order are

$$\begin{pmatrix}x_1\\ y_1\\ z_1\end{pmatrix}=\begin{pmatrix}x_{10}\\ y_{10}\\ z_{10}\end{pmatrix}+\frac{1}{2}A\begin{pmatrix}i\mathcal{S}_x\\ i\mathcal{S}_y\\ 1\end{pmatrix}e^{iS}e^{\kappa c}+(*) \qquad (III.3.24)$$

where $A(a_1,b_1,t_1,a_2,b_2,t_2)$ is the slowly varying short wave amplitude and κ stands for κ^+.

3.2. Governing Equations at Arbitrary Orders

Next, we generalize $(III.3.24)$ to the Lagrangian displacement at any order $\mathcal{O}(\epsilon^j)$

$$\begin{pmatrix} x_j \\ y_j \\ z_j \end{pmatrix} = \begin{pmatrix} x_{j0} \\ y_{j0} \\ z_{j0} \end{pmatrix} + \frac{1}{2} \sum_{\ell \neq 0} \begin{pmatrix} i x_{j\ell} \\ i y_{j\ell} \\ z_{j\ell} \end{pmatrix} e^{i\ell S} + (*) \qquad (III.3.25)$$

where x_{j0}, y_{j0}, z_{j0}, $x_{j\ell}$, $y_{j\ell}$ and $z_{j\ell}$ are all functions of c yet to be found.

3.2.1. *Non-zero harmonic displacements*

Substitution of $(III.3.25)$ in the three $\mathcal{O}(\epsilon^j)$ governing equations yields the following set of ordinary differential equations

$$-iKB\sin\phi\frac{\partial x_{j\ell}}{\partial c} + (1 - KB\cos\phi)\frac{\partial z_{j\ell}}{\partial c} = \ell k(1 + KB\cos\phi)\cos\theta\ x_{j\ell} +$$

$$+\ell k(1 - K^2B^2)\sin\theta\ y_{j\ell} + i\ell kKB\sin\phi\cos\theta\ z_{j\ell} + E_{j\ell} \qquad (III.3.26a)$$

$$(1 - KB\cos\phi)\frac{\partial x_{j\ell}}{\partial c} - iKB\sin\phi\frac{\partial z_{j\ell}}{\partial c} = i\ell kKB\sin\phi\cos\theta\ x_{j\ell} +$$

$$+\ell k(1 + KB\cos\phi)\cos\theta\ z_{j\ell} + G_{j\ell} \qquad (III.3.26b)$$

and

$$0 = -ik(1 - KB\cos\phi)\sin\theta\ x_{j\ell} + ik\cos\theta\ y_{j\ell} - kKB\sin\phi\sin\theta\ z_{j\ell} + H_{j\ell} \quad (III.3.26c)$$

and similarly for the free surface boundary conditions

$$\left[\ell R(1 - KB\cos\phi) + iKB\sin\phi\cos\theta\right] x_{j\ell} +$$

$$-\left[(1 - KB\cos\phi)\cos\theta + i\ell RKB\sin\phi\right] z_{j\ell} = I_{j\ell} \qquad c = 0 \qquad (III.3.27a)$$

and

$$iKB\sin\phi\sin\theta x_{j\ell} + \ell R y_{j\ell} - (1 - KB\cos\phi)\sin\theta\ z_{j\ell} = J_{j\ell} \qquad c = 0 \quad (III.3.27b)$$

3.2.2. *The zeroth harmonic displacements*

The governing equations for the zeroth harmonic cannot be obtained by setting $\ell = 0$ in $(III.3.26a-c)$ and $(III.3.27a-b)$. They are instead given by

$$-KB\sin\phi\frac{\partial x_{j0}}{\partial c} + (1 - KB\cos\phi)\frac{\partial z_{j0}}{\partial c} = E_{j0} \qquad (III.3.28a)$$

$$\frac{\partial^3 y_{j0}}{\partial c \partial t_1^2} = F_{j0} \qquad (III.3.28b)$$

$$(1 - KB\cos\phi)\frac{\partial^3 x_{j0}}{\partial c \partial t_1^2} + KB\sin\phi\frac{\partial^3 z_{j0}}{\partial c \partial t_1^2} - \Omega^2 KB\Big(\cos\phi\frac{\partial x_{j0}}{\partial c} - \sin\phi\frac{\partial z_{j0}}{\partial c}\Big) = G_{j0} \qquad (III.3.28c)$$

Unlike the governing equations for non-zeroth harmonics, eqs. $(III.3.28a)$ and $(III.3.28b-c)$ are obtained respectively at $\mathcal{O}(\epsilon^j)$ and $\mathcal{O}(\epsilon^{j+2})$. The two boundary conditions obtained at $\mathcal{O}(\epsilon^{j+1})$ read

$$-KB\sin\phi\frac{\partial x_{j0}}{\partial a_1} + (1 - KB\cos\phi)\frac{\partial z_{j0}}{\partial a_1} = I_{j0} \qquad c = 0 \qquad (III.3.29a)$$

$$-KB\sin\phi\frac{\partial x_{j0}}{\partial b_1} + (1 - KB\cos\phi)\frac{\partial z_{j0}}{\partial b_1} = J_{j0} \qquad c = 0 \qquad (III.3.29b)$$

With these governing equations, we now deduce evolutions equations for the short wave amplitude A.

3.3. Linear Evolution of Short Waves for Finite Incidence Angles

The first harmonic component of the short wave displacements at $\mathcal{O}(\epsilon^2)$ are governed by $(III.3.26a-c)$ with E_{21}, G_{21} and H_{21} given by

$$\begin{aligned} E_{21} = i\Big\{ & k(\cos\theta + i\mathcal{S}_y KB\sin\phi\sin\theta)\frac{\partial x_{10}}{\partial c}A + \\ & + k\sin\theta(1 - KB\cos\phi - i\mathcal{S}_x KB\sin\phi)\frac{\partial y_{10}}{\partial c}A + \\ & - ik\big[\mathcal{S}_x\cos\theta + \mathcal{S}_y(1 - KB\cos\phi)\sin\theta\big]\frac{\partial z_{10}}{\partial c}A + \\ & - \big[\mathcal{S}_x(1 + KB\cos\phi) + iKB\sin\phi\big]\frac{\partial A}{\partial a_1} - (1 - K^2B^2)\mathcal{S}_y\frac{\partial A}{\partial b_1}\Big\}e^{\kappa c} \end{aligned} \qquad (III.3.30a)$$

$$G_{21} = i\Big\{ k\cos\theta(\mathcal{S}_x\frac{\partial x_{10}}{\partial c} + \mathcal{S}_y\frac{\partial y_{10}}{\partial c} - i\frac{\partial z_{10}}{\partial c})A - (1 + KB\cos\phi + i\mathcal{S}_x KB\sin\phi)\frac{\partial A}{\partial a_1} +$$

$$-2\frac{\Omega}{\sigma}\Big[(1-KB\cos\phi)\mathcal{S}_x - iKB\sin\phi\Big]\frac{\partial\kappa}{\partial\phi}A+$$

$$-2\frac{\Omega}{\sigma}\Big[(1-KB\cos\phi)\kappa - ikKB\sin\phi\cos\theta\Big]\frac{\partial\mathcal{S}_x}{\partial\phi}A\Big\}e^{\kappa c} \qquad (III.3.30b)$$

and

$$H_{21} = \Big\{\mathcal{S}_y\frac{\partial A}{\partial a_1} - \big[(1-KB\cos\phi)\mathcal{S}_x - iKB\sin\phi\big]\frac{\partial A}{\partial b_1}+$$

$$+2\frac{\Omega}{\sigma}k(1-KB\cos\phi)\sin\theta\frac{\partial\mathcal{S}_x}{\partial\phi}A - 2\frac{\Omega}{\sigma}k\cos\theta\frac{\partial\mathcal{S}_y}{\partial\phi}A\Big\}e^{\kappa c} \qquad (III.3.30c)$$

Introducing the new vector of unknowns $U \equiv [x_{21}, z_{21}]^T$, we deduce the following inhomogeneous ordinary differential system for U

$$M\frac{\partial U}{\partial c} = kNU + \begin{pmatrix} E'_{21} \\ G_{21} \end{pmatrix} \qquad (III.3.31a)$$

where E'_{21} defined by

$$E'_{21} \equiv E_{21} + i(1-K^2B^2)\frac{\sin\theta}{\cos\theta}H_{21} \qquad (III.3.31b)$$

arises after the elimination of y_{21} from the continuity equation $(III.3.26a)$ and the Z-component of the vorticity equation $(III.3.26c)$.

The homogeneous part of $(III.3.31a)$ still admits a general solution in the form

$$U = \beta^+\begin{pmatrix} \mathcal{S}_x \\ 1 \end{pmatrix}e^{(\kappa_r+i\kappa_i)c} + \beta^-\begin{pmatrix} \mathcal{S}_x^* \\ -1 \end{pmatrix}e^{(-\kappa_r+i\kappa_i)c} \qquad (III.3.32)$$

where $\beta^{\pm}$ are unknown functions of c. After substituting $(III.3.32)$ in $(III.3.31a)$, we get

$$\frac{\partial\beta^+}{\partial c}\begin{pmatrix} \mathcal{S}_x \\ 1 \end{pmatrix}e^{(\kappa_r+i\kappa_i)c} + \frac{\partial\beta^-}{\partial c}\begin{pmatrix} \mathcal{S}_x^* \\ -1 \end{pmatrix}e^{(-\kappa_r+i\kappa_i)c} = M^{-1}\begin{pmatrix} E'_{21} \\ G_{21} \end{pmatrix} \qquad (III.3.33)$$

which can be solved and then integrated

$$\beta^+(c) = \int^c \frac{RG_{21}(x) + \cos\theta E_{21}(x) + i\sin\theta(1-K^2B^2)H_{21}(x)}{\Xi\big[R(1-KB\cos\phi) - iKB\sin\phi\cos\theta\big]}e^{-(\kappa_r+i\kappa_i)x}dx \qquad (III.3.34a)$$

$$\beta^-(c) = \int_{-\infty}^c \frac{RG_{21}(x) - \cos\theta E_{21}(x) - i\sin\theta(1-K^2B^2)H_{21}(x)}{\Xi\big[R(1-KB\cos\phi) + iKB\sin\phi\cos\theta\big]}e^{(\kappa_r-i\kappa_i)x}dx \qquad (III.3.34b)$$

where

$$\Xi \equiv \mathcal{S}_x + \mathcal{S}_x^* = \frac{2R\cos\theta}{1+(K^2B^2\cos^2\phi - 2KB\cos\phi)\sin^2\theta} \qquad (III.3.34c)$$

Note that the lower bound of integration in $(III.3.34a)$ is left unspecified pending further analysis of the integrand in the vicinity of $c = -\infty$. The integrand in $(III.3.34b)$, however, decreases with depth as $e^{2\kappa_r c}$, in view of $(III.3.30a-c)$, thus justifying the lower bound. No integration constant is allowed in $(III.3.34b)$ to ensure boundedness in $(III.3.32)$ as c goes to $-\infty$.

Having formally solved for U, we must enforce the two boundary conditions. It can be shown (cf. Appendix K) that both boundary conditions give the same result. We shall therefore enforce $(III.3.27a)$ alone. Upon recalling the definition $(III.3.10c)$ of $\mathcal{S}_x$, $(III.3.27a)$ can be rewritten in the form

$$\left[R(1-KB\cos\phi) + iKB\sin\phi\cos\theta\right](x_{21} - \mathcal{S}_x z_{21}) = I_{21} \qquad c=0 \qquad (III.3.35)$$

Upon substitution of $(III.3.32)$ in $(III.3.35)$, only the second eigenmode yields a non-zero contribution

$$\left[R(1-KB\cos\phi) + iKB\sin\phi\cos\theta\right](\mathcal{S}_x + \mathcal{S}_x^*)\beta^- = I_{21} \qquad c=0 \qquad (III.3.36)$$

Comparison of $(III.3.36)$ with $(III.3.34b)$ and $(III.3.34c)$ yields the solvability condition expressed here for the $\mathcal{O}(\epsilon^2)$ displacements:

$$\int_{-\infty}^{0}\left[RG_{21}(c) - \cos\theta E_{21}(c) - i\sin\theta(1-K^2B^2)H_{21}(c)\right]e^{(\kappa_r - i\kappa_i)c}dc = I_{21} \quad (III.3.37)$$

with I_{21} given by

$$I_{21} = -\frac{2i\sigma}{gk}\left[\mathcal{S}_x(1-KB\cos\phi) - iKB\sin\phi\right]\left\{\frac{\partial A}{\partial t_1} + \frac{\Omega}{\sigma}\frac{\partial\sigma}{\partial\phi}A\right\} +$$

$$-\frac{i}{k}(1-KB\cos\phi - iKB\sin\phi\mathcal{S}_x)\frac{\partial A}{\partial a_1} - \frac{2i\sigma\Omega}{gk}(1-KB\cos\phi)\frac{\partial\mathcal{S}_x}{\partial\phi}A \quad (III.3.38)$$

Note that the solvability condition is obtained without solving explicitly for the $\mathcal{O}(\epsilon^2)$ displacements. Upon substituting in the integrand of $(III.3.37)$ the expression of E_{21}, G_{21} and H_{21}, the slowly varying displacements x_{10}, y_{10} and z_{10} cancel. After performing the integration in $(III.3.37)$ and some algebra, we obtain

$$\frac{\partial A}{\partial t_1} + \frac{\sigma\cos\theta}{2R^2k}\frac{\partial A}{\partial a_1} + \frac{\sigma\sin\theta}{2R^2k}(1+K^2B^2 - 2KB\cos\phi)\frac{\partial A}{\partial b_1} - \frac{\Omega}{2\kappa_r}\frac{\partial\kappa}{\partial\phi}A + \frac{\Omega}{\sigma}\frac{\partial\sigma}{\partial\phi}A +$$

$$+\frac{\Omega}{2R^2}\left[R\cos\theta - iKB\sin\phi(1-KB\cos\phi)\sin^2\theta\right]\frac{\partial \mathcal{S}_x}{\partial\phi}A+$$

$$+\frac{\Omega}{2R^2}\left[R(1-KB\cos\phi)+iKB\sin\phi\cos\theta\right]\sin\theta\frac{\partial \mathcal{S}_y}{\partial\phi}A=0 \qquad (III.3.39)$$

In the limit of normal incidence, R and $\mathcal{S}_x$ reduce to unity, $\mathcal{S}_y$ to zero and σ becomes a constant; eq. $(III.3.39)$ reduces to

$$\frac{\partial A}{\partial t_1}+\frac{\sigma}{2k}\frac{\partial A}{\partial a_1}-\frac{\Omega}{2\kappa_r}\frac{\partial\kappa}{\partial\phi}A=0 \qquad (III.3.40)$$

in agreement with Chapter II. In the absence of long waves ($R=1$, $KB=\frac{\partial}{\partial\phi}=0$), and we recover a familiar result:

$$\frac{\partial A}{\partial t_1}+\frac{\sigma\cos\theta}{2k}\frac{\partial A}{\partial a_1}+\frac{\sigma\sin\theta}{2k}\frac{\partial A}{\partial b_1}=0 \qquad (III.3.41)$$

where σ now represents the absolute frequency. Upon substituting in $(III.3.39)$ the expression of κ, κ_r, $\mathcal{S}_x$ and $\mathcal{S}_y$, we obtain

$$\frac{\partial A}{\partial t_1}+\frac{\sigma\cos\theta}{2R^2k}\frac{\partial A}{\partial a_1}+\frac{\sigma\sin\theta}{2R^2k}(1+K^2B^2-2KB\cos\phi)\frac{\partial A}{\partial b_1}+\Omega(D_r+iD_i)A=0 \qquad (III.3.42a)$$

where D_r affects the amplitude of A

$$D_r=\frac{KB\sin\phi}{1+K^2B^2-2KB\cos\phi}+\frac{KB\sin\phi\sin^2\theta}{1+(K^2B^2-2KB\cos\phi)\sin^2\theta}+$$

$$-\frac{KB\sin\phi(1-KB\cos\phi)\sin^2\theta}{1+(K^2B^2\cos^2\phi-2KB\cos\phi)\sin^2\theta} \qquad (III.3.42b)$$

while D_i affects the phase of A:

$$D_i=\frac{-KB\cos\theta}{R(1-K^2B^2)(1+K^2B^2-2KB\cos\phi)[1+(K^2B^2\cos^2\phi-2KB\,\mathrm{ccs}\,\phi)\sin^2\theta]}$$

$$\Big\{(1+K^2B^2)\cos\phi-2KB+\sin^2\theta\big[-KB(1+\cos^2\phi)+K^2B^2(6\cos\phi-\cos^3\phi)+$$

$$-4K^3B^3\cos^2\phi+K^4B^4(3\cos^3\phi-2\cos\phi)\big]\Big\} \qquad (III.3.42c)$$

Eqs. $(III.3.42a-b)$ will be the basis of a thorough study, in §III.4, of the modulation of the complex amplitude A due to the long wave.

3.4. Short Wave Displacements at the Second Order

3.4.1. *The first harmonic displacements*

Once the solvability condition is derived, the first harmonic displacements at $\mathcal{O}(\epsilon^2)$ for a finite incidence angle θ are obtained by integrating $(III.3.34a-b)$ and substituting the result in $(III.3.32)$.

Considering the daunting algebra associated with the case of finite θ, the simpler situation of slight obliqueness is considered here, *i.e.* θ is set to zero while still allowing for a spanwise slow modulation of the short wave amplitude A. Mathematically, this translates into the dependence of A upon the scale b_1. With the above simplification, we turn to the evaluation of x_{21}, y_{21} and z_{21}.

To this end, we must first specify the lower bound of $(III.3.34a)$. It is clear from $(III.3.30a-c)$, that the integrand is *not* attenuated at great depths. With the above simplifications, we may rewrite $(III.3.34a)$ as

$$\beta^+(c) = \int_0^c \frac{G_{21}(x)+E_{21}(x)}{1-KB\cos\phi - iKB\sin\phi} e^{-(\kappa_r+i\kappa_i)x} dx + \beta_h^+ \qquad (III.3.43)$$

where β_h^+ represents a homogeneous solution which can be combined to A without loss of generality. The expression of x_{21} and z_{21} is easily obtained

$$x_{21}(c) = \left\{ i\sigma k^2 \int_0^{t_1} |A|^2 e^{2\kappa_r c} dt_1 \; A \; - ic\left(\frac{\kappa}{k}\frac{\partial A}{\partial a_1} + \frac{\Omega}{\sigma}\frac{\partial \kappa}{\partial \phi}A\right) + \right.$$

$$\left. -i\frac{\Omega}{\sigma}\frac{1-KB\cos\phi - iKB\sin\phi}{2\kappa_r(1-KB\cos\phi+iKB\sin\phi)}\frac{\partial\kappa}{\partial\phi}A \right\} e^{\kappa c} \qquad (III.3.44a)$$

$$z_{21}(c) = \left\{ i\sigma k^2 \int_0^{t_1} |A|^2 e^{2\kappa_r c} dt_1 \; A \; - ic\left(\frac{\kappa}{k}\frac{\partial A}{\partial a_1} + \frac{\Omega}{\sigma}\frac{\partial \kappa}{\partial \phi}A\right) + \right.$$

$$\left. +i\frac{\Omega}{\sigma}\frac{1-KB\cos\phi - iKB\sin\phi}{2\kappa_r(1-KB\cos\phi+iKB\sin\phi)}\frac{\partial\kappa}{\partial\phi}A \right\} e^{\kappa c} \qquad (III.3.44b)$$

The expression of y_{21} is then deduced from $(III.3.26c)$ as

$$y_{21} = \frac{i}{k} H_{21}(c) \qquad (III.3.45)$$

i.e. after substituting $(III.3.30c)$ for H_{21},

$$y_{21}(c) = -\frac{i}{k}(1-KB\cos\phi - iKB\sin\phi)\frac{\partial A}{\partial b_1} \qquad (III.3.46)$$

The expressions of x_{21} and z_{21} are identical to those in Chapter II. Note, however, the presence of a transverse displacement, y_{21}, arising from the slow modulation of the short wave amplitude in that direction.

3.4.2. *The second harmonic displacements*

Next, we solve for the second harmonic displacement at $\mathcal{O}(\epsilon^2)$. The governing equations are given by $(III.3.26a-c)$, the boundary conditions by $(III.3.27a-b)$ with $j=\ell=2$ and the following forcing terms

$$E_{22}=G_{22}=H_{22}=I_{22}=J_{22}=0 \qquad (III.3.47a-f)$$

We thus have a set of homogeneous equations with homogeneous boundary conditions. The solution is therefore $x_{22}=y_{22}=z_{22}=0$ †.

3.4.3. *The zeroth harmonic displacements*

We have pointed out earlier that x_{10}, y_{10} and z_{10} cancel out from the integrand in the linear evolution equation. It is therefore expected that the expression of x_{20}, y_{20} and z_{20} is not needed to derive the nonlinear evolution equation.

3.5. Nonlinear Evolution Equation for Slightly Oblique Incidence

The solvability condition for the first harmonic $\mathcal{O}(\epsilon^3)$ displacements is deduced from $(III.3.37)$ by setting $\theta=0$ and $R=1$:

$$\int_{-\infty}^{0}\left[G_{31}(c)-E_{31}(c)\right]e^{(\kappa_r-i\kappa_i)c}=I_{31} \qquad (III.3.48)$$

where the integrand is given by

$$G_{31}(c)-E_{31}(c)=i(1+KB\cos\phi-iKB\sin\phi)\Big\{\frac{\partial x_{21}}{\partial a_1}-\frac{\partial z_{21}}{\partial a_1}\Big\}-\frac{2kKB\sin\phi}{\sigma}\frac{\partial x_{21}}{\partial t_1}+$$

$$-\frac{2i}{\sigma}(1-KB\cos\phi)\frac{\partial^2 x_{21}}{\partial c\partial t_1}-\frac{2KB\sin\phi}{\sigma}\frac{\partial^2 z_{21}}{\partial c\partial t_1}+\frac{2ik}{\sigma}(1+KB\cos\phi)\frac{\partial z_{21}}{\partial t_1}+$$

† This result is in fact true for an arbitrary angle θ.

$$+ik(x_{21}-z_{21})\{\frac{\partial x_{10}}{\partial c}+i\frac{\partial z_{10}}{\partial c}\}-\frac{2k}{\sigma}(\frac{\partial A}{\partial t_1}+c\Omega\frac{\partial \kappa}{\partial \phi}A)(\frac{\partial x_{10}}{\partial c}-i\frac{\partial z_{10}}{\partial c})e^{\kappa_r c}e^{i\kappa_i c}+$$

$$+\Big\{\frac{2c\Omega}{\sigma}(1+KB\cos\phi+iKB\sin\phi)\frac{\partial\kappa}{\partial\phi}\frac{\partial A}{\partial a_1}+\frac{2}{\sigma}(1+KB\cos\phi+iKB\sin\phi)\frac{\partial^2 A}{\partial a_1\partial t_1}+$$

$$+\frac{\Omega}{\sigma^2}(1-KB\cos\phi-iKB\sin\phi)(\Omega\frac{\partial^2\kappa}{\partial\phi^2}A+2\Omega c(\frac{\partial\kappa}{\partial\phi})^2A+2\frac{\partial\kappa}{\partial\phi}\frac{\partial A}{\partial t_1})+$$

$$-\frac{2k\Omega^2KB(\cos\phi+i\sin\phi)}{\sigma^2(1-KB\cos\phi+iKB\sin\phi)}A+$$

$$+\frac{1-K^2B^2}{2k\kappa_r}(1-KB\cos\phi-iKB\sin\phi)\frac{\partial^2 A}{\partial b_1^2}\Big\}e^{\kappa_r c}e^{i\kappa_i c} \qquad (III.3.49)$$

and I_{31} by

$$I_{31}=-\frac{2i}{\sigma}(1-KB\cos\phi)\frac{\partial x_{21}}{\partial t_1}-\frac{2KB\sin\phi}{\sigma}\frac{\partial z_{21}}{\partial t_1}+$$

$$-\frac{KB\sin\phi}{k}\frac{\partial x_{21}}{\partial a_1}-\frac{i}{k}(1-KB\cos\phi)\frac{\partial z_{21}}{\partial a_1}-(\frac{\partial x_{10}}{\partial a_1}-i\frac{\partial z_{10}}{\partial a_1})A+$$

$$-\frac{2i}{\sigma}(1-KB\cos\phi-iKB\sin\phi)(\frac{\partial A}{\partial t_2}+\frac{\sigma}{2k}\frac{\partial A}{\partial t_2}+\frac{i}{2\sigma}\frac{\partial^2 A}{\partial t_1^2}) \qquad c=0 \quad (III.3.50)$$

After performing the integration and some algebra, both with the help of MACSYMA, we obtain the following nonlinear Schrödinger equation

$$\frac{\partial A}{\partial t_2}+\frac{\sigma}{2k}\frac{\partial A}{\partial a_2}+\frac{i\sigma}{8k^2}\frac{\partial^2 A}{\partial a_1^2}-\frac{i\sigma}{4k^2}(1+K^2B^2-2KB\cos\phi)\frac{\partial^2 A}{\partial b_1^2}+$$

$$+\frac{i\sigma k^2|A|^2A}{2(1+K^2B^2-2KB\cos\phi)}-\frac{i\Omega^2}{4\sigma\kappa_r^2}\frac{\partial\kappa}{\partial\phi}\frac{\partial\kappa_r}{\partial\phi}A-\frac{i\Omega^2}{8\sigma\kappa_r^2}(\frac{\partial\kappa}{\partial\phi})^2A+\frac{i\Omega^2}{2\sigma\kappa_r}\frac{\partial^2\kappa}{\partial\phi^2}A+$$

$$+\frac{iKB\Omega^2(\cos\phi-KB+i\sin\phi)}{\sigma(1-K^2B^2)(1-KB\cos\phi-iKB\sin\phi)}A=0 \qquad (III.3.51)$$

If the short wave is strictly long crested, $\frac{\partial A}{\partial b_1}=0$ and we recover the equation derived in Chapter II. Next, we combine the linear evolution equation $(III.3.40)$ for $\theta=0$ with $(III.3.51)$. Making use of the chain rule of derivatives, we obtain

$$\frac{\partial A}{\partial t_1}+\frac{\sigma}{2k}\frac{\partial A}{\partial a_1}-\frac{\Omega}{2\kappa_r}\frac{\partial\kappa}{\partial\phi}A+\epsilon\Big\{\frac{i\sigma}{8k^2}\frac{\partial^2 A}{\partial a_1^2}-\frac{i\sigma}{4k^2}(1+K^2B^2-2KB\cos\phi)\frac{\partial^2 A}{\partial b_1^2}+$$

$$+\frac{i\sigma k^2|A|^2A}{2(1+K^2B^2-2KB\cos\phi)}-\frac{i\Omega^2}{4\sigma\kappa_r^2}\frac{\partial\kappa}{\partial\phi}\frac{\partial\kappa_r}{\partial\phi}A-\frac{i\Omega^2}{8\sigma\kappa_r^2}(\frac{\partial\kappa}{\partial\phi})^2A+\frac{i\Omega^2}{2\sigma\kappa_r}\frac{\partial^2\kappa}{\partial\phi^2}A+$$

$$+\frac{iKB\Omega^2(\cos\phi-KB+i\sin\phi)}{\sigma(1-K^2B^2)(1-KB\cos\phi-iKB\sin\phi)}A\Big\}=0 \qquad (III.3.52)$$

Let us introduce the following change of variables

$$\xi = k^2\overline{A}(a_1 - \frac{\sigma}{2k}t_1) \qquad \eta = k^2\overline{A}b_1 \qquad (III.3.53a-b)$$

$$\phi = \Omega t_1 - \epsilon K a_1 \quad \text{and} \qquad \overline{A}A = \mathcal{A}e^{i\Gamma(\phi)} \qquad (III.3.53c-d)$$

where $\overline{A}$ is the value of A in the absence of long waves ($KB = 0$) and $\Gamma(\phi, KB, \epsilon\frac{\Omega}{\sigma})$ corresponds to the linear phase terms and is still given by $(II.4.52)$. In the new set of variables $(III.3.52)$ reads

$$\frac{\partial\mathcal{A}}{\partial\phi} = -\frac{1}{\delta}\frac{KB\sin\phi}{1+K^2B^2-2KB\cos\phi}\left[1+\epsilon\frac{\Omega}{\sigma}\frac{1-3K^2B^2+2KB\cos\phi}{1+K^2B^2-2KB\cos\phi}\right]\mathcal{A}+$$

$$-\frac{i\alpha}{4}\frac{\partial^2\mathcal{A}}{\partial\xi^2}+\frac{i\alpha}{2}(1+K^2B^2-2KB\cos\phi)\frac{\partial^2\mathcal{A}}{\partial\eta^2}-\frac{i\alpha|\mathcal{A}|^2\mathcal{A}}{1+K^2B^2-2KB\cos\phi}+\mathcal{O}(\epsilon^2) \qquad (III.3.54)$$

with δ and α defined consistently with Chapter II as

$$\delta = 1-\epsilon\frac{\Omega}{\sigma} \qquad \alpha = \frac{\epsilon}{2\delta}\frac{(k\overline{A})^2}{\frac{\Omega}{\sigma}} \qquad (III.3.55a-b)$$

Eq. $(III.3.54)$ is a two-dimensional nonlinear Schrödinger equation with periodic coefficient. The modulation of the amplitude, wavenumber and frequency of the short wave for finite angle θ is first analysed. We shall then examine the linearized stability of a Stokes wave solution of $(III.3.54)$ to sideband disturbances.

4. MODULATION OF SHORT WAVES FOR FINITE INCIDENCE ANGLES

We have shown in §III.3 that the short waves are affected by the presence of the long wave at the leading order. The frequency σ is an explicit function of ϕ and so is the vertical component of the Lagrangian wavenumber κ_i. Apart from the new component of the Lagrangian displacement, the technique to transform to the Eulerian frame is the same as that described in Chapter II.

We shall first analyse the modulation of the amplitude, wavenumber and the relation between absolute and intrinsic frequencies and then comment on the existence of caustics and the reflection of a short wave riding on a steep Gertsner wave.

4.1. Modulation of the Short Wave Amplitude

We first recall the linear evolution equation $(III.3.42a)$ for the complex amplitude A. Let us then introduce the following reduced coordinates

$$\xi_1 = a_1 - \int^{t_1} \frac{\sigma \cos\theta}{2kR^2} dt_1 \qquad (III.4.1a)$$

$$\xi_2 = b_1 - \int^{t_1} \frac{\sigma \sin\theta}{2kR^2}(1 + K^2B^2 - 2KB\cos\phi)dt_1 \qquad (III.4.1b)$$

and the approximation

$$\phi = \Omega t_1 + \mathcal{O}(\epsilon) \qquad (III.4.1c)$$

Substitution of $(III.4.1a-c)$ in $(III.3.40a)$ yields

$$\frac{\partial A}{\partial \phi} = -(D_r + iD_i)A \qquad (III.4.2)$$

where D_r and D_i are defined by $(III.3.42b-c)$. Let $|A|$ and γ represent respectively the real amplitude and phase of A. It follows from $(III.4.2)$ that

$$\frac{\partial |A|}{\partial \phi} = -\left\{ \frac{KB\sin\phi}{1 + K^2B^2 - 2KB\cos\phi} + \frac{KB\sin\phi\sin^2\theta}{1 + (K^2B^2 - 2KB\cos\phi)\sin^2\theta} + \right.$$

$$\left. - \frac{KB\sin\phi(1 - KB\cos\phi)\sin^2\theta}{1 + (K^2B^2\cos^2\phi - 2KB\cos\phi)\sin^2\theta} \right\} |A| \qquad (III.4.3)$$

Term by term integration of $(III.4.3)$ yields

$$\frac{|A|}{\overline{A}} = (1 + K^2B^2 - 2KB\cos\phi)^{-\frac{1}{2}} \left[\frac{1 + (K^2B^2\cos^2\phi - 2KB\cos\phi)\sin^2\theta}{1 + (K^2B^2 - 2KB\cos\phi)\sin^2\theta}\right]^{\frac{1}{2}} \qquad (III.4.4)$$

where $\overline{A}$ represents the short wave amplitude in the absence of long waves ($KB = 0$). Note that the amplitude modulation ratio for arbitrary θ is the product of two factors: the first is the modulation ratio for colinear long/short waves ($\theta = 0$) and the second represents the effect of θ.

Of interest is the amplitude modulation at the crest ($\phi = 0$) and trough ($\phi = \pi$) of the long wave:

$$\frac{|A|_{\text{crest}}}{\overline{A}} = \frac{1}{1 - KB} \qquad \frac{|A|_{\text{trough}}}{\overline{A}} = \frac{1}{1 + KB} \qquad (III.4.5a - b)$$

Note that these values are identical to the colinear case ($\theta = 0$). The modulation range obtained by subtracting $(III.4.5b)$ from $(III.4.5a)$ is independent of θ. We have shown in Chapter II that the location of the mean sea level crossing, for Gerstner's wave, is characterized by $\cos\phi = -\frac{KB}{2}$. Thus, the amplitude modulation at that location is

$$\frac{|A|_{\text{crossing}}}{\overline{A}} = (1 + 2K^2B^2)^{-\frac{1}{2}} \left[\frac{1 + K^2B^2(1 + \frac{1}{4}K^2B^2)\sin^2\theta}{1 + 2K^2B^2\sin^2\theta}\right]^{\frac{1}{2}} \qquad (III.4.5c)$$

In figure 4.1, The amplitude modulation at the free surface crossing $(III.4.5c)$ is plotted against θ for several values of KB. $|A|_{\text{crossing}}$ decreases slowly with increasing incidence angles.

From $(III.4.4)$, it is clear that short waves incident at right angle with respect to the long waves are modulated in amplitude:

$$\frac{|A|}{\overline{A}} = (1 + K^2B^2 - 2KB\cos\phi)^{-\frac{1}{2}} \left[\frac{1 + K^2B^2\cos^2\phi - 2KB\cos\phi}{1 + K^2B^2 - 2KB\cos\phi}\right]^{\frac{1}{2}} \qquad (III.4.6)$$

unlike the well known result for short waves on a steady current. This is because a long wave with a finite period is transient and provides an effective gravity regardless to its direction of propagation. In appendix L, an elementary argument is given for a wave train propagating on calm water, and subjected to an oscillatory gravity

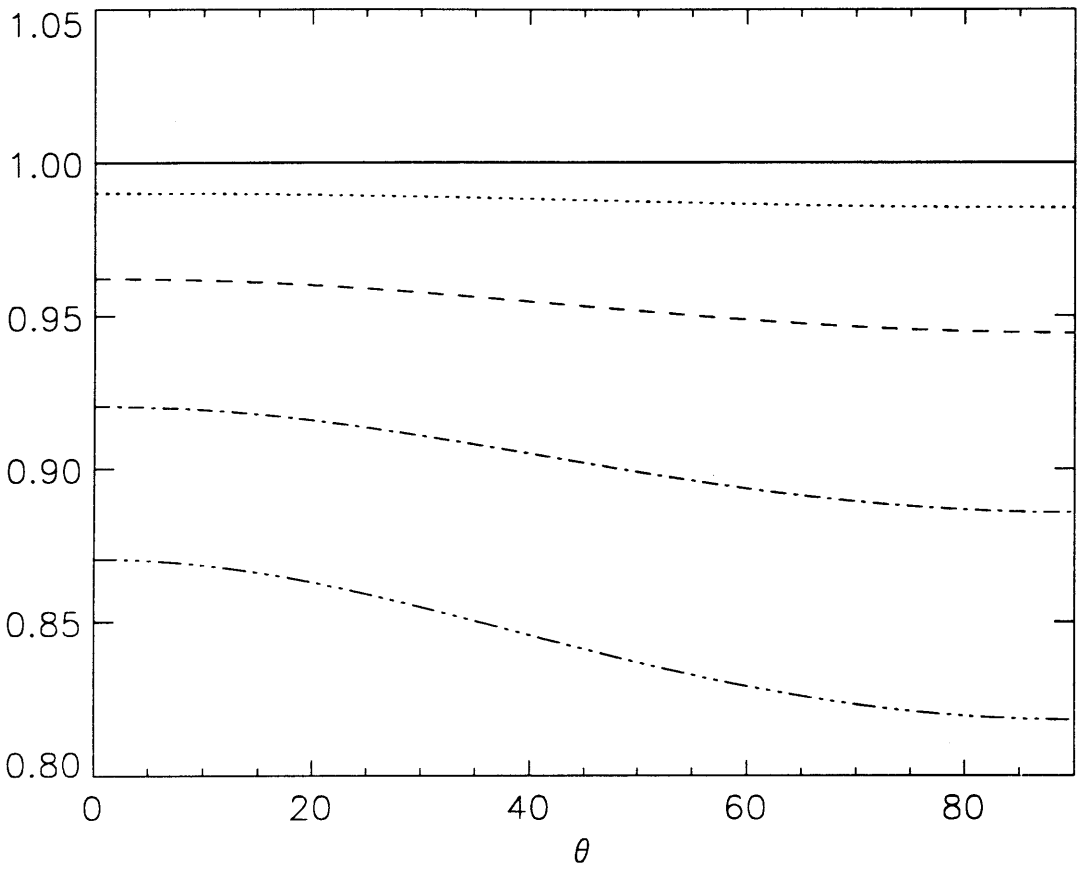

Figure III.4.1: Amplitude modulation ratio at the mean surface crossing for $KB = 0$ (——), $KB = 0.1$ (· · · · ·), $KB = 0.2$ (– – –), $KB = 0.3$ (–·–·–) and $KB = 0.4$ (—· · —· · —).

field. Its amplitude modulation is shown to be inversaly proportional to the square root of the time-dependent gravitational acceleration.

For small long wave slopes ($III.4.4$) can be approximated by

$$\frac{|A|}{\overline{A}} \simeq 1 + KB\cos\phi + \frac{K^2B^2}{2}\left[-(1+\sin^2\theta)+(3+\sin^2\theta)\cos^2\phi)\right] + \mathcal{O}(K^3B^3) \quad (III.4.6)$$

To leading order , the modulation of the amplitude is unaffected by the obliqueness of the short wave.

Next, we plot for $KB = 0.3$ the amplitude ($III.4.4$) normalized by its constant value ($III.4.5b$) at the trough against the long wave phase for several incidence angles. We observe on figure 4.2, for $KB = 0.3$ that these curves differ somewhat only in the vicinity of the surface crossings. This is expected in view of ($III.4.5a-c$).

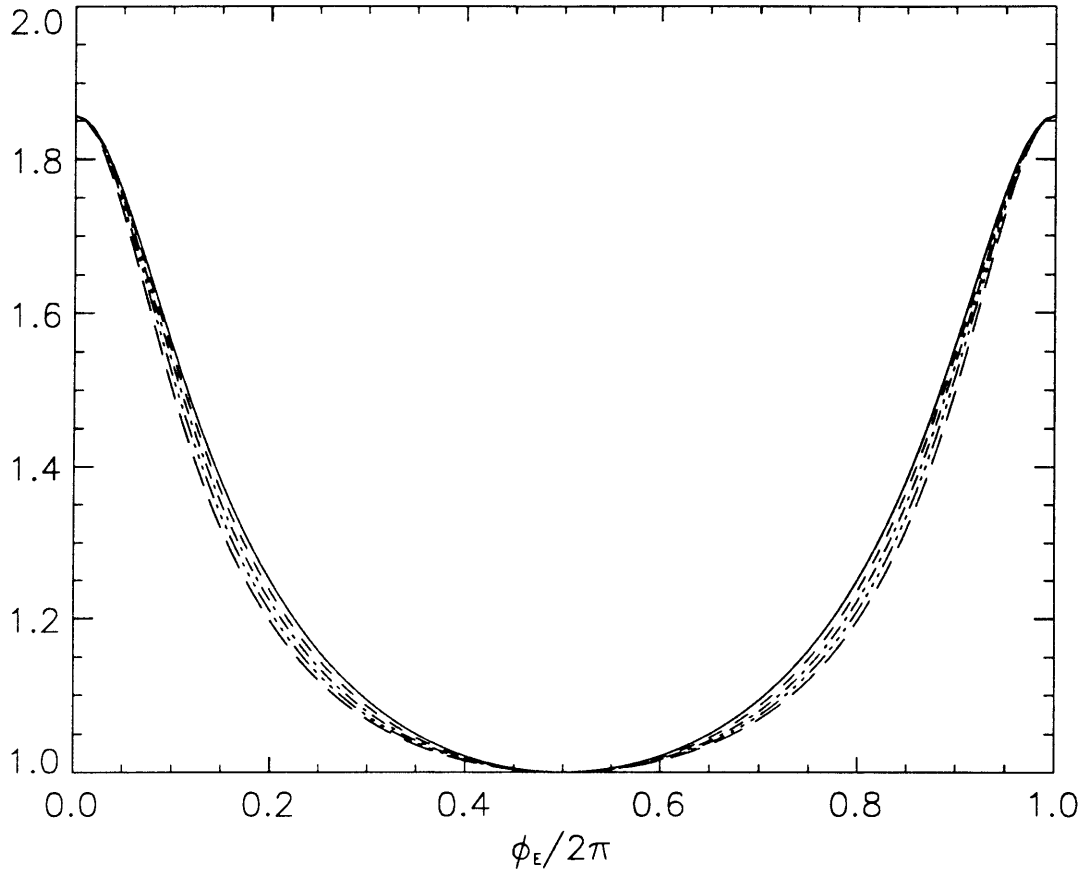

Figure III.4.2: Amplitude modulation ratio normalized by its value at the trough ($\phi = \phi_E = \pi$) with $KB = 0.3$ and $\theta = 0$, 30°, 45°, 60° and 75°, from upper to lower curve.

As pointed out earlier, the range of amplitude modulation does not vanish when the short waves propagate normally to Gerstner's wave.

4.2. Modulation of the Short Wave Wavenumber

4.2.1. *Derivation of the Eulerian wavenumber*

The phase of the short waves was first defined in $(III.3.3a-c)$ by its gradients and time rate of change in anticipation of variable wavenumber k and frequency σ. It was demonstrated that k is constant while σ is a function of ϕ only. Based on this knowldege, we may integrate $(III.3.3a-c)$ for S:

$$S = ka\cos\theta + kb\sin\theta - \int^t \sigma(t)dt \qquad (III.4.7)$$

The solution of the leading order short waves and the linear evolution equation for A suggest that S must be corrected and the true phase should read

$$\tilde{S} = S + \kappa_i c + \gamma(\phi, KB, \theta) \qquad (III.4.8)$$

where $\gamma(\phi, KB, \theta)$ corresponds to the phase term in $(III.4.2)$. Adopting a method similar to that developped in Chapter II, we deduce from $(III.2.10a-c)$ the leading order version of the Eulerian-Lagrangian mapping:

$$a = X - \frac{B}{\epsilon^2}\sin\phi e^{Kc_2} + \mathcal{O}(\epsilon) \qquad b = Y + \mathcal{O}(\epsilon) \qquad c = Z - \frac{B}{\epsilon^2}\cos\phi e^{Kc_2} + \mathcal{O}(\epsilon) \qquad (III.4.9a-c)$$

Substitution of $(III.4.9a-c)$ in $(III.4.8)$ yields the following series

$$\tilde{S} = \frac{1}{\epsilon^2}\tilde{S}_{-2} + \tilde{S}_0 + \mathcal{O}(\epsilon) \qquad (III.4.10a)$$

with

$$\tilde{S}_{-2} = -k\cos\theta\frac{B(1+K^2B^2)\sin\phi}{1+K^2B^2-2KB\cos\phi}e^{Kc_2} \qquad (III.4.10b)$$

and

$$\tilde{S}_0 = k\cos\theta\Big[X + \frac{2KB\sin\phi}{1+K^2B^2-2KB\cos\phi}Z\Big] + kY\sin\theta - \int^t \sigma(\tau)d\tau + \gamma(\phi, KB, \theta) \qquad (III.4.10c)$$

Note the resemblance of $(III.4.10b-c)$ to their counterpart in Chapter II, if k is replaced by $k\cos\theta$. A transverse component $k\sin\theta\, Y$ arises due to the obliqueness. The Eulerian wavenumber vector is then

$$\vec{k}^e = \nabla\tilde{S} + \epsilon\nabla_1\tilde{S} + \epsilon^2\nabla_2\tilde{S} + \ldots \qquad (III.4.11)$$

where $\nabla \equiv (\partial_X, \partial_Y, \partial_Z)$ and $\nabla_i \equiv (\partial_{X_i}, \partial_{Y_i}, \partial_{Z_i})$. Upon substituting $(III.4.10a)$ in $(III.4.11)$, we obtain

$$\vec{k}^e = \nabla\tilde{S}_0 + \nabla_2\tilde{S}_{-2} + \mathcal{O}(\epsilon) \qquad (III.4.12)$$

Recalling that $\tilde{S}_{-2}$ is a function of ϕ (thus of a_2) and c_2, $(III.4.12)$ can be rewritten as

$$\vec{k}^e = \nabla\tilde{S}_0 + \frac{\partial\tilde{S}_{-2}}{\partial\phi}\nabla_2\phi + \frac{\partial\tilde{S}_{-2}}{\partial c_2}\nabla_2 c_2 + \mathcal{O}(\epsilon) \qquad (III.4.13)$$

since $\phi = \Omega t_1 - Ka_2$, we apply the chain rule and find

$$\vec{k}^e = \nabla\tilde{S}_0 + K\Big[\tilde{S}_{-2}\nabla_2 c_2(X_2, Y_2, Z_2) - \frac{\partial\tilde{S}_{-2}}{\partial\phi}\nabla_2 a_2(X_2, Y_2, Z_2)\Big] + \mathcal{O}(\epsilon) \qquad (III.4.14)$$

The expression of $\nabla_2 a_2$ and $\nabla_2 c_2$ are needed. To this end, we first deduce from $(III.2.5)$ and $(III.2.9)$

$$\begin{cases} X_2 = a_2 + B\sin\phi\ e^{Kc_2} \\ Y_2 = b_2 \\ Z_2 = c_2 + B\cos\phi\ e^{Kc_2} \end{cases} \qquad (III.4.15)$$

after omitting $\mathcal{O}(\epsilon^3)$ terms. If use is made of Appendix I's eqs. $(6a-c)$, $(7a-c)$ and $(8a-c)$, with (X_2, Y_2, Z_2) and (a_2, b_2, c_2) instead of (X, Y, Z) and (a, b, c) respectively, along with $(III.4.15)$, we deduce the components of $\nabla_2 a_2$

$$\frac{\partial a_2}{\partial X_2} = \frac{1}{J}\frac{\partial Z_2}{\partial c_2} = \frac{1 + KB\cos\phi\ e^{Kc_2}}{1 - K^2B^2e^{2Kc_2}} \qquad \frac{\partial a_2}{\partial Y_2} = 0 \qquad (III.4.16a-b)$$

and

$$\frac{\partial a_2}{\partial Z_2} = -\frac{1}{J}\frac{\partial X_2}{\partial c_2} = -\frac{KB\sin\phi\ e^{Kc_2}}{1 - K^2B^2e^{2Kc_2}} \qquad (III.4.16c)$$

and similarly, the components of $\nabla_2 c_2$:

$$\frac{\partial c_2}{\partial X_2} = -\frac{1}{J}\frac{\partial Z_2}{\partial a_2} = -\frac{KB\sin\phi\ e^{Kc_2}}{1 - K^2B^2e^{2Kc_2}} \qquad \frac{\partial c_2}{\partial Y_2} = 0 \qquad (III.4.17a-b)$$

and

$$\frac{\partial c_2}{\partial Z_2} = \frac{1}{J}\frac{\partial X_2}{\partial a_2} = \frac{1 - KB\cos\phi\ e^{Kc_2}}{1 - K^2B^2e^{2Kc_2}} \qquad (III.4.17c)$$

Substitution of $(III.4.16a-c)$ and $(III.4.17a-c)$ with $c_2 = 0$ in $(III.4.14)$ yields the three components of $\vec{k}^e$

$$k_x^e = k\cos\theta\frac{1 - 3KB\cos\phi + 4K^2B^2\cos^2\phi - 2K^3B^3\sin^2\phi\cos\phi}{(1 - K^2B^2)(1 + K^2B^2 - 2KB\cos\phi)^2} +$$

$$+k\cos\theta\frac{-K^4B^4(1 + 4\cos^2\phi) + K^5B^5(1 + 2\cos^2\phi)\cos\phi}{(1 - K^2B^2)(1 + K^2B^2 - 2KB\cos\phi)^2} + \mathcal{O}(\epsilon) \qquad (III.4.18a)$$

$$k_y^e = k\sin\theta + \mathcal{O}(\epsilon) \qquad (III.4.18b)$$

and

$$k_z^e = k\cos\theta\frac{KB\sin\phi}{(1 - K^2B^2)(1 + K^2B^2 - 2KB\cos\phi)^2}$$

$$\left[1 - 2KB\cos\phi - 2K^2B^2\cos^2\phi + 6K^3B^3\cos\phi - K^4B^4(1 + 2\cos^2\phi)\right] + \mathcal{O}(\epsilon) \qquad (III.4.18c)$$

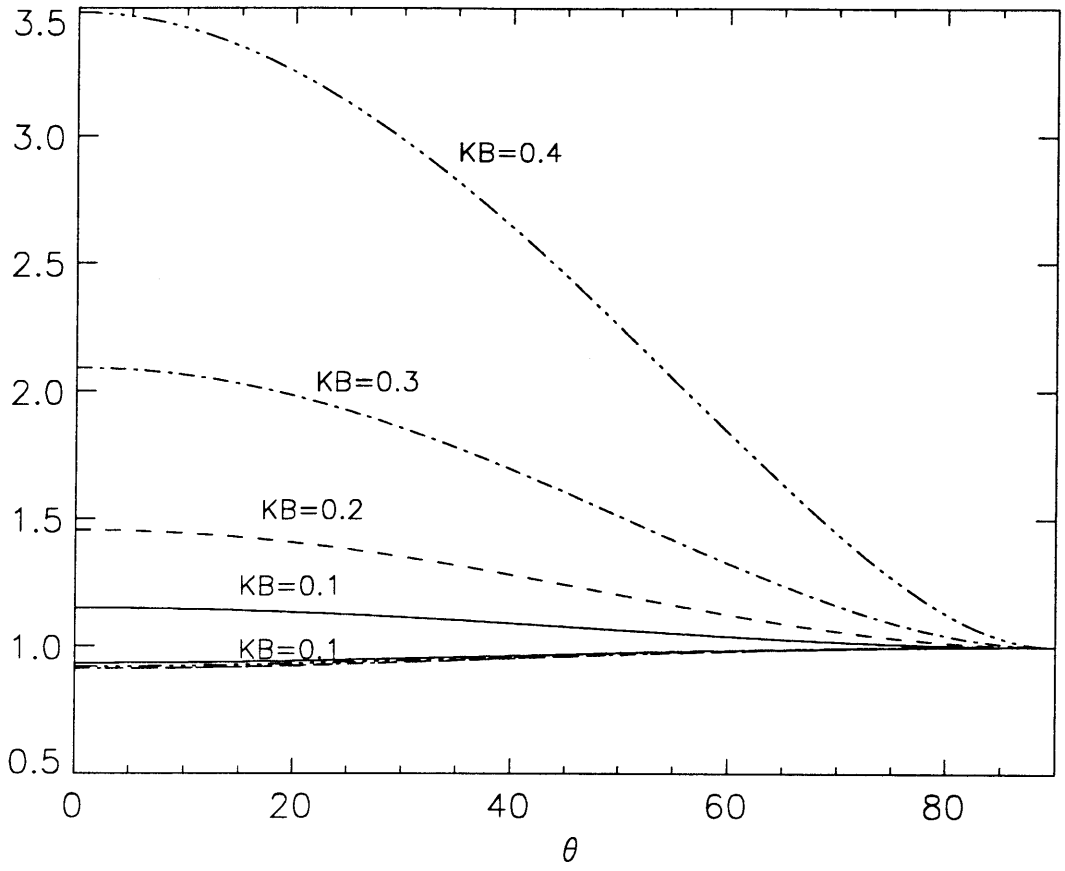

Figure III.4.3: Wavenumber modulation ratio (normalized by its value at the surface crossing) at the crest (top curves) and at the trough (bottom curves) for $KB = 0.1$, 0.2, 0.3 and 0.4.

Expressions $(III.4.18a)$ and $(III.4.18-c)$ clearly reduce to $(II.5.26)$ and $(II.5.30)$ when θ vanishes.

4.2.2. *Modulation of the Eulerian wavenumber*

We first calculate the modulation of k^e at the crest and trough of the long wave and normalize both quantities by the value of k^e at the surface crossing ($\cos\phi = -\frac{KB}{2}$). Figure 4.3. shows the two quantities plotted against the incidence angle θ for $KB = 0.1$, 0.2, 0.3 and 0.4. Larger slopes cause stronger modulation. Note however that, as θ increases the modulation range diminishes reaching zero at $\theta = 90°$. At normal incidence, the wavenumber $\vec{k}^e$ has no component in the vertical (X, Z) plane. This result is the same as if the short waves were just propagating on a perpendicular

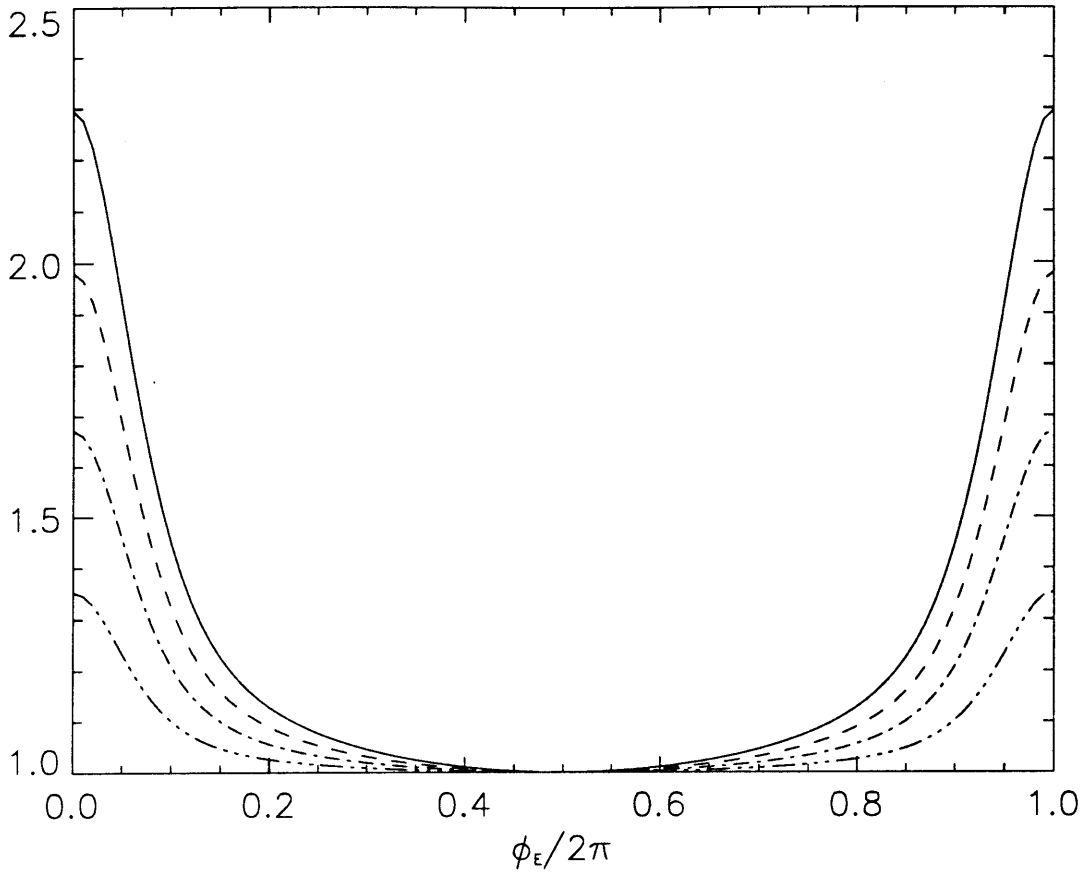

Figure III.4.4: Wavenumber modulation ratio normalized by its value at the trough ($\phi_E = \pi$) with $KB = 0.3$ and $\theta = 0$ (——), 30° (- - -), 45° (-·-·-), 60° (—· · —· · —) and 90° (horizontal axis).

current. In figure 4.4, the variations of the wavenumber k^e now normalized by its value at the trough are plotted against the long wave phase for several incidence angles and $KB = 0.3$. Modulation is at its largest for $\theta = 0$. Note that the profile for $\theta = 90°$ is undistinguishable from the horizontal axis.

It is worthwhile to investigate how the direction of $\vec{k}^e$ is affected by the presence of the long wave. We illustrate these variations in figure 4.5 for $\theta = 30°$. In the absence of long waves ($KB = 0$), the direction of $\vec{k}^e$ is unchanged. Upon increasing KB, the forward particle velocity at the crest of the long wave contributes to shifting the direction of $\vec{k}^e$ towards the X-axis, while at the trough the obliqueness is enhanced. For $KB \neq 0$, there are always two symmetrically located phases for which the direction of $\vec{k}^e$ is exactly θ and which approach respectively 0 and 2π as

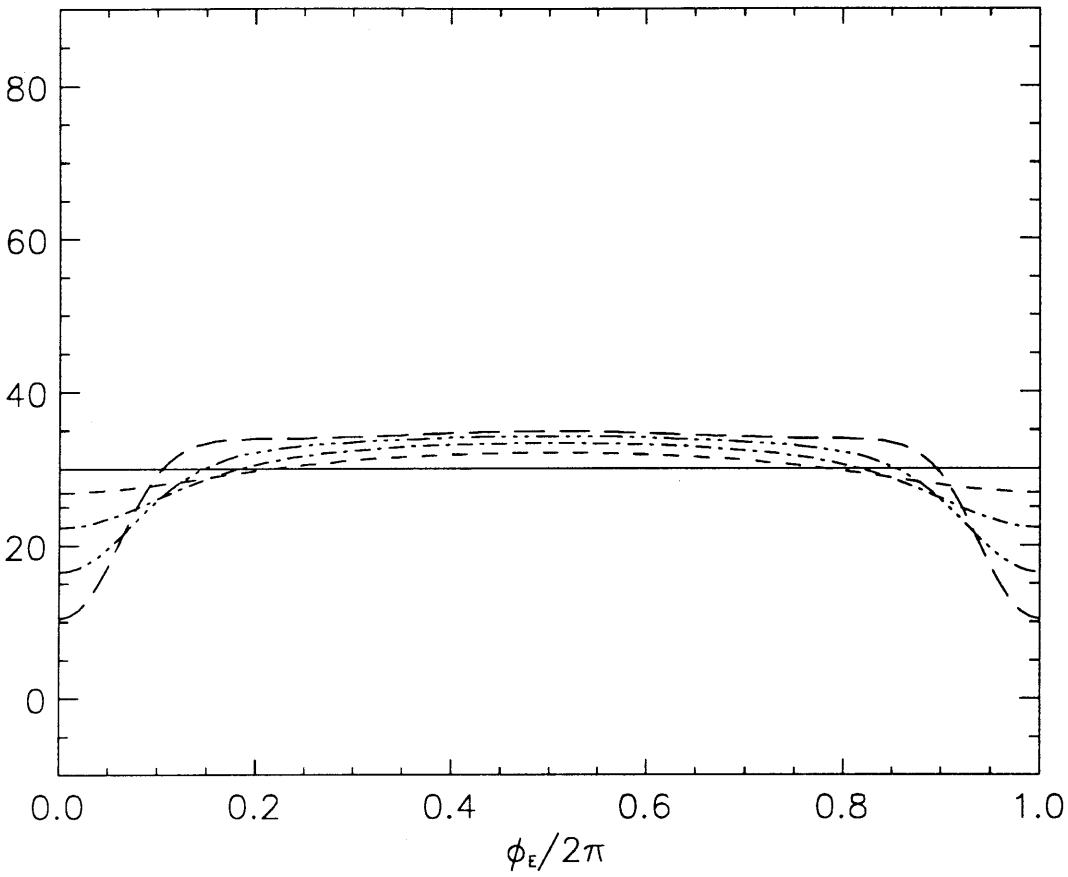

Figure III.4.5: Direction of propagation of the Eulerian short carrier wave (in degrees with respect to the X-axis) with $\theta = 30°$ for $KB = 0$ (——), $KB = 0.1$ (– – –), $KB = 0.2$ (—·—·—), $KB = 0.3$ (—· · ·—· · ·—) and $KB = 0.4$ (— — —).

KB increases.

Finally, we show in figure 4.6 for various incidence angles and $KB = 0.3$, the variations of the direction of $\vec{k}^e$. If the short wave is colinear or perpendicular to the X-axis, it remains so of course. Otherwise, there is a large modulation range reaching 20° for $\theta = 60°$.

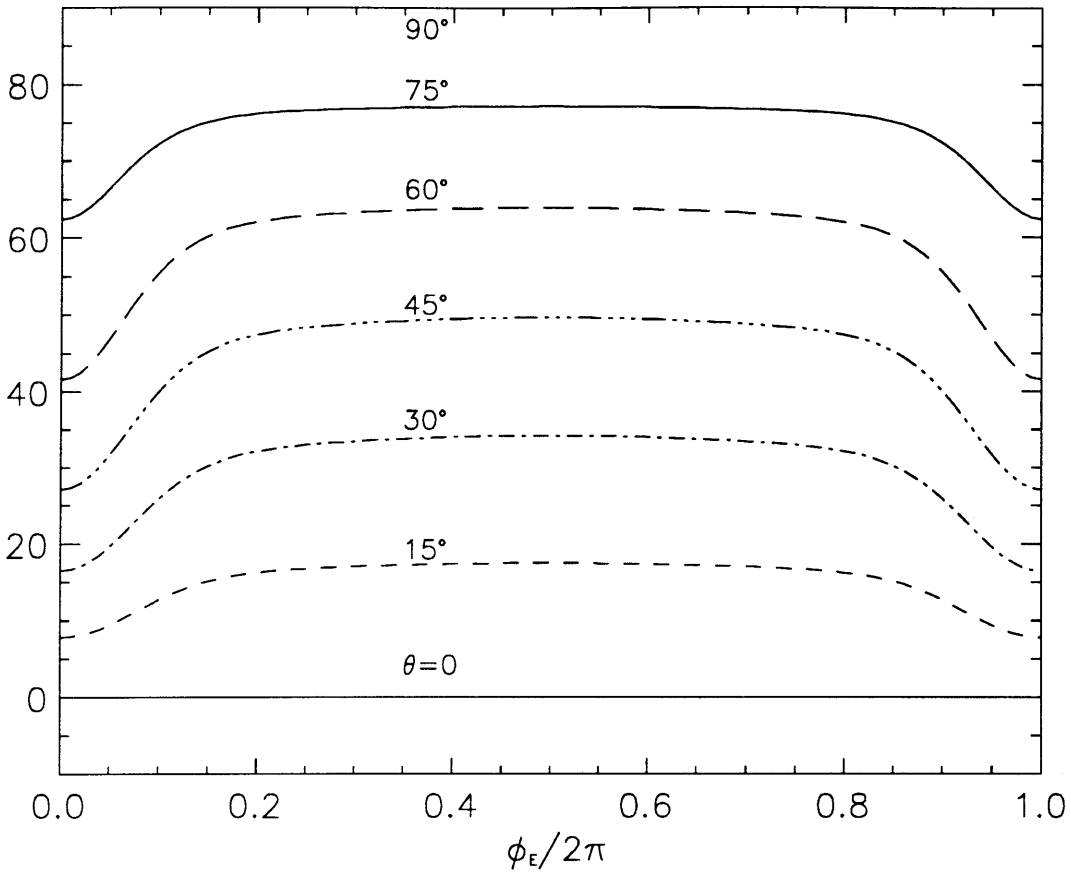

Figure III.4.6: Direction of propagation of the Eulerian short carrier wave for $KB = 0.3$ and incidence angle $\theta = 0$, 15°, 30°, 45°, 60°, 75° and 90°.

4.3. Absolute and Intrinsic Frequencies

The absolute frequency ω, or the frequency seen by a fixed observer, is defined in terms of $\tilde{S}$ as

$$\omega = -\left.\frac{\partial \tilde{S}}{\partial t}\right|_{X,X_1} - \epsilon \left.\frac{\partial \tilde{S}}{\partial t_1}\right|_{X,X_1} + \mathcal{O}(\epsilon) \qquad (III.4.19)$$

where the time derivative must be taken while keeping X, X_1 constant. Substitution of $(III.4.10a)$ in $(III.4.19)$ yields

$$\omega = -\left.\frac{\partial \tilde{S}_0}{\partial t}\right|_{X,X_1} - \frac{1}{\epsilon}\left.\frac{\partial \tilde{S}_{-2}}{\partial t_1}\right|_{X,X_1} + \mathcal{O}(\epsilon) = -\left.\frac{\partial \tilde{S}_0}{\partial t}\right|_{X,X_1} - \frac{1}{\epsilon}\frac{\Omega}{1 - KB\cos\phi}\frac{\partial \tilde{S}_{-2}}{\partial \phi} + \mathcal{O}(\epsilon) \qquad (III.4.20)$$

after making use of $(II.5.43)$. Upon invoking the definition of $\tilde{S}_{-2}$ and the dispersion

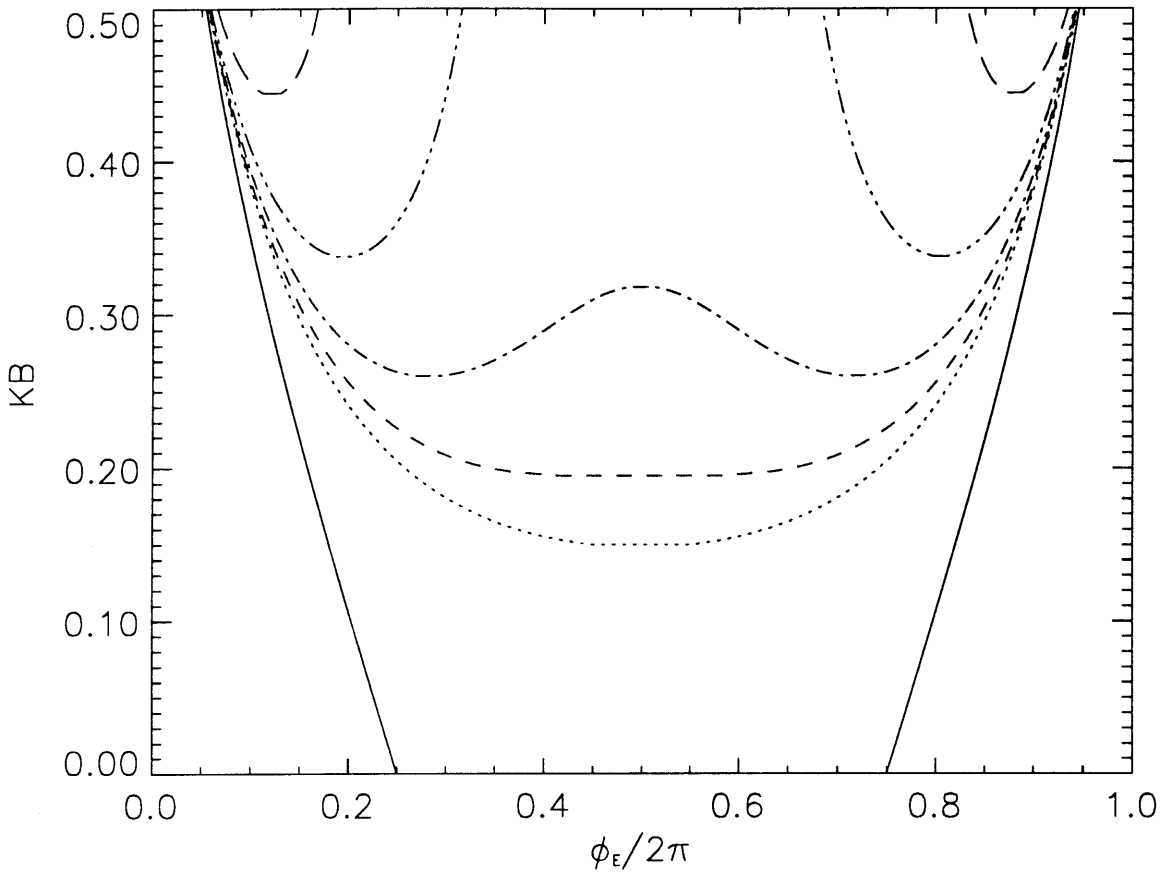

Figure III.4.7: Contours of $\frac{\omega}{\sigma}(\phi_E, KB, \epsilon\frac{\Omega}{\sigma})$, $\frac{\omega}{\sigma} = 1$ (solid lines); $\frac{\omega}{\sigma} = 0$ with $\epsilon\frac{\Omega}{\sigma_0} = 0.1$ and $\theta = 0$ ($\cdots\cdots$), $30°$ ($- - -$), $45°$ ($-\cdot-\cdot-$), $60°$ ($—\cdot\cdot—\cdot\cdot—$) and $75°$ ($— \ — \ —$).

relations for the short and long waves, the absolute frequency becomes

$$\frac{\omega}{\sigma} = 1 + \frac{KB}{\epsilon\frac{\Omega}{\sigma}} \frac{1 + K^2B^2}{1 - KB\cos\phi} \frac{\cos\theta}{R} \frac{(1 + K^2B^2)\cos\phi - 2KB}{(1 + K^2B^2 - 2KB\cos\phi)^2} + \mathcal{O}(\epsilon) \qquad (III.4.21)$$

Next, we recall that $\sigma = \sqrt{R}\sigma_0$ where $\sigma_0 = \sqrt{gk}$. Eq. $(III.4.21)$ thus becomes

$$\frac{\omega}{\sigma} = 1 + \frac{KB}{\epsilon\frac{\Omega}{\sigma_0}} \frac{1 + K^2B^2}{1 - KB\cos\phi} \frac{\cos\theta}{\sqrt{R}} \frac{(1 + K^2B^2)\cos\phi - 2KB}{(1 + K^2B^2 - 2KB\cos\phi)^2} + \mathcal{O}(\epsilon) \qquad (III.4.22)$$

Note that apart from the ratio $\frac{\cos\theta}{\sqrt{R}}$, $(III.4.22)$ is identical to $(II.5.26)$. There are two interesting special cases of $(III.4.22)$. One corresponding to $\omega = \sigma$; this occurs either when

$$\cos\phi = \frac{2KB}{1 + K^2B^2} \qquad (III.4.23)$$

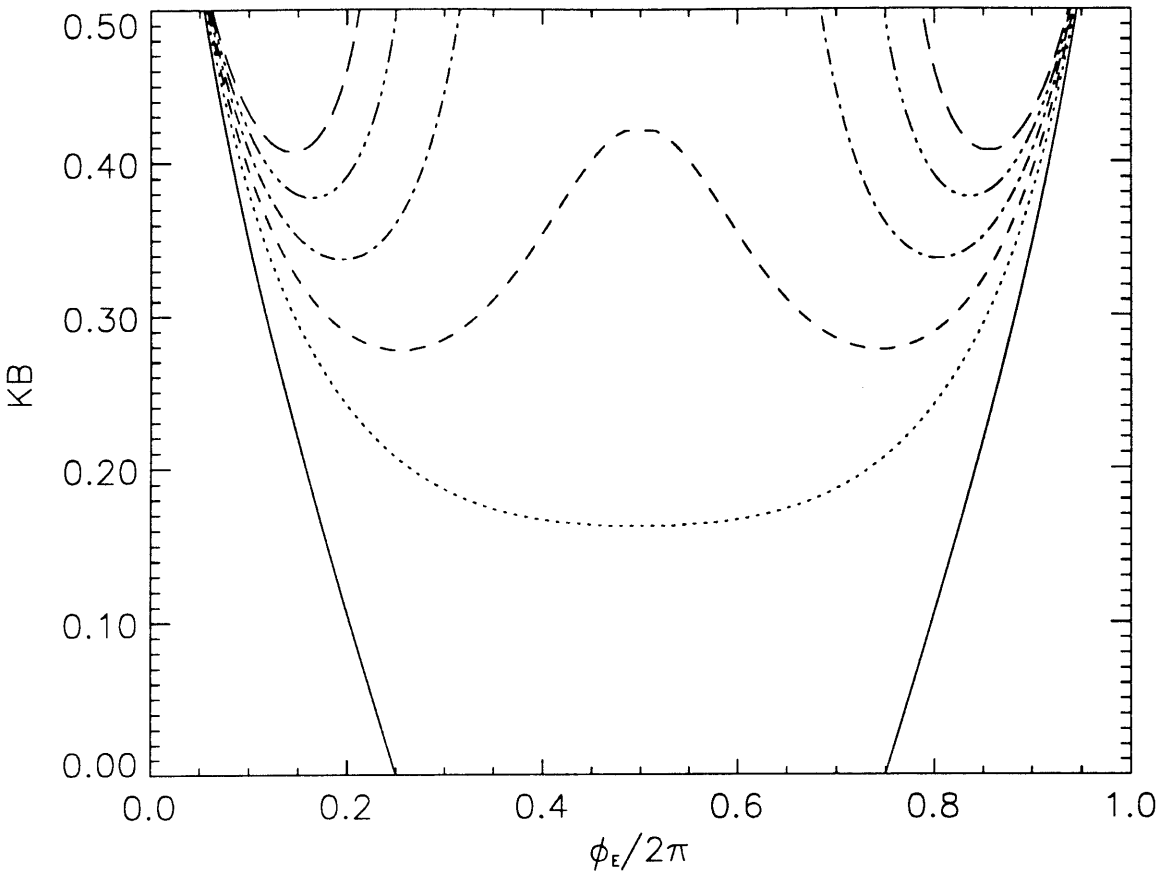

Figure III.4.8: Contours of $\frac{\omega}{\sigma}(\phi_E, KB, \epsilon\frac{\Omega}{\sigma})$, $\frac{\omega}{\sigma} = 1$ (solid lines); $\frac{\omega}{\sigma} = 0$ with $\theta = 60°$ and $\epsilon\frac{\Omega}{\sigma_0} = 0.05$ (· · · · ·), $\epsilon\frac{\Omega}{\sigma_0} = 0.075$ (– – –), $\epsilon\frac{\Omega}{\sigma_0} = 0.1$ (–·–·–), $\epsilon\frac{\Omega}{\sigma_0} = 0.125$ (—· · ·—· · ·—) and $\epsilon\frac{\Omega}{\sigma_0} = 0.15$ (— — —).

as in §II.5 or when $\theta = 90°$. The second special case corresponds to $\omega = 0$. The presence of $\sqrt{R}$ in $(III.4.22)$ precludes a simple analytical solution for ϕ; the contour $\omega = 0$ is therefore found numerically. We plot in figure 4.7 the two branches associated with $(III.4.23)$ (solide lines), along with the contour $\omega = 0$ for $\epsilon\frac{\Omega}{\sigma_0} = 0.1$, $\theta = 0$, 30°, 45°, 60° and 75° (discontinuous lines). The area below (above) a given curve $\omega = 0$ corresponds to $\omega < 0$ ($\omega > 0$). As the incidence angle increases, the contour $\omega = 0$ in the (ϕ_E, KB) plane moves towards larger values of KB, thus making it less probable that a short wave train be perceived by a fixed observer as propagating to the left. Note also that for small incidence angles, left-going short waves first appear at the trough of the long waves. However, as θ increases past 45°, left going short waves are first observed for much steeper long waves, in the

vicinity of the free surface crossing.

Finally, we plot in figure 4.8 the two contour lines $\omega = \sigma$ and $\omega = 0$ with $\theta = 60°$ and $\epsilon\frac{\Omega}{\sigma_0} = 0.05$, 0.075, 0.1, 0.125 and 0.15. Small frequency ratios *i.e.* larger scale contrast between the short and long wave lead to left going short waves for comparatively small KB. In particular, for $\epsilon\frac{\Omega}{\sigma_0} = 0.15$, KB must be greater than 0.4 to allow reflected short waves in the vicinity of the crest.

4.4. Group Velocity, Caustics and Reflection

4.4.1. *Derivation of the absolute group velocity*

It is well known that when a wave train propagates over a variable topography or current, the envelope and the carrier wave may propagate in different directions. We have just found in §4.3 evidence that, under certain circumstances, the carrier waves in the short wave train can be reflected to the left. The objective of this section is to see whether similar conclusions can be reached for the envelope of the short waves riding on long waves. To this end we recall the linear evolution equation $(III.3.42a)$

$$\frac{\partial A}{\partial t_1}+\frac{\sigma\cos\theta}{2R^2k}\frac{\partial A}{\partial a_1}+\frac{\sigma\sin\theta}{2R^2k}(1+K^2B^2-2KB\cos\phi)\frac{\partial A}{\partial b_1}+\Omega(D_r+iD_i)=0 \quad (III.4.24)$$

The direction of propagation of the amplitude (and energy) is dictated by the components of the group velocity evaluated in a fixed frame of reference. Thus, we first need to express the gradients in $(III.4.24)$ in terms of Eulerian derivatives, that is

$$\frac{\partial A}{\partial a_1}=\frac{\partial A}{\partial X_1}\frac{\partial X_1}{\partial a_1}+\frac{\partial A}{\partial Y_1}\frac{\partial Y_1}{\partial a_1} \qquad \frac{\partial A}{\partial b_1}=\frac{\partial A}{\partial X_1}\frac{\partial X_1}{\partial b_1}+\frac{\partial A}{\partial Y_1}\frac{\partial Y_1}{\partial b_1} \qquad (III.4.25a-b)$$

according to the chain rule. From $(III.2.10a-b)$, we deduce

$$X_1 = a_1 + \frac{1}{\epsilon}x_{-2} + \mathcal{O}(\epsilon^2) \qquad Y_1 = b_1 + \mathcal{O}(\epsilon^2) \qquad (III.4.26a-b)$$

and obtain for $(III.4.25a-b)$

$$\frac{\partial A}{\partial a_1}=\frac{\partial A}{\partial X_1}+\mathcal{O}(\epsilon^2) \qquad \frac{\partial A}{\partial b_1}=\frac{\partial A}{\partial Y_1}+\mathcal{O}(\epsilon^2) \qquad (III.4.27a-b)$$

Next, we must rewrite the Lagrangian time derivative

$$\left.\frac{\partial A}{\partial t_1}\right|_{a,a_1}=\left.\frac{\partial A}{\partial t_1}\right|_{X,X_1}+\left.\frac{\partial A}{\partial X_1}\frac{\partial X_1}{\partial t_1}\right|_{a,a_1}+\left.\frac{\partial A}{\partial Y_1}\frac{\partial Y_1}{\partial t_1}\right|_{a,a_1} \qquad (III.4.28)$$

Evaluation of the velocity components yields

$$\left.\frac{\partial A}{\partial t_1}\right|_{a,a_1} = \left.\frac{\partial A}{\partial t_1}\right|_{X,X_1} + \left.\frac{1}{\epsilon}\frac{\partial A}{\partial X_1}\frac{\partial x_{-2}}{\partial t_1}\right|_{a,a_1} + \mathcal{O}(\epsilon^2) = \left.\frac{\partial A}{\partial t_1}\right|_{X,X_1} + \frac{1}{\epsilon}\Omega B\cos\phi\frac{\partial A}{\partial X_1} + \mathcal{O}(\epsilon^2) \tag{III.4.29}$$

Substitution of $(III.4.27a-b)$ and $(III.4.29)$ in $(III.4.24)$ yields the components of the group velocity

$$C_{gX} = \frac{\sigma\cos\theta}{2R^2k} + \frac{1}{\epsilon}\Omega B\cos\phi \tag{III.4.30a}$$

and

$$C_{gY} = \frac{\sigma\sin\theta}{2R^2k}(1 + K^2B^2 - 2KB\cos\phi) \tag{III.4.30b}$$

The direction Θ of the group velocity is therefore given by

$$\Theta \equiv \tan^{-1}\frac{C_{gY}}{C_{gX}} = \tan^{-1}\left\{\frac{\sin\theta(1 + K^2B^2 - 2KB\cos\phi)}{\cos\theta + \frac{2R^{\frac{5}{2}}}{\epsilon\frac{\Omega}{\sigma_0}}KB\cos\phi}\right\} \tag{III.4.31}$$

4.4.2. *Description of results*

We show in figure 4.9 the variations of Θ against ϕ_E for $\theta = 30°$, $\epsilon\frac{\Omega}{\sigma_0} = 0.1$ and several values of KB. As expected, when $KB = 0$ the carrier wave and its amplitude propagate in the same direction. Consider a short wave located at the crest, $\phi = 2\pi$, of a steep long wave. The group velocity of the short waves is almost parallel to the long wave particle velocity *i.e.* the short waves are moving to the right. As time elapses, the short wave train is overtaken by the crest and is now in the section $\phi \in [\frac{3\pi}{2}, 2\pi]$ where, as the particle velocity decreases, the direction Θ of the group velocity (of the short waves which are still propagating to the right) is shifted away from the long wave axis. In the vicinity of the free surface crossing $\phi \simeq \frac{3\pi}{2}$, the a-component of the group velocity in the particle frame of reference is the negative of the long wave particle velocity resulting in $C_{g_x} = 0$, *i.e.* $\Theta = 90°$. The short wave energy propagates along the Y-axis. As the long wave propagates further to the right, the short wave train is now closer to the trough and the negative long wave particle velocity easily overcomes C_{g_a}, inducing the energy of the short waves to propagate to the left. The phase ϕ_E such that $\Theta(\phi_E) = 90°$ clearly corresponds to a caustic. When $\phi_E = \pi$, Θ reaches a maximum and the ray experiences an inflexion

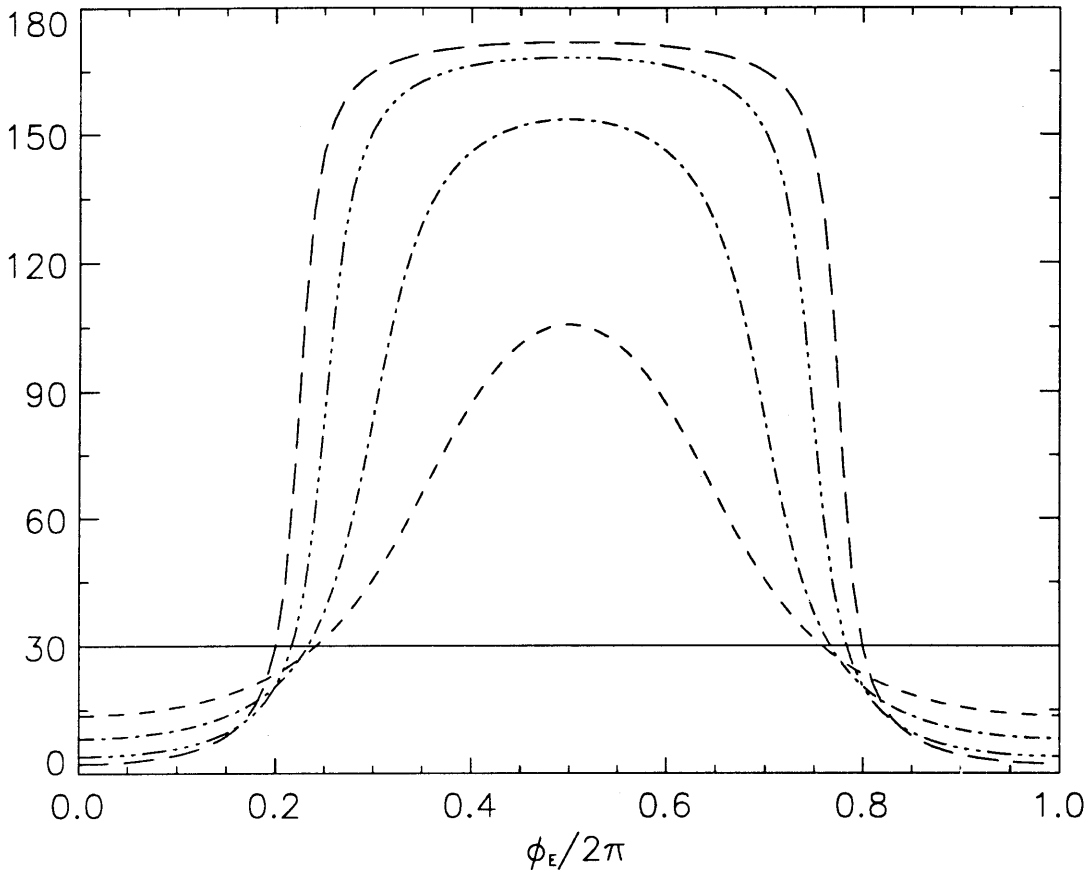

Figure III.4.9: Direction of propagation of the short wave envelope Θ (in degrees with respect to the X-axis) with $\theta = 30°$ and $\epsilon\frac{\Omega}{\sigma_0} = 0.1$ for $KB = 0$ (——), $KB = 0.05$ (– – –), $KB = 0.1$ (–·–·–), $KB = 0.2$ (——·——·——) and $KB = 0.3$ (— — —).

point. As ϕ_E decreases further, the particle velocity of the long wave increases, causing the angle Θ to decrease. In the vicinity of $\phi_E = \frac{\pi}{2}$ the short wave energy encounters a second caustic as Θ decreases from above to below 90°. The energy of the short wave is unable to climb the slope of the long wave and instead turns back and is advected by the increasing positive long wave particle velocity.

5. LINEAR INSTABILITY OF A SHORT STOKES WAVE TO TWO-DIMENSIONAL DISTURBANCES

We have shown in Chapter II for colinear waves, that the presence of a steep Gerstner wave affects drastically the stability of short Stokes wave trains to sideband disturbances. In particular, a new feature is the presence of multiple bands of instability which increases the likelyhood that higher harmonics of sideband wavenumbers in the main instability lobe are also unstable.

It is well known that, in a calm sea, Stokes waves are also unstable to two-dimensional disturbances. With a formulation based on the narrow band assumption, Benney & Roskes(1969) have proved the existence of an infinite instability strip in the wavenumber domain, see figure 5.1b. If the Zakharov formulation is adopted, on the other hand, the unstable region becomes bounded and is shaped like a crescent cf. Crawford *et al*(1981). In this section, we extend the theory of Benney & Roskes by adding a long wave.

The uniform short Stokes wave, $\mathcal{A}_s$, derived in Chapter II is still, by definition, a solution of $(III.3.54)$. The details of $\mathcal{A}_s$ may be found in §II.6.1.

5.1. Formulation of the Linearized Instability Problem

Let us rewrite $\mathcal{A}$ by factoring out the uniform solution $\mathcal{A}_s$

$$\mathcal{A}(\xi,\eta,\phi) = \mathcal{A}_s(\phi)\tilde{\mathcal{A}}(\xi,\eta,\phi) \qquad (III.5.1)$$

Substitution of $(III.5.1)$ in $(III.3.46)$ yields an evolution equation for $\tilde{\mathcal{A}}$:

$$\frac{\partial\tilde{\mathcal{A}}}{\partial\phi} = -i\frac{\alpha}{4}\frac{\partial^2\tilde{\mathcal{A}}}{\partial\xi^2} + i\frac{\alpha}{2}(1+K^2B^2-2KB\cos\phi)\frac{\partial^2\tilde{\mathcal{A}}}{\partial\eta^2} - i\alpha G(\phi)|\tilde{\mathcal{A}}|^2\tilde{\mathcal{A}} \qquad (III.5.2)$$

where $G(\phi)$ is defined by $(II.6.4-5)$. This will be regarded as the canonical form. In the absence of modulation in the transverse direction, $\frac{\partial}{\partial\eta} = 0$, we recover $(II.6.12)$. Next, we decompose the complex amplitude $\tilde{\mathcal{A}}$ as

$$\tilde{\mathcal{A}} = d(\xi,\eta,\phi)e^{iW(\xi,\eta,\phi)} \qquad (III.5.3)$$

where both d and W are real. Substitution of $(III.5.3)$ in $(III.5.2)$ yields two

equations after separation of the real and imaginary parts

$$\frac{\partial d}{\partial \phi} = \frac{\alpha}{4}\left[\frac{\partial}{\partial \xi}(d\frac{\partial W}{\partial \xi}) + \frac{\partial d}{\partial \xi}\frac{\partial W}{\partial \xi}\right] - \frac{\alpha}{2}(1 + K^2B^2 - 2KB\cos\phi)\left[\frac{\partial}{\partial \eta}(d\frac{\partial W}{\partial \eta}) + \frac{\partial d}{\partial \eta}\frac{\partial W}{\partial \eta}\right] \qquad (III.5.4a)$$

and

$$\frac{\partial W}{\partial \phi} = -\frac{\alpha}{4}\left[\frac{1}{d}\frac{\partial^2 d}{\partial \xi^2} - (\frac{\partial W}{\partial \xi})^2\right] + \frac{\alpha}{2}(1 + K^2B^2 - 2KB\cos\phi)\left[\frac{1}{d}\frac{\partial^2 d}{\partial \eta^2} - (\frac{\partial W}{\partial \eta})^2\right] +$$

$$-\alpha G(\phi)d^2 \qquad (III.5.4b)$$

The uniform Stokes wave solution derived in §II.6.1 is characterized by an amplitude $d_0 = 1$ and a phase $W_0 = W_0(\phi)$ which satisfies

$$\frac{\partial W_0}{\partial \phi} = -\alpha G(\phi) \qquad (III.5.5a)$$

i.e.

$$W_0(\phi) = -\alpha \int^{\phi} G(\phi')d\phi' \qquad (III.5.5b)$$

As observed in Chapter II, W_0 cannot be integrated analytically. Let us now perturb around this solution and assume

$$d = 1 + d' \qquad W = W_0(\phi) + W' \qquad (d', W') \ll 1 \qquad (III.5.6a - b)$$

Substitution of $(III.5.6a - b)$ in $(III.5.4a - b)$ yields

$$\frac{\partial d'}{\partial \phi} = \alpha\left[\frac{1}{4}\frac{\partial^2 W'}{\partial \xi^2} - \frac{1}{2}(1 + K^2B^2 - 2KB\cos\phi)\frac{\partial^2 W'}{\partial \eta^2}\right] \qquad (III.5.7a)$$

$$\frac{\partial W'}{\partial \phi} = -\alpha\left[\frac{1}{4}\frac{\partial^2 d'}{\partial \xi^2} - \frac{1}{2}(1 + K^2B^2 - 2KB\cos\phi)\frac{\partial^2 d'}{\partial \eta^2} + 2G(\phi)d'\right] \qquad (III.5.7b)$$

after invoking $(III.5.5a)$ and discarding terms quadratic in the disturbance. We then assume the disturbances d' and W' to be in the form of plane waves

$$d' = \tilde{d}e^{i(\nu_x\xi + \nu_y\eta)} \qquad W' = \tilde{W}e^{i(\nu_x\xi + \nu_y\eta)} \qquad (III.5.8a - b)$$

where $\tilde{d}$ and $\tilde{W}$ are only functions of ϕ. Eqs. $(III.5.7a - b)$ can be expressed in terms of $\tilde{d}$ and $\tilde{W}$

$$\frac{\partial \tilde{d}}{\partial \phi} = \frac{\alpha}{2}\left[-\frac{\nu_x^2}{2} + (1 + K^2B^2 - 2KB\cos\phi)\nu_y^2\right]\tilde{W} \qquad (III.5.9a)$$

$$\frac{\partial \tilde{W}}{\partial \phi} = -2\alpha\left[G(\phi) - \frac{\nu_x^2}{8} + \frac{1}{4}(1 + K^2B^2 - 2KB\cos\phi)\nu_y^2\right]\,\tilde{d} \qquad (III.5.9b)$$

As in Chapter II, we obtain a set of two coupled non-autonomous ordinary differential equations with periodic coefficients. If $\mathbf{M}$ is the coefficient matrix of $(III.5.9a-b)$, we simply have

$$\frac{\partial}{\partial \phi}\begin{pmatrix} \tilde{d} \\ \tilde{W} \end{pmatrix} = \mathbf{M}\begin{pmatrix} \tilde{d} \\ \tilde{W} \end{pmatrix} \qquad (III.5.10)$$

We again invoke Floquet theory and deduce the growth rate from the Floquet multipliers $\mu_{1,2}$

$$g_r = \max\{\Re(\log\mu_1), \Re(\log\mu_2)\} \qquad (III.5.11)$$

Note that the trace of the matrix in $(III.5.10)$ is zero and consequently the two multipliers satisfy $\mu_1\mu_2 = 1$ (cf. Appendix G). This provides a check of the accuracy of the numerical integration.

5.2. Results of Stability Analysis

For the sake of reference and to allow further comparison, we have plotted in figure 5.1a the growth rate of a two-dimensional sideband disturbance to a Stokes wave propagating on a calm sea (Benney & Roskes; 1969). Figure 5.1b shows the boundary of instability in the (ν_x, ν_y) plane †. The upper boundary is the straight line $\nu_x - \sqrt{2}\nu_y = 0$ while the lower boundary is a parabola. In these and the remaining computations, the product $\mu_1\mu_2$ never departed from unity by more than 10^{-8}.

We now assume the presence of a long wave ($KB \neq 0$). In a first step, we investigate the behavior of the Floquet multipliers as the wavenumber of the sideband disturbance varies. Next, we analyse the effect of the long slope KB and finally the effect of both the short wave slope and the frequency ratio through α.

5.2.1. *Influence of the sideband wavenumber ν*

The growth rates are first computed for $(\nu_x, \nu_y) \in [0,6] \times [0,6]$ and $KB = 0.1$, $\epsilon kA = 0.13$ and $\alpha = 0.125$. The three-dimensional display of growth rates and the

† This boundary is obtained by plotting the contour line $g_r = 10^{-5}$.

boundaries of instability are shown in figure 5.2a-b respectively. As conjectured earlier, new instability zones appear.

In the region $\nu_x > \sqrt{2}\nu_y$, the new instability zones consist of concave bands. In the region $\nu_x < \sqrt{2}\nu_y$, however they are convex. Note that some of these bands appear to be non-contiguous. Upon magnifying the upper left quadrant, we obtain figure 5.3a-b, where a contiguous instability band replaces the string of "islands" originating near $\nu_y = 3.75$.

In order to elucidate the structure of the string of "islands", we magnify a portion of figure 5.2b corresponding to $\nu_x = 0.5$ and $\nu_y \in [0, 6]$. Figure 5.4a shows the locus of the Floquet multiplier μ_1 as ν_y is varied. The locus of μ_2 is easily deduced from $\mu_1\mu_2 = 1$. As in Chapter II, the Floquet multipliers are either real and reciprocal of each other or a pair of complex conjugates on the unit circle. In the former case, there is instability since either $|\mu_1|$ or $|\mu_2|$ is greater than unity, while in the latter case there is neutral stability as $|\mu_1| = |\mu_2| = 1$. The transition between the two states occurs at $\mu = \pm 1$.

From figure 5.4a, it is difficult to track in the complex plane the position of μ_1 as ν_y is varied. We thus plot in figure 5.4b $\log|\mu_1|$ and $\arg(\mu_1)$ as a function of ν_y with $\nu_x = 0.5$. For small values of ν_y, $\arg(\mu_1) = 0$ and the growth rate $g_r = \log|\mu_1|$ is non-zero corresponding to the main band observed in figure 5.2a-b. Upon increasing ν_y, the system goes through neutral stability with $\mu_1 = \mu_2 = 1$, *ie* $g_r = 0$. μ_1 then traces the upper-half unit circle, as its argument increases from 0 to π as shown by the chain line in figure 5.4b. For $\nu_y \simeq 2.5$, both μ_1 and μ_2 reach the value -1 before instability arises as μ_1 approaches the origin on the real axis in figure 5.4a. While μ_1 corresponds to the stable manifold (negative growth rate), μ_2 gives rise to the second instability lobe in figure 5.2a. A further increase of ν_y restabilizes the disturbance as μ_1 moves back to -1 and retraces the upper half circle to reach 1 at $\nu_y \simeq 3.75$. If ν_y is further increased, μ_1 leaves the unit circle and thus causes the third and last band of instability shown in figure 5.2b. Note in figure 5.4b the presence of a small instability lobe in the vicinity of $\nu_y = 4.75$. This numerical observation confirms that the "islands" in figure 5.2a are in fact merely the most prominent tips of a continuous ridge whose width and height are too small

to be captured by the surface and contour plots. We present below a theoretical proof of these observations.

Let us reduce $(III.5.10a-b)$ to a Mathieu equation in canonical form

$$\frac{\partial^2 y}{\partial \phi^2} + (\Upsilon + \Delta \cos\phi) y = 0 \qquad (III.5.12)$$

To this end, we take the ϕ derivative of $(III.5.9a)$, subsitute $(III.5.9b)$ in to obtain

$$\tilde{d}_{\phi\phi} - \alpha\nu_y^2 KB \sin\phi\, \tilde{W} + \alpha^2 \left[(1 + K^2B^2 - 2KB\cos\phi)\nu_y^2 - \frac{\nu_x^2}{2}\right] \times$$

$$\left[G(\phi) - \frac{\nu_x^2}{8} + \frac{1}{4}(1 + K^2B^2 - 2KB\cos\phi)\nu_y^2\right]\tilde{d} = 0 \qquad (III.5.13)$$

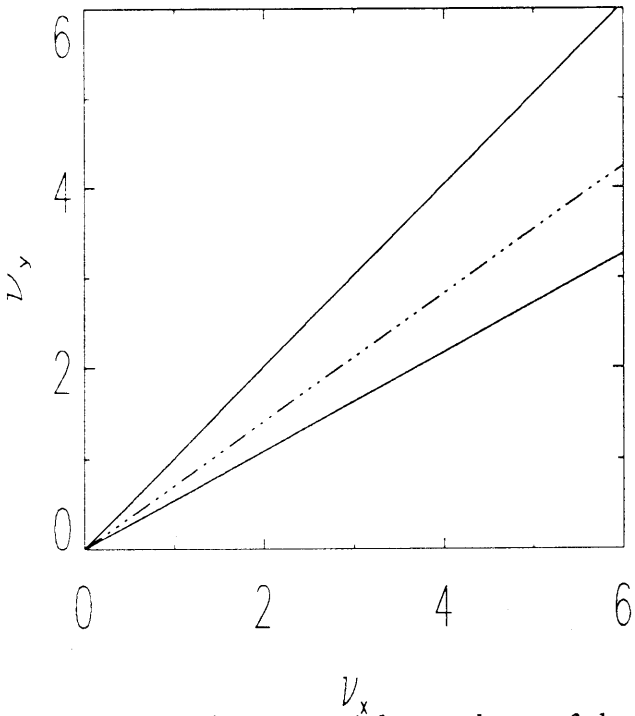

Figure III.5.5: Wedge in the upper right quadrant of the (ν_x, ν_y) plane where the reduction to a Mathieu equation is not possible with $KB = 0.3$.

In order to eliminate $\tilde{W}$, we need to ascertain that its coefficient in $(III.5.9a)$ does not vanish for any value of ϕ. It can easily be shown that

$$-\frac{\nu_x^2}{2} + (1 + K^2B^2 - 2KB\cos\phi)\nu_y^2 \quad \gtrless \quad 0 \qquad \forall\phi \qquad (III.5.14a-b)$$

provided that

$$\nu_x^2 - 2(1 \mp KB)^2 \nu_y^2 \quad \lessgtr \quad 0 \qquad (III.5.15a-b)$$

Eqs. $(III.5.15a-b)$ mean that provided (ν_x, ν_y) is outside the two wedges centered respectively on $\nu_x = \pm\sqrt{2}\nu_y$ (cf. figure 5.5 for the wedge in the upper right quadrant), the coefficient of $\tilde{W}$ in $(III.5.9a)$ never changes sign. We may then eliminate $\tilde{W}$ and obtain

$$\tilde{d}_{\phi\phi} + \frac{2\nu_y^2 KB \sin\phi}{\frac{\nu_x^2}{2} - (1 + K^2B^2 - 2KB\cos\phi)\nu_y^2}\tilde{d}_\phi + \alpha^2\left[(1 + K^2B^2 - 2KB\cos\phi)\nu_y^2 - \frac{\nu_x^2}{2}\right]$$

$$\left[G(\phi) - \frac{\nu_x^2}{8} + \frac{1}{4}(1 + K^2B^2 - 2KB\cos\phi)\nu_y^2\right]\tilde{d} = 0 \qquad (III.5.16)$$

Next, we eliminate the first derivative term by introducing a new dependent variable y

$$\tilde{d} = \sqrt{\left|\frac{\nu_x^2}{2} - (1 + K^2B^2 - 2KB\cos\phi)\nu_y^2\right|}\; y \qquad (III.5.17)$$

Substitution of $(III.5.15)$ in $(III.5.11)$ yields after simplifications

$$y_{\phi\phi} + \left\{\frac{\nu_y^2 KB\cos\phi\left[(1 + K^2B^2)\nu_y^2 - \frac{\nu_x^2}{2}\right] - K^2B^2\nu_y^4(2 + \sin^2\phi)}{\left[\frac{\nu_x^2}{2} - (1 + K^2B^2 - 2KB\cos\phi)\nu_y^2\right]^2} + \right.$$

$$+\alpha^2\left[(1 + K^2B^2 - 2KB\cos\phi)\nu_y^2 - \frac{\nu_x^2}{2}\right]\times$$

$$\left.\left[G(\phi) - \frac{\nu_x^2}{8} + \frac{1}{4}(1 + K^2B^2 - 2KB\cos\phi)\nu_y^2\right]\right\} y = 0 \qquad (III.5.18)$$

which is a Hill equation. We now assume the long wave slope to be small *i.e.* $KB \ll 1$. The expression within curly brackets is simplified to

$$G(\phi) = 1 - 2KB + 4KB\cos\phi + \mathcal{O}(\epsilon KB, K^2B^2) \qquad (III.5.19)$$

and may be subsituted in $(III.5.18)$. Comparison of the resulting equation with the canonical form $(III.5.12)$ yields the expression of Υ and Δ:

$$\Upsilon(\nu_x, \nu_y, KB, \alpha) = \alpha^2(\nu_y^2 - \frac{\nu_x^2}{2})(1 - 2KB - \frac{\nu_x^2}{8} + \frac{\nu_y^2}{4}) \qquad (III.5.20a)$$

and

$$\Delta(\nu_x, \nu_y, KB, \alpha) = KB\left\{\frac{\nu_y^2}{\nu_y^2 - \frac{\nu_x^2}{2}} + \alpha^2\left[2(\nu_y^2 - \nu_x^2) + \frac{1}{2}\nu_y^2(\nu_x^2 - 2\nu_y^2)\right]\right\} \qquad (III.5.20b)$$

In particular, in the absence of long waves ($KB = 0$), we recover the well known criterion of stability for 2-dimensional disturbances

$$(\nu_y^2 - \frac{\nu_x^2}{2})(1 - \frac{\nu_x^2}{8} + \frac{\nu_y^2}{4}) > 0 \qquad (III.5.21)$$

corresponding to the domain of stability first given by Benney & Roskes as shown in figure 5.1a-b. When KB is small and non-zero, the stability of $(III.5.9a-b)$ has been reduced to the stability of a Mathieu equation whose characteristic parameters are given by $(III.5.20a-b)$.

The stability bands of Mathieu's equation are well known and usually displayed in the (Υ, Δ) plane. We have superimposed in figure 5.6a these stability boundaries (solid lines) with the curve $(\Upsilon(\nu_y), \Delta(\nu_y))$ (dotted line) computed from $(III.5.20a-b)$ for $\nu_x = 0.5$, $\nu_y \in [1,6]$, $KB = 0.1$ and $\alpha = 0.125$. Any intersection of the dotted line with an instability zone corresponds to a lobe in figure 5.2a-b. The corresponding value of ν_y at these intersections can be calculated from $(III.5.9a)$ and are plotted for $\nu_x = 0.5$ in figure 5.6b. It is clear from figure 5.6a that segments of the continuous line within successive instability zones shorten very rapidly. In particular, the last two intersections in the vicinity of $\Upsilon = \frac{9}{4}$ and 4 correspond to very narrow ranges of ν_y, as suggested by figure 5.6b.

We conclude that, for non-zero KB, the diagram of stability of a short Stokes wave to 2-dimensional disturbances consists, in addition to the usual parabolic branch, of several instability bands which are convex (concave) in the region $\nu_x - \sqrt{2}\nu_y < 0$ $(\nu_x - \sqrt{2}\nu_y > 0)$.

Next, we examine the behavior of the maximum growth rate in an instability band as ν_x increases. To this end, we take a section of figure 5.2b in a straight line between the two points (0.0,3.5) and (6.0,5.25). Since this line intersects twice the second instability band in the region $\nu_x - \sqrt{2}\nu_y < 0$, as observed in figure 5.7b, the trend in the growth rate can be deduced. The first and lower instability band occurs around $\nu_x = 1.5$ and $\nu_y = 3.85$. The second instability lobe has a larger maximum growth rate.

This confirms that the peak growth rate is an increasing function of ν_x in any instability band belonging to the region $\nu_x - \sqrt{2}\nu_y < 0$. In the region $\nu_x - \sqrt{2}\nu_y > 0$

however, the peak growth rate in a given instability band decreases with increasing ν_x.

5.2.2. *Influence of the long wave slope KB*

We now consider steeper long waves with $KB = 0.2$ and 0.3 and compute the growth rates associated with disturbance wavenumbers $(\nu_x, \nu_y) \in [0,6] \times [0,6]$. The results are presented in figure 5.8a-b and 5.9a-b respectively. The smallest stable longitudinal disturbance decreases with increasing KB. It is worth pointing out that the position of the new instability bands identified in figure 5.2a-b have not changed significantly. However, both their width and height (*i.e.* maximum growth rate) increase drastically.

5.2.3. *Influence of* α

Finally, we present in figures 5.10a-b, 5.11a-b, 5.12a-b and 5.13a-b the stability diagrams for $\alpha = 0.05$, 0.07, 0.1 and 0.15 respectively. Increasing α † causes the bands of instability to approach the main instability branch. The number of bands on each side of this branch, their width and height all increase with α.

† This amounts to increasing the short wave slope ϵkA or decreasing the frequency ratio $\epsilon\frac{\Omega}{\sigma}$.

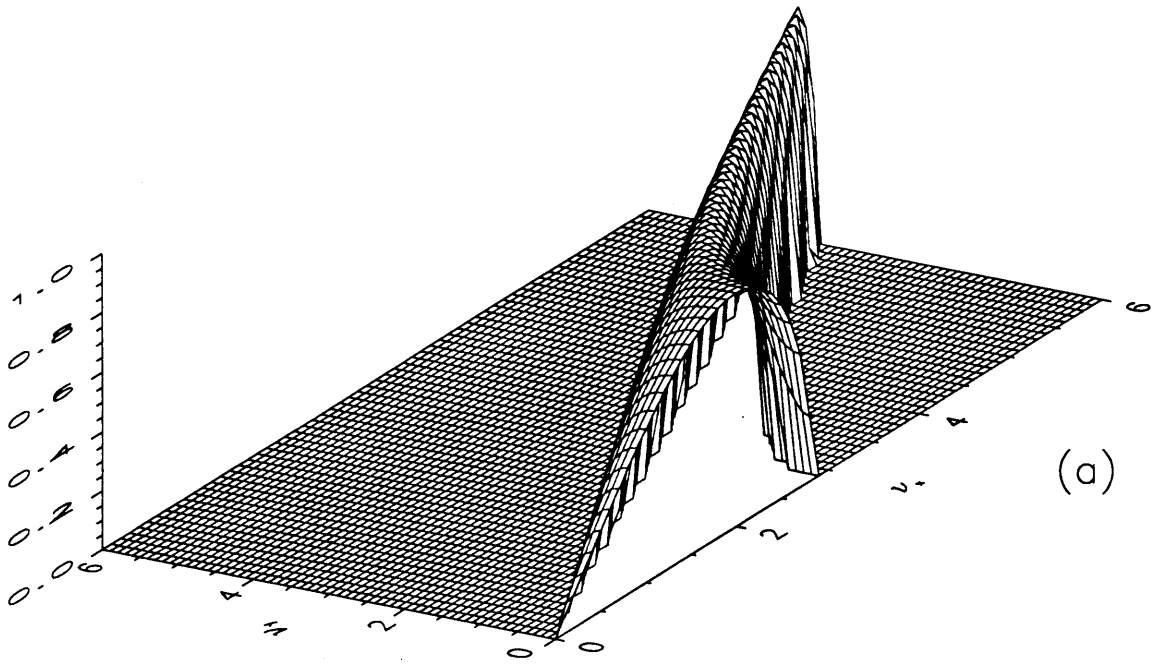

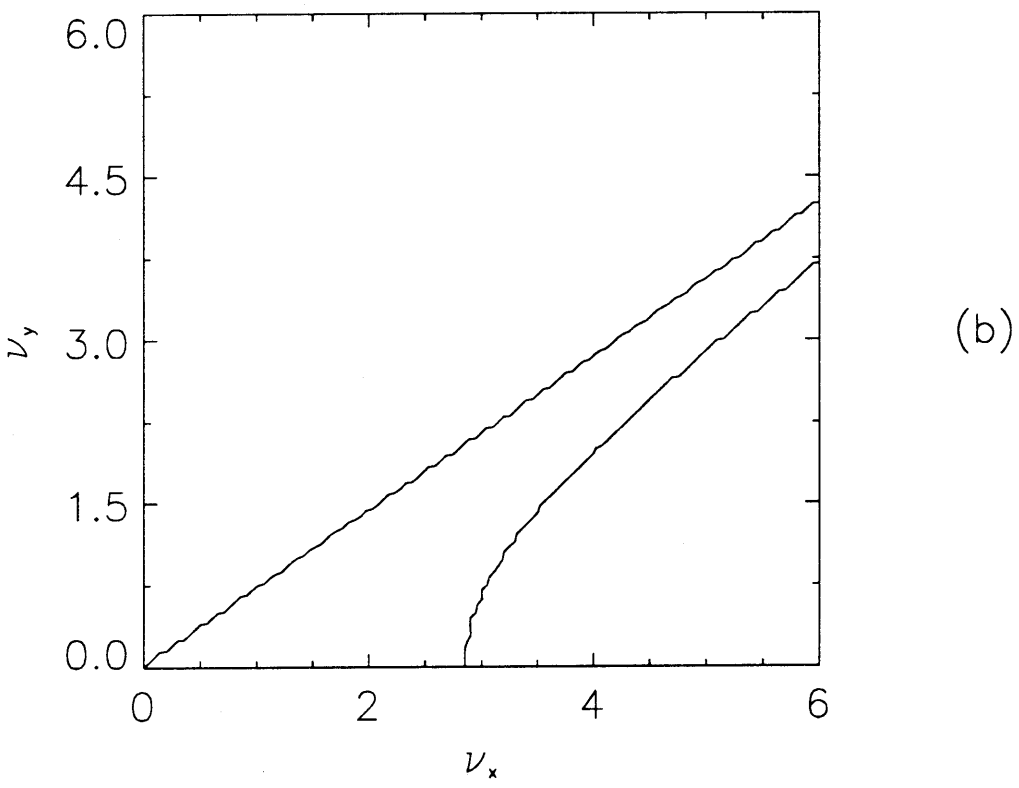

Figures III.5.1a-b: Growth rate for two-dimensional disturbances (ν_x, ν_y) in the absence of long waves (Benney & Roskes, 1969) with $\epsilon k \overline{A} = 0.13$ and $\alpha = 0.125$. (a) Three-dimensional view, (b) Stability boundaries

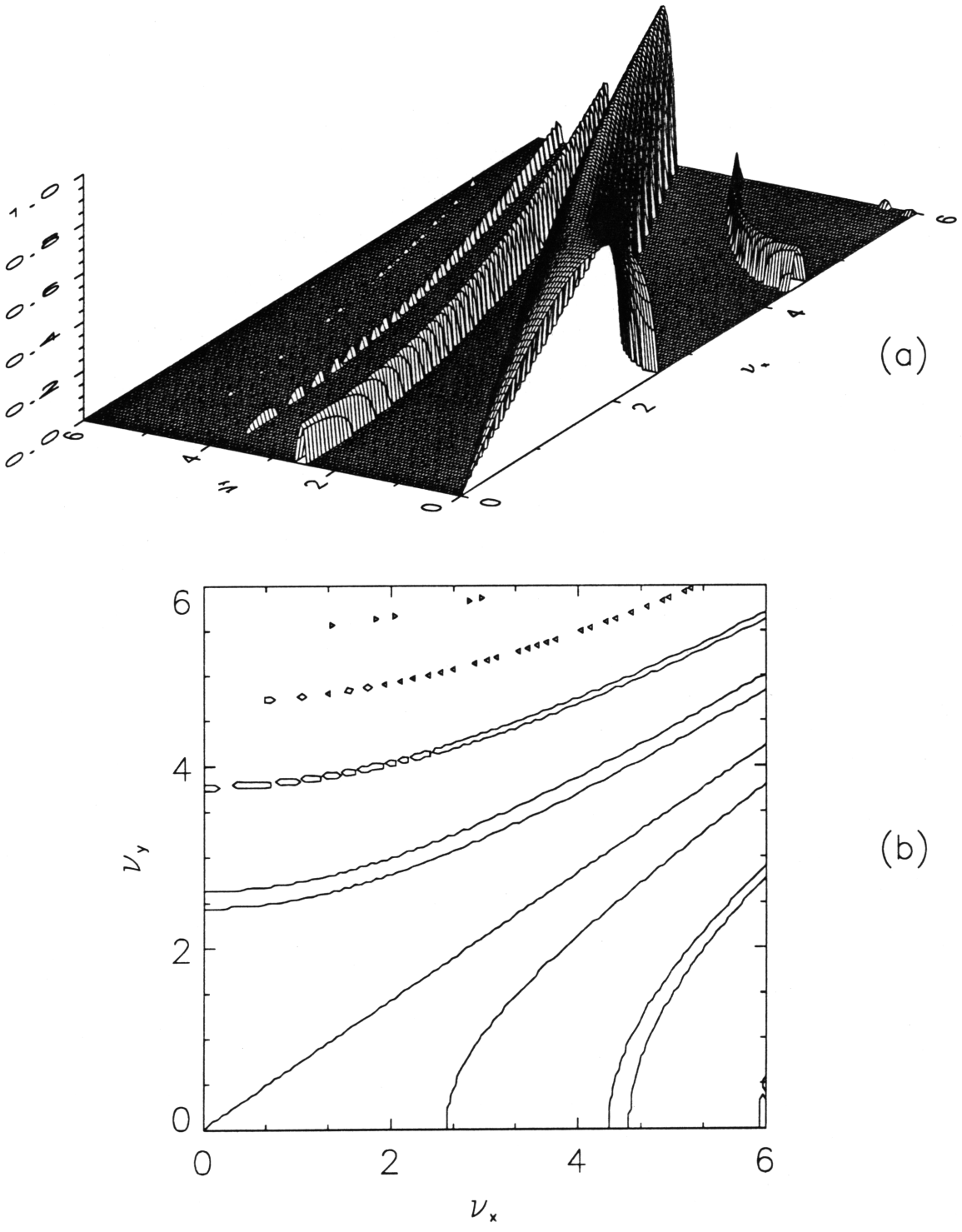

Figures III.5.2a-b: Growth rate for two-dimensional sidebands $(\nu_x, \nu_y) \in [0,6] \times [0,6]$ with $KB = 0.1$ $\epsilon k \overline{A} = 0.13$ and $\alpha = 0.125$. (a) Three-dimensional view, (b) Stability boundaries, the dotted line refers to the section of the (ν_x, ν_y) plane analysed in figures III.5.7a-b.

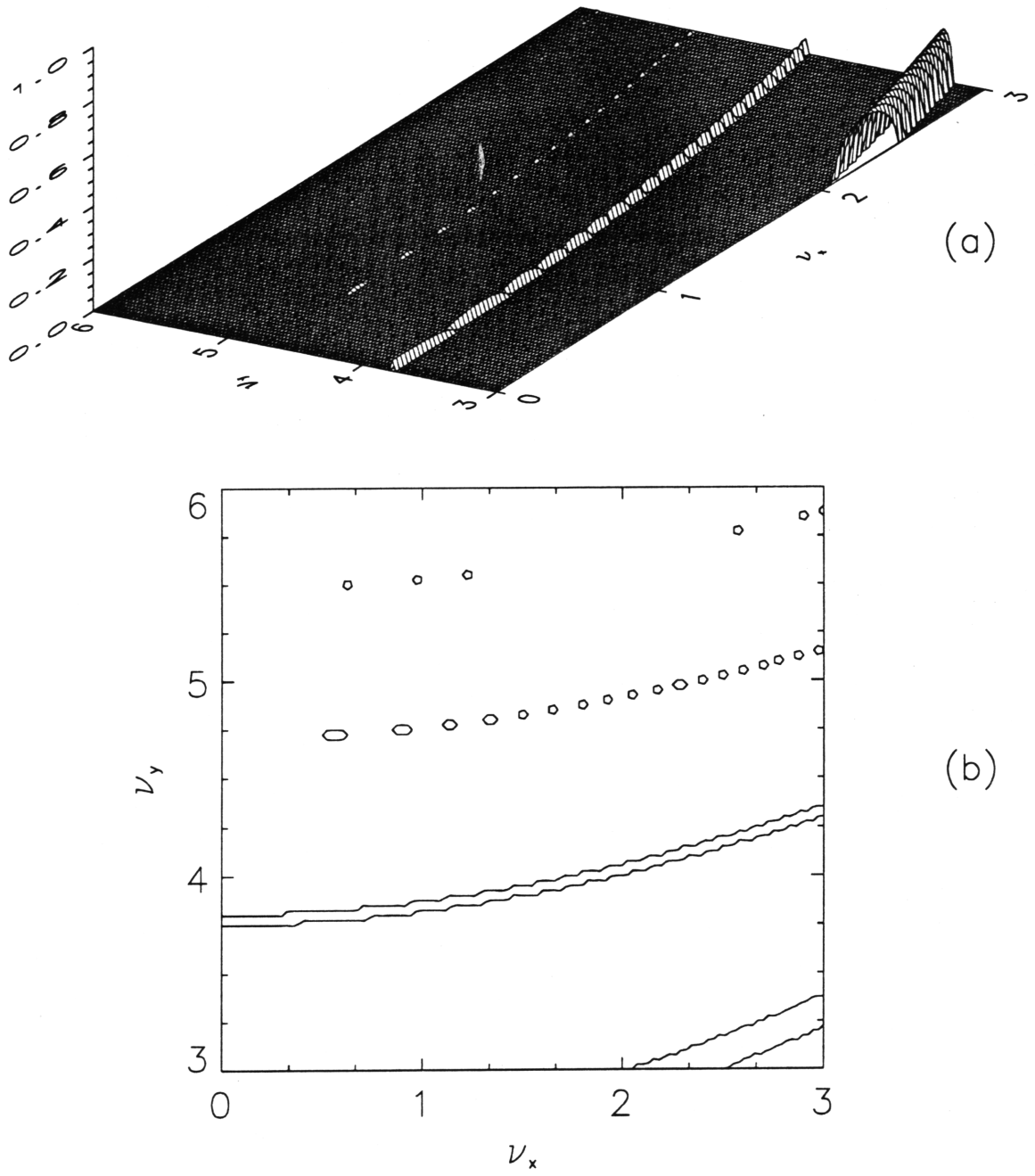

Figures III.5.3a-b: Growth rate for two-dimensional sidebands $(\nu_x, \nu_y) \in [1,3] \times [3,6]$ with $KB = 0.1$ $\epsilon k \overline{A} = 0.13$ and $\alpha = 0.125$. (a) Three-dimensional view, (b) Stability boundaries.

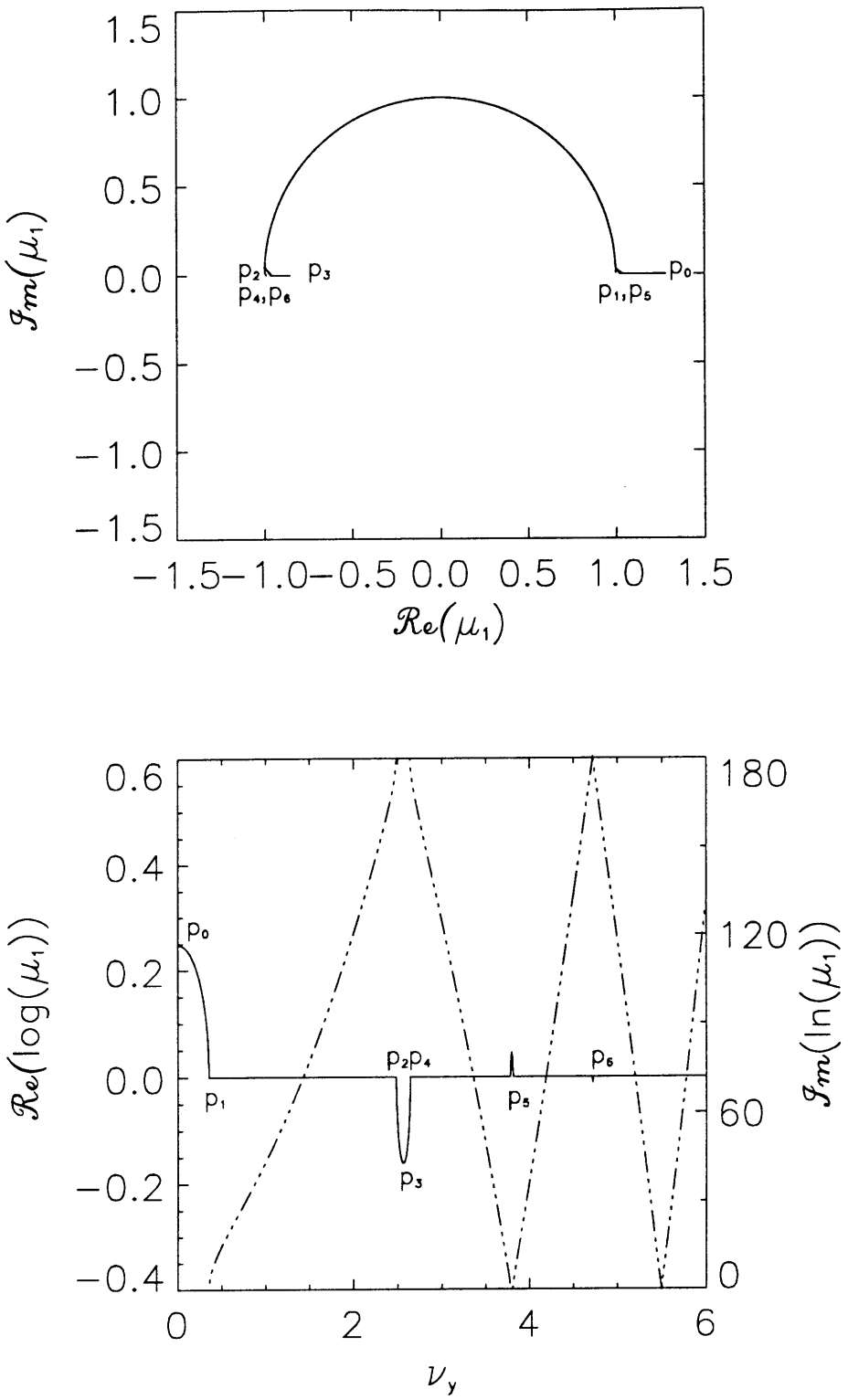

Figure III.5.4: Floquet multiplier μ_1 with $\nu_x = 0.5$, $KB = 0.1$, $\epsilon k\overline{A} = 0.13$ and $\alpha = 0.125$. The sequence of points $p_{0,1,...}$ corresponds to increasing values of $\nu_y \in [0,6]$; (Top) locus of μ_1 in the complex μ plane, (Bottom) $\Re\{\ln(\mu_1)\}$ (solid line) and $\Im\{\ln(\mu_1)\}$ (chain line).

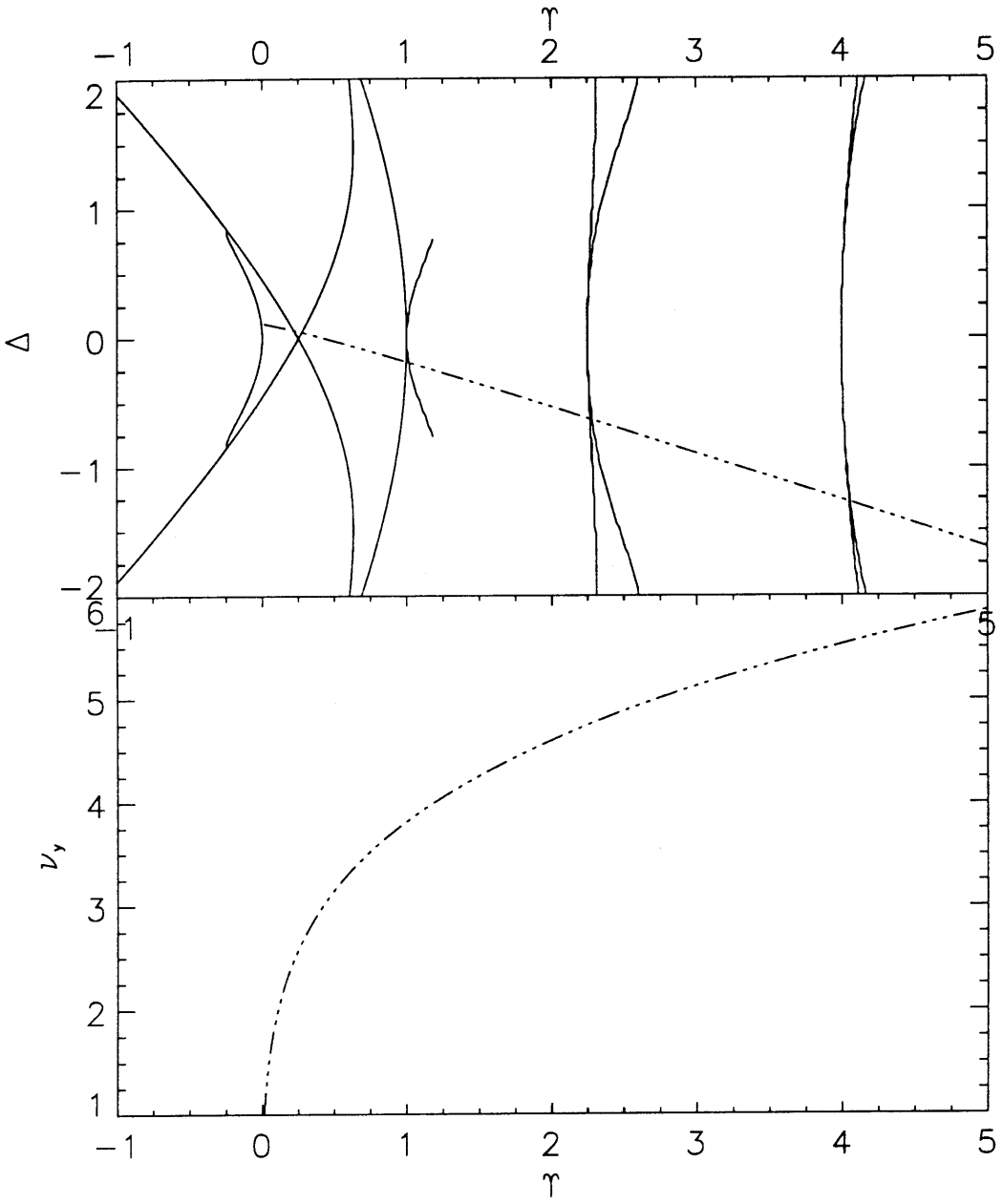

Figure III.5.6: Linearized stability and Strutt diagram with $\nu_x = 0.5$, $\nu_y \in [1, 6]$, $KB = 0.1$, $\epsilon k \overline{A} = 0.13$ and $\alpha = 0.125$; (Top) stability boundaries of Mathieu equation (solid line), $(\Upsilon(\nu_y), \Delta(\nu_y))$ (chain line); (bottom) $\nu_y(\Upsilon)$.

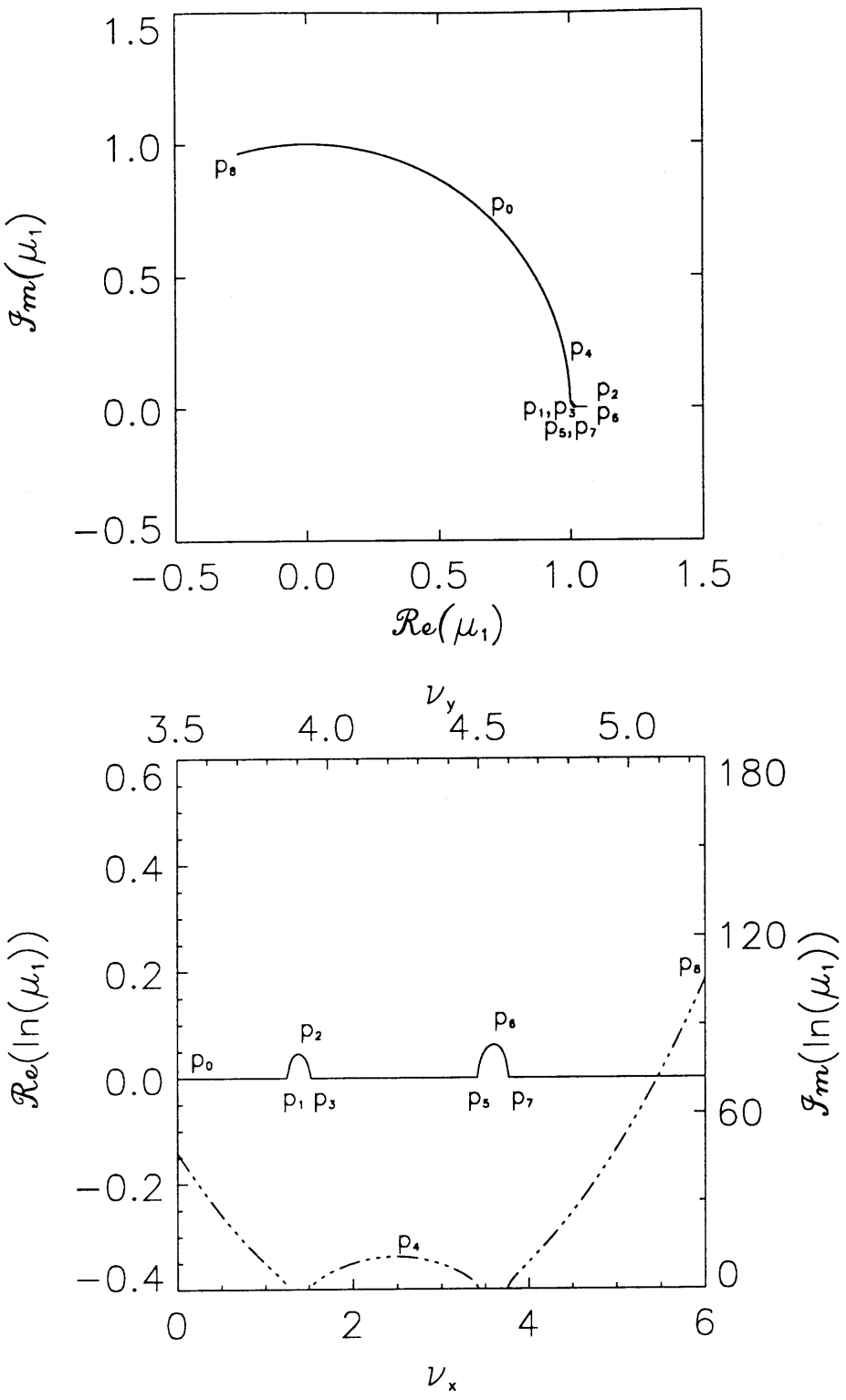

Figure III.5.7: Floquet multiplier μ_1 with $\nu_x \in [0,6]$, $\nu_y \in [3.5, 5.25]$, $KB = 0.1$, $\epsilon k\overline{A} = 0.13$ and $\alpha = 0.125$. The sequence of points $p_{0,1,...}$ corresponds to increasing values of ν_x and ν_y along the dotted line in figure III.5.2b; (Top) locus of μ_1 in the complex μ plane, (Bottom) $\Re\{\ln(\mu_1)\}$ (solid line) and $\Im\{\ln(\mu_1)\}$ (chain line).

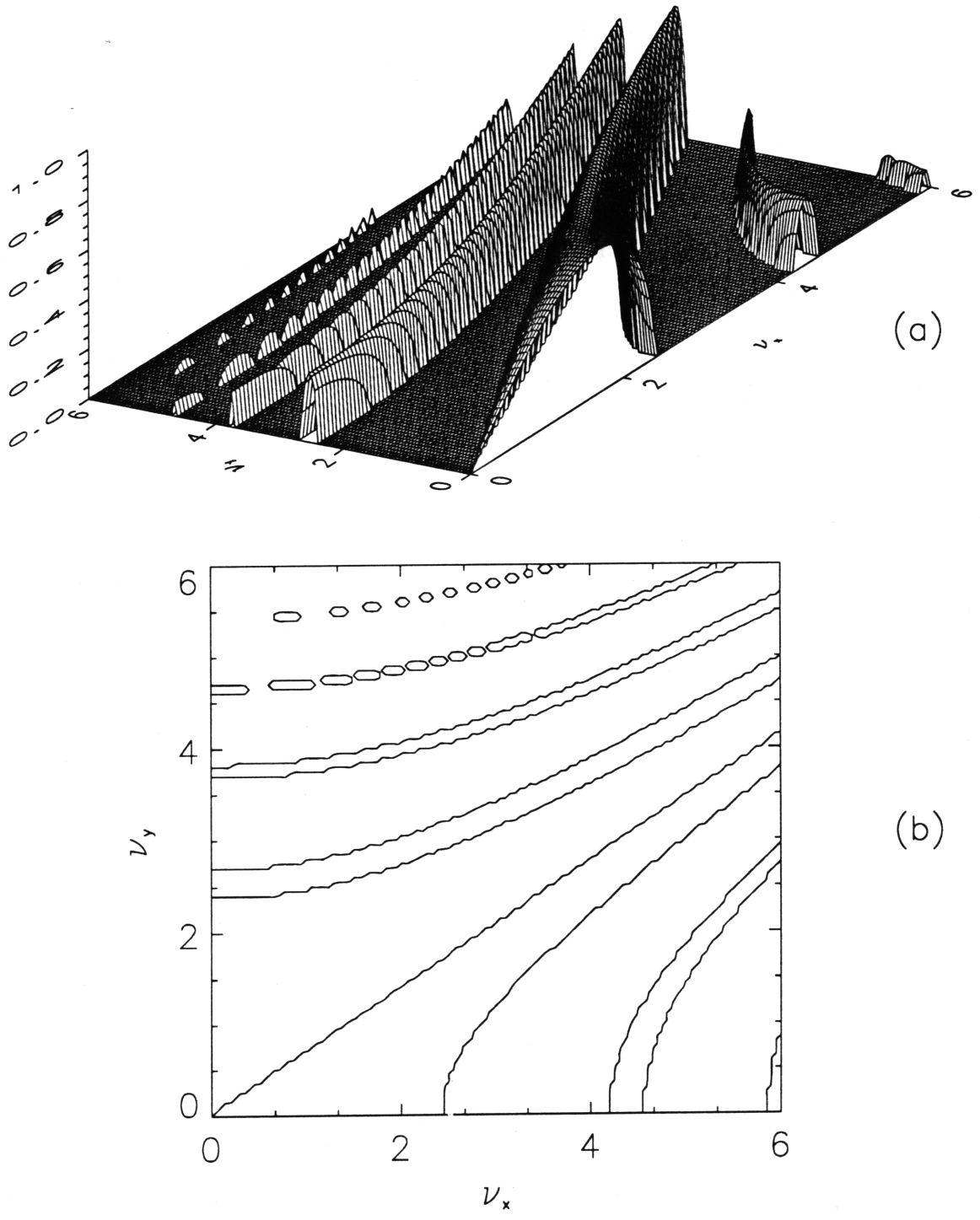

Figures III.5.8a-b: Growth rate for two-dimensional sidebands $(\nu_x, \nu_y) \in [0,6] \times [0,6]$ with $KB = 0.2$ $\epsilon k \overline{A} = 0.13$ and $\alpha = 0.125$. (a) Three-dimensional view, (b) Stability boundaries.

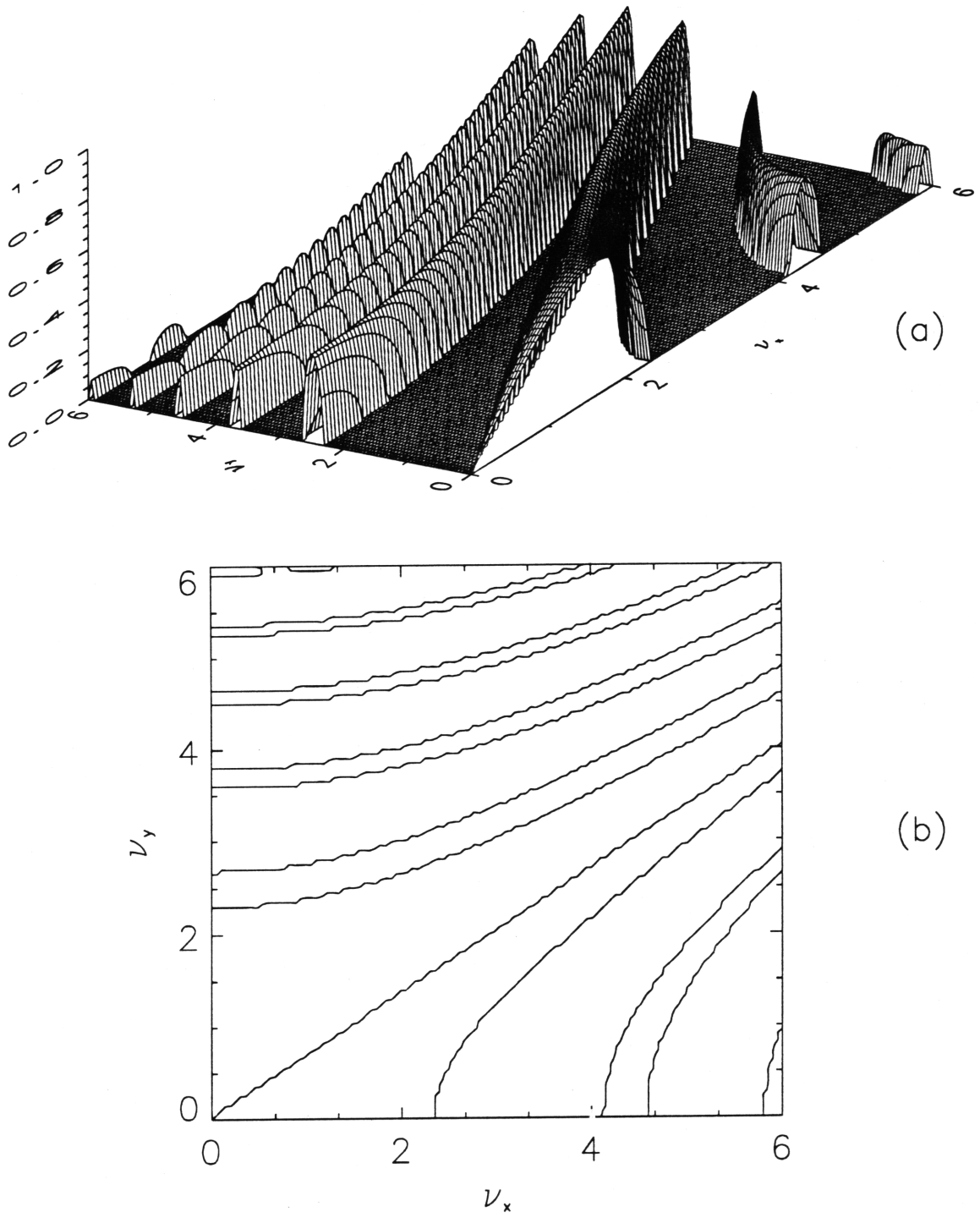

Figures III.5.9a-b: Growth rate for two-dimensional sidebands $(\nu_x, \nu_y) \in [0,6] \times [0,6]$ with $KB = 0.3$ $\epsilon k \overline{A} = 0.13$ and $\alpha = 0.125$. (a) Three-dimensional view, (b) Stability boundaries.

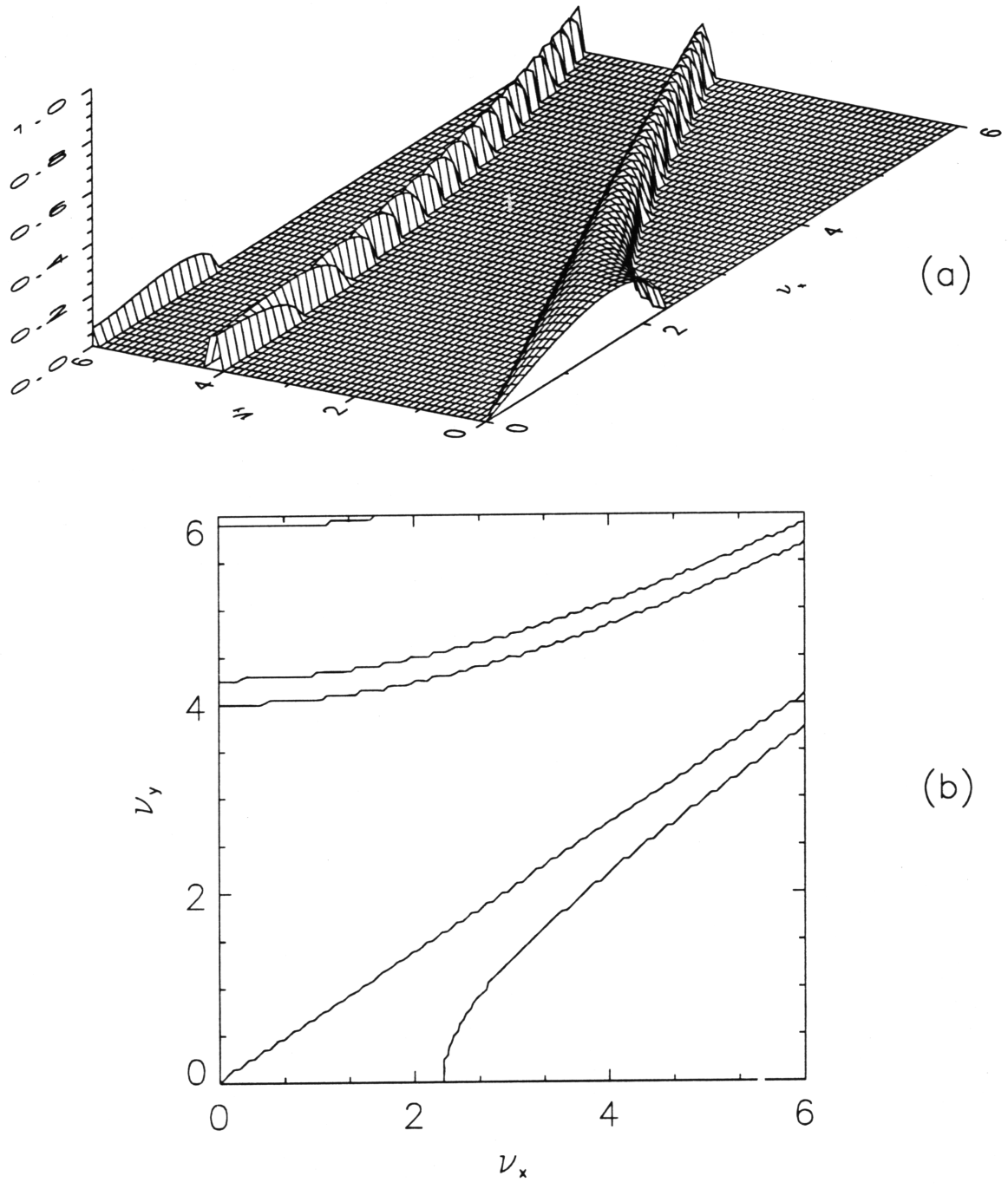

Figures III.5.10a-b: Growth rate for two-dimensional disturbances $(\nu_x, \nu_y) \in [0,6] \times [0,6]$ with $KB = 0.3$ $\epsilon k \overline{A} = 0.13$ and $\alpha = 0.05$. (a) Three-dimensional view, (b) Stability boundaries.

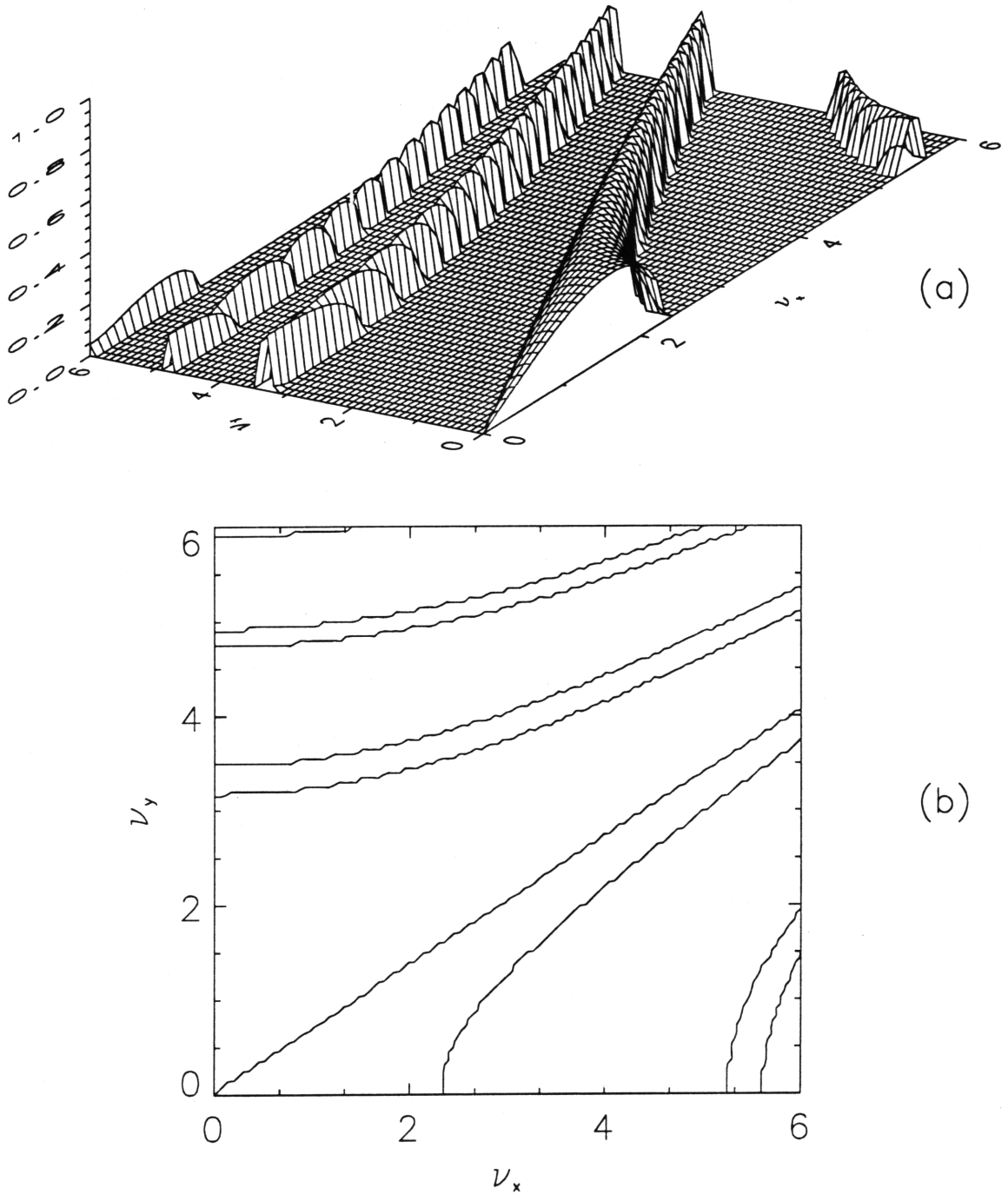

Figures III.5.11a-b: Growth rate for two-dimensional disturbances $(\nu_x, \nu_y) \in [0,6] \times [0,6]$ with $KB = 0.3$ $\epsilon k \overline{A} = 0.13$ and $\alpha = 0.075$. (a) Three-dimensional view, (b) Stability boundaries.

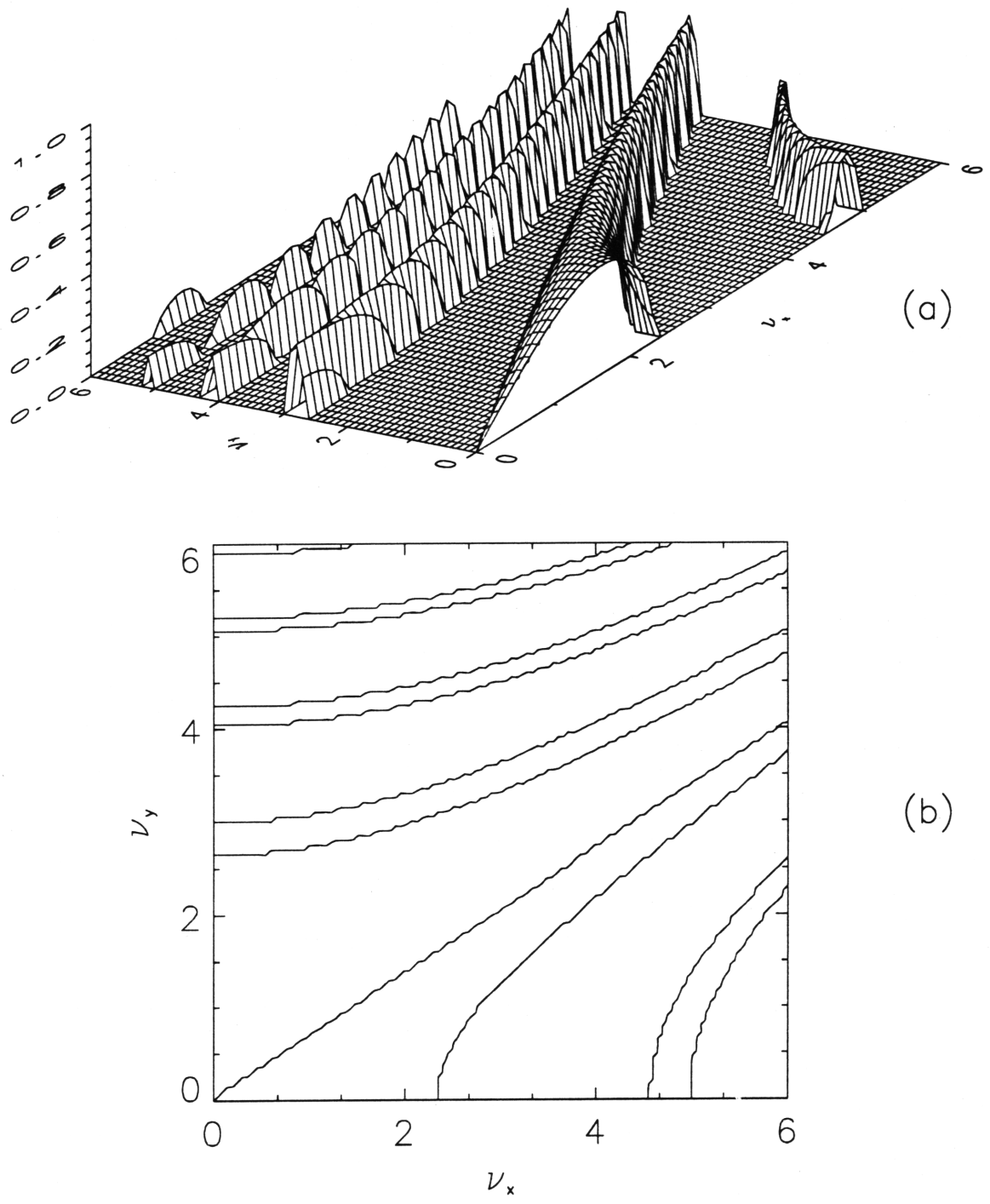

Figures III.5.12a-b: Growth rate for two-dimensional disturbances $(\nu_x, \nu_y) \in [0,6] \times [0,6]$ with $KB = 0.3$ $\epsilon k\overline{A} = 0.13$ and $\alpha = 0.1$. (a) Three-dimensional view, (b) Stability boundaries.

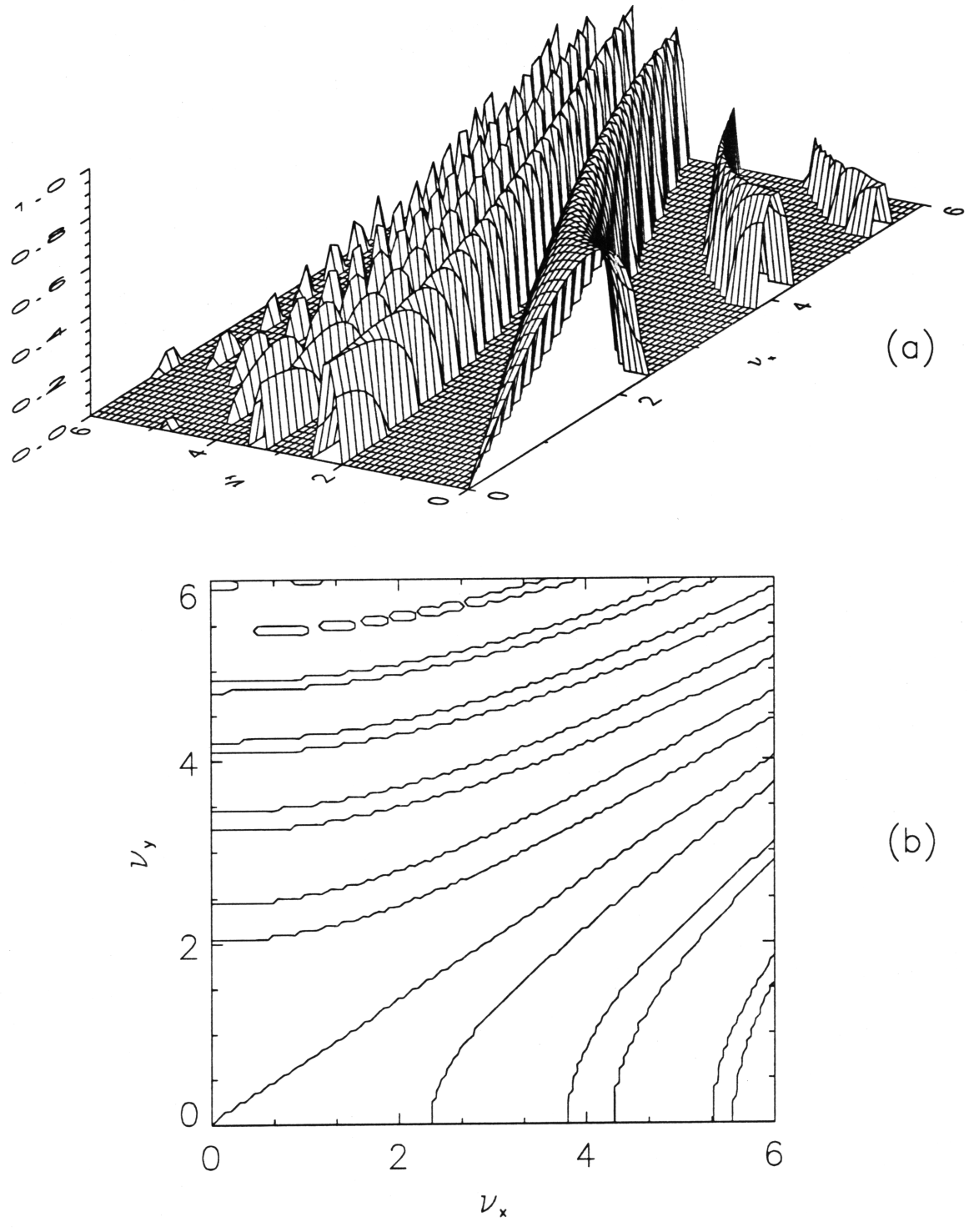

Figures III.5.13a-b: Growth rate for two-dimensional disturbances $(\nu_x, \nu_y) \in [0,6] \times [0,6]$ with $KB = 0.3$ $\epsilon k \overline{A} = 0.13$ and $\alpha = 0.15$. (a) Three-dimensional view, (b) Stability boundaries.

6. CONCLUSIONS

We have analyzed in this Chapter the linear stage of Benjamin & Feir sideband instability of a train of short wave slightly oblique relative to and riding on a long Gerster wave of finite amplitude.

It is found that the intrinsic frequency of an oblique short wave train is a function of the position ϕ on the long wave. The modulation of short waves is sought for an arbitrary angle θ. The short wave amplitude is only mildly affected by θ and this is primarily a function of ϕ. In particular, short waves propagating perpendicularly to the long waves are still modulated in amplitude. Examination of the absolute frequency and group velocity shows that both the carrier short wave and its envelope may propagate to the left after encountering a caustic provided that the long wave is steep enough.

When θ is small, the short wave envelope is governed by a two-dimensional nonlinear Schrödinger equation with time-periodic coefficients. The linearized stability of a uniform solution to two-dimensional sidebands is examined with Floquet theory. It is also found that new instability bands appear near the infinite instability strip of Benney & Roskes(1969) in the (ν_x, ν_y) plane. The instability bands are concave (convex) below (above) this strip with a peak growth rate decreasing (increasing) with increasing ν_x and ν_y. The width, and peak height of these bands both increase with α as their position shifts towards to the main instability strip. Thus, with increasing values of α, it becomes more likely that higher harmonics of a stable disturbance may be unstable. Furthermore, harmonics of an unstable disturbance are likely to become unstable too, thus yielding very complex interactions. When the range of wavenumbers taking part in these interactions becomes very large, thermalization occurs thus violating the narrow band assumption.

GENERAL SUMMARY AND CONCLUSIONS

We have examined in Part 2 the nonlinear interactions between two deep water gravity waves. Three problems have been studied in detail under the common assumptions of weak nonlinearity of the shorter wave, ($kA = \mathcal{O}(\epsilon)$ where $\epsilon \ll 1$), and of a small ratio of the long to short wave wavenumbers, $\frac{K}{k} = \mathcal{O}(\epsilon^2)$. We have employed the Lagrangian formulation. Governing equations in terms of Lagrangian variables are deduced from basic principles. Owing to the contrast in time and spatial scales inherent to the problem, a cascade of slow independent variables is introduced. Solutions are sought in terms of the Lagrangian displacement vector which is decomposed in a perturbation series expansion of the small parameter ϵ. At each order, a harmonic decomposition is then assumed. Approximate governing equations for the displacement vectors are derived. Solvability conditions are enforced and evolution equations for wave amplitudes are deduced. We now summarize each problem separately.

In Chapter I, the long wave is modelled by an irrotational weakly nonlinear Stokes wave ($KB = \mathcal{O}(\epsilon)$). The wavenumber modulation of the short waves is consistent with Longuet-Higgins & Stewart(1960). However, the amplitude modulation is the product of two terms: one corresponding to the theory of Longuet-Higgins & Stewart, the other to a solution of the nonlinear Schrödinger equation in the moving Lagrangian frame. The scaling assumptions are such that the short wave group velocity and the long wave particle velocity are comparable. Examination of the absolute frequency ω, *i.e.* the frequency in a fixed frame of reference, shows that ω is greater than the intrinsic frequency σ in the neighborhood of the crests and less than σ near the trough. For steep enough long waves (see figure I.4.2), ω may become negative near the trough; this implies that the short carrier waves are propagating to the left. Likewise, the group velocity in a fixed frame of reference can change sign signalling the reflection of the short wave energy. The nonlinear evolution of the short wave amplitude, although simple in the moving Lagrangian frame, must be examined in a fixed frame. To this end, a translation to Eulerian

coordinates is performed. The nonlinear effects are then examined for long waves passing a soliton group of short waves. Three long waves are examined corresponding respectively to a uniform, a sinusoidally modulated and a Gaussian envelope B. We have found that the location of the soliton peak in a fixed frame oscillates as a result of the passage of successive long wave crests and troughs while drifting due to the long wave Stokes drift (see figures I.5.1 to I.5.3).

In order to examine stronger interactions between the short and long waves, a finite amplitude long wave ($KB \leq \mathcal{O}(1)$) is considered in Chapters II and III. To avoid tedious complex algebra and minimize numerical work, the simple and exact solution of Gerstner(1802) is chosen for the long wave. The leading order modulation of the short wave envelope and wavenumber is found analytically and compares well with the numerical theories of Longuet-Higgins(1987) and Zhang & Melville(1990) (see figures II.5.3 and II.5.4). We also compare the short wave dispersion relation with the well known Eulerian result $\sigma^2 = g_{\text{eff}} k^e$ (Phillips(1981)) where g_{eff} and k^e are respectively the effective gravity field experienced by the short waves and the Eulerian short wave wavenumber. Differences are small and consistent with the differences in vorticity in the Stokes and Gerstner waves (see §II.5.4).

Because of the time-periodic effective gravity field due to the long waves, the short waves are subjected to parametric excitations. The stability of a uniform short wave train to sideband disturbances is investigated by Floquet theory. The emergence of new bands of instability is observed and then proved theoretically (see figure II.6.4). As α increases (*i.e.* as the short wave slope ϵkA increases and/or the scale contrast decreases) the new instability bands proliferate near the main Benjamin & Feir instability lobe, and both their width and peak growth rates increase (see figure II.6.5). For moderately large α, the harmonics of an unstable sideband may also be unstable. Thus, thermalization may occur whereby energy is leaked to very high wavenumbers in contradiction to the narrow band assumption.

With the knowledge of the linear instability, we examine the nonlinear stage by integrating numerically the evolution equation. For small values of α. Fermi-Pasta-Ulam recurrence is observed (see figure II.7.2). However, when α becomes moderately large, the short wave amplitude evolves chaotically (see figure II.7.6).

The Fourier spectrum remains nevertheless confined to the first 10 modes thus the characterization of "confined chaos" (see figures II.7.6a-b). In order to shed some light on the nonlinear evolution and to assess the importance of the harmonics of the sideband, a simpler problem is examined. The short wave envelope is approximated by a two mode expansion involving the uniform carrier wave and its unstable symmetric sidebands. Using Hamiltonian theory, a set of two coupled ordinary differential equations is derived. Integration of the dynamical system shows chaotic trajectories for moderate α (see figure II.8.7a-e). The importance of the initial conditions as a trigger to chaos is emphasized. We may conclude that the presence of higher harmonics of the sideband is not essential to trigger chaos. In contrast, Yuen & Ferguson(1978) and Caponi *et al*(1982) have found, for short waves without long waves, that at least two unstable sidebands are necessary for chaos to arise.

In Chapter III, we consider the more general situation where the short waves are propagating at an angle θ relative to the steep long wave. The effect of θ on the leading order modulation of the short wave is thoroughly studied. The amplitude modulation is found to be mainly a function of the position ϕ along the profile of the long wave (see figure III.4.2). In contrast, the range of wavenumber modulation depends strongly on θ and vanishes for normal incidence (see figure III.4.3). The absolute frequency ω is also investigated. For large incidence angles θ, the short carrier waves are reflected to the left for a comparatively steeper long wave (see figure III.4.7). Examination of the two components of the group velocity C_g, in a fixed frame, shows the existence of caustics; short wave energy is then reflected (see figure III.4.9).

For small incidence $\theta \ll 1$ the nonlinear evolution of the short wave envelope is found to obey a two-dimensional Schrödinger equation with ϕ-periodic coefficients. The initial stage of the Benjamin & Feir stability of a uniform short wave to two-dimensional sidebands is analysed here for the first time. The growth rates are again obtained using Floquet theory. In the disturbance wavenumber plane, instability bands proliferate near the single strip of Benney & Roskes(1969) (see figure III.5.9). With increasing α, the number of bands, their bandwidth and peak growth rate all increase (see figures III.5.10 to III.5.13).

Extensions of this work are worthwhile in many directions. First, one may extend Chapter I and consider a steeper irrotational Stokes wave with a slope $KB = \mathcal{O}(\epsilon^{\frac{1}{2}})$. The results for uniform long waves can then be compared to the more numerical theory of Zhang & Melville(1990). The evolution of short waves riding on a moderately steep and modulated long wave could also be investigated. It is also worthwhile to investigate to what extent the chaotic evolution of short waves is contingent on the exact periodicity of the long wave.

The confined chaos observed for large values of α (see figures II.7.6 and II.7.7) clearly violates the narrow band assumption. A formulation based on the third order Zakharov theory would be fruitful. Furthermore, the evolution of steeper short waves can also be considered.

Extensions of Chapter III are seen in several directions. Based on the knowledge of the linear instability of two-dimensional sidebands, the nonlinear stage can be investigated numerically with the two-dimensional Schrödinger equation. Further insight can be gained by considering again a two-term Fourier expansion for the short wave envelope. A lower order dynamical system may be derived following the steps of §II.8. The influence of the transverse component of the sideband wavenumber must be investigated. A comparison of the fully nonlinear and lower order model is then worthwhile.

Extension of the two-dimensional Schrödinger equation to an arbitrary incidence angle θ involves complex and lengthy algebra. It can however be a stepping stone towards the more complex problem of a resonant quartet on a steep long wave.

In nature, the short gravity waves are affected by dissipation which becomes important when long time evolution is considered. It is worthwhile to incorporate a dissipation acting over a time scale $\sigma t_2 = \mathcal{O}(1)$ comparable to the evolution scales considered here. The analysis of the truncated dynamical system should lead to very different results.

Bibliography for Part 2

Armstrong, J. A., Bloembergen, N., Ducuing, J., & Pershan, P. S., 1962. Interactions between light waves in a nonlinear dielectric. *Phy. Rev.* 127: 1818-1939.

Benjamin, T. B., & Feir, J. E., 1967. The disintegration of wave trains on deep water. *J. Fluid Mech.* 27, 417-430.

Benney, D.J. & Roskes, G.J. 1969. Wave instabilities. *Studies Appl. Math*, 48, 377-385.

Bretherton F.P., & Garrett, C. J. R. 1969, Wavetrains in inhomogeneous moving media, *Proc. Roy. soc. Lond.* A 302, 529-544.

Bryant, P. J., 1976. Periodic waves in shallow water. *J. Fluid Mech.* 59, 625-644.

Caponi, E.A., Saffman P.G. & Yuen, H.C., 1982. *Phys. Fluids* 25, 2159.

Crawford, D.R., Lake, B.M., Saffman P.G. & Yuen, H.C., 1981. Stability of weakly nonlinear deep-water waves in two and three dimensions. *J. Fluid Mech.* 105, 177-191.

Disthe, K., Henyey, F.S., Longuet-Higgins, M.S. and Schult, R.L. 1988 The orbiting double pendulum: an analogue to interacting gravity waves. *Proc. R. Soc. Lond.* A 418, 281-299.

Gerstner, F. J. von, 1802. Theorie der wellen. *Abb. d. k. böhm. Ges. d. Wiss.*,

Henyey, F.S., Creamer, D.B., Dysthe, K, Schult, R.L. & Wright, J.A., 1988. The energy and action of small waves riding on large waves. *J. Fluid Mech.*, 189, 443-462.

Infeld, E., 1981. Quantitative theory of the Fermi-Pasta-Ulam recurrence in the nonlinear Schrödinger equation. *Phy. Rev. Lett.* 47(10), 717-718.

Iooss, G. & Joseph, D. D., 1980. *Elementary Stability and Bifurcation Theory,* Springer-Verlag.

Kharif, C., 1990, Some aspects of the kinematics of short waves over longer gravity waves on deep water. In *Water Wave Kinematics*, ed. by A. Tørum, Kluwer. 265-279.

Kochin, N. E., Kibel I. A., & Roze, N. V., 1965. *Theoretical Hydrodynamics.* Interscience. 2nd ed.

Lo, E., & Mei, C. C., 1985. A numerical study of water-wave modulation based on a higher-order nonlinear Schrödinger equation. *J. Fluid Mech.* 150, 395-416.

Longuet-Higgins, M. S., 1985. Accelerations in steep gravity waves. *J. Phys. Oceanog.* 15, 1570-1579.

Longuet-Higgins, M. S., 1987. The propagation of short surface waves on longer gravity waves, *J. Fluid Mech.* 177, 293-306.

Longuet-Higgins, M. S., & Stewart, R. W., 1960. Changes in the form of short gravity waves on long waves and tidal currents. *J. Fluid Mech.* 8, 566-583.

Longuet-Higgins, M. S., & Stewart, R. W., 1961. The changes in amplitude of short gravity waves on steady non-uniform currents. *J. Fluid Mech.* 10, 529-549.

Mei, C. C., & Ünlüata, Ü., 1973 Harmonic generation in shallow water waves, in *Waves on Beaches*, 181-202, ed. by R. E. Meyer, Academic.

Nayfeh, A. H., & Mook, D. T., 1979. *Nonlinear Oscillations* Wiley-Interscience.

Phillips, O.M., 1981. The dispersion of short wavelets in the presence of a dominant long wave. *J. Fluid Mech.* 107. 465-485.

Schwartz, L. W., 1974. Computer extension and analytic continuation of Stokes expansion for gravity waves. *J. Fluid Mech* . 62, 553-578.

Shampine, L.F. Gordon, M.K., 1975. *Computer solution of ordinary differential equations. The initial value problem.* W.H. Freeman. San Francisco.

Shirer, H.N. 1987 *Nonlinear Hydrodynamic Modeling. A Mathematical Introduction* ed. by H.N.S. Springer-Verlag .

Stiassnie, M., & Kroszynski, U. I., 1982. Long-time evolution of an unstable water-wave train. *J. Fluid Mech.* 116, 207-225.

Stoker, J.J. 1957. *Water Waves. The mathematical theory with applications.* Interscience, New York.

Tappert, F.D. 1974. Numerical solutions of the Korteweg-de-Vries equation and its generalizations by the split-step Fourier method. *Lectures Appl. Math.* 15, 215-=216.

Strutt, M.J.O. (1928). *Ann. de Phys.* lxxxiv.

Yoshinaga, T., Wakamiya, M. & Kakutani, T. 1991. Recurrence and chaotic behavior resulting from nonlinear interaction between long and short waves. *Phys. Fluids.* A 3(1), 83-89.

Yuen, H.C. & Ferguson, W.E., Jr. (1978). Relationship between Benjamin-Feir instability and recurrence in the nonlinear Schrödinger equation. *Phys. Fluids*, 21, 1275-1278.

Zhang, J., 1990. Nonlinear interactions between short and long waves - evolution of short waves on long waves. O.T.R.C. Report No 6/90-A-3-100. Texas A& M University.

Zhang, J., & Melville, W. K., 1990. Evolution of weakly nonlinear short waves riding on long gravity waves. *J. Fluid Mech.* 214. 321-346.

Zhang, J., & Melville, W. K., 1991. On the stability of weakly nonlinear short waves on finite-amplitude long gravity waves. *Sub. J. Fluid Mech.*.

Figure Captions for Part 2

Chapter I

Figure I.4.1: Contours of $\frac{\omega}{\sigma}(\phi_E, \epsilon KB)$, $\frac{\omega}{\sigma} = 1$ (——); $\frac{\omega}{\sigma} = 0$ with $\epsilon\frac{\Omega}{\sigma} = 0.05$ (· · · · ··), 0.075 (- - - - -), 0.1 (–·–·–·–) and 0.125 (—· · —· · —· · —).

Figure I.4.2: Absolute frequency and group velocity. $\frac{\omega}{\sigma} = 1$ (——-), $\frac{\omega}{\sigma} = 0$ (· · · · ·), and $C_g = 0$ (- - - -) with $\epsilon\frac{\Omega}{\sigma} = 0.1$.

Figure I.5.1: Displacement of the peak of a short wave soliton riding on a long wave with uniform amplitude (case (a)) with $\epsilon k\overline{A} = 0.1$, $\epsilon K\overline{B} = 0.1$ and $\epsilon\frac{\Omega}{\sigma} = 0.1$.

Figure I.5.2: Displacement of the peak of a short wave soliton riding on a long wave with sinusoidally modulated amplitude (case (b)) with $\chi = 8\pi$, $\epsilon k\overline{A} = 0.1$, $\epsilon K\overline{B} = 0.1$ and $\epsilon\frac{\Omega}{\sigma} = 0.1$.

Figure I.5.3: Displacement of the peak of a short wave soliton riding on a long wave with a Gaussian amplitude (case (c)) with $\chi = 8\pi$, $\phi_0 = 30\pi$, $\epsilon k\overline{A} = 0.1$, $\epsilon K\overline{B} = 0.1$ and $\epsilon\frac{\Omega}{\sigma} = 0.1$.

Chapter II

Figure II.3.1: Comparison of Gerstner wave (——) and Stokes wave(- - -) profiles for (a) $KB = 0.1$, (b) $KB = 0.2$ and (c) $KB = 0.3$.

Figure II.3.2: Comparison of mean sea level crossing locations. In the Lagrangian frame: Gerstner (——), Stokes (· · · · ·); In the Eulerian frame: Gerstner (– – –), Stokes (–·–·–).

Figure II.5.1: Effective gravity for Gerstner wave: $KB = 0.1$ (——), $KB = 0.2$ (– – –), and $KB = 0.3$ (·-·-·-·-); Stokes wave (from Longuet-Higgins, 1987): $KB = 0.1$ (○), $KB = 0.2$ (△) and $KB = 0.3$ (◇).

Figure II.5.2: Comparison of inclination of the free surface of Gerstner's wave (——) with the inclination of $\vec{k}^e$ (· · · · ·).

Figures II.5.3a-c: Modulation of linearized short waves riding on a Gerstner wave and a Stokes wave (○, from Longuet-Higgins, 1987). (a) Wavenumber modulation at the crest (· · · · ·) and at the trough (– – –); (b) likewise for the wave steepness; (c) Wave steepness for $KB = 0.1$ (——), $KB = 0.2$ (– – –) and $KB = 0.3$ (· · · · ·). Normalization based on zero-crossing of the Gerstner wave.

Figures II.5.4a-c: Modulation of linearized short waves riding on a Gerstner wave and a Stokes wave (○, from Longuet-Higgins, 1987). (a) Wavenumber modulation at the crest (· · · · ·) and at the trough (– – –); (b) likewise for the wave steepness; (c) Wave steepness for $KB = 0.1$ (——), $KB = 0.2$ (– – –) and $KB = 0.3$ (· · · · ·). Normalization based on zero-crossing of the Stokes wave.

Figure II.5.5: Contours of $\frac{\omega}{\sigma}(\phi_E, KB, \epsilon\frac{\Omega}{\sigma})$, $\frac{\omega}{\sigma} = 1$ (solid lines); $\frac{\omega}{\sigma} = 0$ with $\epsilon\frac{\Omega}{\sigma} = 0.05$ ($\cdots\cdots$), $\epsilon\frac{\Omega}{\sigma} = 0.075$ (- - -), $\epsilon\frac{\Omega}{\sigma} = 0.1$ (-·-·-), $\epsilon\frac{\Omega}{\sigma} = 0.125$ (—· · ·—· · ·—) and $\epsilon\frac{\Omega}{\sigma_0} = 0.15$ (— — —).

Figure II.6.1: Amplitude of uniform Stokes wave (——) and amplitude modulation according to the linear evolution equation (- - - -).

Figures II.6.2a-c: Floquet multipliers and Poincaré map iterates, (a) Neutral stability: phase locking, (b) Neutral stability: quasiperiodicity, (c) Instability.

Figures II.6.3a-d: Floquet multipliers, (a) locus of μ_1 in the complex μ plane, (b) $\ln(\rho_1)$ (——) and $\frac{\eta_1}{2\pi}$ (- - -), (c) locus of μ_2 in the complex μ plane, (d) $\ln(\rho_2)$ (——) and $\frac{\eta_2}{2\pi}$ (- - -).

Figures II.6.4a-b: Growth rate as a function of ν and KB, with $\epsilon k\overline{A} = 0.13$ and $\alpha = 0.125$. (a) Three dimensional view, (b) Stability boundaries, ($\times$) symbol refers to $\nu = 2.2$ and its second harmonic $2\nu = 4.4$.

Figures II.6.5a-b: Growth rate as a function of ν and α, with $KB = 0.3$ and $\epsilon k\bar{A} = 0.13$. (a) Three dimensional view, (b) Stability boundaries, symbols refer, for a given α, to the most unstable disturbance and its second and third harmonics.

Figure II.6.6: Linearized stability and Strutt diagram. (Top) Strutt stability boundaries (——), $\mathcal{C}$ with $KB = 0.1$ ($\cdots\cdots$), with $KB = 0.2$ (- - - - -), with $\nu \in [0, 6]$ and $\alpha = 0.125$; (Bottom) Disturbance wavenumber ν vs. Υ, with the same conventions.

Figure II.7.1: Nonlinear evolution of short wave amplitudes in (a) the Fourier domain (b) the physical domain with $KB = 0.3$, $\epsilon k\bar{A} = 0.13$, $\alpha = 0.125$, $\nu = 2.2$ and $\theta_1(0) = -0.344$.

Figure II.7.2: Nonlinear evolution of short wave amplitudes in (a) the Fourier domain (b) the physical domain with $KB = 0.3$, $\epsilon k\bar{A} = 0.13$, $\alpha = 0.05$, $\nu = 1.60$ and $\theta_1(0) = -0.789$.

Figure II.7.3: Nonlinear evolution of short wave amplitudes in (a) the Fourier domain (b) the physical domain with $KB = 0.3$, $\epsilon k\bar{A} = 0.13$, $\alpha = 0.07$, $\nu = 1.63$ and $\theta_1(0) = -0.792$.

Figure II.7.4: Nonlinear evolution of short wave amplitudes in (a) the Fourier domain (b) the physical domain with $KB = 0\ 3$, $\epsilon k\bar{A} = 0.13$, $\alpha = 0.1$, $\nu = 1.64$ and $\theta_1(0) = -0.80$.

Figure II.7.5: Nonlinear evolution of short wave amplitudes in (a) the Fourier domain (b) the physical domain with $KB = 0.3$, $\epsilon k\bar{A} = 0.13$, $\alpha = 0.125$, $\nu = 1.64$ and $\theta_1(0) = -0.8089$.

Figure II.7.6: Nonlinear evolution of short wave amplitudes in (a) the Fourier domain (b) the physical domain with $KB = 0.3$, $\epsilon k\bar{A} = 0.13$, $\alpha = 0.15$, $\nu = 1.64$ and $\theta_1(0) = -0.817$.

Figure II.7.7: Nonlinear evolution of short wave amplitudes in (a) the Fourier domain (b) the physical domain with $KB = 0.3$, $\epsilon k\bar{A} = 0.13$, $\alpha = 0.25$, $\nu = 1.62$ and $\theta_1(0) = -0.865$.

Figure II.7.8: Nonlinear evolution of short wave amplitudes in (a) the Fourier domain (b) the physical domain with $KB = 0.2$, $\epsilon k\bar{A} = 0.13$, $\alpha = 0.15$, $\nu = 1.70$ and $\theta_1(0) = -0.811$.

Figure II.7.9: Nonlinear evolution of short wave amplitudes in (a) the Fourier domain (b) the physical domain with $KB = 0.1$, $\epsilon k\bar{A} = 0.13$, $\alpha = 0.15$, $\nu = 1.80$ and $\theta_1(0) = -0.811$.

Figures II.8.1a-b: Poincaré maps in the $(J_0, \dot{J}_0)$ plane with $KB = 0.3$, $\epsilon k\overline{A} = 0.13$, $\alpha = 0.125$; (a) $\nu = 2.5$ (stable), (b) $\nu = 1.65$ (unstable).

Figures II.8.1c-d: Poincaré maps in the $(\psi_0, \dot{\psi}_0)$ plane with $KB = 0.3$, $\epsilon k\overline{A} = 0.13$, $\alpha = 0.125$; (c) $\nu = 2.5$ (stable), (d) $\nu = 1.65$ (unstable).

Figure II.8.2a: Frequency spectra of J_0 with $KB = 0.3$, $\epsilon k\overline{A} = 0.13$, $\alpha = 0.125$ and $\nu = 2.5$ (stable).

Figure II.8.2b: Frequency spectra of J_0 with $KB = 0.3$, $\epsilon k\overline{A} = 0.13$, $\alpha = 0.125$ and $\nu = 1.65$ (unstable).

Figure II.8.3: Superposition of three Poincaré maps in the $(J_0, \dot{J}_0)$ plane with $KB = 0.3$, $\epsilon k\overline{A} = 0.13$, $\alpha = 0.125$ for three unstable disturbances $\nu = 1.65$, 1.85 and 2.05.

Figures II.8.4a-b: Poincaré maps in the $(\psi_0, \dot{\psi}_0)$ plane at the transition between instability ($\nu = 2.3185$) and stability ($\nu = 2.3186$). Parameters are $KB = 0.3$, $\epsilon k\overline{A} = 0.13$ and $\alpha = 0.125$; (a) global view, (b) detail.

Figure II.8.5: Directions of growth and decay in Floquet theory (unstable and stable manifolds) in the $(\tilde{d}, \tilde{W})$ plane.

Figures II.8.6a-b: Poincaré maps in the $(\psi_0, \dot{\psi}_0)$ plane and the effect of the intial phase. (a) superposition of three maps for $\psi_0(0) = \frac{\pi}{6}, \frac{\pi}{2}$ and π, (b) superposition of 63 values of the initial phase: $\psi_0(0) = 0., 0.1, \ldots, 6.2$.

Figures II.8.7a-b: Poincaré maps in the $(\psi_0, \dot{\psi}_0)$ plane with $KB = 0.3$, $\epsilon k\overline{A} = 0.13$, $\alpha = 0.125$, $\nu = 1.639$ and $\psi_0(0) = 0.8084$; (a) global view, (b) detail of left-most intersection.

Figures II.8.7c-d: Poincaré maps in the $(J_0, \dot{J}_0)$ plane with $KB = 0.3$, $\epsilon k\overline{A} = 0.13$, $\alpha = 0.125$, $\nu = 1.639$ and $\psi_0(0) = 0.8084$; (a) global view, (b) detail of the corner.

Figure II.8.7e: Frequency spectrum of J_0 with $KB = 0.3$, $\epsilon k\overline{A} = 0.13$, $\alpha = 0.125$, $\nu = 1.639$ and $\psi_0(0) = 0.8084$

Figures II.8.8a-b: Poincaré map in the plane $(J_0, \dot{J}_0)$ with $KB = 0.3$, $\epsilon k\bar{A} = 0.13$, $\alpha = 0.125$, $\nu_{\max} = 1.639$ and $\psi_0(0) = 0.8081$; (a) global view, (b) detail of Poincaré

map in the vicinity of corner.

Figures II.8.9a-b: Poincaré map in the plane $(J_0, \dot{J}_0)$ with $KB = 0.3$, $\epsilon k\bar{A} = 0.13$, $\alpha = 0.125$, $\nu_{\max} = 1.639$ and $\psi_0(0) = 0.8080$; (a) global view, (b) detail of Poincaré map in the vicinity of corner.

Figures II.8.10a-b: (a) Poincaré maps in the $(J_0, \dot{J}_0)$ plane (b) Detail of Poincaré map in the vicinity of corner with $KB = 0.3$, $\epsilon k\bar{A} = 0.13$, $\alpha = 0.05$, $\nu_{\max} = 1.604$ and $\psi_0(0) = 0.789$.

Figure II.8.10c: Frequency spectrum of J_0 with $KB = 0.3$, $\epsilon k\bar{A} = 0.13$, $\alpha = 0.05$, $\nu_{\max} = 1.604$ and $\psi_0(0) = 0.789$.

Figures II.8.11a-b: (a) Poincaré maps in the $(J_0, \dot{J}_0)$ plane (b) Detail of Poincaré map in the vicinity of corner with $KB = 0.3$, $\epsilon k\bar{A} = 0.13$, $\alpha = 0.15$, $\nu_{\max} = 1.638$ and $\psi_0(0) = 0.817$.

Figures II.8.11c: Frequency spectrum of J_0 with $KB = 0.3$, $\epsilon k\bar{A} = 0.13$, $\alpha = 0.15$, $\nu_{\max} = 1.638$ and $\psi_0(0) = 0.817$.

Figures II.8.12a-b: (a) Poincaré map in the $(J_0, \dot{J}_0)$ plane (b) Poincaré map in the $(\psi_0, \dot{\psi}_0)$ plane with $KB = 0.3$, $\epsilon k\bar{A} = 0.13$, $\alpha = 0.25$, $\nu_{\max} = 1.62$ and $\psi_0(0) = 0.865$.

Figures II.8.13a-b: (a) Poincaré map in the $(J_0, \dot{J}_0)$ plane (b) Poincaré map in the $(\psi_0, \dot{\psi}_0)$ plane with $KB = 0.3$, $\epsilon k\bar{A} = 0.13$, $\alpha = 0.30$, $\nu_{\max} = 1.60$ and $\psi_0(0) = 0.892$.

Figures II.8.14a-b: (a) Poincaré maps in the $(J_0, \dot{J}_0)$ plane (b) Poincaré map in the $(\psi_0, \dot{\psi}_0)$ plane with $KB = 0.3$, $\epsilon k\bar{A} = 0.13$, $\alpha = 0.45$, $\nu_{\max} = 1.55$ and $\psi_0(0) = 0.970$.

Figure II.8.15: Basin of chaos for various parameters α.

Figure II.8.16: Poincaré map in the $(J_0, \dot{J}_0)$ plane for $KB = 0.1$, 0.2 and 0.3, with $\epsilon k\bar{A} = 0.13$, $\alpha = 0.15$, $\nu = \nu_{\max}$ and $\psi_0(0) = \psi_0^u$.

Figures II.8.17a-b: (a) Poincaré maps in the $(J_0, \dot{J}_0)$ plane (b) Detail of Poincaré map in the vicinity of corner with $KB = 0.2$, $\epsilon k\bar{A} = 0.13$, $\alpha = 0.15$, $\nu_{\max} = 1.7$ and $\psi_0(0) = 0.811$.

Figures II.8.18a-b: (a) Poincaré maps in the $(J_0, \dot{J}_0)$ plane (b) Detail of Poincaré map in the vicinity of corner with $KB = 0.1$, $\epsilon k\bar{A} = 0.13$, $\alpha = 0.15$, $\nu_{\text{n ax}} = 1.8$ and $\psi_0(0) = 0.811$.

Chapter III

Figure III.3.1: Variations of the intrinsic frequency with the long wave phase ϕ and the incidence angle θ with $KB = 0.3$.

Figure III.4.1: Amplitude modulation ratio at the mean surface crossing for

$KB = 0$ (——), $KB = 0.1$ (· · · · ·), $KB = 0.2$ (- - -), $KB = 0.3$ (-·-·-·-) and $KB = 0.4$ (—· · ·—· · ·—).

Figure III.4.2: Amplitude modulation ratio normalized by its value at the trough ($\phi = \phi_E = \pi$) with $KB = 0.3$ and $\theta = 0$, 30°, 45°, 60° and 75°, from upper to lower curve.

Figure III.4.3: Wavenumber modulation ratio (normalized by its value at the surface crossing) at the crest (top curves) and at the trough (bottom curves) for $KB = 0.1$, 0.2, 0.3 and 0.4.

Figure III.4.4: Wavenumber modulation ratio normalized by its value at the trough ($\phi_E = \pi$) with $KB = 0.3$ and $\theta = 0$ (——), 30° (- - -), 45° (-·-·-), 60° (—· · ·—· · ·—) and 90° (horizontal axis).

Figure III.4.5: Direction of propagation of the Eulerian short carrier wave (in degrees with respect to the X-axis) with $\theta = 30°$ for $KB = 0$ (——), $KB = 0.1$ (- - -), $KB = 0.2$ (—·—·—), $KB = 0.3$ (—· · ·—· · ·—) and $KB = 0.4$ (— — —).

Figure III.4.6: Direction of propagation of the Eulerian short carrier wave for $KB = 0.3$ and incidence angle $\theta = 0$, 15°, 30°, 45°, 60°, 75° and 90°.

Figure III.4.7: Contours of $\frac{\omega}{\sigma}(\phi_E, KB, \epsilon\frac{\Omega}{\sigma})$, $\frac{\omega}{\sigma} = 1$ (solid lines); $\frac{\omega}{\sigma} = 0$ with $\epsilon\frac{\Omega}{\sigma_0} = 0.1$ and $\theta = 0$ (· · · · ·), 30° (- - -), 45° (-·-·-), 60° (—· · ·—· · ·—) and 75° (— — —).

Figure III.4.8: Contours of $\frac{\omega}{\sigma}(\phi_E, KB, \epsilon\frac{\Omega}{\sigma})$, $\frac{\omega}{\sigma} = 1$ (solid lines); $\frac{\omega}{\sigma} = 0$ with $\theta = 60°$ and $\epsilon\frac{\Omega}{\sigma_0} = 0.05$ (· · · · ·), $\epsilon\frac{\Omega}{\sigma_0} = 0.075$ (- - -), $\epsilon\frac{\Omega}{\sigma_0} = 0.1$ (-·-·-), $\epsilon\frac{\Omega}{\sigma_0} = 0.125$ (—· · ·—· · ·—) and $\epsilon\frac{\Omega}{\sigma_0} = 0.15$ (— — —).

Figure III.4.9: Direction of propagation of the short wave envelope Θ (in degrees with respect to the X-axis) with $\theta = 30°$ and $\epsilon\frac{\Omega}{\sigma_0} = 0.1$ for $KB = 0$ (——), $KB = 0.05$ (- - -), $KB = 0.1$ (-·-·-), $KB = 0.2$ (—· · ·—· · ·—) and $KB = 0.3$ (— — —).

Figures III.5.1a-b: Growth rate for two-dimensional disturbances (ν_x, ν_y) in the absence of long waves (Benney & Roskes, 1969) with $\epsilon k\overline{A} = 0.13$ and $\alpha = 0.125$. (a) Three-dimensional view, (b) Stability boundaries

Figures III.5.2a-b: Growth rate for two-dimensional disturbances $(\nu_x, \nu_y) \in [0,6] \times [0,6]$ with $KB = 0.1$ $\epsilon k\overline{A} = 0.13$ and $\alpha = 0.125$. (a) Three-dimensional view, (b) Stability boundaries, the dotted line refers to the section of the (ν_x, ν_y) plane analysed in figures III.5.7a-b.

Figures III.5.3a-b: Growth rate for two-dimensional disturbances $(\nu_x, \nu_y) \in [1,3] \times [3,6]$ with $KB = 0.1$ $\epsilon k\overline{A} = 0.13$ and $\alpha = 0.125$. (a) Three-dimensional view, (b) Stability boundaries.

Figure III.5.4: Floquet multiplier μ_1 with $\nu_x = 0.5$, $KB = 0.1$, $\epsilon k\overline{A} = 0.13$ and $\alpha = 0.125$. The sequence of points $p_{0,1,...}$ corresponds to increasing values of $\nu_y \in [0,6]$; (Top) locus of μ_1 in the complex μ plane, (Bottom) $\Re\{\ln(\mu_1)\}$ (solid line) and $\Im\{\ln(\mu_1)\}$ (chain line).

Figure III.5.5: Wedge in the upper right quadrant of the (ν_x, ν_y) plane where the reduction to a Mathieu equation is not possible with $KB = 0.3$.

Figure III.5.6: Linearized stability and Strutt diagram with $\nu_x = 0.5$, $\nu_y \in [1, 6]$, $KB = 0.1$, $\epsilon k\overline{A} = 0.13$ and $\alpha = 0.125$; (Top) stability boundaries of Mathieu equation (solid line), $(\Upsilon(\nu_y), \Delta(\nu_y))$ (chain line); (bottom) $\nu_y(\Upsilon)$.

Figure III.5.7: Floquet multiplier μ_1 with $\nu_x \in [0, 6]$, $\nu_y \in [3.5, 5.25]$, $KB = 0.1$, $\epsilon k\overline{A} = 0.13$ and $\alpha = 0.125$. The sequence of points $p_{0,1,...}$ corresponds to increasing values of ν_x and ν_y along the dotted line in figure III.5.2b; (Top) locus of μ_1 in the complex μ plane, (Bottom) $\Re\{\ln(\mu_1)\}$ (solid line) and $\Im\{\ln(\mu_1)\}$ (chain line).

Figures III.5.8a-b: Growth rate for two-dimensional disturbances $(\nu_x, \nu_y) \in [0, 6] \times [0, 6]$ with $KB = 0.2$ $\epsilon k\overline{A} = 0.13$ and $\alpha = 0.125$. (a) Three-dimensional view, (b) Stability boundaries.

Figures III.5.9a-b: Growth rate for two-dimensional disturbances $(\nu_x, \nu_y) \in [0, 6] \times [0, 6]$ with $KB = 0.3$ $\epsilon k\overline{A} = 0.13$ and $\alpha = 0.125$. (a) Three-dimensional view, (b) Stability boundaries.

Figures III.5.10a-b: Growth rate for two-dimensional disturbances $(\nu_x, \nu_y) \in [0, 6] \times [0, 6]$ with $KB = 0.3$ $\epsilon k\overline{A} = 0.13$ and $\alpha = 0.05$. (a) Three-dimensional view, (b) Stability boundaries.

Figures III.5.11a-b: Growth rate for two-dimensional disturbances $(\nu_x, \nu_y) \in [0, 6] \times [0, 6]$ with $KB = 0.3$ $\epsilon k\overline{A} = 0.13$ and $\alpha = 0.075$. (a) Three-dimensional view, (b) Stability boundaries.

Figures III.5.12a-b: Growth rate for two-dimensional disturbances $(\nu_x, \nu_y) \in [0, 6] \times [0, 6]$ with $KB = 0.3$ $\epsilon k\overline{A} = 0.13$ and $\alpha = 0.1$. (a) Three-dimensional view, (b) Stability boundaries.

Figures III.5.13a-b: Growth rate for two-dimensional disturbances $(\nu_x, \nu_y) \in [0, 6] \times [0, 6]$ with $KB = 0.3$ $\epsilon k\overline{A} = 0.13$ and $\alpha = 0.15$. (a) Three-dimensional view, (b) Stability boundaries.

APPENDICES FOR CHAPTERS I, II & III

Appendix A: Vorticity in Lagrangian Coordinates:

We first introduce the two-dimensional velocity field $\mathbf{U} = (u, w)$

$$u \equiv \frac{\partial X}{\partial t} \qquad w \equiv \frac{\partial Z}{\partial t} \tag{A.1}$$

The vorticity ϖ is then given by

$$\varpi = \frac{\partial u}{\partial Z} - \frac{\partial w}{\partial X} = \frac{\partial u}{\partial a}\frac{\partial a}{\partial Z} + \frac{\partial u}{\partial c}\frac{\partial c}{\partial Z} - \frac{\partial w}{\partial a}\frac{\partial a}{\partial X} - \frac{\partial w}{\partial c}\frac{\partial c}{\partial X} \tag{A.2}$$

where $X = X(a, c, t)$ and $Z = Z(a, c, t)$. Upon differentiating these two equations with respect to X, we obtain

$$1 = \frac{\partial X}{\partial a}\frac{\partial a}{\partial X} + \frac{\partial X}{\partial c}\frac{\partial c}{\partial X} \tag{A.3a}$$

$$0 = \frac{\partial Z}{\partial a}\frac{\partial a}{\partial X} + \frac{\partial Z}{\partial c}\frac{\partial c}{\partial X} \tag{A.3b}$$

and with respect to Z,

$$0 = \frac{\partial X}{\partial a}\frac{\partial a}{\partial Z} + \frac{\partial X}{\partial c}\frac{\partial c}{\partial Z} \tag{A.4a}$$

$$1 = \frac{\partial Z}{\partial a}\frac{\partial a}{\partial Z} + \frac{\partial Z}{\partial c}\frac{\partial c}{\partial Z} \tag{A.4b}$$

We first solve $(A.3a - b)$ for $\frac{\partial a}{\partial X}$ and $\frac{\partial c}{\partial X}$:

$$(\frac{\partial a}{\partial X}, \frac{\partial c}{\partial X}) = \frac{1}{J}(\frac{\partial Z}{\partial c}, -\frac{\partial Z}{\partial a}) \tag{A.5a - b}$$

and then $(A.4a - b)$ for $\frac{\partial a}{\partial Z}$ and $\frac{\partial c}{\partial Z}$:

$$(\frac{\partial a}{\partial Z}, \frac{\partial c}{\partial Z}) = \frac{1}{J}(-\frac{\partial X}{\partial c}, \frac{\partial X}{\partial a}) \tag{A.6a - b}$$

Substitution of $(A.5a - b)$ and $(A.6a - b)$ into $(A.2)$ yields the expression of the vorticity field in the Lagrangian variables:

$$\varpi = \frac{1}{J}\{\frac{\partial X}{\partial a}\frac{\partial^2 X}{\partial c \partial t} - \frac{\partial X}{\partial c}\frac{\partial^2 X}{\partial a \partial t} + \frac{\partial Z}{\partial a}\frac{\partial^2 Z}{\partial c \partial t} - \frac{\partial Z}{\partial c}\frac{\partial^2 Z}{\partial a \partial t}\} \tag{A.7}$$

where the Jacobian J is given by $(I.2.1)$.

Appendix B: Governing Equations at $\mathcal{O}(\epsilon^3)$

Continuity:

$$\frac{\partial x_3}{\partial a}+\frac{\partial z_3}{\partial c}+\frac{\partial x_2}{\partial a_1}+\frac{\partial z_2}{\partial c_1}+\frac{\partial x_1}{\partial a_2}+\frac{\partial z_1}{\partial c_2}+\frac{\partial x_0}{\partial a_3}+\frac{\partial z_0}{\partial c_3}+\frac{\partial x_{-1}}{\partial a_4}+\frac{\partial z_{-1}}{\partial c_4}+$$

$$+\frac{\partial x_{-1}}{\partial a_2}\frac{\partial z_0}{\partial c_2}+\frac{\partial x_1}{\partial a}\frac{\partial z_0}{\partial c_2}-\frac{\partial x_{-1}}{\partial c_2}\frac{\partial z_0}{\partial a_2}-\frac{\partial x_1}{\partial c}\frac{\partial z_0}{\partial a_2}+$$

$$+\frac{\partial x_{-1}}{\partial a_2}\frac{\partial z_{-1}}{\partial c_3}+\frac{\partial x_1}{\partial a}\frac{\partial z_{-1}}{\partial c_3}+\frac{\partial x_0}{\partial a_2}\frac{\partial z_{-1}}{\partial c_2}+\frac{\partial x_{-1}}{\partial a_3}\frac{\partial z_{-1}}{\partial c_2}+$$

$$+\frac{\partial x_2}{\partial a}\frac{\partial z_{-1}}{\partial c_2}+\frac{\partial x_1}{\partial a_1}\frac{\partial z_{-1}}{\partial c_2}-\frac{\partial x_{-1}}{\partial c_2}\frac{\partial z_{-1}}{\partial a_3}-\frac{\partial x_1}{\partial c}\frac{\partial z_{-1}}{\partial a_3}+$$

$$-\frac{\partial x_0}{\partial c_2}\frac{\partial z_{-1}}{\partial a_2}-\frac{\partial x_{-1}}{\partial c_3}\frac{\partial z_{-1}}{\partial a_2}-\frac{\partial x_2}{\partial c}\frac{\partial z_{-1}}{\partial a_2}-\frac{\partial x_1}{\partial c_1}\frac{\partial z_{-1}}{\partial a_2}+$$

$$+\frac{\partial x_{-1}}{\partial a_2}\frac{\partial z_2}{\partial c}+\frac{\partial x_1}{\partial a}\frac{\partial z_2}{\partial c}-\frac{\partial x_{-1}}{\partial c_2}\frac{\partial z_2}{\partial a}-\frac{\partial x_1}{\partial c}\frac{\partial z_2}{\partial a}+$$

$$+\frac{\partial x_{-1}}{\partial a_2}\frac{\partial z_1}{\partial c_1}+\frac{\partial x_1}{\partial a}\frac{\partial z_1}{\partial c_1}+\frac{\partial x_0}{\partial a_2}\frac{\partial z_1}{\partial c}+\frac{\partial x_{-1}}{\partial a_3}\frac{\partial z_1}{\partial c}+$$

$$+\frac{\partial x_2}{\partial a}\frac{\partial z_1}{\partial c}+\frac{\partial x_1}{\partial a_1}\frac{\partial z_1}{\partial c}-\frac{\partial x_{-1}}{\partial c_2}\frac{\partial z_1}{\partial a_1}-\frac{\partial x_1}{\partial c}\frac{\partial z_1}{\partial a_1}+$$

$$-\frac{\partial x_0}{\partial c_2}\frac{\partial z_1}{\partial a}-\frac{\partial x_{-1}}{\partial c_3}\frac{\partial z_1}{\partial a}-\frac{\partial x_2}{\partial c}\frac{\partial z_1}{\partial a}-\frac{\partial x_1}{\partial c_1}\frac{\partial z_1}{\partial a}=0 \qquad (B.1a)$$

Irrotationality:

$$\frac{\partial^3 x_3}{\partial c\partial t^2}-\frac{\partial^3 z_3}{\partial a\partial t^2}+\frac{\partial^3 x_2}{\partial c_1\partial t^2}-\frac{\partial^3 z_2}{\partial a_1\partial t^2}+2\frac{\partial^3 x_2}{\partial c\partial t\partial t_1}-2\frac{\partial^3 z_2}{\partial a\partial t\partial t_1}+\frac{\partial^3 x_1}{\partial c\partial {t_1}^2}-\frac{\partial^3 z_1}{\partial a\partial {t_1}^2}+$$

$$+2\frac{\partial^3 x_1}{\partial c\partial t\partial t_2}-2\frac{\partial^3 z_1}{\partial a\partial t\partial t_2}+2\frac{\partial^3 x_1}{\partial c_1\partial t\partial t_1}-2\frac{\partial^3 z_1}{\partial a_1\partial t\partial t_1}+$$

$$+\frac{\partial^3 x_1}{\partial c_2\partial t^2}-\frac{\partial^3 z_1}{\partial a_2\partial t^2}+\frac{\partial^3 x_{-1}}{\partial c_2\partial {t_1}^2}-\frac{\partial^3 z_{-1}}{\partial a_2\partial {t_1}^2}$$

$$-\frac{\partial^3 z_1}{\partial a\partial t^2}\frac{\partial z_0}{\partial c_2}+\frac{\partial^3 z_1}{\partial c\partial t^2}\frac{\partial z_0}{\partial a_2}-\frac{\partial^3 z_1}{\partial a\partial t^2}\frac{\partial z_{-1}}{\partial c_3}+$$

$$-\frac{\partial^3 z_2}{\partial a\partial t^2}\frac{\partial z_{-1}}{\partial c_2}-\frac{\partial^3 z_1}{\partial a_1\partial t^2}\frac{\partial z_{-1}}{\partial c_2}-2\frac{\partial^3 z_1}{\partial a\partial t\partial t_1}\frac{\partial z_{-1}}{\partial c_2}+\frac{\partial^3 z_1}{\partial c\partial t^2}\frac{\partial z_{-1}}{\partial a_3}+$$

$$+\frac{\partial^3 z_2}{\partial c\partial t^2}\frac{\partial z_{-1}}{\partial a_2}+\frac{\partial^3 z_1}{\partial c_1\partial t^2}\frac{\partial z_{-1}}{\partial a_2}+2\frac{\partial^3 z_1}{\partial c\partial t\partial t_1}\frac{\partial z_{-1}}{\partial a_2}+\frac{\partial z_1}{\partial a}\frac{\partial^3 z_2}{\partial c\partial t^2}-\frac{\partial^3 z_1}{\partial a\partial t^2}\frac{\partial z_2}{\partial c}+$$

$$-\frac{\partial z_1}{\partial c}\frac{\partial^3 z_2}{\partial a \partial t^2}+\frac{\partial^3 z_1}{\partial c \partial t^2}\frac{\partial z_2}{\partial a}+\frac{\partial z_1}{\partial a}\frac{\partial^3 z_1}{\partial c_1 \partial t^2}-\frac{\partial^3 z_1}{\partial a \partial t^2}\frac{\partial z_1}{\partial c_1}+\frac{\partial z_1}{\partial a_1}\frac{\partial^3 z_1}{\partial c \partial t^2}+$$

$$+2\frac{\partial z_1}{\partial a}\frac{\partial^3 z_1}{\partial c \partial t \partial t_1}-\frac{\partial^3 z_1}{\partial a_1 \partial t^2}\frac{\partial z_1}{\partial c}-2\frac{\partial^3 z_1}{\partial a \partial t \partial t_1}\frac{\partial z_1}{\partial c}-\frac{\partial^3 x_1}{\partial a \partial t^2}\frac{\partial x_0}{\partial c_2}+$$

$$+\frac{\partial^3 x_1}{\partial c \partial t^2}\frac{\partial x_0}{\partial a_2}-\frac{\partial^3 x_1}{\partial a \partial t^2}\frac{\partial x_{-1}}{\partial c_3}-\frac{\partial^3 x_2}{\partial a \partial t^2}\frac{\partial x_{-1}}{\partial c_2}-\frac{\partial^3 x_1}{\partial a_1 \partial t^2}\frac{\partial x_{-1}}{\partial c_2}+$$

$$-2\frac{\partial^3 x_1}{\partial a \partial t \partial t_1}\frac{\partial x_{-1}}{\partial c_2}+\frac{\partial^3 x_1}{\partial c \partial t^2}\frac{\partial x_{-1}}{\partial a_3}+\frac{\partial^3 x_2}{\partial c \partial t^2}\frac{\partial x_{-1}}{\partial a_2}+\frac{\partial^3 x_1}{\partial c_1 \partial t^2}\frac{\partial x_{-1}}{\partial a_2}+2\frac{\partial^3 x_1}{\partial c \partial t \partial t_1}\frac{\partial x_{-1}}{\partial a_2}+$$

$$+\frac{\partial x_1}{\partial a}\frac{\partial^3 x_2}{\partial c \partial t^2}-\frac{\partial^3 x_1}{\partial a \partial t^2}\frac{\partial x_2}{\partial c}-\frac{\partial x_1}{\partial c}\frac{\partial^3 x_2}{\partial a \partial t^2}+\frac{\partial^3 x_1}{\partial c \partial t^2}\frac{\partial x_2}{\partial a}+\frac{\partial x_1}{\partial a}\frac{\partial^3 x_1}{\partial c_1 \partial t^2}-\frac{\partial^3 x_1}{\partial a \partial t^2}\frac{\partial x_1}{\partial c_1}$$

$$+\frac{\partial x_1}{\partial a_1}\frac{\partial^3 x_1}{\partial c \partial t^2}+2\frac{\partial x_1}{\partial a}\frac{\partial^3 x_1}{\partial c \partial t \partial t_1}-\frac{\partial^3 x_1}{\partial a_1 \partial t^2}\frac{\partial x_1}{\partial c}-2\frac{\partial^3 x_1}{\partial a \partial t \partial t_1}\frac{\partial x_1}{\partial c}=0 \qquad (B.1b)$$

Free surface dynamic boundary condition

$$\frac{\partial^2 x_3}{\partial t^2}+g\frac{\partial z_3}{\partial a}+2\frac{\partial^2 x_2}{\partial t \partial t_1}+g\frac{\partial z_2}{\partial a_1}+\frac{\partial^2 x_1}{\partial {t_1}^2}+2\frac{\partial^2 x_1}{\partial t \partial t_2}+$$

$$+g\frac{\partial z_1}{\partial a_2}+2\frac{\partial^2 x_0}{\partial t_1 \partial t_2}+g\frac{\partial z_0}{\partial a_3}+2\frac{\partial^2 x_{-1}}{\partial t_1 \partial t_3}+\frac{\partial^2 x_{-1}}{\partial {t_2}^2}+g\frac{\partial z_{-1}}{\partial a_4}+$$

$$+\frac{\partial z_{-1}}{\partial a_2}\frac{\partial^2 z_0}{\partial {t_1}^2}+\frac{\partial z_1}{\partial a}\frac{\partial^2 z_0}{\partial {t_1}^2}+\frac{\partial^2 z_{-1}}{\partial {t_1}^2}\frac{\partial z_0}{\partial a_2}+\frac{\partial^2 z_1}{\partial t^2}\frac{\partial z_0}{\partial a_2}+$$

$$+\frac{\partial z_{-1}}{\partial a_3}\frac{\partial^2 z_{-1}}{\partial {t_1}^2}+\frac{\partial z_2}{\partial a}\frac{\partial^2 z_{-1}}{\partial {t_1}^2}+\frac{\partial z_1}{\partial a_1}\frac{\partial^2 z_{-1}}{\partial {t_1}^2}+2\frac{\partial z_{-1}}{\partial a_2}\frac{\partial^2 z_{-1}}{\partial t_1 \partial t_2}+$$

$$+2\frac{\partial z_1}{\partial a}\frac{\partial^2 z_{-1}}{\partial t_1 \partial t_2}+\frac{\partial^2 z_1}{\partial t^2}\frac{\partial z_{-1}}{\partial a_3}+\frac{\partial^2 z_2}{\partial t^2}\frac{\partial z_{-1}}{\partial a_2}+2\frac{\partial^2 z_1}{\partial t \partial t_1}\frac{\partial z_{-1}}{\partial a_2}+\frac{\partial z_1}{\partial a}\frac{\partial^2 z_2}{\partial t^2}+\frac{\partial^2 z_1}{\partial t^2}\frac{\partial z_2}{\partial a}+$$

$$+\frac{\partial z_1}{\partial a_1}\frac{\partial^2 z_1}{\partial t^2}+2\frac{\partial z_1}{\partial a}\frac{\partial^2 z_1}{\partial t \partial t_1}+\frac{\partial x_0}{\partial a_1}\frac{\partial^2 x_0}{\partial {t_1}^2}+\frac{\partial x_{-1}}{\partial a_2}\frac{\partial^2 x_0}{\partial {t_1}^2}+\frac{\partial x_1}{\partial a}\frac{\partial^2 x_0}{\partial {t_1}^2}+\frac{\partial^2 x_{-1}}{\partial {t_1}^2}\frac{\partial x_0}{\partial a_2}+$$

$$+\frac{\partial^2 x_1}{\partial t^2}\frac{\partial x_0}{\partial a_2}+\frac{\partial x_{-1}}{\partial a_3}\frac{\partial^2 x_{-1}}{\partial {t_1}^2}+\frac{\partial x_2}{\partial a}\frac{\partial^2 x_{-1}}{\partial {t_1}^2}+\frac{\partial x_1}{\partial a_1}\frac{\partial^2 x_{-1}}{\partial {t_1}^2}+$$

$$+2\frac{\partial x_{-1}}{\partial a_2}\frac{\partial^2 x_{-1}}{\partial t_1 \partial t_2}+2\frac{\partial x_1}{\partial a}\frac{\partial^2 x_{-1}}{\partial t_1 \partial t_2}+\frac{\partial^2 x_1}{\partial t^2}\frac{\partial x_{-1}}{\partial a_3}+\frac{\partial^2 x_2}{\partial t^2}\frac{\partial x_{-1}}{\partial a_2}+2\frac{\partial^2 x_1}{\partial t \partial t_1}\frac{\partial x_{-1}}{\partial a_2}+$$

$$+\frac{\partial x_1}{\partial a}\frac{\partial^2 x_2}{\partial t^2}+\frac{\partial^2 x_1}{\partial t^2}\frac{\partial x_2}{\partial a}+\frac{\partial x_1}{\partial a_1}\frac{\partial^2 x_1}{\partial t^2}+2\frac{\partial x_1}{\partial a}\frac{\partial^2 x_1}{\partial t \partial t_1}=0 \qquad (B.1c)$$

Appendix C: Alternate Form of Solvability Condition

Consider two dependent variables $x(c)$ and $z(c)$ satisfying the following two equations

$$\frac{\partial z}{\partial c} - k\, x = E(c) \qquad \frac{\partial x}{\partial c} - k\, z = G(c) \qquad (C.1a-b)$$

where the forcing terms E and G contain terms proportional to e^{kc}. The boundary condition at the free surface $c = 0$ is

$$x - z = I \qquad c = 0 \qquad (C.1c)$$

Elimination of $z(c)$ from $(C.1a-b)$ yields

$$\frac{\partial^2 x}{\partial c^2} - k^2 x = \frac{\partial G}{\partial c} + kE \qquad (C.2a)$$

and likewise from $(C.1c)$

$$\frac{\partial x}{\partial c} - kx = -kI + G \qquad c = 0 \qquad (C.2b)$$

Since e^{kc} is a solution of the homogeneous form of $(C.2a)$, the existence of a solution requires that the Green formula be satisfied, *i.e.*

$$\int_{-\infty}^{0} \left[\frac{\partial^2 x}{\partial c^2} - k^2 x\right] e^{kc} dc = \left[e^{kc}\frac{\partial x}{\partial c} - k e^{kc} x\right]_{-\infty}^{0} \qquad (C.3)$$

After $(C.2a)$ is substituted in $(C.3)$, we may integrate by parts and obtain

$$\left[G e^{kc}\right]_{-\infty}^{0} + k\int_{-\infty}^{0} [E - G] e^{kc} dc = -kI + G(0) \qquad (C.4)$$

i.e. after simplifications

$$\int_{-\infty}^{0} \left[G(c) - E(c)\right] e^{kc} dc = I \qquad (C.5)$$

Eq. $(C.5)$ is equivalent to the Green solvability condition for the Laplacian operator.

Appendix D: Governing Equations at $\mathcal{O}(\epsilon^3)$:

Continuity:

$$\frac{\partial x_3}{\partial a}+\frac{\partial z_3}{\partial c}+\frac{\partial x_2}{\partial a_1}+\frac{\partial z_2}{\partial c_1}+\frac{\partial x_1}{\partial a_2}+\frac{\partial z_1}{\partial c_2}+$$
$$+\frac{\partial x_1}{\partial a}\frac{\partial z_2}{\partial c}-\frac{\partial x_1}{\partial c}\frac{\partial z_2}{\partial a}+\frac{\partial x_2}{\partial a}\frac{\partial z_1}{\partial c}+\frac{\partial x_1}{\partial a_1}\frac{\partial z_1}{\partial c}+$$
$$-\frac{\partial x_2}{\partial c}\frac{\partial z_1}{\partial a}-\frac{\partial x_1}{\partial c_1}\frac{\partial z_1}{\partial a}+\frac{\partial x_1}{\partial a}\frac{\partial z_1}{\partial c_1}-\frac{\partial x_1}{\partial c}\frac{\partial z_1}{\partial a_1}+$$
$$+\frac{\partial x_3}{\partial a}\frac{\partial z_{-2}}{\partial c_2}+\frac{\partial x_2}{\partial a_1}\frac{\partial z_{-2}}{\partial c_2}+\frac{\partial x_1}{\partial a_2}\frac{\partial z_{-2}}{\partial c_2}-\frac{\partial x_3}{\partial c}\frac{\partial z_{-2}}{\partial a_2}-\frac{\partial x_2}{\partial c_1}\frac{\partial z_{-2}}{\partial a_2}-\frac{\partial x_1}{\partial c_2}\frac{\partial z_{-2}}{\partial a_2}+$$
$$+\frac{\partial x_{-2}}{\partial a_2}\frac{\partial z_3}{\partial c}-\frac{\partial x_{-2}}{\partial c_2}\frac{\partial z_3}{\partial a}+\frac{\partial x_{-2}}{\partial a_2}\frac{\partial z_2}{\partial c_1}-\frac{\partial x_{-2}}{\partial c_2}\frac{\partial z_2}{\partial a_1}+\frac{\partial x_{-2}}{\partial a_2}\frac{\partial z_1}{\partial c_2}-\frac{\partial x_{-2}}{\partial c_2}\frac{\partial z_1}{\partial a_2}=0 \tag{D.1a}$$

Vorticity:

$$\frac{\partial^3 x_3}{\partial c\partial t^2}-\frac{\partial^3 z_3}{\partial a\partial t^2}+2\frac{\partial^3 x_2}{\partial t_1\partial c\partial t}-2\frac{\partial^3 z_2}{\partial t_1\partial a\partial t}+\frac{\partial^3 x_2}{\partial c_1\partial t^2}-\frac{\partial^3 z_2}{\partial a_1\partial t^2}+$$
$$+2\frac{\partial^3 x_1}{\partial t_2\partial c\partial t}+\frac{\partial^3 x_1}{\partial c_2\partial t^2}+\frac{\partial^3 x_1}{\partial t_1^2\partial c}+2\frac{\partial^3 x_1}{\partial c_1\partial t_1\partial t}+$$
$$-2\frac{\partial^3 z_1}{\partial t_2\partial a\partial t}-\frac{\partial^3 z_1}{\partial a_2\partial t^2}-\frac{\partial^3 z_1}{\partial t_1^2\partial a}-2\frac{\partial^3 z_1}{\partial a_1\partial t_1\partial t}+$$
$$+\frac{\partial x_1}{\partial a}\frac{\partial^3 x_2}{\partial c\partial t^2}+\frac{\partial^3 x_1}{\partial c\partial t^2}\frac{\partial x_2}{\partial a}+\frac{\partial x_1}{\partial a_1}\frac{\partial^3 x_1}{\partial c\partial t^2}+2\frac{\partial^3 x_1}{\partial t_1\partial c\partial t}\frac{\partial x_1}{\partial a}+\frac{\partial^3 x_1}{\partial c_1\partial t^2}\frac{\partial x_1}{\partial a}+$$
$$-\frac{\partial^3 x_1}{\partial a\partial t^2}\frac{\partial x_2}{\partial c}-\frac{\partial x_1}{\partial c}\frac{\partial^3 x_2}{\partial a\partial t^2}-2\frac{\partial^3 x_1}{\partial t_1\partial a\partial t}\frac{\partial x_1}{\partial c}-\frac{\partial^3 x_1}{\partial a_1\partial t^2}\frac{\partial x_1}{\partial c}-\frac{\partial x_1}{\partial c_1}\frac{\partial^3 x_1}{\partial a\partial t^2}+$$
$$+\frac{\partial z_1}{\partial a}\frac{\partial^3 z_2}{\partial c\partial t^2}+\frac{\partial^3 z_1}{\partial c\partial t^2}\frac{\partial z_2}{\partial a}+\frac{\partial^3 z_1}{\partial c_1\partial t^2}\frac{\partial z_1}{\partial a}+\frac{\partial z_1}{\partial a_1}\frac{\partial^3 z_1}{\partial c\partial t^2}+2\frac{\partial^3 z_1}{\partial t_1\partial c\partial t}\frac{\partial z_1}{\partial a}+$$
$$-\frac{\partial^3 z_1}{\partial a\partial t^2}\frac{\partial z_2}{\partial c}-\frac{\partial z_1}{\partial c}\frac{\partial^3 z_2}{\partial a\partial t^2}-\frac{\partial z_1}{\partial c_1}\frac{\partial^3 z_1}{\partial a\partial t^2}-2\frac{\partial^3 z_1}{\partial t_1\partial a\partial t}\frac{\partial z_1}{\partial c}-\frac{\partial^3 z_1}{\partial a_1\partial t^2}\frac{\partial z_1}{\partial c}+$$
$$+\frac{\partial x_1}{\partial a}\frac{\partial^3 x_{-2}}{\partial t_1^2\partial c_2}+\frac{\partial^3 x_3}{\partial c\partial t^2}\frac{\partial x_{-2}}{\partial a_2}+\frac{\partial^3 x_2}{\partial c_1\partial t^2}\frac{\partial x_{-2}}{\partial a_2}+\frac{\partial^3 x_1}{\partial c_2\partial t^2}\frac{\partial x_{-2}}{\partial a_2}+\frac{\partial^3 x_1}{\partial t_1^2\partial c}\frac{\partial x_{-2}}{\partial a_2}+$$
$$-\frac{\partial^3 x_3}{\partial a\partial t^2}\frac{\partial x_{-2}}{\partial c_2}-\frac{\partial^3 x_2}{\partial a_1\partial t^2}\frac{\partial x_{-2}}{\partial c_2}-\frac{\partial^3 x_1}{\partial a_2\partial t^2}\frac{\partial x_{-2}}{\partial c_2}-\frac{\partial^3 x_1}{\partial t_1^2\partial a}\frac{\partial x_{-2}}{\partial c_2}-\frac{\partial x_1}{\partial c}\frac{\partial^3 x_{-2}}{\partial t_1^2\partial a_2}+$$
$$+2\frac{\partial^3 x_2}{\partial t_1\partial c\partial t}\frac{\partial x_{-2}}{\partial a_2}+2\frac{\partial^3 x_1}{\partial t_2\partial c\partial t}\frac{\partial x_{-2}}{\partial a_2}+2\frac{\partial^3 x_1}{\partial c_1\partial t_1\partial t}\frac{\partial x_{-2}}{\partial a_2}+$$

$$-2\frac{\partial^3 x_2}{\partial t_1 \partial a \partial t}\frac{\partial x_{-2}}{\partial c_2} - 2\frac{\partial^3 x_1}{\partial t_2 \partial a \partial t}\frac{\partial x_{-2}}{\partial c_2} - 2\frac{\partial^3 x_1}{\partial a_1 \partial t_1 \partial t}\frac{\partial x_{-2}}{\partial c_2} +$$

$$+\frac{\partial z_1}{\partial a}\frac{\partial^3 z_{-2}}{\partial t_1^2 \partial c_2} + \frac{\partial^3 z_3}{\partial c \partial t^2}\frac{\partial z_{-2}}{\partial a_2} + \frac{\partial^3 z_2}{\partial c_1 \partial t^2}\frac{\partial z_{-2}}{\partial a_2} + \frac{\partial^3 z_1}{\partial c_2 \partial t^2}\frac{\partial z_{-2}}{\partial a_2} + \frac{\partial^3 z_1}{\partial t_1^2 \partial c}\frac{\partial z_{-2}}{\partial a_2} +$$

$$-\frac{\partial^3 z_3}{\partial a \partial t^2}\frac{\partial z_{-2}}{\partial c_2} - \frac{\partial^3 z_2}{\partial a_1 \partial t^2}\frac{\partial z_{-2}}{\partial c_2} - \frac{\partial^3 z_1}{\partial a_2 \partial t^2}\frac{\partial z_{-2}}{\partial c_2} - \frac{\partial^3 z_1}{\partial t_1^2 \partial a}\frac{\partial z_{-2}}{\partial c_2} - \frac{\partial z_1}{\partial c}\frac{\partial^3 z_{-2}}{\partial t_1^2 \partial a_2} +$$

$$+2\frac{\partial^3 z_2}{\partial t_1 \partial c \partial t}\frac{\partial z_{-2}}{\partial a_2} + 2\frac{\partial^3 z_1}{\partial t_2 \partial c \partial t}\frac{\partial z_{-2}}{\partial a_2} + 2\frac{\partial^3 z_1}{\partial c_1 \partial t_1 \partial t}\frac{\partial z_{-2}}{\partial a_2} +$$

$$-2\frac{\partial^3 z_2}{\partial t_1 \partial a \partial t}\frac{\partial z_{-2}}{\partial c_2} - 2\frac{\partial^3 z_1}{\partial t_2 \partial a \partial t}\frac{\partial z_{-2}}{\partial c_2} - 2\frac{\partial^3 z_1}{\partial a_1 \partial t_1 \partial t}\frac{\partial z_{-2}}{\partial c_2} = 0 \qquad (D.1b)$$

Free surface boundary condition:

$$\frac{\partial^2 x_3}{\partial t^2} + g\frac{\partial z_3}{\partial a} + 2\frac{\partial^2 x_2}{\partial t_1 \partial t} + g\frac{\partial z_2}{\partial a_1} + \frac{\partial^2 x_1}{\partial t_1^2} + 2\frac{\partial^2 x_1}{\partial t_2 \partial t} + g\frac{\partial z_1}{\partial a_2} +$$

$$+\frac{\partial x_1}{\partial a}\frac{\partial^2 x_2}{\partial t^2} + \frac{\partial^2 x_1}{\partial t^2}\frac{\partial x_2}{\partial a} + \frac{\partial x_1}{\partial a_1}\frac{\partial^2 x_1}{\partial t^2} + 2\frac{\partial^2 x_1}{\partial t_1 \partial t}\frac{\partial x_1}{\partial a} +$$

$$+\frac{\partial z_1}{\partial a}\frac{\partial^2 z_2}{\partial t^2} + \frac{\partial^2 z_1}{\partial t^2}\frac{\partial z_2}{\partial a} + \frac{\partial z_1}{\partial a_1}\frac{\partial^2 z_1}{\partial t^2} + 2\frac{\partial^2 z_1}{\partial t_1 \partial t}\frac{\partial z_1}{\partial a} +$$

$$+\frac{\partial^2 x_3}{\partial t^2}\frac{\partial x_{-2}}{\partial a_2} + \frac{\partial x_3}{\partial a}\frac{\partial^2 x_{-2}}{\partial t_1^2} + \frac{\partial x_2}{\partial a_1}\frac{\partial^2 x_{-2}}{\partial t_1^2} + \frac{\partial^2 x_1}{\partial t_1^2}\frac{\partial x_{-2}}{\partial a_2} + \frac{\partial x_1}{\partial a_2}\frac{\partial^2 x_{-2}}{\partial t_1^2} +$$

$$+\frac{\partial^2 z_3}{\partial t^2}\frac{\partial z_{-2}}{\partial a_2} + \frac{\partial z_3}{\partial a}\frac{\partial^2 z_{-2}}{\partial t_1^2} + \frac{\partial z_2}{\partial a_1}\frac{\partial^2 z_{-2}}{\partial t_1^2} + \frac{\partial^2 z_1}{\partial t_1^2}\frac{\partial z_{-2}}{\partial a_2} + \frac{\partial z_1}{\partial a_2}\frac{\partial^2 z_{-2}}{\partial t_1^2} +$$

$$+2\frac{\partial^2 x_2}{\partial t_1 \partial t}\frac{\partial x_{-2}}{\partial a_2} + 2\frac{\partial^2 x_1}{\partial t_2 \partial t}\frac{\partial x_{-2}}{\partial a_2} + 2\frac{\partial^2 z_2}{\partial t_1 \partial t}\frac{\partial z_{-2}}{\partial a_2} + 2\frac{\partial^2 z_1}{\partial t_2 \partial t}\frac{\partial z_{-2}}{\partial a_2} = 0 \qquad c = 0$$

$$(D.1c)$$

Appendix E: Transformation from Lagrangian to Eulerian Coordinates

To permit comparison with existing Eulerian theories, it is necessary to express our results in terms of Eulerian coordinates. Thanks to the Laurent series ($II.2.11a-b$):

$$X = a + \epsilon^{-2}x_{-2} + \epsilon x_1 + \epsilon^2 x_2 + \epsilon^3 x_3 + \mathcal{O}(\epsilon^4) \qquad (E.1a)$$

$$Z = c + \epsilon^{-2}z_{-2} + \epsilon z_1 + \epsilon^2 z_2 + \epsilon^3 z_3 + \mathcal{O}(\epsilon^4) \qquad (E.1b)$$

it is possible to deduce at any time the position of a given particle characterized by (a, c). The objective now is to identify the particles going through a given location (X, Z) as time elapses. Equivalently, we must invert the map defined by $(E.1)$. Before dealing with this problem, two important issues are raised

• The inversion is possible because one and only one particle goes through a given location at a given time. Mathematically, this is equivalent to the condition

$$J = \frac{D(X,Z)}{D(a,c)} \neq 0, \infty \qquad (E.2)$$

for all times. This is guaranteed by the continuity equation.

• The presence of multiple scales $(a_i, c_i)_{i=1,2}$ suggests the introduction of the corresponding Eulerian stretched scales:

$$(X_i, Z_i) = \epsilon^i (X, Z) \qquad i = 1, 2 \qquad (E.3)$$

For instance, multiplication of $(E.1)$ by ϵ^2 yields

$$X_2 = a_2 + x_{-2} + \mathcal{O}(\epsilon^3) \qquad Z_2 = c_2 + z_{-2} + \mathcal{O}(\epsilon^3) \qquad (E.4)$$

where use has been made of $(II.2.9)$.

We are concerned with the leading order, $\mathcal{O}(1)$, modulation of the short wave amplitude and wavenumber. Let the Eulerian long wave phase be $\phi_E = \Omega t_1 - K X_2$. Substitution of $(II.3.2)$ in $(E.4)$ yields, after simple manipulations

$$\phi_E = \phi - KB\sin\phi, \qquad Z_2 = B\cos\phi \quad c_2 = 0 \qquad (E.5a-b)$$

We plot in figure E.1 ϕ as a function of ϕ_E for 3 values of KB. Note that the crests $(\phi = 2n\pi)$ and troughs $(\phi = (2n+1)\pi)$ are both invariant in the Lagrangian to

Eulerian transformation. Once ϕ is found, the surface elevation can be obtained through $(E.5b)$.

Now, a and c can be expressed solely in terms of Eulerian coordinates, within an error of $\mathcal{O}(\epsilon)$:

$$a = X - \epsilon^{-2} B \sin\phi(\phi_E) + \mathcal{O}(\epsilon) \qquad c = Z - \epsilon^{-2} B \cos\phi(\phi_E) + \mathcal{O}(\epsilon) \quad (E.6a - b)$$

This relationship is used in the derivation of the leading order modulation of the wavenumber in the Eulerian frame.

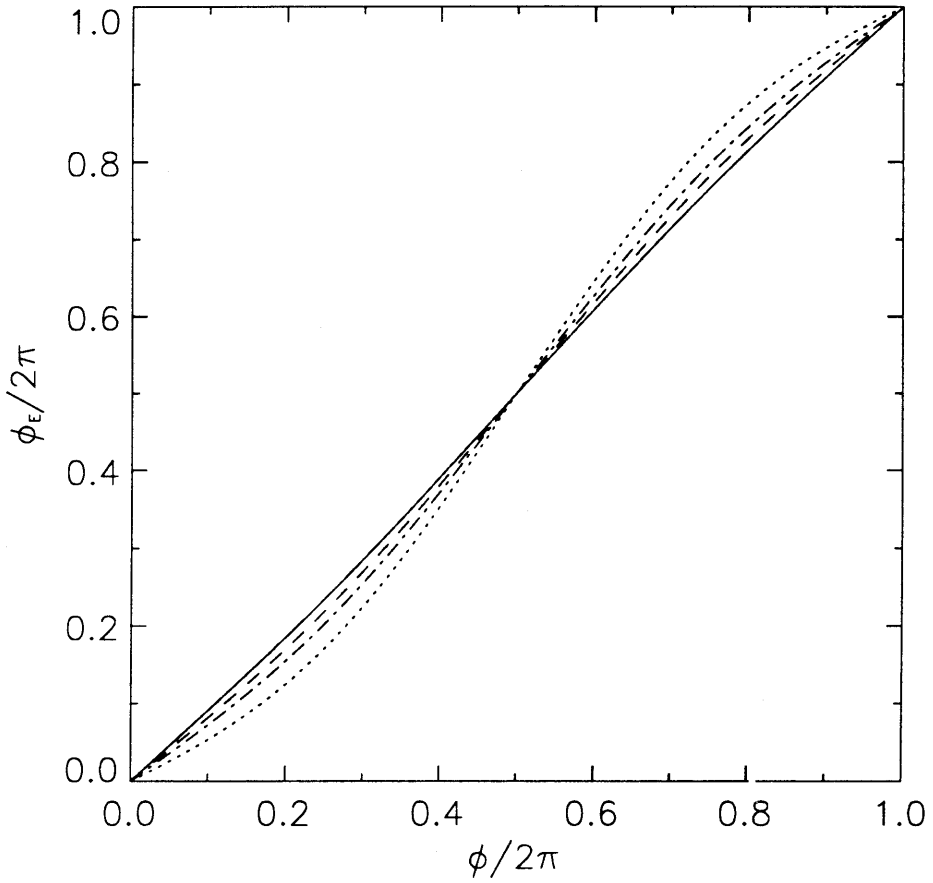

Figure E.1: Relationship between Lagrangian and Eulerian phases of the long Gerstner wave for $KB = 0.1$ (——), $KB = 0.2$ (- - - - -), $KB = 0.3$ (·····) and $KB = 0.5$ (· · · · ·).

Appendix F: Zero-crossings of the Stokes Wave

Following the notation of Schwartz(1974), the free surface elevation of a deep water Stokes wave is given parametrically by

$$y(\chi) = a_1 \cos\chi + \frac{a_2}{2}\cos 2\chi + \ldots + \frac{a_n}{n}\cos n\chi + \ldots \qquad (F.1a)$$

$$-x(\chi) = \chi + a_1 \sin\chi + \frac{a_2}{2}\sin 2\chi + \ldots + \frac{a_n}{n}\sin n\chi + \ldots \qquad (F.1b)$$

where χ represents the Eulerian phase (ϕ_{E} in this paper) along the Stokes wave profile and the a_j's are expressed in powers series of the slope h (KB in this paper) as follows:

$$a_1 = h - \frac{3}{2}h^3 - \frac{1}{24}h^5 + \mathcal{O}(h^7) \qquad a_2 = 2h^2 - 5h^4 + \frac{19}{6}h^6 + \mathcal{O}(h^8)$$

$$a_3 = \frac{9}{2}h^3 - \frac{31}{2}h^5 + \mathcal{O}(h^7) \qquad a_4 = \frac{32}{3}h^4 - \frac{839}{18}h^6 + \mathcal{O}(h^8)$$

and

$$a_5 = \frac{625}{24}h^5 + \mathcal{O}(h^7) \qquad a_6 = \frac{324}{5}h^6 + \mathcal{O}(h^8) \qquad (F.2)$$

The mean surface elevation $\overline{y}$ is also given in power series of h by

$$\overline{y} = \frac{1}{2}h^2 - \frac{1}{2}h^4 - \frac{13}{24}h^6 + \mathcal{O}(h^8) \qquad (F.3)$$

The zero-crossings χ_{crossing} are solutions of

$$y(\chi) = \overline{y} \qquad (F.4)$$

In the interval $[0, 2\pi]$, $(F.4)$ admits two solutions in the vicinity of $\frac{\pi}{2}$ and $\frac{3\pi}{2}$. By symmetry, it is sufficient to examine the vicinity of $\frac{\pi}{2}$ and let

$$\chi_{\mathrm{crossing}} = \frac{\pi}{2} + \sum_{i=1}^{5} p_i h^i \qquad (F.5)$$

Substitution of $(F.5)$ in $(F.4)$ with the help of $(F.2)$ and $(F.3)$ yields the values of $(p_i)_{i=1,5}$ and

$$\chi_{\mathrm{crossing}} = \frac{\pi}{2} - \frac{3}{2}h + \frac{29}{48}h^3 + \frac{5743}{11520}h^5 + \mathcal{O}(h^7) \qquad (F.6)$$

In our notation, $\chi = \phi_{\mathrm{E}}$ and $h = KB$.

Appendix G: Outline of Floquet Theory

We quote for convenience certain key results of the Floquet theory in the form directly useful for our problem. Additional details can be found in Nayfeh & Mook(1979), Iooss & Joseph(1980) and Shirer(1987). The system of ordinary differential equations $(I.5.18a-b)$ is written in the following matrix form

$$\frac{\partial U}{\partial \phi} = MU \qquad U = \begin{pmatrix} \tilde{d} \\ \tilde{W} \end{pmatrix} \tag{G.1}$$

where $M = (m_{i,j})$ is the time dependent 2π-periodic coefficient matrix of $(II.6.18a-b)$. The values of $\tilde{d}$ and $\tilde{W}$ are entirely determined by the initial condition $U^0 = U(\phi = \phi_0)$. This complex vector lies in a plane and is clearly a linear combination of the following two basis vectors $U_1^0 = \begin{pmatrix} 1 \\ 0 \end{pmatrix}$ and $U_2^0 = \begin{pmatrix} 0 \\ 1 \end{pmatrix}$. Let us define the corresponding solutions to $(G.1)$ by

$$U_1(\phi) = \begin{pmatrix} v_{1,1}(\phi) \\ v_{2,1}(\phi) \end{pmatrix} \quad \text{and} \quad U_2(\phi) = \begin{pmatrix} v_{1,2}(\phi) \\ v_{2,2}(\phi) \end{pmatrix} \tag{G.2}$$

Consequently, there exists one pair of complex parameters (q_1, q_2) such that

$$U(\phi) = q_1 U_1(\phi) + q_2 U_2(\phi) \tag{G.3}$$

Next, since $U_1(\phi)$ and $U_2(\phi)$ are solutions of $(G.1)$ so are $U_1(\phi+T)$ and $U_2(\phi+T)$. As a result, they can be decomposed uniquely along $U_1(\phi)$ and $U_2(\phi)$ as

$$\begin{pmatrix} v_{1,1}(\phi+T) \\ v_{2,1}(\phi+T) \end{pmatrix} = n_{1,1} \begin{pmatrix} v_{1,1}(\phi) \\ v_{2,1}(\phi) \end{pmatrix} + n_{2,1} \begin{pmatrix} v_{1,2}(\phi) \\ v_{2,2}(\phi) \end{pmatrix} = \begin{pmatrix} v_{1,1}(\phi) & v_{1,2}(\phi) \\ v_{2,1}(\phi) & v_{2,2}(\phi) \end{pmatrix} \begin{pmatrix} n_{1,1} \\ n_{2,1} \end{pmatrix} \tag{G.4a}$$

and

$$\begin{pmatrix} v_{1,2}(\phi+T) \\ v_{2,2}(\phi+T) \end{pmatrix} = \begin{pmatrix} v_{1,1}(\phi) & v_{1,2}(\phi) \\ v_{2,1}(\phi) & v_{2,2}(\phi) \end{pmatrix} \begin{pmatrix} n_{1,2} \\ n_{2,2} \end{pmatrix} \tag{G.4b}$$

$(G.4a-b)$ can be summarized by

$$\begin{pmatrix} v_{1,1}(\phi+T) & v_{1,2}(\phi+T) \\ v_{2,1}(\phi+T) & v_{2,2}(\phi+T) \end{pmatrix} = \begin{pmatrix} v_{1,1}(\phi) & v_{1,2}(\phi) \\ v_{2,1}(\phi) & v_{2,2}(\phi) \end{pmatrix} \begin{pmatrix} n_{1,1} & n_{1,2} \\ n_{2,1} & n_{2,2} \end{pmatrix} \tag{G.5}$$

where complex matrix $N = \{n_{i,j}\}$ has constant coefficients. Let us introduce a complex quantity μ such that

$$\tilde{d}(\phi+T) = \mu \tilde{d}(\phi) \tag{G.6}$$

Because of $(G.3)$, the left hand side of $(G.24)$ may be written as

$$\tilde{d}(\phi+T)=\sum_{k=1}^{2}q_k v_{1,k}(\phi+T)=\sum_{k=1}^{2}q_k\sum_{l=1}^{2}n_{l,k}v_{1,l}(\phi) \qquad (G.7a)$$

where use has been made of $(G.4)$. Similarly, the right hand side yields

$$\tilde{d}(\phi)=\sum_{k=1}^{2}q_k v_{1,k}(\phi)=\sum_{k=1}^{2}q_k\sum_{l=1}^{2}\delta_{l,k}v_{1,l}(\phi) \qquad (G.7b)$$

where $\delta_{i,j}$ designates Kronecker delta. Upon combining $(G.7a-b)$, we get

$$\sum_{k=1}^{2}\sum_{l=1}^{2}q_k(n_{l,k}-\mu\delta_{l,k})v_{1,l}(\phi)=0 \qquad (G.8)$$

Since the two functions $v_{1,l}$'s are linearly independent, $(G.8)$ implies

$$\sum_{k=1}^{2}q_k(n_{1,k}-\mu\delta_{1,k})=0 \qquad \sum_{k=1}^{2}q_k(n_{2,k}-\mu\delta_{2,k})=0 \qquad (G.9a-b)$$

The existence of non-trivial solutions (q_1,q_2) for $(G.9)$ requires that

$$\det\begin{vmatrix} n_{1,1}-\mu & n_{1,2} \\ n_{2,1} & n_{2,2}-\mu \end{vmatrix}=0 \qquad (G.10)$$

This determines the two characteristic multipliers $\mu_{1,2}$. Upon recalling $(G.5)$ and the initial conditions, N may be rewritten as:

$$\begin{pmatrix} n_{1,1} & n_{1,2} \\ n_{2,1} & n_{2,2} \end{pmatrix}=\begin{pmatrix} v_{1,1}(\phi_0+T) & v_{1,2}(\phi_0+T) \\ v_{2,1}(\phi_0+T) & v_{2,2}(\phi_0+T) \end{pmatrix} \qquad (G.11)$$

The system $(G.1)$ is solved numerically for the two initial conditions $U^0_{1,2}$ up to $\phi=\phi_0+T=\phi_0+2\pi$. This is done by the Runge-Kutta 4^{th} order time stepping scheme. Afterwards, N is found and the μ_j's can be calculated. To check the accuracy of our computations, we use an exact property of $(G.1)$. Let $v(\phi)$ be the matrix with coefficients $\{v_{i,j}(\phi)\}$ and $\Upsilon(\phi)$ its determinant. It is straightforward to obtain

$$\frac{d\Upsilon}{d\phi}=\{\mathrm{Tr}(M(\phi))\}\Upsilon \qquad (G.12)$$

which can be integrated to yield

$$\Upsilon(\phi)=\Upsilon(0)\exp\Big[\int_0^{\phi}\mathrm{Tr}(M(t))dt\Big] \qquad (G.13)$$

where $\Upsilon(0)$ is clearly unity. Evaluation of $(G.13)$ at $\phi = T$ yields $\det(N)$ - also equal to the product of N's eigenvalues:

$$\mu_1\mu_2 = \exp\Big[\int_0^{2\pi} \mathrm{Tr}(M(\phi))d\phi\Big] \qquad (G.14)$$

It is clear from $(I.5.18a-b)$ that $\mathrm{Tr}M(\phi) = 0$, this implies the following identity

$$\mu_1\mu_2 = 1 \qquad (G.15)$$

Our computations performed in double precision led to a maximum error of the order of 10^{-8}.

Appendix H: Governing Equations at $\mathcal{O}(\epsilon^3)$:

In the following, we quote for completeness the governing equations deduced at $\mathcal{O}(\epsilon^3)$ in Chapter III. These include a continuity equation, two vorticity equations and two dynamic free surface boundary conditions.

Continuity:

$$\frac{\partial x_3}{\partial a}+\frac{\partial y_3}{\partial b}+\frac{\partial z_3}{\partial c}+\frac{\partial x_2}{\partial a_1}+\frac{\partial y_2}{\partial b_1}+\frac{\partial z_2}{\partial c_1}+\frac{\partial x_1}{\partial a_2}+\frac{\partial y_1}{\partial b_2}+\frac{\partial z_1}{\partial c_2}+$$

$$-\frac{\partial y_1}{\partial c_1}\frac{\partial z_1}{\partial b}-\frac{\partial x_{-2}}{\partial c_2}\frac{\partial z_1}{\partial a_2}-\frac{\partial x_1}{\partial c}\frac{\partial z_1}{\partial a_1}-\frac{\partial x_2}{\partial c}\frac{\partial z_1}{\partial a}-\frac{\partial x_1}{\partial c_1}\frac{\partial z_1}{\partial a}+\frac{\partial x_{-2}}{\partial a_2}\frac{\partial y_3}{\partial b}+$$

$$+\frac{\partial x_{-2}}{\partial a_2}\frac{\partial y_2}{\partial b_1}+\frac{\partial x_1}{\partial a}\frac{\partial y_2}{\partial b}-\frac{\partial x_1}{\partial b}\frac{\partial y_2}{\partial a}+\frac{\partial x_{-2}}{\partial a_2}\frac{\partial y_1}{\partial b_2}+\frac{\partial x_1}{\partial a}\frac{\partial y_1}{\partial b_1}+\frac{\partial x_2}{\partial a}\frac{\partial y_1}{\partial b}+$$

$$+\frac{\partial x_1}{\partial a_1}\frac{\partial y_1}{\partial b}-\frac{\partial x_1}{\partial b}\frac{\partial y_1}{\partial a_1}-\frac{\partial x_2}{\partial b}\frac{\partial y_1}{\partial a}-\frac{\partial x_1}{\partial b_1}\frac{\partial y_1}{\partial a}+\frac{\partial y_1}{\partial b_1}\frac{\partial z_1}{\partial c}+\frac{\partial x_2}{\partial a}\frac{\partial z_1}{\partial c}+$$

$$+\frac{\partial x_1}{\partial a_1}\frac{\partial z_1}{\partial c}-\frac{\partial y_1}{\partial c}\frac{\partial z_1}{\partial b_1}-\frac{\partial y_2}{\partial c}\frac{\partial z_1}{\partial b}+\frac{\partial y_3}{\partial b}\frac{\partial z_{-2}}{\partial c_2}+\frac{\partial y_2}{\partial b_1}\frac{\partial z_{-2}}{\partial c_2}+\frac{\partial y_1}{\partial b_2}\frac{\partial z_{-2}}{\partial c_2}+$$

$$+\frac{\partial x_3}{\partial a}\frac{\partial z_{-2}}{\partial c_2}+\frac{\partial x_2}{\partial a_1}\frac{\partial z_{-2}}{\partial c_2}+\frac{\partial x_1}{\partial a_2}\frac{\partial z_{-2}}{\partial c_2}-\frac{\partial x_3}{\partial c}\frac{\partial z_{-2}}{\partial a_2}-\frac{\partial x_2}{\partial c_1}\frac{\partial z_{-2}}{\partial a_2}-\frac{\partial x_1}{\partial c_2}\frac{\partial z_{-2}}{\partial a_2}+$$

$$+\frac{\partial x_{-2}}{\partial a_2}\frac{\partial z_3}{\partial c}-\frac{\partial x_{-2}}{\partial c_2}\frac{\partial z_3}{\partial a}+\frac{\partial x_{-2}}{\partial a_2}\frac{\partial z_2}{\partial c_1}+\frac{\partial y_1}{\partial b}\frac{\partial z_2}{\partial c}+\frac{\partial x_1}{\partial a}\frac{\partial z_2}{\partial c}-\frac{\partial y_1}{\partial c}\frac{\partial z_2}{\partial b}+$$

$$-\frac{\partial x_{-2}}{\partial c_2}\frac{\partial z_2}{\partial a_1}-\frac{\partial x_1}{\partial c}\frac{\partial z_2}{\partial a}+\frac{\partial x_{-2}}{\partial a_2}\frac{\partial z_1}{\partial c_2}+\frac{\partial y_1}{\partial b}\frac{\partial z_1}{\partial c_1}+\frac{\partial x_1}{\partial a}\frac{\partial z_1}{\partial c_1}+\frac{\partial y_2}{\partial b}\frac{\partial z_1}{\partial c}+$$

$$\frac{\partial x_{-2}}{\partial a_2}\frac{\partial y_3}{\partial b}\frac{\partial z_{-2}}{\partial c_2}+\frac{\partial x_{-2}}{\partial a_2}\frac{\partial y_2}{\partial b_1}\frac{\partial z_{-2}}{\partial c_2}+\frac{\partial x_1}{\partial a}\frac{\partial y_2}{\partial b}\frac{\partial z_{-2}}{\partial c_2}-\frac{\partial x_1}{\partial b}\frac{\partial y_2}{\partial a}\frac{\partial z_{-2}}{\partial c_2}+$$

$$+\frac{\partial x_{-2}}{\partial a_2}\frac{\partial y_1}{\partial b_2}\frac{\partial z_{-2}}{\partial c_2}+\frac{\partial x_1}{\partial a}\frac{\partial y_1}{\partial b_1}\frac{\partial z_{-2}}{\partial c_2}+\frac{\partial x_2}{\partial a}\frac{\partial y_1}{\partial b}\frac{\partial z_{-2}}{\partial c_2}+\frac{\partial x_1}{\partial a_1}\frac{\partial y_1}{\partial b}\frac{\partial z_{-2}}{\partial c_2}+$$

$$-\frac{\partial x_1}{\partial b}\frac{\partial y_1}{\partial a_1}\frac{\partial z_{-2}}{\partial c_2}-\frac{\partial x_2}{\partial b}\frac{\partial y_1}{\partial a}\frac{\partial z_{-2}}{\partial c_2}-\frac{\partial x_1}{\partial b_1}\frac{\partial y_1}{\partial a}\frac{\partial z_{-2}}{\partial c_2}-\frac{\partial x_{-2}}{\partial c_2}\frac{\partial y_3}{\partial b}\frac{\partial z_{-2}}{\partial a_2}+$$

$$+\frac{\partial x_1}{\partial b}\frac{\partial y_2}{\partial c}\frac{\partial z_{-2}}{\partial a_2}-\frac{\partial x_{-2}}{\partial c_2}\frac{\partial y_2}{\partial b_1}\frac{\partial z_{-2}}{\partial a_2}-\frac{\partial x_1}{\partial c}\frac{\partial y_2}{\partial b}\frac{\partial z_{-2}}{\partial a_2}+\frac{\partial x_1}{\partial b}\frac{\partial y_1}{\partial c_1}\frac{\partial z_{-2}}{\partial a_2}+$$

$$+\frac{\partial x_2}{\partial b}\frac{\partial y_1}{\partial c}\frac{\partial z_{-2}}{\partial a_2}+\frac{\partial x_1}{\partial b_1}\frac{\partial y_1}{\partial c}\frac{\partial z_{-2}}{\partial a_2}-\frac{\partial x_{-2}}{\partial c_2}\frac{\partial y_1}{\partial b_2}\frac{\partial z_{-2}}{\partial a_2}-\frac{\partial x_1}{\partial c}\frac{\partial y_1}{\partial b_1}\frac{\partial z_{-2}}{\partial a_2}+$$

$$-\frac{\partial x_2}{\partial c}\frac{\partial y_1}{\partial b}\frac{\partial z_{-2}}{\partial a_2}-\frac{\partial x_1}{\partial c_1}\frac{\partial y_1}{\partial b}\frac{\partial z_{-2}}{\partial a_2}+\frac{\partial x_{-2}}{\partial a_2}\frac{\partial y_1}{\partial b}\frac{\partial z_2}{\partial c}-\frac{\partial x_{-2}}{\partial a_2}\frac{\partial y_1}{\partial c}\frac{\partial z_2}{\partial b}+$$

$$+\frac{\partial x_{-2}}{\partial c_2}\frac{\partial y_1}{\partial a}\frac{\partial z_2}{\partial b}-\frac{\partial x_{-2}}{\partial c_2}\frac{\partial y_1}{\partial b}\frac{\partial z_2}{\partial a}+\frac{\partial x_{-2}}{\partial a_2}\frac{\partial y_1}{\partial b}\frac{\partial z_1}{\partial c_1}+\frac{\partial x_{-2}}{\partial a_2}\frac{\partial y_2}{\partial b}\frac{\partial z_1}{\partial c}+$$

$$+\frac{\partial x_{-2}}{\partial a_2}\frac{\partial y_1}{\partial b_1}\frac{\partial z_1}{\partial c}+\frac{\partial x_1}{\partial a}\frac{\partial y_1}{\partial b}\frac{\partial z_1}{\partial c}-\frac{\partial x_1}{\partial b}\frac{\partial y_1}{\partial a}\frac{\partial z_1}{\partial c}-\frac{\partial x_{-2}}{\partial a_2}\frac{\partial y_1}{\partial c}\frac{\partial z_1}{\partial b_1}+$$

$$+\frac{\partial x_{-2}}{\partial c_2}\frac{\partial y_1}{\partial a}\frac{\partial z_1}{\partial b_1}-\frac{\partial x_{-2}}{\partial a_2}\frac{\partial y_2}{\partial c}\frac{\partial z_1}{\partial b}+\frac{\partial x_{-2}}{\partial c_2}\frac{\partial y_2}{\partial a}\frac{\partial z_1}{\partial b}-\frac{\partial x_{-2}}{\partial a_2}\frac{\partial y_1}{\partial c_1}\frac{\partial z_1}{\partial b}+$$

$$-\frac{\partial x_1}{\partial a}\frac{\partial y_1}{\partial c}\frac{\partial z_1}{\partial b}+\frac{\partial x_{-2}}{\partial c_2}\frac{\partial y_1}{\partial a_1}\frac{\partial z_1}{\partial b}+\frac{\partial x_1}{\partial c}\frac{\partial y_1}{\partial a}\frac{\partial z_1}{\partial b}-\frac{\partial x_{-2}}{\partial c_2}\frac{\partial y_1}{\partial b}\frac{\partial z_1}{\partial a_1}+$$

$$-\frac{\partial x_{-2}}{\partial c_2}\frac{\partial y_2}{\partial b}\frac{\partial z_1}{\partial a}+\frac{\partial x_1}{\partial b}\frac{\partial y_1}{\partial c}\frac{\partial z_1}{\partial a}-\frac{\partial x_{-2}}{\partial c_2}\frac{\partial y_1}{\partial b_1}\frac{\partial z_1}{\partial a}-\frac{\partial x_1}{\partial c}\frac{\partial y_1}{\partial b}\frac{\partial z_1}{\partial a}=0 \qquad (H.1)$$

Y-Vorticity equation:

$$\frac{\partial^3 x_3}{\partial c\partial t^2}-\frac{\partial^3 z_3}{\partial a\partial t^2}+\frac{\partial^3 x_2}{\partial c_1\partial t^2}+2\frac{\partial^3 x_2}{\partial c\partial t\partial t_1}-\frac{\partial^3 z2}{\partial a_1\partial t^2}-2\frac{\partial^3 z2}{\partial a\partial t\partial t_1}+$$

$$+\frac{\partial^3 x_1}{\partial c_2\partial t^2}+\frac{\partial^3 x_1}{\partial c{\partial t_1}^2}+2\frac{\partial^3 x_1}{\partial c\partial t\partial t_2}+2\frac{\partial^3 x_1}{\partial c_1\partial t\partial t_1}+$$

$$-\frac{\partial^3 z_1}{\partial a_2\partial t^2}-2\frac{\partial^3 z_1}{\partial a_1\partial t\partial t_1}-\frac{\partial^3 z_1}{\partial a{\partial t_1}^2}-2\frac{\partial^3 z_1}{\partial a\partial t\partial t_2}+$$

$$+\frac{\partial^3 z_{-2}}{\partial c_2{\partial t_1}^2}\frac{\partial z_1}{\partial a}-\frac{\partial z_{-2}}{\partial c_2}\frac{\partial^3 z_3}{\partial a\partial t^2}-\frac{\partial z_{-2}}{\partial c_2}\frac{\partial^3 z2}{\partial a_1\partial t^2}-2\frac{\partial z_{-2}}{\partial c_2}\frac{\partial^3 z2}{\partial a\partial t\partial t_1}-\frac{\partial^3 z_1}{\partial a_2\partial t^2}\frac{\partial z_{-2}}{\partial c_2}+$$

$$-2\frac{\partial^3 z_1}{\partial a_1\partial t\partial t_1}\frac{\partial z_{-2}}{\partial c_2}-\frac{\partial^3 z_1}{\partial a{\partial t_1}^2}\frac{\partial z_{-2}}{\partial c_2}-2\frac{\partial^3 z_1}{\partial a\partial t\partial t_2}\frac{\partial z_{-2}}{\partial c_2}-\frac{\partial z_1}{\partial c}\frac{\partial^3 z_{-2}}{\partial a_2{\partial t_1}^2}+\frac{\partial^3 z_3}{\partial c\partial t^2}\frac{\partial z_{-2}}{\partial a_2}+$$

$$+\frac{\partial^3 z2}{\partial c_1\partial t^2}\frac{\partial z_{-2}}{\partial a_2}+2\frac{\partial^3 z2}{\partial c\partial t\partial t_1}\frac{\partial z_{-2}}{\partial a_2}+\frac{\partial^3 z_1}{\partial c_2\partial t^2}\frac{\partial z_{-2}}{\partial a_2}+2\frac{\partial^3 z_1}{\partial c_1\partial t\partial t_1}\frac{\partial z_{-2}}{\partial a_2}+\frac{\partial^3 z_1}{\partial c{\partial t_1}^2}\frac{\partial z_{-2}}{\partial a_2}+$$

$$+2\frac{\partial^3 z_1}{\partial c\partial t\partial t_2}\frac{\partial z_{-2}}{\partial a_2}+\frac{\partial z_1}{\partial a}\frac{\partial^3 z2}{\partial c\partial t^2}-\frac{\partial^3 z_1}{\partial a\partial t^2}\frac{\partial z2}{\partial c}-\frac{\partial z_1}{\partial c}\frac{\partial^3 z2}{\partial a\partial t^2}+\frac{\partial^3 z_1}{\partial c\partial t^2}\frac{\partial z2}{\partial a}+$$

$$+\frac{\partial z_1}{\partial a}\frac{\partial^3 z_1}{\partial c_1\partial t^2}-\frac{\partial^3 z_1}{\partial a\partial t^2}\frac{\partial z_1}{\partial c_1}+\frac{\partial z_1}{\partial a_1}\frac{\partial^3 z_1}{\partial c\partial t^2}+2\frac{\partial z_1}{\partial a}\frac{\partial^3 z_1}{\partial c\partial t\partial t_1}-\frac{\partial^3 z_1}{\partial a_1\partial t^2}\frac{\partial z_1}{\partial c}+$$

$$-2\frac{\partial^3 z_1}{\partial a\partial t\partial t_1}\frac{\partial z_1}{\partial c}+\frac{\partial y_1}{\partial a}\frac{\partial^3 y_2}{\partial c\partial t^2}-\frac{\partial^3 y_1}{\partial a\partial t^2}\frac{\partial y_2}{\partial c}-\frac{\partial y_1}{\partial c}\frac{\partial^3 y_2}{\partial a\partial t^2}+\frac{\partial^3 y_1}{\partial c\partial t^2}\frac{\partial y_2}{\partial a}+$$

$$+\frac{\partial y_1}{\partial a}\frac{\partial^3 y_1}{\partial c_1\partial t^2}-\frac{\partial^3 y_1}{\partial a\partial t^2}\frac{\partial y_1}{\partial c_1}+\frac{\partial y_1}{\partial a_1}\frac{\partial^3 y_1}{\partial c\partial t^2}+2\frac{\partial y_1}{\partial a}\frac{\partial^3 y_1}{\partial c\partial t\partial t_1}-\frac{\partial^3 y_1}{\partial a_1\partial t^2}\frac{\partial y_1}{\partial c}+$$

$$-2\frac{\partial^3 y_1}{\partial a\partial t\partial t_1}\frac{\partial y_1}{\partial c}+\frac{\partial x_1}{\partial a}\frac{\partial^3 x_{-2}}{\partial c_2{\partial t_1}^2}-\frac{\partial^3 x_3}{\partial a\partial t^2}\frac{\partial x_{-2}}{\partial c_2}-\frac{\partial^3 x_2}{\partial a_1\partial t^2}\frac{\partial x_{-2}}{\partial c_2}-2\frac{\partial^3 x_2}{\partial a\partial t\partial t_1}\frac{\partial x_{-2}}{\partial c_2}+$$

$$-\frac{\partial^3 x_1}{\partial a_2\partial t^2}\frac{\partial x_{-2}}{\partial c_2}-2\frac{\partial^3 x_1}{\partial a_1\partial t\partial t_1}\frac{\partial x_{-2}}{\partial c_2}-\frac{\partial^3 x_1}{\partial a{\partial t_1}^2}\frac{\partial x_{-2}}{\partial c_2}-2\frac{\partial^3 x_1}{\partial a\partial t\partial t_2}\frac{\partial x_{-2}}{\partial c_2}+$$

$$-\frac{\partial x_1}{\partial c}\frac{\partial^3 x_{-2}}{\partial a_2 \partial {t_1}^2}+\frac{\partial^3 x_3}{\partial c \partial t^2}\frac{\partial x_{-2}}{\partial a_2}+\frac{\partial^3 x_2}{\partial c_1 \partial t^2}\frac{\partial x_{-2}}{\partial a_2}+2\frac{\partial^3 x_2}{\partial c \partial t \partial t_1}\frac{\partial x_{-2}}{\partial a_2}+\frac{\partial^3 x_1}{\partial c_2 \partial t^2}\frac{\partial x_{-2}}{\partial a_2}+$$
$$+2\frac{\partial^3 x_1}{\partial c_1 \partial t \partial t_1}\frac{\partial x_{-2}}{\partial a_2}+\frac{\partial^3 x_1}{\partial c \partial {t_1}^2}\frac{\partial x_{-2}}{\partial a_2}+2\frac{\partial^3 x_1}{\partial c \partial t \partial t_2}\frac{\partial x_{-2}}{\partial a_2}+\frac{\partial x_1}{\partial a}\frac{\partial^3 x_2}{\partial c \partial t^2}-\frac{\partial^3 x_1}{\partial a \partial t^2}\frac{\partial x_2}{\partial c}+$$
$$-\frac{\partial x_1}{\partial c}\frac{\partial^3 x_2}{\partial a \partial t^2}+\frac{\partial^3 x_1}{\partial c \partial t^2}\frac{\partial x_2}{\partial a}+\frac{\partial x_1}{\partial a}\frac{\partial^3 x_1}{\partial c_1 \partial t^2}-\frac{\partial^3 x_1}{\partial a \partial t^2}\frac{\partial x_1}{\partial c_1}+\frac{\partial x_1}{\partial a_1}\frac{\partial^3 x_1}{\partial c \partial t^2}+$$
$$+2\frac{\partial x_1}{\partial a}\frac{\partial^3 x_1}{\partial c \partial t \partial t_1}-\frac{\partial^3 x_1}{\partial a_1 \partial t^2}\frac{\partial x_1}{\partial c}-2\frac{\partial^3 x_1}{\partial a \partial t \partial t_1}\frac{\partial x_1}{\partial c}=0 \qquad (H.2)$$

Z-Vorticity equation:

$$\frac{\partial^3 x_3}{\partial b \partial t^2}-\frac{\partial^3 y_3}{\partial a \partial t^2}+\frac{\partial^3 x_2}{\partial b_1 \partial t^2}+2\frac{\partial^3 x_2}{\partial b \partial t \partial t_1}-\frac{\partial^3 y_2}{\partial a_1 \partial t^2}-2\frac{\partial^3 y_2}{\partial a \partial t \partial t_1}+$$
$$+\frac{\partial^3 x_1}{\partial b_2 \partial t^2}+2\frac{\partial^3 x_1}{\partial b_1 \partial t \partial t_1}+\frac{\partial^3 x_1}{\partial b \partial {t_1}^2}+2\frac{\partial^3 x_1}{\partial b \partial t \partial t_2}+$$
$$-\frac{\partial^3 y_1}{\partial a_2 \partial t^2}-2\frac{\partial^3 y_1}{\partial a_1 \partial t \partial t_1}-\frac{\partial^3 y_1}{\partial a \partial {t_1}^2}-2\frac{\partial^3 y_1}{\partial a \partial t \partial t_2}+$$
$$-\frac{\partial z_1}{\partial b}\frac{\partial^3 z_{-2}}{\partial a_2 \partial {t_1}^2}+\frac{\partial^3 z_3}{\partial b \partial t^2}\frac{\partial z_{-2}}{\partial a_2}+\frac{\partial^3 z_2}{\partial b_1 \partial t^2}\frac{\partial z_{-2}}{\partial a_2}+2\frac{\partial^3 z_2}{\partial b \partial t \partial t_1}\frac{\partial z_{-2}}{\partial a_2}+\frac{\partial^3 z_1}{\partial b_2 \partial t^2}\frac{\partial z_{-2}}{\partial a_2}+$$
$$+2\frac{\partial^3 z_1}{\partial b_1 \partial t \partial t_1}\frac{\partial z_{-2}}{\partial a_2}+\frac{\partial^3 z_1}{\partial b \partial {t_1}^2}\frac{\partial z_{-2}}{\partial a_2}+2\frac{\partial^3 z_1}{\partial b \partial t \partial t_2}\frac{\partial z_{-2}}{\partial a_2}+\frac{\partial z_1}{\partial a}\frac{\partial^3 z_2}{\partial b \partial t^2}-\frac{\partial^3 z_1}{\partial a \partial t^2}\frac{\partial z_2}{\partial b}+$$
$$-\frac{\partial z_1}{\partial b}\frac{\partial^3 z_2}{\partial a \partial t^2}+\frac{\partial^3 z_1}{\partial b \partial t^2}\frac{\partial z_2}{\partial a}+\frac{\partial z_1}{\partial a}\frac{\partial^3 z_1}{\partial b_1 \partial t^2}-\frac{\partial^3 z_1}{\partial a \partial t^2}\frac{\partial z_1}{\partial b_1}+\frac{\partial z_1}{\partial a_1}\frac{\partial^3 z_1}{\partial b \partial t^2}+$$
$$+2\frac{\partial z_1}{\partial a}\frac{\partial^3 z_1}{\partial b \partial t \partial t_1}-\frac{\partial^3 z_1}{\partial a_1 \partial t^2}\frac{\partial z_1}{\partial b}-2\frac{\partial^3 z_1}{\partial a \partial t \partial t_1}\frac{\partial z_1}{\partial b}+\frac{\partial y_1}{\partial a}\frac{\partial^3 y_2}{\partial b \partial t^2}-\frac{\partial^3 y_1}{\partial a \partial t^2}\frac{\partial y_2}{\partial b}+$$
$$-\frac{\partial y_1}{\partial b}\frac{\partial^3 y_2}{\partial a \partial t^2}+\frac{\partial^3 y_1}{\partial b \partial t^2}\frac{\partial y_2}{\partial a}+\frac{\partial y_1}{\partial a}\frac{\partial^3 y_1}{\partial b_1 \partial t^2}-\frac{\partial^3 y_1}{\partial a \partial t^2}\frac{\partial y_1}{\partial b_1}+\frac{\partial y_1}{\partial a_1}\frac{\partial^3 y_1}{\partial b \partial t^2}+$$
$$+2\frac{\partial y_1}{\partial a}\frac{\partial^3 y_1}{\partial b \partial t \partial t_1}-\frac{\partial^3 y_1}{\partial a_1 \partial t^2}\frac{\partial y_1}{\partial b}-2\frac{\partial^3 y_1}{\partial a \partial t \partial t_1}\frac{\partial y_1}{\partial b}-\frac{\partial x_1}{\partial b}\frac{\partial^3 x_{-2}}{\partial a_2 \partial {t_1}^2}+\frac{\partial^3 x_3}{\partial b \partial t^2}\frac{\partial x_{-2}}{\partial a_2}+$$
$$+\frac{\partial^3 x_2}{\partial b_1 \partial t^2}\frac{\partial x_{-2}}{\partial a_2}+2\frac{\partial^3 x_2}{\partial b \partial t \partial t_1}\frac{\partial x_{-2}}{\partial a_2}+\frac{\partial^3 x_1}{\partial b_2 \partial t^2}\frac{\partial x_{-2}}{\partial a_2}+2\frac{\partial^3 x_1}{\partial b_1 \partial t \partial t_1}\frac{\partial x_{-2}}{\partial a_2}+\frac{\partial^3 x_1}{\partial b \partial {t_1}^2}\frac{\partial x_{-2}}{\partial a_2}+$$
$$+2\frac{\partial^3 x_1}{\partial b \partial t \partial t_2}\frac{\partial x_{-2}}{\partial a_2}+\frac{\partial x_1}{\partial a}\frac{\partial^3 x_2}{\partial b \partial t^2}-\frac{\partial^3 x_1}{\partial a \partial t^2}\frac{\partial x_2}{\partial b}-\frac{\partial x_1}{\partial b}\frac{\partial^3 x_2}{\partial a \partial t^2}+\frac{\partial^3 x_1}{\partial b \partial t^2}\frac{\partial x_2}{\partial a}+$$
$$+\frac{\partial x_1}{\partial a}\frac{\partial^3 x_1}{\partial b_1 \partial t^2}-\frac{\partial^3 x_1}{\partial a \partial t^2}\frac{\partial x_1}{\partial b_1}+\frac{\partial x_1}{\partial a_1}\frac{\partial^3 x_1}{\partial b \partial t^2}+$$
$$+2\frac{\partial x_1}{\partial a}\frac{\partial^3 x_1}{\partial b \partial t \partial t_1}-\frac{\partial^3 x_1}{\partial a_1 \partial t^2}\frac{\partial x_1}{\partial b}-2\frac{\partial^3 x_1}{\partial a \partial t \partial t_1}\frac{\partial x_1}{\partial b}=0 \qquad (H.3)$$

First free surface dynamic boundary condition:

$$\frac{\partial^2 x_3}{\partial t^2} + g\frac{\partial z_3}{\partial a} + 2\frac{\partial^2 x_2}{\partial t \partial t_1} + g\frac{\partial z_2}{\partial a_1} + \frac{\partial^2 x_1}{\partial {t_1}^2} + 2\frac{\partial^2 x_1}{\partial t \partial t_2} + g\frac{\partial z_1}{\partial a_2} +$$

$$+\frac{\partial z_3}{\partial a}\frac{\partial^2 z_{-2}}{\partial {t_1}^2} + \frac{\partial z_2}{\partial a_1}\frac{\partial^2 z_{-2}}{\partial {t_1}^2} + \frac{\partial z_1}{\partial a_2}\frac{\partial^2 z_{-2}}{\partial {t_1}^2} + \frac{\partial^2 z_3}{\partial t^2}\frac{\partial z_{-2}}{\partial a_2} + 2\frac{\partial^2 z_2}{\partial t \partial t_1}\frac{\partial z_{-2}}{\partial a_2} +$$

$$+\frac{\partial^2 z_1}{\partial {t_1}^2}\frac{\partial z_{-2}}{\partial a_2} + 2\frac{\partial^2 z_1}{\partial t \partial t_2}\frac{\partial z_{-2}}{\partial a_2} + \frac{\partial z_1}{\partial a}\frac{\partial^2 z_2}{\partial t^2} + \frac{\partial^2 z_1}{\partial t^2}\frac{\partial z_2}{\partial a} + \frac{\partial z_1}{\partial a_1}\frac{\partial^2 z_1}{\partial t^2} +$$

$$+2\frac{\partial z_1}{\partial a}\frac{\partial^2 z_1}{\partial t \partial t_1} + \frac{\partial y_1}{\partial a}\frac{\partial^2 y_2}{\partial t^2} + \frac{\partial^2 y_1}{\partial t^2}\frac{\partial y_2}{\partial a} + \frac{\partial y_1}{\partial a_1}\frac{\partial^2 y_1}{\partial t^2} + 2\frac{\partial y_1}{\partial a}\frac{\partial^2 y_1}{\partial t \partial t_1} +$$

$$+\frac{\partial x_3}{\partial a}\frac{\partial^2 x_{-2}}{\partial {t_1}^2} + \frac{\partial x_2}{\partial a_1}\frac{\partial^2 x_{-2}}{\partial {t_1}^2} + \frac{\partial x_1}{\partial a_2}\frac{\partial^2 x_{-2}}{\partial {t_1}^2} + \frac{\partial^2 x_3}{\partial t^2}\frac{\partial x_{-2}}{\partial a_2} + 2\frac{\partial^2 x_2}{\partial t \partial t_1}\frac{\partial x_{-2}}{\partial a_2} + \frac{\partial^2 x_1}{\partial {t_1}^2}\frac{\partial x_{-2}}{\partial a_2} +$$

$$+2\frac{\partial^2 x_1}{\partial t \partial t_2}\frac{\partial x_{-2}}{\partial a_2} + \frac{\partial x_1}{\partial a}\frac{\partial^2 x_2}{\partial t^2} + \frac{\partial^2 x_1}{\partial t^2}\frac{\partial x_2}{\partial a} + \frac{\partial x_1}{\partial a_1}\frac{\partial^2 x_1}{\partial t^2} + 2\frac{\partial x_1}{\partial a}\frac{\partial^2 x_1}{\partial t \partial t_1} = 0 \quad c = 0 \tag{H.4}$$

Second free surface dynamic boundary condition:

$$\frac{\partial^2 y_3}{\partial t^2} + g\frac{\partial z_3}{\partial b} + 2\frac{\partial^2 y_2}{\partial t \partial t_1} + g\frac{\partial z_2}{\partial b_1} + \frac{\partial^2 y_1}{\partial {t_1}^2} + 2\frac{\partial^2 y_1}{\partial t \partial t_2} + g\frac{\partial z_1}{\partial b_2} +$$

$$+\frac{\partial z_3}{\partial b}\frac{\partial^2 z_{-2}}{\partial {t_1}^2} + \frac{\partial z_2}{\partial b_1}\frac{\partial^2 z_{-2}}{\partial {t_1}^2} + \frac{\partial z_1}{\partial b_2}\frac{\partial^2 z_{-2}}{\partial {t_1}^2} + \frac{\partial z_1}{\partial b}\frac{\partial^2 z_2}{\partial t^2} + \frac{\partial^2 z_1}{\partial t^2}\frac{\partial z_2}{\partial b} +$$

$$+\frac{\partial z_1}{\partial b_1}\frac{\partial^2 z_1}{\partial t^2} + 2\frac{\partial z_1}{\partial b}\frac{\partial^2 z_1}{\partial t \partial t_1} + \frac{\partial y_1}{\partial b}\frac{\partial^2 y_2}{\partial t^2} + \frac{\partial^2 y_1}{\partial t^2}\frac{\partial y_2}{\partial b} + \frac{\partial y_1}{\partial b_1}\frac{\partial^2 y_1}{\partial t^2} +$$

$$+2\frac{\partial y_1}{\partial b}\frac{\partial^2 y_1}{\partial t \partial t_1} + \frac{\partial x_3}{\partial b}\frac{\partial^2 x_{-2}}{\partial {t_1}^2} + \frac{\partial x_2}{\partial b_1}\frac{\partial^2 x_{-2}}{\partial {t_1}^2} + \frac{\partial x_1}{\partial b_2}\frac{\partial^2 x_{-2}}{\partial {t_1}^2} + \frac{\partial x_1}{\partial b}\frac{\partial^2 x_2}{\partial t^2} +$$

$$+\frac{\partial^2 x_1}{\partial t^2}\frac{\partial x_2}{\partial b} + \frac{\partial x_1}{\partial b_1}\frac{\partial^2 x_1}{\partial t^2} + 2\frac{\partial x_1}{\partial b}\frac{\partial^2 x_1}{\partial t \partial t_1} = 0 \quad c = 0 \tag{H.5}$$

Appendix I: A Property of the Vorticity Vector in Lagrangian Coordinates:

Consider in a three-dimensional space a velocity field **U** with components (u, v, w). These components are related to the Eulerian coordinates (X, Y, Z) by

$$u \equiv \frac{\partial X}{\partial t} \qquad v \equiv \frac{\partial Y}{\partial t} \qquad w \equiv \frac{\partial Z}{\partial t} \tag{I.1}$$

The three components of the vorticity vector $\vec{\varpi}$ are then

$$\vec{\varpi} = \begin{pmatrix} \frac{\partial w}{\partial Y} - \frac{\partial v}{\partial Z} \\ \frac{\partial u}{\partial Z} - \frac{\partial w}{\partial X} \\ \frac{\partial v}{\partial X} - \frac{\partial u}{\partial Y} \end{pmatrix} \tag{I.2}$$

If use is made of the chain rule of derivative, we find

$$\varpi_X = \frac{\partial W}{\partial a}\frac{\partial a}{\partial Y} + \frac{\partial W}{\partial b}\frac{\partial b}{\partial Y} + \frac{\partial W}{\partial c}\frac{\partial c}{\partial Y} - \frac{\partial V}{\partial a}\frac{\partial a}{\partial Z} - \frac{\partial V}{\partial b}\frac{\partial b}{\partial Z} - \frac{\partial V}{\partial c}\frac{\partial c}{\partial Z} \tag{I.3a}$$

for the first component, and for the remaining two

$$\varpi_Y = \frac{\partial U}{\partial a}\frac{\partial a}{\partial Z} + \frac{\partial U}{\partial b}\frac{\partial b}{\partial Z} + \frac{\partial U}{\partial c}\frac{\partial c}{\partial Z} - \frac{\partial W}{\partial a}\frac{\partial a}{\partial X} - \frac{\partial W}{\partial b}\frac{\partial b}{\partial X} - \frac{\partial W}{\partial c}\frac{\partial c}{\partial X} \tag{I.3b}$$

and

$$\varpi_Z = \frac{\partial V}{\partial a}\frac{\partial a}{\partial X} + \frac{\partial V}{\partial b}\frac{\partial b}{\partial X} + \frac{\partial V}{\partial c}\frac{\partial c}{\partial X} - \frac{\partial U}{\partial a}\frac{\partial a}{\partial Y} - \frac{\partial U}{\partial b}\frac{\partial b}{\partial Y} - \frac{\partial U}{\partial c}\frac{\partial c}{\partial Y} \tag{I.3c}$$

To evaluate the derivatives of the Lagrangian parameters (a, b, c) with respect to the Eulerian coordinates, we consider

$$X = X(a, b, c, t) \quad Y = Y(a, b, c, t) \quad Z = Z(a, b, c, t) \tag{I.4a-c}$$

and differentiate first with respect to X. We obtain a system of equations for $\frac{\partial a}{\partial X}$, $\frac{\partial b}{\partial X}$ and $\frac{\partial c}{\partial X}$

$$\frac{\partial X}{\partial a}\frac{\partial a}{\partial X} + \frac{\partial X}{\partial b}\frac{\partial b}{\partial X} + \frac{\partial X}{\partial c}\frac{\partial c}{\partial X} = 1 \tag{I.5a}$$

$$\frac{\partial Y}{\partial a}\frac{\partial a}{\partial X} + \frac{\partial Y}{\partial b}\frac{\partial b}{\partial X} + \frac{\partial Y}{\partial c}\frac{\partial c}{\partial X} = 0 \tag{I.5b}$$

$$\frac{\partial Z}{\partial a}\frac{\partial a}{\partial X} + \frac{\partial Z}{\partial b}\frac{\partial b}{\partial X} + \frac{\partial Z}{\partial c}\frac{\partial c}{\partial X} = 0 \tag{I.5c}$$

whose determinant - equal by definition to the Jacobian J introduced in §2 - is finite and non-zero. We find

$$\frac{\partial a}{\partial X} = \frac{1}{J}\left(\frac{\partial Y}{\partial b}\frac{\partial Z}{\partial c} - \frac{\partial Y}{\partial c}\frac{\partial Z}{\partial b}\right) \tag{I.6a}$$

$$\frac{\partial b}{\partial X} = \frac{1}{J}\left(\frac{\partial Y}{\partial c}\frac{\partial Z}{\partial a} - \frac{\partial Y}{\partial a}\frac{\partial Z}{\partial c}\right) \tag{I.6b}$$

$$\frac{\partial c}{\partial X} = \frac{1}{J}\left(\frac{\partial Y}{\partial a}\frac{\partial Z}{\partial b} - \frac{\partial Y}{\partial b}\frac{\partial Z}{\partial a}\right) \tag{I.6c}$$

Similarly, differentiation of $(I.4a-c)$ with respect to Y and Z yields respectively

$$\frac{\partial a}{\partial Y} = \frac{1}{J}\left(\frac{\partial X}{\partial c}\frac{\partial Z}{\partial b} - \frac{\partial X}{\partial b}\frac{\partial Z}{\partial c}\right) \tag{I.7a}$$

$$\frac{\partial b}{\partial Y} = \frac{1}{J}\left(\frac{\partial X}{\partial a}\frac{\partial Z}{\partial c} - \frac{\partial X}{\partial c}\frac{\partial Z}{\partial a}\right) \tag{I.7b}$$

$$\frac{\partial c}{\partial Y} = \frac{1}{J}\left(\frac{\partial X}{\partial b}\frac{\partial Z}{\partial a} - \frac{\partial X}{\partial a}\frac{\partial Z}{\partial b}\right) \tag{I.7c}$$

and

$$\frac{\partial a}{\partial Z} = \frac{1}{J}\left(\frac{\partial X}{\partial b}\frac{\partial Y}{\partial c} - \frac{\partial X}{\partial c}\frac{\partial Y}{\partial b}\right) \tag{I.8a}$$

$$\frac{\partial b}{\partial Z} = \frac{1}{J}\left(\frac{\partial X}{\partial c}\frac{\partial Y}{\partial a} - \frac{\partial X}{\partial a}\frac{\partial Y}{\partial c}\right) \tag{I.8b}$$

$$\frac{\partial c}{\partial Z} = \frac{1}{J}\left(\frac{\partial X}{\partial a}\frac{\partial Y}{\partial b} - \frac{\partial X}{\partial b}\frac{\partial Y}{\partial a}\right) \tag{I.8c}$$

Substitution of $(I.6a-c)$, $(I.7a-c)$ and $(I.8a-c)$ in $(I.3a-c)$ yields after invoking $(I.1)$ the following expression for the components of the vorticity vector:

$$\begin{aligned} J\varpi_X = {} & \frac{\partial X}{\partial a}\left[\frac{\partial Y}{\partial c}\frac{\partial^2 Y}{\partial b\partial t} - \frac{\partial Y}{\partial b}\frac{\partial^2 Y}{\partial c\partial t} + \frac{\partial Z}{\partial c}\frac{\partial^2 Z}{\partial b\partial t} - \frac{\partial Z}{\partial b}\frac{\partial^2 Z}{\partial c\partial t}\right] + \\ & + \frac{\partial X}{\partial b}\left[\frac{\partial Y}{\partial a}\frac{\partial^2 Y}{\partial c\partial t} - \frac{\partial Y}{\partial c}\frac{\partial^2 Y}{\partial a\partial t} + \frac{\partial Z}{\partial a}\frac{\partial^2 Z}{\partial c\partial t} - \frac{\partial Z}{\partial c}\frac{\partial^2 Z}{\partial a\partial t}\right] + \\ & + \frac{\partial X}{\partial c}\left[\frac{\partial Y}{\partial b}\frac{\partial^2 Y}{\partial a\partial t} - \frac{\partial Y}{\partial a}\frac{\partial^2 Y}{\partial b\partial t} + \frac{\partial Z}{\partial b}\frac{\partial^2 Z}{\partial a\partial t} - \frac{\partial Z}{\partial a}\frac{\partial^2 Z}{\partial b\partial t}\right] \end{aligned} \tag{I.9a}$$

$$\begin{aligned} J\varpi_Y = {} & \frac{\partial Y}{\partial a}\left[\frac{\partial X}{\partial c}\frac{\partial^2 X}{\partial b\partial t} - \frac{\partial X}{\partial b}\frac{\partial^2 X}{\partial c\partial t} + \frac{\partial Z}{\partial c}\frac{\partial^2 Z}{\partial b\partial t} - \frac{\partial Z}{\partial b}\frac{\partial^2 Z}{\partial c\partial t}\right] + \\ & + \frac{\partial Y}{\partial b}\left[\frac{\partial X}{\partial a}\frac{\partial^2 X}{\partial c\partial t} - \frac{\partial X}{\partial c}\frac{\partial^2 X}{\partial a\partial t} + \frac{\partial Z}{\partial a}\frac{\partial^2 Z}{\partial c\partial t} - \frac{\partial Z}{\partial c}\frac{\partial^2 Z}{\partial a\partial t}\right] + \\ & + \frac{\partial Y}{\partial c}\left[\frac{\partial X}{\partial b}\frac{\partial^2 X}{\partial a\partial t} - \frac{\partial X}{\partial a}\frac{\partial^2 X}{\partial b\partial t} + \frac{\partial Z}{\partial b}\frac{\partial^2 Z}{\partial a\partial t} - \frac{\partial Z}{\partial a}\frac{\partial^2 Z}{\partial b\partial t}\right] \end{aligned} \tag{I.9b}$$

and

$$\begin{aligned} J\varpi_Z = {} & \frac{\partial Z}{\partial a}\left[\frac{\partial X}{\partial c}\frac{\partial^2 X}{\partial b\partial t} - \frac{\partial X}{\partial b}\frac{\partial^2 X}{\partial c\partial t} + \frac{\partial Y}{\partial c}\frac{\partial^2 Y}{\partial b\partial t} - \frac{\partial Y}{\partial b}\frac{\partial^2 Y}{\partial c\partial t}\right] + \\ & + \frac{\partial Z}{\partial b}\left[\frac{\partial X}{\partial a}\frac{\partial^2 X}{\partial c\partial t} - \frac{\partial X}{\partial c}\frac{\partial^2 X}{\partial a\partial t} + \frac{\partial Y}{\partial a}\frac{\partial^2 Y}{\partial c\partial t} - \frac{\partial Y}{\partial c}\frac{\partial^2 Y}{\partial a\partial t}\right] + \end{aligned}$$

$$+\frac{\partial Z}{\partial c}\left[\frac{\partial X}{\partial b}\frac{\partial^2 X}{\partial a \partial t}-\frac{\partial X}{\partial a}\frac{\partial^2 X}{\partial b \partial t}+\frac{\partial Y}{\partial b}\frac{\partial^2 Y}{\partial a \partial t}-\frac{\partial Y}{\partial a}\frac{\partial^2 Y}{\partial b \partial t}\right] \qquad (I.9c)$$

The first square bracket in $(I.9a)$ can be simplified using the definition $(III.2.3a)$ of $\mathcal{U}(a,b,c)$ and similarly for the remaining two brackets and two equations. The vorticity vector components take up the form

$$J\varpi_X = \mathcal{U}(a,b,c)\frac{\partial X}{\partial a}+\mathcal{V}(a,b,c)\frac{\partial X}{\partial b}+\mathcal{W}(a,b,c)\frac{\partial X}{\partial c} \qquad (I.10a)$$

$$J\varpi_Y = \mathcal{U}(a,b,c)\frac{\partial Y}{\partial a}+\mathcal{V}(a,b,c)\frac{\partial Y}{\partial b}+\mathcal{W}(a,b,c)\frac{\partial Y}{\partial c} \qquad (I.10b)$$

$$J\varpi_Z = \mathcal{U}(a,b,c)\frac{\partial Z}{\partial a}+\mathcal{V}(a,b,c)\frac{\partial Z}{\partial b}+\mathcal{W}(a,b,c)\frac{\partial Z}{\partial c} \qquad (I.10c)$$

i.e. in a matrix form

$$\begin{pmatrix}\varpi_X\\ \varpi_Y\\ \varpi_Z\end{pmatrix}=\frac{1}{J}\begin{pmatrix}\frac{\partial X}{\partial a} & \frac{\partial X}{\partial b} & \frac{\partial X}{\partial c}\\ \frac{\partial Y}{\partial a} & \frac{\partial Y}{\partial b} & \frac{\partial Y}{\partial c}\\ \frac{\partial Z}{\partial a} & \frac{\partial Z}{\partial b} & \frac{\partial Z}{\partial c}\end{pmatrix}\begin{pmatrix}\mathcal{U}(a,b,c)\\ \mathcal{V}(a,b,c)\\ \mathcal{W}(a,b,c)\end{pmatrix} \qquad (I.11)$$

The determinant of the 3×3 matrix is by definition equal to $J(a,b,c)$. For exemple, the requirement of zero vorticity is equivalent to the statement

$$\mathcal{U}(a,b,c)=\mathcal{V}(a,b,c)=\mathcal{W}(a,b,c)=0 \qquad (I.12)$$

Appendix J: On the Time Rate of Change of the Vorticity Vector:

We need only prove that the first component of the vector relation (*III*.2.20) is true. The same argument holds true for the remaining two components. Recalling the definition (I.1) of the velocity field, the first component of (*III*.2.19) yields:

$$\frac{\partial \varpi^X}{\partial t} = \frac{1}{J}\left[\frac{\partial u}{\partial a}\mathcal{U} + \frac{\partial u}{\partial b}\mathcal{V} + \frac{\partial u}{\partial c}\mathcal{W}\right] \tag{J.1}$$

Upon expressing the Lagrangian derivatives of u in terms of Eulerian derivatives, we obtain

$$\frac{\partial \varpi^X}{\partial t} = \frac{1}{J}\left[\frac{\partial u}{\partial X}\left(\frac{\partial X}{\partial a}\mathcal{U} + \frac{\partial X}{\partial b}\mathcal{V} + \frac{\partial X}{\partial c}\mathcal{W}\right) + \right.$$

$$\left. + \frac{\partial u}{\partial Y}\left(\frac{\partial Y}{\partial a}\mathcal{U} + \frac{\partial Y}{\partial b}\mathcal{V} + \frac{\partial Y}{\partial c}\mathcal{W}\right) + \frac{\partial u}{\partial Z}\left(\frac{\partial Z}{\partial a}\mathcal{U} + \frac{\partial Z}{\partial b}\mathcal{V} + \frac{\partial Z}{\partial c}\mathcal{W}\right)\right] \tag{J.2}$$

i.e. after making use of (I.11)

$$\frac{\partial \varpi^X}{\partial t} = \varpi^X \frac{\partial u}{\partial X} + \varpi^Y \frac{\partial u}{\partial Y} + \varpi^Z \frac{\partial u}{\partial Z} \tag{J.3}$$

which is precisely the first component of (*III*.2.20).

Appendix K: On the Equivalence of Two Free Surface Boundary Conditions:

Recall the free surface boundary condition $(III.2.13a)$ for the first harmonic

$$\big[R(1-KB\cos\phi)+iKB\sin\phi\cos\theta\big]x_{j1}+$$

$$-\big[(1-KB\cos\phi)\cos\theta+iRKB\sin\phi\big]z_{j1}=I_{j1}\quad c=0 \qquad (K.1)$$

Elimination of y_{j1} from the second free surface boundary condition $(III.2.13b)$ is performed using $(III.2.12c)$. We then obtain

$$\frac{\sin\theta}{\cos\theta}\Big\{\big[R(1-KB\cos\phi)+iKB\sin\phi\cos\theta\big]x_{j1}+$$

$$-\big[(1-KB\cos\phi)\cos\theta+iRKB\sin\phi\big]z_{j1}\Big\}=J_{j1}-\frac{iRH_{j1}(c=0)}{k\cos\theta}\quad c=0 \quad (K.2)$$

We thus have a system of two equations in the two unknowns x_{j1} and z_{j1}. The determinant clearly vanishes and the two equations are compatible provided that

$$Q_{j1}=\sin\theta I_{j1}-\cos\theta J_{j1}+i\frac{R}{k}H_{j1}(c=0) \qquad (K.3)$$

is identically zero. For $j=2$, we substitute the expression of I_{21}, J_{21} and $H_{21}(c=0)$ in $(K.3)$ and obtain

$$Q_{21}=\frac{2iR}{\sigma}\Big[\mathcal{S}_y\cos\theta-\sin\theta\big\{(1-KB\cos\phi)\mathcal{S}_x-iKB\sin\phi\big\}\Big]\frac{\partial A}{\partial t_1}+$$

$$+\frac{i}{k}\big[R\mathcal{S}_y-\sin\theta(1-KB\cos\phi\mathcal{S}_x-iKB\sin\phi\mathcal{S}_x)\big]\frac{\partial A}{\partial a_1}+$$

$$-\frac{i}{k}\Big[R\big\{(1-KB\cos\phi)\mathcal{S}_x-iKB\sin\phi\big\}-\cos\theta(1-KB\cos\phi-iKB\sin\phi\mathcal{S}_x)\Big]\frac{\partial A}{\partial b_1} \qquad (K.4)$$

Substitution of the expression of $\mathcal{S}_x$, $\mathcal{S}_y$ in $(K.4)$ reduces the coefficient of the three derivatives of A to zero identically. We conclude that $Q_{21}=0$ and the two boundary conditions are equivalent.

Appendix L: Evolution of a Wave Train on an Oscillatory Gravity Field

We investigate the evolution of a train of gravity waves assuming that the magnitude of the gravitational acceleration is slowly varying and oscillatory in time. We again assume a Lagrangian description with

$$X = a + x \qquad Z = c + z \tag{L.1a - b}$$

where the X-axis is chosen to be the direction of propagation. The short wave train is weakly nonlinear thus allowing the expansion of the Lagrangian displacements (x, z) in the form

$$x = \epsilon x_1 + \epsilon^2 x_2 + \mathcal{O}(\epsilon^3) \qquad z = \epsilon z_1 + \epsilon^2 z_2 + \mathcal{O}(\epsilon^3) \tag{L.2a - b}$$

Substitution of these equations in $(III.2.6a)$, $(III.2.6b)$ and $(III.2.7a)$ yields two equations and a boundary condition governing x_1 and z_1

$$\frac{\partial x_1}{\partial a} + \frac{\partial z_1}{\partial c} = 0 \qquad \frac{\partial^3 x_1}{\partial c \partial t^2} - \frac{\partial^3 z_1}{\partial a \partial t^2} = 0 \tag{L.3a - b}$$

and

$$\frac{\partial^2 x_1}{\partial t^2} + g\frac{\partial z_1}{\partial a} = 0 \qquad c = 0 \tag{L.3c}$$

where g is the slowly varying gravitational acceleration:

$$g = g_0 g'(\Omega t_1) \tag{L.4}$$

A solution is sought in the form

$$x_1 = x_{10} + i x_{11} e^{iS} + c.c. \qquad z_1 = z_{10} + z_{11} e^{iS} + c.c. \tag{L.5a - b}$$

where x_{10}, z_{10}, x_{11} and z_{11} are functions of c and of slow variables and S satisfies

$$k = \frac{\partial S}{\partial a} \qquad \sigma = -\frac{\partial S}{\partial t} \tag{L.5c - d}$$

Note that k and σ are functions of t_1. Substitution of $(L.5a - d)$ in $(L.3a - b)$ yields

$$x_1 = x_{10} + iAe^{iS}\, e^{kc} + c.c. \qquad z_1 = Ae^{iS}\, e^{kc} + c.c. \tag{L.6a - b}$$

where $x_{10} = x_{10}(a_1, c, t_1)$ and $A = A(a_1, t_1)$ is the slowly varying amplitude of the wave train. Upon enforcing the dynamic free surface boundary condition $(L.3c)$, we obtain the dispersion relation

$$\sigma^2 = gk = g_0 k g'(\Omega t_1) \tag{L.7}$$

Next, we invoke the conservation of phase derived from $(L.5c - d)$

$$\frac{\partial k}{\partial t} + \frac{\partial \sigma}{\partial a} = 0 \tag{L.8}$$

Upon expanding $(L.8)$ according to multiple scale rules, we deduce from the $\mathcal{O}(\epsilon)$ contribution

$$\frac{\partial k}{\partial t_1} = -\frac{\partial \sigma}{\partial a_1} = 0 \tag{L.9}$$

Comparison of $(L.9)$ and $(L.7)$ yields that σ is alone time dependent. Next, we consider the $\mathcal{O}(\epsilon^2)$ governing equations and deduce the corresponding solvability condition (cf. Part I):

$$\sigma \frac{\partial A}{\partial t_1} + \frac{g}{2}\frac{\partial A}{\partial a_1} + \frac{\partial \sigma}{\partial t_1} A = 0 \tag{L.10}$$

We then introduce the reduced coordinates

$$\xi = a_1 - \int^{t_1} \frac{g}{2\sigma} dt_1 \qquad \tau = t_1 \tag{L.11a - b}$$

Substitution of the new variables $(L.11a - b)$ in $(L.10)$ yields

$$\frac{\partial A}{\partial \tau} = -\frac{1}{\sigma}\frac{\partial \sigma}{\partial \tau} A \tag{L.12a}$$

Comparison of $(L.12a)$ with $(L.7)$ yields

$$A\sqrt{g'(\Omega t_1)} = \text{const.} \tag{L.12b}$$

The amplitude is therefore modulated in time with the same period as that of the gravity field.

Appendix M: MACSYMA Command Files for Chapter II

The symbolic algebra package MACSYMA has been used extensively in Part 2 to derive the approximate governing equations, solve for the short wave displacements at the leading and first order and to deduce from the $\mathcal{O}(\epsilon^2)$ and $\mathcal{O}(\epsilon^3)$ solvability conditions, linear and nonlinear evolution equations for the short wave amplitude A. Although MACSYMA has been instrumental in all three chapters of Part 2, the algebra pertaining to Chapter II only is presented here, for brevity.

In the following pages, we present several command files recognizable by the extension **.mac**. Command file **eqs.mac**, for instance, can be executed at once (batch mode) by typing at the prompt (c1):

batch ("eqs.mac")$

Alternately, each command in file **eqs.mac** can be entered interactively. In either case, the summary of the session including the commands as well as the corresponding result will be stored in **eqs.out**. A semi-colon at the end of a command line causes the result to be displayed. With a dollar sign, however, no result is displayed. The **.out** files are not included here for brevity. Finally, a third extension **.sav** refers to a lisp file containing some of the results of the current session which are saved for later use.

Each of the following twelve command files is documented and preceeded by a brief summary.

Appendix M.1: Command file EQS.MAC

Introduction of multiple scales and perturbation analyses in the governing equations. Deduction of approximate equations at $\mathcal{O}(1)$, $\mathcal{O}(\epsilon)$, $\mathcal{O}(\epsilon^2)$ and $\mathcal{O}(\epsilon^3)$.

```
inchar:m$
outchar:n$
kill(all)$
linel:80$
bothcases:true$
loadprint:false$
writefile("eqs.out")$
timedate();
/*——Defining the dependencies————————————*/
depends([X,Z,x,z],[a,c,t])$
/*——Defining the multiple scale transformation rules-*/
gradef(a1,a,e)$
gradef(a2,a,e^2)$
gradef(c1,c,e)$
gradef(c2,c,e^2)$
gradef(t1,t,e)$
gradef(t2,t,e^2)$
/*————Continuity equation————————————————*/
diff(X,a)*diff(Z,c)-diff(X,c)*diff(Z,a);
CONT:ev(%,X=a+x,Z=c+z,diff,expand);
/*————Irrotationality equation————————-*/
diff(diff(X,a)*diff(X,c,1,t,1)+diff(Z,a)*diff(Z,c,1,t,1),t)-
diff(diff(X,c)*diff(X,a,1,t,1)+diff(Z,c)*diff(Z,a,1,t,1),t);
IRR:ev(%,X=a+x,Z=c+z,diff,expand);
/*————Free surface dynamic boundary condition—-*/
diff(X,t,2)*diff(X,a)+(diff(Z,t,2)+g)*diff(Z,a);
```

```
SBC:ev(%,X=a+x,Z=c+z,diff,expand);
/*————————Declaring dependencies————————————*/
depends([xm2,zm2],[a2,c2,t1])$
depends([x1,z1],[a,a1,a2,c,c1,c2,t,t1,t2])$
depends([x2,z2],[a,a1,c,c1,t,t1])$
depends([x3,z3],[a,c,t])$
dependencies;
showtime:true$
/*————————CONTINUITY————————————————————*/
/*————————Linear terms————————————————-*/
part(CONT,[2,4]);
ev(%,x=xm2/e^2+e*x1+e^2*x2+e^3*x3,
z=zm2/e^2+e*z1+e^2*z2+e^3*z3,diff)$
TERM1:taylor(%,e,0,3)$
/*————————Quadratic terms————————————————-*/
part(CONT,allbut(2,4));
ev(%,x=xm2/e^2+e*x1+e^2*x2+e^3*x3,
z=zm2/e^2+e*z1+e^2*z2+e^3*z3,diff)$
TERM2:taylor(%,e,0,3)$
C:expand(TERM1+TERM2)$
nterms(%);
kill(TERM1,TERM2)$
/*————————IRROTATIONALITY————————————————-*/
/*————————Linear terms————————————————-*/
part(IRR,[3,5]);
ev(%,x=xm2/e^2+e*x1+e^2*x2+e^3*x3,
z=zm2/e^2+e*z1+e^2*z2+e^3*z3,diff)$
TERM1:taylor(%,e,0,3)$
/*————————Quadratic terms————————————————-*/
part(IRR,allbut(3,5));
ev(%,x=xm2/e^2+e*x1+e^2*x2+e^3*x3,
z=zm2/e^2+e*z1+e^2*z2+e^3*z3,diff)$
```

```
TERM2:taylor(%,e,0,3)$
/**/
I:expand(TERM1+TERM2)$
nterms(%);
kill(TERM1,TERM2)$
/*--------FREE SURFACE BOUNDARY CONDITION--------*/
/*--------linear terms----------------------*/
part(SBC,[2,4]);
ev(%,x=xm2/e^2+e*x1+e^2*x2+e^3*x3,
z=zm2/e^2+e*z1+e^2*z2+e^3*z3,diff)$
TERM1:taylor(%,e,0,3)$
/*--------Quadratic terms--------------------*/
part(SBC,allbut(2,4));
ev(%,x=xm2/e^2+e*x1+e^2*x2+e^3*x3,
z=zm2/e^2+e*z1+e^2*z2+e^3*z3,diff)$
TERM2:taylor(%,e,0,3)$
S:expand(TERM1+TERM2)$
nterms(%);
kill(TERM1,TERM2)$
remove(all,atomgrad)$
/*--------------------------------------*/
/*--------Leading Order O(1) equations--------*/
/*--------Continuity----------------------*/
CONT0:coeff(C,e,0);
nterms(expand(%));
/*--------Irrotationality--------------------*/
I0:coeff(I,e,0);
nterms(expand(%));
/*--------Free Surface Boundary Condition--------*/
BC0:coeff(S,e,0);
nterms(expand(%));
/*--------------------------------------*/
```

```
/*--------Leading Order O(e) equations---------*/
/*--------Continuity-----------------------*/
CONT1:coeff(C,e,1);
nterms(expand(%));
/*--------Irrotationality-------------------*/
I1:coeff(I,e,1);
nterms(expand(%));
/*--------Free Surface Boundary Condition-------*/
BC1:coeff(S,e,1);
nterms(expand(%));
/*-------------------------------------------*/
/*--------O(e^2) equations-----------------*/
/*--------Continuity-----------------------*/
CONT2:coeff(C,e,2);
nterms(expand(%));
/*--------Irrotationality-------------------*/
I2:coeff(I,e,2);
nterms(expand(%));
/*--------Free Surface Boundary Condition-------*/
BC2:coeff(S,e,2);
nterms(expand(%));
/*-------------------------------------------*/
/*--------O(e^3) equations-----------------*/
/*--------Continuity-----------------------*/
CONT3:coeff(C,e,3);
nterms(expand(%));
/*--------Irrotationality-------------------*/
I3:coeff(I,e,3);
nterms(expand(%));
/*--------Free Surface Boundary Condition-------*/
BC3:coeff(S,e,3);
nterms(expand(%));
```

```
/*————————-Saving the results————————————————*/
save("eqs.sav",CONT0,CONT1,CONT2,CONT3,I0,I1,I2,
I3,BC0,BC1,BC2,BC3)$
closefile();
```

Appendix M.2: Command file LONG_0.MAC

Introduction of the Gerstner wave. Substitution of this solution in the governing equations.

```
inchar:m$
outchar:n$
kill(all)$
bothcases:true$
writefile("long_0.out")$
timedate();
loadfile("eqs.sav")$
depends([xm2,zm2],[a2,c2,t1])$
depends([x1,z1],[a,a1,c,c1,t,t1])$
depends([x2,z2],[a,c,t])$
/*——Governing Equations for leading order Long Waves——*/
eq[1]:ev(CONT0,diff);
eq[2]:ev(part(I2,[1,2,6,15,16,17]),diff);
eq[3]:ev(BC0,diff);
/*————————————————————————————————————————*/
/*———-Introducing Gerstner wave solution————————-*/
Sxm2:xm2=B*sin(PHI)*exp(K*c2);
Szm2:zm2=B*cos(PHI)*exp(K*c2);
gradef(PHI,a2,-K)$
gradef(PHI,t1,OM)$
```

```
/*-----checking the solution----------------------*/
ev(eq[1],Sxm2,Szm2,diff)$
ratsubst(1-cos(PHI)^2,sin(PHI)^2,%)$
expand(%);
ev(eq[2],Sxm2,Szm2,diff)$
ratexpand(%);
ev(eq[3],Sxm2,Szm2,diff)$
ev(%,c=0)$
factor(%)=0;
closefile();
```

Appendix M.3: Command file SHORT_1.MAC

Determination of the governing equations for the short wave displacements at the leading order. Solution for these displacements. Dispersion relation for the short waves.

```
inchar:m$
outchar:n$
kill(all)$
bothcases:true$
writefile("short_1.out")$
timedate();
/*-----Recall governing equations saved in eqs.sav—*/
loadfile("eqs.sav")$
depends([x1,z1],[a,c,t])$
depends([xm2,zm2],[a2,c2,t1])$
/*-----Definition of the displacements of Gerstner's wave—-*/
Sxm2:xm2=B*sin(PHI)*exp(K*c2);
Szm2:zm2=B*cos(PHI)*exp(K*c2);
```

```
/*-----Defining phase function (φ) by its gradients—*/
gradef(PHI,a2,-K)$
gradef(PHI,t1,OM)$
/*-----Governing Equations for leading order Short Waves—*/
ev(CONT1,diff);
ev(%,Sxm2,Szm2,diff)$
EQ[1]:ev(%,c2=0);
ev(I1,diff);
ev(%,Sxm2,Szm2,diff)$
EQ[2]:ev(%,c2=0);
ev(BC1,diff);
ev(%,Sxm2,Szm2,diff)$
EQ[3]:ev(%,c2=0);
/*-------Short Wave Solution is sought in the form-----*/
Sx1:x1=%i*X*exp(%i*(k*a-om*t)+kappa*c);
Sz1:z1=Z*exp(%i*(k*a-om*t)+kappa*c);
/*-------om stands for σ in Chapter II-------*/
/*-------Substitute the above form in equations-------*/
/*-------Continuity equation-------------------*/
ev(EQ[1],Sx1,Sz1,diff)$
ev(%,a=0,c=0,t=0)$
eq[1]:expand(%);
/*-------Irrotationality equation---------------*/
ev(EQ[2],Sx1,Sz1,diff)$
ev(%,a=0,c=0,t=0)$
eq[2]:expand(%*%i/om);
/*-------Define the coefficient matrix----------*/
/*-------and solve for kappa (κ)----------*/
MM:coefmatrix([eq[1],eq[2]],[X,Z]);
determinant(%)$
expand(%)$
subst(1-cos(PHI)^2,sin(PHI)^2,%)$
```

```
expand(%);
solve(%,kappa)$
subst(1-cos(PHI)^2,sin(PHI)^2,%)$
ratsimp(%);
/*———————Retain only kappa+ ———————————————-*/
part(%,2)$
subst(1-(K*B)^2,sqrt((K*B)^4-2*(K*B)^2+1),%)$
Skappa:ratsimp(%);
/*———————Reevaluate the continuity equation————————*/
/*———————to determine the eigenvector————————————*/
ev(eq[1],Skappa)$
expand(%)$
solve(%,X)$
subst(1-cos(PHI)^2,sin(PHI)^2,%)$
SOL:ratsimp(%);
/*———————Substitute solution in dynamic boundary condition-*/
ev(EQ[3],Sx1,Sz1,diff)$
ev(%,a=0,c=0,t=0)$
ev(%,SOL)$
ratsubst(g*K,OM^2,%)$
eq[3]:expand(%);
factor(realpart(%));
factor(imagpart(%th(2)));
/*———————Check the solution———————————————-*/
/*———————Substitute it in continuity———————————-*/
ev(eq[1],SOL,Skappa)$
ratsimp(%)$
subst(1-cos(PHI)^2,sin(PHI)^2,%)$
ratsimp(%);
/*———————Substitute it in irrotationality————————*/
ev(eq[2],SOL,Skappa)$
ratsimp(%)$
```

```
subst(1-cos(PHI)^2,sin(PHI)^2,%)$
ratsimp(%);
closefile();
```

Appendix M.4: Command file SHORT_2.MAC

Determination of the governing equations for the short wave displacements at $\mathcal{O}(\epsilon^2)$. Harmonic decomposition of leading order and $\mathcal{O}(\epsilon^2)$ short waves. Note that x21 and x21s refer respectively to x_{21} and its complex conjugate $x_{21}^{\star}$.

```
inchar:m$
outchar:n$
kill(all)$
bothcases:true$
loadprint:false$
writefile("short_2.out")$
timedate();
loadfile("eqs.sav")$
/*------Specify dependences of displacements----------*/
depends([xm2,zm2],[a2,c2,t1])$
depends([x1,z1],[a,a1,c,c1,t,t1])$
depends([x2,z2],[a,c,t])$
depends([A,As],[a1,t1])$
depends([x10,z10],[a1,c,c1,t1])$
depends([x20,z20,x21,x21s,z21,z21s,x22,x22s,z22,z22s],[a1,c,c1,t1])$
depends([kappai,kappar],[t1,a2])$
/*------Define Lagrangian phase of short waves by gradients-*/
gradef(e,a,%i*k*e)$
gradef(e,t,-%i*om*e)$
```

```
/*-----Define Gerstner's wave----------*/
Sxm2:xm2=B*sin(PHI)*exp(K*c2);
Szm2:zm2=B*cos(PHI)*exp(K*c2);
gradef(PHI,a2,-K)$
gradef(PHI,t1,OM)$
/*-----Define rela and imaginary parts of kappa----------*/
Skappai:kappai=2*k*K*B*sin(PHI)/(1-2*K*B*cos(PHI)+(K*B)^2);
Skappar:kappar=k*(1-(K*B)^2)/(1-2*K*B*cos(PHI)+(K*B)^2);
/*-----------------------------------------*/
/*-----Continuity for short wave at O(e^2)----------*/
ev(CONT2,diff)$
nterms(%);
ev(%th(2),Sxm2,Szm2,diff)$
ev(%,c2=0)$
ev(%,x1=x10+1/2*%i*(A*e*exp(%i*kappai*c)-
As*exp(-%i*kappai*c)/e)*exp(kappar*c),
z1=z10+1/2*(A*e*exp(%i*kappai*c)+
As*exp(-%i*kappai*c)/e)*exp(kappar*c),diff,expand)$
ev(%,x2=x20+1/2*%i*(x21*e-x21s/e)+1/2*%i*(x22*e^2-x22s/e^2),
z2=z20+1/2*(z21*e+z21s/e)+1/2*(z22*e^2+z22s/e^2),diff,expand)$
C:expand(%)$
/*-----------------------------------------*/
/*-----Harmonic decomposition of continuity equation-----*/
/*-----First harmonic----------*/
coeff(C,e,1)$
expand(%*2)$
e21_1:part(%,[1,2,3,5,6,7])=-part(%,allbut(1,2,3,5,6,7));
/*-----Second harmonic----------*/
coeff(C,e,2)$
e22_1:expand(%*2)=0;
/*-----Zeroth harmonic----------*/
e20_1:coeff(C,e,0)=0;
```

```
/*-------------------------------------------------*/
/*-----Irrotationality for short wave at O(e^2)-------*/
ev(I2,diff)$
nterms(%);
ev(%th(2),Sxm2,Szm2,diff)$
ev(%,c2=0)$
ev(%,x1=x10+1/2*%i*(A*e*exp(%i*kappai*c)-
As*exp(-%i*kappai*c)/e)*exp(kappar*c),
z1=z10+1/2*(A*e*exp(%i*kappai*c)+
As*exp(-%i*kappai*c)/e)*exp(kappar*c),diff,expand)$
ev(%,x2=x20+1/2*%i*(x21*e-x21s/e)+1/2*%i*(x22*e^2-x22s/e^2),
z2=z20+1/2*(z21*e+z21s/e)+1/2*(z22*e^2+z22s/e^2),diff,expand)$
I:expand(%)$
/*-------------------------------------------------*/
/*-----Harmonic decomposition of irrotationality equation-*/
/*-----First harmonic-----------------------------*/
coeff(I,e,1)$
expand(%*2/om^2/%i*(-1))$
e21_2:part(%,[1,2,3,5,6,7])=-part(%,allbut(1,2,3,5,6,7));
/*-----Second harmonic----------------------------*/
coeff(I,e,2)$
e22_2:expand(%/2/om^2/%i*(-1))=0;
/*-----Zeroth harmonic----------------------------*/
e20_2:coeff(I,e,0)=0;
/*-------------------------------------------------*/
/*-----Free Surface dynamic boundary condition O(e^2) */
ev(BC2,diff)$
nterms(%);
ev(%th(2),Sxm2,Szm2,diff)$
ev(%,c2=0)$
ev(%,x1=x10+1/2*%i*(A*e*exp(%i*kappai*c)-
As*exp(-%i*kappai*c)/e)*exp(kappar*c),
```

```
z1=z10+1/2*(A*e*exp(%i*kappai*c)+
As*exp(-%i*kappai*c)/e)*exp(kappar*c),diff,expand)$
ev(%,x2=x20+1/2*%i*(x21*e-x21s/e)+1/2*%i*(x22*e^2-x22s/e^2),
z2=z20+1/2*(z21*e+z21s/e)+1/2*(z22*e^2+z22s/e^2),diff,expand)$
S:expand(%)$
/*-----------------------------------------*/
/*-----Harmonic decomposition of boundary condition-----*/
/*-----First harmonic-----------------------*/
coeff(S,e,1)$
ratsubst(g*K,OM^2,%)$
ratsubst(om^2,g*k,%)$
ev(%,c=0)$
expand(%*2/om^2*%i)$
e21_3:factor(part(%,[1,2,3,4,5,6]))=-part(%,allbut(1,2,3,4,5,6));
/*-----Second harmonic----------------------*/
coeff(S,e,2)$
ratsubst(g*K,OM^2,%)$
ratsubst(om^2,g*k,%)$
expand(%/om^2*%i)$
e22_3:factor(%)=0;
/*-----Zeroth harmonic----------------------*/
coeff(S,e,0)$
ratsubst(g*K,OM^2,%)$
e20_3:expand(%/g)=0;
/*-----------------------------------------*/
/*---Deriving the coefficient matrices------*/
/*-----First harmonic-----------------------*/
M1:coefmatrix([lhs(e21_1),lhs(e21_2)],[diff(x21,c),diff(z21,c)]);
determinant(%);
N1:coefmatrix([lhs(e21_1),lhs(e21_2)],[x21,z21]);
expand(invert(M1).N1)$
ratsubst(1-sin(PHI)^2,cos(PHI)^2,%)$
```

```
ratsimp(%);
/*-----Second harmonic-----------------------------*/
M2:coefmatrix([lhs(e22_1),lhs(e22_2)],[diff(x22,c),diff(z22,c)]);
N2:coefmatrix([lhs(e22_1),lhs(e22_2)],[x22,z22]);
expand(invert(M2).N2)$
ratsubst(1-sin(PHI)^2,cos(PHI)^2,%)$
ratsimp(%);
/*-----Saving results-----------------------------*/
save("short_2.sav",e21_1,e21_2,e21_3,e22_1,e22_2,e22_3,
e20_1,e20_2,e20_3)$
closefile();
```

Appendix M.5: Command file SHORT_3.MAC

Determination of the governing equations for the short wave displacements at $\mathcal{O}(\epsilon^3)$. Harmonic decomposition of leading order, $\mathcal{O}(\epsilon^2)$ and $\mathcal{O}(\epsilon^3)$ short waves.

```
inchar:m$
outchar:n$
kill(all)$
loadprint:false$
bothcases:true$
writefile("short_3.out")$
timedate();
loadfile("eqs.sav")$
/*-----Scale dependence of displacements-----------*/
depends([xm2,zm2],[a2,c2,t1])$
depends([x1,z1],[a,a1,a2,c,c1,c2,t,t1,t2])$
depends([x2,z2],[a,a1,c,c1,t,t1])$
```

```
depends([x3,z3],[a,c,t])$
depends([A,As],[a1,a2,t1,t2])$
depends(sumA2,[a1,a2,c,t1,t2])$
depends([x10,z10],[a1,a2,c,t1,t2])$
depends([x20,z20,x21,x21s,z21,z21s],[a1,c,t1])$
depends([x30,z30,x31,z31,x32,z32],[a1,c,c1,t1])$
depends([kappai,kappar],[t1,a2])$
/**/
gradef(e,a,%i*k*e)$
gradef(e,t,-%i*om*e)$
/* Gerstner Swell */
Sxm2:xm2=B*sin(PHI)*exp(K*c2);
Szm2:zm2=B*cos(PHI)*exp(K*c2);
gradef(PHI,a2,-K)$
gradef(PHI,t1,OM)$
/**/
Skappai:kappai=2*k*K*B*sin(PHI)/(1-2*K*B*cos(PHI)+(K*B)^2);
Skappar:kappar=k*(1-(K*B)^2)/(1-2*K*B*cos(PHI)+(K*B)^2);
/*-----------------------------------------*/
/*-----Continuity for short wave at O(e^3)---------*/
ev(CONT3,diff)$
nterms(%);
ev(%th(2),Sxm2,Szm2,diff)$
ratsubst(1,exp(K*c2),%)$
ev(%,x1=x10+1/2*%i*(A*e*exp(%i*kappai*c)-
As*exp(-%i*kappai*c)/e)*exp(kappar*c),
z1=z10+1/2*(A*e*exp(%i*kappai*c)+
As*exp(-%i*kappai*c)/e)*exp(kappar*c),diff,expand)$
ev(%,x2=x20+1/2*%i*(x21*e-x21s/e),z2=z20+1/2*(z21*e+z21s/e),
diff,expand)$
ev(%,x3=x30+1/2*%i*x31*e+1/2*%i*x32*e^2,
z3=z30+1/2*z31*e+1/2*z32*e^2,diff,expand)$
```

```
C:expand(%)$
/*-----------------------------------------------*/
/*-----Harmonic decomposition of continuity equation-----*/
/*-----First harmonic-----------------------------*/
coeff(C,e,1)$
expand(%*2)$
e31_1:part(%,[1,2,3,11,12,13])=-part(%,allbut(1,2,3,11,12,13));
/*-----Second harmonic----------------------------*/
coeff(C,e,2)$
expand(%*2)$
e32_1:part(%,[1,2,3,7,8,9])=-part(%,allbut(1,2,3,7,8,9));
/*-----Zeroth harmonic----------------------------*/
coeff(C,e,0)$
expand(%)$
e30_1:part(%,2)=-part(%,allbut(2));
/*-----------------------------------------------*/
/*-----Irrotationality for short wave at O(e^3)-----*/
ev(I3,diff)$
nterms(%);
ev(%th(2),Sxm2,Szm2,diff)$
ratsubst(1,exp(K*c2),%)$
ratsubst(1,exp(K*c2),%)$
ev(%,x1=x10+1/2*%i*(A*e*exp(%i*kappai*c)-
As*exp(-%i*kappai*c)/e)*exp(kappar*c),
z1=z10+1/2*(A*e*exp(%i*kappai*c)+
As*exp(-%i*kappai*c)/e)*exp(kappar*c),diff,expand)$
ev(%,x2=x20+1/2*%i*(x21*e-x21s/e),z2=z20+1/2*(z21*e+z21s/e),
diff,expand)$
ev(%,x3=x30+1/2*%i*x31*e+1/2*%i*x32*e^2,
z3=z30+1/2*z31*e+1/2*z32*e^2,diff,expand)$
I:expand(%)$
/*-----------------------------------------------*/
```

```
/*-----Harmonic decomposition of irrotationality equation-*/
/*-----First harmonic-------------------------------*/
coeff(I,e,1)$
expand(%*2/om^2*%i)$
e31_2:part(%,[1,2,3,17,18,19])=-part(%,allbut(1,2,3,17,18,19));
/*-----Second harmonic-------------------------------*/
coeff(I,e,2)$
e32_2:expand(%*%i/2/om^2)=0;
/*-----Zeroth harmonic-------------------------------*/
coeff(I,e,0)$
e30_2:expand(%)=0;
/*-------------------------------------------------*/
/*-----Free Surface dynamic boundary condition O(e^2) */
ev(BC3,diff)$
nterms(%);
ev(%th(2),Sxm2,Szm2,diff)$
ratsubst(1,exp(K*c2),%)$
ratsubst(1,exp(K*c2),%)$
ev(%,x1=x10+1/2*%i*(A*e*exp(%i*kappai*c)-
As*exp(-%i*kappai*c)/e)*exp(kappar*c),
z1=z10+1/2*(A*e*exp(%i*kappai*c)+
As*exp(-%i*kappai*c)/e)*exp(kappar*c),diff,expand)$
ev(%,x2=x20+1/2*%i*(x21*e-x21s/e),z2=z20+1/2*(z21*e+z21s/e),
diff,expand)$
ev(%,x3=x30+1/2*%i*x31*e+1/2*%i*x32*e^2,
z3=z30+1/2*z31*e+1/2*z32*e^2,diff,expand)$
S:expand(%)$
/*-------------------------------------------------*/
/*-----Harmonic decomposition of boundary condition-----*/
/*-----First harmonic-------------------------------*/
coeff(S,e,1)$
ratsubst(g*K,OM^2,%)$
```

```
ratsubst(om^2,g*k,%)$
ev(%,c=0)$
expand(%*2*%i/om^2)$
e31_3:factor(part(%,[1,2,3,8,9,10]))=-part(%,allbut(1,2,3,8,9,10));
/*-----Second harmonic-----------------------*/
coeff(S,e,2)$
ratsubst(g*K,OM^2,%)$
ratsubst(om^2,g*k,%)$
ev(%,c=0)$
e32_3:expand(%*%i/om^2);
/*-----Zeroth harmonic-----------------------*/
coeff(S,e,0)$
ev(%,c=0)$
e30_3:expand(%)=0;
/*-----Saving results-----------------------*/
save("short_3.sav",e30_1,e30_2,e30_3,e31_1,e31_2,e31_3,e32_1,
e32_2,e32_3)$
closefile();
```

Appendix M.6: Command file WAVE_ACTION.MAC

Derivation of the linear evolution equation at $\mathcal{O}(\epsilon^2)$.

```
inchar:m$
outchar:n$
kill(all)$
bothcases:true$
loadprint:false$
writefile("wave_action.out")$
/*-----------------------------------------*/
```

```
timedate();
loadfile("short_2.sav")$
/*-----Scale dependence-----------------------------*/
depends([A,As],[a1,t1])$
depends([x10,z10],[a1,c,c1,t1])$
depends([x21,x21s,z21,z21s],[a1,c,c1,t1])$
depends([PHI,kappar,kappai],[t1,a2])$
/*-----------------------------------------------*/
Skappai:kappai=2*k*K*B*sin(PHI)/(1-2*K*B*cos(PHI)+(K*B)^2);
Skappar:kappar=k*(1-(K*B)^2)/(1-2*K*B*cos(PHI)+(K*B)^2);
/*-----------------------------------------------*/
gradef(PHI,a2,-K)$
gradef(PHI,t1,OM)$
/*-----Evaluating the integrand in solvability condition-----*/
ev(rhs(e21_2)-rhs(e21_1),diff)$
%*exp(kappar*c)*exp(-%i*kappai*c)$
ratexpand(%)$
primitive(%,c)$
ev(%,Skappar,Skappai,diff)$
ratsimp(%)$
ratsubst(1-cos(PHI)^2,sin(PHI)^2,%)$
ratsimp(%);
/*-----Making use of definition of kappa-----------------*/
top:factor(part(part(%,1),1))*exp(2*kappar*c);
bottom:part(%th(2),2);
gg:top/bottom;
/*-----------------------------------------------*/
/*-----Evaluating the right hand side of solvability condition-*/
e21_3;
/*-----Left hand side is simply gg @ c=0-----------------*/
factor(ev(gg,c=0))$
%-rhs(%th(2))$
```

```
EQ:ratexpand(%*om/%i)$
/*-----Simplifying the solvability condition----------*/
coeff(EQ,diff(A,t1))$
coef1:ratsimp(%);
/**/
coeff(EQ,diff(A,a1))$
coef2:ratsimp(%/coef1);
/**/
coeff(EQ,A)$
coef3:ratsimp(%/coef1)$
/**/
realpart(coef3)$
ratsimp(%)$
subst(1-cos(PHI)^2,sin(PHI)^2,%)$
coef4:ratsimp(%);
/**/
imagpart(coef3)$
ratsimp(%)$
subst(1-cos(PHI)^2,sin(PHI)^2,%)$
ratsimp(%)$
coef5:factor(%);
/*-----Displaying wave action equation---------- */
Green_1:diff(A,t1)+coef2*diff(A,a1)+A*coef4+%i*A*coef5=0;
/*-----Saving results----------*/
save("wave_action.sav",Green_1)$
closefile();
```

Appendix M.7: Command file SOLVE_2.MAC

Solution of first and second harmonic displacements of the short waves at

$\mathcal{O}(\epsilon^2)$.

```
inchar:m$
outchar:n$
kill(all)$
loadprint:false$
bcthcases:true$
writefile("solve_2.out")$
timedate();
loadfile("short_2.sav")$
loadfile("wave_action.sav")$
/**/
depends([A,As],[a1,t1])$
depends(sumA2,[a1,a2,c,t1])$
depends([x10,z10],[a1,c,c1,t1])$
depends([x21,x21s,z21,z21s],[a1,c,c1,t1])$
depends([PHI,kappai,kappar],[t1,a2])$
/*——sumA2 refers to ∫_0^t1 |A|^2 e^(2Kc2) dt1———-*/
Sx10:x10=om*k*(1-K*B*cos(PHI))*sumA2;
Sz10:z10=om*k*K*B*sin(PHI)*sumA2;
/**/
Skappai:kappai=2*k*K*B*sin(PHI)/(1-2*K*B*cos(PHI)+(K*B)^2);
Skappar:kappar=k*(1-(K*B)^2)/(1-2*K*B*cos(PHI)+(K*B)^2);
/**/
gradef(PHI,a2,-K)$
gradef(PHI,t1,OM)$
/*——Integrand of β+ in thesis————————————-*/
declare(integrate,linear)$
EQ:rhs(e21_1)+rhs(e21_2)$
/*——First, integrate terms involving x10 and z10————-*/
part(EQ,[1,2])$
expand(%*exp(-kappar*c)*exp(-%i*kappai*c))$
```

```
primitive(%,c)$
ev(%,integrate)$
ev(%,Sx10,Sz10)$
factor(%);
/*——Factor out the -%i————————————————————*/
expand(%*%i)$
ff[1]:-%i*factor(%);
FF[1]:ratsimp(%/2/(1-K*B*cos(PHI)+%i*K*B*sin(PHI)));
/*——Second, integrate the remaining terms————————*/
part(EQ,allbut(1,2))$
%*exp(-kappar*c)*exp(-%i*kappai*c)$
ratexpand(%)$
primitive(%,c)$
ev(%,Skappai,Skappar,diff)$
ratsubst(1-cos(PHI)^2,sin(PHI)^2,%)$
ratexpand(%);
ff[2]:factor(part(%,[1,2,3]))$
FF[2]:%/2/(1-K*B*cos(PHI)+%i*K*B*sin(PHI));
/**/
ratsimp(part(%th(3),allbut(1,2,3)))$
ff[3]:factor(%)$
FF[3]:%/2/(1-K*B*cos(PHI)+%i*K*B*sin(PHI));
/**/
ff[1]+ff[2]+ff[3];
/*——Second integral computed in WAVE_ACTION.MAC————*/
gg;
%/2/(1-K*B*cos(PHI)-%i*K*B*sin(PHI));
top:part(%,1);
bottom:part(%th(2),2);
exp:part(top,5)/part(bottom,2)$
/**/
realpart(%)$
```

```
subst(1-cos(PHI)^2,sin(PHI)^2,%)$
ggr:ratsimp(%);
/**/
imagpart(exp)$
subst(1-cos(PHI)^2,sin(PHI)^2,%)$
ggi:ratsimp(%);
GG:(ggr+%i*ggi)*part(top,allbut(5))/part(bottom,allbut(2));
/*-----------------------------------------*/
/*----Definition of x21 and z21----------------------*/
Sx21:x21= FF[1]*exp(kappar*c)*exp(%i*kappai*c)+
FF[2]*exp(kappar*c)*exp(%i*kappai*c)+
FF[3]*exp(kappar*c)*exp(%i*kappai*c)+
GG*exp(-kappar*c)*exp(%i*kappai*c);
subst(-%i,%i,rhs(%))$
subst(As,A,%)$
Sx21s:x21s=%;
/**/
Sz21:z21= FF[1]*exp(kappar*c)*exp(%i*kappai*c)+
FF[2]*exp(kappar*c)*exp(%i*kappai*c)+
FF[3]*exp(kappar*c)*exp(%i*kappai*c)-
GG*exp(-kappar*c)*exp(%i*kappai*c);
subst(-%i,%i,rhs(%))$
subst(As,A,%)$
Sz21s:z21s=%;
/*----Saving results-------------------------*/
save("solve_2.sav",Skappai,Skappar,Sx10,Sz10,
Sx21,Sx21s,Sz21,Sz21s)$
closefile();
```

Appendix M.8: Command file SCHR.MAC

Integrand in the solvability condition for the short wave displacements at $\mathcal{O}(\epsilon^3)$ is broken in two components: term[1] includes all terms depending on either x10, z10, x21 and z21, and term[2] includes all terms explicit in A. term[3] refers to the right hand side of the solvability condition.

```
inchar:m$
outchar:n$
kill(all)$
loadprint:false$
bothcases:true$
writefile("schr.out")$
timedate();
loadfile("short_3.sav")$
loadfile("solve_2.sav")$
/**/
depends([A,As],[a1,a2,t1,t2])$
depends(sumA2,[a1,a2,c,t1,t2])$
depends([x10,z10],[a1,a2,c,t1,t2])$
depends([x20,z20,x21,z21],[a1,c,c1,t1])$
depends([x30,z30,x31,z31],c)$
depends([PHI,kappai,kappar],[t1,a2])$
/*-----------------------------------------------*/
rhs(e31_2)-rhs(e31_1)$
%*exp(kappar*c)*exp(-%i*kappai*c)$
EQ:ratexpand(%)$
n:nterms(%);
/*-----------------------------------------------*/
/*----Splitting the above integral in two terms----------*/
/*-----------------------------------------------*/
```

```
/* term[1] contains the terms involving x10, z10, x21 and z21 */
/* term[2] contains the terms explicit in A A. */
/*-------------------------------------------------------*/
/*----and right hand side of the free surface boundary condition----*/
/*----term[3] contains all terms-------------------------*/
/*-------------------------------------------------------*/
/*----Extracting term[1]---------------------------------*/
term[1]:0$
for i:1 thru 22 do term[1]:term[1]+part(EQ,i);
term[1];
nterms(%);
/*-------------------------------------------------------*/
/*----Extracting term[2]---------------------------------*/
term[2]:0$
for i:23 thru n do term[2]:term[2]+part(EQ,i)$
nterms(term[2]);
/*-------------------------------------------------------*/
/*----Defining term[3]-----------------------------------*/
/*-------------------------------------------------------*/
term[3]:rhs(e31_3);
nterms(term[3]);
/*-----Saving results------------------------------------*/
save("schr.sav",term)$
closefile();
```

Appendix M.9: Command file SCHR_1.MAC

Integration of term[1] is performed.

```
inchar:m$
```

```
outchar:n$
kill(all)$
loadprint:false$
bothcases:true$
derivsubst:true$
writefile("schr_1.out")$
/*-----------------------------------------------*/
/*-------Integration of term[1]-------------------*/
timedate();
loadfile("wave_action.sav")$
loadfile("solve_2.sav")$
loadfile("schr.sav")$
/**/
depends([A,As],[a1,a2,t1,t2])$
depends(sumA2,[a1,a2,c,t1,t2])$
depends([x10,z10],[a1,a2,c,t1,t2])$
depends([x20,z20,x21,z21],[a1,c,c1,t1])$
depends([x30,z30,x31,z31],c)$
depends([PHI,kappai,kappar],[t1,a2])$
/*-----------------------------------------------*/
Skappai:kappai=2*k*K*B*sin(PHI)/(1-2*K*B*cos(PHI)+(K*B)^2);
Skappar:kappar=k*(1-(K*B)^2)/(1-2*K*B*cos(PHI)+(K*B)^2);
/*-----------------------------------------------*/
gradef(PHI,a2,-K)$
gradef(PHI,t1,OM)$
/*----t1-derivative of kappai and kappar---------*/
diff(Skappai,t1)$
ratsubst(1-cos(PHI)^2,sin(PHI)^2,%)$
factor(%);
substpart(k*(1-(K*B)^2)/kappar,%,2,2,1)$
Sdkappai:factor(%);
/**/
```

```
diff(Skappar,t1)$
ratsubst(kappar,k*(1-(K*B)^2)/(1-2*K*B*cos(PHI)+(K*B)^2),%)$
Sdkappar:ratsubst(kappai/k,2*K*B*sin(PHI)/
(1-2*K*B*cos(PHI)+(K*B)^2),%);
/*-----------------------------------------------*/
/*-----Define x10 and z10-------------------------*/
Sx10:x10=om*k*(1-K*B*cos(PHI))*sumA2;
Sz10:z10=om*k*K*B*sin(PHI)*sumA2;
gradef(sumA2,t1,A*As*exp(2*kappar*c)/(1-2*K*B*cos(PHI)+(K*B)^2))$
/**/
Q:rhs(Sx21)-rhs(Sz21);
/*-----------------------------------------------*/
/*-----Expressing diff(A,t1) interms of diff(A,a1) and A-----*/
rule1:diff(A,t1)=-part(lhs(Green_1),allbut(4));
/*-----------------------------------------------*/
/*-----Breaking down term[1] in pieces-----------*/
/*-----------------------------------------------*/
/*-----EQ1 corresponds to terms with x21 or z21 only in term[1]---*/
/*--------after transformation of z21 in terms of x21--------*/
/*-----EQ2 corresponds to terms in term[1] involving x10 and z10--*/
/*--------Integration for EQ2 is done by hand !!!-------------*/
nterms(term[1]);
part(term[1],[1,2,3,4,5,6,13,14,15,16,17,18]);
ev(%,z21=x21-Q,diff)$
EQ1:expand(%)$
nterms(%);
/*-----------------------------------------------*/
part(term[1],allbut(1,2,3,4,5,6,13,14,15,16,17,18));
ev(%,z21=x21-Q,diff)$
EQ2:ratsimp(%,diff(x10,c),diff(z10,c));
/*-----------------------------------------------*/
/*-----EQ11 is the contribution of EQ1 involving x21-------*/
```

```
/*----EQ12 is the contribution of EQ1 not involving x21----*/
/*-------------------------------------------------------*/
EQ11:part(EQ1,[1,2,3,4,5,6])$
diff(x21,t1)*ratcoef(%,diff(x21,t1))+
diff(x21,t1,1,c,1)*ratcoef(%,diff(x21,t1,1,c,1));
/*-----Rearranging the above expression-----------------*/
ss*part(%,1,1,3)*(part(%,2,1,3)+part(%,1,1,[1,2,4])/part(%,2,1,1));
/*---with---*/
ss:part(%th(2),2,1,1)/part(%th(2),2,2);
/*-----Integration wrt c yields-----------------------*/
at(diff(x21,t1),c=0)-2*kappar*'integrate(diff(x21(c),t1)
*exp(kappar*c-%i*kappai*c),c);
/*-------------------------------------------------------*/
EQ12:part(EQ1,allbut(1,2,3,4,5,6))$
nterms(%);
/*-------------------------------------------------------*/
/*-----EQ111 is the contribution to EQ11( to the above-----*/
/*---------intregral) from the first term in the---------*/
/*---------definition of x21 (depending on sumA2)--------*/
/*---------The integration is done by hand !!! ----------*/
/*-----EQ112 is the contribution to EQ11 from all the-----*/
/*---------other terms in the definition of x21.---------*/
/*---------The integration is performed by MACSYMA-------*/
/*-------------------------------------------------------*/
/*---------for EQ111 only the first term in x21 ---------*/
x21=part(rhs(Sx21),1);
diff(%,t1)$
expand(%*exp(kappar*c-%i*kappai*c));
/*---------for EQ112 all but the first term ------------*/
depends([F1,F2,F3],t1)$
x21=part(rhs(Sx21),allbut(1));
/*-----Assigning names to subexpressions----------------*/
```

```
part(rhs(Sx21),2)$
SF1:F1=part(%,1,allbut(2,7,9))/part(%,2);
part(rhs(Sx21),3)$
SF2:F2=part(%,1,allbut(1,6))/part(%,2);
part(rhs(Sx21),4)$
SF3:F3=-part(%,1,1,allbut(1,3,4))/part(%,1,2);
/*-----------------------------------------------*/
/*----Rewriting x21 with the new notations ------------*/
x21=(A*F1+diff(A,a1)*F3)*c*exp(kappar*c+%i*kappai*c)+
F2*A*exp(kappar*c+%i*kappai*c);
exp:diff(%,t1)$
expand(%*exp(kappar*c-%i*kappai*c))$
primitive(rhs(%),c)$
ev(%,c=0)$
expand(ev(rhs(exp),c=0)-2*kappar*%)$
subst(rhs(rule1),diff(A,t1),%)$
ev(%,diff)$
EQ:multthru(part(%,1))+multthru(part(%,2))+part(%,allbut(1,2))$
nterms(%);
for i:1 thru 10 do eq[i]:0$
/*-----------------------------------------------*/
/*-----proportional to diff(A,a1) ------------------*/
coeff(EQ,diff(A,a1));
nterms(%);
ev(%th(2),Sdkappai,Sdkappar)$
ev(%,SF1,SF3,diff)$
ev(%,Skappai,Skappar)$
ratsubst(1-cos(PHI)^2,sin(PHI)^2,%)$
ratsubst(om^2,g*k,%)$
eq[3]:ss*factor(%);
/*-----------------------------------------------*/
/*-----proportional to diff(A,a1,2) ----------------*/
```

```
coeff(EQ,diff(A,a1,2));
nterms(%);
ev(%th(2),SF3,Skappar)$
eq[4]:ss*factor(%);
/*-----------------------------------------------*/
/*-----proportional to A ------------------------*/
coeff(EQ,A);
nterms(%);
ev(%th(2),Sdkappai,Sdkappar)$
ev(%,SF1,SF2,diff)$
exp:ev(%,Skappai,Skappar)$
/**/
ratsimp(realpart(exp))$
ratsubst(1-cos(PHI)^2,sin(PHI)^2,%)$
eq[6]:ss*factor(%);
/**/
ratsimp(imagpart(exp))$
ratsubst(1-cos(PHI)^2,sin(PHI)^2,%)$
eq[7]:ss*factor(%);
/*-----Combining the results ---------------------*/
RES_MACSYMA_1:eq[1]*diff(A,t2)+eq[2]*diff(A,a2)+eq[3]*diff(A,a1)+
eq[4]*diff(A,a1,2)+eq[5]*A^2+eq[6]*A+%i*eq[7]*A;
/*-----------------------------------------------*/
RES_HAND:k^2*A^2*As/(1-K*B*cos(PHI)-%i*K*B*sin(PHI)) +
2*k^2*K*B*OM*A/(1-(K*B)^2)*(%i*cos(PHI)+sin(PHI)-%i*K*B)*sumA2;
eq[5]:coeff(%,A,2);
eq[8]:coeff(%th(2),sumA2);
/*-----------------------------------------------*/
/*-----Performing the integration for EQ12-------*/
/*-----and then factoring-----------------------*/
primitive(EQ12,c)$
ev(%,c=0)$
```

```
subst(rhs(rule1),diff(A,t1),%)$
ev(%,diff)$
EQ:expand(%)$
nterms(%);
/*-----------------------------------------------*/
/*-----proportional to diff(A,t2) ----------------*/
eq1[1]:coeff(EQ,diff(A,t2))$
nn[1]:nterms(%);
/*-----------------------------------------------*/
/*-----proportional to diff(A,a2) ----------------*/
eq1[2]:coeff(EQ,diff(A,a2))$
nn[2]:nterms(%);
/*-----------------------------------------------*/
/*-----proportional to diff(A,a1) ----------------*/
coeff(EQ,diff(A,a1))$
nn[3]:nterms(%);
ev(%th(2),Skappai,Skappar,diff)$
ratsimp(%)$
ratsubst(1-cos(PHI)^2,sin(PHI)^2,%)$
ratsubst(om^2,g*k,%)$
eq1[3]:factor(%);
/*-----------------------------------------------*/
/*-----proportional to diff(A,a1,2) ----------------*/
coeff(EQ,diff(A,a1,2))$
nn[4]:nterms(%);
ev(%th(2),Skappai,Skappar,diff)$
ratsimp(%)$
ratsubst(1-cos(PHI)^2,sin(PHI)^2,%)$
eq1[4]:ratsimp(%);
/*-----------------------------------------------*/
/*-----proportional to A^2 ----------------------*/
eq1[5]:coeff(EQ,A,2)$
```

```
nn[5]:nterms(%);
/*-----------------------------------------------*/
/*-----proportional to A-------------------------*/
exp:coeff(EQ,A)$
/*---real part ---*/
realpart(exp)$
nn[6]:nterms(%);
ev(%th(2),Skappai,Skappar,diff)$
ratsimp(%)$
ratsubst(1-cos(PHI)^2,sin(PHI)^2,%)$
eq1[6]:factor(%);
/*-----------------------------------------------*/
/*---imaginary part ---*/
imagpart(exp)$
nn[7]:nterms(%);
ev(%th(2),Skappai,Skappar,diff)$
ratsimp(%)$
ratsubst(1-cos(PHI)^2,sin(PHI)^2,%)$
eq1[7]:factor(%);
/*-----Checking the number of terms--------------*/
nt:0$
for i:1 thru 7 do nt:nt+nn[i]$
nt;
/*-----------------------------------------------*/
/*-----Results from the Macsyma integration------*/
RES_MACSYMA_2:eq1[1]*diff(A,t2)+eq1[2]*diff(A,a2)+eq1[3]*diff(A,a1)+
eq1[4]*diff(A,a1,2)+eq1[5]*A^2+eq1[6]*A+%i*eq1[7]*A;
/*-----------------------------------------------*/
/*-----Total contribution of term[1] to the integral is-----*/
/*-----------------------------------------------*/
part1:RES_HAND+RES_MACSYMA_1+RES_MACSYMA_2$
/*-----Saving the results-----------------------*/
```

```
save("schr_1.sav",part1,eq,eq1)$
closefile();
```

Appendix M.10: Command file SCHR_2.MAC

Integration of term[2] is performed

```
inchar:m$
outchar:n$
kill(all)$
loadprint:false$
bothcases:true$
derivsubst:true$
writefile("schr_2.out")$
/*-----------------------------------------------------*/
/*-------Integrating terms[2]--------------------------*/
timedate();
loadfile("wave_action.sav")$
loadfile("schr.sav")$
kill(term[1],term[3])$
/**/
depends([A,As],[a1,a2,t1,t2])$
depends(sumA2,[a1,a2,c,t1,t2])$
depends([x10,z10],[a1,a2,c,t1,t2])$
depends([x20,z20,x21,z21],[a1,c,c1,t1])$
depends([x30,z30,x31,z31],c)$
depends([PHI,kappai,kappar],[t1,a2])$
/**/
Skappai:kappai=2*k*K*B*sin(PHI)/(1-2*K*B*cos(PHI)+(K*B)^2);
Skappar:kappar=k*(1-(K*B)^2)/(1-2*K*B*cos(PHI)+(K*B)^2);
```

```
gradef(PHI,a2,-K)$
gradef(PHI,t1,OM)$
/*-----------------------------------------------------*/
/*-------Expressing diff(A,t1) interms of diff(A,a1) and A--------*/
rule1:diff(A,t1)=-part(lhs(Green_1),allbut(4));
/*-----------------------------------------------------*/
/*-------Expressing diff(A,t1,2) interms of a1 derivatives of A----*/
diff(rule1,t1)$
subst(rhs(rule1),diff(A,t1),%)$
ev(rhs(%),diff);
rule2:diff(A,t1,2)=multthru(part(%,1))+multthru(part(%,2))+
multthru(part(%,3))+part(%,allbut(1,2,3));
/*-----------------------------------------------------*/
nterms(term[2]);
primitive(term[2],c)$
ev(%,c=0)$
ev(%,rule2)$
subst(rhs(rule1),diff(A,t1),%)$
ev(%,diff)$
EQ:expand(%)$
nterms(EQ);
/*-----------------------------------------------------*/
/*-------Proportional to diff(A,t2) ----------------------*/
coeff(EQ,diff(A,t2))$
nn[1]:nterms(%);
ev(%th(2),Skappai,Skappar,diff)$
ratsimp(%)$
ratsubst(1-cos(PHI)^2,sin(PHI)^2,%)$
eq2[1]:ratsimp(%);
/*-----------------------------------------------------*/
/*-------Proportional to diff(A,a2) ----------------------*/
eq2[2]:coeff(EQ,diff(A,a2));
```

```
nn[2]:nterms(%);
/*-----------------------------------------------------*/
/*-------Proportional to diff(A,a1) ---------------------*/
coeff(EQ,diff(A,a1))$
nn[3]:nterms(%);
ev(%th(2),Skappai,Skappar,diff)$
ratsimp(%)$
ratsubst(1-cos(PHI)^2,sin(PHI)^2,%)$
eq2[3]:ratsimp(%);
/*-----------------------------------------------------*/
/*-------Proportional to diff(A,a1,2) ---------------------*/
coeff(EQ,diff(A,a1,2))$
nn[4]:nterms(%);
ev(%th(2),Skappai,Skappar,diff)$
ratsimp(%)$
ratsubst(1-cos(PHI)^2,sin(PHI)^2,%)$
eq2[4]:factor(%);
/*-----------------------------------------------------*/
/*-------Proportional to A^2 ---------------------*/
eq2[5]:coeff(EQ,A,2)$
nn[5]:nterms(%);
/*-----------------------------------------------------*/
/*-------Proportional to A---------------------*/
exp:coeff(EQ,A)$
/*--real part --*/
realpart(exp)$
nn[6]:nterms(%);
ev(%th(2),Skappai,Skappar,diff)$
ratsimp(%)$
ratsubst(1-cos(PHI)^2,sin(PHI)^2,%)$
eq2[6]:ratsimp(%);
/*-----------------------------------------------------*/
```

```
/*—-imaginary part —*/
imagpart(exp)$
nn[7]:nterms(%);
ev(%th(2),Skappai,Skappar,diff)$
ratsimp(%)$
ratsubst(1-cos(PHI)^2,sin(PHI)^2,%)$
eq2[7]:ratsimp(%);
/*———Checking the number of terms for term[2]————————*/
nt:0$
for i:1 thru 7 do nt:nt+nn[i]$
nt;
/*———Forming the contribution of term[2]————————————-*/
part2:eq2[1]*diff(A,t2)+eq2[2]*diff(A,a2)+eq2[3]*diff(A,a1)+
eq2[4]*diff(A,a1,2)+eq2[5]*A^2+eq2[6]*A+%i*eq2[7]*A;
/*———Saving the results———————————————————*/
save("schr_2.sav",part2,eq2)$
closefile();
```

Appendix M.11: Command file SCHR_3.MAC

Substitution of $\mathcal{O}(\epsilon)$ and $\mathcal{O}(\epsilon^2)$ displacements in term[3].

```
inchar:m$
outchar:n$
kill(all)$
loadprint:false$
bothcases:true$
derivsubst:true$
writefile("schr_3.out")$
timedate();
```

```
/*-----------------------------------------------*/
/*--------Dealing with the right hand side of solvability---*/
loadfile("schr.sav")$
kill(term[1],term[2])$
loadfile("solve_2.sav")$
loadfile("wave_action.sav")$
/**/
depends([A,As],[a1,a2,t1,t2])$
depends(sumA2,[a1,a2,c,t1,t2])$
depends([x10,z10],[a1,a2,c,t1,t2])$
depends([x20,z20,x21,z21],[a1,c,c1,t1])$
depends([x30,z30,x31,z31],c)$
depends([PHI,kappai,kappar],[t1,a2])$
/**/
Skappai:kappai=2*k*K*B*sin(PHI)/(1-2*K*B*cos(PHI)+(K*B)^2);
Skappar:kappar=k*(1-(K*B)^2)/(1-2*K*B*cos(PHI)+(K*B)^2);
gradef(PHI,a2,-K)$
gradef(PHI,t1,OM)$
/**/
Sx10:x10=om*k*(1-K*B*cos(PHI))*sumA2;
Sz10:z10=om*k*K*B*sin(PHI)*sumA2;
gradef(sumA2,t1,A*As*exp(2*kappar*c)/(1-2*K*B*cos(PHI)+(K*B)^2))$
/*-----------------------------------------------*/
/*-----Expressing diff(A,t1) in terms of diff(A,a1) and A---*/
rule1:diff(A,t1)=-part(lhs(Green_1),allbut(4));
/*-----------------------------------------------*/
/*-----Expressing diff(A,t1,2) in terms of diff(A,a1)-----*
diff(rule1,t1)$
subst(rhs(rule1),diff(A,t1),%)$
ev(rhs(%),diff);
rule2:diff(A,t1,2)=multthru(part(%,1))+multthru(part(%,2))+
multthru(part(%,3))+part(%,allbut(1,2,3));
```

```
/**/
Q:rhs(Sx21)-rhs(Sz21);
/*-----------------------------------------------------*/
/*-----EQ1 corresponds to the first 8 terms needing evaluation-*/
/*-----EQ2 corresponds to the remaining terms-----------------*/
/*-----------------------------------------------------*/
nterms(term[3]);
/*-----Dealing with EQ1 ------------------------------*/
part(term[3],[1,2,3,4,5,6,7,8]);
ev(%,Sx10,Sz10,diff)$
ev(%,z21=x21-Q,diff)$
ev(%,Sx21,diff)$
ev(%,c=0)$
ev(%,Skappai,Skappar,diff)$
ev(%,rule1)$
ratsubst(1-cos(PHI)^2,sin(PHI)^2,%)$
EQ1:expand(%)$
/*-----Dealing with EQ2 ------------------------------*/
part(term[3],allbut(1,2,3,4,5,6,7,8))$
ratsimp(%,diff(A,t1,2),diff(A,a2),diff(a,t2))$
ev(%,rule2)$
EQ2:expand(%)$
/*-----Combining the contributions ---------------------*/
EQ:expand(EQ1+EQ2)$
nterms(%);
/*----- ------------------------------------*/
/*-----Proportional to diff(A,t2) ------------------*/
coeff(EQ,diff(A,t2))$
nn[1]:nterms(%);
ev(%th(2),Skappai,Skappar,diff)$
ratsimp(%)$
ratsubst(1-cos(PHI)^2,sin(PHI)^2,%)$
```

```
eq3[1]:factor(%);
/*-----------------------------------------------*/
/*-----Proportional to diff(A,a2) ----------------*/
coeff(EQ,diff(A,a2))$
nn[2]:nterms(%);
ev(%th(2),Skappai,Skappar,diff)$
ratsimp(%)$
ratsubst(1-cos(PHI)^2,sin(PHI)^2,%)$
eq3[2]:factor(%);
/*-----------------------------------------------*/
/*-----Proportional to diff(A,a1) ----------------*/
coeff(EQ,diff(A,a1))$
nn[3]:nterms(%);
ev(%th(2),Skappai,Skappar,diff)$
ratsimp(%)$
ratsubst(1-cos(PHI)^2,sin(PHI)^2,%)$
eq3[3]:factor(%);
/*-----------------------------------------------*/
/*-----Proportional to diff(A,a1,2) ----------------*/
coeff(EQ,diff(A,a1,2))$
nn[4]:nterms(%);
ev(%th(2),Skappai,Skappar,diff)$
ratsimp(%)$
ratsubst(1-cos(PHI)^2,sin(PHI)^2,%)$
eq3[4]:factor(%);
/*-----------------------------------------------*/
/*-----Proportional to A^2 ----------------*/
coeff(EQ,A,2)$
nn[5]:nterms(%);
ev(%th(2),Skappai,Skappar,diff)$
ratsimp(%)$
ratsubst(1-cos(PHI)^2,sin(PHI)^2,%)$
```

```
eq3[5]:factor(%);
/*-----------------------------------------------*/
/*-----Proportional to A-------------------------*/
coeff(EQ,A)$
ev(%,sumA2=0,diff)$
exp:expand(%)$
/*---real part ---*/
realpart(exp)$
nn[6]:nterms(%);
ev(%th(2),Skappai,Skappar,diff)$
ratsimp(%)$
ratsubst(1-cos(PHI)^2,sin(PHI)^2,%)$
eq3[6]:factor(%);
/*-----------------------------------------------*/
/*---imaginary part ---*/
imagpart(exp)$
nn[7]:nterms(%);
ev(%th(2),Skappai,Skappar,diff)$
ratsimp(%)$
ratsubst(1-cos(PHI)^2,sin(PHI)^2,%)$
eq3[7]:factor(%);
/*-----------------------------------------------*/
/*-----Proportional to sumA2 ---------------------*/
coeff(EQ,sumA2)$
nn[8]:nterms(%);
ev(%th(2),Skappai,Skappar,diff)$
ratsimp(%)$
ratsubst(1-cos(PHI)^2,sin(PHI)^2,%)$
eq3[8]:factor(%);
/*-----------------------------------------------*/
/*-----Proportional to diff(sumA2,a1) ------------*/
coeff(EQ,diff(sumA2,a1))$
```

```
nn[9]:nterms(%);
ev(%th(2),Skappai,Skappar,diff)$
ratsimp(%)$
ratsubst(g*k,om^2,%)$
ratsubst(1-cos(PHI)^2,sin(PHI)^2,%)$
eq3[9]:ratsimp(%);
/*-----Checking the number of terms for term[2]----------*/
nt:0$
for i:1 thru 9 do nt:nt+nn[i]$
nt;
/*-----Forming the contribution of term[3]----------*/
part3:eq3[1]*diff(A,t2)+eq3[2]*diff(A,a2)+eq3[3]*diff(A,a1)+
eq3[4]*diff(A,a1,2)+eq3[5]*A^2+eq3[6]*A+%i*eq3[7]*A +
eq3[8]*sumA2+eq3[9]*diff(sumA2,a1);
/*-----Saving the results----------*/
save("schr_3.sav",part3,eq3)$
closefile();
```

Appendix M.12: Command file SCHRODINGER.MAC

Derivation of the nonlinear Schrödinger equation for the short wave amplitude. Terms are combined from SCHR_1.SAV, SCHR_2.SAV and SCHR_3.SAV.

```
inchar:m$
outchar:n$
kill(all)$
loadprint:false$
bothcases:true$
writefile("schrodinger.out")$
```

```
/*-------------------------------------------------------*/
timedate();
loadfile("schr_1.sav")$
loadfile("schr_2.sav")$
loadfile("schr_3.sav")$
/**/
depends([A,As],[a1,a2,t1,t2])$
depends(sumA2,[a1,a2,c,t1,t2])$
F:-%i*om/2;
/*-------------------------------------------------------*/
/*-----Proportional to diff(A,t2) ------------------------*/
eq[1]+eq1[1]+eq2[1]-eq3[1]$
expand(%*F)$
C[1]:factor(%);
/*-------------------------------------------------------*/
/*-----Proportional to diff(A,a2) ------------------------*/
eq[2]+eq1[2]+eq2[2]-eq3[2]$
expand(%*F)$
C[2]:factor(%);
/*-------------------------------------------------------*/
/*-----Proportional to diff(A,a1) ------------------------*/
/*-----Simplifying eq2[3] and eq3[3] ---------------------*/
eq2[3];
ratsubst(g*k,om^2,%)$
eq2[3]:factor(%);
/**/
eq3[3];
ratsubst(g*k,om^2,%)$
eq3[3]:factor(%);
/*-----Combining the contributions ----------------------*/
eq[3]+eq1[3]+eq2[3]-eq3[3]$
expand(%*F)$
```

```
ratsubst(1-cos(PHI)^2,sin(PHI)^2,%)$
C[3]:factor(%);
/*-----------------------------------------------------*/
/*-----Proportional to diff(A,a1,2) ---------------------*/
eq[4]+eq1[4]+eq2[4]-eq3[4]$
expand(%*F)$
ratsubst(om^2/k,g,%)$
ratsubst(1-cos(PHI)^2,sin(PHI)^2,%)$
C[4]:factor(%);
/*-----------------------------------------------------*/
/*-----Proportional to A^2-------------------------------*/
eq[5]+eq1[5]+eq2[5]-eq3[5]$
expand(%*F)$
ratsubst(1-cos(PHI)^2,sin(PHI)^2,%)$
C[5]:factor(%);
/*-----------------------------------------------------*/
/*-----Proportional to A---------------------------------*/
/*-----Real part -----------------------------------------*/
/*-----Simplifying some terms ----------------------------*/
eq2[6]:factor(eq2[6]);
/*-----Combining the four contributions -----------------*/
eq[6]+eq1[6]+eq2[6]-eq3[6]$
expand(%*F)$
ratsubst(1-cos(PHI)^2,sin(PHI)^2,%)$
C[6]:factor(%);
/*--imaginary part --*/
eq[7]+eq1[7]+eq2[7]-eq3[7]$
expand(%*F)$
ratsubst(1-cos(PHI)^2,sin(PHI)^2,%)$
C[7]:factor(%);
/*-----------------------------------------------------*/
/*-----Proportional to sumA2-----------------------------*/
```

```
/*------Checking two contributions ------------------------*/
eq1[8];
eq2[8];
eq[8]-eq3[8]$
expand(%*F)$
C[8]:factor(%);
/*-------------------------------------------------------*/
/*------Proportional to diff(sumA2,a1) --------------------*/
/*------Checking two contributions ------------------------*/
eq1[9];
eq2[9];
eq[9]-eq3[9]$
expand(%*F)$
C[9]:factor(%);
/*-------------------------------------------------------*/
/*------Normalizing each coefficient by C[1] and simplyfying them---*/
/*------Proportional to diff(A,t2) ------------------------*/
D[1]:1;
/*-------------------------------------------------------*/
/*------Proportional to diff(A,a2) ------------------------*/
D[2]:C[2]/C[1];
/*-------------------------------------------------------*/
/*------Proportional to diff(A,a1) ------------------------*/
D[3]:C[3]/C[1];
/*-------------------------------------------------------*/
/*------Proportional to diff(A,a1,2) ----------------------*/
eq:C[4]/C[1]$
factor(realpart(%))$
ratsubst(1-cos(PHI)^2,sin(PHI)^2,%);
/*---*/
factor(imagpart(eq))$
ratsubst(1-cos(PHI)^2,sin(PHI)^2,%)$
```

```
D[4]:%i*factor(%);
/*-----------------------------------------------------*/
/*-----Proportional to A^2-------------------------------*/
eq:C[5]/C[1]$
factor(realpart(%))$
ratsubst(1-cos(PHI)^2,sin(PHI)^2,%);
/*---*/
factor(imagpart(eq))$
ratsubst(1-cos(PHI)^2,sin(PHI)^2,%)$
D[5]:%i*factor(%);
/*-----------------------------------------------------*/
/*-----Proportional to A---------------------------------*/
eq:(C[6]+%i*C[7])/C[1]$
/*---real part ---*/
factor(realpart(%))$
ratsubst(1-cos(PHI)^2,sin(PHI)^2,%)$
D[6]:factor(%);
/*---imaginary part ---*/
factor(imagpart(eq))$
ratsubst(1-cos(PHI)^2,sin(PHI)^2,%)$
D[7]:factor(%);
/*-----------------------------------------------------*/
Green_2:diff(A,t2)+D[2]*diff(A,a2)+D[4]*diff(A,a1,2)+D[5]*A^2+
D[6]*A +%i*D[7]*A=0;
/*-----Save results--------------------------------------*/
save("schrodinger.sav",Green_2,D)$
closefile();
```

Appendix N: FORTRAN Implementation of Floquet Theory in Chapter II:

This program computes the Floquet multipliers in the sideband instability of a uniform short wave. A large set of multiplier pairs can be computed when either of ν or α is varied while keeping the other parameters constant. The following notations have been used:

bk	long wave slope KB
ak	short wave slope $\epsilon k\overline{A}$
om	frequency ratio $\epsilon\frac{\Omega}{\sigma}$
alpha	parameter α
nu	disturbance wavenumber ν
mu(1), mu(2)	Floquet multipliers $\mu_{1,2}$
arg	Initial phase of the most unstable disturbance
errmax	maximum departure from $\mu_1\mu_2 = 1$
k	integration time step in Runge-Kutta routine

```
      program floq2d
      implicit real*8 (a-h,o-z)
      complex*16 a11,a12,a21,a22,ci,cone,czero
     &, aa11,bb11,cc11,dd11
     &, aa12,bb12,cc12,dd12
     &, aa21,bb21,cc21,dd21
     &, aa22,bb22,cc22,dd22
     &, sum,prod,det,mu(2),z
      real*8 k,nu
      character*15 filnam
c
      zero=0.0d0
      one=1.0d0
      two=2.0d0
      pi=3.14159265359d0
      twopi=two*pi
      ci=dcmplx(zero,one)
      cone=dcmplx(one,zero)
      czero=dcmplx(zero,zero)
      errmax=zero
```

```
      tau0=0.0d0
      k=1.0d-3
      iter=1000
      k=twopi*k
c
      write(6,*)
      write(6,*) '—— Floquet Analysis ——'
      write(6,*)
      write(6,*) ' change in nu: 1'
      write(6,*) ' change in alpha (variable kA): 2'
      write(6,*) ' change in alpha (variable OM/om): 3'
      read(5,*) nopt
c
      if(nopt-2) 10,20,30
c
 10   write(6,*) ' enter KB, kA and OM/om'
      read(5,*) bk,ak,om
      write(6,*) ' enter minimum, maximum and # values for nu'
      read(5,*) parmin,parmax,npt
c
      delta=one-om/two
      alpha=(ak**2)/om/delta/2.0d0
      q0=one-two*bk*dcos(tau0)+bk**2
      g0=dexp(om*(one-bk**2)/delta/q0)/q0
      goto 40
c
 20   write(6,*) ' enter KB, OM/om and nu'
      read(5,*) bk,om,nu
      write(6,*) ' enter minimum, maximum and # values for alpha'
      read(5,*) parmin,parmax,npt
c
      delta=one-om/two
      q0=one-two*bk*dcos(tau0)+bk**2
      g0=dexp(om*(one-bk**2)/delta/q0)/q0
      goto 40
```

```
c
 30 write(6,*) ' enter KB, kA and nu'
    read(5,*) bk,ak,nu
    write(6,*) ' enter minimum, maximum and # values for alpha'
    read(5,*) parmin,parmax,npt
c
    q0=one-two*bk*dcos(tau0)+bk**2
c
 40 write(6,*) ' enter filnam'
    read(5,50) filnam
 50 format(a15)
    open(unit=10,file=filnam,status='new',form='formatted')
c
c-> some parameters
c
    do 200 id=1,npt
    if(nopt-2) 60,70,80
c
 60 nu=parmin+dble(id-1)*(parmax-parmin)/dble(npt-1)
    goto 90
c
 70 alpha=parmin+dble(id-1)*(parmax-parmin)/dble(npt-1)
    ak=dsqrt(two*alpha*om*delta)
    goto 90
c
 80 alpha=parmin+dble(id-1)*(parmax-parmin)/dble(npt-1)
    om=one-dsqrt(one-ak**2/alpha)
    delta=one-om/two
    g0=dexp(om*(one-bk**2)/delta/q0)/q0
c
c-> initial data for basis functions
c
 90 a11=cone
    a12=czero
    a21=czero
    a22=cone
```

```
      tau=tau0
c
c-> 4th order Runge Kutta
c
      do 100 i=1,iter
      q1=one-two*bk*dcos(tau)+bk**2
      q12=one-two*bk*dcos(tau+k/two)+bk**2
      q2=one-two*bk*dcos(tau+k)+bk**2
c
      g1=dexp(om*(one-bk**2)/delta/q1)/q1**2
      g12=dexp(om*(one-bk**2)/delta/q12)/q12**2
      g2=dexp(om*(one-bk**2)/delta/q2)/q2**2
c
c-> computing the first stage
c
      aa11= k * ci * alpha * nu * a21 / 4.0d0
      aa21= k * two * ci * alpha * nu * ( nu**2/8.0d0 - g1/g0 ) * a11
      aa12= k * ci * alpha * nu * a22 / 4.0d0
      aa22= k * two * ci * alpha * nu * ( nu**2/8.0d0 - g1/g0 ) * a12
c
c-> computing the second stage
c
      tau=tau+k/two
c
      bb11= k * ci * alpha * nu * ( a21 + aa21/two ) / 4.0d0
      bb21= k * two * ci * alpha * nu * ( nu**2/8.0d0 - g12/g0 ) *
     & ( a11 + aa11/two )
      bb12= k * ci * alpha * nu * ( a22 + aa22/two ) / 4.0d0
      bb22= k * two * ci * alpha * nu * ( nu**2/8.0d0 - g12/g0 ) *
     & ( a12 + aa12/two )
c
c-> computing the third stage
c
      cc11= k * ci * alpha * nu * ( a21 + bb21/two ) / 4.0d0
      cc21= k * two * ci * alpha * nu * ( nu**2/8.0d0 - g12/g0 ) *
     & ( a11 + bb11/two )
```

```
      cc12= k * ci * alpha * nu * ( a22 + bb22/two ) / 4.0d0
      cc22= k * two * ci * alpha * nu * ( nu**2/8.0d0 - g12/g0 ) *
     & ( a12 + bb12/two )
c
c-> computing the fourth stage
c
      tau=tau+k/two
      dd11= k * ci * alpha * nu * ( a21 + cc21 ) / 4.0d0
      dd21= k * two * ci * alpha * nu * ( nu**2/8.0d0 - g2/g0 ) *
     & ( a11 + cc11 )
      dd12= k * ci * alpha * nu * ( a22 + cc22 ) / 4.0d0
      dd22= k * two * ci * alpha * nu * ( nu**2/8.0d0 - g2/g0 ) *
     & ( a12 + cc12 )
c
c-> combining the results
c
      a11=a11+(aa11+two*(bb11+cc11)+dd11)/6.0d0
      a12=a12+(aa12+two*(bb12+cc12)+dd12)/6.0d0
      a21=a21+(aa21+two*(bb21+cc21)+dd21)/6.0d0
      a22=a22+(aa22+two*(bb22+cc22)+dd22)/6.0d0
100 continue
c
      sum=a11+a22
      prod=a11*a22-a21*a12
      det=sum**2-4.0d0*prod
      mu(1)=(sum+zsqrt(det))/two
      mu(2)=(sum-zsqrt(det))/two
      errmax=dmax1(errmax,zabs(prod-one))
      if(dreal(det) .le. 0.0d0) then
      write(10,1000) ak,om,alpha,nu,(mu(j),j=1,2)
      else
      if(zabs(mu(1)) .gt. 1.0) then
      z=-(a11-mu(1))/a12
      else
```

```
      z=-(a11-mu(2))/a12
      endif
      arg=carg(1.0+z/nu)
      write(10,1000) ak,om,alpha,nu,(mu(j),j=1,2),arg
      endif
200 continue
c
      write(10,2000) errmax
      write(10,*)
      close(unit=10)
c
      noindent 1000 format(x,f5.3,x,f7.5,x,f5.3,x,f5.3,x,2(f8.5,x,f8.5,x)
     &,f8.5)
1010 format((x,3(i4,2x)))
1100 format(x,f6.4,x,f8.5,2(x,2e11.4),x,e11.4)
2000 format(x,e10.3)
3000 format(2x,i1)
      stop
      end
ccc
c Finding the argument of a complex quantity
c234567
      real*8 function carg(z)
      complex*16 z
c
      if(zabs(z) .eq. 0.0d0) then
      write(6,*) 'argument is undefined !!'
      else
      carg=dimag(zlog(z/zabs(z)))
      endif
      return
      end
```

Appendix O: FORTRAN Program for Nonlinear Schrödinger Evolution:

This program numerically computes the evolution of the sound envelope using the split-step method. Space-time results for the complex amplitude are stored in "file1", the Fourier spectrum evolution in "file2", energy conservation in "file3" and aliasing in "file4". Each of these file bears the run number. File "c3.d" contains the parameters used in the program "c3.f". A standard double precision Fast Fourier transform is used. The following notations have been used:

bk	long wave slope KB
ak	short wave slope $\epsilon k\overline{A}$
om	frequency ratio $\epsilon\frac{\Omega}{\sigma}$
alpha	parameter α
nu	disturbance wavenumber ν
theta1	Phase of the initial sideband disturbance θ_1
h	spatial grid size h
dt	integration time step in Runge-Kutta routine

```
      program c3
      implicit real*8 (a-h,o-z)
      complex*16 a(4096),at(4096),datat0,ci,aa,bb
      integer iwk(15),imode(1024)
      logical flag1,flag2,flag3
      character*10 file1,file2,file3
      character*12 file4
      real*8 k,d1(4096),d2(4096),nu
      common /idata/ nu,theta1
      common /spdiff/ d1,d2,scale
c
      one=1.0d0
      two=2.0d0
      zero=0.0d0
      pi=3.14159265359d0
      twopi=two*pi
      ci=dcmplx(zero,one)
      flag1=.false.
      flag2=.false.
```

```
      flag3=.false.
      file1='p3d .dat'
      file2='fou .dat'
      file3='nrg .dat'
      file4='alias .dat'
c
c-> reading data file
c
      open(unit=10,file='c3.d',status='old',form='formatted')
      read(10,1000) bk,ak,om
      read(10,1000) nu,theta1
      read(10,1000) tmax
      tmax=twopi*tmax
c
      read(10,1010) m
      npnt=2**m
      npd2=npnt/2
      scale=nu
c
      h=twopi/scale/dble(npnt)
      read(10,1000) dt
      dt=twopi*dt
c
      read(10,1010) nopt1,nopt2,nopt3
      if(nopt2 .eq. 1) then
      read(10,1010) nmode
      if(nmode .lt. 6) then
      read(10,1010) (imode(i),i=1,nmode)
      else
      nmode=npd2
      do 5 i=1,npd2
      imode(i)=i
    5 continue
      endif
      endif
```

```
      read(10,1010) nplot1, nplot2, nplot3
      read(10,1010) necho
      close(unit=10)
c
c-> deriving some parameters
c
      delta=one-om/two
      alpha=(ak**2)/delta/om/two
      dtcrit=4.0d0/alpha/nu**2/float(npd2)**2
      if(dt .gt. dtcrit) then
      write(6,*) ' Time step must be smaller than ',dtcrit
      stop
      endif
c
c-> updating the run number
c
      open(unit=10,file='run.dat',status='old',form='formatted')
      read(10,10) nrun
      close(unit=10,status='delete')
      nrun=nrun+1
      open(unit=10,file='run.dat',status='new',form='formatted')
      write(10,10) nrun
      close(unit=10)
   10 format(2x,i3.3)
c
      write(6,*) ' — Nonlinear Stability of a Stokes wave —'
      write(6,*) ' - to sideband disturbances -'
      write(6,*) ' Run # ', nrun
      write(6,*)
c
      if(nopt1 .eq. 1) then
      flag1=.true.
      write(file1(4:6),15) nrun
      open(unit=11,file=file1,status='new',form='formatted')
```

```
      endif
      if(nopt2 .eq. 1) then
      flag2=.true.
      write(file2(4:6),15) nrun
      open(unit=12,file=file2,status='new',form='formatted')
      endif
      if(nopt3 .eq. 1) then
      flag3=.true.
      write(file3(4:6),15) nrun
      open(unit=13,file=file3,status='new',form='formatted')
      endif
   15 format(i3.3)
c
c-> defining the initial data
c
      call spectral(m)
      do 20 i=1,npnt
      xi=-pi/scale+h*dble(i-1)
      a(i)=datat0(xi)
   20 continue
c
      if (flag1) write(11,2000) (zabs(a(i)),i=1,npnt)
      if (flag2) then
      do 30 i=1,npnt
      at(i)=a(i)
   30 continue
      call forfft(at,m,iwk)
      peak=zabs(at(1))
      write(12,2000) (zabs(at(imode(j)))/peak,j=1,nmode)
      endif
      if (flag3) then
      sum10=zero
      do 40 i=1,npnt
      sum10=sum10+zabs(a(i))**2
   40 continue
```

```
      write(13,2000) zero,one,-10.0d0
      endif
cccc
c PART II
c time stepping begins
cccc
      it=0
      k=dt/two
      tau=0.0d0
      q0=one-two*bk*dcos(tau)+bk**2
      g0=dexp(om*(one-bk**2)/delta/q0)/q0
      u=one+bk**2
      v=one-bk**2
c
      nter=idnint(tmax/dt)
c
      do 200 iter=1,nter
      it=it+1
      if(mod(it,necho) .eq. 0) write(6,*) ' ... tau = '
     &, sngl((tau+dt)/twopi)
c
      q1=u-two*bk*dcos(tau)
      q14=u-two*bk*dcos(tau+k/two)
      q12=u-two*bk*dcos(tau+k)
      q34=u-two*bk*dcos(tau+3.0d0*k/two)
      q2=u-two*bk*dcos(tau+dt)
c
      g1=dexp(om*v/delta/q1)/q1**2/g0
      g14=dexp(om*v/delta/q14)/q14**2/g0
      g12=dexp(om*v/delta/q12)/q12**2/g0
      g34=dexp(om*v/delta/q34)/q34**2/g0
      g2=dexp(om*v/delta/q2)/q2**2/g0
c
c-> Modified Euler Scheme for Nonlinear part
c
      do 50 i=1,npnt
```

```
      aa= -k*ci*alpha*g1*a(i)*zabs(a(i))**2
      bb= -k*ci*alpha*g14*(a(i)+aa/two)*zabs(a(i)+aa/two)**2
      at(i)=a(i)+bb
   50 continue
c
c-> Exact integration of Linear part
c-> Fourier transform of Nonlinear solution
c
      call forfft(at,m,iwk)
c
c-> integrating exactly for a dt step
c
      do 60 i=1,npd2-1
      at(i)=at(i)*zexp(ci*alpha/4.0d0*d2(i)*dt)
   60 continue
c
      do 70 i=npd2,npd2+2
      at(i)=at(i)/(one-ci*alpha/4.0d0*d2(i)*dt)
   70 continue
c
      do 80 i=npd2+3,npnt
      at(i)=at(i)*zexp(ci*alpha/4.0d0*d2(i)*dt)
   80 continue
c
c-> return to physical space
c
      call invfft(at,m,iwk)
c
c-> Modified Euler Scheme for Nonlinear part
c
      do 90 i=1,npnt
      aa= -k*ci*alpha*g12*at(i)*zabs(at(i))**2
      bb= -k*ci*alpha*g34*(at(i)+aa/two)*zabs(at(i)+aa/two)**2
      a(i)=at(i)+bb
   90 continue
c
      tau=tau+dt
```

```
ccccc
c PART III
c Data collection
ccccc
c-> amplitudes
c
      if(flag1 .and. mod(it,nplot1) .eq. 0) then
      write(11,2000) (zabs(a(i)),i=1,npnt)
      endif
c-> Fourier amplitudes
c
      if(flag2 .and. mod(it,nplot2) .eq. 0) then
      do 100 i=1,npnt
      at(i)=a(i)
100 continue
      call forfft(at,m,iwk)
      write(12,2000) (zabs(at(imode(j)))/peak,j=1,nmode)
      endif
c-> Recording the total energy
c
      if (flag3 .and. mod(it,nplot3) .eq. 0) then
      sum1=zero
      do 110 i=1,npnt
      sum1=sum1+zabs(a(i))**2
      at(i)=a(i)
110 continue
      sum1=sum1/sum10
c
      err1=dlog10(dabs(one-sum1))
      write(13,2000) tau/pi,sum1,err1
      endif
200 continue
c
c-> checking aliasing
c
      call forfft(a,m,iwk)
      amax=zero
```

```
      do 210 i=1,npnt
      amax=dmax1(amax,zabs(a(i)))
210 continue
c
      write(file4(6:8),15) nrun
      open(unit=14,file=file4,status='new',form='formatted')
      write(14,2000) (zabs(a(i))/amax,i=1,npd2)
      close(unit=14)
c
1000 format((t6,5(d11.4,2x)))
1010 format(t6,5(i4,2x))
2000 format((2x,6(d11.4,x)))
      stop
      end
cccc
c defines initial data for short wave amplitude
c234567
      function datat0(xi)
      real*8 xi,nu,theta1
      complex*16 datat0,ci
      common /idata/ nu,theta1
      ci=dcmplx(0.0d0,1.0d0)
c
      datat0=1.0d0+0.1d0*dcos(nu*xi)*zexp(ci*theta1)
      return
      end
cccc
c computing the coefficients multiplying the fourier modes to get
c the spectral second derivative
c234567
      subroutine spectral(m)
      real*8 d1(4096),d2(4096),scale
      integer i,m,npnt,npd2
      common /spdiff/ d1,d2,scale
c
```

```
      npnt=2**m
      npd2=npnt/2
c
      do 5 i=1,npnt
      if( i - npd2 -1 ) 1,2,3
    1 d2(i)=(dble(i-1)*scale)**2
      d1(i)=dble(i-1)*scale
      goto 5
    2 d2(i)=(dble(i-1)*scale)**2
      d1(i)=0.0d0
      goto 5
    3 d2(i)=(dble(i-1-npnt)*scale)**2
      d1(i)=dble(i-1-npnt)*scale
    5 continue
      return
      end
```